TECTONIC AND SEDIMENTARY HISTORY OF THE MID NATAL VALLEY (S.W. INDIAN OCEAN)

by

STEPHEN W. GOODLAD

Thesis submitted in fulfilment of the requirements for the degree of Doctor of Philosophy in the Faculty of Science at the University of Cape Town

February 1986

ABSTRACT

The Natal Valley is a sediment-filled marine basin situated between the east coast of southern Africa (Natal) and the Mozambique Ridge. Geophysical and sedimentological techniques are used in a broad geological study of the mid Natal Valley. Major emphasis is directed to: (a) basin history and tectonic evolution; (b) seismic stratigraphy of the basin fill; (c) recent sedimentary processes and responses.

General basin morphology is defined by five major physiographic provinces: continental shelf and slope, Tugela Cone, Central Terrace, Mozambique Ridge and deep basin plain. Thinned (20-25 km) continental crust, attenuated and subsided in response to Gondwana rifting and drifting, underlies the Central Terrace, Tugela Cone and Mozambique Ridge. Southern margins of the Central Terrace and Tugela Cone are cored by a series of sub-sea floor ridge and pinnacle complexes (Naude, East Tugela and South Tugela Ridges). Geochemical analyses of East Tugela Ridge basalts suggest a transitional origin but with continental affinities. These volcanic marginal ridges may approximately delineate the continental-oceanic crust boundary (COB) in the Natal Valley. To the south, the deep basin plain is underlain by oceanic crust.

Recognition of Mesozoic magnetic anomalies M0-M12 in the southern Natal Valley constrains the early relative motion between the Falkland Plateau (South America) and Africa. Optimum continuity of inter-continental structural lineaments is achieved by overlapping anomaly M10N of the Natal Valley and Georgia Basin. Simultaneously, the leading apex of the Falkland Plateau

is rotated against the South Tugela Ridge, a marginal ridge suspected to have been emplaced within continental crust immediately north of the COB. It is implied that, in this zone of SW Gondwana, sea floor spreading commenced at ~125 Myr.

With improvement in definition of the COB of the Mozambique Ridge and Natal Valley, morphological fits suggest that the southern Mozambique Ridge may presently be situated 160 km east of its pre-drift palaeo-position. Palaeo-fracture zone trends (S72°W) accommodating the translation are recognised by basement morphology, magnetic lineaments, non-magnetic fracture ridges and bathymetric offsets on the Mozambique Ridge flanks. Crustal thickness and structural style, East Tugela Ridge basalt geochemistry and the absence of demonstrable magnetic and fracture zone lineaments suggest that the northern Natal Valley is underlain by subsided attenuated continental crust. This crustal status invalidates Gondwana refits in which East Antarctica is abutted against the Lebombo Line.

Seismic stratigraphic analysis of the basin fill is established relative to four regional depositional sequence boundaries: acoustic basement, horizon McDuff (Cenomanian-Turonian), Angus (early Oligocene) and Jimmy (early Pliocene). These sequence boundaries define the four major depositional sequences (sediment units A-D). Time-depth and time-thickness maps for the sequence boundaries and depositional sequences respectively help reconstruct the basin sedimentary history.

Over basement-high zones (Central Terrace and Mozambique Ridge), sediment unit A (pre-McDuff) growth-faulted onlap fill has aggraded to >1,0 secs time-thickness in irregular graben. In the deep basin, unit A onlap fill is locally >1,2 secs thick.

Major progradational growth of the Tugela Cone during deposition of unit B (McDuff-Angus) permitted thick (max >2,0 secs) delta and deep-sea fan aggradation. Unit B deep-sea fans over the Central Terrace flanks are locally thicker than 1,0 secs. Mixed offlap and onlap sequences within unit C (Angus-Jimmy) and unit D (post-Jimmy) indicate periodic Tugela Cone growth and inactive phases. Both units are locally thicker than 0,6 secs. Within units C and D, local deep-sea fan growth continued along the flanks of the Central Terrace although low-energy onlap fill and sheet drape facies characterises the Central Terrace crest and deep basin plain. Contourite mounds within the uppermost sequences of units B and C and throughout unit D are important indicators of extant current-control on sedimentation.

Depositional style evolution from onlap fill (unit A) through mixed offlap, onlap and onlap fill (units B-C) to offlap and sheet drape (unit D) is typical of early rift basin fill and post-rift passive offlap fill. Total sediment thickness reaches a maximum of 7,25 km under the upper Tugela Cone declining to 2,8-3,5 km under the eastern Tugela Cone/deep basin. Structural configurations of the major provinces have changed little since the early Oligocene. Sedimentation rates for unit A are fast (41-119 m/my) declining through units B and C (14-53 m/my) before dramatically increasing in unit D (18-132 m/my). Major controls over this trend include: the balance between sediment supply and basin subsidence, climatic change and relative sea-level. Modern sediment supply to the basin is 5-8 times higher than average rates in the geologic past, probably as a result of poor modern land management.

The Agulhas Current has strongly influenced sedimentation

processes through time by initiating: (1) slow post-Angus net sedimentation rates in scoured zones; (2) local exposure of units B and C strata in scoured zones; (3) generation of current-controlled microtopography and large-scale bedforms; (4) asymmetric sedimentation and scour moating; (5) sediment reworking and winnowing. Regions subjected to strong Agulhas Current flow include the Central Terrace, Mozambique Ridge and eastern and upper slopes of the Tugela Cone. Below 2500 m, North Atlantic Deep Water flow around the deep basin margins inhibits fast sedimentation by inducing winnowing and redistribution processes.

Invigorated deep current action is invoked to explain generation of the major early Oligocene (Angus) and early Pliocene (Jimmy) erosive hiatuses. Sea-level low stands may have initiated the equivalent coastal/shelf hiatuses. A low sea-level stand allied to regional tectonism may have triggered the non-depositional Cenomanian-Turonian hiatus (McDuff).

The Tugela Canyon is an erosional feature that was formed during a post-early Pliocene (Jimmy) low sea-level stand. In contrast, the 29° 25'S Canyon has acted as the major distributary fan valley on the Tugela Cone since at least the early Oligocene fostering significant levee/fan complex aggradation over the eastern Tugela Cone. Post-Jimmy (unit D) sediment instability over the northernmost Tugela Cone has resulted in generation of four sediment slides, each 200-1100 km^2 in areal extent. Instability in this region is a response to fast sedimentation rates and slope oversteepening. Seismic shocks may have acted as the final trigger.

Analysis of core and grab samples recovered at 54 stations

forms the basis for a regional discussion of sedimentology, lithofacies and sediment dispersal. Modern sediment composition and carbonate content is strongly controlled by the influx and dispersal of terrigenous detritus. Major terrigenous depocentres and dispersal routes are characterised by low carbonate contents and abundant detrital minerals. Pelagic environments are dominated by foram and coccolith oozes.

Hinterland-sourced illite is the dominant marine clay mineral group and is concentrated in the terrigenous depocentres. Smectites and kaolinites are locally hinterland-derived but there is significant import from the Mozambique/Madagascar area by Agulhas Current flow.

Textural analyses reveal five major provinces related to energy regime and detrital type. Equilibrium mud deposition is active over the south Tugela Cone terrigenous depocentre. Pelagic provinces are coarser-grained because of the large sand-size foram population. Winnowing and sand-enrichment occurs beneath regions of vigorous current flow. Sand fraction size-frequency distributions verify the presence of two overlapping and mixing hydraulic populations within the basin: medium-fine sand (biogenic) and very fine sand (terrigenous). Progressive mixing is best developed over the south Tugela Cone and adjacent deep basin.

Five modern lithofacies are discriminated: turbidite, hemipelagite, pelagite, muddy contourite and sandy contourite. Facies assemblage distributions are primarily controlled by proximity to terrigenous sources, dispersal routes and the strength of current influences.

forms the basis for a regional discussion of sedimentology, lithofacies and sediment dispersal. Modern sediment composition and carbonate content is strongly controlled by the influx and dispersal of terrigenous detritus. Major terrigenous depocentres and dispersal routes are characterised by low carbonate contents and abundant detrital minerals. Pelagic environments are dominated by foram and coccolith oozes.

Hinterland-sourced illite is the dominant marine clay mineral group and is concentrated in the terrigenous depocentres. Smectites and kaolinites are locally hinterland-derived but there is significant import from the Mozambique/Madagascar area by Agulhas Current flow.

Textural analyses reveal five major provinces related to energy regime and detrital type. Equilibrium mud deposition is active over the south Tugela Cone terrigenous depocentre. Pelagic provinces are coarser-grained because of the large sand-size foram population. Winnowing and sand-enrichment occurs beneath regions of vigorous current flow. Sand fraction size-frequency distributions verify the presence of two overlapping and mixing hydraulic populations within the basin: medium-fine sand (biogenic) and very fine sand (terrigenous). Progressive mixing is best developed over the south Tugela Cone and adjacent deep basin.

Five modern lithofacies are discriminated: turbidite, hemipelagite, pelagite, muddy contourite and sandy contourite. Facies assemblage distributions are primarily controlled by proximity to terrigenous sources, dispersal routes and the strength of current influences.

Modern sediment input to the basin has four main sources: (1) hinterland-sourced bedload detritus; (2) hinterland-derived suspended muds; (3) bedload and suspensates introduced from the north by current flow; (4) pelagic rain. Terrigenous bedload is funnelled to modern basin depocentres under Agulhas Current traction while suspensates are more widely distributed. Areas remote from the hinterland are dominated by pelagic and hemipelagic sedimentation. Winnowing and redispersal of muds and very fine sands is common in current-scoured areas. Only suspended muds have the potential for significant export from the Natal Valley basin.

Development of the Tugela Fan (Tugela Cone and deep basin) has followed standard models of deep-sea fan evolution with the 29° 25'S Canyon acting as the major mid fan distributary channel/levee system. Major fan growth has probably taken place during low sea-level stands and/or phases of deltaic progradation to the outer shelf. Large regions of the fan are temporarily inactive because of the modern high sea-level stand and changes in canyon status. The large size (upper-mid fan is 230 x 170 km in dimension) but atypical morphology of the Tugela Fan favours its classification as an hybrid fan type but with close affinities to the elongate fan type end-member.

ACKNOWLEDGEMENTS

Professor R.V. Dingle, my supervisor, deserves special thanks for inviting me out to South Africa to participate in the Natal Valley project, guiding my early progress and critically reviewing the final manuscript. Richard also acted as chief scientist on the data-collection cruises during which he introduced me to many basic principles of basin analysis, seismic stratigraphy and sedimentology.

Principal project funding and support facilities were provided by the Geological Survey of South Africa through André du Plessis and Robbie Kleywegt. More recently, personal financial support was granted by the University of Cape Town and the Southern Oil Corporation (SOEKOR).

The officers and crews of the research vessels Thomas B. Davie and Meiring Naude are thanked for their assistance and patience during long cruises. Without the technical expertise of Jack Engelbrecht and Tom Fitton (seismic profiling systems) and Eric Bryce (piston corer), the acquisition of marine geophysical data and sediment cores would have been a much more painful exercise. Help from Bill Siesser, Frances Westall and particularly Keith Martin ensured successful data collection at sea. Keith deserves special acknowledgement for his collaboration and discussion of many preliminary aspects of this project including data compilation, early bathymetric and seismic interpretation and core handling.

Thanks are also due to the many people who in some way assisted me during the project including: Burg Flemming

(sedimentology), André du Plessis (magnetics), Donne Murray (magnetics and computer applications), Gavin Birch and Mike Bremner (lab techniques and clay mineralogy), Dave Salmon (foram identification), Stuart Smith and John Bristow (geochemistry), Dave Crawford (SEM) and Maurice Gidlow (computer applications). Over the years, Richard Dingle, Burg Flemming, Gavin Birch, Mike Bremner and André du Plessis gave freely of their time and knowledge during many stimulating discussions which helped direct the project evolution. The draughting skills of Sue Sayers, Shirley Smith, Debbie Jenner and Sally Baumann eased a daunting burden while Matthew Smith provided welcome assistance in the sedimentology lab. Grace Krummeck deserves a special thank-you for typing many manuscripts over the years including the final version of this thesis.

Finally, to Sue Parker, for providing technical assistance, moral support, unlimited tolerance and for cracking the whip when necessary, a very appreciative thank-you.

CONTENTS

LIST OF FIGURES

LIST OF TABLES

LIST OF PLATES

CHAPTER 1 INTRODUCTION

1.1 INTRODUCTION AND REGIONAL SETTING

The Natal Valley project was initiated to promote geological and geophysical study of the continental slope and adjacent deep basin off the east coast of southern Africa, a region considered to be poorly known in recent Indian Ocean geological syntheses (Nairn and Stehli, 1982). The Natal Valley is a N-S trending, sediment-filled submarine basin within the SW Indian Ocean (Fig.1.1). To the west, the Natal Valley is bordered by the southern African continental margin while the basement-cored Mozambique Ridge forms a natural eastern boundary. From north to south, the valley floor descends from the SE Mozambique coastal plain to the abyssal Transkei Basin. Two large submarine fans (Tugela and Limpopo Cones) have been constructed within the Natal Valley. The investigation area of this thesis (mid Natal Valley) was roughly delineated to accommodate multidisciplinary study of the Tugela Cone and adjacent physiographic provinces (Fig.1.1). Data collection phases of the project included shooting a regional grid of seismic reflection, bathymetric and magnetic profiles together with retrieval of a representative suite of sediment cores.

From a broad spectrum of possible topics, three major aspects of the mid Natal Valley geology are focussed on within this study: (1) basin history, tectonism and configuration; (2) basin in-fill including seismic-stratigraphic analysis, deep current influences, hiatus formation and allochthonous processes; and (3) sedimentology and modern sedimentary processes and responses. Emphasis has been placed on sedimentology and

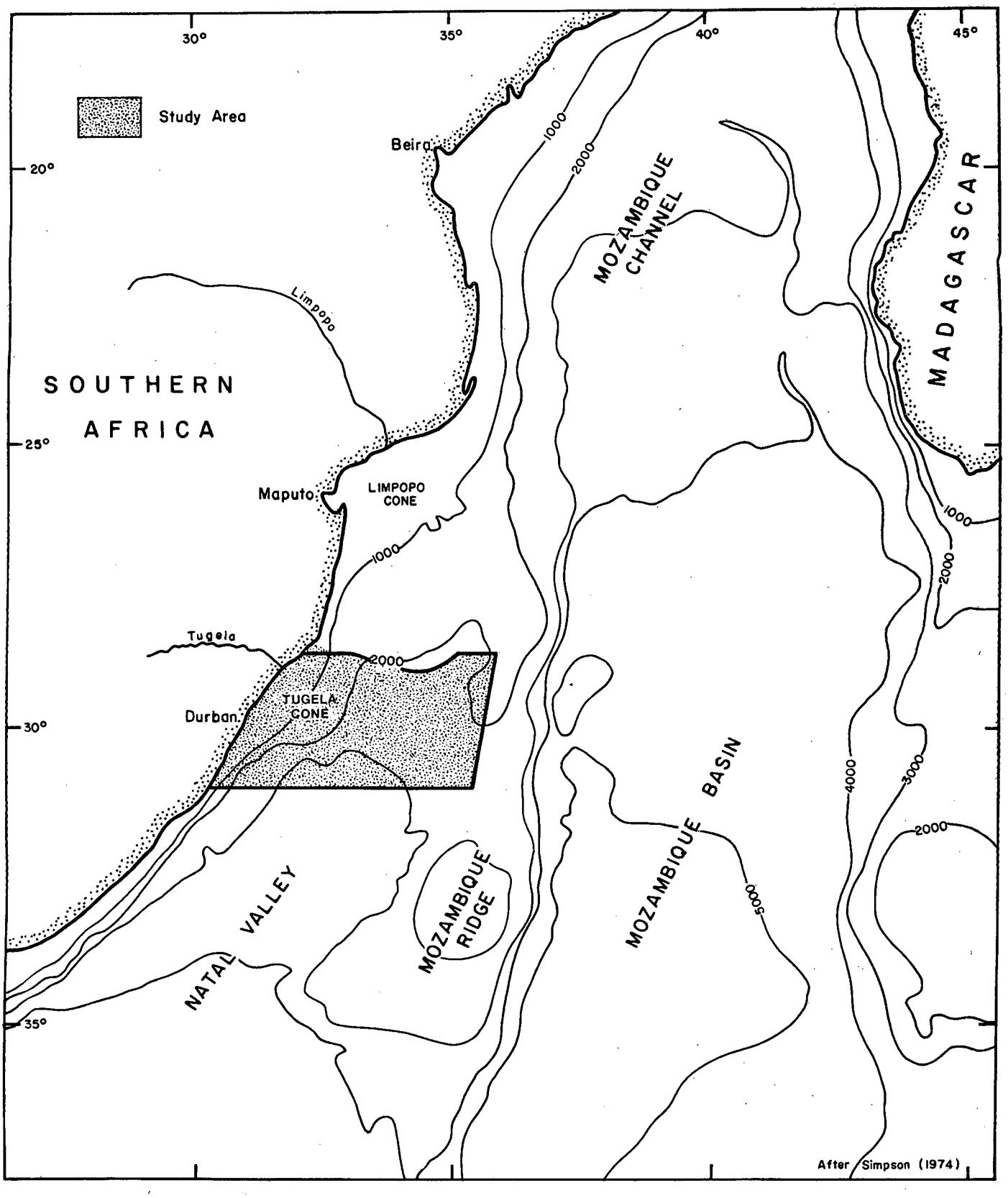

Fig. 1.1 STUDY AREA RELATIVE TO S.W. INDIAN OCEAN AND SOUTHERN AFRICA

seismic-stratigraphic analysis since knowledge of sedimentary processes and responses over the continental slope assumes increasing importance as the search for hydrocarbons intensifies in deep-water provinces. Previous work in the Natal Valley area is outlined within the relevant sections.

The study commences with a summary of the hinterland regional setting (Chapter 1). Physical oceanography of the Agulhas Current and North Atlantic Deep Water flow regimes, both major sedimentation controls, is assessed in Chapter 3. The tectonic/structural framework and Mesozoic sedimentary history of the Natal Valley basin and the application of continental rifting models are reviewed in Chapter 4. In Chapter 5, basement configuration and major crustal elements are defined leading to discussion of subsidence, microplate readjustment of the Mozambique Ridge and the tectonic status of the northern Natal Valley.

A seismic-stratigraphic analysis of the basin fill comprising assessment of depositional sequences, sequence boundaries, depositional styles and systems, sediment distribution and sedimentation rates and budgets is contained in Chapter 6. Major controls on sedimentation dynamics including the influence of geostrophic currents, hiatus generation, canyon formation and allochthonous sedimentation are considered in Chapter 7.

The sedimentology of surficial deposits is examined in Chapter 8. The relationships of chemical, compositional and textural trends together with lithofacies information enables evaluation of modern sedimentary processes and responses and sediment dispersal. In Chapter 9, seismic stratigraphy and

sedimentology are combined to relate Tugela Cone evolution to standard models of deep-sea fan development.

This thesis represents an initial phase to the understanding of the geological history of the mid Natal Valley and is intended to serve as a basis for future study in the area.

1.2 THE HINTERLAND

The regional hinterland setting, to a large extent, controls volume and composition of terrigenous sediment supply to the adjacent marine basin. Brief reviews of hinterland physiography, geology, climate and hydrology provide information from which terrigenous sediment yield to the mid Natal Valley can be assessed.

1.2.1 Physiography

The hinterland, defined by the extent of the regional watershed, comprises an area of 72 000 km^2 (Flemming and Hay, 1983) within the province of Natal including Zululand. The watershed follows the summits of the Drakensberg escarpment while northern and southern boundaries approximately coincide with the 27^oS and 31^oS lines of latitude (Fig.1.2). The landscape of Natal and Zululand is complex but can be divided into four main geomorphologic provinces (Fig.1.2): (1) Drakensberg escarpment (>2000m); (2) highland plateau (1200-2000m); (3) intermediate benchland (300-1200m); and (4) coastal lowlands. All of these provinces are variably incised by the drainage system with most severe dissection occurring in the Drakensberg escarpment zone. Coastwards, the terrain becomes more undulating finally grading into the coastal lowlands, a physiographic zone best developed in the Zululand area.

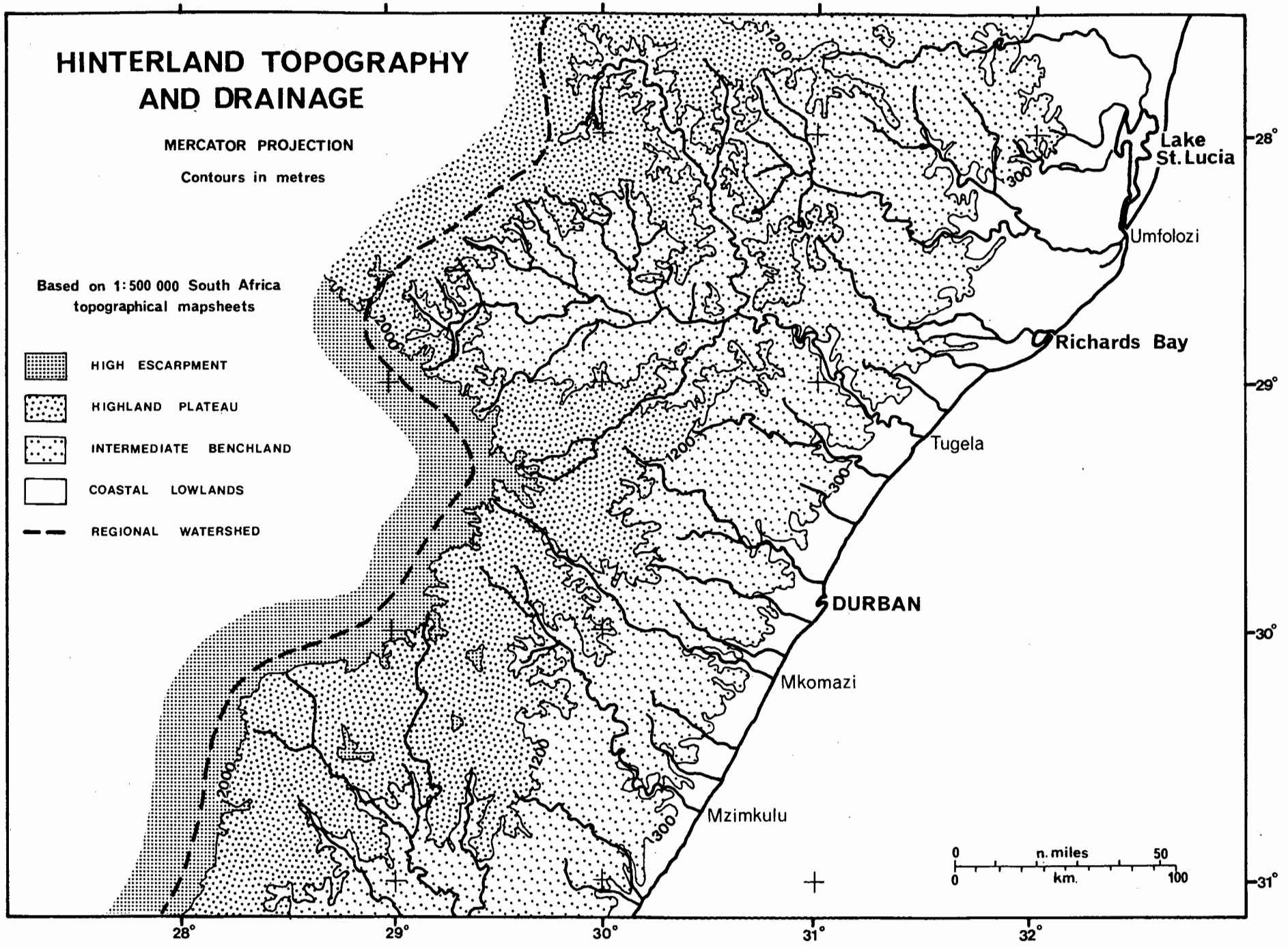
HINTERLAND TOPOGRAPHY AND DRAINAGE
MERCATOR PROJECTION
Contours in metres
Based on 1:500 000 South Africa topographical mapsheets
HIGH ESCARPMENT
HIGHLAND PLATEAU
INTERMEDIATE BENCHLAND
COASTAL LOWLANDS
REGIONAL WATERSHED
Lake St. Lucia
Umfolozi
Richards Bay
Tugela
DURBAN
Mkomazi
Mzimkulu
0 n. miles 50
0 km. 100
28°
29°
30°
31°
32°

Fig. 1.2

1.2.2 Geology

The geological succession of Natal/Zululand may be subdivided into four principal sequences: Archaean basement, Table Mountain Group, Karoo Supergroup and the Cretaceous-Cainozoic sequence. The distribution of the sequences (Fig.1.3) is approximately coincident with the major geomorphologic provinces.

Basement rocks of Natal and Zululand comprise Archaean crystalline granites, gneisses and schists, primarily outcropping along the axis of the Natal monocline (King, 1972), which corresponds to the intermediate benchland area. Stratigraphically-higher sandstones and shales of the Table Mountain Group are also distributed along the monocline axis.

Unconformably overlying the Table Mountain Group, the Karoo Supergroup outcrops over large areas of the interior hinterland (Fig.1.3). Glacial tillites of the Dwyka Group outcrop along the monocline trend. Sandstones and shales of the Ecca and Beaufort Groups together are dominant in the highland plateau area. The high Drakensberg escarpment is formed of sandstones and shales of the Stormberg Group capped by a thick volcanic pile (Drakensberg basalt).

The final geological sequence includes relatively undeformed Cretaceous and Cainozoic sediments of aeolian, fluvial and marine origin. A very variable range of lithofacies underlies the Zululand coastal plain and to the south, outcrops along the coastal lowlands.

(After King, 1972)

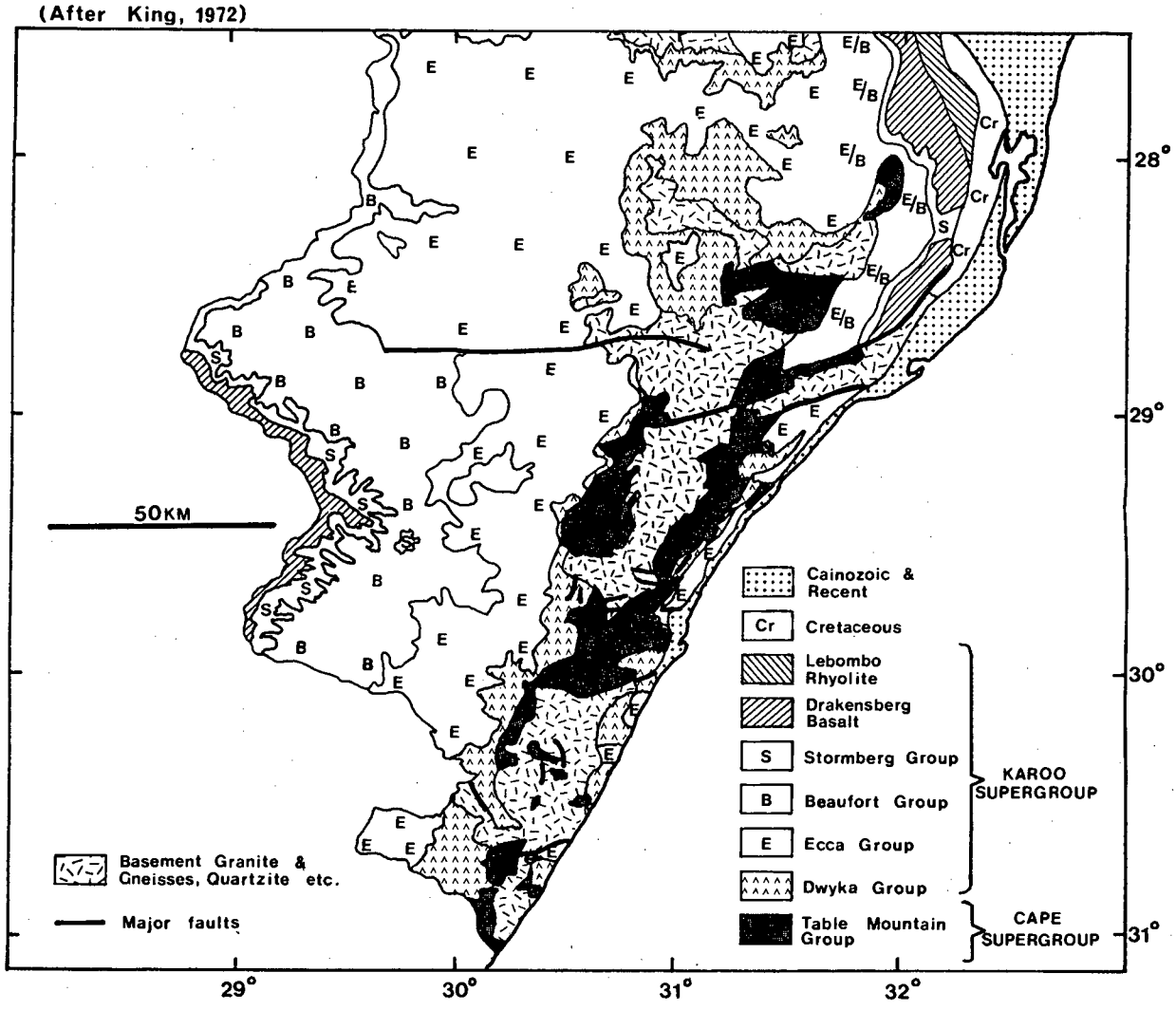

Fig. 1.3 SIMPLIFIED HINTERLAND GEOLOGY

(After Van Zinderen Bakker, 1976)

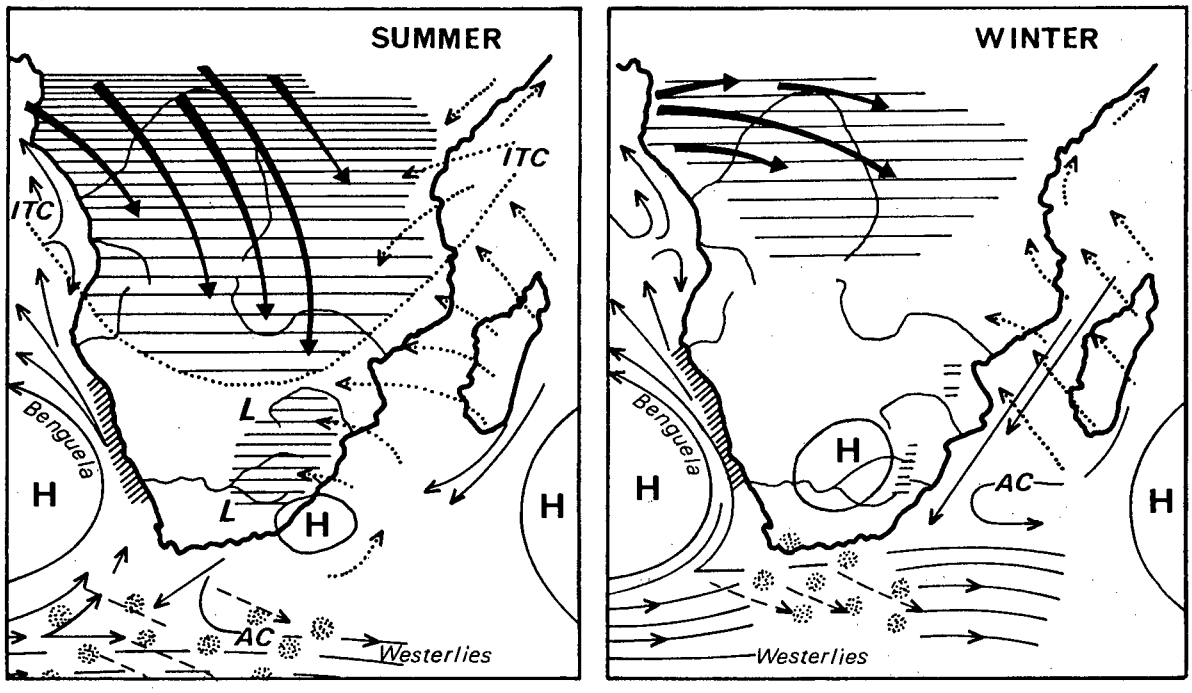

Fig. 1.4 CLIMATIC REGIME OF SOUTHERN AFRICA

1.2.3 Climate

The climatic regime of the hinterland is dominated by the subtropical high pressure belt (Fig.1.4) which discontinuously straddles the subcontinent (Schulze, 1965; van Zinderen Bakker, 1976). The summer situation, with typical southeastward displacement of the central high pressure anticyclone (Fig.1.4), allows humid maritime air to penetrate to the Drakensberg escarpment (van Zinderen Bakker, 1976) where orographic rain falls in the upper hinterland catchment. Summer rainfall of this type accounts for the majority of annual precipitation. Winter rainfall, associated with the passage of NE travelling cyclonic depressions, is widespread but minor proportionately.

Natal receives a mean annual rainfall of 907mm (Orme, 1974) but distribution over the province is very asymmetric. Precipitation over the Drakensberg escarpment and coastal regions annually exceeds 1250mm. Central interior regions receive average rainfall but low precipitation rates are recorded over the upper Tugela basin and north Zululand. Run-off and potential erosion and transportation rates are therefore highly variable within the different catchment zones of the hinterland.

1.2.4 Hydrology

On hydrological character, Orme (1974) subdivided the hinterland into three regional systems (Fig.1.5). Zones I and II in the south receive significant stream-flow from the Drakensberg region and thus perennial flow is maintained. Perennial flow is rare in the Zululand catchment (zone III) due to a combination of reduced precipitation and high soil infiltration although in coastal regions of zone III, clay and iron pans impede

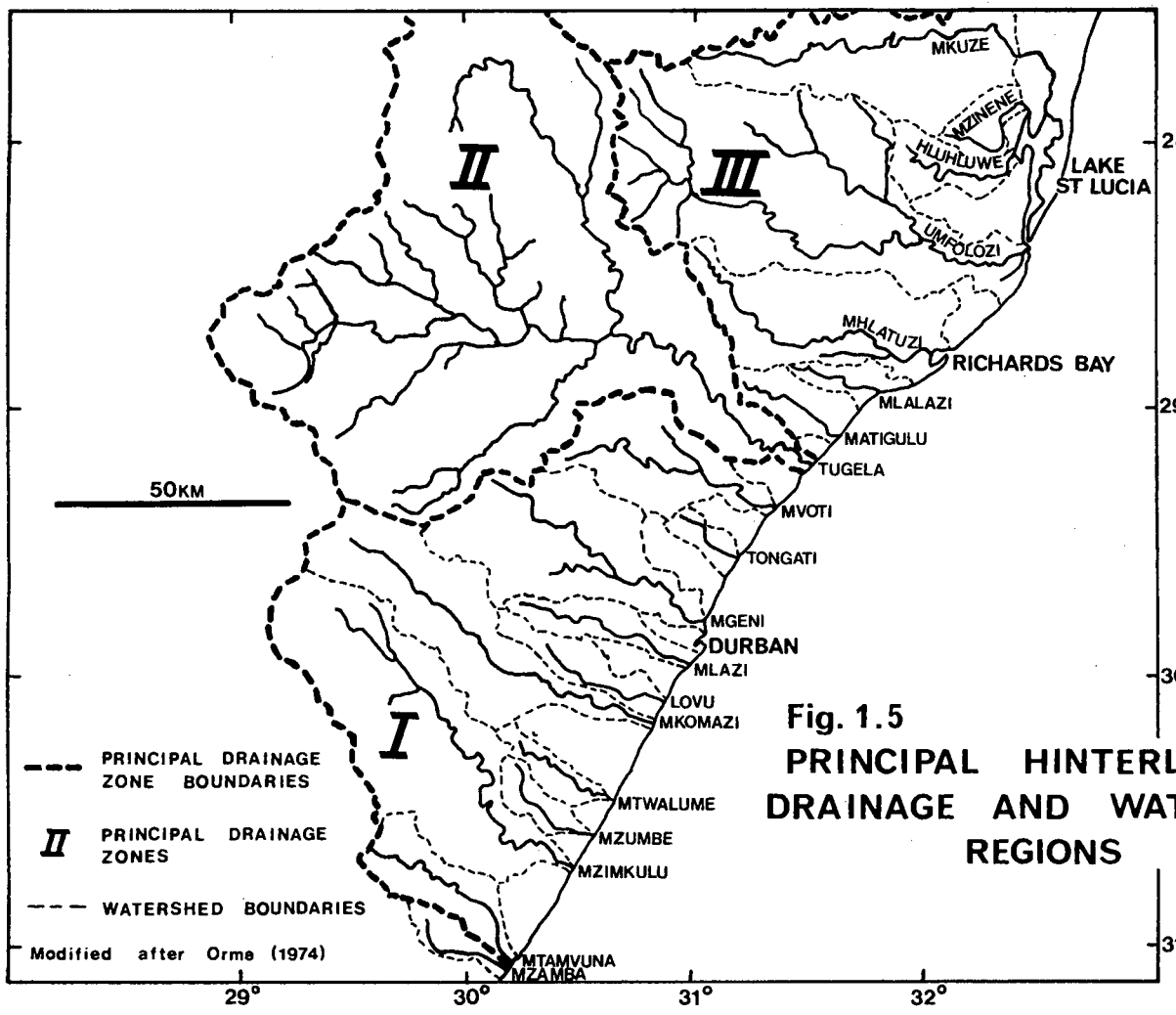

Fig. 1.5
PRINCIPAL HINTERLAND DRAINAGE AND WATERSHED REGIONS

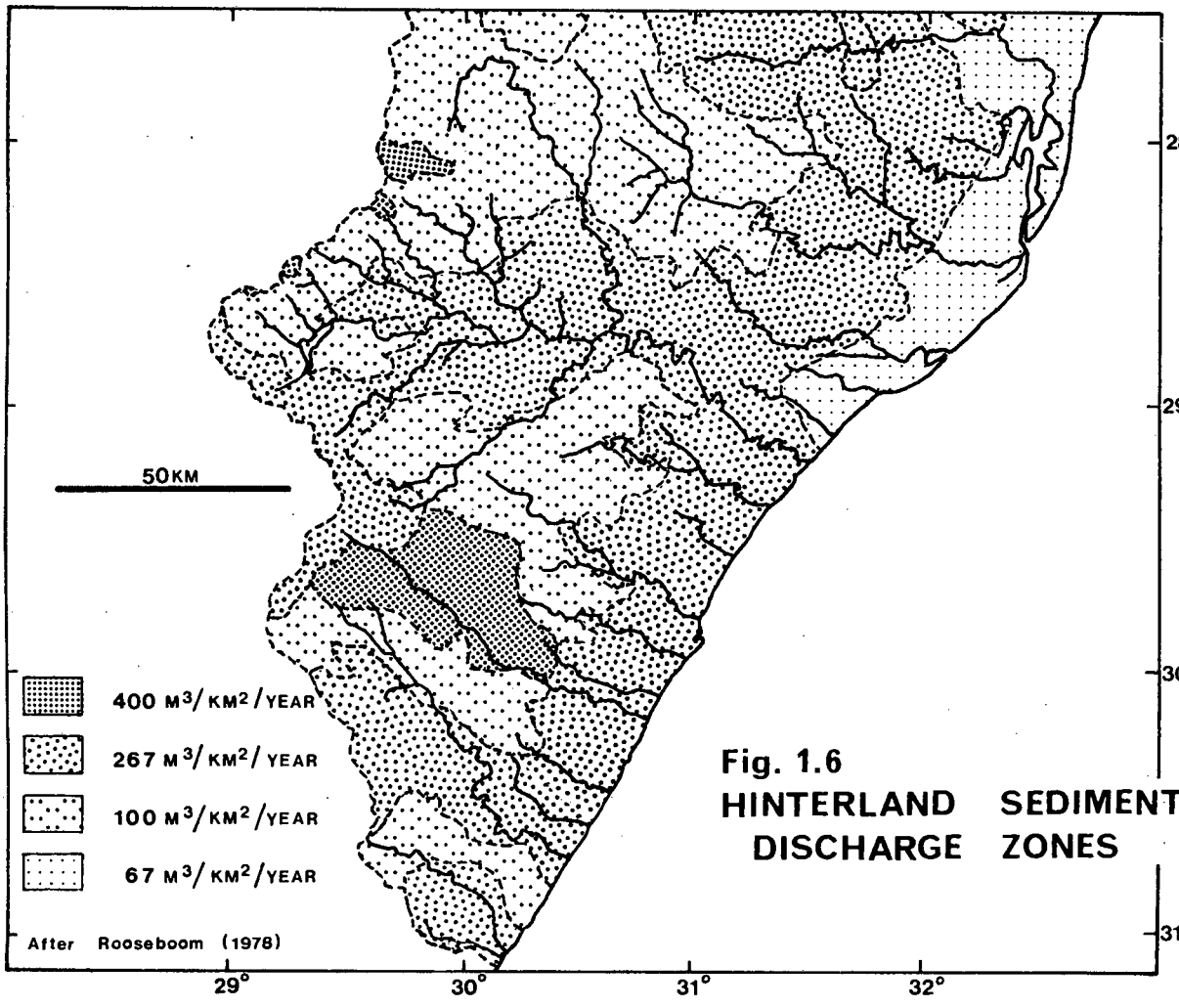

Fig. 1.6
HINTERLAND SEDIMENT DISCHARGE ZONES

infiltration inducing swamp conditions.

With a summer rainfall regime, Natal rivers reach their highest flow rates between October and March. As a result, run-off, erosion and yield to the offshore basin is extremely seasonal. During the summer months large volumes of detritus are discharged directly into the offshore basin from drainage zones I and II. To the north, in zone III, the majority of sediment is dumped into the coastal lagoon system. Reduced stream-flow rates in winter permit closure of the river mouths by littoral drift and little detritus is supplied to the marine basin.

1.2.5 Sediment Erosion and Yield

The subtropical climatic conditions within the hinterland have fostered development of a deep weathering zone. In the Archaean basement, Table Mountain Group and Karoo Supergroup sequences, the weathering profile within sandstones and granites is commonly 200m thick (Orme, 1974), while shale, tillite and some sandstones are mechanically weak (King, 1972). Younger Cretaceous-Cainozoic sediments are poorly-lithified or unconsolidated and are easily eroded. Deep weathering together with accelerated stream-flow and sheet-flood during thunderstorm conditions favours widespread and vigorous hinterland erosion.

Denudational rates have been estimated by Rooseboom (1978) and are presented in Figure 1.6. Erosional rates vary from 67 $m^3/km^2/annum$ in areas of low rainfall and gentle gradient to >267 $m^3/km^2/annum$ in regions of steep gradient and high precipitation. The denudation pattern appears to be primarily governed by the location of the major catchments. Overprinted on this, effects of physiography and rainfall lead to a secondary coast-parallel

zonation (Fig.1.6). Estimates of the annual mechanical denudation in the Tugela catchment area (Fig.1.5; zone II) have varied between 250 m^3/km^2 (Orme, 1974) and 309 m^3/km^2 (Rooseboom 1978), significantly higher than many of the major rivers world-wide (e.g. Zambesi, Mississippi and Nile; Milliman and Meade, 1983).

Sediment yields for the Natal and Zululand hinterland (Table 1.1) have been computed by Flemming and Hay (1983). The most prominent detrital source is the river Tugela (5.874 x $10^6 m^3$/annum) which alone supplies 39,3% of the total terrigenous yield. Although the yield from other river catchments is less, erosion may still be considerable following high intensity summer storms.

The river Limpopo annually discharges 65,1 x $10^6 m^3$ of terrigenous detritus (Flemming and Hay, 1983) into the northern Natal Valley (Fig.1.1). The majority of this volume is directly deposited over the Limpopo Cone and Inharrime Terrace (Dingle et al, 1978). However, axial valley transport stimulated by Agulhas Current flow may result in long distance sediment transportation to depocentres of the mid Natal Valley.

Table 1.1 Annual Terrigenous Sediment Yield of the Hinterland

HYDROLOGICAL ZONE	MAJOR RIVERS	CATCHMENT AREA (km^2)	TERRIGENOUS YIELD ($x10^6 m^3$)	PROPORTION OF YIELD (%)
I	Mzimkulu Mkomazi Mgeni Mvoti	19335	4,845	32,4
II	Tugela	29101	5,874	39,3
III	Mhlatuzi Umfolozi Mkuze	23331	4,243	28,3
TOTAL		71767	14,962	100,0

- data modified after Flemming and Hay (1983).

CHAPTER 2 PHYSICAL OCEANOGRAPHY

2.1 INTRODUCTION

Detailed topography, seismic stratigraphy and sedimentology studies have revealed that sedimentation dynamics within the Natal Valley are strongly influenced by the action of both surface and deep-water oceanic currents. The recognition of current-moulded mounds, scour moats, exposed pre-Quaternary strata, sediment reworking and contourite lithofacies in all water depths is conclusive evidence that vigorous deep-sea current action is a major agent in sediment erosion/deposition and dispersal. To provide background information, therefore, it is necessary to review oceanographic literature summarising gross circulation features of the SW Indian Ocean and local current dynamics of the Natal Valley. Water mass circulation in the Natal Valley is dominated by western boundary currents of the Indian Ocean (Agulhas Current) with subsidiary influence of deep undercurrent inflow (North Atlantic Deep Water).

2.2 SURFACE WATER MASSES AND CIRCULATION

2.2.1 Introduction

Early oceanographic work in the area has been fully reviewed by Lutjeharms (1971), van Foreest (1977) and Pearce (1977). Satellite-tracked drifter buoys (Stavropoulos and Duncan, 1974; Grundlingh, 1977; Lutjeharms et al, 1981) and satellite imagery (Harris and van Foreest, 1977; Harris et al, 1978; Malan and Schumann, 1979) together with inertial jet modelling (van

Foreest, 1977) have provided extensive new data, often confirming earlier interpretations. These new data have also emphasised the complexity and short-term variability of the flow regime, in particular the Agulhas Current system.

2.2.2 Large Scale Circulation and Agulhas Current Sources

Oceanic scale circulation in the southern Indian Ocean is dominated by a large sub-tropical anti-cyclonic gyre. This gyre comprises: (1) westerly flow of the South Equatorial Current; (2) southerly flow of the western boundary current system (including the Agulhas Current) developed along the SE African continental margin; (3) easterly flow along the sub-tropical convergence zone; and (4) northerly return flow off west Australia (Bang and Pearce, 1978).

Three possible sources of the Agulhas Current (Fig.2.1) have been identified by Harris and van Foreest (1977). These sources are: (a) Mozambique Current waters ('tropical') flowing south through the Mozambique Channel; (b) East Madagascar Current waters ('tropical') meandering westwards from the southern tip of Madagascar; and (c) recycled 'sub-tropical' waters comprising discrete eddies advecting north and west through the Mozambique Basin towards the convergence zone. The three water masses converge around 35°E, 25°S in the northern Natal Valley (Fig.2.1), the source region for the two components of the Agulhas Current.

2.2.3 The Agulhas Current

Southerly flow from the source zone may follow either of two

Fig.2.1 SCHEMATIC INDICATION OF MAJOR SOURCES AND FLOWPATHS OF AGULHAS CURRENT

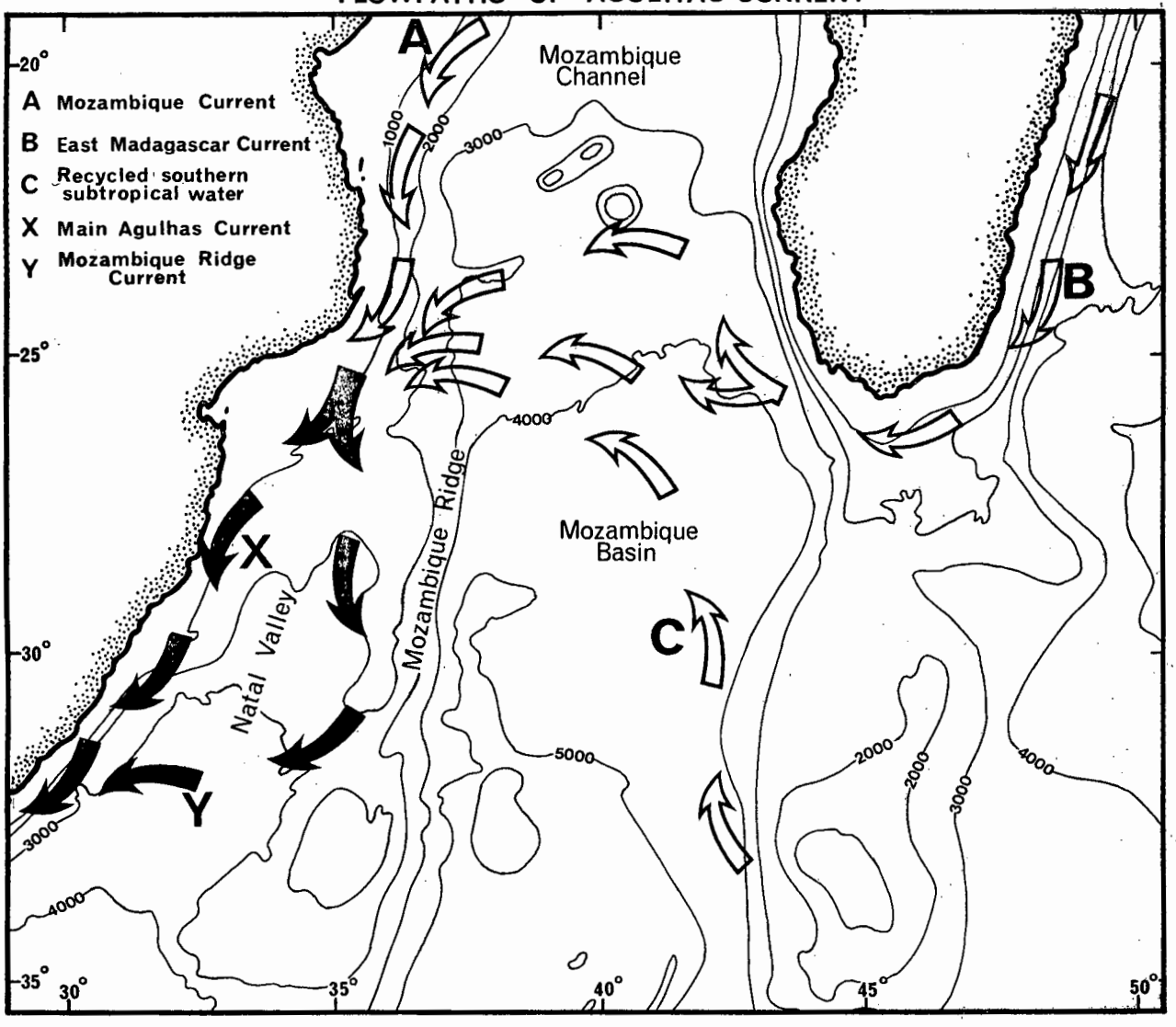

alternative routes (Harris and van Foreest, 1977; Grundlingh and Lutjeharms, 1979) before confluxing again south of Durban (Fig.2.1). The Agulhas Current core (route X) traverses the northern Natal Valley from NE to SW to impinge on the east coast continental margin around 28°S. The subordinate Mozambique Ridge Current (route Y) follows a southerly course parallel to the Mozambique Ridge swinging westwards between 29°S and 32°S to conflux with the core Agulhas flow (route X) near the continental margin (Fig.2.1).

The Agulhas Current core (route X), the most vigorous sub-system of the southern Indian Ocean gyre, gains its identity between 25°S and 30°S but is only properly developed as a deep western boundary current south of Durban (van Foreest, 1977). South of Durban, flow velocities of 1 - 1,5 m/s are typical and speeds in excess of 2,5 m/s have been recorded (Harris and van Foreest, 1977).

The Agulhas Current is generally accepted as being a fast, deep current (Duncan, 1970; Lutjeharms, 1971; van Foreest, 1977). Based on current measurements, Duncan (1970) traced motion to a depth of 2500m in a perspective view of the current (Fig.2.2). Direct current velocity measurements (van Foreest, 1977) have shown the Agulhas Current to be remarkably homogeneous with depth. Computed velocity sections and profiles (Lutjeharms, 1971; Harris, 1972; van Foreest, 1977) indicate current velocities of 20 cm/s at 2000m. Lutjeharms (1971) concluded that the major water transport zone of the Agulhas Current lies between 500 and 750m below sea level. Water transport volumes are large and vary seasonally from 80-100 megatons/sec (Duncan, 1970) to designate the Agulhas Current as being one of the major

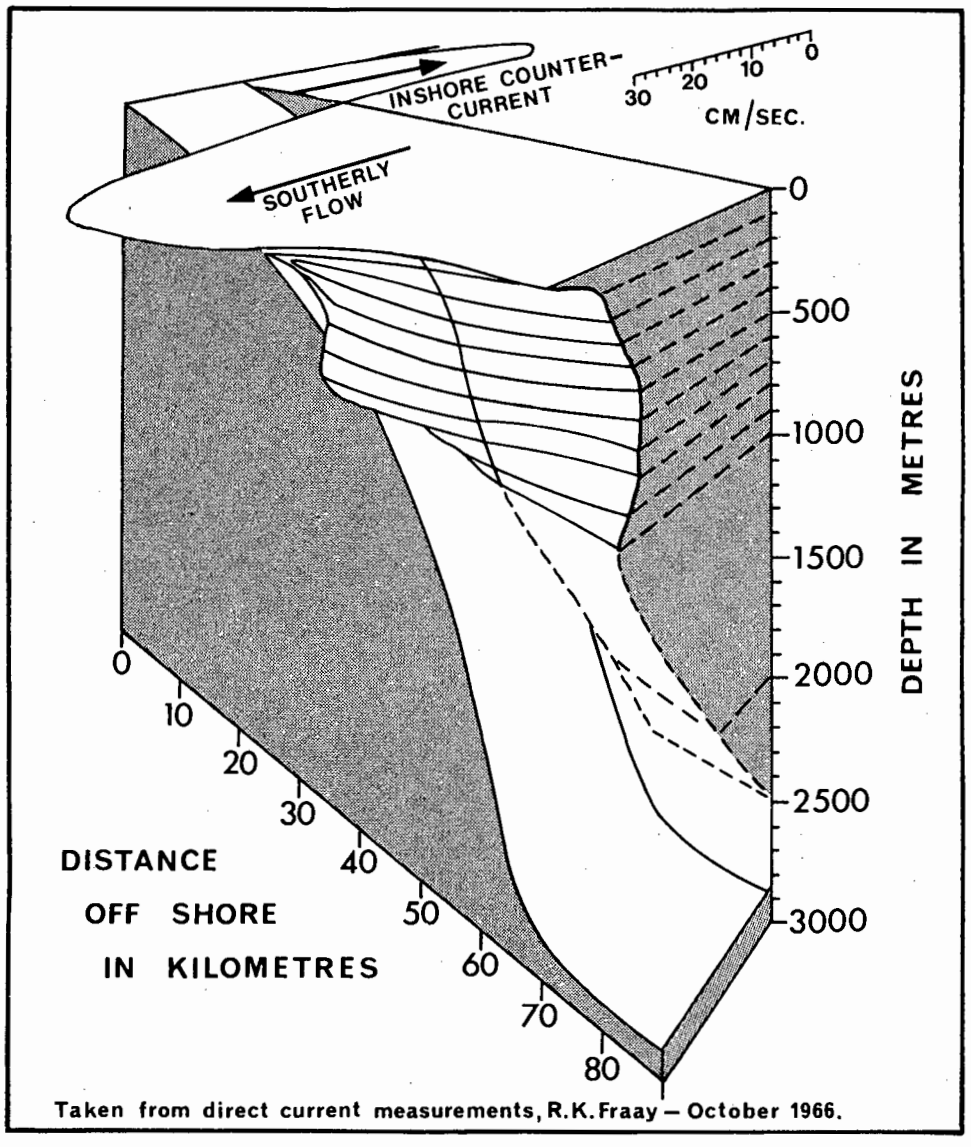

Fig. 2.2 PERSPECTIVE VIEW OF THE AGULHAS CURRENT SOUTH-SOUTH EAST FROM DURBAN

(After Duncan, 1970)

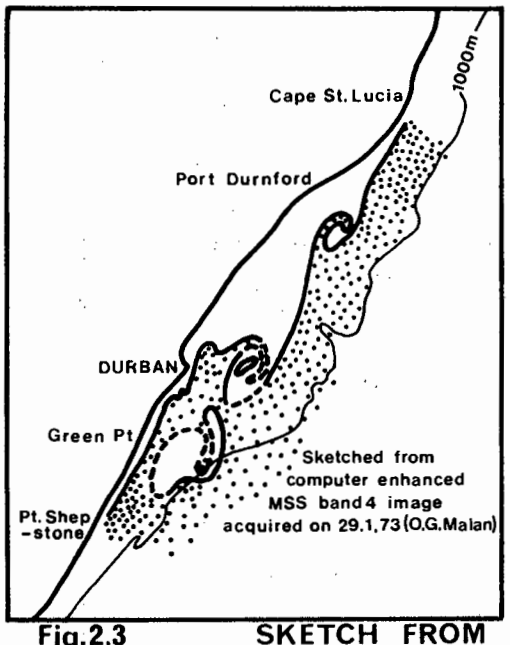

Fig. 2.3 SKETCH FROM LANDSAT IMAGE

(after Harris, 1978)

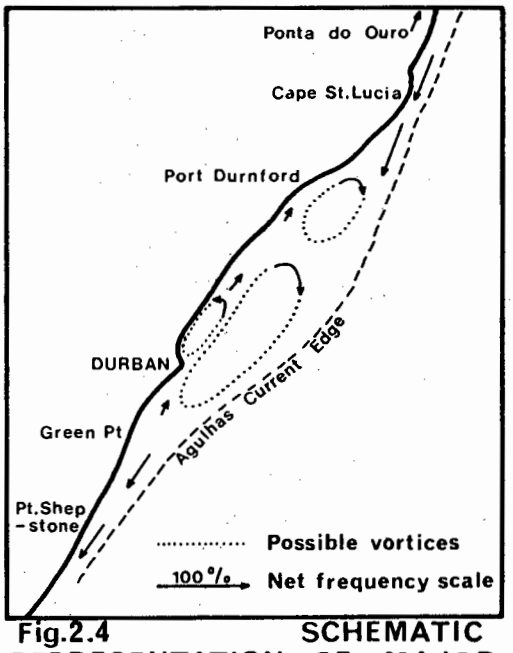

Fig. 2.4 SCHEMATIC REPRESENTATION OF MAJOR SHELF CIRCULATION ELEMENTS

(after Harris, 1978)

western boundary current systems of the world. The Mozambique Ridge Current (route Y) can be considered as a minor western boundary current.

Early work (Darbyshire, 1964; Tripp, 1967) emphasised the seasonal bias in the SW Indian Ocean flow regime. More recent studies of synoptic data and satellite imagery data (Harris and van Foreest, 1977) have demonstrated the importance of short-lived phenomena, with major changes in the Agulhas Current system occurring over a period of several days to 3-4 weeks. The Agulhas Current core flow (route X) and the Mozambique Ridge Current (route Y) may assume intermittent flow dominance (van Foreest, 1977) within the mid Natal Valley.

2.2.4 Coastal Circulation Patterns and Upwelling Processes

Coastal waters are typically cooler and less saline than Agulhas Current waters (Bang and Pearce, 1978) enabling easy recognition on temperature and salinity data. The Agulhas Current acts as an outer boundary to shelf circulation; this boundary is typically demarcated in surface waters by a region of intense cyclonic shear (Figs.2.3 and 2.4).

Shelf circulation exhibits two contrasting configurations dependent upon shelf width (Fig.2.4). North of Cape St. Lucia and south of Green Point, the continental shelf is narrow and thus the Agulhas Current core flows close to the coast. Coastal waters tend to move in sympathy with the Agulhas Current and consequently, southerly flow predominates (Fig.2.4). In contrast, in the 'Natal Bight' (Cape St. Lucia to Green Point), the Agulhas Current diverges from the coast generating a series of south-advecting cyclonic gyres over the shelf (Figs.2.3 and

2.4). Elements of this 'Natal Gyre' are considered semi-permanent but locally exhibit highly variable configurations in time and space (Harris, 1978).

Dynamics of the Agulhas Current system leads to mild but continuous upwelling of water onto the east coast continental shelf (Pearce, 1977). Superimposed on this, mesoscale upwelling events are recognised along the shelf break north of Durban on the basis of nutrient (silicate and nitrate) increase and temperature decrease (Pearce, 1977). In conjunction, these upwelling events are significant processes within east coast circulation dynamics.

2.3 DEEP WATER CIRCULATION

2.3.1 Introduction

Recent interpretations of abyssal flow have confirmed the presence of a well-defined, northward-flowing, deep western boundary current system within the SW Indian Ocean (Kolla et al, 1976a; Jacobs and Georgi, 1977; Ellwood et al, 1979; Johnson and Damuth, 1979; Kolla et al, 1980a; Westall, 1984). These studies suggest that the deep current system comprises a two-layer structure, both layers originating from distinct high latitude source areas. These two water masses are North Atlantic Deep Water (NADW) and Antarctic Bottom Water (AABW). Dynamic sedimentological effects of western boundary undercurrents in the SW Indian Ocean have been investigated in the Amirante Passage (Johnson and Damuth, 1979), Mozambique Basin (Kolla et al, 1980a) and Agulhas Passage (Westall, 1984). The effects of NADW flow in the mid Natal Valley have not previously been documented. The

characteristics and circulation patterns of NADW are summarised in this section since it directly influences sedimentation processes in the Natal Valley basin.

Antarctic Bottom Water is restricted to depths greater than 4000m (Kolla et al, 1980a) and thus does not affect sedimentation processes in the mid Natal Valley.

2.3.2 North Atlantic Deep Water (NADW)

The important role of NADW in deep circulation of the SW Indian Ocean has long been recognised (Clowes and Deacon, 1935; Le Pichon, 1960; Lutjeharms, 1971; Kolla et al, 1976a) although there is little published work on its effect on sedimentation processes. Kolla et al (1976a) document intense erosion, old outcrops, manganese nodule pavements and a rippled sea floor on sectors of the Agulhas Plateau and attribute these to NADW flow with velocities greater than 20 cm/s. Few bottom current measurements or photographs have been obtained from abyssal zones of the Natal Valley, but those published (Kolla et al, 1976a) suggest at least intermittent strong deep flow. High bottom-water particle concentrations measured in the Natal Valley (Fig.2.5) confirm the presence of a well-developed nepheloid layer implying active deep current flow.

The core layer of NADW is distinguished on three main criteria (Wyrtki et al, 1971; Kolla et al, 1980a): potential temperature (1,2 - 2,2^{o}C); salinity (34,78 - 34,84$^{o}/_{oo}$; and oxygen content (5 ml/l). As NADW flow turns eastwards and northwards into the SW Indian Ocean, it is identifiable as a salinity maximum from 2500-3000m (Warren, 1974; Jacobs and Georgi, 1977). Lutjeharms (1971) has suggested that NADW may

Fig.2.5 DISTRIBUTION OF NEPHELOID LAYER

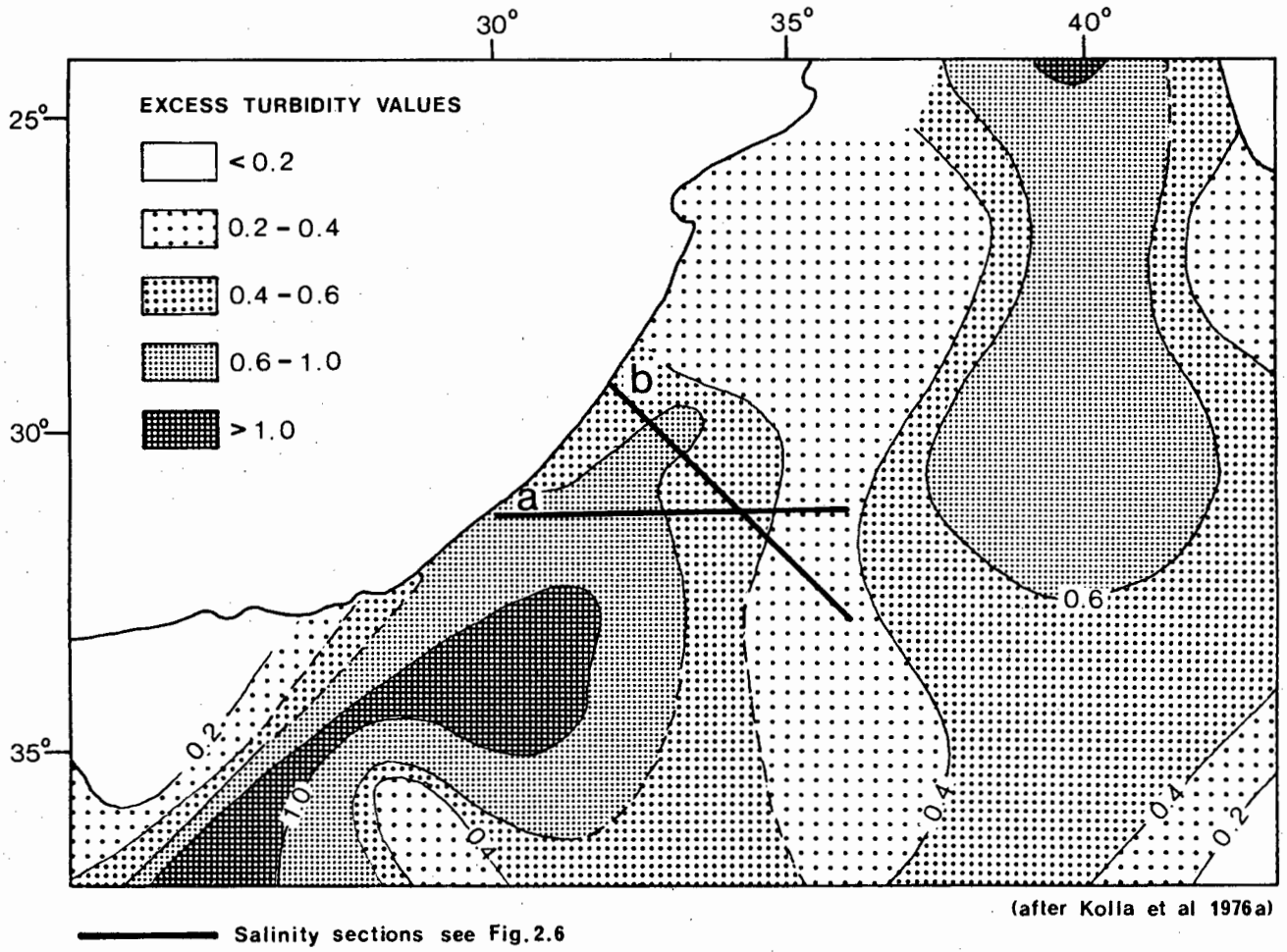

Fig.2.6 DEEP SALINITY SECTIONS ACROSS THE NATAL VALLEY

(after Wyrtki et al, 1971)

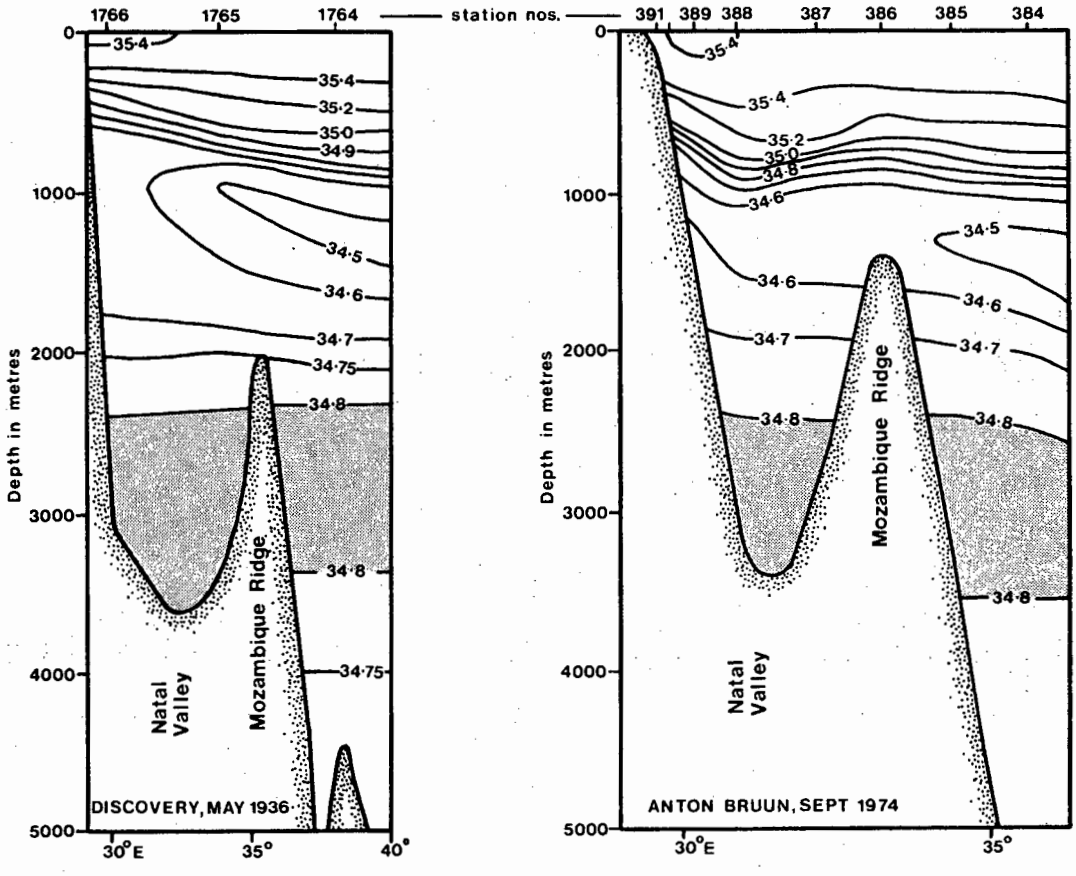

rise as shallow as 2400m. The presence of NADW in the Natal Valley is indicated by the deep salinity maximum portrayed on hydrographic sections (Fig.2.6; section locations in Fig.2.5). In addition, Le Pichon (1960) interpreted the distribution of the deep salinity maximum (Fig.2.7) as showing northward passage of an undercurrent (NADW) beneath the south-flowing Agulhas Current.

NADW flow in the Natal Valley may be analogous to deep undercurrent flow described by Kolla et al (1980a) in the adjacent and geometrically-similar Mozambique Basin (Fig.2.8). It is postulated that NADW enters the Natal Valley to flow north along the continental slope and Tugela Cone margins as a Coriolis-intensified boundary current below 2400m (Fig.2.8). On encountering the shallow Central Terrace plateau, flow is deflected south along the western Mozambique Ridge to exit from the basin.

In summary, circulation of deep water masses within the SW Indian Ocean is strongly depth-dependent. Below 4000 m, cold Antarctic Bottom Water (AABW) circulation is dominant but cannot penetrate the Natal Valley (Fig.2.8). Above AABW, NADW flow is developed but is restricted to depths greater than 2400 m within the Natal Valley by water mass physical characteristics (Fig.2.6). Shoaler than 2400 m, Agulhas Current deep water masses dominate the flow regime.

Fig.2.7 LAYER OF THE DEEP SALINITY MAXIMUM
(modified after Le Pichon, 1960)

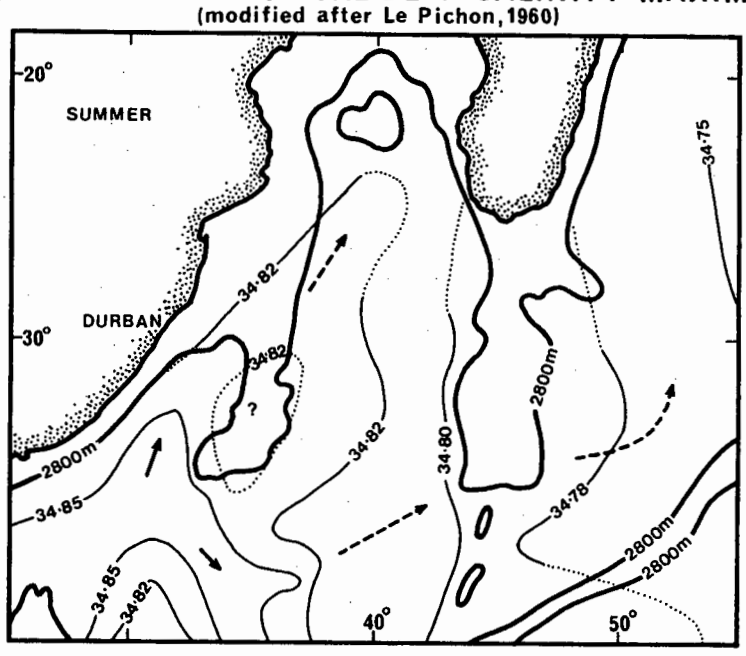

Fig 2.8 COMPOSITE DEEP FLOW IN THE SOUTHWEST INDIAN OCEAN

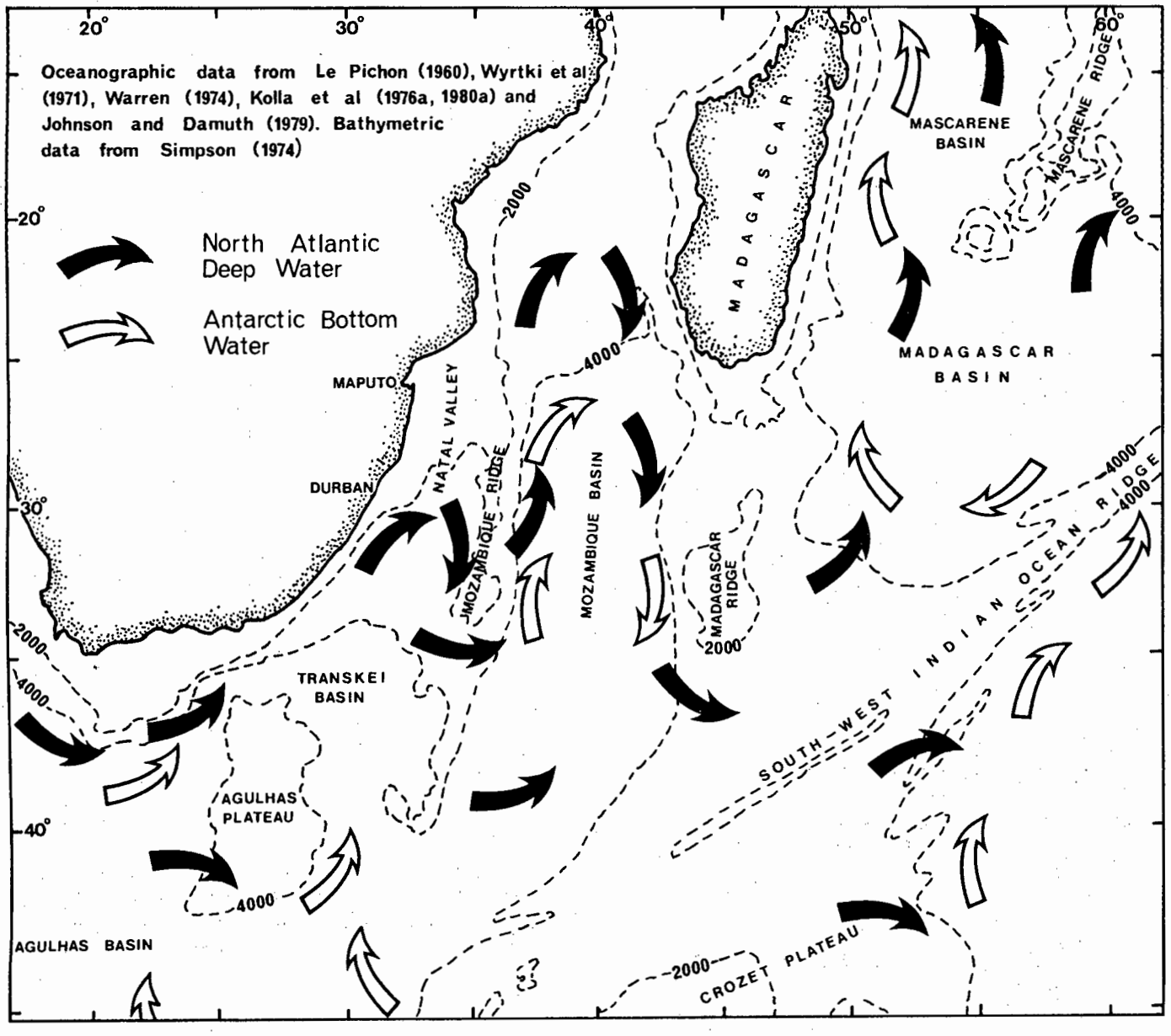

CHAPTER 3 BATHYMETRY AND PHYSIOGRAPHY

3.1 INTRODUCTION

An important early phase in any regional geological study is compilation of a detailed bathymetric chart. Previous bathymetric work in the Natal Valley has been very limited focussing mainly on the continental shelf and upper slope zones (Bang, 1968; Moir, 1975; Flemming, 1980). The first regional bathymetric map was compiled by Simpson (1974) but only at a 500m isobath interval. At an early stage in this project, Dingle et al (1978) presented a preliminary bathymetric map laying a basis for further stratigraphic and sedimentological studies.

In total, 18 560 km of bathymetric traverses have been collected in the study area. Satellite-navigated tracks (7380 km) provide an accurate traverse framework to which tie lines with cross-over discrepancies have been adjusted. Traverse ground coverage is shown in Figure 3.1a. Contouring was performed at 20m intervals except in areas of complex relief (SW continental slope) and poor data quality-control (Tugela Cone upper slope).

In this chapter, the first 20m interval bathymetry chart of the mid Natal Valley is presented (Fig.3.2). Based on the bathymetry map and cross-section profiles (Figs.3.3 and 3.4), six major physiographic provinces are delineated: continental shelf, continental slope, Tugela Cone, Central Terrace, Mozambique Ridge and the deep ocean basin (Fig.3.5). All can be related to specific geological features and their boundaries represent facies or sediment thickness discontinuities (Dingle et al, 1978). In addition, a topography classification based on sea floor microrelief and providing information on depositional

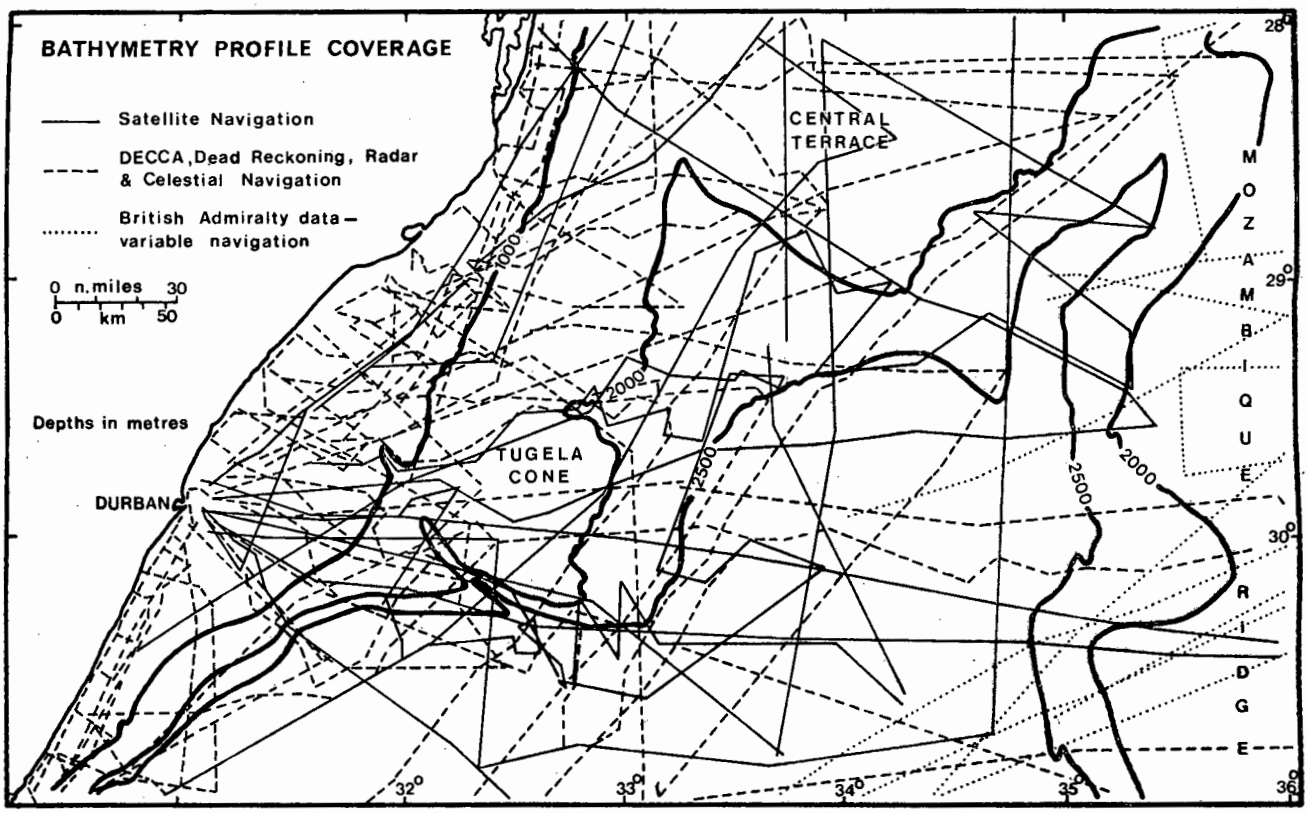

Fig. 3.1a BATHYMETRY PROFILE LOCATION

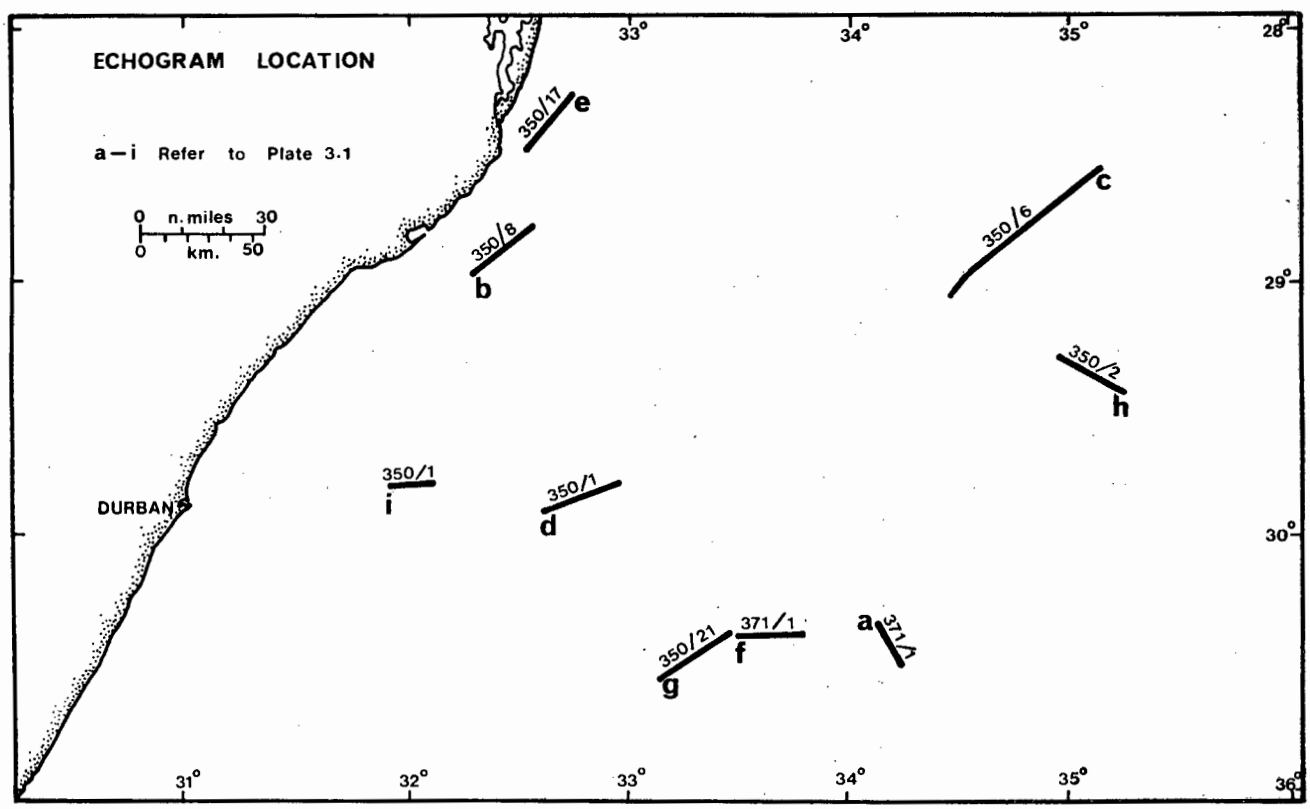

Fig. 3.1b ECHOGRAM LOCATION

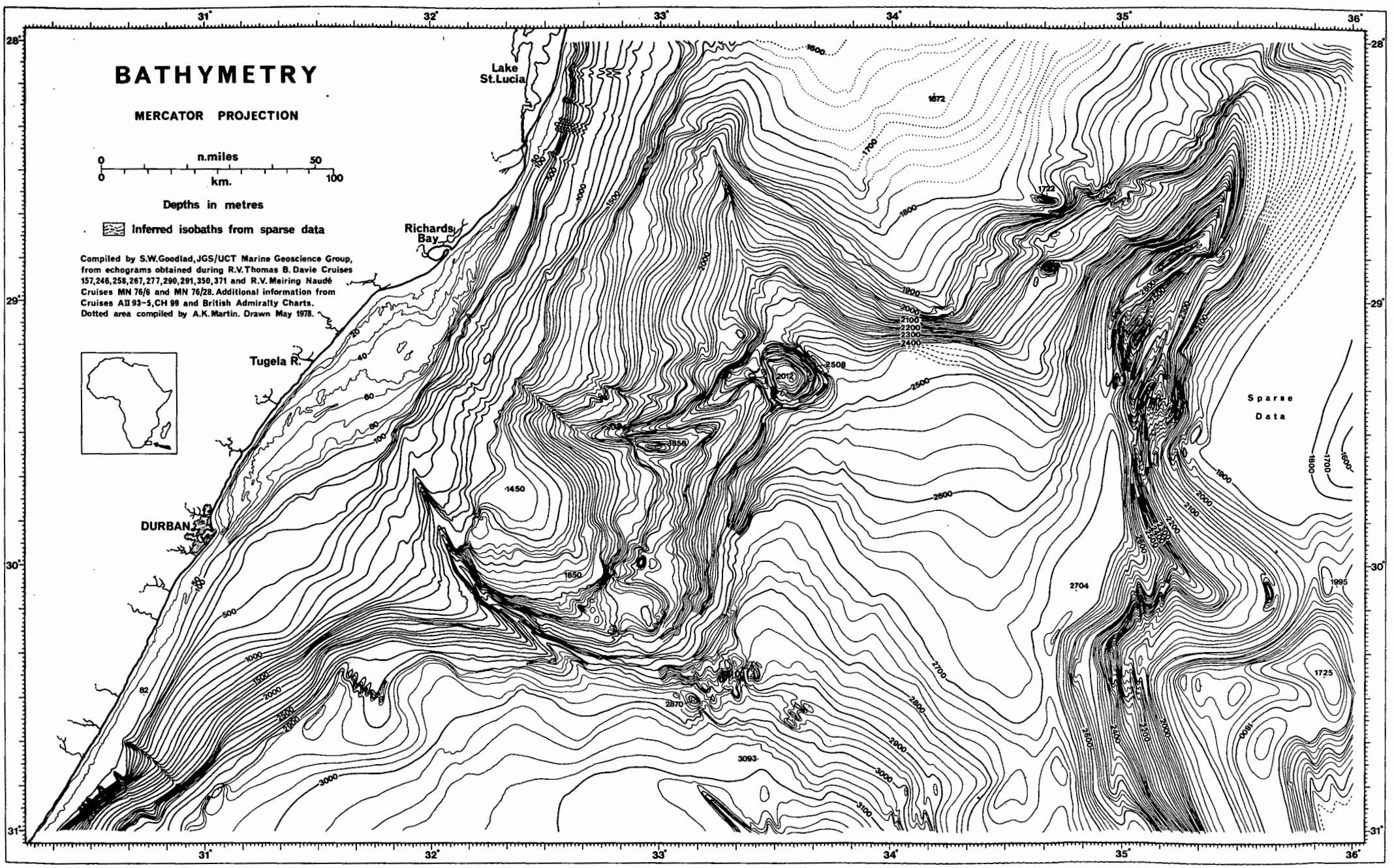
BATHYMETRY
MERCATOR PROJECTION
0 n.miles 50
0 km. 100
Depths in metres
Inferred isobaths from sparse data
Compiled by S.W.Goodlad, JGS/UCT Marine Geoscience Group, from echograms obtained during R.V.Thomas B. Davie Cruises 157,246,258,267,277,290,291,350,371 and R.V. Meiring Naudé Cruises MN 76/6 and MN 76/28. Additional information from Cruises AII 93-5, CH 99 and British Admiralty Charts. Dotted area compiled by A.K.Martin. Drawn May 1978.
Lake St.Lucia
Richards Bay
Tugela R.
DURBAN
Sparse Data
31°
32°
33°
34°
35°
36°
28°
29°
30°
31°

Fig. 3. 2

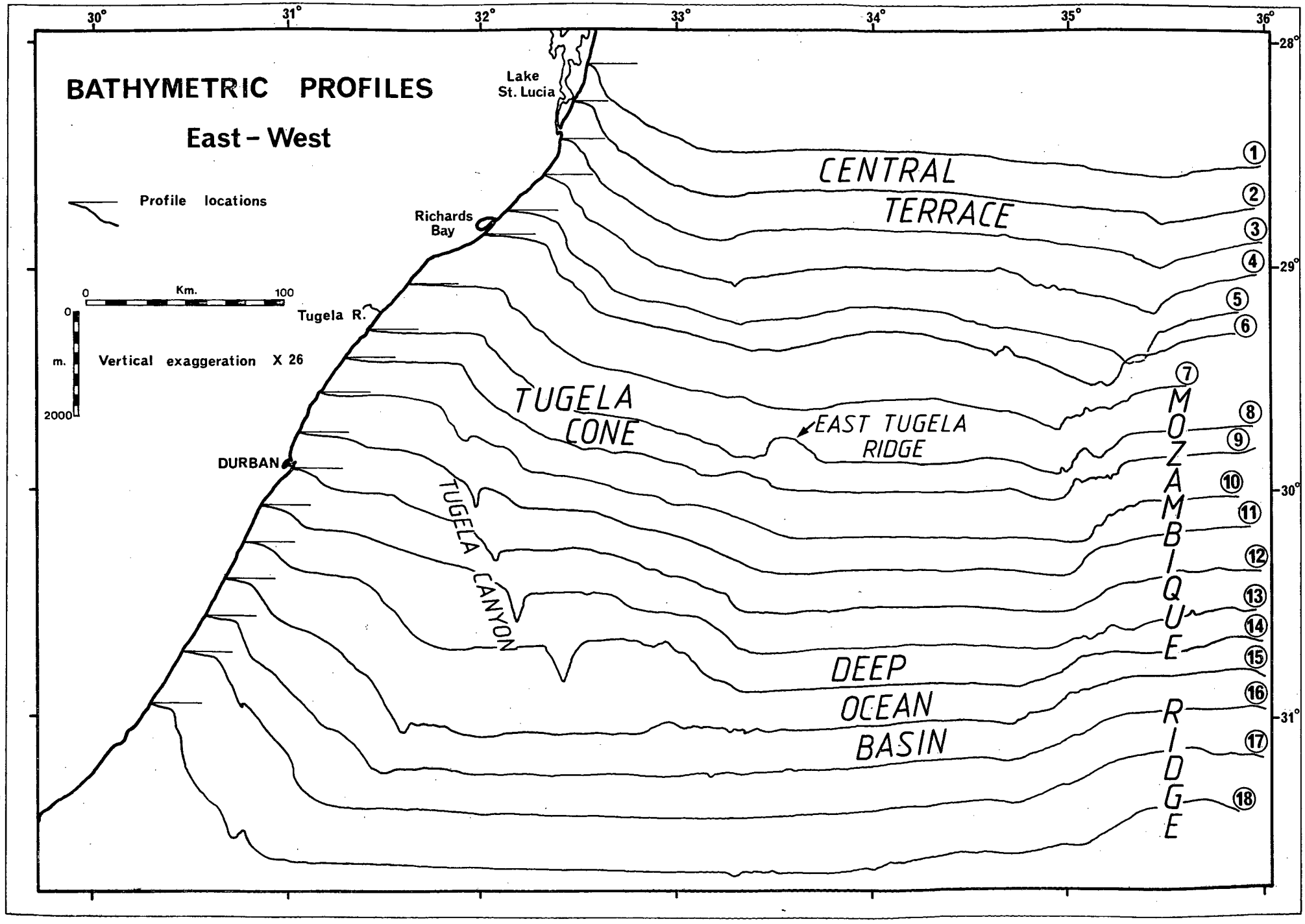
BATHYMETRIC PROFILES
East – West
Profile locations
Lake St. Lucia
Richards Bay
Tugela R.
DURBAN
0 Km. 100
0
m.
2000
Vertical exaggeration X 26
CENTRAL TERRACE
TUGELA CONE
EAST TUGELA RIDGE
TUGELA CANYON
DEEP OCEAN BASIN
MOZAMBIQUE RIDGE
1
2
3
4
5
6
7
8
9
10
11
12
13
14
15
16
17
18
30°
31°
32°
33°
34°
35°
36°
28°
29°
30°
31°

Fig. 3.3

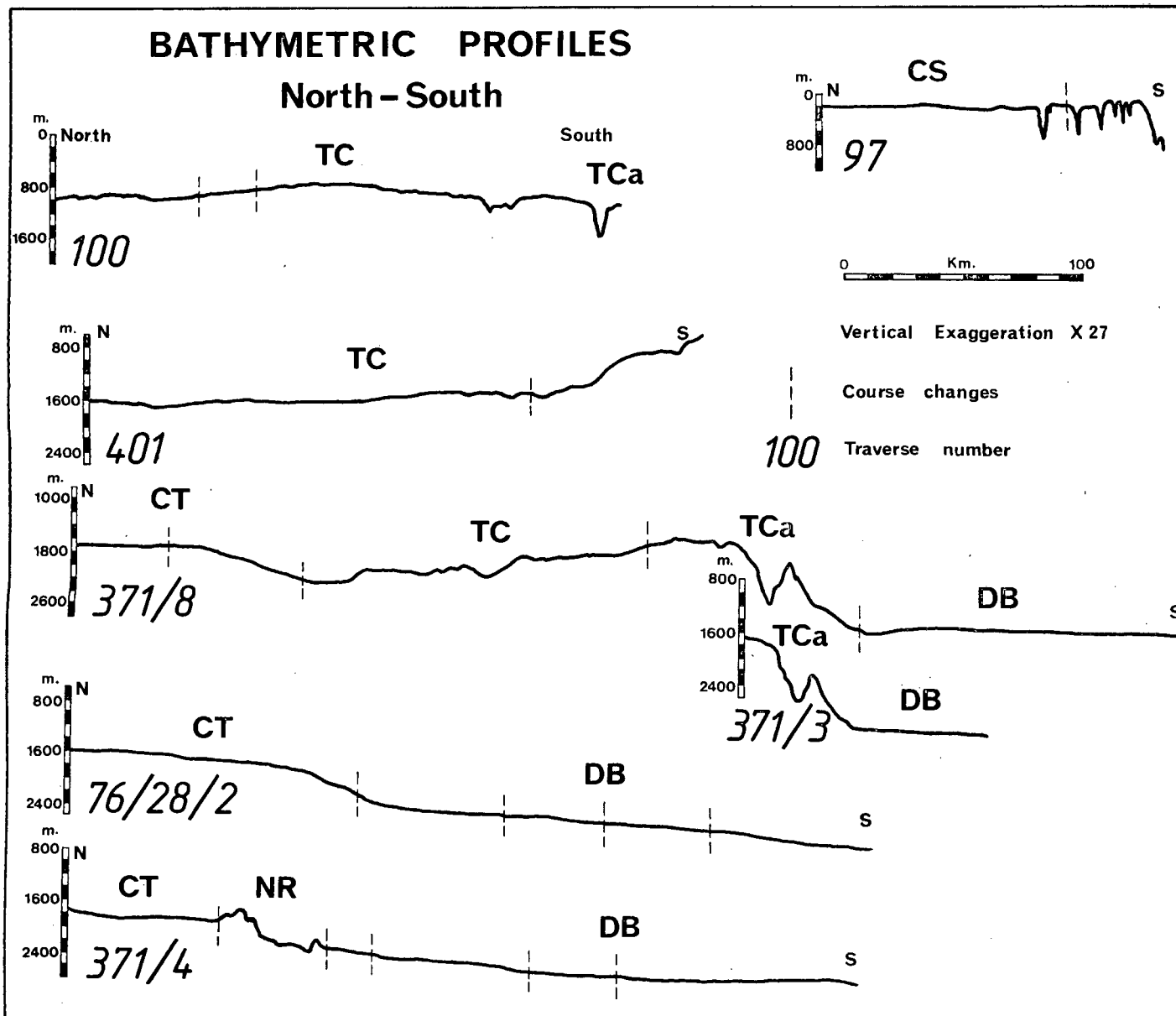
BATHYMETRIC PROFILES
North – South
m.
0 North
800
1600
100
TC
TCa
South
CS
m.
0 N
800
97
S
0 Km. 100
Vertical Exaggeration X 27
Course changes
100 Traverse number
m.
800 N
1600
2400
401
TC
S
m.
1000 N
1800
2600
371/8
CT
TC
TCa
m.
800
1600
2400
371/3
TCa
DB
S
DB
m.
800 N
1600
2400
76/28/2
CT
DB
S
m.
800 N
1600
2400
371/4
CT
NR
DB
S
TC Tugela Cone
TCa Tugela Canyon
CT Central Terrace
DB Deep Ocean Basin
CS Continental Shelf
NR Naudé Ridge
TRACK CHART
Course changes
DURBAN
97
100
401
TC
TCa
TBD 371/8
TBD 371/3
1000
1500
2000
2500
3000
CT
NR
MN 76/28/2
DB
TBD 371/4
2000
29°
30°
31°
32°
33°
34°
35°

Fig. 3. 4

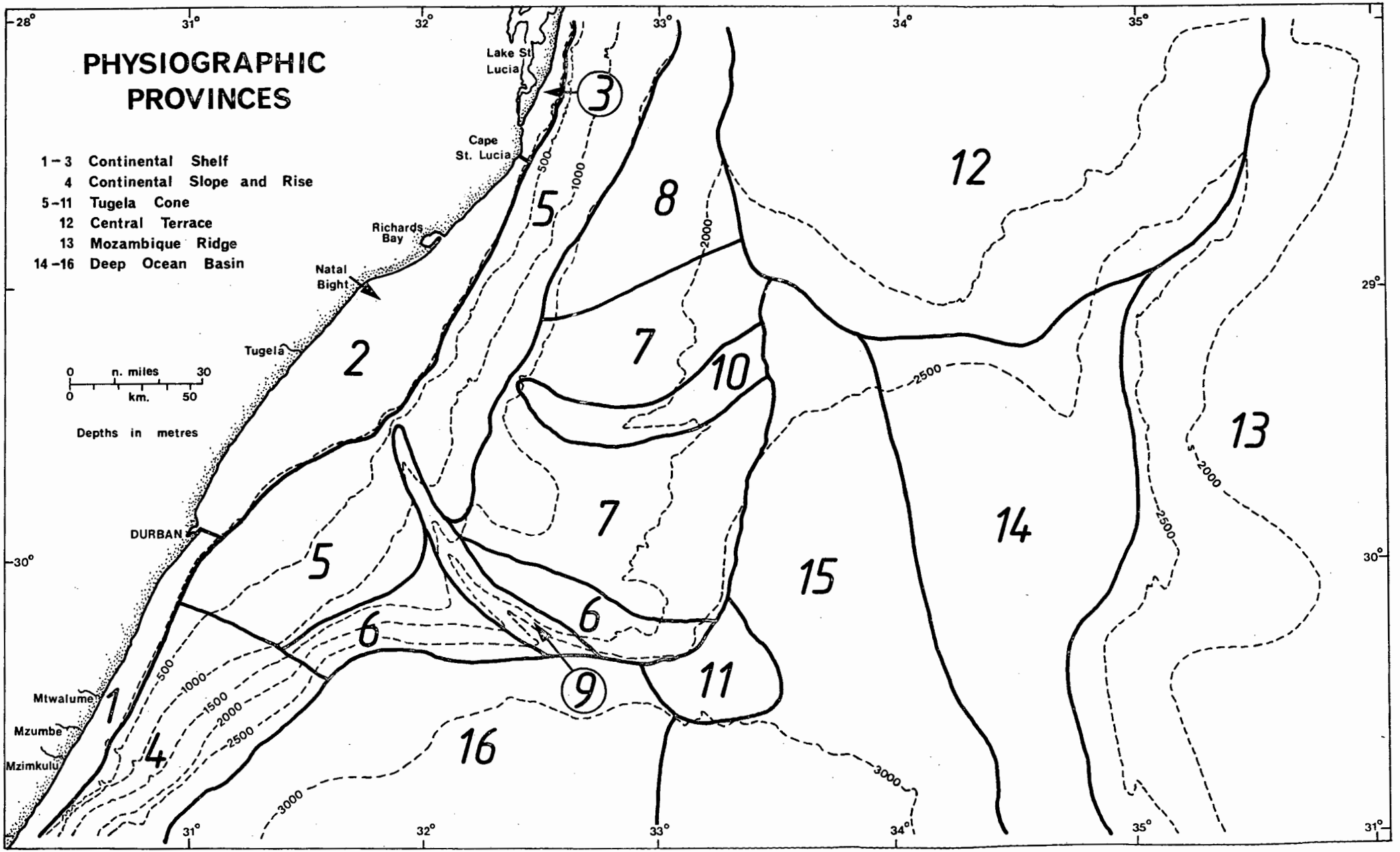
PHYSIOGRAPHIC PROVINCES
1 – 3 Continental Shelf
4 Continental Slope and Rise
5 – 11 Tugela Cone
12 Central Terrace
13 Mozambique Ridge
14 – 16 Deep Ocean Basin
Depths in metres
0 n. miles 30
0 km. 50
Lake St Lucia
Cape St. Lucia
Richards Bay
Natal Bight
Tugela
DURBAN
Mtwalume
Mzumbe
Mzimkulu
28°
31°
32°
33°
34°
35°
29°
30°
500
1000
1500
2000
2500
3000

Fig. 3.5

processes is constructed and discussed (sections 3.3 and 7.2.4). Quantitative bathymetric data are listed in Table 3.1. Methods employed in data acquisition and reduction are described in Appendix A1.

3.2 PHYSIOGRAPHIC PROVINCES

3.2.1 Continental Shelf

The continental shelf in the mid Natal Valley may be subdivided into three units (Fig.3.5; units 1-3) based on morphology. South of Durban (unit 1), the shelf break is sharply defined 10-12 km offshore at a depth of 100m. Between Durban and Cape St. Lucia (unit 2), the shelf widens to a maximum of 45 km in response to structural offset of the coastline (Dingle, 1973) and progradation of the Tugela Cone. Because of sediment draping, the shelf break is poorly defined at a depth of 100m. North of Cape St. Lucia (unit 3), the shelf is extremely narrow averaging only 5 km width. The shelf break shoals northwards from 100m at Cape St. Lucia to 60m at 28°S. Bathymetric statistics (Table 3.1) indicate that the Natal Valley continental shelf is narrow, steep and shallow in comparison to the world average (Shepard, 1963).

3.2.2 Continental Slope

A typical smooth continental slope profile is developed south of the Tugela Cone (Fig.3.5; unit 4) in the SW zone of the study area. Over the slope, gradients vary from 1:8 to 1:16 similar to world averages (Heezen, 1974), decreasing to 1:50 towards marginal areas of the Tugela Cone. Scarp slopes are

Table 3.1 Quantitative Bathymetric Data

	Aver.Gradient	Max. Gradient	Shelf Width (km)	Shelf Depth (m)
CONTINENTAL SHELF				
*Unit 1	1:120(0,5°)	1:80(0,7°)	10-12	100
Unit 2	1:320(0,2°)	1:120(0,5°)	4,5-45	100
Unit 3	1:60(0,95°)	1:40(1,4°)	5	60-100
+World Average	1:500(0,12°)	-	73	130
CONTINENTAL SLOPE				
Unit 4	1:14(4,1°)	1:8(7,1°)		
+World Average	1:13(4,28°)			
TUGELA CONE				
Unit 5	1:33(1,7°)	1:15(3,8°)		
Unit 6	1:27(2,1°)	1:17(3,4°)		
Unit 7	1:125(0,5°)	1:40(1,4°)		
Unit 8	1:85(0,7°)	1:40(1,4°)		
Unit 9 axis	1:53(1,1°)	1:26(2,2°)		
Unit 9 wall	1:8(7,1°)	1:4(13,7°)		
Unit 10 axis	1:130(0,4°)	-		
Unit 10 wall	1:70(0,8°)	1:36(1,6°)		
DEEP OCEAN BASIN				
Unit 14	1:500(0,12°)	1:250(0,2°)		
Unit 15	1:200(0,3°)	-		
Unit 16	1:600(0,1°)	1:200(0,3°)		

* - physiographic units refer to Fig.3.5

\+ - data from Shepard (1963)

prominent between 200-1000m and 2000-2500m. South of 30° 40'S, the slope is dissected by a series of narrow, V-shaped canyons with axial relief of up to 350m (Figs.3.2 and 3.4, profile 97). Axial depths decrease seawards and the canyons possibly coalesce in a dendritic pattern. The continental rise is very poorly developed or absent along the SW continental slope and an abrupt slope break at 2920m marks transition into the deep ocean basin plain.

3.2.3 Tugela Cone

The continental margin of the mid Natal Valley is dominated by the Tugela Cone, a large asymmetric feature approximately 230 x 170 km in size. To the south and east, the cone is delimited by the deep basin plain. To the NE, a wide prominent valley separates the Tugela Cone from the Central Terrace. The Tugela Cone is subdivided into seven physiographic units (Fig.3.5; units 5-11).

The upper slope (unit 5) is bounded by the shelf break and the 1500m isobath. Gradients range from 1:15 to 1:36 over this concave-upward physiographic unit (Figs.3.2 and 3.3) corresponding to the upper fan zone of Damuth and Kumar (1975). Several terraces, sediment wedges and canyons break regularity of the relatively uniform slope. North of Cape St. Lucia, a series of steep-sided gullies and canyons (Bang, 1968) dissect the upper slope. Axial depths of these canyons range from 30-100m and they appear to coalesce into a dendritic pattern. The present day hinterland drainage system shows no association to canyon location in this area. However, Hill (1975) established links

between former terrestrial drainage and the offshore canyons.

The east-west oriented southern margin of the Tugela Cone (unit 6) is straight and relatively smooth and is thus atypical for a prograding sediment wedge. Only minor corrugations and slump scars locally disrupt the steep gradient of 1:27. Shallower regions of unit 6 are more undulating and hummocky grading into units 5 and 7. Obliquely slicing across unit 6, the Tugela Canyon delineates a large prismatic sediment body on its SW margin (Figs.3.2 and 3.4).

Complex surface relief on a less steep slope contrasts the eastern margin (unit 7) with unit 6. Slope gradients range from 1:40 to 1:160 in this region characterised by numerous large hummocks, levees, valleys and scarps. Several terraces break regularity to give the slope a stepped appearance. A major canyon (29^{o} 25'S Canyon) cross-cuts unit 7 dividing it into northern and southern sub-units.

Sea floor topography of the NE margin (unit 8) contrasts with the adjacent eastern margin (unit 7) and displays a relatively smooth, regular (1:85) slope disrupted by occasional scarps, terraces and tributary gullies to the wide valley separating the Central Terrace and Tugela Cone.

The Tugela Cone apex (unit 11) comprises a zone of steep-sided dome-shaped mounds, frequently separated by small sinuous valleys and closed depressions. Average mound relief is 60m, although peaks of 120m elevation occur (Fig.3.2). No obvious directional trends in mound attitude are recognisable and mound relief becomes progressively subdued towards marginal areas of the unit (Fig.3.2).

3.2.4 Tugela Canyon

The Tugela Canyon (Fig.3.5; unit 9) has been the subject of a more detailed bathymetry investigation (Figs.3.6 - 3.8). The Tugela Canyon heads 50 km offshore opposite the Tugela river to obliquely cross-cut the southern Tugela Cone (unit 6) from NW to SE. The canyon is 120 km long and typically deeply incised and V-shaped although locally, U-shaped and bifurcate cross sections occur (Fig.3.7). Originating as a wide 20m deep valley at 500m below sea level, the canyon progressively deepens to a maximum axial relief of 800m midway along its length. Thalweg gradients vary from 1:26 to 1:150 imparting a stepped character to the canyon axis longtitudinal profile. Canyon walls are much steeper (1:8 average) with hummocks, ? slump scars and tributary canyons disrupting the slopes (Fig.3.6). Cross sections (Fig.3.7) show the narrow (<500m) canyon floor to have a highly variable morphology with flat, sloping and dissected bifurcate configurations. The Tugela Canyon is sinuous in plan view (Fig.3.6), but unlike a 'typical' erosive submarine canyon (Shepard, 1963), only a few shallow, minor tributary valleys are delineated. Levee development is restricted to the NE canyon flank where a large asymmetric levee has substantially heightened the canyon wall (Fig.3.7; profiles d-g). With increasing distance from source there is progressive eastward deflection of the Tugela Canyon axis.

3.2.5 29° 25'S Canyon

Physiographically, the 29° 25'S Canyon (Fig.3.5; unit 10) strongly contrasts with the Tugela Canyon. Originating as a wide, shallow valley 1400m below sea level, the canyon gradually

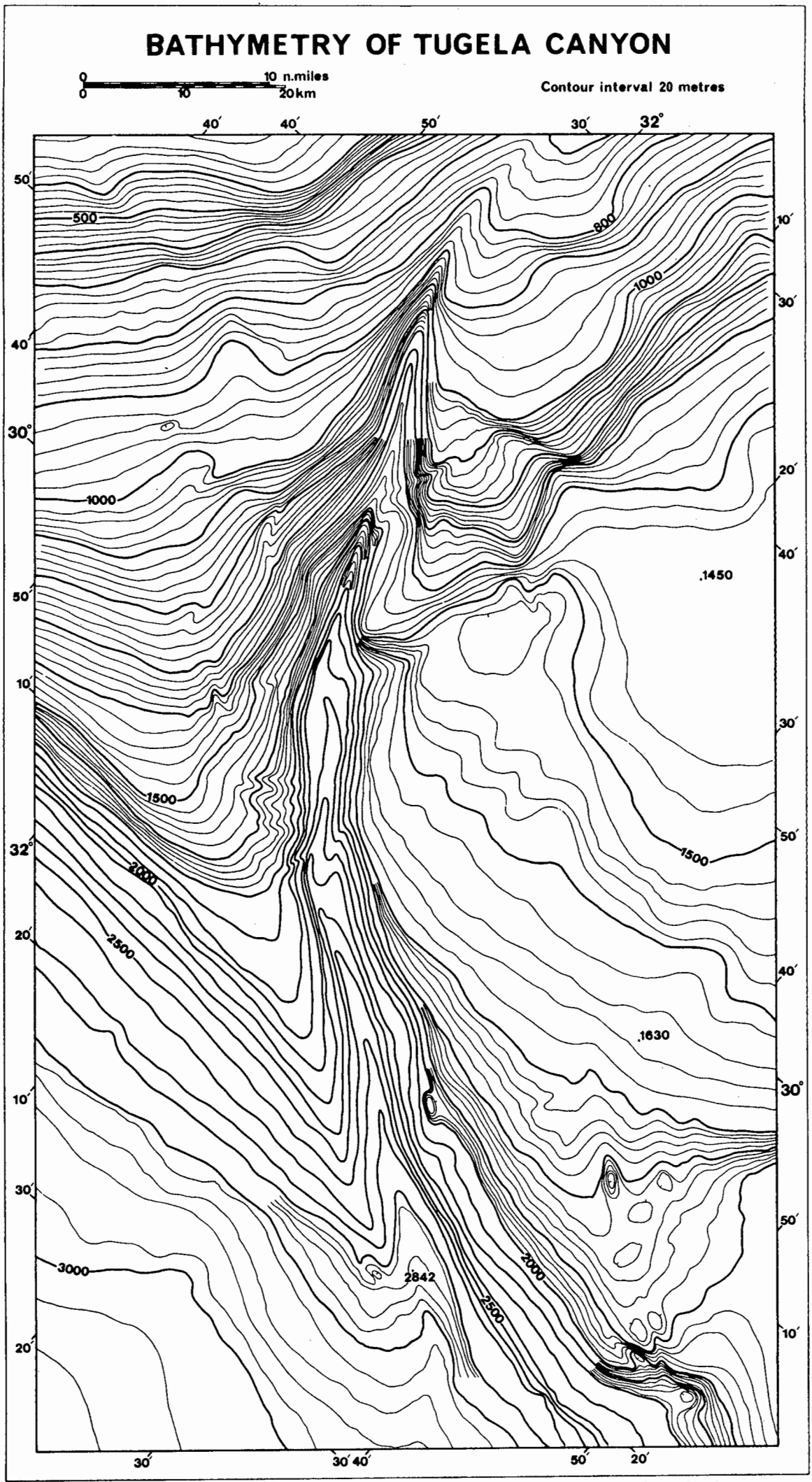
BATHYMETRY OF TUGELA CANYON
0 10 n.miles
0 10 20km
Contour interval 20 metres
40′ 40′ 50′ 30′ 32°
50′
40′
30°
50′
10′
32°
20′
10′
30′
3000
500
1000
1500
2000
2500
800
1000
1500
2000
2500
.1450
.1630
2842
10′
30′
50′
20′
30′
30′ 40′
50′
20′

Fig. 3.6

TUGELA CANYON-CROSS SECTIONS

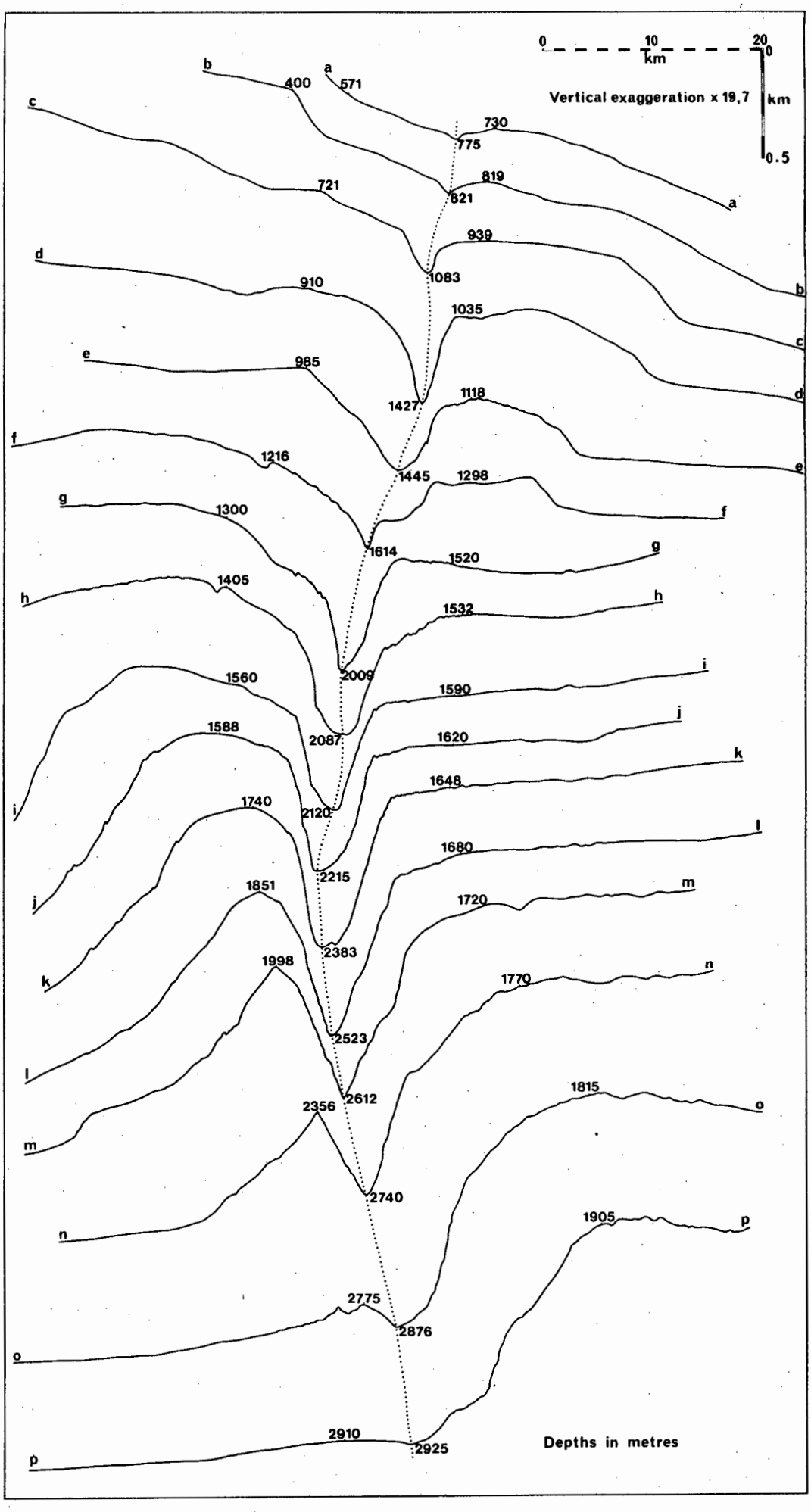

Fig. 3.7

TUGELA CANYON TRACK CHART

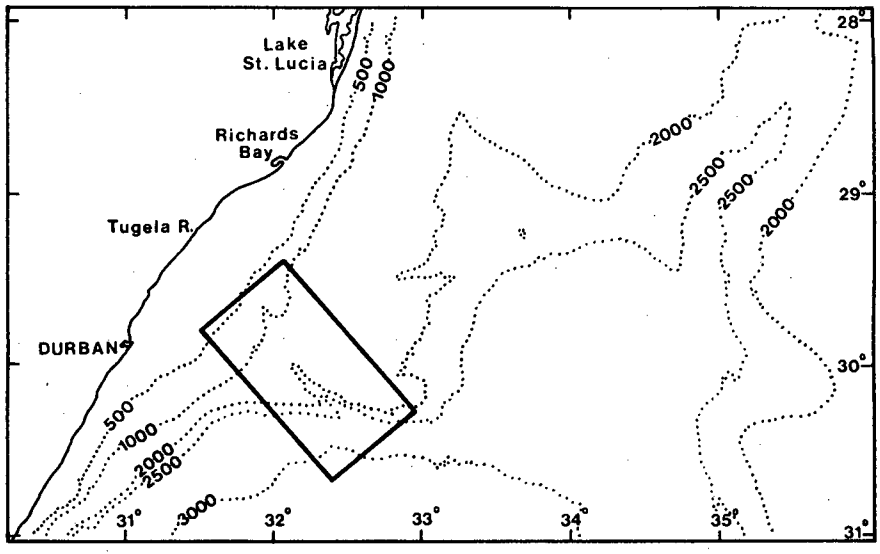

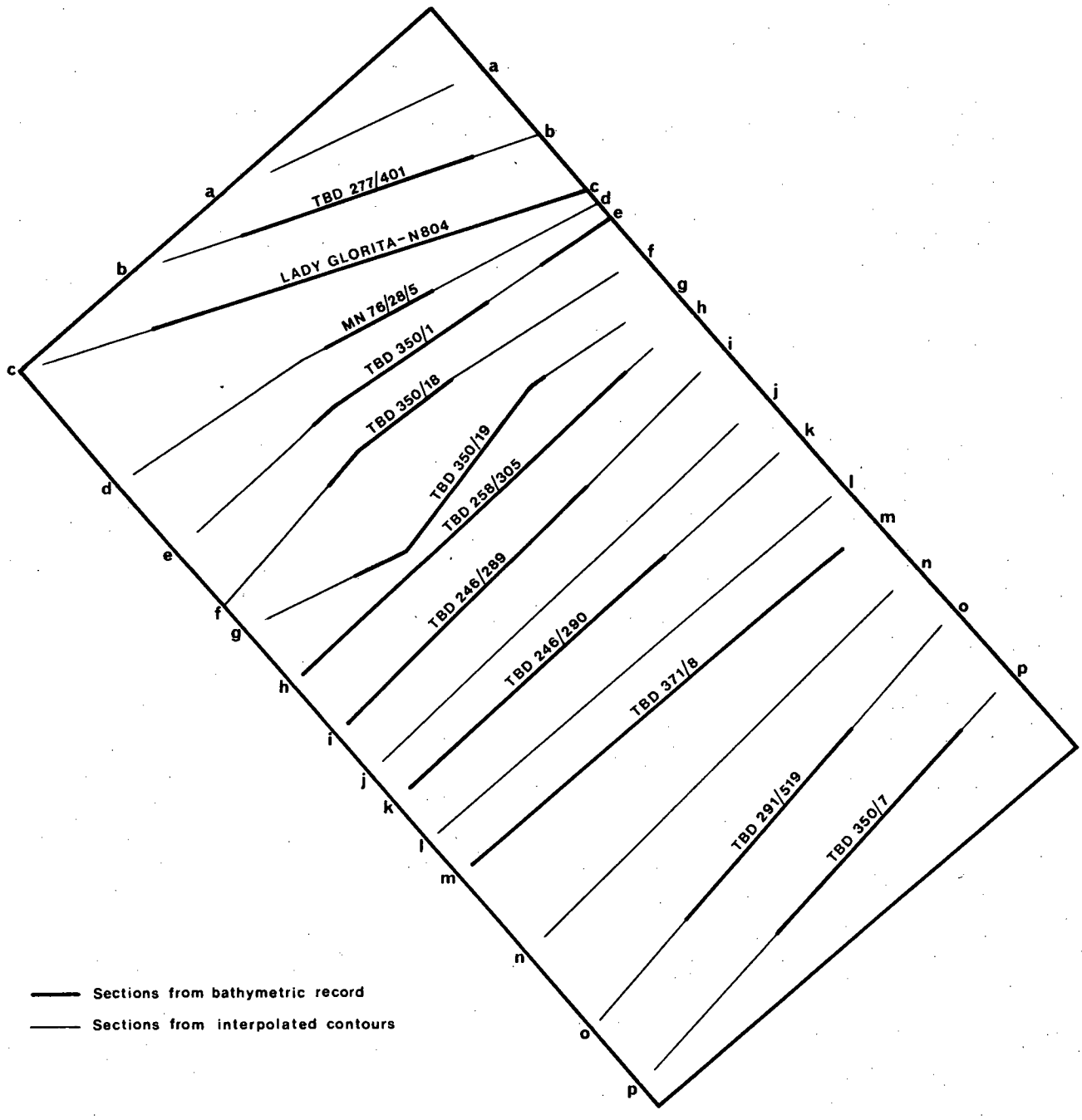

Fig. 3.8

widens and deepens down-slope to attain a maximum axial depth of 250m. Both the axial (1:130) and side wall (1:70) gradients are less than for the Tugela Canyon (Table 3.1). Tributary valleys are characteristic of the 29° 25'S Canyon, particularly on the northern side wall. Showing sinuous form, the canyon emerges from the cone at 2320m where depressions, scour moats and sediment ridges are developed around the East Tugela Ridge basement high (Fig.3.3; profile 8). Like the Tugela Canyon, with increasing distance from source, the 29° 25'S Canyon is progressively deflected to the left (looking down-canyon).

3.2.6 Central Terrace

Situated NE of the Tugela Cone, the southern Central Terrace (Fig.3.5; unit 12) slopes gently southward at 1:400 from 1600-2000m. The terrace crest forms a smooth convex surface with a N-S central axis which bifurcates and swings NNW-SSE towards its southern extension. The terrace is flanked to the east and west by prominent valleys separating it from the Mozambique Ridge and Tugela Cone respectively. The southern flank is steep and straight with an abrupt transition to the deep basin plain at 2400m. Around 28° 35'S, 34° 50'E, a zone of peaks, ridges and gullies is an expression of outcropping indurated Tertiary strata. A moated basement pinnacle of the Naude Ridge complex protrudes 200m through the surrounding sediment drape at 28° 52'S, 34° 41'E.

3.2.7 Mozambique Ridge

The sediment-draped Mozambique Ridge (Fig.3.5; unit 13) forms an eastern boundary to the mid Natal Valley. The

undulating ridge crest area comprises numerous basement peaks, sediment mounds and ponded valleys. The steep (1:25 to 1:100) western margin of the ridge is typically smooth and undulatory with a relief in excess of 800m. In the vicinity of 29°S, the slope becomes more rugged and incised (Figs.3.2 and 3.3; profiles 7-10) and is dominated by steep basement/sediment mounds and ridges up to 140m amplitude. A wide transverse valley and saddle cross-cuts the ridge crest at 30°S (Fig.3.2). A sharp topographic discontinuity at 2700m marks transition into the deep ocean basin plain.

3.2.8 Deep Ocean Basin Plain

The deep ocean basin has been subdivided into three units (Fig.3.5; units 14-16) based on physiographic character.

The eastern section (unit 14) comprises an elongate asymmetrical lobe of sediment with a south-trending apex. The smooth and slightly undulating lobe slopes very gently (1:500) southwards with slight steepening on both flanks (Fig.3.2). A flat-floored moat, 20-60m in depth and ranging from 5-20 km in width, is a persistent feature along the Mozambique Ridge base.

Westwards into unit 15, gradients steepen to 1:200 and echograms indicate a corrugated microtopography locally incised by narrow channels. South of 30° 30'S, microrelief is more chaotic with numerous small valleys and hummocks. The largest of these valleys, 60m in axial depth, trends NW-SE in line with the Tugela Canyon (Fig.3.2) and may constitute a now largely-inactive extension of the Tugela Canyon. The East Tugela Ridge basement high protrudes 400m through basinal sediments in the NW region of unit 15 at 29° 18'S, 33° 34'E (Fig.3.2).

Central areas of the SW deep basin (unit 16) are smooth with a low gradient (1:600). Towards the Tugela Cone and continental margin gradients steepen to 1:200 and the sea floor becomes increasingly corrugated. Immediately south of the Tugela Canyon mouth, southward isobath deflection (Fig.3.2) probably delineates a depositional fan. Farther west at 30^{o} 31'S, 31^{o} 45'E, a large dissected sediment lobe probably represents a slumped mass.

3.3 SEA FLOOR TOPOGRAPHY

3.3.1 Introduction

In recent years an increasing number of studies have demonstrated that high frequency (3,5-12kHz) echograms are an invaluable tool in evaluation of ocean floor depositional/erosional processes (Damuth, 1975; Damuth and Hayes, 1977; Embley et al, 1978; Damuth, 1978; Kolla et al, 1980a; Damuth, 1980). A similar approach, leading to echogram classification, has been attempted in the mid Natal Valley.

Bathymetric data from the mid Natal Valley has been almost exclusively retrieved using a 12kHz transducer. This prevents an approach identical to Damuth and co-workers who restrict their data base to 3,5kHz echograms wherever possible. As a consequence, Natal Valley echograms are categorised on sea floor shape and form alone, discounting any reference to sub-bottom reflectors. Close cognizance of inter-related factors including seismic stratigraphy (Chapters 6 and 7) and sedimentology (Chapter 8) aided development of the topography classification scheme (Damuth, 1980).

3.3.2 Classification and Distribution of Topographic Zones

Based on 12kHz echograms, sea floor topography can be allocated to two principal classes: (1) smooth topography; and (2) rough topography. These two classes can be further subdivided into twelve discrete groups, which are often locally intergradational. Photographically-reduced examples of ten of the echogram categories are presented in Plate 3.1 with locations being shown in Fig.3.1b. The areal distribution of topographic groups is mapped in Figure 3.9.

3.3.2.1 Smooth Topography (Class I)

Within this class only one major type is recognised in the mid Natal Valley:

Type IA A very smooth sea floor with almost complete absence of bottom corrugation characterises type IA. Three subsidiary groups are delineated:

(IA-1) - smooth sea floor exhibiting occasional very low amplitude, long wavelength undulations (Plate 3.1a). This echo group is restricted to low gradient (<1:500) areas of the deep basin plain.

(IA-2) - smooth sea floor with infrequent corrugations and undulations (Plate 3.1b). This echo group dominates the Central Terrace crest with isolated patches mapped over the upper Tugela Cone and SW Central Terrace (Fig.3.9).

(IA-3) - smooth sea floor, characterised by common long wavelength (20 km), low amplitude (<20m) undulations (Plate 3.1c), is mapped over the Mozambique Ridge crest and east Central Terrace.

3.3.2.2 Rough Topography (Class II)

This class can be divided into four major types, each subdivisable depending on form and dimension of sea floor relief:

Type IIA (Corrugations) This type is distinguished on existence of low amplitude (<10m) asymmetric corrugations with short wavelength and frequency. Presence or absence of long frequency undulations permits subdivision:

(IIA-1) - short wavelength (<1-2 km), low amplitude corrugations with occasional irregular channels (<10m axial depth) superimposed on a smooth sea floor (Plate 3.1b and c). This microrelief style is widespread over the continental shelf, upper and northern Tugela Cone and the west Central Terrace.

(IIA-2) - short wavelength, infrequent low amplitude corrugations superimposed on a sea floor characterised by long wavelength, low undulations (Plate 3.1f). This topographic style is restricted to the deep basin plain adjacent to the eastern Tugela Cone and SW continental slope (Fig.3.9).

Type IIB (Hummocks) Type IIB sea floors are distinguished by the prevalence of broad hummocks of variable wavelength and symmetry ranging from 10-40m in amplitude. Two subsidiary groups are defined:

(IIB-1) - asymmetric to strongly asymmetric hummocks which are smooth in surface detail. Individual hummocks with wavelengths of 1-10 km may be isolated or closely spaced (Plate 3.1d). This major category dominates the southern and eastern Tugela Cone.

SEA FLOOR ECHOGRAMS — MICROTOPOGRAPHY CLASSIFICATION

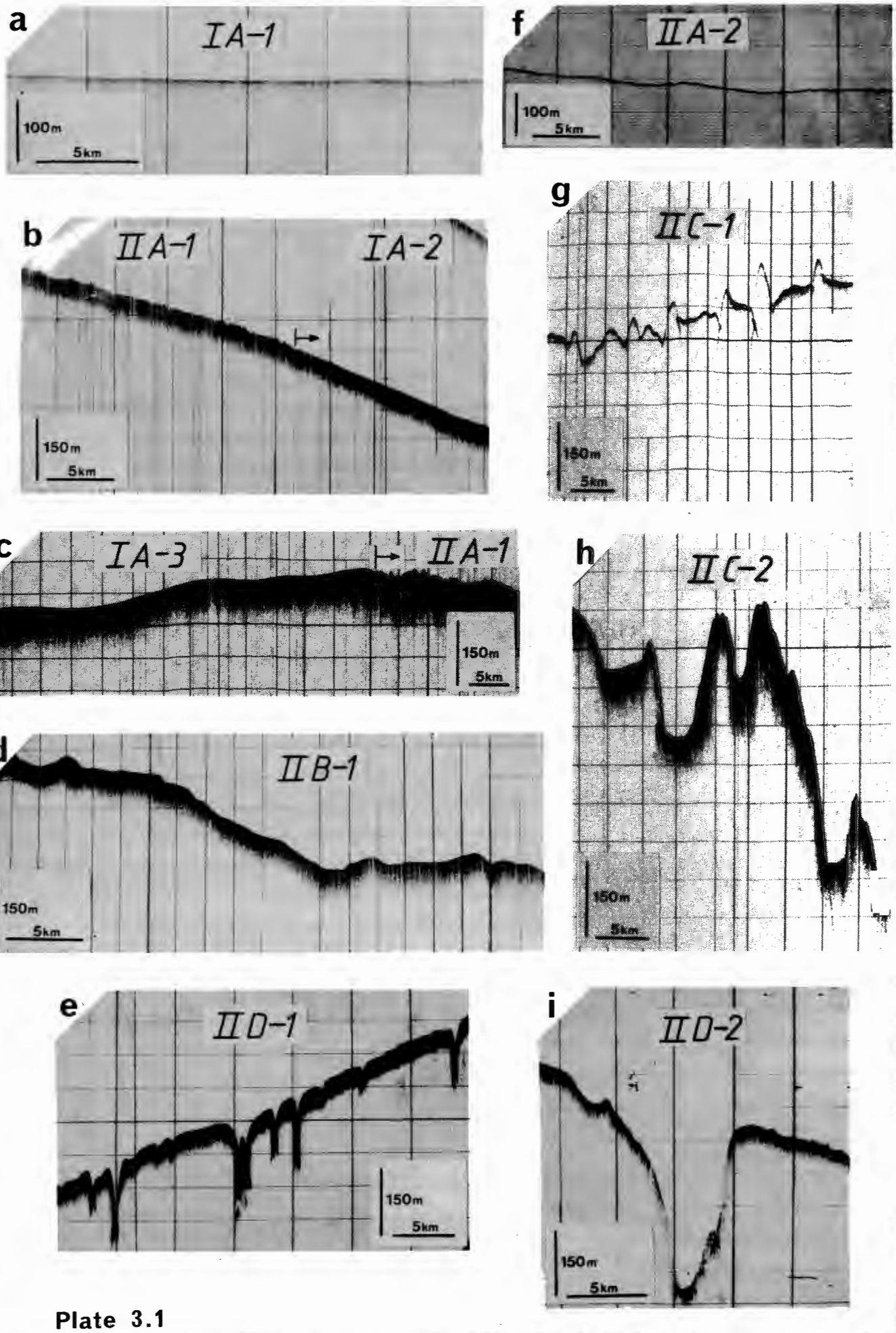

Plate 3.1

Plate 3.1 Sea Floor Echograms - Microtopography Classification

a IA-1 Smooth sea floor showing occasional very low amplitude, long wavelength undulations (TBD 371/1).

b IA-2 Smooth sea floor with very minor, infrequent corrugations and undulations.

IIA-1 Short wavelength, low amplitude corrugations with occasional shallow irregular channels (TBD 350/8).

c IA-3 Smooth sea floor characterised by long wavelength, low amplitude undulations.

IIA-1 see caption b (TBD 350/6)

d IIB-1 Hummocky terrain; individual asymmetric hummocks up to 40 m in amplitude and with wavelengths of 1-5 km (TBD 350/1).

e IID-1 Dissected sea floor; canyon axial depth varies from 10-150 m in this example (TBD 350/17).

f IIA-2 Short wavelength, infrequent low amplitude corrugations superimposed on long wavelength undulations (TBD 371/1).

g IIC-1 Steep sided, largely symmetrical, peaked mounds from 40-80 m in amplitude with intervening corrugated sea floor (TBD 350/21).

h IIC-2 Super-large asymmetric, corrugated mounds from 50-200 m in amplitude (TBD 350/2).

i IID-2 Large solitary canyon (Tugela Canyon) (TBD 350/1)

Echogram locations presented in Fig.3.1b.

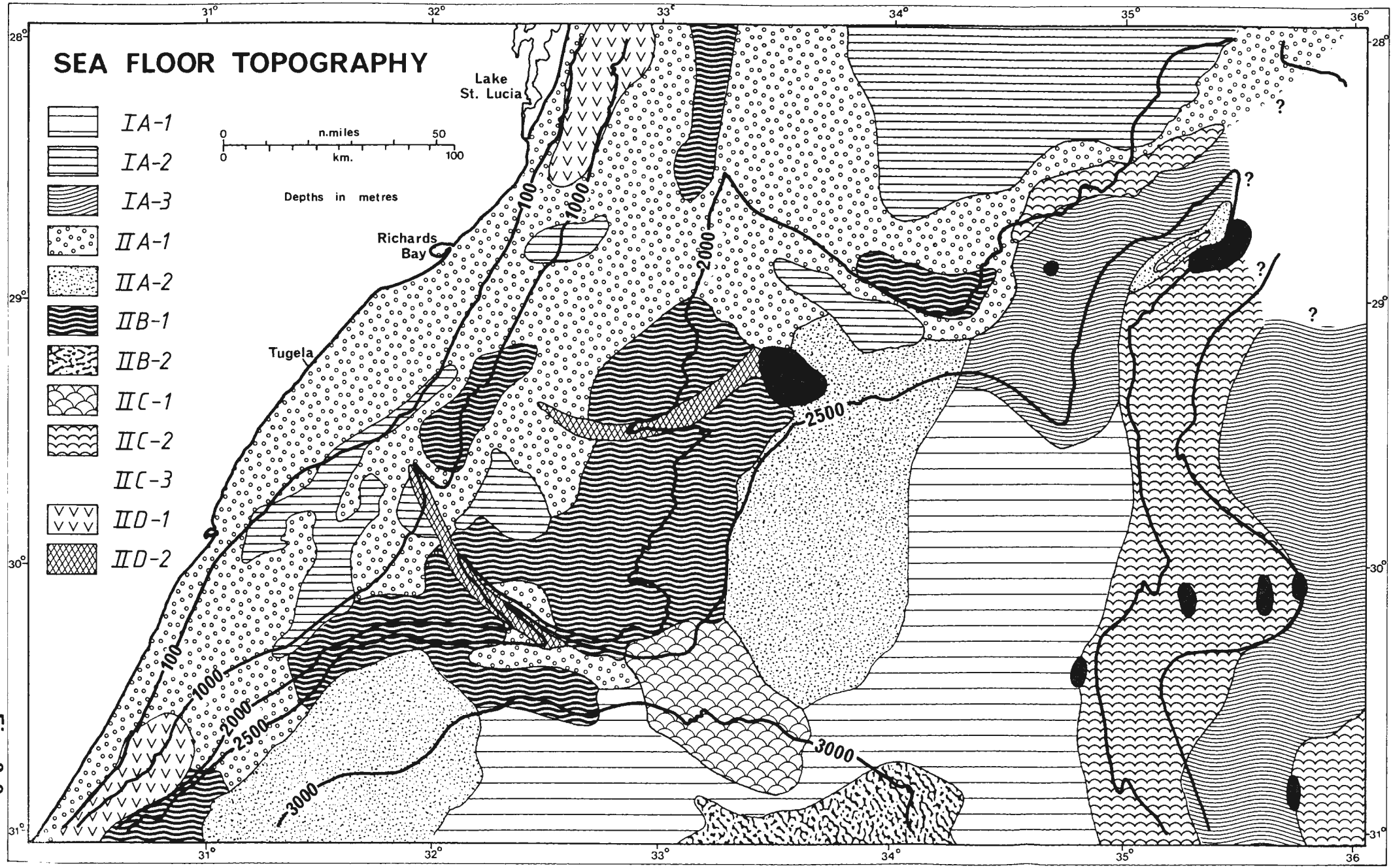
SEA FLOOR TOPOGRAPHY
IA-1
IA-2
IA-3
IIA-1
IIA-2
IIB-1
IIB-2
IIC-1
IIC-2
IIC-3
IID-1
IID-2
0 n.miles 50
0 km. 100
Depths in metres
Lake St. Lucia
Richards Bay
Tugela
100
1000
2000
2500
3000
?
28°
29°
30°
31°
31°
32°
33°
34°
35°
36

Fig. 3.9

(IIB-2) - infrequent hummocks separated by a corrugated sea floor and cross-cut by intermittent deep-sea valleys. Seismic profile 371/3 (Plate B3.3c) shows a section of group IIB-2 from the south deep basin plain.

Type IIC (Large Mounds) Presence of mounds greater than 40m in amplitude define type IIC topographies. Three subdivisions are recognised:

(IIC-1) - steep-sided, smooth, symmetric to slightly asymmetric, peaked mounds ranging from 40-80m in amplitude. Mounds are solitary or closely spaced and show moated margins. Between isolated mounds, the sea floor is typically corrugated (Plate 3.1g). Group IIC-1 topographies are restricted to the Tugela Cone apex (Figs.3.9 and 3.5 unit 11).

(IIC-2) - super-large mounds with an amplitude range of 50-200m. Mounds of this group are rarely symmetrical and are corrugated on their flanks. Deep flat-floored valleys separate the mounds (Plate 3.1h) which are common over the western Mozambique Ridge flanks. Similar topographies have been recognised over the eastern Mozambique Ridge (Kolla et al, 1980a).

(IIC-3) - rugged basement protrusions of group IIC-3 are primarily restricted to the Mozambique Ridge province, although sections of the East Tugela and Naude Ridges also outcrop at the sea floor.

Type IID (Canyons) Two groups of canyon terrain are recognised within the study area:

(IID-1) - numerous steep-sided canyons (50-300m axial

depth), probably coalescing in a dendritic pattern, dissect the IID-1 sea floor (Plate 3.1e) over the upper slope zones of the SW continental slope and northern Tugela Cone (Fig.3.9).

(IID-2) - large solitary canyons with minor tributary systems (Tugela and 29° 25'S Canyons) cross-cutting the Tugela Cone (Plate 3.1i shows the Tugela Canyon).

3.3.3 Comparison with Existing Echo Classification Schemes

The topography classifications reviewed by Damuth (1980) are not directly comparable to the scheme presented in the preceding section since this study relies solely on surface morphology with no reference to sub-bottom reflections. However, many of the bathymetric traverses are backed up by 40 in^3 airgun seismic profiles in which numerous shallow sub-bottom reflectors are visible. Because of this, it is possible to qualitatively correlate the echo categories of this study to those of previous compilations (Damuth, 1980). Results of this visual correlation are shown in Table 3.2. Because of the minor reliance on sub-bottom reflections, categories of the present study, in some cases, do not exclusively correspond to classes defined by Damuth and his colleagues. For example, category IIA-1 is analogous to classes IA-2 and IIIC of Damuth (1978).

With these limitations in mind, correlation to existing studies is of considerable use in relating the Natal Valley topographic zonation to extant oceanographic and sedimentary processes. Discussion of the relevance of several of the topography classes is contained in section 7.2.4.

Table 3.2 Correlation of Echo Categories with Previous Nomenclature*

THIS STUDY	NORWEGIAN-GREENLAND SEA+	EAST BRAZILIAN MARGIN**	NORTH BRAZILIAN MARGIN***
IA-1	IB or IIA	IB or IIA	IB or IIA-2
IIA-1	IA-2 or IIIC	IIIC	IIB-2
IIA-2	-	IIID	IIB-3
IIB-1	IIID	-	IIB-5
IIC-1	IIIB	IIIB	IIB-4
IIC-3	IIIA	IIIA	IIB-1

* part of this table previously published by Damuth (1978)

\+ data from Damuth (1978)

** data from Damuth and Hayes (1977)

*** data from Damuth (1975)

CHAPTER 4 TECTONIC AND EARLY SEDIMENTATION HISTORY

4.1 INTRODUCTION

Development of sedimentary basins along the SE African continental margin has been constrained by tectonic structures initiated during the rifting and drifting phases of Gondwanaland break-up (Dingle and Scrutton, 1974). Consideration of Gondwana reconstructions is therefore important in discussion of the early geological history of the Natal Valley. Combination of the break-up tectonic history with published regional lithostratigraphic profiles permits speculation on facies and provenance of early basinal sediments of the Natal Valley.

In this chapter, some Gondwana reconstructions are briefly reviewed and the chronological sequence of events during break-up and continental separation is outlined. The tectonic history and structural development of the SE African margin and pre-drift contiguous Falkland Plateau is presented and utilised in application of passive continental margin rifting models to the Natal Valley region. Finally, the Natal Valley pre-drift and early post-drift sedimentation history is considered taking cognizance of the tectonic history and hinterland lithostratigraphic data.

4.2 GONDWANALAND RECONSTRUCTIONS

Following almost universal acceptance of plate tectonic and sea floor spreading theory, several different Gondwana reconstructions have been proposed. Geometric reconstructions of Africa and South America were published by Bullard et al (1965). Following this, utilising a similar method but reinforced by

geological constraints, Smith and Hallam (1970) proposed their widely-accepted Gondwana refit (Fig.4.1). There is general agreement over many aspects of most 'modern' reconstructions. The South America to Africa (West Gondwana) refit is successfully restricted on several lines of evidence (Smith and Hallam, 1970; Siedner and Mitchell, 1976; Rabinowitz and LaBrecque, 1979; Martin, Hartnady and Goodlad, 1981). Australia and Antarctica have also been confidently reconstructed (Wiessel et al, 1977). However, refit positions of Madagascar, India, Antarctic peninsula and the general reconstruction of East and West Gondwana continue to generate controversy.

Using the South Atlantic spreading history described by Ladd (1976) and Rabinowitz and LaBrecque (1979) and incorporating all available information on magnetic lineations, fracture zone trends, location of spreading centres and topographic features within the Indian Ocean, Norton and Sclater (1979) have presented an updated reconstruction for the Gondwana continents (Fig.4.2). This fit emplaces Dronning Maud Land (Antarctica) in juxtaposition with southern Mozambique while Madagascar is positioned in a northerly site against Kenya. India and Antarctica are refitted in accordance with Smith and Hallam (1970). East Gondwana (Antarctica - India - Madagascar) is relocated against Africa using a best visual fit but without overlapping the Mozambique Ridge which is inferred to be a pre-drift continental fragment. This reconstruction, however, retains untenable overlap of continental basement portions of the Falkland Plateau and Antarctic peninsula. The reconstructed position of peninsular Antarctica may be resolved either by: (1) placing it west of South America in the Andean province (Harrison

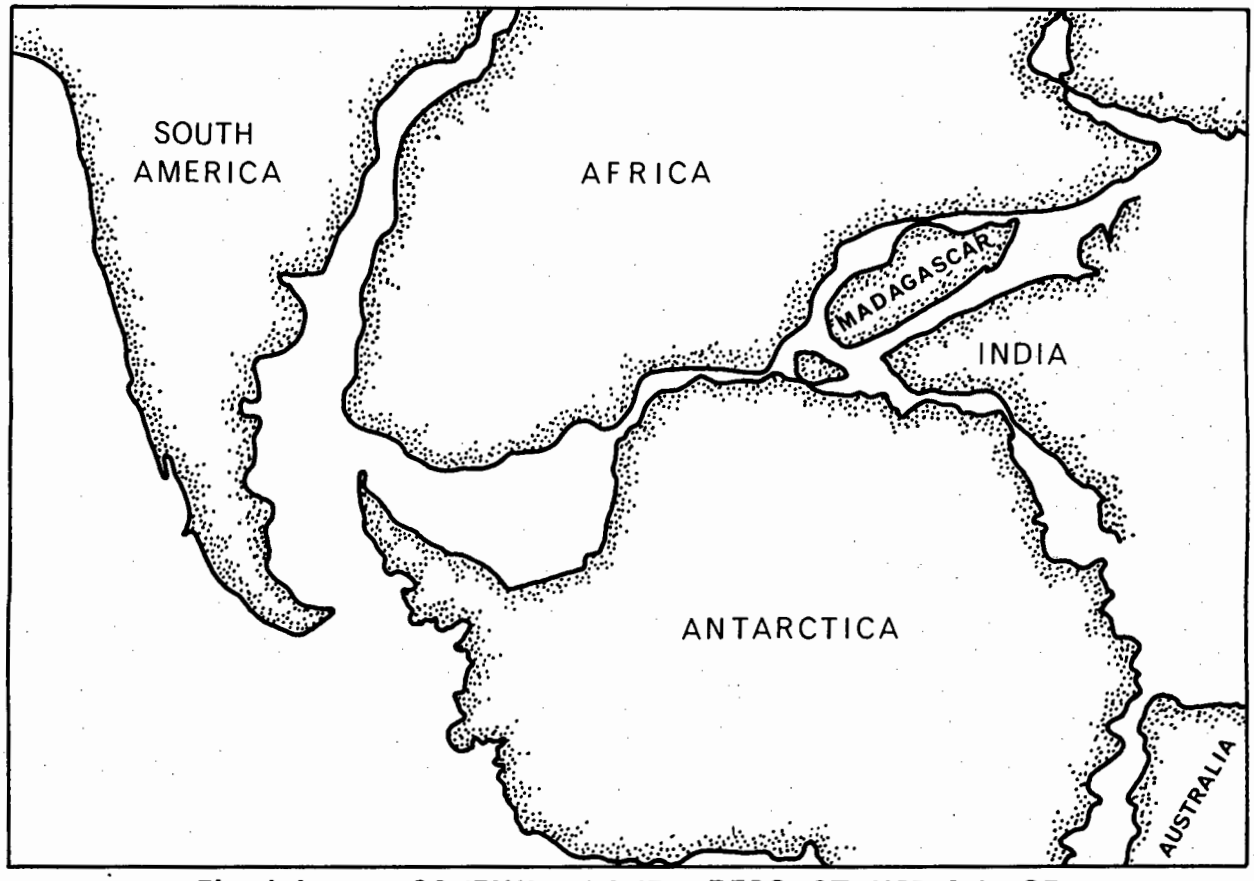

Fig. 4.1 GONDWANALAND RECONSTRUCTION OF SMITH AND HALLAM (1970)

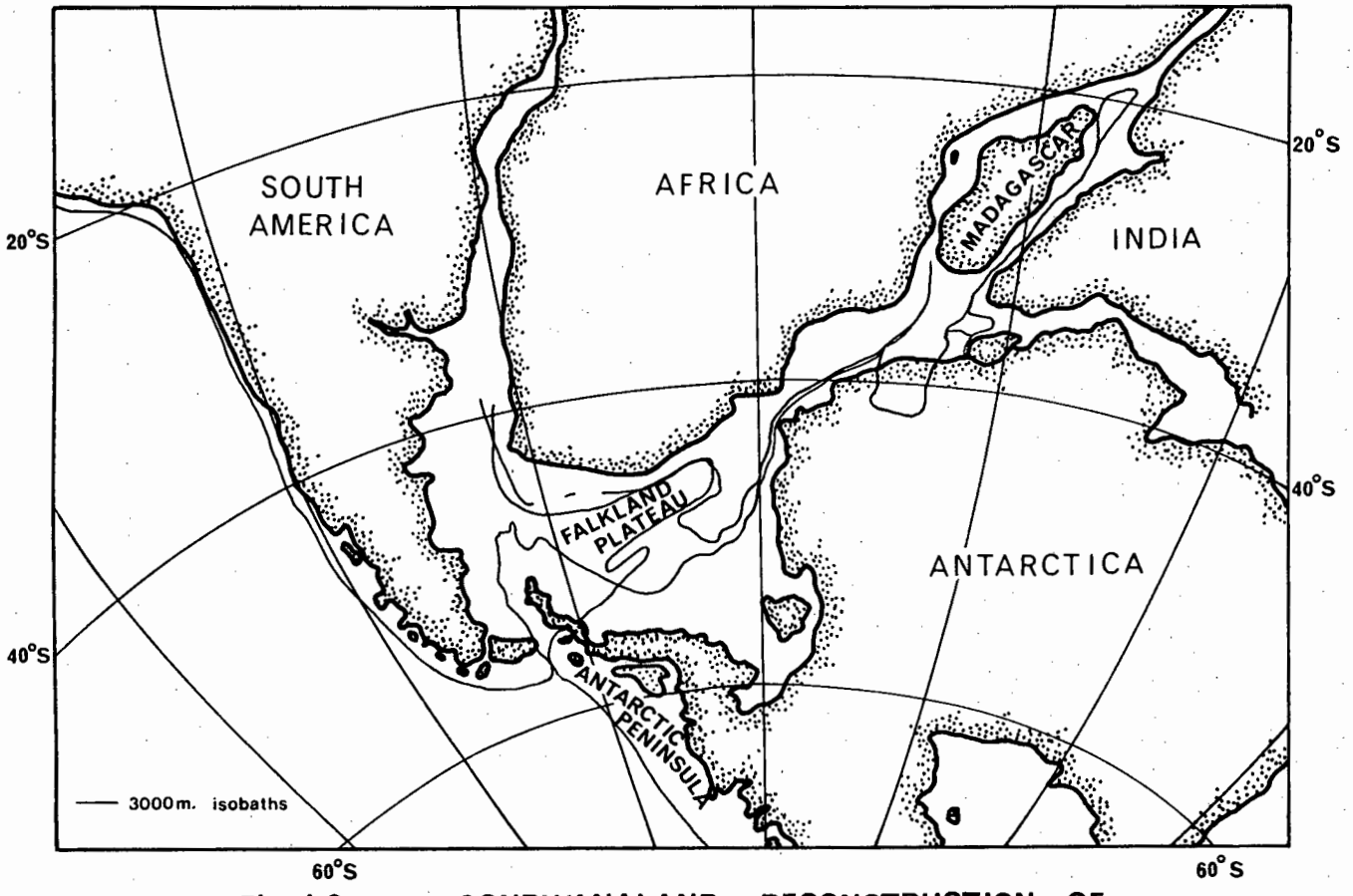

Fig. 4.2 GONDWANALAND RECONSTRUCTION OF NORTON AND SCLATER (1979)

et al, 1979); (2) invoking post-drift oroclinal bending (Dalziel and Elliot, 1971); or (3) invoking post-drift microplate rotation (de Wit, 1977).

Accepting that evidence from some problematical areas is yet equivocal, the Gondwana reconstruction of Norton and Sclater (1979) merged with Antarctic peninsula microplate rotation (de Wit, 1977) is adopted in discussion of the tectonic and sedimentary history of the Natal Valley (Fig.4.3).

4.3 TIMING OF GONDWANALAND BREAK-UP

Onset of continental separation is marked by uplift, intrusion and extrusion of basic and alkaline igneous rocks, rift formation and initiation of marine sedimentation (Barron et al, 1978). Timing of these events together with palaeomagnetic constraints has established a chronological order for Gondwana break-up (e.g. Smith and Hallam, 1970; Scrutton, 1973a; McElhinny, 1973).

Initial tectonism may precede the final separation by a considerable period of time (Barron et al, 1978). Widespread Jurassic volcanism in the southern Andes, Antarctic peninsula and Karoo basin (Adie, 1972; Cox, 1978) and Late Carboniferous tectonic activity in East Africa have been related to initial separation of East and West Gondwana. Palaeomagnetic poles for the Gondwana continents show significant divergence by the Late Jurassic confirming that relative movement had already occurred (Norton and Sclater, 1979).

Palaeogeographic reconstructions for the sedimentary basins of eastern Africa also provide information on timing of continental separation. A progressively southward-encroaching

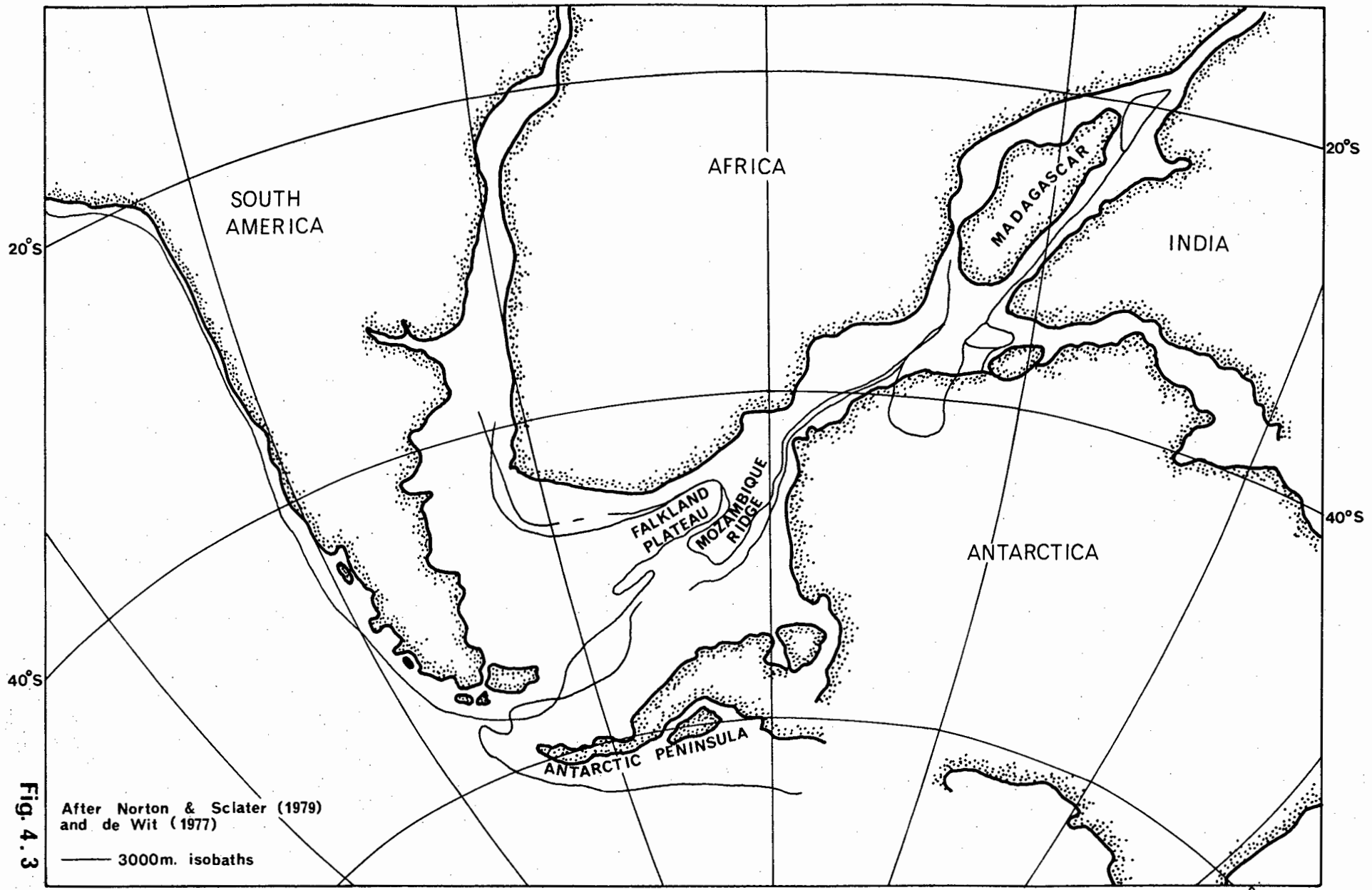

Fig. 4.3

GONDWANALAND RECONSTRUCTION OF NORTON AND SCLATER (1979) MODIFIED BY ANTARCTIC PENINSULA ROTATION

Jurassic transgression, recorded by identification of Tethyan fauna, finally reached the Falkland Plateau (DSDP 330) in the middle Jurassic (Barker, Dalziel et al, 1976) and persisted in the central Outeniqua Basin throughout the late Jurassic (Dingle, 1978). Recognition of southward-transgressing marine sediments is consistent with the East/West Gondwana separation model of Norton and Sclater (1979), whereby Sri Lanka and the Mozambique Ridge acted as obstructions to open marine circulation, constraining marine incursion to penetrate from the north. Norton and Sclater (1979) suggest that the earliest break-up tectonics primarily consisted of vertical and transcurrent displacements with only minor ridge spreading, also limiting the size of the early marine basins. Accordingly, the early taphrogenic phase of East/West Gondwana fragmentation is placed in the Late Triassic or Early Jurassic (~200-180 Myr).

In the SW Indian Ocean, the earliest recognised sea floor spreading magnetic anomaly is the Late Jurassic anomaly M22 (141 Myr) which Segoufin (1978) delineated in the Mozambique Channel, thus prompting Norton and Sclater (1979) to infer an East/West Gondwana split by that time. Similarly, Barron et al (1978) conclude that separation of East and West Gondwana occurred in the time interval 140-160 Myr.

Initial opening of the South Atlantic has been confidently dated in the range 125-130 Myr. This is substantiated by marine magnetic anomalies (Larson and Ladd, 1973; Goodlad et al, 1982) and further supported by palaeomagnetic evidence (Creer, 1973), radiometric age determinations (Siedner and Miller, 1968) and igneous rock distributions (Marsh, 1973). South Atlantic opening was the last major continental separation event which had direct

effect on the structural geometry, morphology and early sedimentary history of the Natal Valley. Falkland Plateau translation past the Mozambique Ridge southern apex removed the last obstruction to open marine circulation within the Natal Valley and full oceanic conditions have prevailed since that event.

4.4 TECTONIC AND STRUCTURAL FRAMEWORK

4.4.1 Introduction

Southeast African continental margins can be subdivided into two major groups, each defined by a distinctive structural style reflecting dominant tectonic processes active during their formation (Dingle and Scrutton, 1974):

(1) Northeast margin (Zululand and Mozambique) - zone of tensional faulting active during separation of East and West Gondwana; and

(2) South and east margins (eastern Agulhas Bank, Transkei and Natal) - zone of transform faulting active during break-up of West Gondwana (Africa and South America).

Both vertical tensional faulting and transform faulting have played important roles in construction of Natal Valley basement geometry and thus these tectonic styles are considered in greater detail.

4.4.2 Northeast Margin - Zone of Vertical Tectonics

This zone incorporates marginal basins of Mozambique and northern Zululand together with adjacent offshore basins: Mozambique Channel, NW Mozambique Basin and northernmost Natal

Valley (Figs.4.4 and 4.5). Large scale crustal fractures initiated during the East/West Gondwana pre-drift taphrogenic phase, defined an approximately N-S regional tectonic grain in generating large graben, horsts and oceanward-stepping faulted blocks in southern Mozambique and Zululand (Sowerbutts, 1972; Flores, 1973; Dingle and Scrutton, 1974). In the East African coastal region, a protracted phase of predominantly vertical crustal movement throughout the Permian, Triassic and Jurassic generated a series of major tectonic dislocations of up to 10 km throw (Kent, 1974a). Resultant graben systems often assumed great complexity as illustrated by the cross-cutting graben of southern Mozambique (Flores, 1973). Large scale block faulting and tilting has also been instrumental in defining gross morphological features of the Mozambique Ridge (Simpson, Schlich et al, 1974).

The 'Lebombo Line' (Fig.4.5) is a major crustal fracture cross-cutting the eastern end of the Kaapvaal Craton. Controversy on genesis of this crustal lineament still exists. The Lebombo Line has been considered as a zone of mid-Mesozoic monoclinal flexure draped by Karoo lavas (King, 1972; Cleverly, 1979). Alternatively, this lineament may be interpreted as the edge of a major Jurassic graben (de Swardt and Bennet, 1974; Bristow, 1980; Dingle, 1980a). Three factors suggest that the latter hypothesis is more plausible: (1) parallelism to other east coast regional graben; (2) extensive development of lavas farther east (Flores, 1973); and (3) recognition of complex, arcuate fault zones colinear with the southern Lebombo Line (Maud, 1961). Consequently, the least controversial explanation is that the Lebombo Line demarcates a western limit to the zone

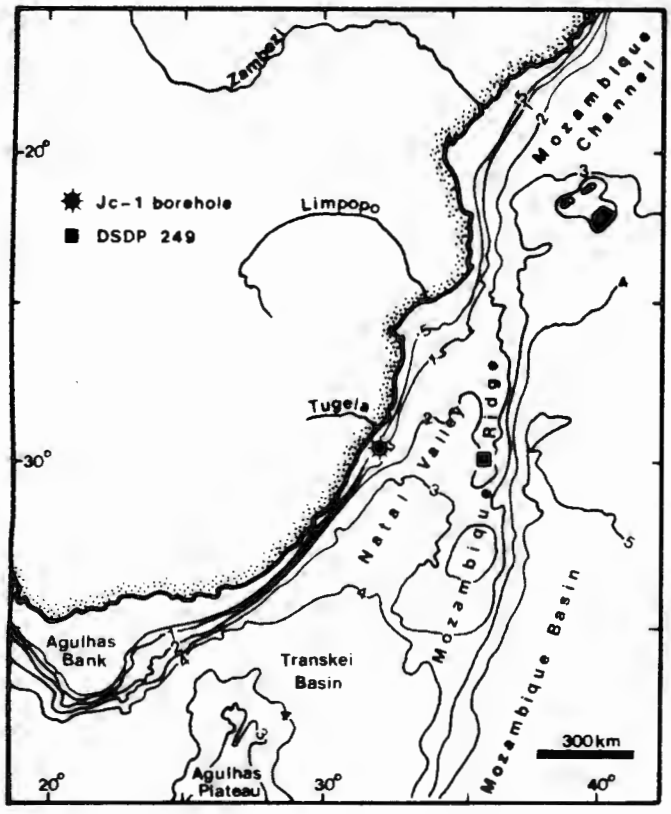

Fig. 4.4 MAJOR BATHYMETRIC FEATURES OF THE S.W. INDIAN OCEAN

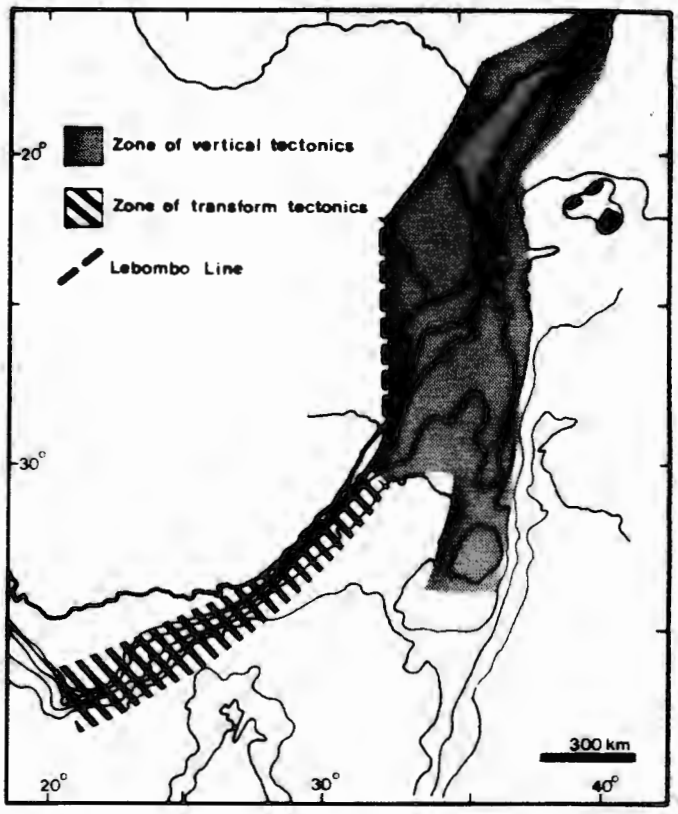

Fig. 4.5 DISTRIBUTION OF VERTICAL AND TRANSFORM TECTONIC ZONES

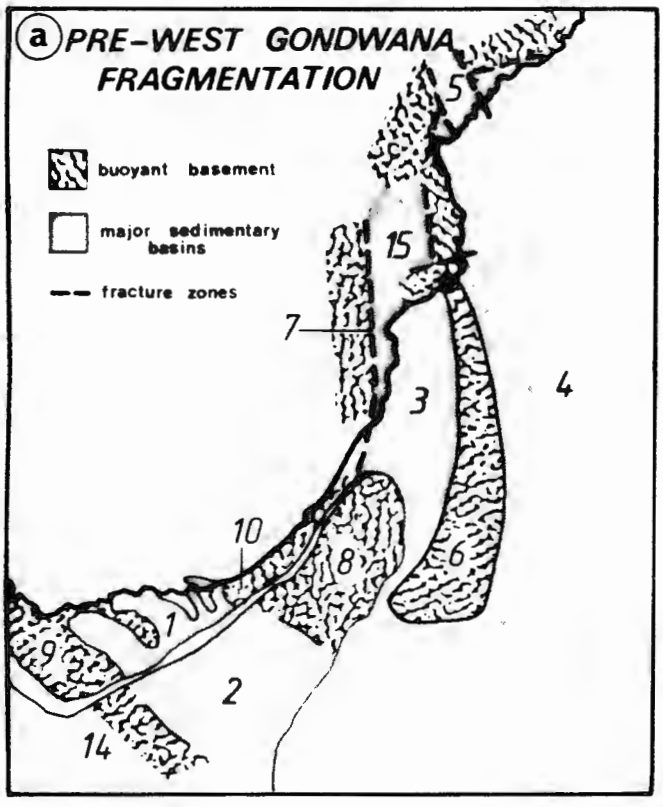

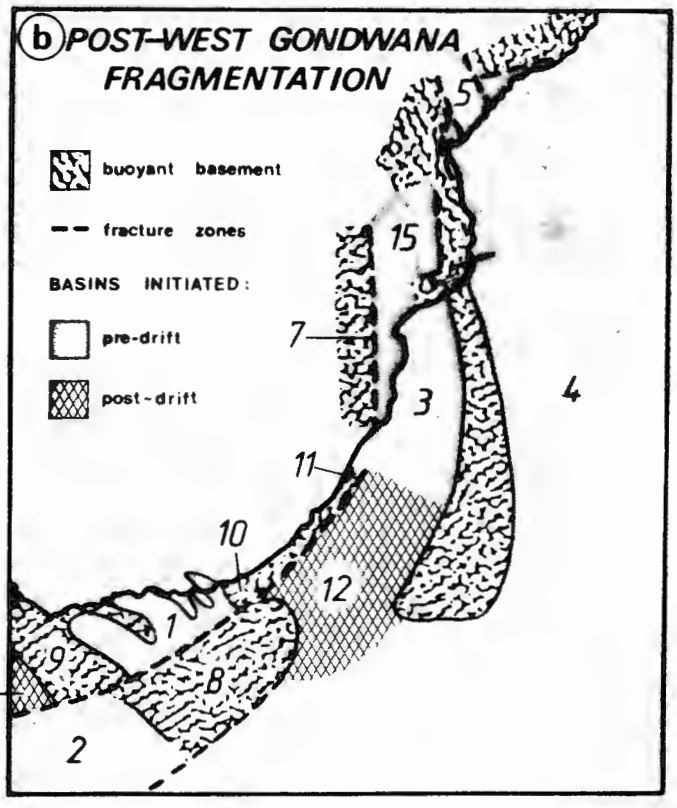

1 Outeniqua Basin
2 Falkland Plateau Basin
3 northern Natal Valley Basin
4 western Mozambique Basin
5 Zambezi Graben
6 Mozambique Ridge
7 Lebombo Line
8 Maurice Ewing Bank
9 Agulhas Arch
10 Port Alfred Arch
11 Agulhas / Falkland Fracture Zone
12 southern Natal Valley
13 Cape Basin
14 South American continental crust
15 Sul do Save graben area

Fig. 4.6 CONFIGURATION OF SEDIMENTARY BASINS – PRE- AND POST- WEST GONDWANA FRAGMENTATION

of vertical tectonics (Fig.4.5), along which lavas were extruded penecontemporaneously to progressive eastward downthrow.

Separated by an intervening northerly extension of the Mozambique Ridge, the onland Jurassic Mozambique sedimentary basins comprise the Zambezi Graben and Sul do Save composite graben (Fig.4.6a; Flores, 1973; Dingle et al, 1983). The western basin, depocentre for detritus from the Limpopo drainage basin and Natal/Zululand rivers, extends from SW Mozambique into the Natal Valley, probably as far south as $\sim 31^{\circ}$S, northernmost extreme of the Falkland Plateau Gondwana palaeoposition. This northern Natal Valley graben is suspected, however, to be composite in nature comprising several subsidiary horst and graben structures. Dredged volcanic rocks from the Almirante Leite Ridge in the northern Natal Valley are typically nephelinitic (A.K.Martin, pers. comm., 1980) corroborating dominance of rift tectonism in this area (Bailey, 1977). During its early history a downwarped composite northern Natal Valley graben was bounded on four sides by more buoyant continental basement (Fig.4.6a): Mozambique Ridge (east); Falkland Plateau (south); Lebombo Line and its offshore continuation (west); and southern Mozambique basement highs (north) (Fig.95 of Dingle et al, 1983). This graben probably served as a proto-depocentre for hinterland erosional yield.

4.4.3 South and East Margins - Zone of Transform Tectonics

Fragmentation of West Gondwana (125-130 Myr) resulted in divergence of the Falkland Plateau from its Natal Valley palaeoposition between the African continent and the Mozambique Ridge (Fig.4.6a and b), perhaps exploiting a southerly extension of the Lebombo Line as a zone of crustal weakness (Dingle and

Scrutton, 1974). Early relative rotation between South America (Falkland Plateau) and Africa was severely constrained by orientation and length of the intervening intracontinental shear zone, the Agulhas/Falkland Fracture Zone (AFFZ). This shear is coincident with a small circle (68°S) about the early pole of rotation (Francheteau and Le Pichon, 1972; Scrutton and du Plessis, 1973), confirming its origin by transform faulting. In formation, the AFFZ truncated pre-existing structural trends including the E-W or SE-NW tectonic grain of the Permo-Triassic Cape Fold Belt and the graben complex of the offshore Outeniqua Basin (Fig.4.6b). Along the Outeniqua Basin truncated margin, a large fracture ridge was emplaced during transform motion and delineates location of the AFFZ (Scrutton and du Plessis, 1973). The SE African continental margin can thus be classified as a zone of transform tectonism (Fig.4.5), with a resultant anomalous physiography compared to world norms (Table 3.1).

The pre-drift taphrogenic phase of basin development, followed by fragmentation of West Gondwana, controlled resultant basement configuration within the Natal Valley. Physiography of this proto-basin was probably largely defined by disposition of marginal basement high zones: the Mozambique Ridge (east); foundered continental basement (north and northeast); and the African continental margin (west). This general framework was later modified by epeirogenic subsidence (Dingle, 1980a) and large scale sediment input.

4.5 CONTINENTAL RIFTING MODELS

4.5.1 Introduction and General Model

In the last decade, several dynamic models for passive

continental margin evolution have been proposed (Falvey, 1974; Kinsman, 1975; Steckler and Watts, 1978; Watts and Thorne, 1984; and others). The causes of uplift and subsidence associated with continental rifting remains controversial although there is general agreement over the gross sequence of margin evolution events. Up to 50 my before continental separation (Falvey, 1974), anomalous mantle thermal activity may initiate crustal arching and erosional thinning along the uplifted incipient rift. This may result in the onset of an extended period of graben subsidence. Hypotheses explaining rift-phase subsidence may be assigned to one of three groups: (1) lithosphere thermal cooling following uplift and erosion (Sleep, 1971) or subcrustal thinning (McKenzie, 1978); (2) crustal stretching through regional extension (Sclater and Christie, 1980) or differential loading (Watts and Thorne, 1984); (3) deep crustal metamorphism (Falvey, 1974). These mechanisms have been reviewed by Steckler and Watts (1978) and Bott (1979). Syn-rift uplift may be a response to asthenospheric upwelling (Rowley and Sahagian, 1986). Rift-phase graben widening and collapse may continue until sea floor spreading commences. After the onset of drift, the newly-created continental margins are subjected to an extended period of epeirogenic subsidence primarily driven by thermal contraction and sediment loading (Watts and Thorne, 1984).

Gondwanaland reconstructions and the timing of the break-up rift and drift phases have been summarised in sections 4.2 and 4.3. To accommodate separation of Antarctica and Africa, strike-slip transform motion along the eastern margin of the Mozambique

Ridge has been inferred (Norton and Sclater, 1979). Transform motion along the AFFZ permitted separation of the Falkland Plateau and Africa. Between these major transform fracture zones, small rift margin segments developed. Regardless of which reconstruction and break-up model is followed, a complex system of rifted and transform margins must border the Natal Valley and Falkland Plateau continental blocks (Fig.4.7).

4.5.2 Application to the Natal Valley/Falkland Plateau

An uplift zone 150-200 km wide, either side of the incipient ridge axis, is predicted by the Falvey (1974) model of rift-associated linear arching, erosion and subsidence. Applying this concept to pre-drift SW Gondwana (Fig.4.8), a major part of the Natal Valley/Falkland Plateau province may have been affected by at least one cycle of rift-associated arching, erosion and subsidence. Assuming initiation of uplift 50 my before onset of sea floor spreading, arching in SE Mozambique, the eastern Mozambique Ridge and the south Falkland Plateau, associated with the East/West Gondwana break-up, may have commenced around 200 Myr (Late Triassic-Early Jurassic). Related to break-up of West Gondwana, a second phase of uplift affecting the Natal Valley and eastern Falkland Plateau may have been instituted around 180 Myr (Early Jurassic). Thus, in the Natal Valley/Falkland Plateau region, two phases of axial arching may have occurred with a possible cumulative effect leading to enhanced uplift, protracted erosion and eventual excessive subsidence. Hot spot mantle plumes may be active at transform-spreading ridge junctions (Kinsman, 1975) and this opens the possibility of additional domal uplift and related erosion and subsidence at two such sites

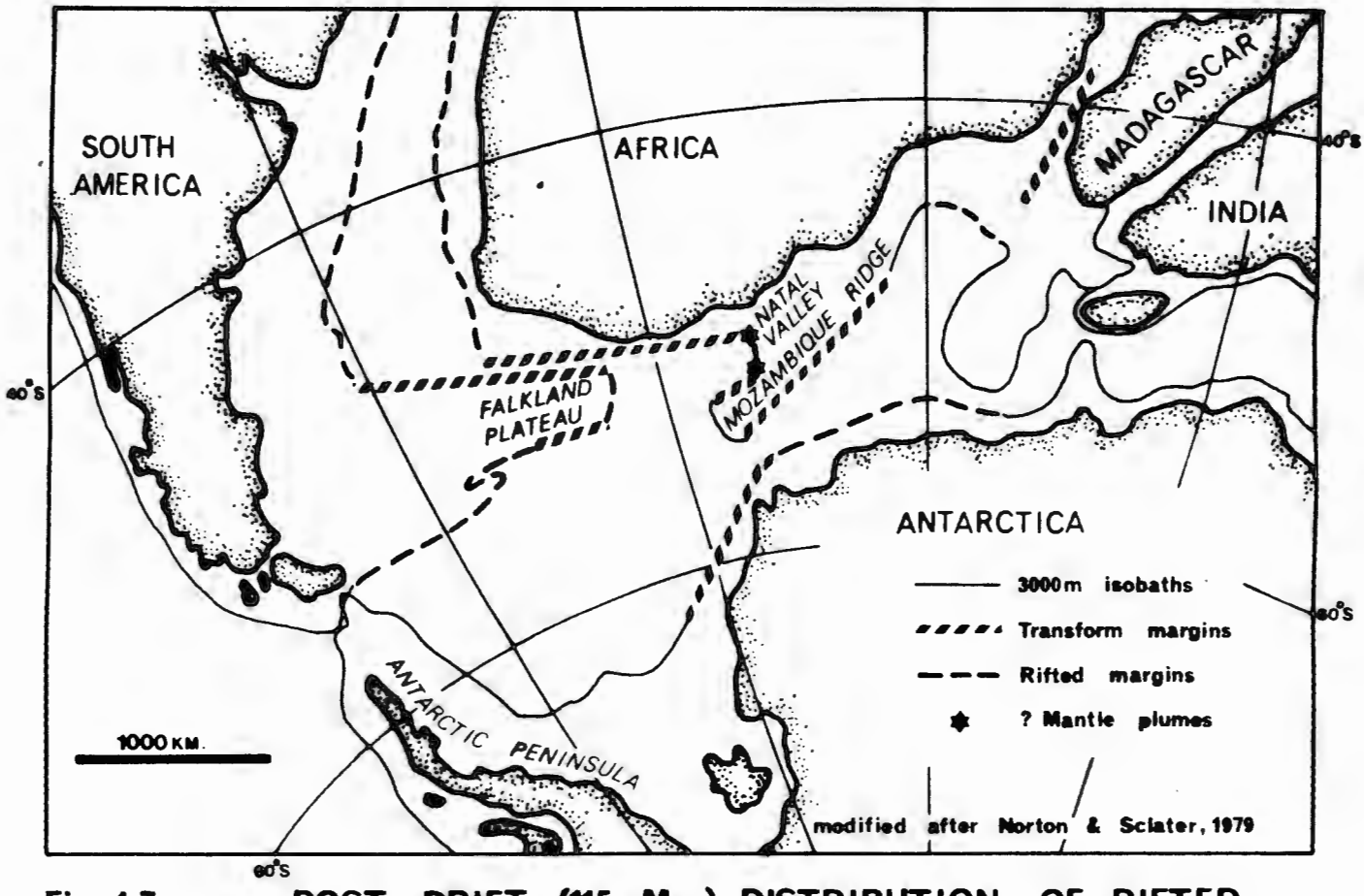

Fig. 4.7 POST-DRIFT (115 Myr) DISTRIBUTION OF RIFTED AND TRANSFORM CONTINENTAL MARGINS

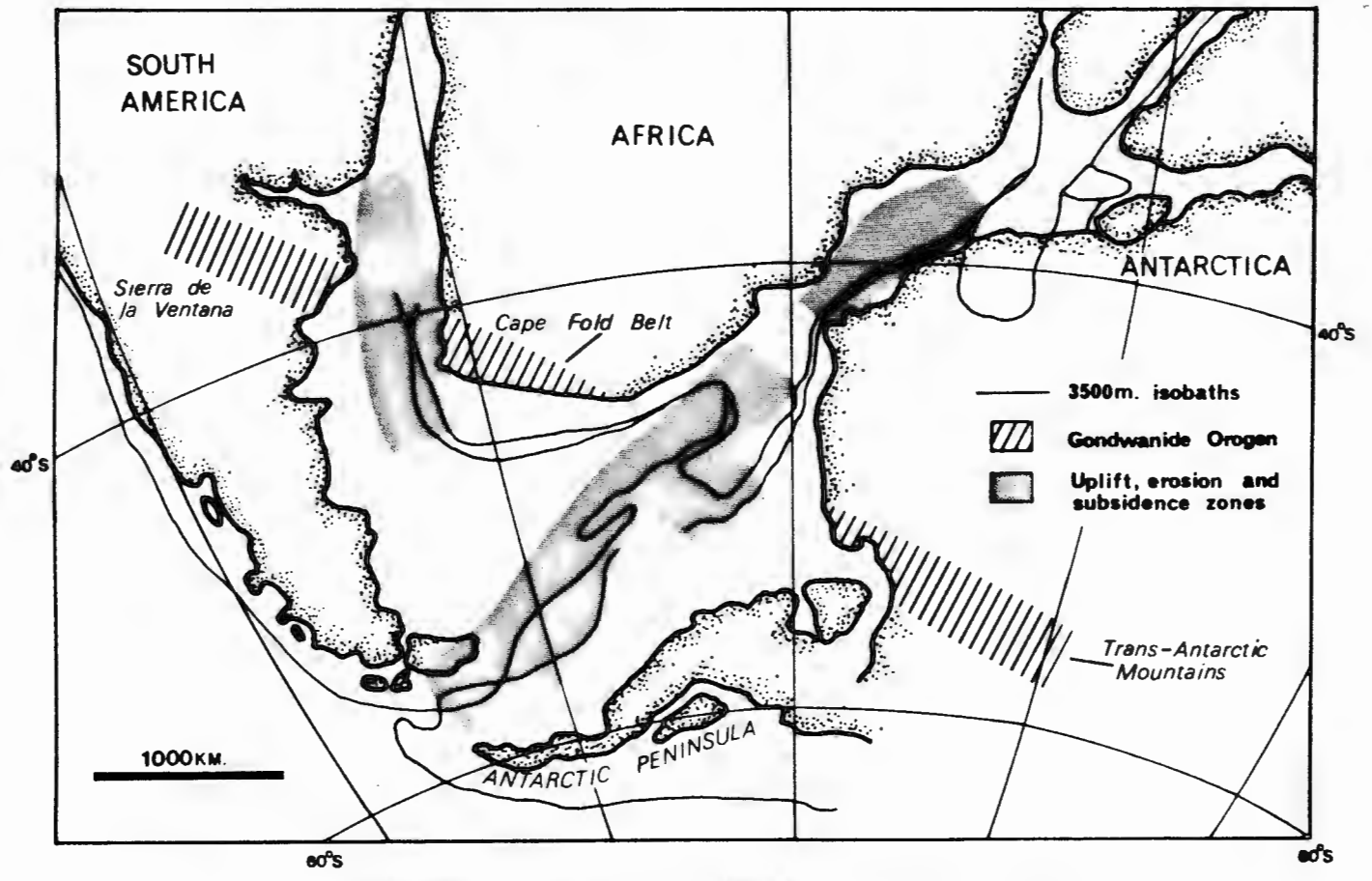

Fig. 4.8 DISTRIBUTION OF ZONES SUBJECTED TO PRE-DRIFT UPLIFT, EROSION AND SUBSIDENCE

within the reconstructed mid Natal Valley (Fig.4.7).

Kinsman (1975) has suggested that there is only minor heating and no uplift along transform continental margins. Since much of the inter-plate motion in the Natal Valley/Falkland Plateau province was transcurrent (Fig.4.7), the expected extent of the uplift, erosion and subsidence mechanism might be diminished. However, an opposing viewpoint has been expressed by Nicolas et al (1977) in that, along intracontinental shear zones, viscous heating during transform shearing may induce metamorphism to amphibolite grade along with local anatexis. With heating and anatexis resulting in uplift and the presence of dense amphibolite grade rocks causing later subsidence, an uplift, erosion and subsidence model may remain valid. Scrutton (1979) has inferred that, as sea floor spreading proceeds, the accreting mid-ocean ridge may instigate a short-life wave of heating and uplift while migrating along the transform margin. Thus, although transform margins border several zones of the Natal Valley/Falkland Plateau province, there may still have been extensive uplift, erosion and subsidence but to a lesser degree than that associated with rifted margins.

The Permo-Triassic Gondwanide orogenic belt is contiguous from South America through southern Africa to Antarctica (Fig.4.8), and must thus traverse part of the Falkland Plateau Dingle et al, 1983). Recent palaeomagnetic studies suggest a new palaeoposition for the Falkland Islands (Mitchell et al, 1986) and imply that they were in part influenced by the Gondwanide orogeny before undergoing complex pre-drift (190-125 Myr) microplate readjustments. Major orogenesis within the Cape Fold Belt has been dated at $\pm$227-217 Myr (Dingle et al, 1983). Cape Fold Belt orogenesis, therefore, either predated or was

contemporaneous to uplift and erosion associated with the break-up of East/West Gondwana and thus, may have enhanced the uplift and erosion processes along southern margins of Africa.

Several lines of geological evidence support the concept of extensive uplift/erosion preceding onset of sea floor spreading with ultimate rifted continental margin subsidence in the Natal Valley/Falkland Plateau regions:

(1) Gneissose and granitic basement rocks drilled at DSDP 330 are capped by a thin calcrete and palaeosol horizon indicating sub-aerial exposure prior to the Middle (?) to Late Jurassic marine transgression (Barker, Dalziel et al, 1976). Early phases of crustal subsidence followed by sediment loading are indicated within the basinal provinces of the Agulhas Bank (Outeniqua Basin) and Falkland Plateau (Falkland Plateau Basin). Barker (1976) concluded that the Falkland Plateau Basin had subsided 1-2 km prior to the Mid - Late Jurassic transgression while sedimentation in the juxtaposed Outeniqua Basin (Fig.4.6a) began either in the Mid Jurassic (Dingle, 1978) or the Late Jurassic (McLachlan and McMillan, 1979). Subsequent thermal contraction and possibly extension-driven subsidence and sediment loading in the Outeniqua Basin has locally depressed continental basement to depths in excess of 10 km (Dingle et al, 1983).

(2) Seismic refraction profiles (Ewing et al, 1971; Hales and Nation, 1972; 1973) have identified a lower crust high-density zone under parts of the Outeniqua Basin and southern Mozambique Ridge. It can be speculated that deep crustal metamorphism in these regions may have enhanced subsidence as in the model of Falvey (1974).

(3) Early faults within the Cape Fold Belt developed with a

northerly downthrow (Newton, 1976) indicating elevated basement to the south. Provenance of the Upper Beaufort and Molteno Formations (Late Permian to Late Triassic) of the Karoo Supergroup likewise imply an uplifted southern sediment source (Truswell, 1970). Reversal of fault style to southerly downthrow in later stages of the Cape Orogeny (Newton, 1976) suggests initiation of subsidence in southern areas (Outeniqua and ? Falkland Plateau Basins).

(4) DSDP 249 on the Mozambique Ridge bottomed in vesicular basalt (Erlank and Reid, 1974). Large vesicle volume (5-10%) and size (up to 1 cm) suggests extrusion in relatively shallow water (Moore and Schilling, 1973). A subsidence phase before deposition of the first Valanginian marine sediments is implied.

In the absence of deep geophysical data, it is impossible to assess the individual effects of mechanisms promoting continental margin subsidence (section 4.5.1) in the Natal Valley region. Subsidence related to thermal contraction was probably widespread because of the protracted (80 my) heating phase while sediment loading effects may have been extensive under thick sediment piles (Tugela Cone, Outeniqua Basin graben). Crustal thinning and subsidence initiated by post-drift crustal extension or creep (Bott, 1976) can, however, be discounted as a major process influencing the Natal Valley (Martin et al, 1981). Pre-drift, rift phase crustal extension may, however, have been operative in SW Gondwana.

Juxtaposition of the Falkland Plateau, Agulhas Bank, Mozambique Ridge and northern Natal Valley in a Gondwana reconstruction composes an elongate zone approximately 1600-1800 km long and 400-600 km wide, which speculatively is cored by subsided continental crust (Fig.4.8). Available models suggest

that these areas were subjected to a protracted phase (~80 my) of repeated heating, uplift and erosion cycles, perhaps initiated by the Triassic major Cape Orogeny, but primarily related to pre-drift Jurassic axial uplift along incipient rifts of the East/West Gondwana break-up and West Gondwana break-up. This mechanism, reinforced by sediment loading and thermal contraction, may provide an explanation for the abnormally large region of subsided continental crust bordering SE Africa and including the Falkland Plateau.

4.6 MESOZOIC SEDIMENTARY HISTORY

4.6.1 Introduction

General stratigraphy and sedimentary histories of coastal east and SE Africa is well documented (Flores, 1973; Dingle and Scrutton, 1974; Kent, 1974b; Forster, 1975; McLachlan and McMillan, 1979; Dingle et al, 1983). Evaluation of the Natal Valley basin sedimentary history is more problematical in the absence of borehole data. Some control is provided by DSDP 249 on the Mozambique Ridge (Simpson, Schlich et al, 1974) and drillsite Jc-1 (du Toit and Leith, 1974) on the east coast continental shelf. Additional information is furnished by DSDP 327, 329, 330 and 511 (Barker, Dalziel et al, 1976; Ludwig, Krasheninnikov et al, 1980; 1983) located on the Falkland Plateau, juxtaposed to the northern Natal Valley in reconstructions of West Gondwana. This section utilises documented east and south coast stratigraphic history, palaeogeography, tectonic evolution and drillsite data to construct an early sedimentary history for the Natal Valley basin.

4.6.2 Pre-Drift Sedimentation History

Prior to final separation of East/West Gondwana, large scale vertical tectonism active in East Africa and Madagascar/Mozambique created a series of approximately N-S trending graben (Flores, 1973; Kent, 1974a), which accumulated thick deposits of fluviatile, lacustrine and aeolian sediments in a Karoo continental environment. In the Madagascar/Mozambique graben, marine sediment intercalations imply temporary penetrations of shallow epi-continental seas (Dingle, 1978). In contrast, marine incursions were not widespread in the southern basins with Triassic sedimentation in Natal being totally continental (Dingle, 1978). It is probable, therefore, that Early-Middle Triassic rift-phase sedimentation within the Natal Valley was almost exclusively continental in character. By the Late Triassic, however, shallow epi-continental seas had ingressed this basin leading to deposition of a dominantly shallow marine lithofacies (Fig.12A of Dingle, 1978). An early stratigraphy of this type is in accord with the Beck and Lehner (1974) general model for sedimentation on a passive continental margin. This model predicts that initial rift-phase block faulting and subsidence on the continental margin is contemporaneous to deposition of a thick sequence of continental clastics, lacustrine shales and interbedded volcanics unconformably overlain by marine clastics and carbonates laid down under conditions of general regional subsidence.

In the Early-Middle Jurassic (~180 Myr), an important new phase of tectonism was initiated as the first rifts between East and West Gondwana began to form, promoting crustal subsidence in the region. Subsidence of the Natal Valley during this period is

substantiated by recognition of extensive faulting in coastal Natal to which Maud (1961) has assigned a Late Jurassic age. Similarly, extrusives of the major Karoo volcanic cycle dated at 190-137 Myr (Cleverly and Bristow, 1979) are draped over the Lebombo Line, indicative of active Late Triassic to Late Jurassic subsidence within the northern Natal Valley basin. Profuse Karoo volcanism and resultant accumulation of thick lava piles throughout this cycle probably terminated sediment deposition in many SE Africa graben. This is corroborated by multi-channel seismic reflection profiles (Beck and Lehner, 1974; Kent, 1974a) which have delineated basalts across the northern Natal Valley and Mozambique Channel in structural continuity with Karoo volcanics of Mozambique (Lebombo) and Madagascar.

Following the Karoo volcanic cycle, regional deposition within the lava-covered marginal basins marked Jurassic resumption of clastic sedimentation (Dingle, 1978). Related to the onset of East/West Gondwana fragmentation, marine sedimentation in these basins became increasingly common towards the Late Jurassic with successive marine incursions progressively expanding in aerial extent. Kent (1974b) and Forster (1975) have recognised a series of southward-overstepping and younging Jurassic marine transgressions in the East Africa region. Similarly, Thompson (1976) suspected a marine transgression from SE to NW across the Falkland Plateau during the (?) Middle to Late Jurassic. In summary, throughout the Middle to Late Jurassic, progressively more extensive marine transgressions, originating from both north and ?south, inundated south and SE Africa. It may be speculated that the Natal Valley basin, being located remote from both transgression sources, would not have

been affected by the earlier Jurassic incursions and thus continental sedimentation could have prevailed. With expansion of transgressions, however, by the Late Jurassic marine sedimentation had probably assumed dominance although interbedded with volcanogenic sediments from still-active Lebombo fissures. During this period, bordering provinces may have retained predominance of continental lacustrine and fluviatile sedimentation.

The inland lava-covered Karoo and Zambesi Basins, Natal, Mozambique and the Maurice Ewing bank (eastern Falkland Plateau) were subjected to uplift during the Jurassic (Dingle and Scrutton, 1974; Dingle, 1978) related to the rifting of East/West Gondwana. Jurassic marine sedimentary sequences are absent in Natal, Zululand and southern Mozambique corroborating existence of an elevated hinterland. Subsequent denudation of this high hinterland (Gondwana erosion cycle of King, 1967) would have supplied vast amounts of terrigenous detritus to an actively subsiding and deepening Natal Valley graben basin. With a high Jurassic erosional rate, increased discharge from the Tugela and Limpopo rivers or their equivalents probably initiated proto-cones on the western and northern margins of the Natal Valley basin respectively. Because the Cretaceous marine succession in north Zululand is transgressive, Kennedy and Klinger (1975) suspected that older sequences should be present farther east. Although the oldest marine strata in borehole Jc-1 are Cenomanian in age (du Toit and Leith, 1974), multi-channel seismic profiles record development of a 3,2 km thick wedge of pre-mid Cretaceous sediment (proto Tugela Cone) at the base of the continental slope (Table 6.2; section 6.4.7). Lowermost marine strata within this

wedge may locally be as old as Middle Jurassic to Oxfordian since marine sequences of this age have been recognised on the palaeogeographically-nearby Maurice Ewing Bank (Barker, Dalziel et al, 1976). Because of the relatively restricted area of deposition within the subsiding Natal Valley graben basin, early turbidite sequences may have accumulated to considerable thickness.

4.6.3 Rift-Drift Phase Euxinic Facies

Euxinic facies sedimentation has been considered a response to either bottom water stagnation (Andrews, 1977; Natland, 1978) or impingement of oxygen-minimum layers on the sediment/water interface (Schlanger and Jenkyns, 1976). Andrews (1977) reasoned that small embryonic ocean basins, with complex rift-generated configuration, would be characterised by restricted circulation and stagnant conditions favouring euxinic sedimentation. As marine sedimentation assumed progressive dominance in east and SE Africa through the Jurassic, the Natal Valley was probably confined in extent by surrounding elevated hinterland or bathymetric sills and therefore characterised by restricted circulation conditions. It can be speculated, therefore, that earliest Natal Valley marine environments were of an anoxic nature, resulting in deposition of euxinic shales intercalated with thick-bedded terrigenous turbidites (high hinterland erosional rate).

Depositional environments of Late Jurassic and Cretaceous regional sedimentation in the South Atlantic and SW Indian Ocean basins (Andrews, 1977) confirm the widespread development of euxinic facies during the rift and early post-drift phases of

Gondwanaland break-up. The regional extent and continuity of anoxic depositional environments has been verified by the intersection of euxinic, sapropelic claystone facies successions during deep drilling in five southern Africa marginal basins and structural highs:

(1) Cape Basin (DSDP 361) - interbedded euxinic shales and terrigenous turbidites of Cretaceous age (Bolli, Ryan et al, 1978);

(2) Maurice Ewing Bank (DSDP 327, 330 and 511) - post-transgressional Late Jurassic to Early Cretaceous dark carbonaceous claystone (Barker, Dalziel et al, 1976; Ludwig, Krasheninnikov et al, 1980);

(3) Mozambique Ridge (DSDP 249) - dark organic carbon -rich silty claystones of Valanginian to Cenomanian age (Simpson, Schlich et al, 1974);

(4) Algoa Basin (sub-basin of the Outeniqua Basin complex) - sapropelic shales of the Late Jurassic to Early Cretaceous Infanta and Sundays River Formations (McLachlan and McMillan, 1979); and

(5) Southeast Mozambique - dark, thin-bedded marly shales of the Albian Domo Formation (Flores, 1973).

In view of the surrounding widespread development of euxinic facies, it can be reasonably concluded that Natal Valley early marine sedimentation occurred in a restricted anoxic environment.

Jenkyns (1980) states that lateral continuity of black shales is related to factors such as emplacement of turbidites or ash falls which locally influence the depositional rate. The same mechanism must also control vertical continuity of euxinic sediments. It can be inferred that on bathymetric highs

(Falkland Plateau - DSDP 327, 330 and 511), euxinic black shales would accumulate largely uninterrupted, while in a restricted basin (Cape Basin - DSDP 361), an intercalated, thicker sequence of turbidites and black shales would be deposited. This simplistic model suggests that Natal Valley euxinic facies, if present, should comprise interbedded black shales and thick turbidites.

Although SE Atlantic and SW Indian Ocean anoxic sedimentation can be considered as a localised phenomenon related to break-up of Gondwanaland, a more world-wide 'Anoxic Event' has been recognised in the Early Toarcian (Hallam and Bradshaw, 1979), correlated to a contemporaneous global transgression. Effects of this global event may have been overprinted on local physiographic and oceanographic conditions already suited to development of an anoxic environment.

4.6.4 Post-Drift Sedimentation History

On fragmentation of West Gondwana, the Falkland Plateau diverged from its Natal Valley palaeoposition and thus progressively created the southern Natal Valley and Transkei Basin. Established sedimentary basins (Outeniqua and South Mozambique/Natal Valley) continued to receive sedimentation following break-up but with extension of the Natal Valley depocentre (Fig.4.6), a large proportion of the detrital input would have been deposited in the newly-created southern Natal Valley basin (Fig.4.6b). Expansion of these proto-oceanic basins would have been accompanied by epeirogenic subsidence of the bordering passive continental margins. This subsidence should be preserved as marine transgressional facies in hinterland coastal

stratigraphic columns. With expansion of the new oceanic basins, pre-drift stagnant environments would have been slowly replaced by open-marine oxygenated conditions. Final full establishment of thermohaline circulation should be demarcated by total disappearance of euxinic claystone facies and establishment of a biogenic-rich marine facies (Andrews, 1977).

Post-drift sedimentation around SE Africa is discussed regionally with reference to a composite Mesozoic lithostratigraphic column for the major basins and structural highs (Fig.4.9). Particular attention is paid to recognition of transgressive cycles and termination of euxinic sedimentation.

Zululand/Northern Natal

Unconformably resting on deeply-weathered Jurassic volcanics, the Cretaceous of this region comprises three transgressive sequences which progressively overlap southwestwards (Fig.9 of Dingle, 1978): Makatini, Mzinene and St. Lucia Formations (Fig.4.9, column 1).

The Makatini Fm. (Barremian-Aptian) comprises basal piedmont fan and fluviatile sands/conglomerates overlain by glauconitic sand/silt deposited in a nearshore to inner shelf environment (McLachlan and McMillan, 1979). The overlying Mzinene Fm. (Albian-Cenomanian) consists of shallow marine glauconitic sands/silts with shelly horizons evidencing a rich marine fauna. Absence of sapropelic units verifies deposition under oxygenated conditions. The major regressional hiatus ending deposition of the Mzinene Fm. may have been related to final separation of the Falkland Plateau and Africa (Dingle and Scrutton, 1974). The St.

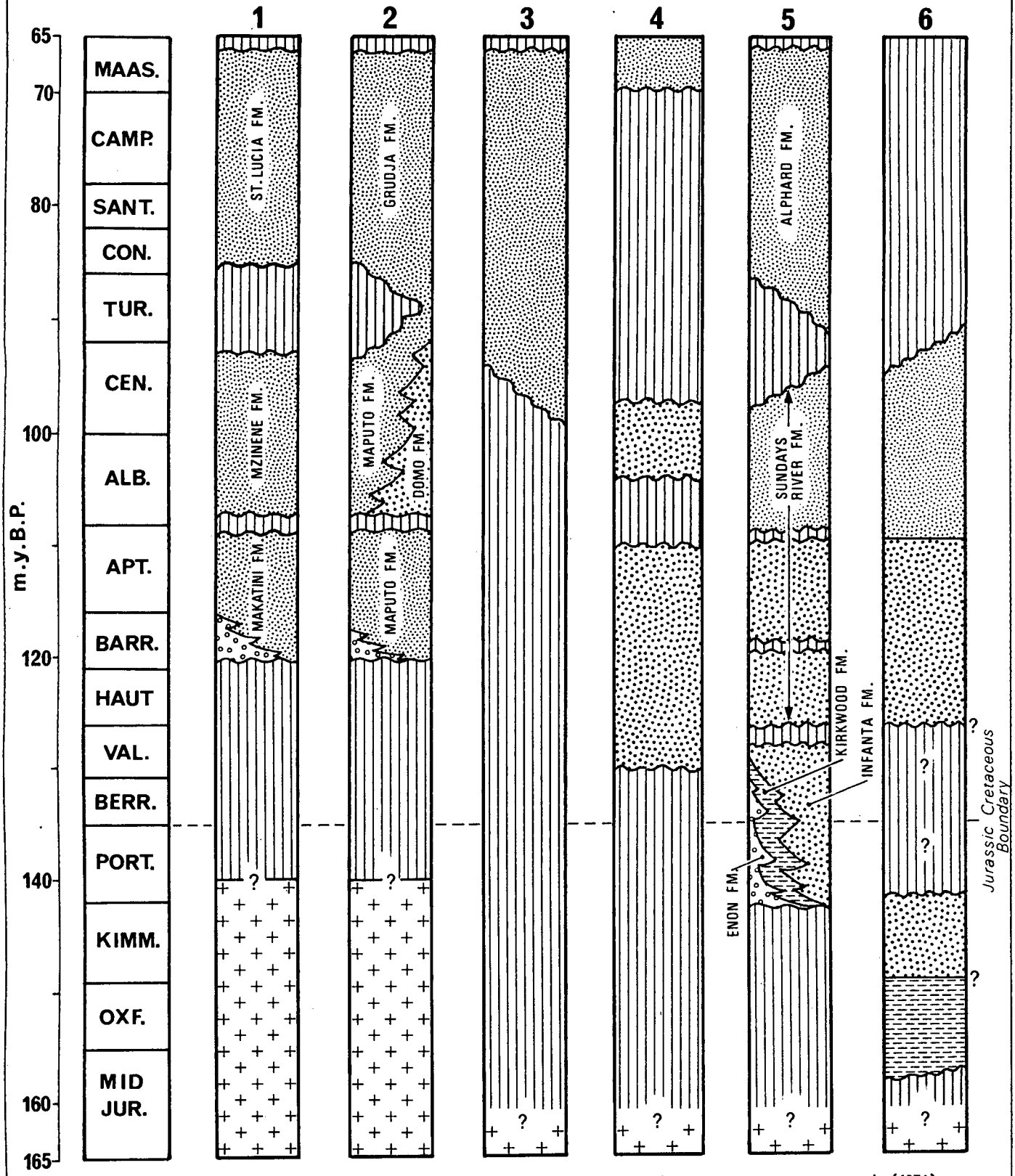

Composite data are from Flores (1973), du Toit and Leith (1974), Simpson, Schlich et al (1974), Forster (1975), Larson and Hilde (1975), Barker, Dalziel et al (1976), Dingle (1978) and McLachlan & McMillan (1979)

basement
continental sediments
paralic sediments
open marine sediments
euxinic marine sediments
hiatus

1 Zululand / Natal
2 South Mozambique
3 drillsite Jc-1
4 Mozambique Ridge (DSDP 249)
5 Outeniqua Basin
6 Falkland Plateau (DSDP 330)

Fig.4.9 MESOZOIC STRATIGRAPHIC FRAMEWORK OF SOUTHEAST AFRICAN SEDIMENTARY BASINS

Lucia Fm. (Coniacian-Maastrichtian) is most extensive in areal development (Dingle, 1978) and constitutes shelly glauconitic silts with occasional limestones and plant fragments characteristic of a shallow, low-energy nearshore environment. A Late Maastrichtian regression, possibly related to commencement of the African cycle of uplift/erosion (King, 1967), terminated this depositional cycle.

Southern Mozambique

In the south Mozambique coastal plain, a similar marine Cretaceous succession to Zululand/Natal has been described by Flores (1973) and Forster (1975). This transgressive sequence progressively onlaps northwards onto the Limpopo-Save uplift which was only finally inundated in post-Maastrichtian times (Forster, 1975).

The early Cretaceous transgression, initiating the Maputo Fm. (Barremian-Cenomanian), deposited glauconitic silty sandstones with occasional sandy limestones on a bedrock of deeply-weathered Karoo lavas. In the western ?shallower segment of the basin there was little variation in sedimentation before the Cenomanian regression (Forster, 1975). Towards eastern deeper sectors of the basin, however, glauconitic siltsones of the Maputo Fm. grade laterally and vertically into the Albian Domo Fm., a sequence of dark marly shales deposited in a restricted anoxic environment (Flores, 1973). Development of Albian-Cenomanian euxinic facies suggests that open marine circulation was late to penetrate into south Mozambique. Existence of a bathymetric sill (?Almirante Leite Ridge - Dingle

et al, 1978), restrictive to circulation, may explain the late development of oxygenated conditions. Following the mid Cretaceous hiatus, marine conditions were re-established in the southern Mozambique with deposition of the Grudja Fm., a sequence of silty sandstones. In the eastern deep-water basin zones, however, the mid Cretaceous hiatus is not developed and Flores (1973) noted a continuous sequence from the euxinic marine Domo Fm. to the open marine Grudja Fm. (Fig.4.9, column 2).

Natal Continental Shelf

Basal sediments recovered from SOEKOR borehole Jc-1 (du Toit and Leith, 1974) on the continental shelf have been dated as Cenomanian (Fig.4.9, column 3), while at Umzamba in the north Transkei, the equivalent transgression commenced in Middle Santonian times. This situation further illustrates the progressive southwest onlap of the Zululand Cretaceous transgression. After the onset of continental drift, slow epeirogenic subsidence would have permitted progressive inundation. A transgression timespan of ~35 my (Barremian-Santonian) demonstrates the very slow progress of post-drift continental margin subsidence.

Borehole Jc-1 penetrated a complete Late Cretaceous succession consisting of claystones with subordinate coarse clastics and minor limestones, deposited a mid-outer shelf environment. Absence of sapropelic horizons verifies that open marine oxygenated conditions had prevailed before the Cenomanian in this region.

Mozambique Ridge

Marine sedimentation on the Mozambique Ridge (DSDP 249)

commenced in the Valanginian (Fig.4.9, column 4) with deposition of olive black silty claystone and volcanogenic siltstone (Simpson, Schlich et al, 1974). Early onset of marine sedimentation suggests that subsidence was initiated soon after the West Gondwana break-up. High percentages of organic carbon and reduced iron along with scarcity of marine fossils are indicative of an euxinic depositional environment. Occurrence of volcanogenic sediments signifies contemporaneous volcanic activity (?Lebombo fissures). An hiatus encompassing the Cenomanian to Campanian marks termination of the anoxic volcanogenic phase and upon resumption of sedimentation, open marine conditions prevailed with deposition of foram-bearing clay-rich nanno chalk (Simpson, Schlich et al, 1974).

Outeniqua Basin

Oldest sediments of the Outeniqua Basin are assigned to the Uitenhage Group and can be subdivided into three major formations: the continental Enon Fm., the paralic Kirkwood Fm, and the marine Infanta Fm. (Fig.4.9, column 5). Euxinic conditions were relatively limited within the Uitenhage Group, probably because of the shallow, high energy depositional environment. One major exception is the Colchester Member, a sequence of grey shales with abundant sapropels (McLachlan and McMillan, 1979), representing a short-lived transgression into the paralic Kirkwood Fm. (Winter, 1973). A Valanginian-Hauterivian hiatus, related to the onset of continental drift (du Toit, 1979), terminated deposition of the Uitenhage Group (Fig.4.9, column 5). Subsequent marine invasion, caused by post-drift epeirogenic subsidence, initiated deposition of the Sundays

River Fm. Throughout this formation, McLachlan and McMillan (1979) recognise numerous sapropelic horizons, especially in deeper parts of the basin, thus implying a protracted euxinic phase. Anoxic conditions may have been preserved by contiguity of the Falkland Plateau (Maurice Ewing Bank) and Agulhas Arch during the early post-drift phase (Fig.4.6b). Bottom anoxia may have been further emphasised by circulation constraint caused by formation of the Agulhas marginal fracture ridge (Dingle and Scrutton, 1974).

Final separation of the Falkland Plateau and Africa occurred at ~100 Myr instigating a Late Albian-Cenomanian regressional hiatus which terminated deposition of the Sundays River Fm. Subsequent inundation started deposition of the marine Alphard Fm., in which complete absence of sapropelic units demonstrates development of an open marine environment following the final Falkland Plateau/Africa split.

Falkland Plateau

Marine conditions were already established on the Maurice Ewing Bank (DSDP 330) prior to initiation of the West Gondwana drift phase. Early taphrogenic subsidence and Middle to Late Jurassic marine invasion may have been related to the earlier rifting of East/West Gondwana. Slow deposition of olive black carbonaceous claystones from the Oxfordian to Late Aptian (Barker, Dalziel et al, 1976) confirms a protracted phase of euxinic sedimentation over the eastern Falkland Plateau (Fig.4.9, column 6), perhaps related to development of the Agulhas marginal fracture ridge (Thompson, 1976).

In the Early-Middle Albian (~100 Myr), as the Falkland

Plateau finally detached from Africa (Dingle and Scrutton, 1974), euxinic conditions were terminated. An open marine environment developed over the Falkland Plateau as suggested by deposition of nannofossil clays, oozes and chalks. Simultaneously, rapid tectonic subsidence of the Falkland Plateau was initiated (Ciesielski and Wise, 1977) with the Cenomanian-Turonian unconformity being attributed to increased bottom current flow and a rise in the carbonate compensation level.

Widespread development of a post-drift transgressional marine facies of Early Cretaceous age around marginal basins of SE Africa is consistent with generalised models of passive continental margin rifting (e.g. Falvey, 1974) in which the post-drift margins are subject to regional epeirogenic subsidence.

Prior to the Aptian/Albian, anoxic conditions caused by restricted circulation were regionally dominant in the marginal basins of SE Africa, and thus early Cretaceous sedimentation in the Natal Valley was probably euxinic. Regional change to biogenic-rich sedimentation in the Albian/Cenomanian marked development of full open marine conditions with thermohaline circulation. This major environmental change was probably initiated by final separation of the Falkland Plateau and southern Africa. Local euxinic conditions may have persisted until the Cenomanian in silled sub-basins of the Natal Valley (e.g. Mozambique Ridge graben).

CHAPTER 5 BASEMENT CONFIGURATION AND CRUSTAL ELEMENTS

5.1 INTRODUCTION

Few crustal geophysical studies have been undertaken in the Natal Valley. Consequently, the exact distribution of continental, transitional and oceanic crust remains controversial. In this critical zone for West Gondwana reconstruction, the continent/ocean crust boundary (COB) has not been conclusively defined with previous publications (e.g. Darracott, 1974; Dingle and Scrutton, 1974; Scrutton, 1976; Rabinowitz and LaBrecque, 1979; Norton and Sclater, 1979; Powell et al, 1980; Veevers et al, 1980; Martin et al, 1981) either directly or indirectly placing the COB in a variety of locations.

In this chapter, recently acquired seismic reflection data, magnetic data and limited geochemical data are presented and utilised to improve definition of basement topography and character. Mesozoic magnetic anomalies M0-M12(G) are recognised within the southern Natal Valley. Important implications of this discovery are outlined. Previous investigations on crustal structure are reviewed and collated with new data enabling amendment of COB location and demarcation of major structural elements. Basement subsidence around the SE Africa margins is evaluated and the concept of Mozambique Ridge micro-plate displacement from Africa is assessed. Finally, the new refit of East Antarctica and Africa (Martin and Hartnady, 1983), with inferences as to the tectonic status of the northern Natal Valley, is critically discussed.

5.2 TIME-DEPTH TO ACOUSTIC BASEMENT

5.2.1 Introduction

Seismic profile data reduction procedures are summarised in Appendix A2 with depth to basement being measured in seconds two-way travel time. On seismic profiles (see Fig.6.1 for coverage), acoustic basement is recognised by its high reflectivity with densely-overlapping, steep-sided hyperbolae and absence of internal reflectors. A time-depth map of acoustic basement, using sea level as a datum, is presented as Figure 5.1.

The majority of seismic traverses were procured using a 40 in^3 airgun single-channel system. Inherent poor penetration precluded recognition of acoustic basement over large tracts of the study area (Tugela Cone, deep basin plain and continental margin). Structural high zones provide the only areas over which conclusive recognition of acoustic basement is possible. Multi-channel profiles (courtesy of SOEKOR) provided depth to basement information from the continental margin north of Durban.

With track coverage limitations in mind, general form and structure of the basement is discussed with reference to Figure 5.1. Selected seismic profiles are depicted in Figure 5.2. Locations of the five profiles are shown in Figure 5.3b.

5.2.2 Mozambique Ridge

Within the Natal Valley, the Mozambique Ridge is the most impressive basement high zone (Fig.5.1). The N-S trending basement core is characterised by undulating topography punctuated by several peaks, scarp slopes and valleys. Drilling into one of these valleys, DSDP 249 (Fig.5.14 for location)

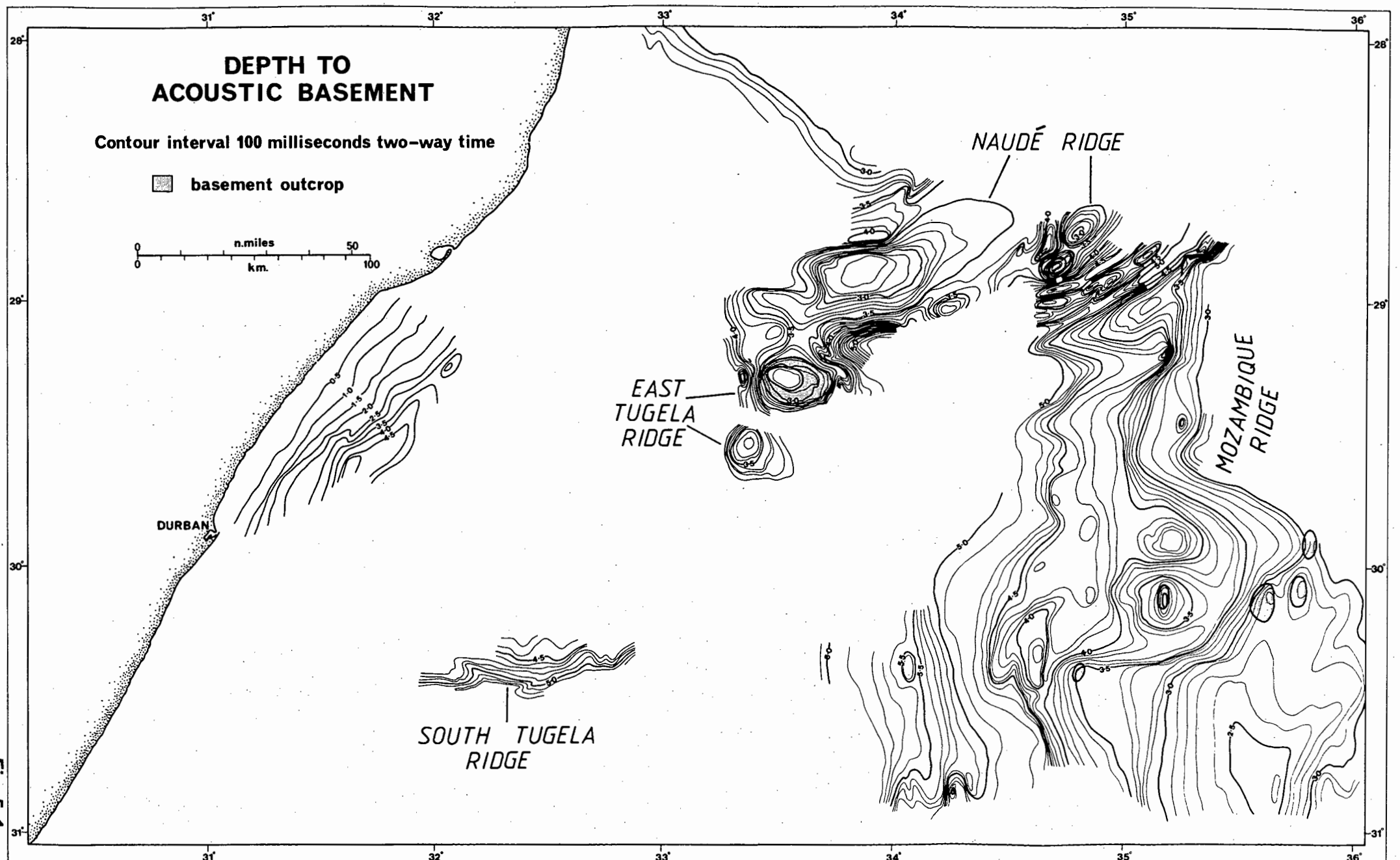
DEPTH TO
ACOUSTIC BASEMENT
Contour interval 100 milliseconds two-way time
basement outcrop
0 n.miles 50
0 km. 100
NAUDÉ RIDGE
EAST
TUGELA
RIDGE
MOZAMBIQUE
RIDGE
SOUTH TUGELA
RIDGE
DURBAN
31°
32°
33°
34°
35°
36°
28°
29°
30°
31°

Fig. 5.1

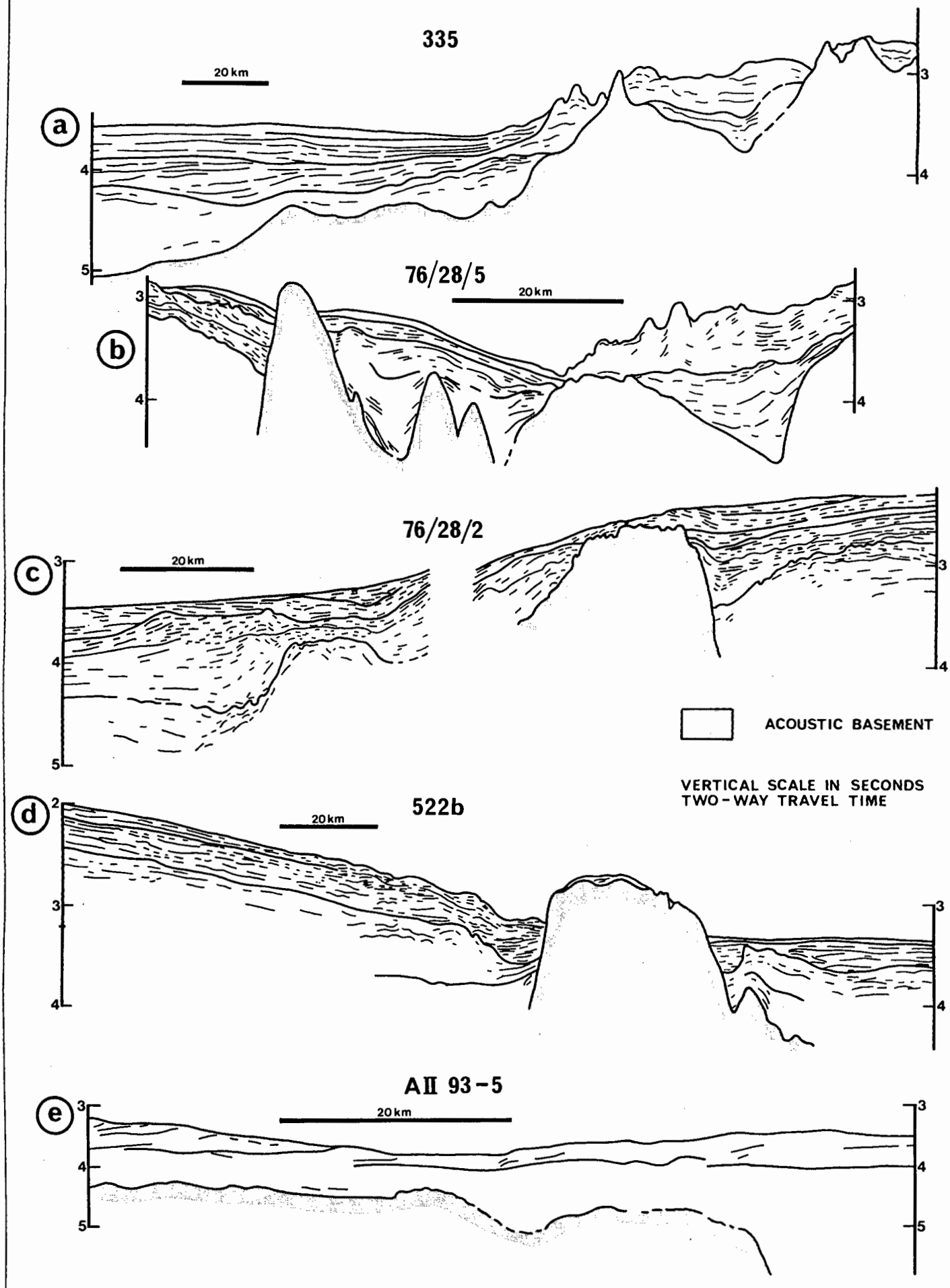

Fig.5.2 SEISMIC PROFILE LINE DRAWINGS ILLUSTRATING BASEMENT TOPOGRAPHY

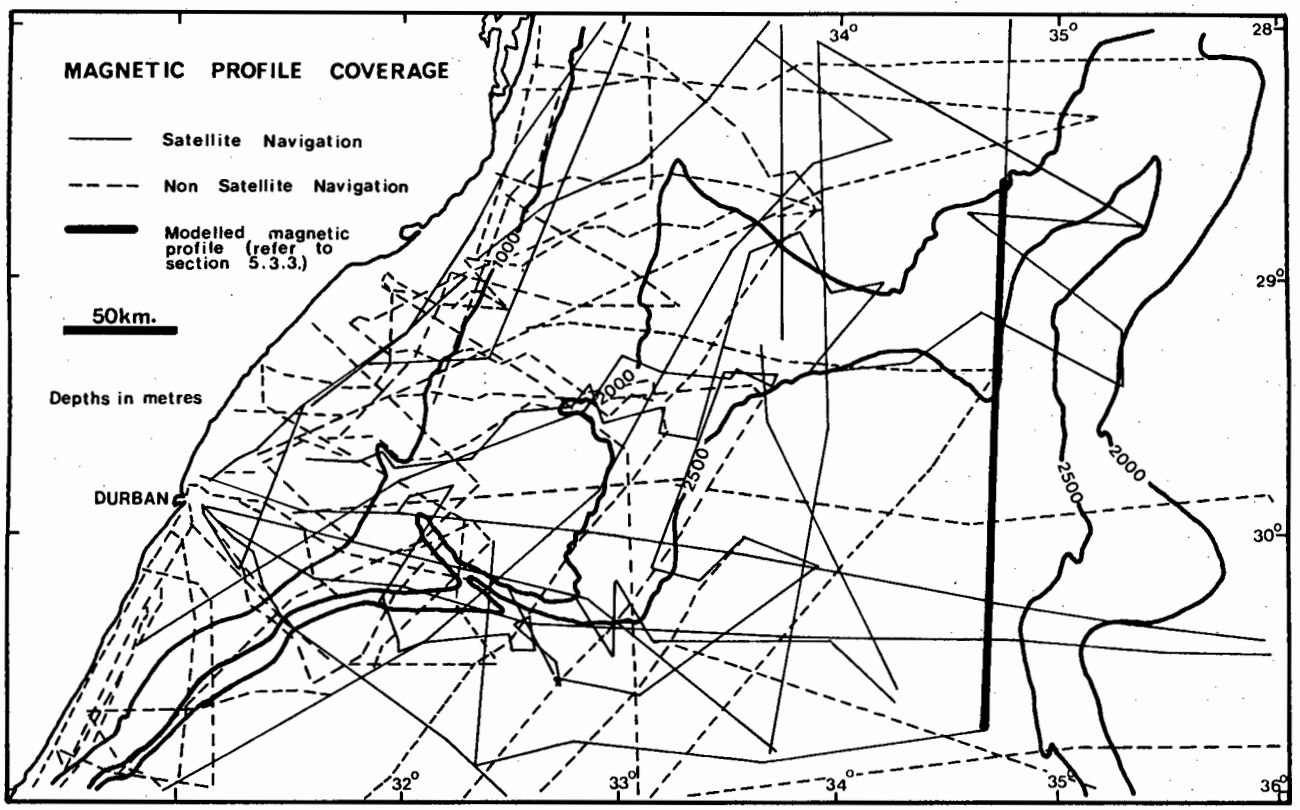

Fig. 5.3a MAGNETIC PROFILE COVERAGE

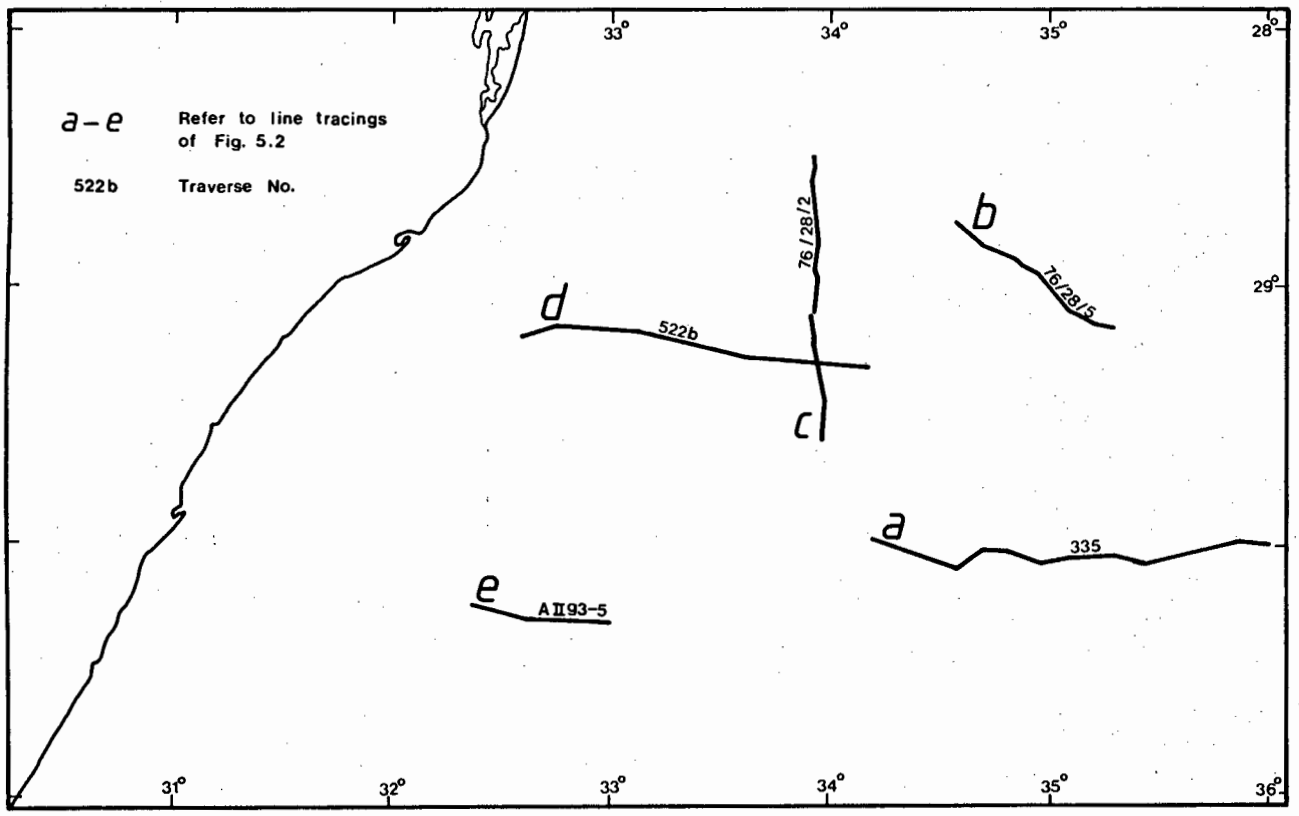

Fig. 5.3b LOCATION OF SEISMIC PROFILE LINE TRACINGS

intersected basalts at 2500m below sea level. Above 3 secs, the ridge crest plateau shows minor relief although three small peaks in the vicinity of 30° 00'S, 35° 45'E outcrop at the sea floor (Figs.5.1 and 5.2a). Shoalest basement time-depths (~2,4 secs) are recorded over the SE section of the ridge.

Westward towards the deep basin plain, basement deepens and becomes more irregular. The steep western flanks are probably fault-controlled and may be related to tectonic uplift of the Mozambique Ridge around 70 my ago (Thompson et al, 1982). Several deep valleys, which trend ENE-WSW (Fig.5.1), dissect the Mozambique Ridge western flank. Major valleys are noted at 28° 55'S, 29° 10'S, 29° 50'S and 30° 20'S (Figs.5.1 and 5.2b). These valleys may demarcate the sites of several transform faults (section 5.5.7). Deeper than 4,3 secs, basement topography smoothens as the Mozambique Ridge merges with the deep basin. Smooth acoustic basement in this zone may be indurated high velocity sediments which mask the underlying basaltic crust. Along one traverse (AII93-5), smooth, deep basin basement can be traced to at least 6,1 sec depth.

5.2.3 Naude Ridge

The structural style of the Naude Ridge basement province (Fig.5.1) contrasts with the Mozambique Ridge. This ridge and pinnacle complex extends 160 km from the east Tugela Cone to the Mozambique Ridge forming a core to the steep southern slope of the Central Terrace. The entire ridge system is sediment-draped except for one small pinnacle outcrop at 28° 52'S, 34° 41'E on the Central Terrace SE flank. Overall, the Naude Ridge trends approximately E-W but can be subdivided into four sub-parallel ridges trending ENE-WSW or NE-SW (Figs.5.1 and 5.14).

The western Naude Ridge segment, 100 by 30 km in dimension, is steep-sided with rugged flanks and crest shoaling centrally to 2,7 secs (Figs.5.1 and 5.2c). The eastern Naude Ridge is more complex comprising numerous steep-sided, smooth pinnacles and ridges separated by deep troughs (Figs.5.1, 5.2b and 5.14). Individual pinnacles are small in areal extent, averaging 10 by 20 km.

The Naude Ridge is separated from the Mozambique Ridge by a deep ENE-WSW trending basement trough centred on 28° 55'S, 35° 05'E. Magnetic modelling (section 5.3.3) implies that basement is elevated over large areas of the southern Central Terrace, north of the Naude Ridge. Basement must thus be closely associated with reflector McDuff (sections 6.2.2 and 6.2.3).

5.2.4 East Tugela Ridge

Southwest of the Naude Ridge, two basement seamounts together comprise the East Tugela Ridge, a structural high beneath the eastern Tugela Cone. The northerly peak, 20 by 30 km in size, protrudes 400m through Tugela Cone sediments and constitutes the largest single exposure of basement within the Natal Valley (Fig.5.1). Although the present bathymetric expression of the seamount is asymmetric due to sediment draping, its basement core is relatively symmetrical, characterised by steep walls and rugged summit smoothed by a thin sediment drape (Fig.5.2d). A deep but narrow trench separates the northern seamount from the smaller, conical and totally-buried southern basement mount. Structural continuity between the East Tugela Ridge and western Naude Ridge, with only a shallow intervening saddle (Fig.5.1), may imply a related genesis.

5.2.5 South Tugela Ridge

Geographically-sited beneath and just south of the steep Tugela Cone southern margin, the South Tugela Ridge is delineated by a relatively steep, south-facing basement scarp (Fig.5.1). The regular but locally rugged scarp slope (Fig.5.10) is broken by several promontaries. Western extent of the ridge is poorly defined on existing data. Eastern ridge limits are however clearly demarcated by a sharp basement discontinuity of 1 sec relief at 32° 55'E (Fig.5.2e), marking transition to deep basin crust. From available data, ridge dimensions are measured as 100 by 25 km.

5.2.6 Continental Margin

Availability of multi-channel seismic data (e.g. L-18 of du Toit and Leith, 1974) has enabled basement recognition over the continental margin north of Durban (Fig.5.1). The steep continental slope exhibits a coast-parallel trend broken by shallow indentations and shoals to 0,5 secs time-depth within 10 km of the present day coastline (Fig.5.1). Below 4,0 secs the scarp slope levels and displays gradient reversals which may be expressions of basement block-tilting during vertical tectonism. However, seismic control is insufficient to determine geometry of basement faults. Farther south on the continental margin, south of borehole Jc-1, Dingle (1979) reports that the basement scarp alignment diverges from the coast to trend in a more NNE-SSW attitude (Fig.5.14).

5.3 MAGNETIC ANOMALIES

5.3.1 Introduction

A total of 13 190 km of continuous magnetic profiles have been recovered from the mid Natal Valley providing good regional coverage (Fig.5.3a). Satellite navigation, operational during 51% (6720 km) of cruise time, enabled construction of a control grid to which poorly-navigated were adjusted. Reduction of magnetic data is fully outlined in Appendix A3. Profiles of total magnetic intensity were plotted as perpendicular projections onto a straight line joining the two end points of each traverse. Removal of the geomagnetic reference field enabled discrimination of positive and negative anomalies relative to a zero datum.

An isomagnetic contour chart (Fig.5.4), supported by a representative selection of traverses (Fig.5.5) is used to describe the regional field and improve basement geometry definition. Basement magnetisation and structure over the Naude Ridge, deep basin and Mozambique Ridge is briefly examined by application of 2D magnetic modelling. The Mesozoic sea floor spreading magnetic anomaly sequence (M0-M12) is for the first time recognised (Appendix C) with important implications for Gondwana reconstruction and timing of fragmentation.

5.3.2 Magnetic Anomaly Character and Distribution

The east coast continental margin generates a broad, coast-subparallel, negative anomaly sited just seaward of the shelf break (Fig.5.4). This discontinuous anomaly attains a magnitude of 300-400γ south of 29^{o}S but is weakly developed to the north

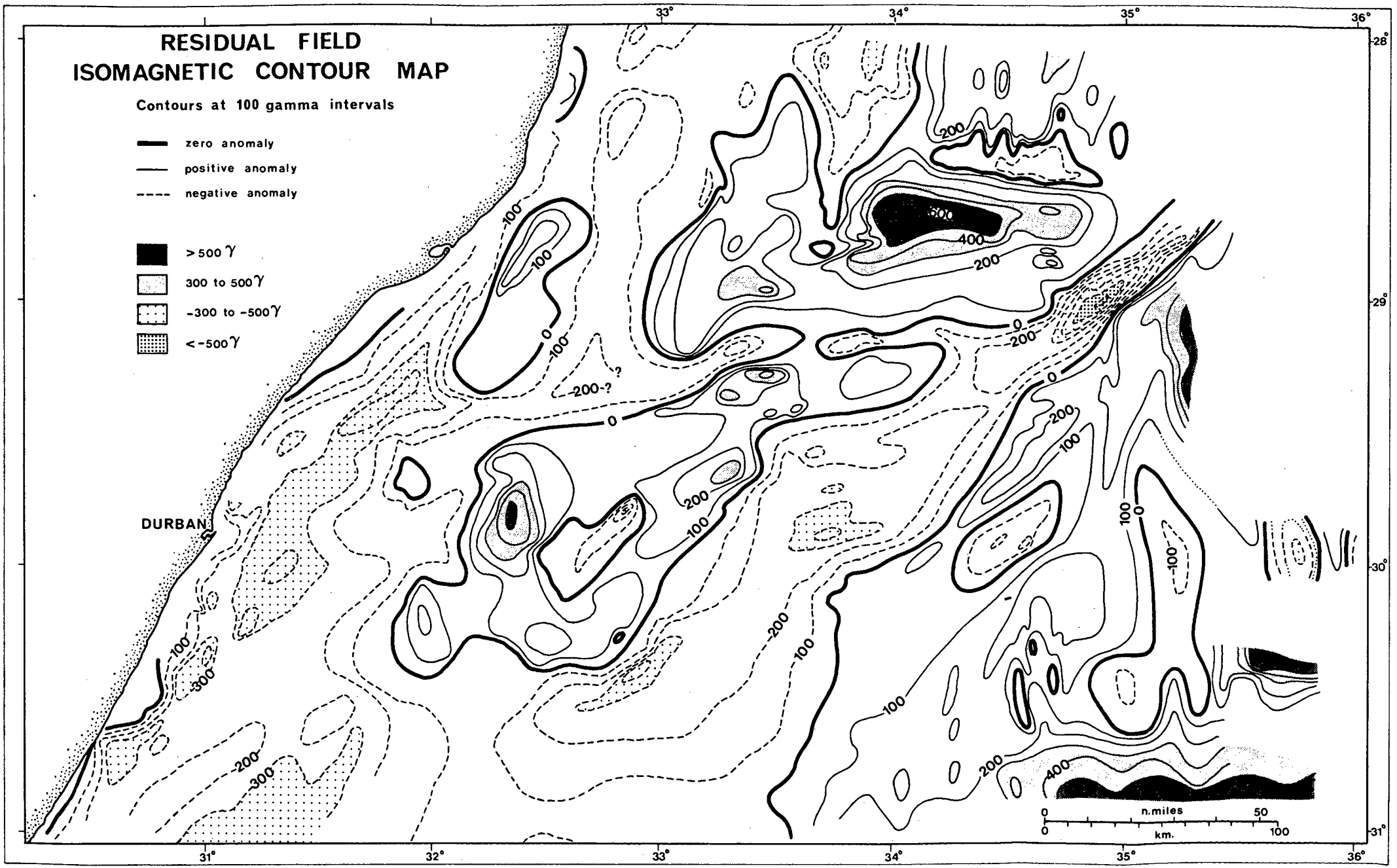
RESIDUAL FIELD
ISOMAGNETIC CONTOUR MAP
Contours at 100 gamma intervals
zero anomaly
positive anomaly
negative anomaly
>500 γ
300 to 500 γ
-300 to -500 γ
<-500 γ
DURBAN
33°
34°
35°
36°
28°
29°
30°
31°
31°
32°
33°
34°
35°
36°
n.miles
km.
0
50
100

Fig. 5.4

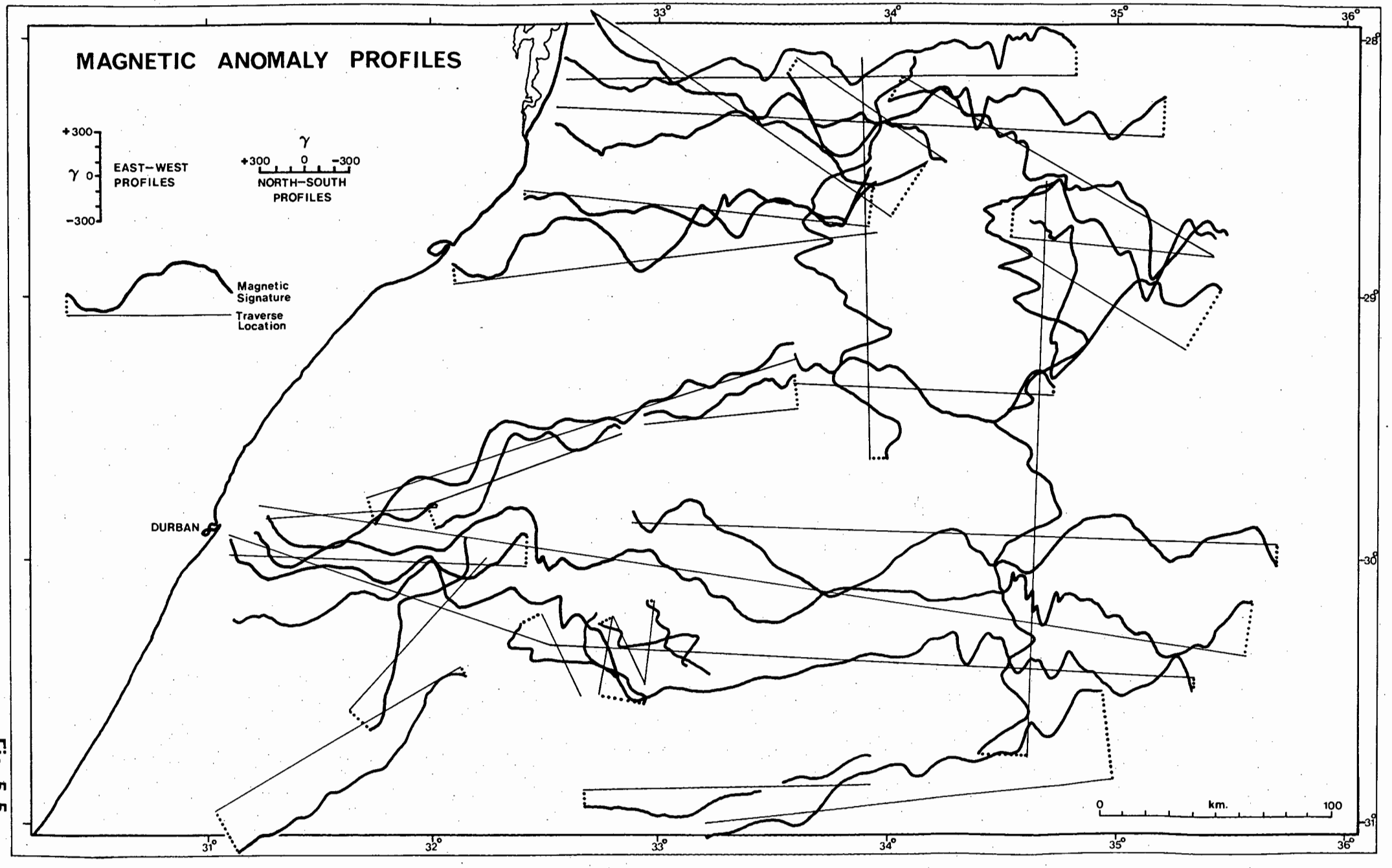
MAGNETIC ANOMALY PROFILES
+300
γ 0
−300
EAST–WEST PROFILES
γ
+300 0 −300
NORTH–SOUTH PROFILES
Magnetic Signature
Traverse Location
DURBAN
33°
34°
35°
36°
28°
29°
30°
31°
0 km. 100

Fig. 5.5

(Figs.5.4 and 5.5). With the data at hand (Fig.5.3a), it is not possible to delineate the northern extremity of the Cape Slope Anomaly of du Plessis and Simpson (1974). A series of discontinuous low amplitude (-100γ to 100γ) anomalies characterise the continental shelf.

Bounded by the NE-SW trending zero anomaly contour, the Mozambique Ridge stands out as a distinct positive magnetic province (Fig.5.4) with subsidiary negative zones. Individual anomalies range up to +600γ in amplitude with variable wavelength and these are superimposed by low amplitude, short wave-length anomalies. A N-S magnetic grain is prevalent over the Mozambique Ridge. Along its western flank, however, the anomalies decrease in amplitude and diverge to assume NE-SW alignment (Figs.5.4 and 5.5).

A second distinctive positive province is generated by the Naude Ridge basement high zone (Figs.5.1 and 5.4). Magnetically, this province is clearly delineated by bordering negative anomalies. The most prominent zone of this province comprises an E-W trending elongate high attaining an amplitude of +600γ. To the west the anomaly is less prominent varying from +200 to +400γ (Fig.5.4). Individual basement peaks within the ridge complex produce positive anomalies up to +200γ in amplitude superimposed on the general positive high. The Naude Ridge positive province lies slightly north of the mapped basement high while its larger dimensions may indicate the presence of magnetised Lebombo basalts over the southern Central Terrace. North of the Naude Ridge positive, irregular N-S trending anomalies characterise the Central Terrace.

A final positive province encompasses the southern and

eastern zones of the Tugela Cone. In these areas poorly-defined positive anomalies of maximum amplitude +400 are north-displaced with respect to the seismically-recognised basement South Tugela and East Tugela Ridges (compare Figs.5.1 and 5.4). Additional positive peaks in this province may delineate as yet undiscovered basement ridges (Fig.5.4; 29° 50'S, 32° 20'E).

A negative field discriminates the deep basin plain from surrounding positive anomalies generated by basement highs of the Mozambique, Naude, South Tugela and East Tugela Ridges (Fig.5.4). Individual profiles (Fig.5.5) show the negative field to consist of a single, long wavelength, low amplitude (-200) anomaly on which is superimposed subsidiary undulations. Sea-floor spreading anomalies are not recognised in the deep basin enclave north of 30° 20'S. Farther south however, in the southern Natal Valley, the Mesozoic anomaly sequence M0-M12 has been discriminated (section 5.3.4).

In summary, basement high zones recognised from seismic profiling and which are suspected to be primarily of a volcanic nature are characterised by prominent positive anomalies. Dimensions of these anomalies improve definition of the areal extent of basement core to the Mozambique, Naude, South Tugela and East Tugela Ridges.

5.3.3 Magnetic Anomaly Models

To further study basement magnetisation in the Natal Valley, 2D magnetic modelling has been attempted on a N-S profile along which basement is continuously observed (TBD 371/4; Plate B3.4c). This profile (Fig.5.3a for location) traverses the SW Mozambique Ridge, the NE enclave of deep basin and the Naude Ridge.

In anomaly simulation, the 2D magnetic interpretation programme "IGS 9" was employed (Vine, 1965). This programme computes the variation in total intensity of the Earth's magnetic field generated by a number of parallel, horizontal prisms of infinite length, arbitrary polygonal cross-section and specified magnetisation. The infinite number of 2D magnetic bodies capable of simulating the observed anomalies along traverse TBD 371/4 has been reduced by applying four assumptions: (1) the upper surfaces of acoustic and magnetic basement were assumed to be coincident; (2) basal depth of the magnetic body in the NE deep basin (oceanic crust) was fixed at -7,4 km. This is a typical value for depth to base Layer 2 in normal oceanic crust (Raitt, 1963); (3) over the SW Mozambique Ridge, the magnetic body base was assigned a depth of -10,0 km; and (4) the magnetisation vector was taken to be co-directional with the present ambient field (declination 20^{o}W of N; inclination -63^{o}). Null values were assigned to non-magnetised blocks.

Velocity data from refraction site 160 (Ludwig et al, 1968) were used in depth conversion of the time-to-basement data. To combat edge effects in modelling, the magnetic body was arbitrarily extended by 50 km both north and south. In constructing the model, a relatively simple and geologically-feasible basement structure was maintained. The optimum model attempt is shown in Figure 5.6 which presents observed and simulated magnetic signatures along with the parent basement body.

Inspection of the modelled profile (Fig.5.6) shows that there are varying degrees of similarity between the observed and simulated signatures dependent on physiographic region.

MAGNETIC ANOMALY MODEL PROFILE

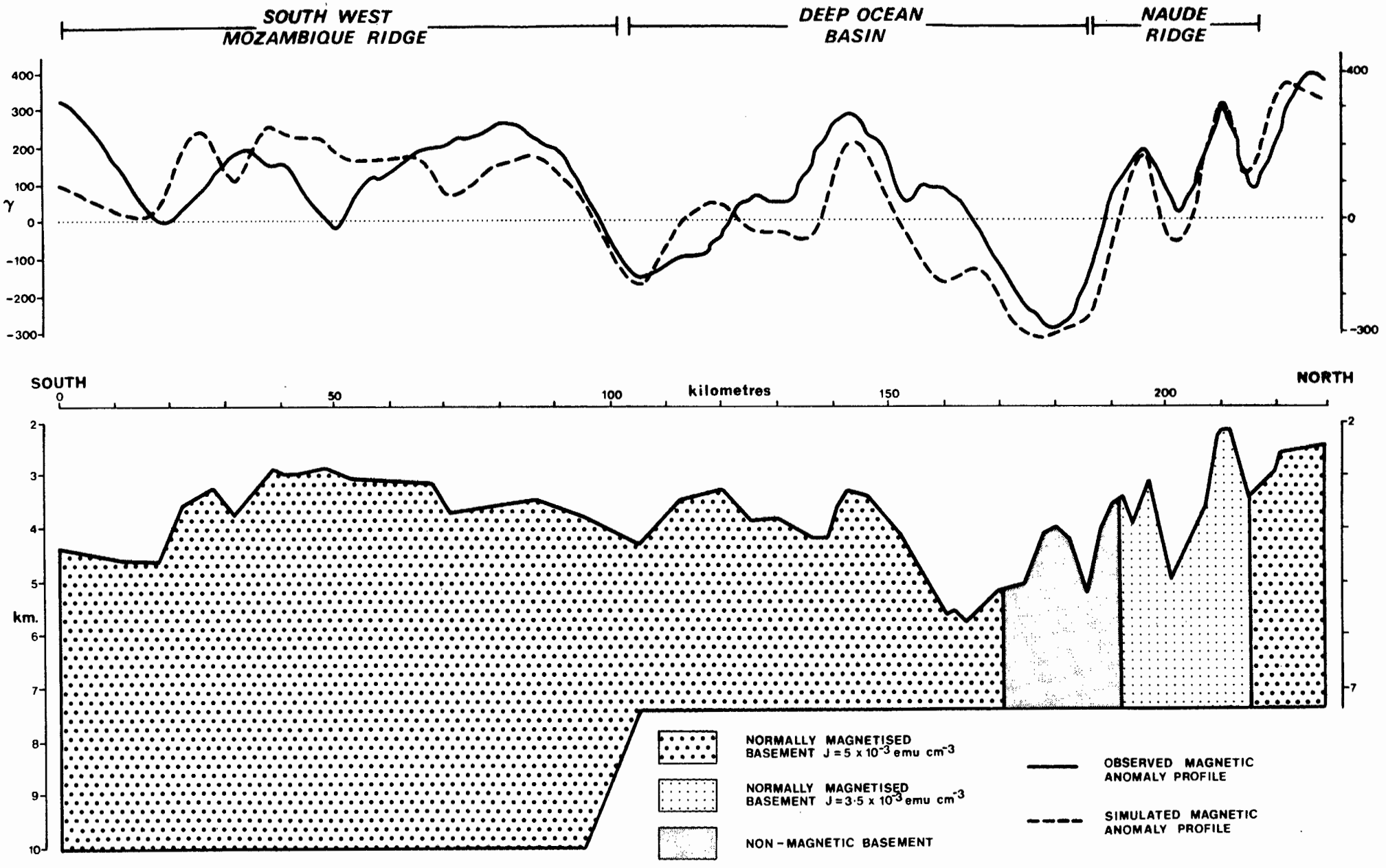

Fig. 5.6

Excellent matching is achieved over the Naude Ridge zone where the simulated and observed anomalies are analogous in shape, amplitude and magnetic gradient. A poorer but still satisfactory match is obtained over the deep basin section where the observed and modelled anomalies are of similar shape, amplitude and gradient although not perfectly matched in peak/trough location. The Mozambique Ridge exhibits the least satisfactory correlation with only minor shape and gradient correspondence (Fig.5.6).

To generate the model, all zones except the Naude Ridge were assigned a magnetisation intensity (J) of $5,0 \times 10^{-3}$ emu cm^{-3}. Naude Ridge magnetisation intensity was set at $3,5 \times 10^{-3}$ emu cm^{-3} (du Plessis, 1978). These values lie centrally within the typical magnetisation intensity range of basalts (Harrison, 1976). Best fit of observed and modelled anomalies was attained by inserting a non-magnetic block ~20 km wide between the deep basin and Naude Ridge (Fig.5.6).

There is good correspondence between basement upper surface topography and the distribution and amplitude of the observed anomaly peaks and troughs over the Naude Ridge and deep basin. This suggests that, in these areas, the upper section of basement is a major contributor to the local magnetic field. Good correlation using a simplistic basement model and basaltic magnetisation intensities argues for a basaltic basement character. Extrusion may have occurred over a relatively short time span since no negative polarity blocks are required in the model.

On the southern flank of the Naude Ridge (Fig.5.6; 180 km), one basement peak has no associated positive magnetic anomaly and is thus assigned a non-magnetic character. Insertion of the non-

magnetic block centred on this peak provides an excellent match of observed and simulated signatures (Fig.5.6). This non-magnetised peak (1200m high) is part of an elongate basement ridge, 50 by 10 km in dimension (Figs.5.1 and 5.14). It is suggested that the entire ridge may comprise non-magnetic basement, the implications of which are discussed in section 5.5.7.

There are no clear correlations between modelled and observed anomalies over the Mozambique Ridge zone, excepting edge effects at 100 km (Fig.5.6) attributable to shoaling of the magnetic body base. Likewise, there is poor correspondence of observed magnetic and basement highs. This is taken to imply that basement may comprise a series of complexly magnetised (positive, negative and non-magnetic) blocks with horizontal to vertical contacts and variable magnetisation intensities. Otherwise, poor correlation may indicate that inherent assumptions of the model are not applicable to this region. In view of the suspected structural complexity within the Mozambique Ridge zone, it was decided not to attempt refinement of the model magnetic fit of Figure 5.6.

An indirect conclusion derived from the modelling study concerns acoustic basement depth immediately north of the Naude Ridge. In this region horizon McDuff is strongly reflective preventing accurate recognition of acoustic basement, although elevated basement is intuitively suspected. Corroborative evidence is supplied by the model study as it is necessary to infer 'high' magnetic basement, sited closely beneath reflector McDuff, to simulate the observed anomaly.

5.3.4 Southern Natal Valley Mesozoic Magnetic Anomalies

Confirmation of the continental nature of the Falkland Plateau (Ewing et al, 1971; Rabinowitz et al, 1976; Barker, Dalziel et al, 1976) necessitates its inclusion in recent reconstructions of SW Gondwana (Barker, Dalziel et al, 1976; Norton and Sclater, 1979; Martin et al, 1981), fitting into the gap between SE Africa and the Mozambique Ridge (Fig.5.7). During the West Gondwana drift phase, the Falkland Plateau moved past Africa constrained by orientation of the Agulhas/Falkland Fracture Zone (Francheteau and Le Pichon, 1972; du Plessis, 1977). Recognition of magnetic anomalies on conjugate margins of the southern South Atlantic has helped to define the sea-floor spreading history of South America and Africa (Rabinowitz and LaBrecque, 1979) north of the Agulhas/Falkland Fracture Zone. In contrast, to the south of the fracture zone, the Natal Valley has been largely ignored as a prospective source of geophysical data for testing reconstruction of West Gondwana. Remote location ($\sim 40^{o}$) from the early rotation pole (Rabinowitz and LaBrecque, 1979; Martin et al, 1981) suggests that sea floor spreading in the Natal Valley may have advanced at a fast rate and thus resultant magnetic anomalies should be widely spaced and easy to recognise. Magnetic anomaly lineations present in the Natal Valley should be aligned approximately perpendicular to the Agulhas Fracture Zone.

Four previously published magnetic traverses (du Plessis, 1977) have been reassessed in conjunction with newly acquired data to reveal a Mesozoic magnetic anomaly lineation pattern (Cape Sequence) within the southern Natal Valley. Du Plessis

Figure 5.7

Revised Falkland Plateau Palaeoposition Relative to the Natal Valley

This reconstruction of SW Gondwana, defined by inter-continental alignment of pre-drift tectonic lineaments and removal of continental basement overlap (Martin et al, 1981), depicts the excellent physiographic match of the Falkland Plateau and SE Africa (Natal Valley).

South African 1000, 2000 and 3000 m isobaths - dashed after Simpson (1977) and Figure 3.2. South American/Falkland Plateau 1830 m (1000 fm) and 2740 m (1500 fm) isobaths - solid after Lonardi and Ewing (1971). Alternative position for the NE apex of the Falkland Plateau (2740 m isobath) in reconstruction utilising Rabinowitz and LaBrecque (1979) rotation parameters is dotted.

Key to physiographic zones : 1 - Tugela Cone, 2 - Natal Valley, 3 - Mozambique Ridge, 4 - Maurice Ewing Bank, 5 - Falkland Plateau Basin, 6 - Agulhas Bank, 7 - Burdwood Bank, 8 - Falkland Islands. Inset A shows the location of magnetic profile SHACKLETON (SH) in the Georgia Basin, east of the Falkland Plateau apex (from Barker, 1979). Inset B presents locations of magnetic profiles 25 and 26 (Rabinowitz and LaBrecque, 1979) from the Cape Basin, SW of South Africa. Inset numbered zones - refer to above key.

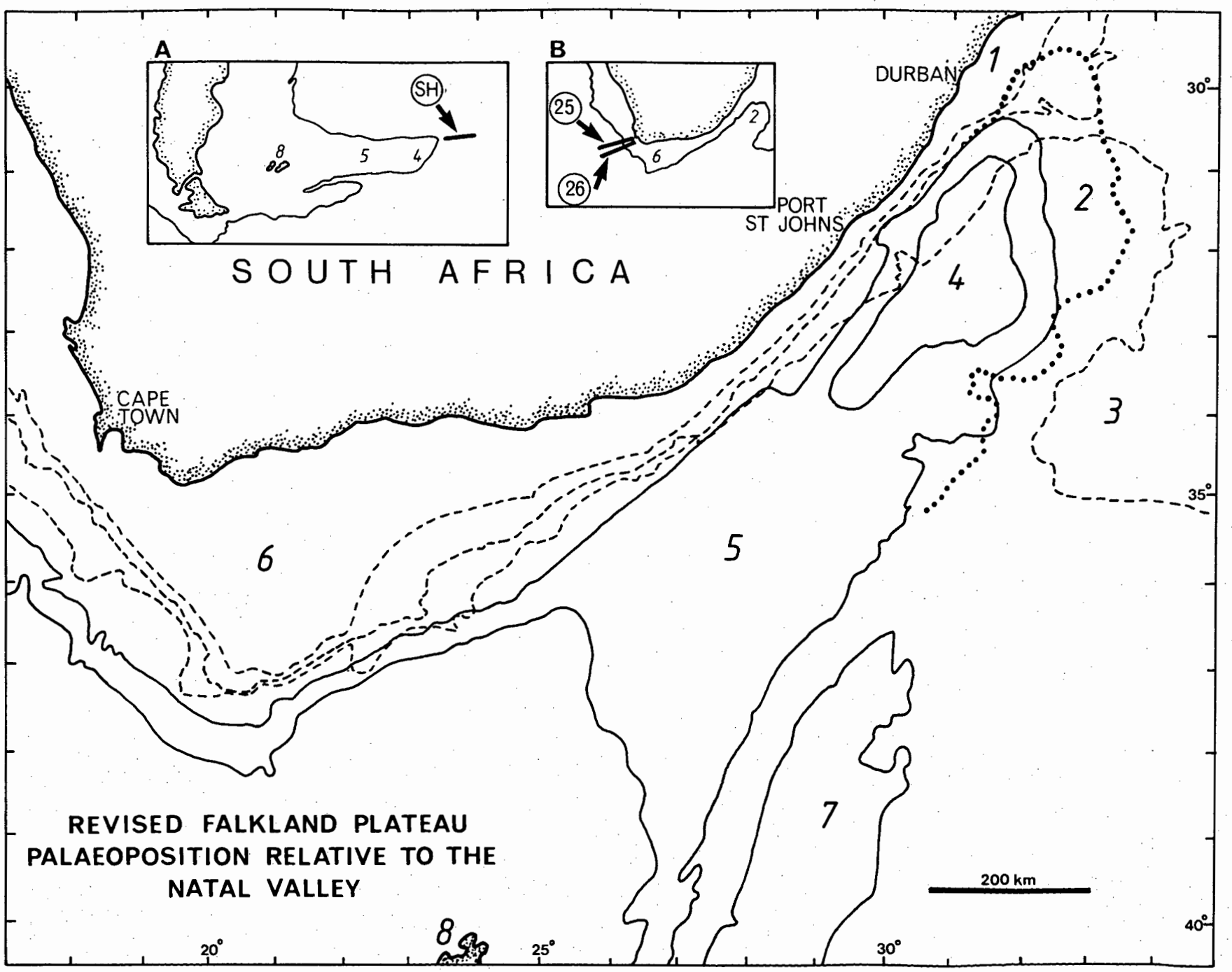

REVISED FALKLAND PLATEAU PALAEOPOSITION RELATIVE TO THE NATAL VALLEY

Fig. 5.7

(1977) recognised coast-normal magnetic lineations but did not reconcile these to standard Mesozoic anomaly models. The reinterpreted profiles (527, 515/518, 519, 371/3, 371/8, AGULHAS 2 and 402) are geographically aligned and compared with the modelled Mesozoic anomaly sequence of Rabinowitz and LaBrecque (1979) in Figure 5.8. Inter-profile correlation and correspondence to the synthetic model is considered to be good. Slight disparity of profile 527 is suspected to be due to navigational inaccuracy. Natal Valley and Cape Basin magnetic signatures parallel to the spreading direction show similarities (Fig.5.8), further confirming correct anomaly sequence identification.

Anomalies M12 to M0 are recognised, correlation being particularly good in the range M4 to M0 (Fig.5.8). Anomaly M4 is prominent in all profiles as a broad positive 250γ in amplitude while the M2 - M0 composite anomaly is conspicuous as a positive triple peak some 200-500γ in amplitude. Lineations defining M11, M9 and M7 are less distinctive but still considered valid (Fig.5.8). However, identification of the Mesozoic Cape Sequence rests primarily on recognition of anomalies M4 to M0.

Observed Natal Valley profiles fit credibly closely to the synthetic model simulated using a half-spreading rate of 1,5 cm/yr (Fig.5.8). Consequently, 1,5 cm/yr is proposed as an average Mesozoic half-spreading rate for the Natal Valley. In detail, however, the M4-M0 rate appears slightly slower than the 1,5 cm/yr model (anomalies more compressed) while a slightly faster spreading speed (~1,7 cm/yr) may be more appropriate to the M11-M4 sequence. These velocities are closely comparable to those calculated for oceanic crust immediately east of the Falkland Plateau in the Georgia Basin (Barker, 1979).

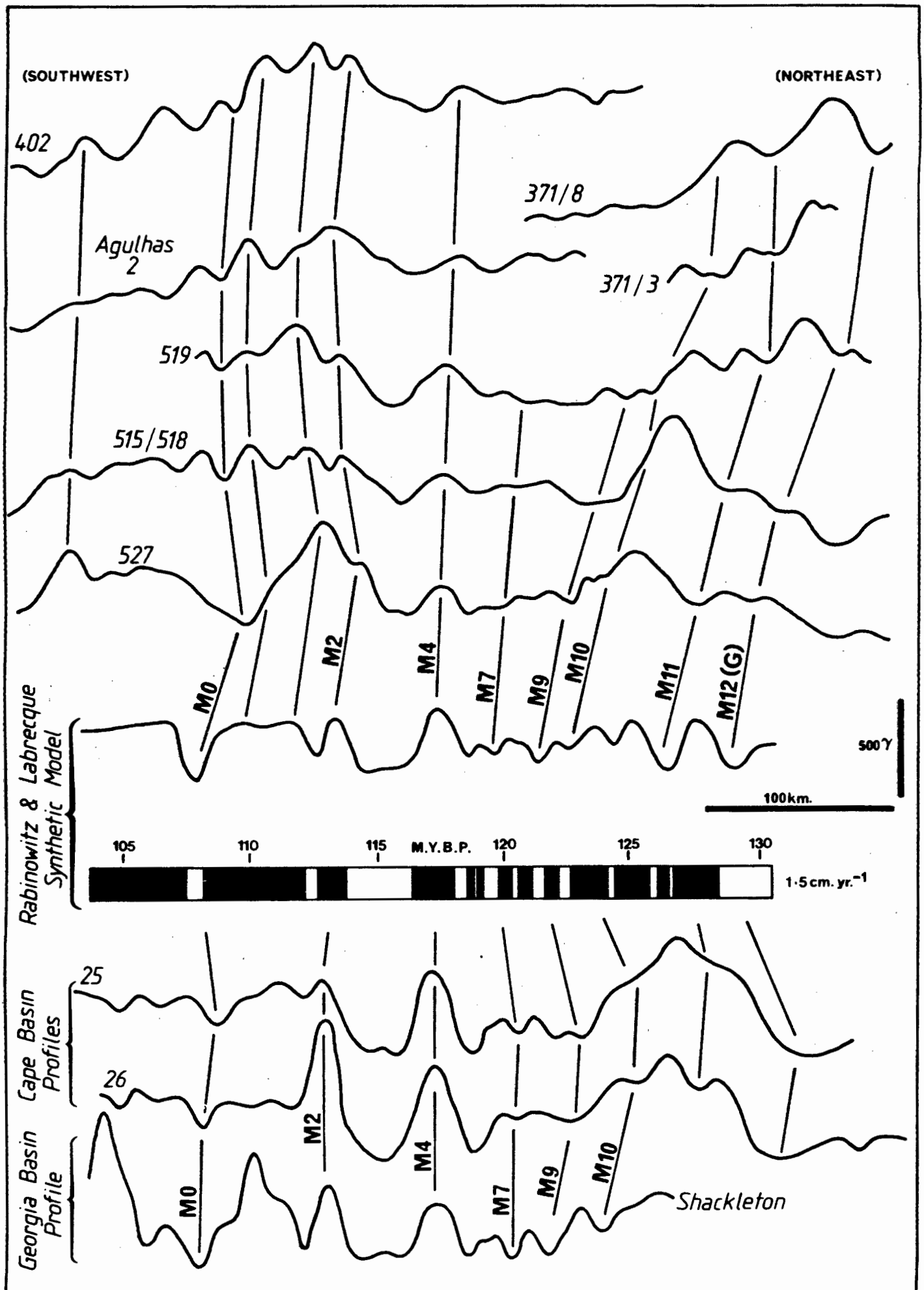

Data from Larson and Hilde (1975), Barker (1979), Rabinowitz and Labrecque (1979) and this study.

Fig. 5.8 SOUTHERN NATAL VALLEY MAGNETIC ANOMALY LINEATIONS

A geographic plot of the magnetic traverse (Fig.5.9) shows that the subparallel anomalies define a strike trend normal to the Agulhas Fracture Zone (delineated by the Cape Slope Anomaly - du Plessis and Simpson, 1974). Oceanic crust created directly east of the Falkland Plateau in the Georgia Basin should theoretically generate mirror images of Natal Valley magnetic profiles although these may now be partially distorted by differing ambient field declination, inclination and skewness. A profile from the Georgia Basin (Barker, 1979), mirror-imaged in Figure 5.8, exhibits the expected degree of symmetry to Natal Valley anomalies.

The revised fit of South America and south Central Africa (Fig.5.7) from Martin, Hartnady and Goodlad (1981) is primarily based on cross-continent alignment of three major pre-drift tectonic features:

(1) eastern and western boundaries of the submarine Jurassic Outeniqua Basin (South Africa) and the Falkland Plateau Basin;

(2) northern tectonic limit of the Triassic Cape Fold Belt (South Africa) and a closely contiguous major morphological feature on the Falkland Plateau; and

(3) Late Precambrian transcurrent fault and mylonite belts of Pernambuco (Brazil) and Foumban (West Africa).

This revised reconstruction (total pole of rotation - 46,75°N, 32,65°W; rotation angle - 56,4°) is close to but slightly looser than the refit of Rabinowitz and LaBrecque (1979) - see Figure 5.7 and thus solves continental basement overlap in the Natal Valley and Precambrian overlap in the Gulf of Benin.

Seismic profiling surveys have discovered and delineated an

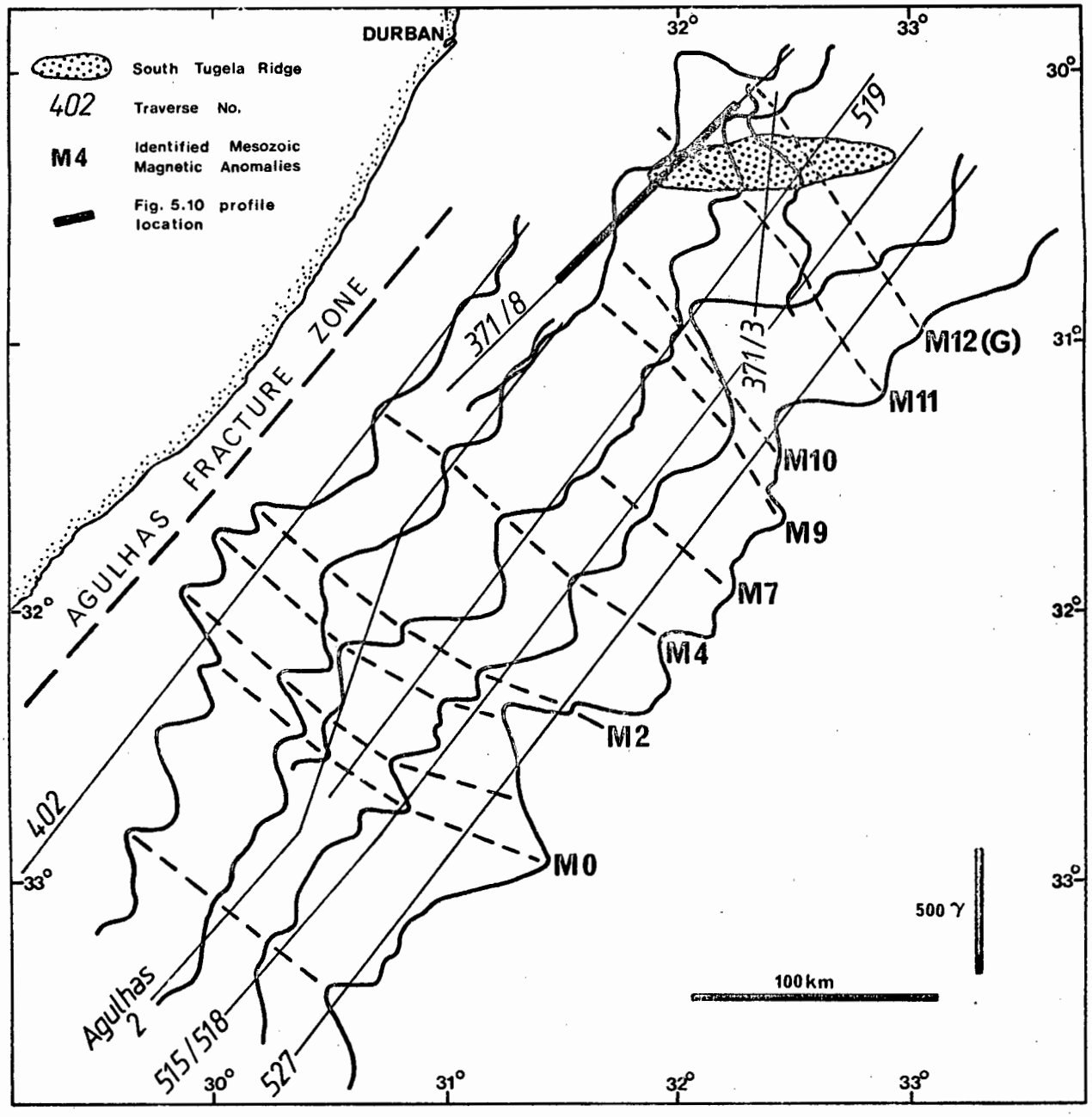

Fig. 5.9 MAGNETIC ANOMALY PROFILES IN THE SOUTHERN NATAL VALLEY

approximately E-W oriented, deeply-buried, basement ridge - the South Tugela Ridge (Fig.5.10) underlying or situated immediately south of the steep Tugela Cone southern flank (section 5.2.5). Ridge location is depicted in Figure 5.9. Significantly, in the revised reconstruction (Martin et al, 1981) the South Tugela Ridge becomes juxtaposed to the continental/oceanic crust boundary (COB) of the Falkland Plateau as approximated by the 1500 fm (2740 m) isobath on seismic refraction results (Ewing et al, 1971). Independent geological/geophysical evidence therefore suggests that the South Tugela Ridge may be sited just north of the Natal Valley COB and is probably a manifestation of initial rift volcanics intercalated with splintered continental blocks.

Within the Natal Valley, the oldest correlative magnetic anomaly is identified as M12 (Figs.5.8 and 5.9 - after the time-scale of Larson and Hilde, 1975) corresponding in character to anomaly G (Rabinowitz, 1976; Rabinowitz and LaBrecque, 1979). Magnetic anomaly G, first mapped along the west coast of Africa (Rabinowitz, 1976; Rabinowitz and LaBrecque, 1979), has been interpreted as a magnetic edge effect separating continental from oceanic basement. Reinforced by isostatic gravity modelling, Rabinowitz and LaBrecque (1979) use anomaly G to demarcate the COB. However, west coast Africa magnetic lineation G, to which Rabinowitz and LaBrecque (1979) assign an M12 age, has previously been dated at M13 by Larson and Ladd (1973) utilising the same raw data; thus dating of this anomaly is not unambiguous.

The revised fit of Martin, Hartnady and Goodlad (1981) suggests that the SW Africa COB may be sited ~40 km seaward of magnetic anomaly G, but still positioned within the landward gradient of the isostatic gravity anomaly. On reconstruction

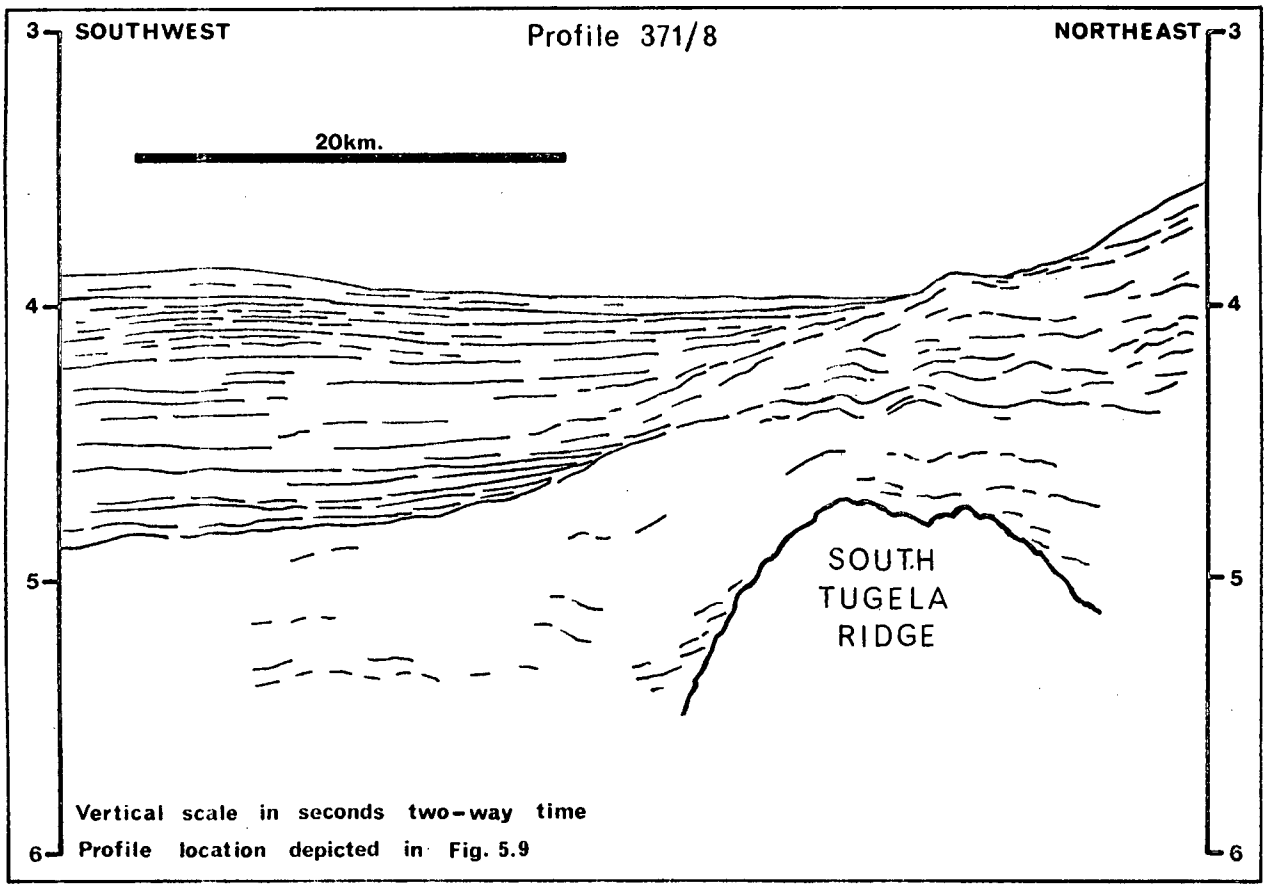

Fig. 5.10 LINE TRACING OF SEISMIC PROFILE OVER THE SOUTH TUGELA RIDGE

evidence, the Natal Valley COB is suspected to be located south of the South Tugela Ridge thus implying that anomaly G is placed on continental crust.

Utilising a new early spreading pole (Martin et al, 1981), rotation of South America towards Africa simultaneously achieves precise juxtaposition of Mesozoic anomalies (M0, M2, M4 and M10) in areas both south and north of the Agulhas/Falkland Fracture Zone. Thus, using one set of rotation parameters, there is concomitant abutment of Cape/Argentine Basin anomalies (Rabinowitz and LaBrecque, 1979) and Natal Valley /Georgia Basin anomalies (Barker, 1979 and this study). Complete kinematic description of the early spreading history is outwith the scope of this study but has been more fully considered in Martin, Goodlad, Hartnady and du Plessis (1982). However, back-rotation to M10N accomplishes optimum contiguity of inter-continental structural lineaments previously described. It is therefore postulated that opening of the South Atlantic commenced at ~125 Myr (M10N using time-scale of Larson and Hilde, 1975).

Accepting this looser reconstruction (see Fig.5.7), it is necessary to explain the existence of recognisable magnetic anomalies (M11 and M12) landward of M10N (approximate COB) as demarcated in Figures 5.8 and 5.9. A possible explanation may be that prior to final separation, crustal rifting allowed extensive intrusion of volcanic lavas, subsequently magnetised in the earth's ambient field. This mechanism, with possible interference from basement topography and non-magnetised splinters of continental crust, may explain the poorer M11 and M12 correlation with the modelled profile (Fig.5.8) and anomaly distension on several profiles. Larson and Ladd (1973) likewise

attribute poor correlation between anomalies older than M7 along the SW Africa continental margin to disruption of the lineation pattern by the initial rifting phenomenon. Basement topography certainly induces modulation of the ambient field in the Natal Valley with high amplitude positive anomalies plotting over the South Tugela Ridge (Fig.5.9 - profiles 371/8, 371/3 and 519).

The collection of multi-channel seismic data off the continental margin of SW Africa (Uchupi and Austin, 1981; Gerrard and Smith, 1983) has cast additional doubt on the 'anomaly G' refit of South America and Africa. In particular, Uchupi and Austin (1981) locate their SW Africa COB at or closely seaward of the 3000 m isobath. This placement is in general agreement with the reconstruction described by Martin et al (1981) which likewise corroborates the new magnetic evidence presented here. Although the SW Africa COB of Gerrard and Smith (1983) is located even farther seaward, constraints on data quality allow for some ambiguity in exact positioning (I. Gerrard, pers. comm., 1981). These new multi-channel data also imply that extensive intracontinental stretching took place along the passive margin of SW Africa during the early opening phase of the South Atlantic (Uchupi and Austin, 1981). However, the reconstruction proposed by Martin et al (1981) in combination with the magnetic data outlined in this section suggests that post-breakup continental crust stretching may not have been widespread over the Falkland Plateau/Natal Valley zone

5.4 BASEMENT ROCK PETROLOGY AND GEOCHEMISTRY

5.4.1 Introduction

To further investigate the nature of basement ridges within

the mid Natal Valley, basement outcrops of the East Tugela Ridge were dredged during cruise TBD 371. In this section, dredge rocks are petrologically and geochemically described. The major and trace element composition of recovered basalts are used in an attempt to discriminate tectonic setting of the East Tugela Ridge at its time of formation. This in turn helps refine location of the COB in the study area. Because of their strongly altered character, it was considered impractical to attempt isotopic dating on the basalts.

5.4.2 Dredge Location and General Description

The northern exposed seamount of the East Tugela Ridge was selected as a dredge target and basement rock recovery was achieved during dredge 5749 which traversed its NE margin. A detailed bathymetric chart of the northern seamount, with site location of dredge 5749, is presented in Figure 5.11. Three satellite navigation fixes provided good navigational control. Dredging operations were carried out over the depth range ~2480-2120 m below sea level.

In total, 4 kg of sample were obtained on dredge retrieval, consisting of two blocks of volcanic rock (maximum size, 140 x 100 x 70 mm) with at least one broken fresh face indicative of local derivation (5749 D1 and D3), together with a more rounded volcanic cobble (5749 D2; size 115 x 58 x 40 mm). Although showing no freshly broken faces, this cobble is still considered to be locally-derived since there are no other known basement outcrops within 100 km. All three rock fragments show substantial secondary alteration as indicated by their yellow-green to red colour range.

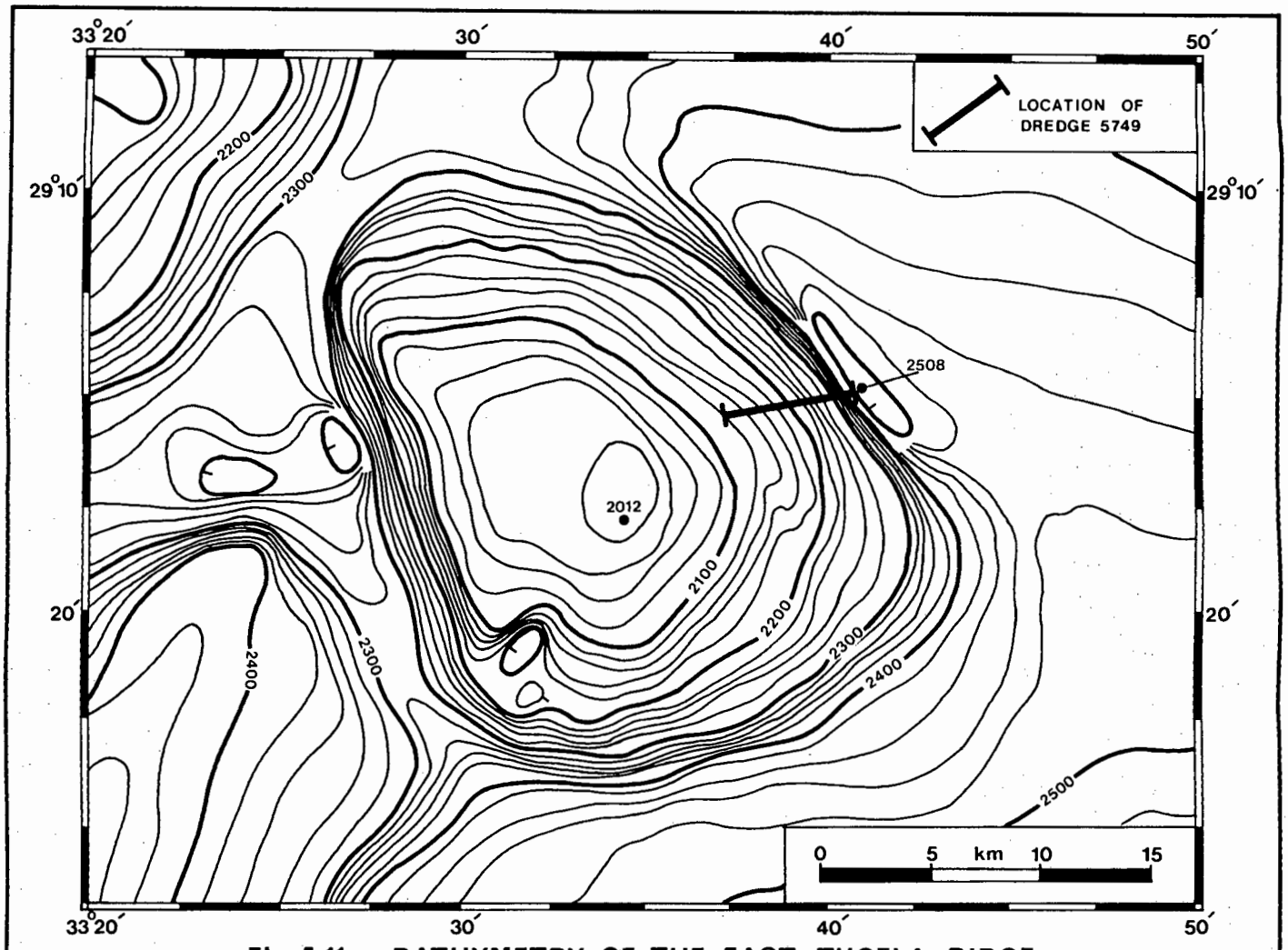

Fig. 5.11 BATHYMETRY OF THE EAST TUGELA RIDGE (NORTHERN SEAMOUNT) AND THE LOCATION OF DREDGE 5749

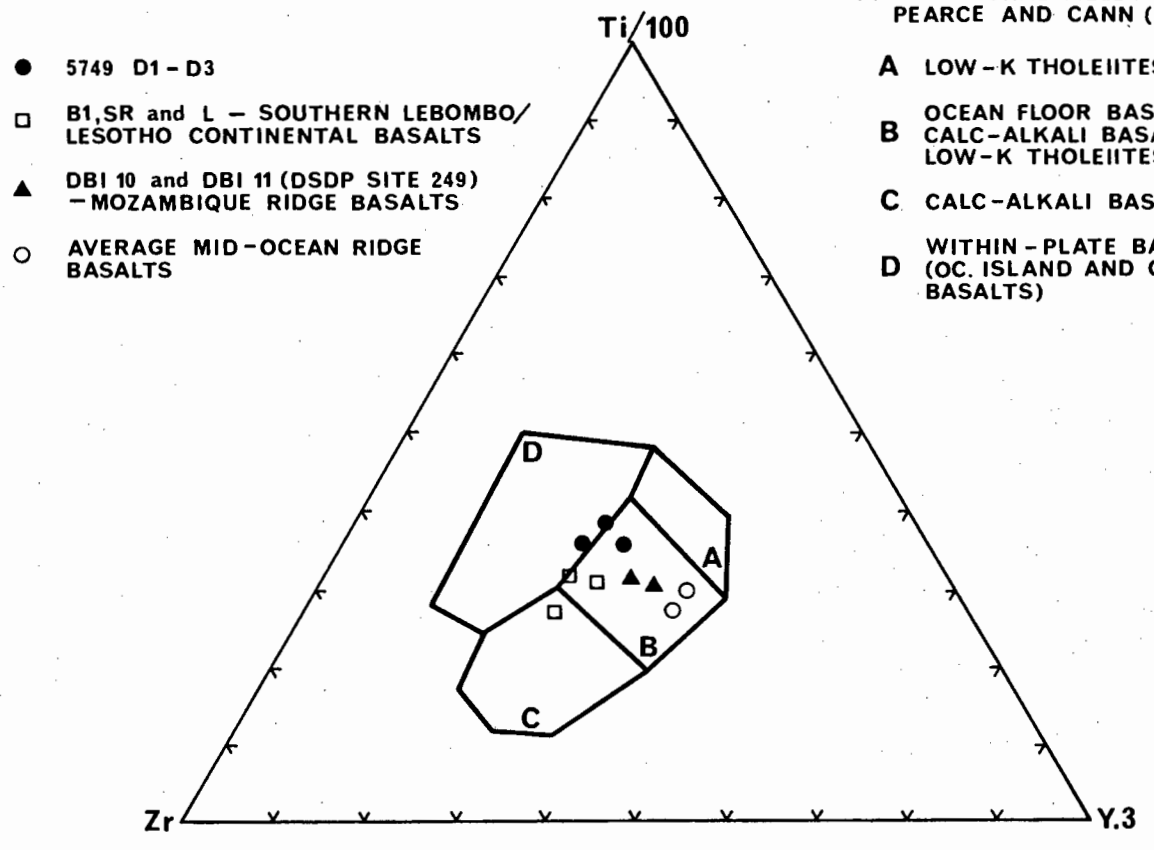

Fig. 5.12 BASALTS 5749 D1 - D3 PLOTTED ON Ti - Zr - Y TRIANGLE

5.4.3 Petrology of the Dredge Rocks

All three dredge sub-samples (5749 D1-D3) are basaltic, although highly carbonatised, oxidised and calcified. Each sub-sample, however, shows a distinctive petrology and accordingly, separate descriptions for all three types are presented. Photomicrographs are compiled in Plate 5.1.

5749 D1 This basaltic rock displays altered olivine as its only phenocryst phase. Showing relict subhedral to euhedral habit (Plate 5.1a and b) and a maximum diameter of 2,0 mm, these phenocrysts are now almost entirely altered to iddingsite, chlorite-serpentine and hematite mixtures. The groundmass is characterised by unoriented slender laths of plagioclase feldspar (0,1 - 0,2 mm in length) enclosed within larger (maximum size - 0,5 mm) equant clinopyroxenes in a typical ophitic texture (Plate 5.1a-c). Minor groundmass phases include microphenocrysts of altered olivine (Plate 5.1c) and magnetite. The groundmass shows extensive secondary alteration to admixtures of clay minerals, sericite, chlorite and iron oxides while calcite is a common replacement phase either pseudomorphing primary volcanic minerals or as a secondary vein mineral (Plate 5.1a).

5749 D2 This porphyritic basalt is characterised by an amygdaloidal texture (Plate 5.1d and c) with vesicles (as large as 1 cm) comprising ~10-15% of the total rock volume. Porphyritic phases comprise small euhedral olivines (maximum diameter - 0,5 mm) invariably altered to a host of secondary minerals including carbonate, chlorite, iddingsite and Fe-oxides

Plate 5.1 Dredge Sample 5749 - Photomicrographs

a-5749 D1 Extensively-altered subhedral olivine phenocrysts sitting in groundmass of plagioclase laths enclosed within larger clinopyroxenes (high relief) in an ophitic texture. Magnetite completes the groundmass phases. Note the cross-cutting secondary calcite vein to the left of the olivine phenocrysts (plane light).

b-5749 D1 Euhedral olivine, altered to iddingsite/chlorite-serpentine/hematite in a groundmass of plagioclase and clinopyroxene (right, high relief) showing ophitic texture. Small subhedral magnetites occur as a groundmass phase (plane light).

c-5749 D1 Clinopyroxene (high relief, top of frame) and plagioclase laths in ophitic texture. Note also several microphenocrysts of altered olivine (plane light).

d-5749 D2 Full view of hand specimen with conspicuous vesicles.

e-5749 D2 Amygdaloidal basalt with dominant crystalline phase plagioclase co-existing with devitrified glass in either hyalopilitic or intersertal texture (plane light).

f-5749 D2 Plagioclase phenocrysts, some of which show quench texture, sitting in a devitrified, altered glassy matrix in a hyalopilitic texture. Note vesicle to the left of the frame (plane light).

g-5749 D2 Large phenocryst of plagioclase surrounded by small plagioclase laths and volcanic glass enclosed by altered subhedral olivines (top right, bottom centre) (plane light).

h-5749 D2 Close up of vesicle enclosed in hyalopilitic matrix of plagioclase/devitrified, altered glass. Vesicle infill includes ? primary zeolite (rims), calcite micrite, detrital quartz/feldspar and foraminifera (plane light).

i-5749 D3 Volcanic breccia with variable size, angular fragments of relatively well crystallised volcanic rock (plagioclase/minor olivine/altered glass) enclosed within devitrified, extensively altered, volcanic glass (plane light).

j-5749 D3 Contact between volcanic fragments and enclosing matrix. Brecciated fragment shows plagioclase laths and glass in hyalopilitic texture. The volcanic matrix, containing a few microphenocrysts of plagioclase, magnetite and olivine, shows a more distinct glassy quenched texture adjoining the breccia fragment (plane light).

DREDGE SAMPLE 5749 — PHOTOMICROGRAPHS

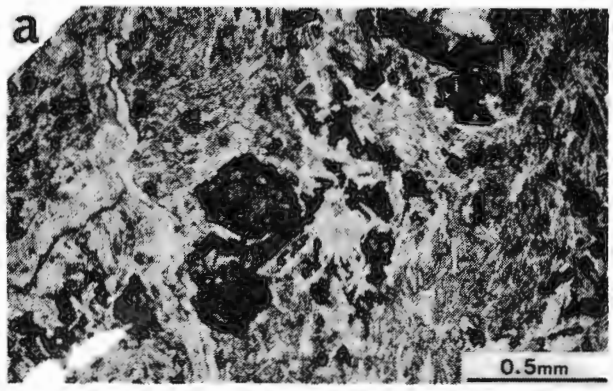

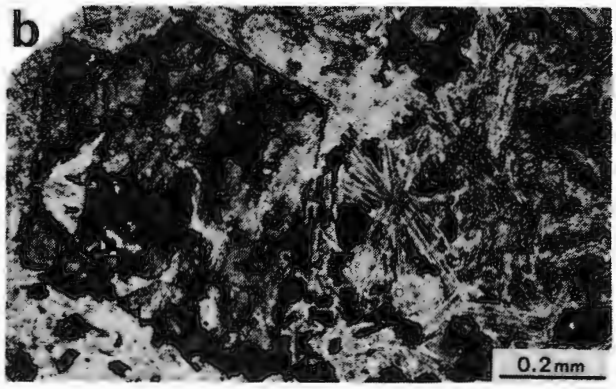

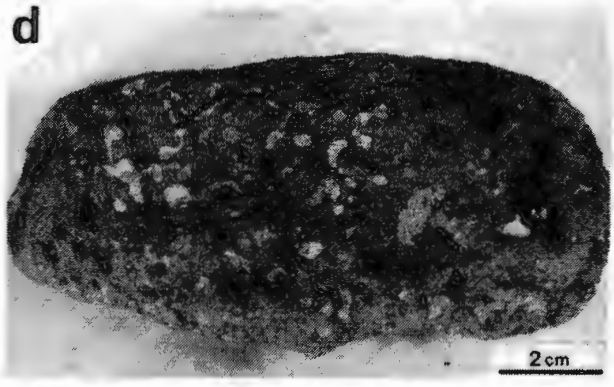

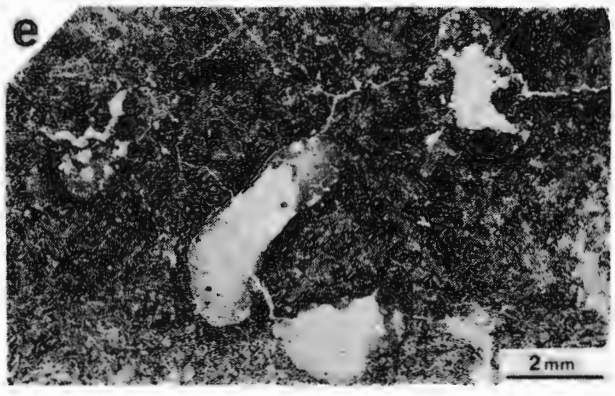

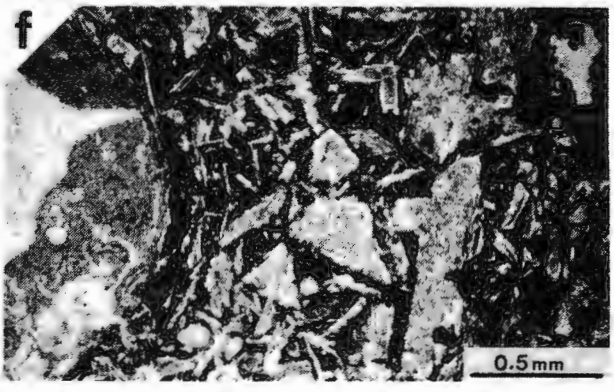

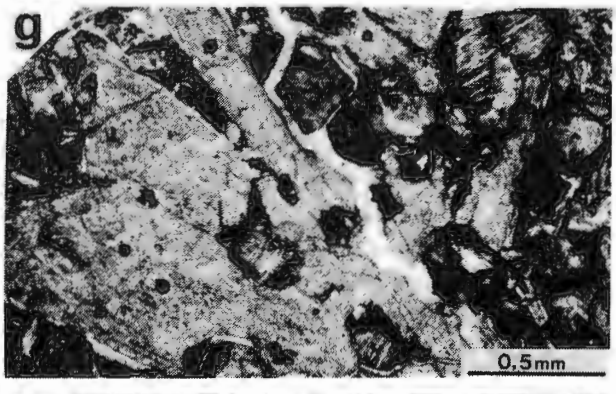

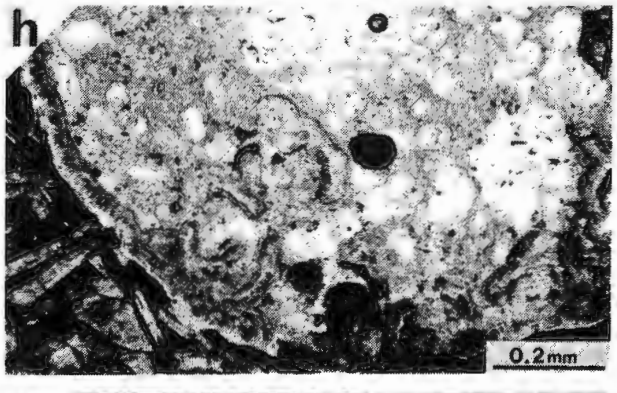

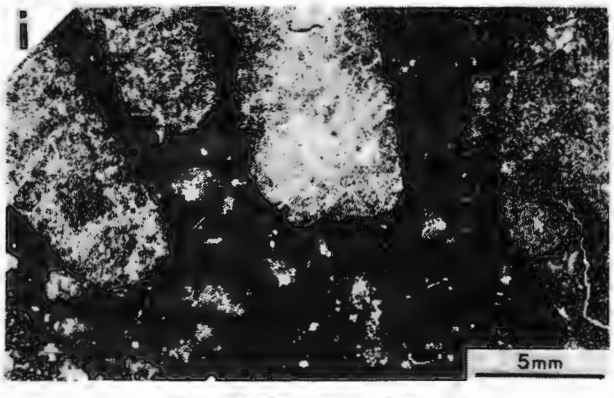

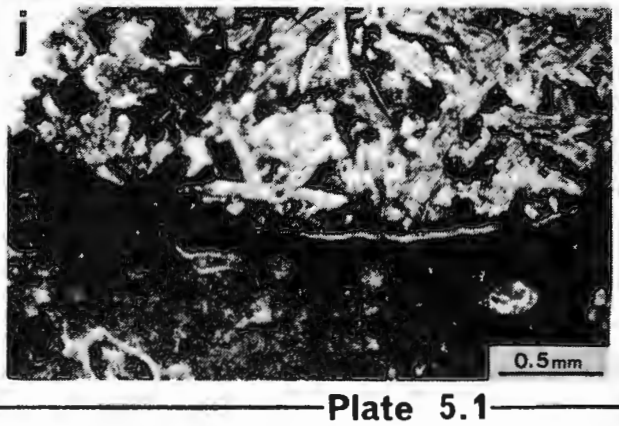

Plate 5.1

(Plate 5.1g) along with relatively fresh, equant or elongate plagioclase feldspars of 1,5 mm maximum dimension (Plate 5.1g). Occurring in acicular or lath habit, plagioclase is the dominant mineral phase in a groundmass typified by hyalopilitic (Plate 5.1e and f) to intersertal (Plate 5.1e) textures. Although commonly sericitised and saussuritised, numerous of these groundmass plagioclases (size range; 0,1 - 0,4 mm) retain quenched textures (Plate 5.1f), indicative of rapid cooling in a submarine environment (Bryan, 1974). Interstitial voids are filled with dark red/brown glassy mesostasis, now devitrified and extensively altered to iron oxides and clay mineral admixtures. Minor magnetite microphenocrysts and secondary calcite complete the groundmass phases in a basalt notable for its total absence of clinopyroxene. It is suspected that mineralisation within the vesicles is almost exclusively secondary in origin with abundant zeolite, calcite and clay minerals (Plate 5.1h). Open exchange with sediment-charged sea water is demonstrated since detrital feldspar, quartz, zircon, hornblende, magnetite, lime micrite and numerous foraminifera (Plate 5.1h) are common constituents in the vesicles.

5749 D3 Classified as an agglomerate, this rock is very distinctive with angular, porphyritic, volcanic blocks of variable size (1 mm to 5 cm) sitting in a glassy, slightly vesicular matrix (Plate 5.1i).

The brecciated blocks are very similar to rock D2 excepting the complete absence of amygdales. Altered olivine and relatively fresh plagioclase phenocrysts are enclosed in a groundmass of slender plagioclase laths and volcanic glass either

in hyalopilitic or intersertal texture. As in rock D2, the groundmass plagioclases often show quench textures. Matrix glass is devitrified and substantially altered to mixtures of clays and Fe-oxides. Rare clinopyroxene phenocrysts of maximum diameter 1 mm (visually estimated at ~1% of the mode) differentiate the brecciated blocks from rock type D2.

The binding matrix of the fragmented blocks is slightly vesicular and fine grained. Originally very glassy, devitrification and heavy alteration has reduced the glass to an opaque mixture of powdery Fe-oxides and undifferentiated clays (Plate 5.1i). Microphenocrysts of altered olivine, magnetite and plagioclase along with occasional small, zeolite/clay-filled vesicles punctuate the glassy matrix comprising ~10% of its volume. Contacts between brecciated fragments and intervening glassy lava are sharp (Plate 5.1j) and quick chilling is evidenced by the increasing glassy character towards these contacts. Secondary calcite is ubiquitous throughout the fragmented blocks and enclosing glassy matrix.

5.4.4 Geochemistry of the Dredge Rocks

Chemical analyses obtained by procedures outlined in Appendix A4 are listed in Tables 5.1 and 5.2 along with comparative data from southern Lebombo basalts (Bristow, 1976; 1980), Lesotho basalts (Cox et al, 1967), Mozambique Ridge DSDP 249 basalts (Erlank and Reid, 1974) and average mid-ocean ridge basalts (Melson and Thompson, 1971; Erlank and Reid, 1974; Engel and Fisher, 1975). Major element concentrations of 5749 D1-D3 show large differences depending on the volume of carbonate-filled vesicles and veins incorporated in the samples (Tables 5.1

Table 5.1 Whole Rock Major Element Chemical Analyses* of Dredge 5749 Samples compared to Average Southern Lebombo and Lesotho Basalts, DSDP Site 249 Basalts and Average Mid-Ocean Ridge Abyssal Basalts

	5749+ D1	5749+ D2	5749+ D3	B1*1	SR*2	L*3	DBI 10*4	DBI 11*4	A*5	MIORB*6
SiO_2	47.11	51.89	42.53	52.97	51.70	51.80	52.86	51.96	49.83	50.74
TiO_2	1.46	2.07	1.47	1.27	1.40	1.13	0.80	0.81	1.41	1.24
Al_2O_3	17.29	18.26	13.72	14.90	15.60	14.80	16.76	17.15	16.01	16.62
Fe_2O_3**	11.64	12.71	10.74	12.00	12.20	11.18	9.33	9.85	9.52	8.58
MnO	0.13	0.10	0.16	0.16	0.20	0.17	0.11	0.13	0.16	0.16
MgO	5.45	4.05	3.62	5.54	5.50	7.10	7.48	7.14	8.64	8.03
CaO	13.21	5.40	22.80	9.33	9.90	10.57	9.66	9.96	11.28	11.60
Na_2O	2.24	2.21	1.49	2.77	2.70	2.40	2.46	2.52	2.74	2.75
K_2O	1.28	2.90	2.97	0.76	0.59	0.74	0.47	0.40	0.26	0.16
P_2O_5	0.20	0.41	0.50	0.32	0.19	0.13	0.07	0.08	0.15	0.11

* calculated anhydrous and CO_2-free; normalised to 100%.

** total iron oxide expressed as Fe_2O_3.

\+ analyst S.W. Goodlad.

*1 average Southern Lebombo basalt (Mfolozi River - 11 samples) - after Bristow (1976).

*2 average Southern Lebombo basalt (Sabie River - 18 samples) - after Bristow (1980)

*3 average Lesotho basalt (21 samples) - after Cox et al. (1967).

*4 DSDP site 249 basalts - after Erlank and Reid (1974).

*5 average mid-ocean ridge basalt - after Melson and Thompson (1971).

*6 average mid-Indian Ocean ridge basalt ($8^{o}S$-$25^{o}S$) - after Engel and Fisher (1975).

Table 5.2 Whole Rock Trace Element Chemical Analyses* of Dredge 5749 Samples compared to Average Southern Lebombo and Lesotho Basalts, DSDP Site 249 Basalts and Average Mid-Ocean Ridge Abyssal Basalts

	5749+ D1	5749+ D2	5749+ D3	B1*1	SR*2	L*3	DBI 10*4	DBI 11*4	A*5	MIORB*6
Ba	37	74	27	330	245	256	77	46	12	17
Co	69	80	49	46	50	34	57	71	32	35
Cr	355	330	252	154	137	317	249	228	296	360
Cu	77	149	66	-	117	-	68	115	87	93
Ga	17	19	12	-	-	-	15	14	18	-
Nb	4	11	9	4	4	11-16	2	3	3	-
Ni	219	197	160	65	100	73	167	178	123	109
Rb	21	33	34	20	17	<50	5	5	1	-
Sc	33	41	28	-	29	-	-	-	-	49
Sr	198	190	142	373	329	190	103	107	123	108
V	372	145	131	241	245	300	191	187	289	250
Y	21	31	26	27	25	23	19	22	43	35
Zn	157	162	105	93	92	-	79	82	122	-
Zr	76	132	82	130	111	85	62	63	100	71
S**	0.031	0.030	0.046	-	-	-	0.005	0.009	-	-

* expressed in ppm

** expressed as wt.%

\- no data available

\+ analyst S.W. Goodlad; trace element standard deviation: Ga(0.3); Y(0.4); Zr,Sc,Rb,Nb(0.5); Zn,Sr(0.6); Cu(0.8); Cr,Ni(1.0); Co(1.2); Ba(1.4); V(2.7)

*1 average Southern Lebombo basalt (Mfolozi River - 11 samples) - after Bristow (1976)

*2 average Southern Lebombo basalt (Sabie River - 18 samples) - after Bristow (1980)

*3 average Lesotho basalt (21 samples) - after Cox et al. (1967)

*4 DSDP site 249 basalts - after Erlank and Reid (1974)

*5 average mid-ocean ridge basalt - data sources listed in Erlank and Reid (1974)

*6 average mid-Indian Ocean ridge basalt - after Engel and Fisher (1975)

and 5.2). To estimate original basalt composition, major element data have been recalculated on an anhydrous and calcite-free basis after the method of Dietrich and Jones (1980). Recalculated data are listed in Table 5.3. Deficiencies of this data processing method are exemplified by the recalculated weight % of CaO in both D2 (4,9%) and D3 (3,6%) which are far below normal basalt CaO concentrations. In turn, other element oxides show concomitant percentage increases.

Examination of major element data listed in Tables 5.1 and 5.3 does not indicate definite compositional affinity between dredge 5749 basalts and any of the other basaltic categories (Lesotho/Lebombo - continental; Mozambique ridge; mid-ocean ridge - oceanic). This is possibly a result of secondary alteration of the dredge 5749 samples, as shown by petrographic examination. Alteration is common in submarine basalts during which most major elements and many trace elements are mobile (Floyd and Winchester, 1975; Hart et al, 1974). Secondary alteration and element mobility in samples 5749 D1-D3 is suggested by the relatively high K, Rb and H_2O^- contents, high Fe_2O_3/FeO ratios (Erlank and Reid, 1974) and low S contents (Moore and Fabbi, 1971). Low K/Rb and high K/Ba and Rb/Sr ratios (Hart et al, 1974) provide corroborative evidence. Geochemical parameters indicative of secondary alteration in samples 5749 D1-D3 are documented in Table 5.4.

The concentrations of the elements Ti, Zr and Y, which are considered immobile during secondary alteration (Hart et al, 1974), may aid in discrimination of tectonic environment during basalt extrusion (Pearce and Cann, 1973; Pearce, 1975; Floyd and Winchester, 1975). In Figure 5.12, the concentrations of Ti, Zr

Table 5.3 Major Element Chemical Analyses Recalculated on an Anhydrous and Calcite-Free Basis*

	5749 D1		5749 D2		5749 D3	
	norm+	calc	norm+	calc	norm+	calc
SiO_2	43,44	48,87	49,04	51,33	35,08	52,41
TiO_2	1,35	1,52	1,96	2,05	1,21	1,81
Al_2O_3	15,99	17,99	17,27	18,08	11,30	16,88
Fe_2O_3**	11,75	13,22	13,23	13,85	9,73	14,54
MnO	0,12	0,13	0,10	0,10	0,13	0,19
MgO	5,13	5,77	3,95	4,13	3,01	4,50
CaO	12,18	8,65	5,00	4,94	19,02	3,56
Na_2O	2,05	2,31	2,10	2,20	1,24	1,85
K_2O	1,19	1,34	2,76	2,89	2,46	3,68
P_2O_5	0,18	0,20	0,40	0,42	0,39	0,58
H_2O^+	3,11	-	3,98	-	3,37	-
CO_2	3,52	-	0,22	-	13,06	-

* after the method of Dietrich and Jones (1980), whereby H_2O^+, CO_2 and the CaO equivalent of CO_2 (calcite composition) is removed from the total before normalising to 100%

** total iron expressed as Fe_2O_3

\+ analyst S.W. Goodlad; data normalised to 100%.

Table 5.4 Geochemical Parameters Indicative of Secondary Alteration in Dredge Sample 5749 Basalts

	5749 D1	5749 D2	5749 D3	A*1
H_2O^-*	3,32	5,58	4,16	-
S*	0,031	0,03	0,046	0,1*2
Fe_2O_3/FeO**	6,3	13,8	11,9	0,31
K^+	10628	24062	24660	1160
Rb^+	21	33	34	1
Ba^+	37	74	27	12
Sr^+	198	190	142	123
K/Rb	506	729	725	1054
K/Ba	287	325	913	97
Rb/Sr	0,106	0,174	0,239	0,009

* expressed as weight %

\+ expressed in ppm

\- no data available

** FeO analyses by Geological Survey of South Africa

*1 average mid-ocean ridge basalt - data sources listed in in Erlank and Reid (1974)

*2 data from Moore and Fabbi (1971)

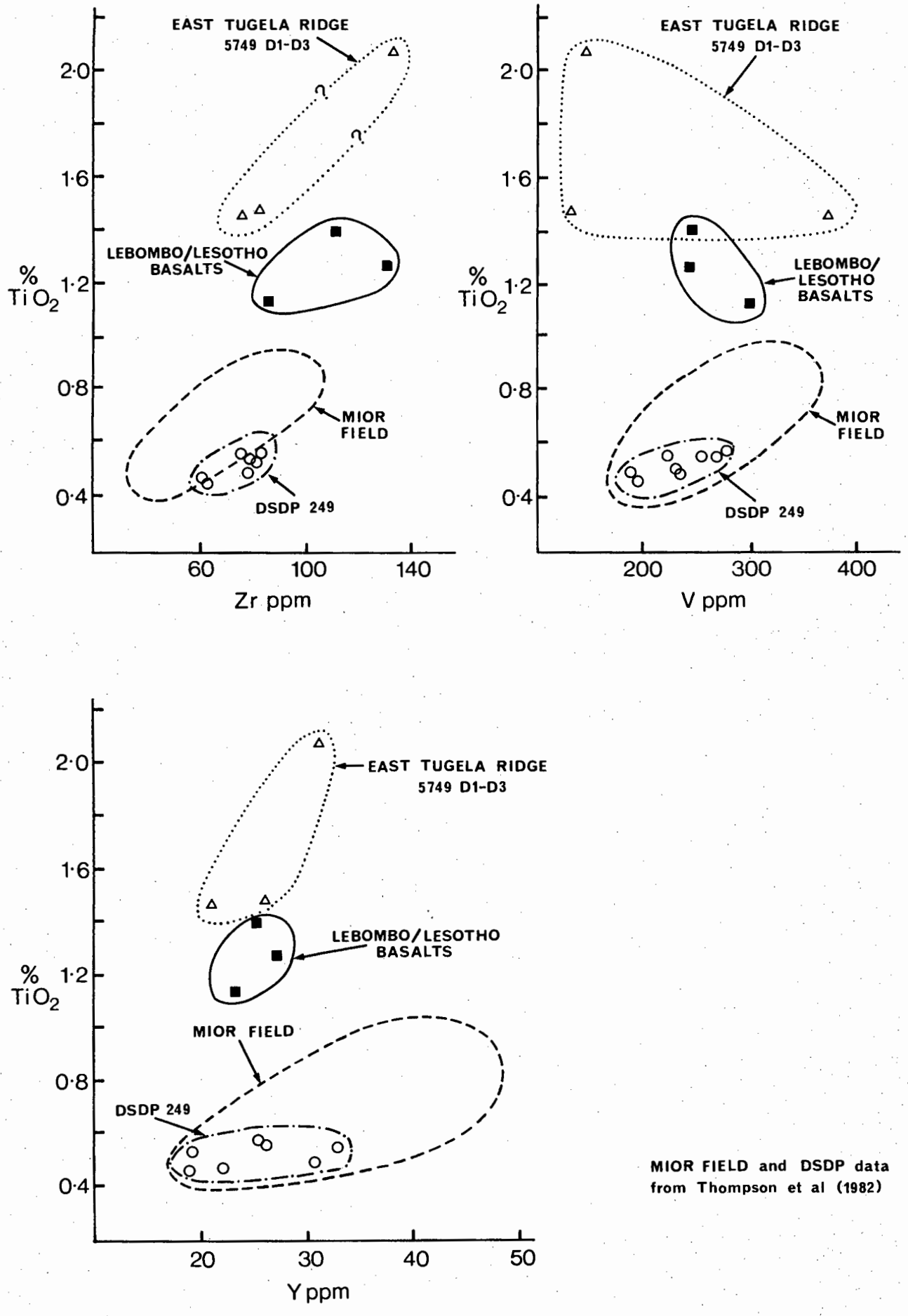

MIOR FIELD and DSDP data from Thompson et al (1982)

Fig. 5.13 INCOMPATIBLE ELEMENTS (Zr,V AND Y) VERSUS TiO_2

and Y are plotted as a ternary diagram after Pearce and Cann (1973). Bivariate plots of the elements V, Zr and Y versus $\%TiO_2$ (Thompson et al, 1982) are presented in Figure 5.13. Comparative data from continental Lebombo/Lesotho basalts, Mozambique Ridge basalts and mid-ocean ridge basalts are included in both figures. The East Tugela Ridge basalts (5749 D1-D3) plot significantly apart from both the continental and mid-ocean ridge basalts (Figs.5.12 and 5.13) suggesting a transitional origin.

Their plot locus over the boundary zone between fields B and D (Fig.5.12) precludes a definite classification as either continental or oceanic. In Figure 5.13 however, the East Tugela Ridge basalts are located much closer to the Lebombo/Lesotho basalts than to the MIOR field indicating that they probably have strong continental affinities. From the chemical data (Figs.5.12 and 5.13), it is evident that the East Tugela Ridge, Lebombo/Lesotho and Mozambique Ridge basalts are genetically distinct and were probably extruded in different tectonic settings from different sources.

Original geochemical analysis (Erlank and Reid, 1974) could not determine a definite continental or oceanic origin for the Mozambique Ridge basalts. Based on new chemical analyses, however, Thompson et al (1982) interpret the DSDP 249 Mozambique Ridge basalts as being of mid-ocean ridge origin, and suggest that their extrusion was related to Early Cretaceous rifting between the eastern Falkland Plateau and Mozambique Ridge continental fragments (Tucholke et al, 1981). It is conceivable that these basalts were extruded during microplate movements of the Mozambique Ridge in the Early Cretaceous (section 5.5.7).

5.5 MAJOR CRUSTAL ELEMENTS

5.5.1 Introduction

Collation of published data with new geophysical data relating to crustal character of the Natal Valley allows recognition of four basement types: continental crust; subsided, thinned continental or transitional crust; marginal ridges and deep basin oceanic crust. Distribution and character of each of these groups is outlined and discussed. Locations of relevant geophysical profiles, refraction sites, drillsites and dredges along with a speculative spatial distribution of the crustal types is presented in Figure 5.14. Brief studies on basement subsidence, Mozambique Ridge micro-plate movement and the tectonic status of the northern Natal Valley complete this section.

5.5.2 Continental Crust

Normal elevated continental basement, typically 35 km thick (Darracott, 1974) is recognised on seismic refraction, magnetic and gravity data (Ludwig et al, 1968; du Plessis and Simpson, 1974; Scrutton, 1976) and the trend of major basement scarps (Fig.5.1; Dingle, 1979). Three major, contiguous, geological lineaments define the eastern extent of normal continental basement: (1) the Agulhas Fracture Zone; (2) the cross-shelf trending steep basement scarp from $\sim 31^{\circ}S$ to $29^{\circ}S$; and (3) the Lebombo Line (see Fig.5.14). In the southern Natal Valley, the Agulhas Fracture Zone is delineated by the Cape Slope Magnetic Anomaly (du Plessis and Simpson, 1974) and demarcates the

Fig. 5.14

Speculative Distribution of Crustal Types and Location of Drillsites, Refraction Sites and Important Geophysical Markers

Crustal types: 1 - "normal" continental crust; 2 - subsided, thinned continental or transitional crust; 3 - marginal ridges; and 4 - oceanic crust.

Eastern limit of "normal" continental crust defined by approximate colinearity of four geophysical markers: the Lebombo Line positive gravity anomaly (Darracott, 1974; Darracott and Kleywegt, 1974); basement marginal scarp "a" from Figure 5.1; basement marginal scarp "b" from Dingle (1979); the Cape Slope Anomaly (CSA) after du Plessis and Simpson (1974). Note that basement scarp "a" is offset from the Lebombo Line.

Southern limit of subsided, thinned continental crust or transitional crust speculatively demarcated by alignment of the southernmost marginal ridges (Fig.5.1) and the non-magnetic ? fracture ridge (section 5.3.3). Western boundary of Mozambique Ridge continental crust may approximate to the 4,3 sec TWT basement isochron (Fig.5.1). At this time-depth, there is an obvious change in basement structural style from rough and uneven on the Mozambique Ridge crest to smooth and regular on the deep basin floor.

Refraction sites 157-160 from Ludwig et al (1968); DSDP 249 from Simpson, Schlich et al (1974); SOEKOR drillsite Jc-1 from du Toit and Leith (1974); dredge site 5749 - see section 5.4; thin dashed line - location of gravity profile (see Fig.5.16 after Darracott, 1974); Empangeni Fault System after Maud (1961).

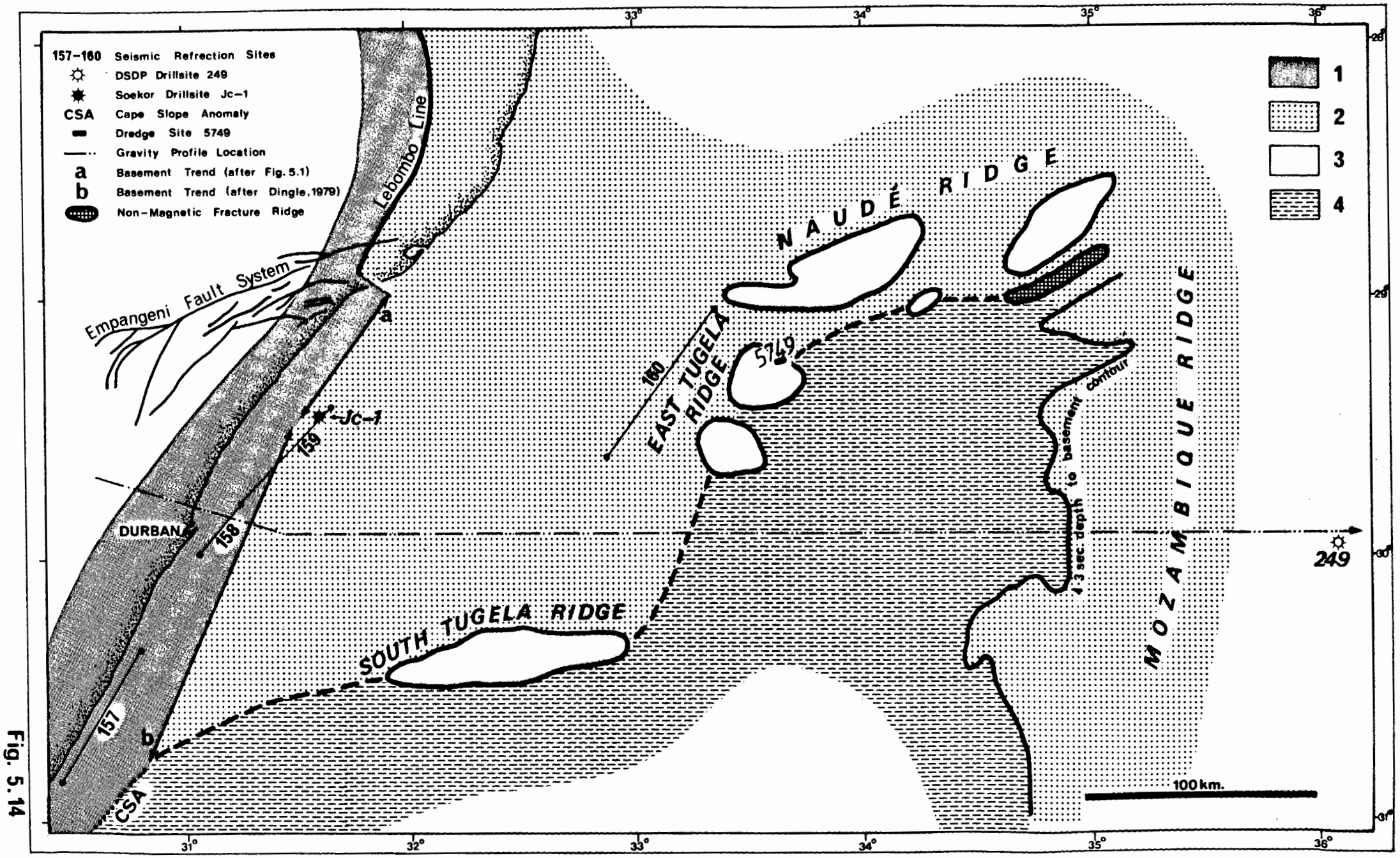
157–160 Seismic Refraction Sites
DSDP Drillsite 249
Soekor Drillsite Jc–1
CSA Cape Slope Anomaly
Dredge Site 5749
Gravity Profile Location
a Basement Trend (after Fig. 5.1)
b Basement Trend (after Dingle, 1979)
Non-Magnetic Fracture Ridge
1
2
3
4
Lebombo Line
Empangeni Fault System
NAUDÉ RIDGE
EAST TUGELA RIDGE
SOUTH TUGELA RIDGE
MOZAMBIQUE RIDGE
5749
160
159
Jc–1
158
157
DURBAN
CSA
249
4·3 sec depth to basement contour
100 km.
33°
34°
35°
36°
31°
32°
33°
34°
35°
36°
28°
29°
30°
31°

Fig. 5.14

continental/oceanic crust boundary (COB). At about 30° 50'S, where this anomaly dies out, the steep basement scarp swings northward cutting across the continental shelf to approximately line up with the Lebombo Line (Dingle and Scrutton, 1974). Misalignment of the basement scarp and the Lebombo Line (Fig.5.14) may indicate structural offset along the Empangeni Fault System (de Swardt and Bennet, 1974). The Lebombo Line follows the crest of a major isostatic gravity anomaly (Darracott, 1974) partly produced by the thick Lebombo volcanic sequence. However, Darracott and Kleywegt (1974) demonstrated a substantial crustal effect implying that the Lebombo Line is a major crustal discontinuity, probably delineating the eastern extent of normal continental crust.

Basement structure of the east coast shelf is not well understood, but a series of refraction sites (Fig.5.14; sites 157-159) have revealed gross features (Fig.5.15). Basement comprises block-faulted segments overlain by units of low-medium velocity indicative of a Cretaceous to Cainozoic age (Dingle, 1979). Up to 2 km of low-medium velocity sediments fill the graben while horst blocks are only thinly-covered (Fig.5.15). Basement, with seismic velocities greater than 4,96 km/sec (Fig.5.15), is classified as Palaeozoic or older (Dingle, 1979) probably belonging to either the Cape or Karoo Supergroups (section 1.2.2). This is verified by recovery of quartzitic sandstone of the Cape Supergroup at a depth of 2324 m below sea level in borehole Jc-1 (du Toit and Leith, 1974).

5.5.3 Subsided Continental or Transitional Crust

This crustal type is suspected to underlie the Tugela Cone,

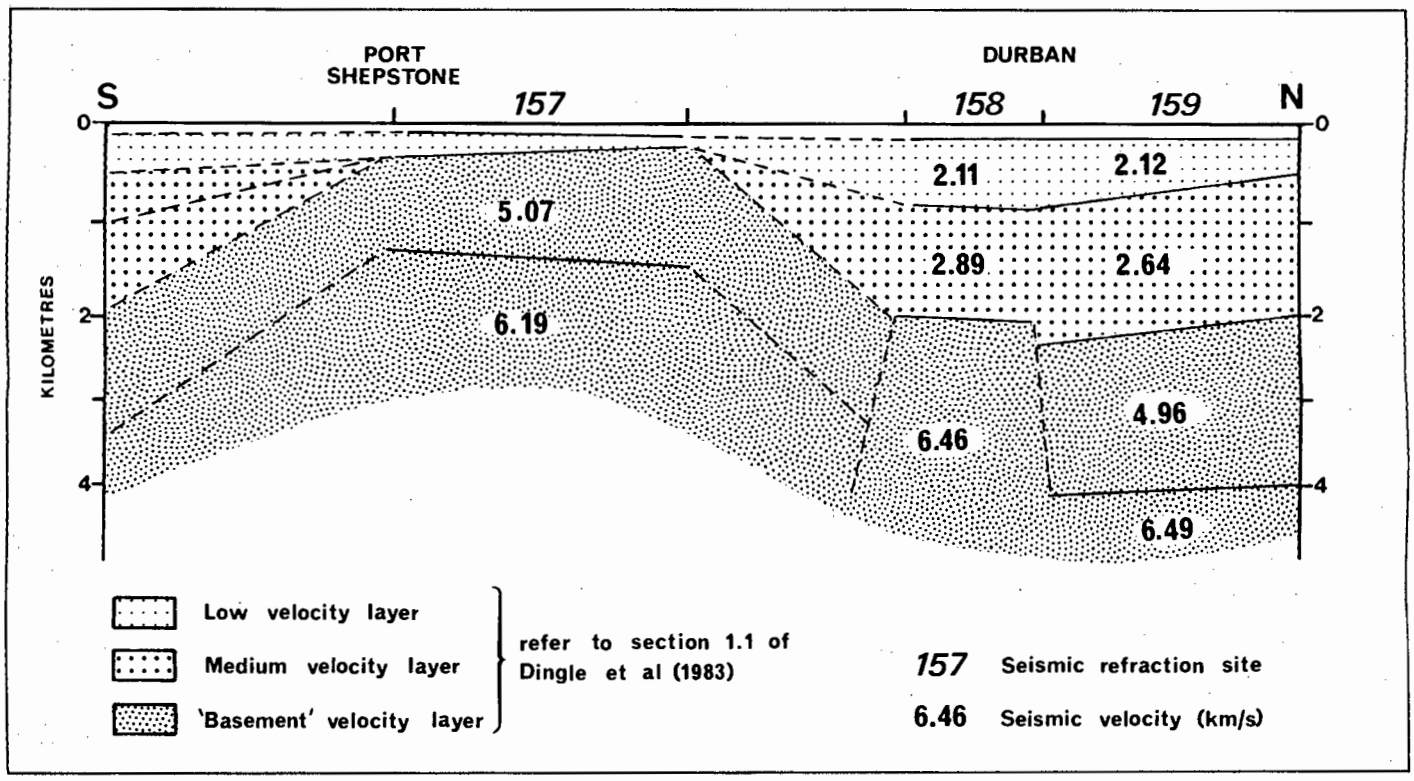

Fig. 5.15 SEISMIC REFRACTION SECTION ALONG EAST COAST CONTINENTAL SHELF
(After Ludwig et al, 1968)

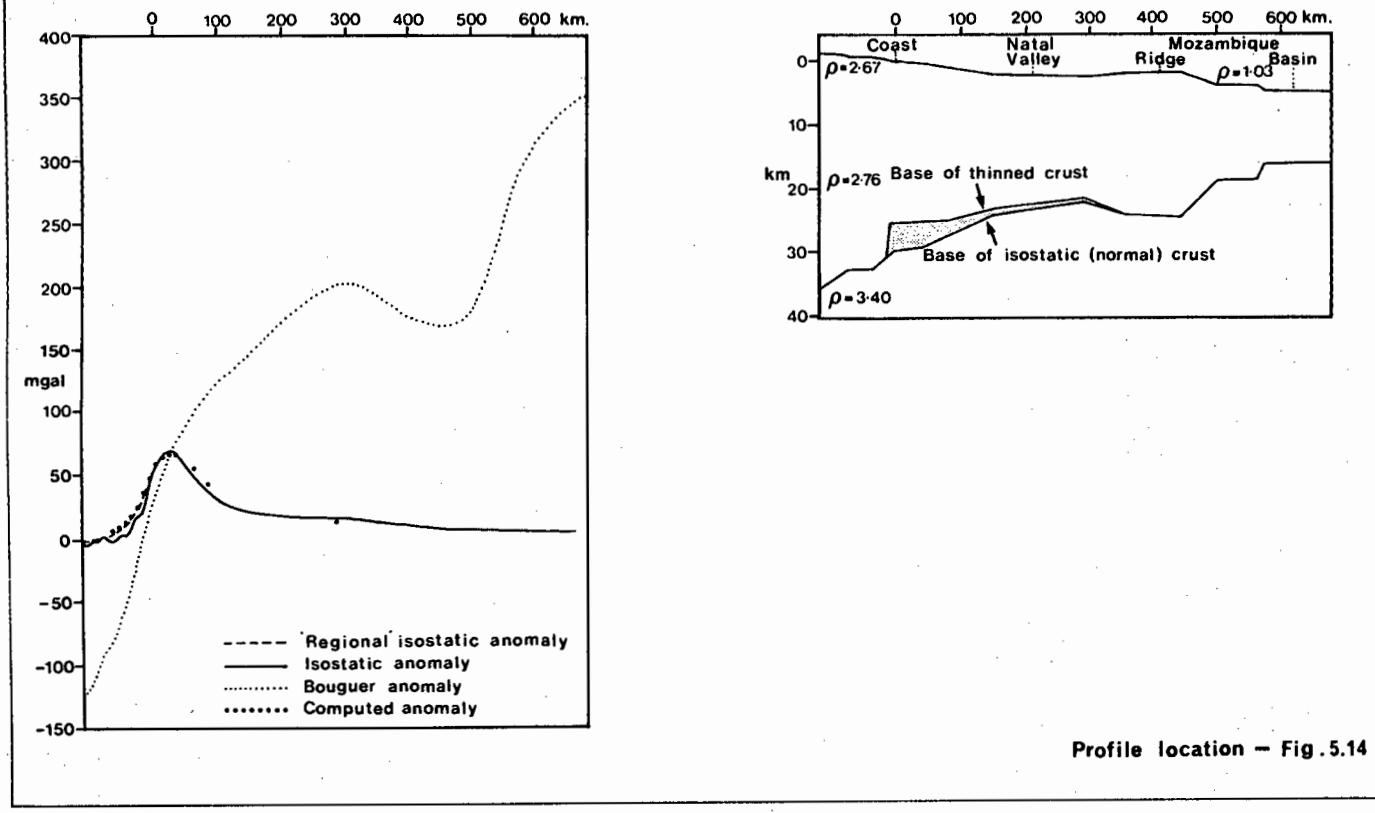

Fig. 5.16 EAST–WEST GRAVITY ANOMALY PROFILE AND MODELLED BASEMENT STRUCTURE
(After Darracott, 1974)

Central Terrace and Mozambique Ridge provinces (Fig.5.14). Darracott (1974) presented gravity profiles across the Natal Valley (Fig.5.16) and from these calculated a crustal thickness of 24-27 km. In the northern Natal Valley, Scrutton (1976) also proposed excessive thinning to explain a crustal thickness of 20 km. Based on these studies, Dingle and Scrutton (1974) suggested that, north of 30°S, the Natal Valley is underlain by thinned continental crust. Structural models for the Lebombo volcanic belt (Darracott and Kleywegt, 1974) portray 5-6 km of crustal depression east of the Lebombo Line. A multi-channel seismic profile across the northern Natal Valley (Beck and Lehner, 1974) showed acoustic basement, at 2-4 km below sea level, to be in seismic continuity with Jurassic volcanics exposed along the Lebombo monocline, verifying offshore basement subsidence. Farther north in south Mozambique, ?early Cretaceous Lebombo-type volcanics were encountered at 1832 m in the Zandemala borehole (Flores, 1973), indicative of northward-shoaling basement (Dingle et al, 1983; Martin, 1984).

The nature and origin of the Mozambique Ridge has been subject to much debate. Seismic refraction (Hales and Nation, 1973) and gravity studies (Darracott, 1974; Scrutton, 1976) have indicated an intermediate crustal thickness of 23 km. The close relationship between the Mozambique Ridge and coastal SE Mozambique favours a continental origin (Laughton et al, 1971) although its varied morphology may indicate a composite origin. In addition, the Mozambique Ridge can be accommodated in Gondwana reconstructions without serious overlap problems suggesting that the bulk of the ridge may comprise continental crust (Dingle et al, 1983). Although recent geochemical studies have confirmed that basement basalts recovered at DSDP 249 are oceanic in origin

(Fig.5.13), Thompson et al (1982) suggest that basalt extrusion was a result of a brief episode of Early Cretaceous rifting which separated the eastern Falkland Plateau and Mozambique Ridge continental fragments (Tucholke et al, 1981). Thus, although not finally resolved, it may be reasoned that the Mozambique Ridge is a continental fragment (Carlson et al, 1980), consisting of either thinned and subsided crust or perhaps transitional crust locally draped by oceanic extrusives. However, other scenarios have been proposed in which the Mozambique Ridge is considered to be an oceanic volcanic ridge (e.g. Martin and Hartnady, 1983). Subsequent discussion (e.g. sections 5.5.4-5.5.8) is based on the premise that the Mozambique Ridge is continental in origin. Detailed geophysical surveys and perhaps IPOD drilling is required to finally resolve this vital problem, critical to precise reconstruction of southern Gondwanaland.

5.5.4 Oceanic Crust

Seismic refraction studies (Hales and Nation, 1973; Nicolaysen, 1973) confirm that the southern Natal Valley is underlain by normal oceanic crust. Recognition of a series of magnetic spreading anomalies (section 5.3.4), east of the COB as defined by the Cape Slope Anomaly (du Plessis and Simpson, 1974), further confirms an oceanic origin for the southern Natal Valley. Exact configuration of the northern limit of oceanic crust is however still indefinite.

Geological and geophysical evidence suggests that the South Tugela Ridge (section 5.3.4) and perhaps the other marginal ridges (East Tugela and Naude Ridges) may approximately delimit the northern extent of oceanic crust within the Natal Valley. Along the Mozambique Ridge western margin, a distinct change in

structural style from rugged basement (Mozambique Ridge) to smooth regular basement (deep basin) occurs at about the 4,3 secs isochron, and may delineate the COB (Fig.5.14). Using these criteria, the 2500 m isobath roughly approximates the northern limit of oceanic crust, defining a large re-entrant into the thinned continental crust zone north of 30° 20'S, bounded by the Naude, Mozambique and East Tugela Ridges. Common to the majority of West Gondwana reconstructions (e.g. Norton and Sclater, 1979), there is a distinct gap between the Falkland Plateau eastern margin and Mozambique Ridge western margin which includes the re-entrant north of 30° 20'S. Geophysical evidence suggests that this gap may be underlain by oceanic crust generated during relative eastward movement of the Mozambique Ridge during early stages of Gondwanaland fragmentation (section 5.5.7).

5.5.5 Marginal Ridges

The distribution of the marginal ridges (Naude, East Tugela and South Tugela Ridges) is presented in Figure 5.14 while their general morphology is outlined in section 5.2. No published refraction or gravity data is available to characterise these previously-undiscovered basement ridges. Geochemistry and petrology of dredge 5749 basalts (section 5.4) suggest the East Tugela Ridge basement core is transitional in nature but with continental affinities. The other marginal ridges may possibly display a similar chemistry on account of their analogous physiography and tectonic environment. Excepting the narrow, elongate SE component of the Naude Ridge complex (Figs.5.1 and 5.14), all marginal ridges generate strong positive magnetic anomalies (section 5.3.2) suggestive of volcanogenic origin. Basaltic petrology displayed by dredge 5749 samples confirms a volcanic origin for the East Tugela Ridge.

It is postulated that these marginal ridges may have been constructed by extensive volcanism during initial sundering of SW Gondwana and their attitude perhaps reflects gross geometry of the COB (Fig.5.14). Formation of the South Tugela Ridge was almost certainly related to fragmentation of the Falkland Plateau and southern Africa. This origin is supported by: (1) its location relative to the revised palaeoposition of the Falkland Plateau in a new refit of West Gondwana (section 5.3.4); (2) southern Natal Valley Mesozoic magnetic lineations (section 5.3.4) which favour a spreading history consistent with the new refit of Martin et al (1981); and (3) recognition of a distinct isostatic gravity anomaly (COB marker of Rabinowitz and LaBrecque, 1979) over the South Tugela Ridge (P. Rabinowitz, pers.comm., Jan. 1980). These data verify that the South Tugela Ridge is sited just north of the COB. At the present time, however, the exact status and tectonic setting of the East Tugela and Naude Ridges cannot be confirmed, although it is thought that their formation was genetically linked to continental fragmentation.

5.5.6 Basement Subsidence

Crustal subsidence may be initiated by a combination of factors (section 4.5) but the primary mechanisms comprise thermal contraction of the lithosphere (Sleep, 1971; McKenzie, 1978) and crustal stretching through extension (Sclater and Christie, 1980) or differential loading (Watts and Thorne, 1984). Compaction, palaeobathymetry, erosion and sea level changes may act as subsidiary controls in the post-drift phase.

In evaluation of basement subsidence within the Natal Valley province, detailed 'backstripping' studies (Steckler and Watts, 1978; Guidish et al, 1984) involving the progressive unloading of

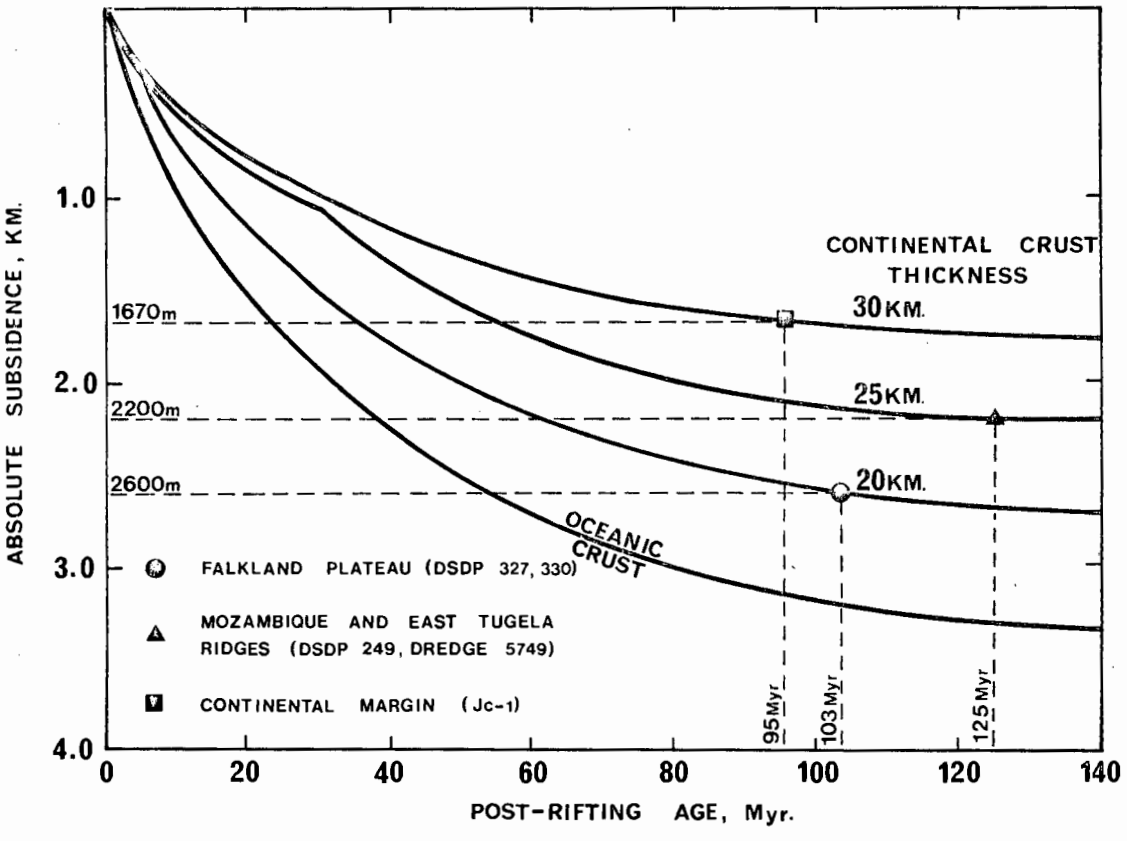

Fig.5.17 ABSOLUTE SUBSIDENCE-TIME CURVES FOR OCEANIC AND CONTINENTAL LITHOSPHERIC COLUMNS OF 30, 25 AND 20 KM. CRUSTAL THICKNESS

(modified after Kinsman, 1975)

Table 5.5 Apparent Basement Subsidence at DSDP, Dredge and Seismic Sites in the Southwest Indian Ocean and Falkland Plateau

Site	Lat/ Long	Water Depth (m)	Sediment Thickness (m)	Sediment Correction (m)*1	Marker Horizon Corrected Depth (m)*2	Marker Horizon Stratigraphic Zone or Datum	Rapid Subsidence Initiation Age (Myr)	Crustal Thickness (km)	Average Subsidence rate (m/my)	Marker Horizon Comments
Mozambique Ridge										
249	29°57'S 36°05'E	2088	408	265	2353	West Gondwana rift	125*7	25	18.8	Vesicular basalt extruded in a shallow water environment
East Tugela Ridge										
5749	29°15'S 33°39'E	2300	-	-	2300	West Gondwana rift	125*7	?25	18.4	Vesicular, quenched basalt extruded in shallow water
Continental Shelf										
Jc-1	29°28'S 31°36'E	72	2203	1542	1614	Cenomanian/ Turonian	95*8	30	17.0	Base of claystone unit resting unconformably on Dwyka tillite *3
Falkland Plateau										
327	50°52'S 46°47'W	2400	325	228	2628	Aptian/Albian	103	-	25.5	Top of shallow water euxinic black shale facies *6
330	50°55'S 46°53'W	2626	200	140	2766	Aptian/Albian	103	-	26.9	Top of shallow water euxinic black shale facies *6
Deep Ocean Basin										
AII93-5*4	30°22'S 33°30'E	2888	2400*5	1680	4568	~West Gondwana rift	~125*7	-	-	Seismically identified acoustic basement

Data are from Simpson, Schlich et al (1974), Detrick et al (1977), Darracott (1974), Barker, Dalziel et al (1976), du Toit and Leith (1974) and this study

*1 After the method of Parsons and Sclater (1977) assuming a sediment velocity of 2.0 km/sec and density of 1.7 g/cm^3.

*2 Marker horizon depth isostatically corrected for sediment loading effect, as calculated in *1.

*3 Marker horizon taken as the base of a claystone facies, assumed to have been deposited in relatively shallow water, which unconformably overlies continental Dwyka tillites (du Toit and Leith, 1974).

*4 Seismic profile retrieved during cruise R.V. Atlantis II 93-5.

*5 Sediment thickness measured from seismic profile assuming a sediment velocity of 2.0 km/sec.

*6 Shallow water environment of this facies inferred from nearby DSDP site 511 (Ludwig, Krasheninnikov et al, 1980).

*7 It is assumed that rapid subsidence of these continental or transitional basement zones was initiated after the West Gondwana rift, dated at ~125 Myr (this study, section 5.3.4).

*8 Subsidence was probably initiated prior to this age. This is, however, the oldest datum age from which subsidence can be calculated.

the sedimentary and water columns are inappropriate with the existing data base. Sea level curves for SE Africa and tight stratigraphic control in the Natal Valley are required to justify 'backstripping' projects but have not been sufficiently refined to date. In addition, the borehole data necessary to establish porosity and density gradients have not yet been released by SOEKOR.

However, in a preliminary attempt to estimate basement subsidence, the less sophisticated approach of Parsons and Sclater (1977) has been employed. Using drillsite, dredge and seismic reflection data, absolute subsidence rates for several Natal Valley provinces have been calculated and are compared to generalised subsidence models (Kinsman, 1975; Parsons and Sclater, 1977). Pertinent data are listed in Table 5.5. Subsidence-time curves are presented in Figure 5.17.

On the Mozambique Ridge, DSDP 249 bottomed in vesicular glassy basalt indicating that extrusion probably took place in a shallow marine environment (Thompson et al, 1978; Viswanatha Reddy et al, 1978; section 4.5.2). Because of its ?continental origin (section 5.5.3), Mozambique Ridge subsidence should be compared to continental crust subsidence models (e.g. Kinsman, 1975). The corrected basement depth of 2353 m at DSDP 249 (Table 5.5) compares closely to the expected subsidence (2200 m) using the 25 km curve (Fig.5.17). In agreement with gravity models (Scrutton, 1976), these calculations suggest that the Mozambique Ridge is a thinned (25 km) continental fragment rather than an oceanic crust plateau. Application of oceanic crust subsidence curves to the Mozambique Ridge has proved unsuccessful (Detrick et al, 1977). Nevertheless, the subsidence history of the Mozambique Ridge is yet unresolved and may have included periods of tectonic uplift. Subsidence calculations (average 18,5 m/my)

must therefore only be considered as absolute, disregarding periods of stability or uplift.

Retrieval of vesicular basalts with quenched plagioclases from dredge 5749 (section 5.4.3) implies a shallow marine extrusive formation for the East Tugela Ridge (Bryan, 1974; Viswanatha Reddy et al, 1978). Vesicle volume (15%) and size (up to 1 cm) confirms a relatively shallow water origin (Moore and Schilling, 1973). Assuming a 25 km thick transitional crust for the East Tugela Ridge, there is excellent correspondence between the measured (2300 m) and expected (2200 m) absolute subsidence (Fig.5.17 and Table 5.5).

Subsidence calculations for the east coast continental margin basement rely on data from borehole Jc-1 (du Toit and Leith, 1974). After correction for sediment loading, the computed depth (1614 m) for the Cenomanian/Turonian marker horizon (Table 5.5) closely matches the expected subsidence (1670 m) derived from Figure 5.17 (30 km thick crust; 95 my subsidence period). This implies that basement on the continental margin bordering the Natal Valley has subsided at normal continental crust rates (Kinsman, 1975).

Data from DSDP 327 and 330 (Barker, Dalziel et al, 1976) are used to compute basement subsidence for the Falkland Plateau. Rapid subsidence, related to final separation of the Falkland Plateau and African continent, is considered to have commenced in the Late Aptian/Early Albian (Ciesielski and Wise, 1977). After correction for sediment loading, absolute subsidences of the marker horizon at sites 327 and 330 are computed as 2628 m and 2766 m respectively (Table 5.5), relatively similar to the expected subsidence (2600 m) derived from Figure 5.17 (20 km thick crust; 103 my subsidence period). It may be tentatively concluded that the Falkland Plateau crust is excessively thin (~

20 km). Such a conclusion is geologically feasible since the Falkland Plateau was probably strongly influenced by a protracted heating, uplift and erosional phase, with resultant enhancement of crustal thinning, induced by East/West Gondwana separation and also West Gondwana fragmentation (section 4.5). Pre-drift crustal stretching may also have thinned the Falkland Plateau crust.

Subsidence calculations have been applied to one oceanic crust site (seismic profile AII93-5). Crust formation in this southern zone of the deep basin must have closely followed commencement of West Gondwana fragmentation and has thus been assigned an age of 125 Myr. After correction for loading, the basement depth (4568 m) is approximately 1500 m shoaler than expected from its age of formation on comparison to the oceanic crust subsidence curve of Parsons and Sclater (1977). Two factors may be combining to explain this discrepancy: (1) oceanic crust in the Natal Valley comprises a narrow enclave bordered on three sides by relatively buoyant continental blocks. Incomplete decoupling of continental and oceanic crust may be effectively hindering oceanic crust subsidence; and (2) formation depth of Natal Valey oceanic crust may have been much shoaler than crust generation depths invoked in the Parsons and Sclater (1977) model.

Seismic reflection profile data show basement to lie at a much greater depth under the Tugela Cone relative to the Central Terrace, even though both provinces are considered to be floored by equivalent crustal types (Fig.5.14). Extreme sediment loading over the Tugela Cone has probably caused the greater apparent subsidence in this area.

5.5.7 Mozambique Ridge Micro-Plate Movement

The tectonic regime responsible for creating the present day distribution of crustal blocks in the Natal Valley has not previously been considered in detail (Dingle and Scrutton, 1974; Scrutton, 1976; Dingle, 1979). In summary, these authors conclude that a rifted margin segment trending approximately NW-SE from the vicinity of Durban separates continental crust to the north from oceanic crust. To the south of the rifted margin, transform motion along the Agulhas Fracture zone (Francheteau and Le Pichon, 1972) and the west side of the Mozambique Ridge (Scrutton, 1976) enabled severance of the Falkland Plateau from SE Africa. The Mozambique Ridge has been denoted a stationary location throughout the early Gondwana fragmentation history.

With improvement in definition of major tectonic boundaries in the Natal Valley (section 5.5; Fig.5.14), several lines of evidence suggest that the Mozambique Ridge may now be situated approximately 160 km east of its pre-drift Gondwana palaeoposition. There is strong morphological similarity between the Falkland Plateau/Tugela Cone eastern margin and the Mozambique Ridge western margin (Martin et al, 1981). Possibility of Mozambique Ridge movement relative to Africa was first suggested on this physiographic similarity. Moreover, in several West Gondwana reconstructions (Scrutton, 1973b; Barker, Dalziel et al, 1976; Rabinowitz and LaBrecque, 1979), there is a consistent but untenable ~160 km wide gap between the Mozambique Ridge and Falkland Plateau/Tugela Cone continental blocks. Suspicion that the narrow enclave between the Tugela Cone and Mozambique Ridge is floored by oceanic crust (section 5.5.4) necessitates a sea-floor spreading phase to explain its origin.

In formulating a best morphological fit between the Mozambique Ridge and Falkland Plateau/Natal Valley continental

Figure 5.18

Speculative Pre-Drift and Post-Drift Configurations of the Major Continental Blocks within the Natal Valley

(a) Pre-Drift:

Reconstruction of major continental crust blocks within the investigation area. Falkland Plateau location and COB from the revised West Gondwana refit of Martin et al (1981). Natal Valley COB speculatively defined as the continuous lineament of marginal ridges (approximate to the present day 2500 m isobath). Mozambique Ridge COB taken as the 4,3 sec basement isochron (Fig.5.1), which approximates the change from rugged to smooth acoustic character.

Reconstruction achieved as a best morphological fit constrained by strike of fracture zones (basement morphology) and attitude of the SE Naude non-magnetic fracture ridge. Reconstruction gap is denoted by shaded zone.

(b) Post-Drift:

Present day configuration of continental blocks showing location of fracture zones, marginal ridges, the non-magnetic fracture ridge and direction of continental block movement relative to the African plate.

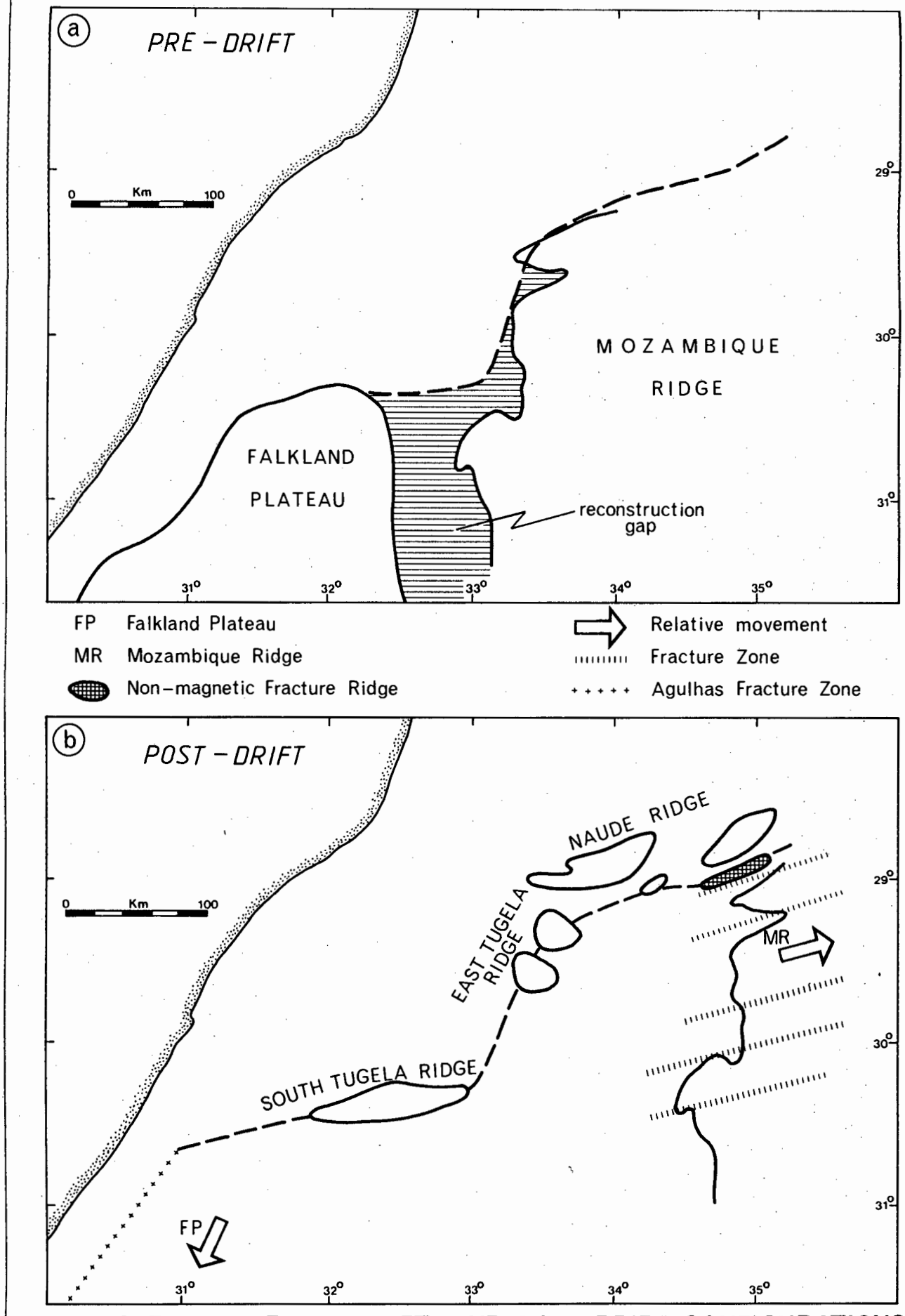

Fig. 5.18 SPECULATIVE PRE-DRIFT AND POST-DRIFT CONFIGURATIONS OF THE MAJOR CONTINENTAL BLOCKS WITHIN THE NATAL VALLEY

blocks, emphasis is placed on the zone between 29°S and 31°S where seismic profiling has provided control on location of the COB (Figs.5.14 and 5.18). Constraint on rotation and reconstruction is provided by the trend of fracture zones on the Mozambique Ridge western flank (Fig.5.18b). These fracture zones are delineated by deep valleys on the acoustic basement surface (Fig.5.1) and the ~NE-SW trend of magnetic lineaments (Fig.5.4). The most southerly of the fracture zones (Fig.5.18b) is clearly delineated by 'necking' of a N-S magnetic anomaly at 30° 20'S (Fig.5.4). Basement exposure is common along the Mozambique Ridge eastern flank and thus bathymetric offsets on this margin (Dingle et al, 1978) are likely additional indicators of fracture zones.

Contemporaneous volcanism related to transform motion is postulated to have constructed the Naude Ridge basement complex. Of basement highs in this complex, only the elongate SE ridge has no associated topography-generated positive magnetic anomaly (Figs.5.1 and 5.4). Magnetic modelling (section 5.3.3) is best satisfied by assigning a non-magnetic character to the narrow basement block centred on this ridge (Fig.5.6). This elongate non-magnetic ridge parallels the fracture zones (Fig.5.18b) and shows close physical similarity to the non-magnetic Agulhas Marginal Fracture Ridge formed during transform motion between the Falkland Plateau and SE Africa (du Plessis and Simpson, 1974). Rabinowitz et al (1976) have postulated that transform tectonics may create a 'core' of non-magnetic basement 50 km wide in which magnetisation is destroyed by intense shearing. By analogy, transform tectonics may provide a plausible model to explain both the fracture zones and the parallel non-magnetic fracture ridge (Fig.5.18) within the Naude Ridge/Mozambique Ridge province.

A good reconstruction within the Natal Valley is achieved on 160 km rotation of the Mozambique Ridge towards the African continent along the fracture zone trend (72° west of south; Fig.5.18a). Because of its association with the fracture ridge, the northernmost fracture zone (approximately 29°S) is considered the major translation domain and is utilised to contain the full 160 km rotation. South of 30° 15'S, a 50 km wide gap exists in the reconstruction, assuming the Mozambique Ridge to have moved as a single unit (Fig.5.18a). Existence of minor fracture zones (Fig.5.18b) may imply local translation within the Mozambique Ridge. Movement of subsidiary blocks could eliminate inherent gaps in the refit of Figure 5.18a. As a cross-check on validity of the reconstruction, the full length of the Mozambique Ridge is rotated against the Falkland Plateau using the S72°W fracture zone trend (Fig.5.19). This morphologic fit, using the Mozambique Ridge 2500 m and Falkland Plateau 2740 m isobaths to define the COB, provides a relatively good reconstruction and thus strengthens the suggested micro-plate movement scheme.

Accepting that the Mozambique Ridge pre-drift palaeoposition was closer to Africa, it is possible to improvise a tectonic regime capable of producing the present day Natal Valley distribution of oceanic and continental crust. A plausible but non-unique scheme is outlined in Figure 5.20. This displays known structural elements (Fig.5.18) allied to a feasible distribution of spreading ridge and fracture zone segments. Existence of a stable RRR triple junction south of the South Tugela Ridge (Fig.5.20) is necessary to accommodate coalescence of the three spreading arms.

Major problems are evident in hypothesising a tectonic regime to exist as depicted in Figure 5.20. The enclave of crust between the East Tugela Ridge and the Mozambique Ridge has not

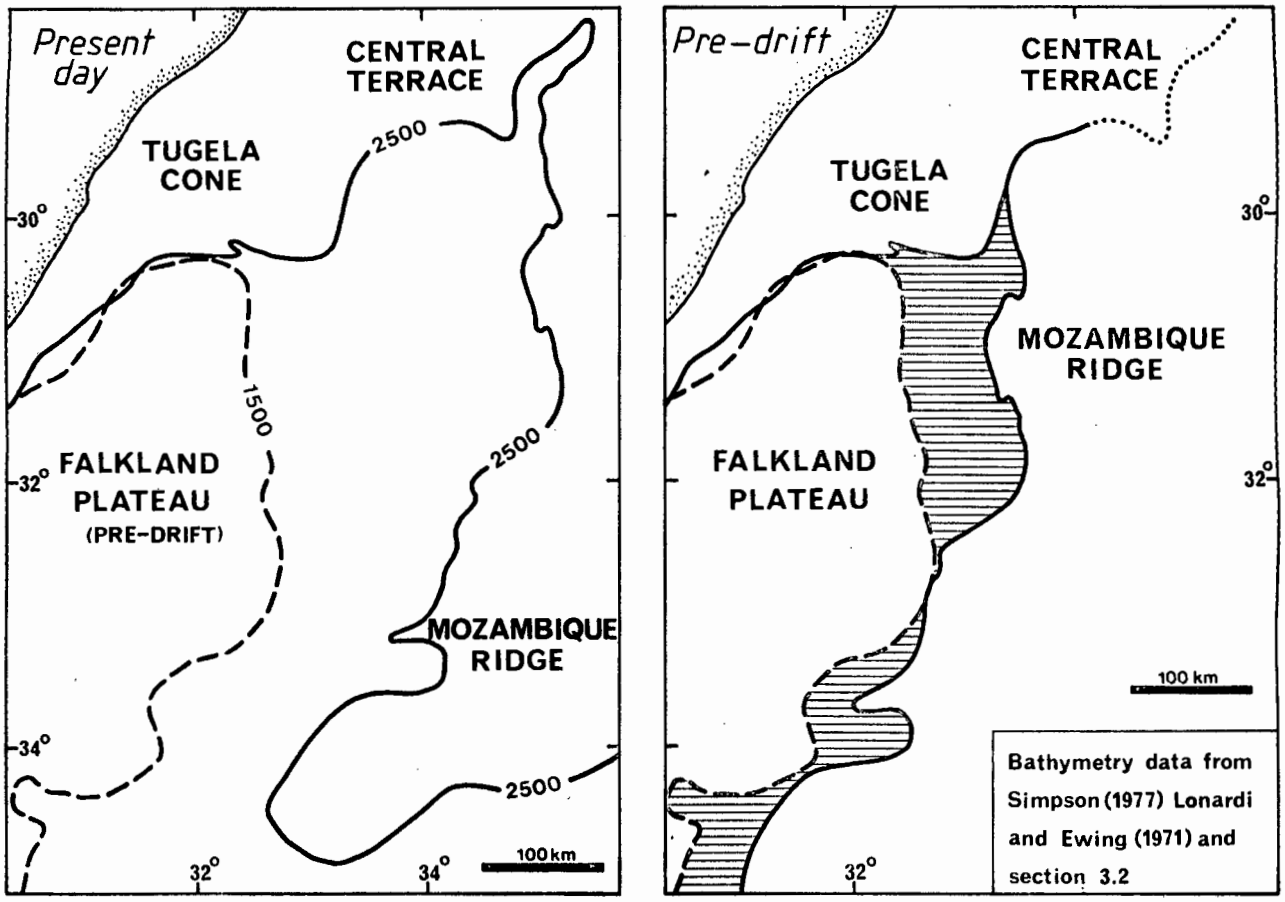

Fig.5.19 MORPHOLOGICAL FIT OF THE MOZAMBIQUE RIDGE (2500m ISOBATH), NATAL VALLEY CONTINENTAL MARGIN (2500m ISOBATH) AND THE FALKLAND PLATEAU (1500 FM. ISOBATH).

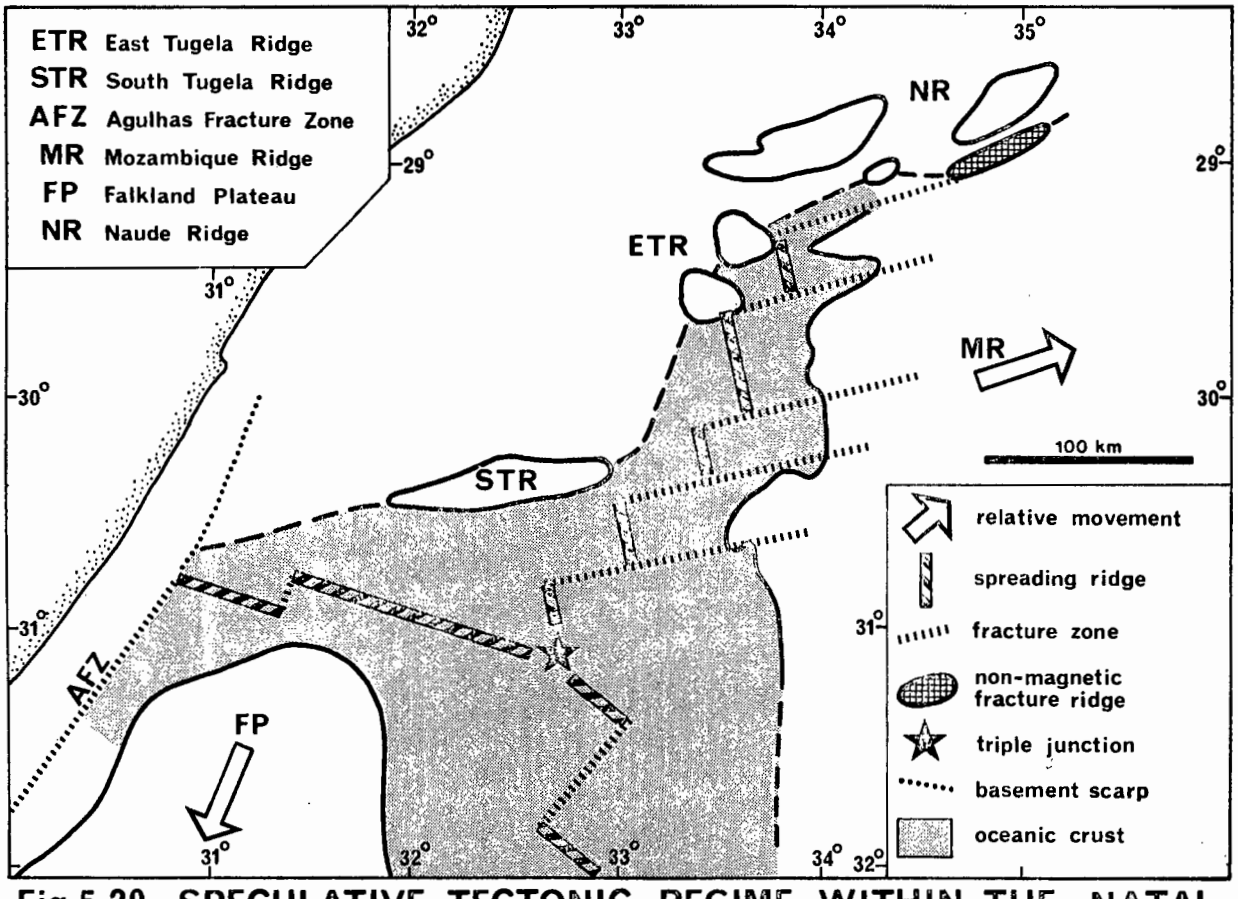

Fig.5.20 SPECULATIVE TECTONIC REGIME WITHIN THE NATAL VALLEY – EARLY SOUTHWEST GONDWANA POST-DRIFT PHASE

been conclusively proven to be of oceanic origin. Available seismic reflection profiles do not have sufficient penetration to substantiate the presence of fossil spreading ridges, with one exception perhaps being the double basement ridge (0,5 sec relief) at 30° 50'S, 34° 15'E (Fig.5.1). Magnetic data are also of minor use, especially in the enclave north of 30°S, where the suspected close proximity of fracture zones and spreading ridges would have rendered spreading lineaments unrecognisable. South of 30°S and east of the Falkland Plateau Gondwana palaeoposition, possible NW-SE lineation is recognised although no symmetry is perceived.

A readjustment of tectonic elements is implied on termination of eastward Mozambique Ridge motion. Following the failed rift-arm model of Dewey and Burke (1974), the triple junction ceased to be active on extinction of the NE spreading arm. The SE arm altered from a ridge/transform section to a single, straight transform fault on decoupling of the Falkland Plateau continental block and newly-formed oceanic crust to the east.

Mozambique Ridge relative eastward movement must have strongly influenced tectonic evolution of its eastern margin. In a model of Antarctica/Africa fragmentation, it is necessary to invoke existence of a 'hole' into which the Mozambique Ridge could move. A simple schematic model is outlined in Figure 5.21. Transposing the Mozambique Ridge to its presumed pre-drift Gondwana palaeoposition would effect a 160 km offset on its eastern margin (Fig.5.21a). Some equivalent offset is likely to exist on the Princess Martha Land coast of Antarctica, juxtaposed to the Mozambique Ridge in Gondwana reconstruction (Norton and

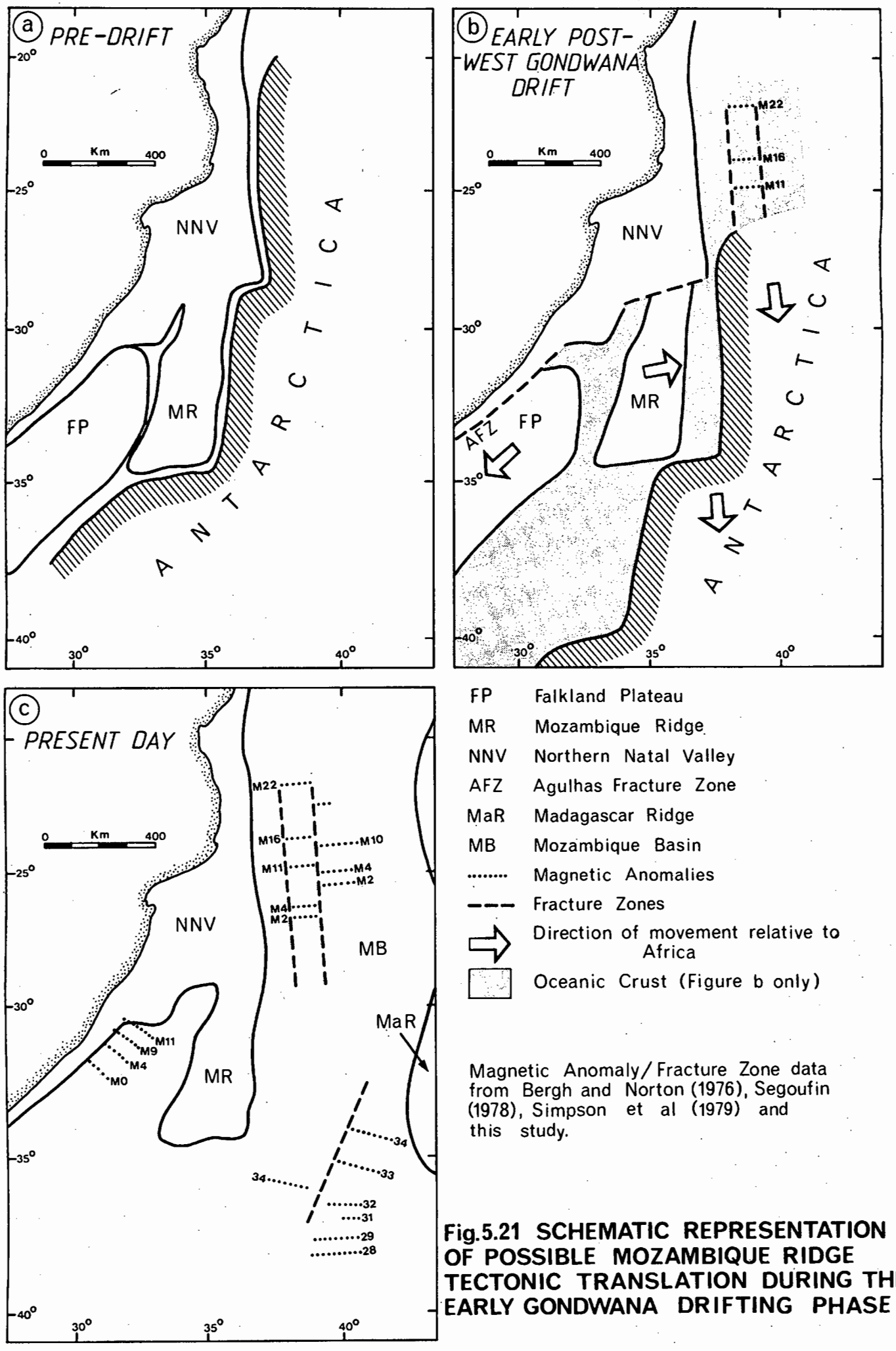

Magnetic Anomaly/Fracture Zone data from Bergh and Norton (1976), Segoufin (1978), Simpson et al (1979) and this study.

Fig.5.21 SCHEMATIC REPRESENTATION OF POSSIBLE MOZAMBIQUE RIDGE TECTONIC TRANSLATION DURING THE EARLY GONDWANA DRIFTING PHASE

Sclater, 1979).

Following break-up of East/West Gondwana around 150 Myr (Bergh, 1977), Antarctica diverged from Africa constrained by trends of fracture zones and magnetic lineaments (Segoufin, 1978; Simpson et al, 1979) within the north Mozambique Basin (Fig.5.21b). By anomaly M16 time Antarctica would have been far enough south to have generated a zone of oceanic crust equivalent in width to the original offset of the Mozambique Ridge (Fig.5.21b). Using the polarity time-scale of Larson and Hilde (1975), this event is dated at 135 Myr. Early Cretaceous West Gondwana rifting (Rabinowitz and LaBrecque, 1979) initiated formation of new oceanic crust in the Natal Valley as the Falkland Plateau diverged from SE Africa, generating a series of NW-SE trending magnetic anomaly lineations (section 5.3.4 and Fig.5.21c). As evidenced by large scale graben formation (sections 4.4 and 4.5) and Lebombo fissure volcanism, SE Africa was characterised by an E-W tensional stress field (Sowerbutts, 1972) during the pre-drift phase of Gondwana fragmentation. Mozambique Ridge translation may have taken place under this E-W tension as a response to additional crustal stress induced by West Gondwana break-up.

5.5.8 Tectonic Status of the Northern Natal Valley

Further attention has been focussed on the plate tectonic status of the northern Natal Valley and Mozambique Ridge by Martin and Hartnady (1983) who have proposed a revised reconstruction of Antarctica and Africa by abutting East Antarctica against the Lebombo Mountains. This new refit is constrained by published magnetic anomaly and fracture zone

trends. In one alternative, the Mozambique Ridge is assumed to be oceanic in origin removing the need for its inclusion in the reconstruction. In another option, the microplate is considered to be continental and on reconstruction is placed into the Nuanetsi region of Zimbabwe/Mozambique on morphological fit alone. Whichever version is favoured, the northern Natal Valley must be underlain by oceanic crust.

The new reconstruction considers several important factors to accurate refitting of East Antarctica and Africa. However, it can only be regarded as speculative for Martin and Hartnady (1983) are not able to present any evidence to support the hypothesis that the northern Natal Valley is in fact underlain by oceanic crust. Major points of contention in their hypothesis include:

(1) despite numerous magnetic surveys in the northern Natal Valley, spreading anomalies equivalent to those of the Mozambique Basin have not been delineated. Over the southern Central Terrace the prevalent magnetic grain is N-S (Fig.5.4; see good N-S correlation between E-W profiles at 28^{o}S, $34^{o}30'$E in Fig.5.5) which is inconsistent with the spreading history outlined by Martin and Hartnady (1983);

(2) there is no geophysical evidence to support the existence of a major transform fault along the eastern margin of the Tugela Cone;

(3) basement rocks of the East Tugela Ridge (dredge site 5749) are transitional in character but with strong continental affinities (section 5.4.4; Fig.5.13). In the refit of Martin and Hartnady (1983), the East Tugela Ridge is inadmissibly overlapped by East Antarctica;

(4) the Lebombo region has long been considered a pre-drift-onset tensional zone (King, 1972) as evidenced by widespread graben formation in southern Mozambique (Flores, 1973);

(5) northern Natal Valley crust is intermediate in thickness (Darracott, 1974), and if floored by oceanic crust, a model for abnormal oceanic crust thickening must be invoked. Martin and Hartnady (1983) offer no suggestions for such a mechanism. Crustal thinning during rift-phase tectonism to produce attenuated continental crust provides a satisfactory model to explain the intermediate thickness (section 4.5.2);

(6) Martin and Hartnady (1983) do not discuss the significant change in basement structure between the northern and mid Natal Valley. North of the Naude Ridge, basement is shallow (2,2 km) and the crust is of intermediate thickness (24-27 km). To the south, thinner crust (10-12 km) has subsided to much greater depths (>5 km). If the Natal Valley is entirely floored by oceanic crust, it is difficult to account for this significant change in structural style, whereas such a change would be expected if the Naude Ridge complex marks the transition from attenuated continental to oceanic crust (Fig.5.14);

(7) multi-channel seismic data across the northern Natal Valley (Beck and Lehner, 1974) indicates that acoustic basement is in seismic continuity with onshore Lebombo Group volcanics. In addition, extension of the Lebombo Group under the Mozambique coastal plain is proven by borehole data (Flores, 1973; Dingle et al, 1983) and it can be inferred that a massive sequence of Karoo volcanics are draped over basement in these areas (Fig.45 of Dingle et al, 1983). With this volcanic pile being dated at 190-

137 Myr (Flores, 1973; Cleverly and Bristow, 1979), it is difficult to envisage a mechanism to emplace oceanic crust (145 my old) beneath such an overlying sequence (i.e. older sequence overlying younger crust) as required by the Martin and Hartnady (1983) model.

These seven points of contention taken together strongly argue against an oceanic crustal status for the northern Natal Valley, severely weakening the case for a refit of East Antarctica against the Lebombo Mountains as proposed by Martin and Hartnady (1983). All seven points can be resolved if it is assumed that the northern Natal Valley and Mozambique Ridge (north of 35^{o}S) are underlain by attenuated continental crust as suggested in section 5.5.3. Accordingly, I support reconstructions which retain the continental status of the northern Natal Valley and in which East Antarctica is abutted against the Mozambique Ridge (e.g. Norton and Sclater, 1979).

CHAPTER 6 SEISMIC STRATIGRAPHY OF THE BASIN FILL

6.1 INTRODUCTION

Previous geophysical studies off the SE African margin have concentrated on crustal structure (e.g. Darracott, 1974; Dingle and Scrutton, 1974) and gross sediment thickness and distribution (e.g. Kidd and Davies, 1978; Dingle, 1979). Published details on the acoustic stratigraphy of the mid Natal Valley basin fill are restricted to the preliminary account of Dingle et al (1978) and expanded by Goodlad (1979).

A data base comprising 10 470 km of single channel seismic profiles (Fig.6.1) are used in this study to establish a seismic-stratigraphic framework. Of these profiles, 60% (6230 km) are located with satellite accuracy. Profile coverage and navigational quality are shown in Figure 6.1. Poorly-navigated tracks have been adjusted to fit the accurate framework of satellite-navigated traverses. Data reduction procedures and details of seismic hardware are summarised in Appendix A2.

In this chapter, the seismic profile data base is compiled with existing offshore borehole and hinterland stratigraphic data to lay basis for a review of the seismic stratigraphy of the mid Natal Valley. Reference reflectors are defined and the configuration, seismic character and time-thickness of the major sediment units and sub-facies are described and discussed. Depositional styles and systems in the basin fill are reviewed and sedimentation rates and budgets are evaluated. Time-depth palaeobathymetry maps of the major depositional sequence boundaries allow basin geometry development to be assessed.

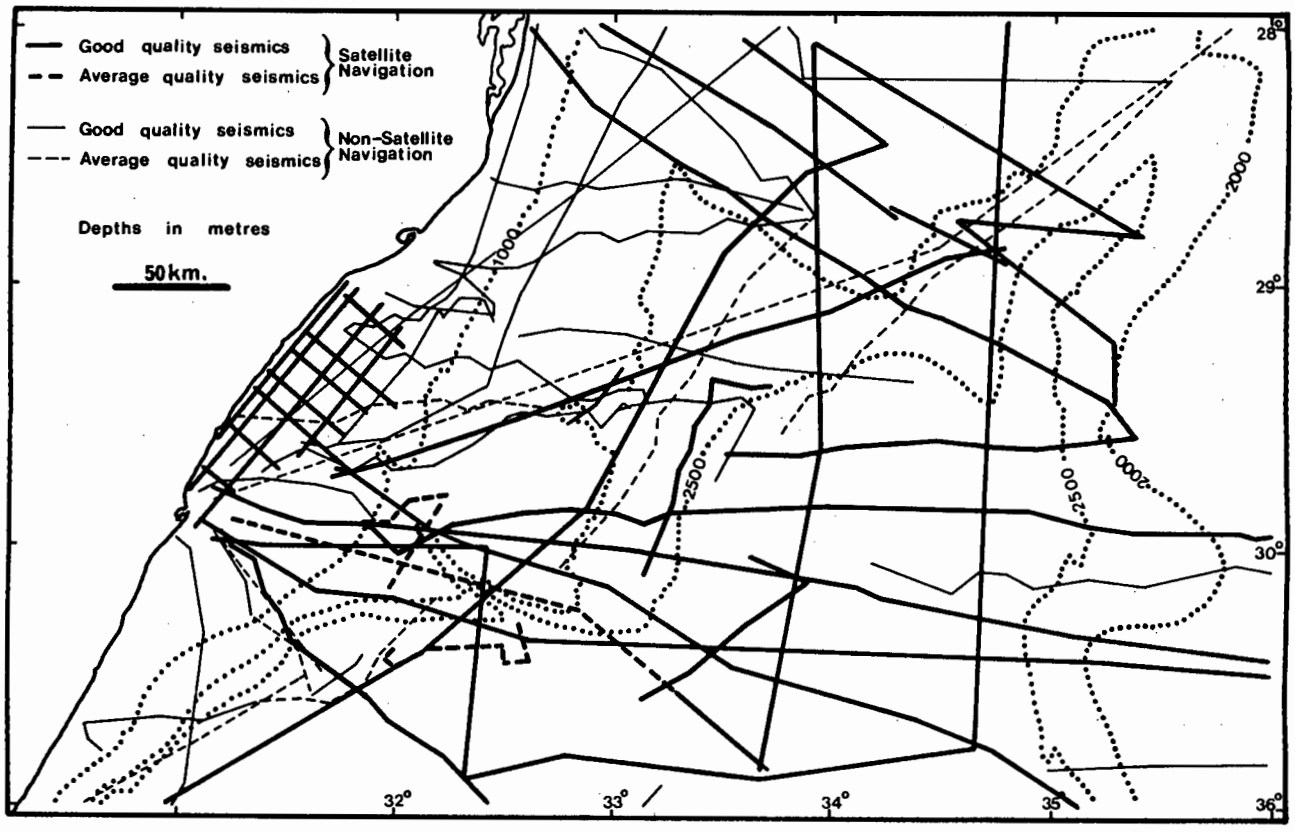

Fig. 6.1 CONTINUOUS SEISMIC PROFILE COVERAGE

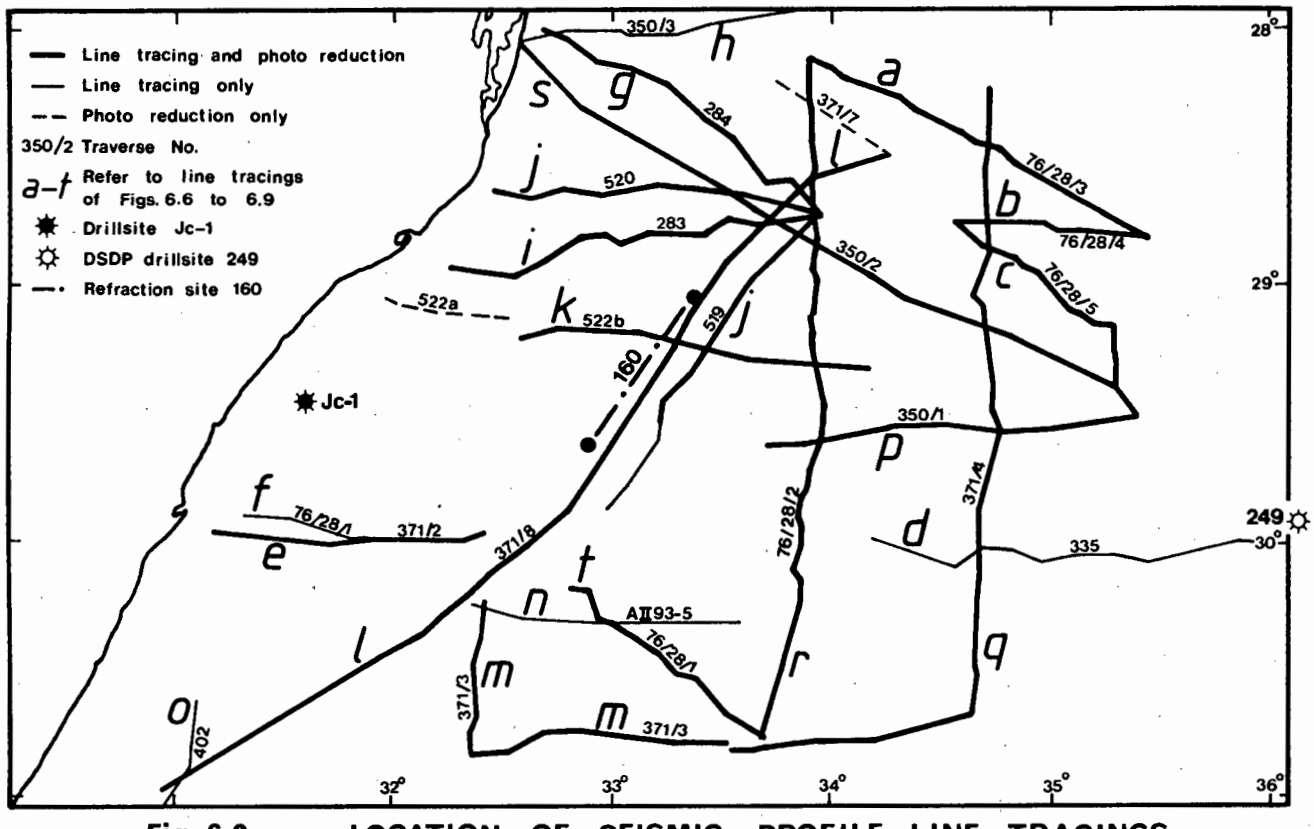

Fig. 6.2 LOCATION OF SEISMIC PROFILE LINE TRACINGS AND PHOTOGRAPHIC REDUCTIONS

6.2 REFERENCE REFLECTOR AGE AND CORRELATION

6.2.1 Introduction

Acoustic stratigraphy of the mid Natal Valley may be conveniently described with reference to three regionally-developed reflecting horizons (McDuff, Angus and Jimmy) and acoustic basement. The stratigraphic significance of these regional reflectors is confirmed through comparison with the onshore Cretaceous and Tertiary succession (Kennedy and Klinger, 1971; Flores, 1973; Forster, 1975; Dingle, 1978; Siesser and Miles, 1979; McLachlan and McMillan, 1979), borehole Jc-1 (du Toit and Leith, 1974), DSDP 249 (Simpson, Schlich et al, 1974) and recently-recovered sea floor samples. Additional control is provided by seismic refraction sites (Ludwig et al, 1968). Locations of the drillsites and refraction sites are shown in Figure 6.2. A tentative correlation of east coast lithostratigraphic units and hiatuses derived from borehole and seismic data is presented as Figure 6.3.

6.2.2 McDuff

Reflector McDuff has been equated (Dingle et al, 1978) with a major seismic horizon which abuts continental basement 7 km east and 0,25 secs stratigraphically below the base of Jc-1 (Fig.6.3, column 2). McDuff is therefore considered to pre-date the Jc-1 basal Cenomanian/Turonian sediments. Farther east, Ludwig et al (1968) identify a strong velocity discontinuity between 2 and 4 km/sec units at refraction site 160, close to the projected depth of McDuff, under the east Tugela Cone. Pre-McDuff sediments may therefore be characterised by a high seismic

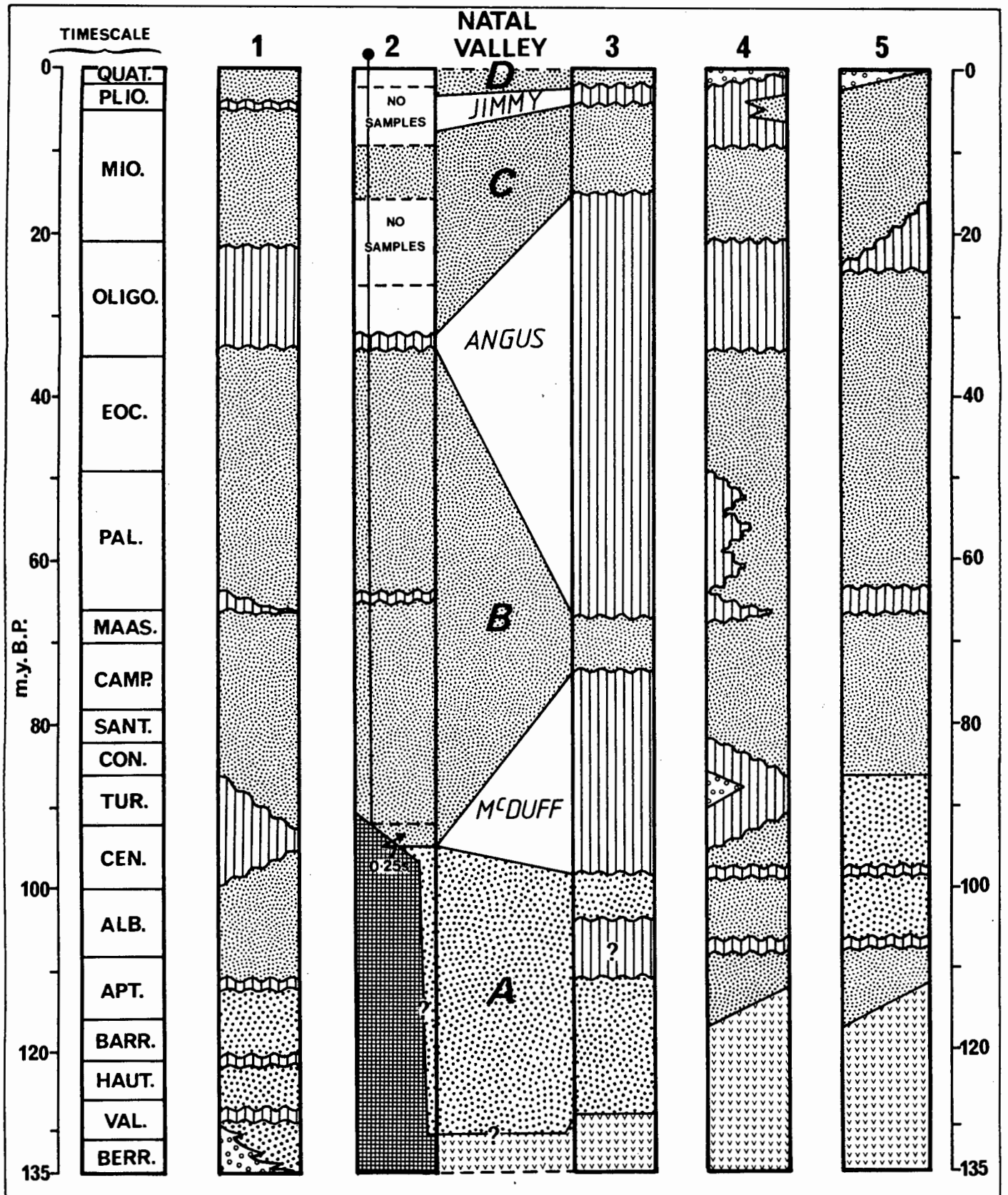

Composite data are from du Toit and Leith (1974), Flores (1973), Simpson, Schlich et al (1974), Forster (1975), Dingle et al (1978), Dingle (1978) and McLachlan and McMillan (1979)

volcanic basement
continental basement
open marine sediments
euxinic marine sediments
continental sediments

1 Outeniqua Basin
2 Continental Shelf (Durban)
3 Mozambique Ridge (DSDP 249)
4 SW Mozambique (Maputo)
5 SE Mozambique (Zandamela/ Domo)

drillsite Jc–1
0·25s. see text
hiatus
A–D sediment units (see text)

Fig. 6.3 TENTATIVE EAST COAST LITHOSTRATIGRAPHIC CORRELATION

velocity. Although direct correlation to DSDP 249 on the Mozambique Ridge is impossible (intervening basement exposure), a prominent reflector with very similar characteristics to McDuff marks a 30 my hiatus between Cenomanian ash-rich euxinic silts and Campanian open-marine nanno-chalk (Simpson, Schlich et al, 1974). In SW Mozambique and Zululand, a conspicuous Late Cenomanian - Late Coniacian hiatus (Kennedy and Klinger, 1971; Dingle, 1978) is probably the lateral equivalent of McDuff. In SE Mozambique, a distinct end-Turonian facies change from euxinic shales to open-marine silty sandstones (Flores, 1973) has been correlated with a similar Mozambique Ridge post-McDuff lithological change (Girdley et al, 1974). Within the Outeniqua Basin (Agulhas Bank), an hiatus of Cenomanian-Turonian duration (McLachlan and McMillan, 1979) is analogous to McDuff (Fig.6.3).

6.2.3 Angus

Age definition of horizon Angus is inexact, but best correlation is achieved on comparison with borehole Jc-1. A prominent base Oligocene unconformity and hiatus, separating deltaic sands from shallow marine clays in the Jc-1 borehole (du Toit and Leith, 1974), closely corresponds to a major reflector which merges with horizon Angus when traced seaward. This early Oligocene hiatus has been correlated (Fig.6.3) with an equivalent Mozambique Ridge hiatus which separates Maastrichtian nanno-chalk from Miocene foram-rich nanno ooze in DSDP 249 (Simpson, Schlich et al, 1974). Micropalaeontological dating of samples from the Angus-Jimmy sequence (D.S. Salmon, pers.comm., 1980) has confirmed that reflector Angus is at least older than Early Miocene and may thus be Oligocene in age. Oligocene hiatuses

have been reported in the successions of SW Mozambique and Zululand (Flores, 1973). In contrast, in SE and E Mozambique and the Mozambique Channel, the Oligocene is complete (Fig.6.3) although an Early Miocene hiatus is developed (Forster, 1975). Strong Oligocene hiatuses have been recognised over the eastern Outeniqua Basin (McLachlan and McMillan, 1979) and in abyssal basins around South Africa (Tucholke and Embley, 1984) confirming the regional importance of the Angus event.

6.2.4 Jimmy

Pre-Jimmy strata are extensively exposed over current-scoured areas in the Natal Valley. Micropalaeontological dating of pre-Jimmy sediments retrieved from the sea floor constrain the hiatus age (Fig.6.4 and Appendix A5) with uppermost pre-Jimmy sediments being Late Miocene/Pliocene in age. As a sequence boundary to these strata, horizon Jimmy is postulated to be an early Pliocene event. A Middle-Late Pliocene hiatus associated with sediment reworking and condensed sequences at DSDP 249 on the Mozambique Ridge is proposed as a lateral equivalent of Jimmy (Fig.6.3). In onshore Zululand, a well-developed Pliocene hiatus (Siesser and Dingle, 1981) is equivalent to offshore hiatus Jimmy. Pre-Jimmy microfauna (Fig.6.4) show close affinity to the Zululand Neogene limestone microfauna described by Siesser and Miles (1979). Over the Outeniqua Basin, a widespread Pliocene hiatus (McLachlan and McMillan, 1979) verifies the regional importance of the Jimmy event. Late Tertiary hiatus definition is more confused in southern Mozambique. In SW Mozambique (Fig.6.3), sediments of Middle Miocene-Pliocene age are unknown (Forster, 1975) and this level of non-deposition may be

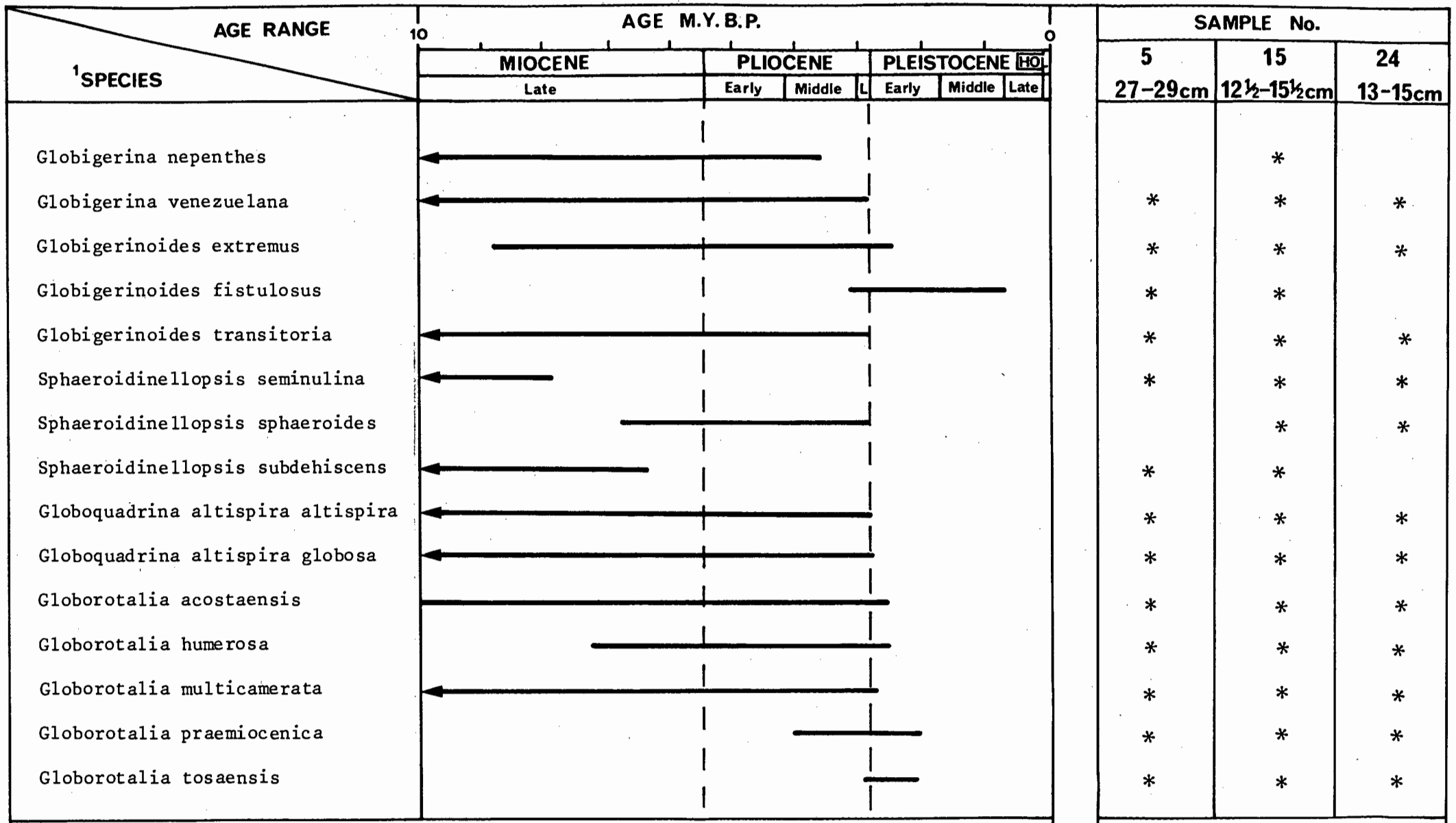

Fig. 6.4 REDUCED SPECIES LIST AND RANGES OF DIAGNOSTIC PLANKTIC FORAMINIFERA

correlative to hiatus Jimmy. In SE Mozambique however the Late Tertiary sequence is complete (Fig.6.3) and an equivalent to Jimmy is not developed.

6.3 DEPOSITIONAL SEQUENCE BOUNDARIES

6.3.1 Introduction

The reference reflectors (McDuff, Angus and Jimmy) and acoustic basement bound the major depositional sequences of the mid Natal Valley (Fig.6.3, sediment units A-D), and thus their seismic character and relationship to adjacent strata warrant brief description. Relationships between the seismic horizons and sediment units are illustrated in Figure 6.5. Seismic profiles are presented as line tracings (Figs.6.6-6.9) while photographic reproductions are contained in Appendix B3. Profile location is shown in Figure 6.2. All terminology is consistent with Mitchum et al (1977a; 1977b). A compilation of strata boundary relations and major prograding clinoform types is presented in Figure 6.10. Acoustic basement has already been discussed in sections 5.2 and 5.5.

6.3.2 Horizon McDuff

The acoustic character of horizon McDuff, a middle Cretaceous hiatus (section 6.2.2), is summarised in Figure 6.5a. McDuff is best developed on the Central Terrace where it terminates a sequence of dense, hyperbolic reflectors. In this area, McDuff is highly reflective and typically crenulated (Plate B3.3a; Fig.6.6a) marking a strong unconformity and major seismic facies change. Numerous normal and growth faults, which

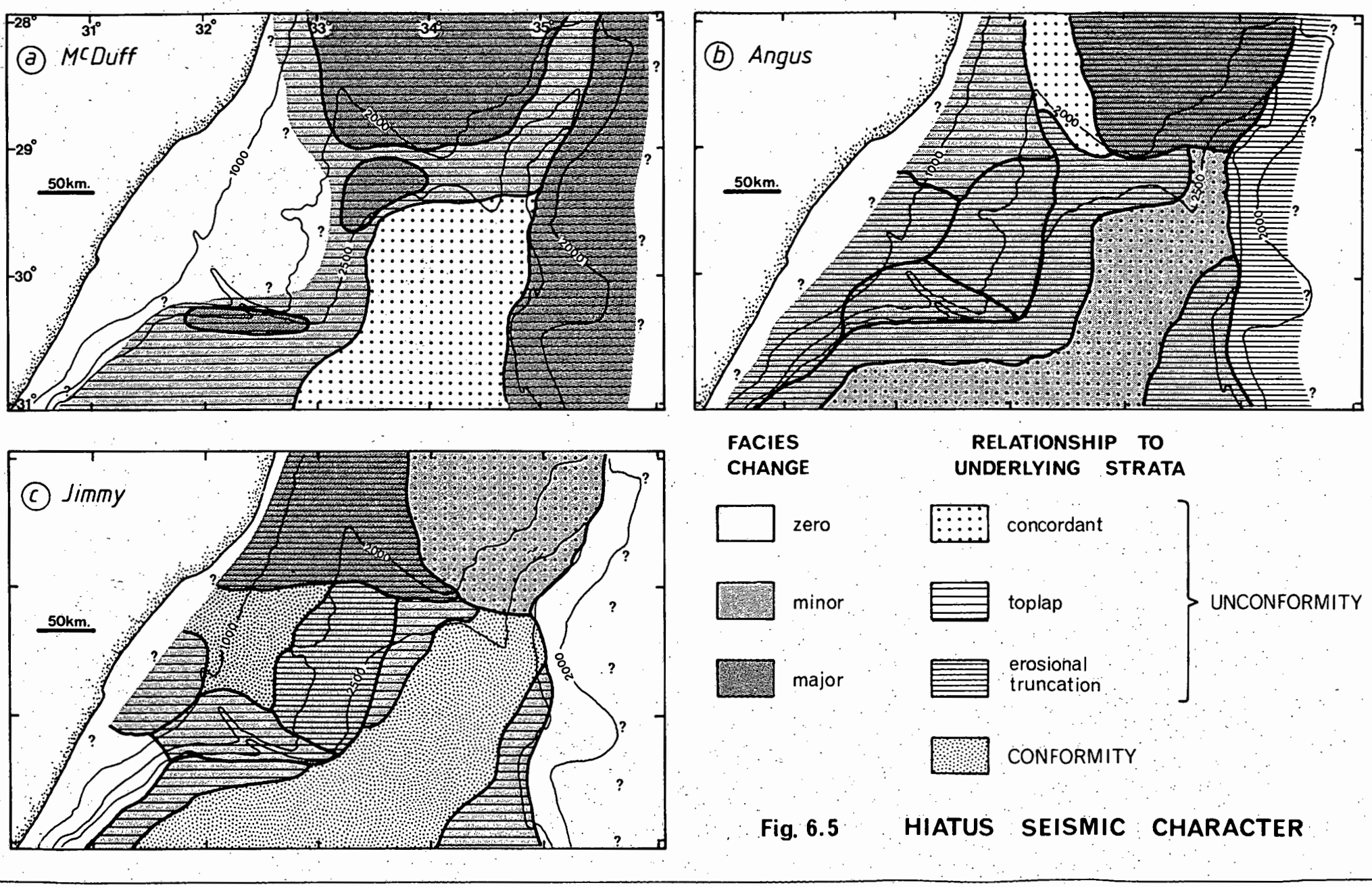

Fig. 6.5 HIATUS SEISMIC CHARACTER

downthrow a maximum of 0,3 secs (±300 m) to the east (Plate B3.1a; Fig.6.7i), extensively disrupt the McDuff surface. Horizon McDuff retains a moderately reflective, crenulated character adjacent to all basement ridges and high zones within the mid Natal Valley (Plate B3.4a; Fig.6.9r). In contrast, traversing onto the Tugela Cone, Mozambique Ridge crest and deep basin plain, McDuff rapidly loses its highly reflective character but remains a smooth, prominent reflector (Plate B3.3c; Fig.6.8m) with either concordant or toplap relationships to sediment unit A strata (Plate B3.2a; Fig.6.8l).

Horizon McDuff recurrently demonstrates both concordant and toplap stratigraphic relationships with pre-McDuff reflectors and therefore appears to represent a non-depositional hiatus with little associated erosional activity.

6.3.3 Horizon Angus

Horizon Angus, dated as Oligocene (section 6.2.3), is a prominent unconformity recognised over the majority of the mid Natal Valley basin (Fig.6.5b). Hummocky or irregular in character, horizon Angus erosionally truncates pre-Angus strata over the Central Terrace in all zones except the west. Pre-Angus strata locally outcrop over the southern Central Terrace (section 7.2). Structural configuration is more diverse over the Tugela Cone. North of 29° 15'S the pre-Angus sequence toplaps under a smooth reflector Angus (Fig.6.7g,h and i). Angus defines strong erosional truncation over the remainder of the Tugela Cone, particularly the upper slope (Figs.6.6e, 6.8l and m), where a wavy, hummocky or irregular acoustic signature is common. Over the deep basin plain, Angus loses its erosional character to

become a smooth, concordant horizon (Figs.6.5b and 6.8m). Adjacent to the basin plain margins, however, horizon Angus is locally erosional with a corrugated or hummocky signature (Fig.7.9t). This character is most pronounced in the SW deep basin (Fig.6.8o) where horizon Angus is sculptured into large mounds (1 km wavelength; 50 m amplitude). Horizon Angus cannot be identified in the acoustically-transparent pelagic facies of the Mozambique Ridge crest.

Angus heralds basin-wide seismic facies change except over the Mozambique Ridge crest. Facies transition is greatest over the Central Terrace (Plate B3.3a; Fig.6.6a). Compared to McDuff, Angus is less important as a level of seismic facies change but high incidence of reflector truncation confirms its association with strong erosive activity. Widespread erosion was probably initiated as a response to increased bottom water flow in the Oligocene (sections 7.2 and 7.3).

6.3.4 Horizon Jimmy

Horizon Jimmy, a prominent early Pliocene unconformity (section 6.2.4), is mappable over most physiographic provinces. Pre-Jimmy strata extensively outcrop over the Central Terrace and lower flanks of the Tugela Cone (section 7.2). Over the west Central Terrace, Jimmy is highly reflective and erosionally truncates sediment unit C (Fig.6.9s). In other zones of the Central Terrace, pre-Jimmy reflectors are concordant to or toplap horizon Jimmy (Fig.6.6a). Jimmy is erosional over the northern and eastern Tugela Cone (Fig.6.5c) and may be smooth to hummocky (Plate B3.3d; Fig.6.7k) but locally disrupted or crumpled in the north beneath slump masses (section 7.5). In the central upper

slope zone, horizon Jimmy defines a conformity (Fig.6.5c) while over the southern upper slope, toplap relations suggest a non-depositional hiatus origin (Fig.6.6e and f). On the deep basin plain, horizon Jimmy is weakly reflective and concordant representing either a conformity or short-duration hiatus. Along the basin margins, Jimmy is locally discordant or erosional. This sequence boundary cannot be mapped over the SW continental slope and Mozambique Ridge, although at DSDP 249 (Simpson, Schlich et al, 1974) a Pliocene hiatus and condensed sequence is its lateral equivalent.

Horizon Jimmy displays erosional truncation, toplap and concordant relations with pre-Jimmy sediment unit C strata and is typically associated with only minor seismic facies change. Increased bottom current activity initiated in the Pliocene (section 7.3) was probably an important control in hiatus development.

6.3.5 Other Major Horizons

Two other reflectors, both locally unconformable sequence boundaries, have been mapped in the mid Natal Valley. Horizon H is developed mid-sequence between McDuff and Angus (sediment unit B) over the north Tugela Cone, Central Terrace and deep basin plain. Displaying toplap or concordant configurations, horizon H probably represents a non-depositional hiatus. Along the SW deep basin margin, horizon H is locally erosional (Fig.6.8m).

Horizon S, close beneath horizon Jimmy in sediment unit C, is very restricted in areal development being confined to the northern Tugela Cone where it is strongly erosional and the Central Terrace where it is more concordant.

Table 6.1 Seismic Facies Characteristics

SEISMIC SUB-FACIES	GEOGRAPHIC LOCATION	DEPOSITIONAL SETTING AND EXTERNAL FORM	FACIES CONFIGURATION	THICKNESS RANGE (SECS TWT)	REFLECTION GEOMETRY AT BOUNDARIES	PRINCIPAL INTERNAL CONFIGURATION	REFLECTION AMPLITUDE	REFLECTION CONTINUITY
A1	Central Terrace	basement valley and graben fill	onlap fill and drape	0-0.6	toplap at top; basal onlap	chaotic; locally sub-parallel to divergent	very high	discontinuous and hyperbolic
A2	deep basin plain	basin floor fill	onlap fill	?<1.2	concordant or toplap at top; basal onlap and downlap	parallel	low to transparent	continuous
A3	Mozambique Ridge & marginal ridges	basement valley and graben fill	onlap fill	0-1.0	toplap at top; basal onlap	sub-parallel to wavy; locally divergent	moderate	variable
B1 pre-H	central and west Central Terrace	basin slope - fan complex and onlap fill	mixed offlap, onlap and onlap fill	0.1-0.7	basal onlap and downlap	parallel to sub-parallel	high	continuous
B1 post-H	central and west Central Terrace	basin slope - modified onlap fill	mounded onlap fill	0.1-0.7	erosional truncation at top	complex mounded to sub-parallel; local erosion surfaces	moderate	discontinuous; locally continuous
B2	south & east Central Terrace	basin slope - fan complex	mixed offlap and onlap	0.1-1.2	erosional truncation at top; basal onlap	sub-parallel; locally hummocky with erosion surfaces	moderate to low; locally very high in current-moulded zones	continuous; locally discontinuous
B3	northern deep basin plain	basin floor fill	onlap fill	0.5-1.05	concordant on top & base; margin baselap and erosional truncation	parallel; complex divergent or hummocky along basin margins	moderate to low	very continuous
B4 pre-H	south & SW deep basin plain	basin floor fill	heterogeneous onlap fill	0.3-1.0	basal onlap	parallel to sub-parallel	low	very continuous
B4 post-H	south & SW deep basin plain	basin floor fill	onlap fill	0.3-1.0	concordant or erosional truncation at top	parallel; locally hummocky	high	continuous
B5	northern Tugela Cone	basin slope - prograding fan complex	offlap; minor onlap	?	toplap at top; basal onlap and downlap	parallel to sub-parallel	moderate	variable
B6	central & southern upper slope of the Tugela Cone	basin slope - oblique prograding clinoform	offlap	~2.0	concordant or toplap at top; unknown basal relations	parallel; locally wavy	moderate to high	continuous; locally discontinuous
B7	eastern Tugela Cone	basin slope - prograding fan complex	offlap; minor onlap	?	erosional truncation at top; basal onlap and downlap	irregular and parallel to hummocky and sub-parallel	moderate to low	continuous; locally variable
C1	Central Terrace	basin slope - fan complex & onlap fill	mixed offlap and onlap fill	0-0.3	toplap or concordant at top; concordant at base	parallel; locally hummocky; locally chaotic	high; moderate in the east	continuous
C2	east Central Terrace	basin slope - fan complex	mixed offlap and onlap	0-0.3	concordant at top and base; local baselap	sub-parallel to parallel	moderate to low	continuous

SEISMIC SUB-FACIES	GEOGRAPHIC LOCATION	DEPOSITIONAL SETTING AND EXTERNAL FORM	FACIES CONFIGURATION	THICKNESS RANGE (SECS TWT)	REFLECTION GEOMETRY AT BOUNDARIES	PRINCIPAL INTERNAL CONFIGURATION	REFLECTION AMPLITUDE	REFLECTION CONTINUITY
C3	deep basin plain	basin floor fill	onlap fill ponded	0.15-0.3	concordant at top and base; local baselap	regular and parallel; locally irregular	moderate to high	very continuous
C4	deep basin plain margins	basin floor fill	onlap fill	0-0.15	toplap at top; basal onlap and downlap	hummocky sub-parallel; local erosion surfaces	high	variable; locally continuous
C5	northern Tugela Cone	basin slope - prograding slope	mixed offlap and onlap	0.2-0.65	erosional truncation at top; basal onlap and downlap	parallel to oblique; locally chaotic	moderate to high	discontinuous to continuous
C6	Tugela Cone upper slope	basin slope - oblique prograding clinoforms	offlap	0.2-0.62	toplap or concordant at top; basal downlap	parallel to oblique; locally irregular	moderate to high	continuous
C7	eastern Tugela Cone	basin slope - prograding slope	mixed offlap and onlap; mounded	0.15-0.52	toplap or erosional truncation at top; basal onlap	sub-parallel to migrating wave mounds; cut and fill	variable	commonly discontinuous; variable
C8	southern Tugela Cone	basin slope - ? fan complex	offlap; local onlap; chaotic	0-0.3	toplap or erosional truncation at top; baselap	irregular to hummocky; locally chaotic	low	variable, disrupted
D1	Central Terrace	basin slope - onlap fill & oblique prograding clinoforms	onlap fill and offlap	0-0.11	concordant	parallel and even; oblique in fan build-up	very high	continuous
D2	east & SE Central Terrace	basin slope - sheet drape	sheet drape	0-0.09	concordant	parallel and even	low	continuous
D3	deep basin plain	basin floor fill	sheet drape	0-0.09	concordant	parallel and even	moderate to low	very continuous
D4	northern Tugela Cone	basin slope - prograding slope	offlap	0.1-0.6	concordant or onlap and downlap	sub-parallel and even; locally contorted	high; locally low	variable
D5	central & southern upper slope of the Tugela Cone	basin slope - oblique prograding clinoforms	offlap	0-0.32	basal downlap; locally concordant	sub-parallel and even; oblique in fan buildup	high	variable
D6	eastern Tugela Cone	basin slope - prograding slope	mixed offlap and onlap; mounded	0-0.42	concordant; local baselap	sub-parallel and wavy; mounded	high to low	variable
D7	southern Tugela Cone	basin slope - prograding slope	mixed offlap and onlap	0-0.3	concordant; local baselap	sub-parallel; even to hummocky; locally mounded or chaotic	low	discontinuous
P (post-Mcduff)	Mozambique Ridge	elevated ridge - asymmetric drape	mounded drape	0-0.5	local baselap	locally sub-parallel or mounded; erosion surfaces	transparent; locally low	variable
S (post-McDuff)	SW continental slope	basin slope - slope wedge	chaotic fill	?	?	chaotic and contorted	high to low	very discontinuous; short contorted segments

Figs.6.7j, 6.9r) infilling basement valleys and graben. Over the deep basin floor, the onlap fill sequence is classified as sub-facies A_2 (Plate B3.3c; Figs.6.6d, 6.8m). Adjacent to basin margins, reflectors converge and onlap basement high zones (Plate B3.3c). Sequences designated as sub-facies A_3 onlap and fill basement graben on the Mozambique Ridge (Plate B3.3b; Figs.6.6c, 6.9q) or form onlapping drape aprons to the marginal ridges (East and South Tugela Ridges).

Lithofacies control on sub-facies A_3 is provided by DSDP 249 which intersected volcanogenic siltstones-silty claystones, rich in volcanic debris and ash layers, deposited in an anoxic basin (Simpson, Schlich et al, 1974). Development of numerous normal and growth faults over the Central Terrace (Fig.6.7i) together with abundant volcanogenic sedimentation on the Mozambique Ridge implies active syn-sedimentary tectonic instability and volcanism in these provinces during unit A deposition.

Time-thickness data for sediment unit A (Table 6.1) are incomplete because of the shortage of deep penetration seismic profiles. Multi-channel seismic data show that a pre-McDuff proto-Tugela Cone had aggraded to at least 3,2 km thickness (Table 6.2). Over the Central Terrace and Mozambique Ridge, unit A thickness is highly variable dependent on basement topography but may locally exceed 1,0 secs. Over the southern deep basin plain, unit A onlap fill has aggraded to 1,2 secs time-thickness.

6.4.3 Sediment Unit B (McDuff-Angus)

Unit B is divided into seven sub-facies (B_1-B_7) on acoustic character (Table 6.1) with the southern Tugela Cone being omitted

Figures 6.6-6.9 Seismic Profile Line Tracings

Province notation: CT - Central Terrace, TC - Tugela Cone, MR - Mozambique Ridge, DBP - deep basin plain, NR - Naude Ridge, ETR - East Tugela Ridge.
Reflector notation: J - horizon Jimmy, S - horizon S, A - horizon Angus, H - horizon H, Mc - horizon McDuff, B - acoustic basement, Mult - sea floor multiple. Profile notation: C/C - major course change, C/S - profile scale change. Vertical scale is in seconds two-way travel time. Photographic reproductions of the majority of reflection profiles are contained in Appendix B3. Profile locations are shown in Figure 6.2.

---

due to lack of data. Sub-facies distributions are shown in Figure 6.11b.

Three sub-facies (B_5-B_7), each dominated by offlap reflector configuration, are mapped over the Tugela Cone. The offlap pattern of deposition implies that sustained sediment supply remained in excess of subsidence resulting in progradation. Sub-facies B_6, mapped over the upper slope, has been constructed as an oblique tangential prograding clinoform (Fig.6.10; Fig.6.6e; Plate B3.2e). Foreset beds are highly reflective and parallel grading eastwards into wavy and locally discontinuous bottomset strata (Plate B3.2e). Borehole Jc-1 (du Toit and Leith, 1974) intersected sub-facies B_6 identifying a terrigenous sequence of pro-delta and delta-fringe clays, upward-coarsening to include numerous regressive sands and sandy limestones. Delta construction took place over an actively subsiding continental margin. The progradational offlap seismic configuration of sub-facies B_5 and B_7 (Fig.6.7g; Plate B3.1a) suggests that deep-water fan complexes were under construction over the northern and

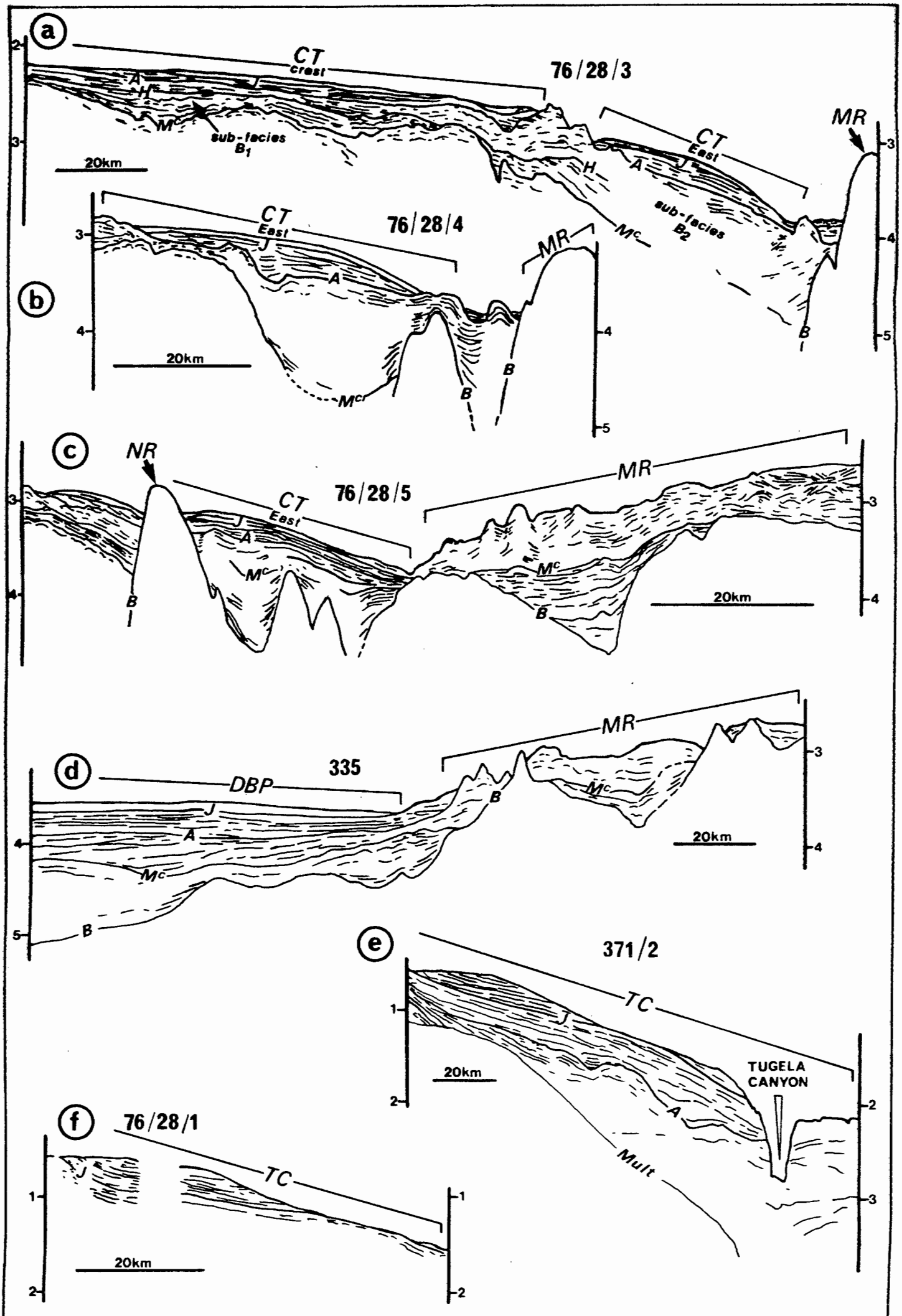

Fig. 6.6 SEISMIC PROFILE LINE TRACINGS

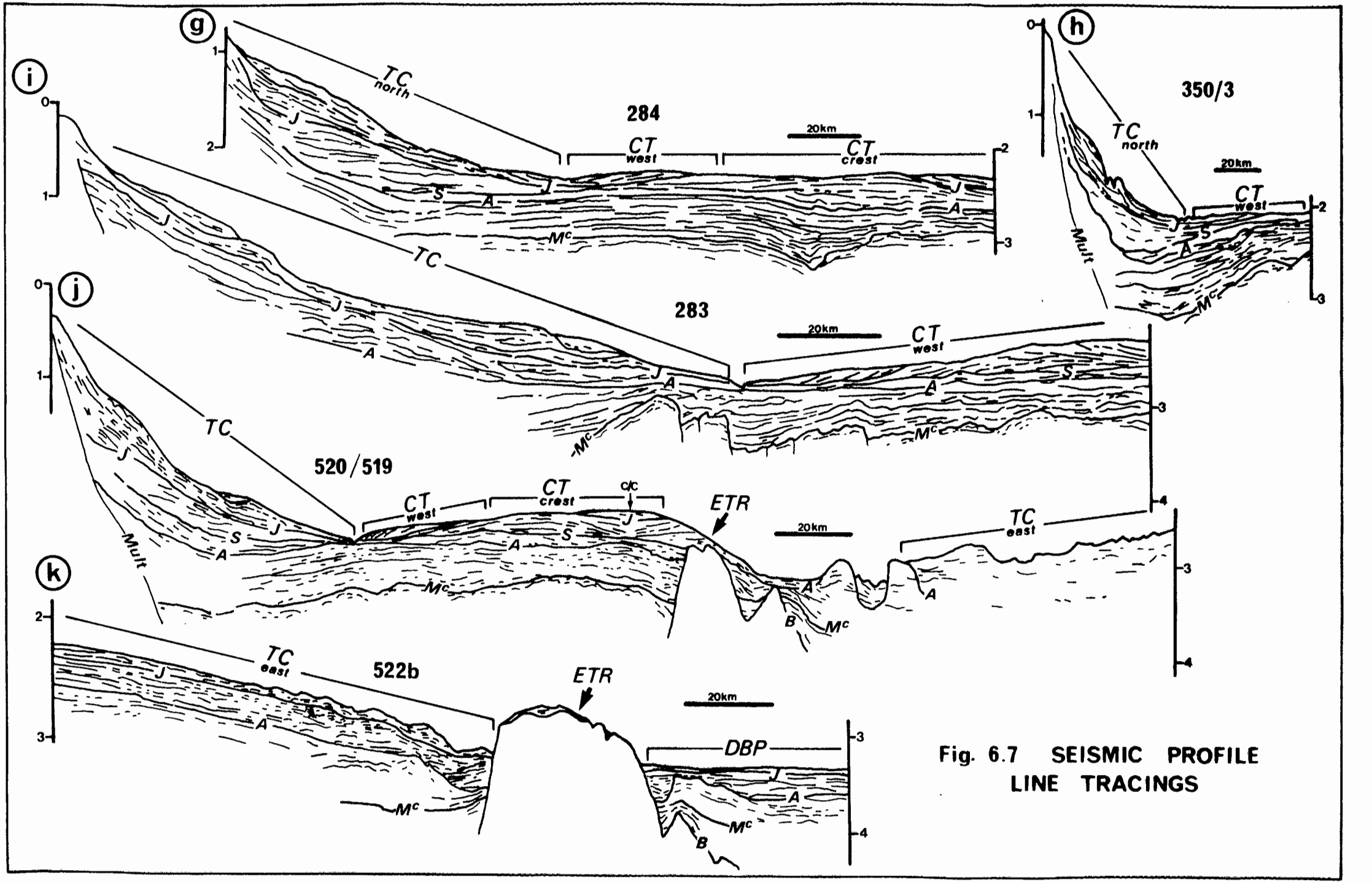

Fig. 6.7 SEISMIC PROFILE LINE TRACINGS

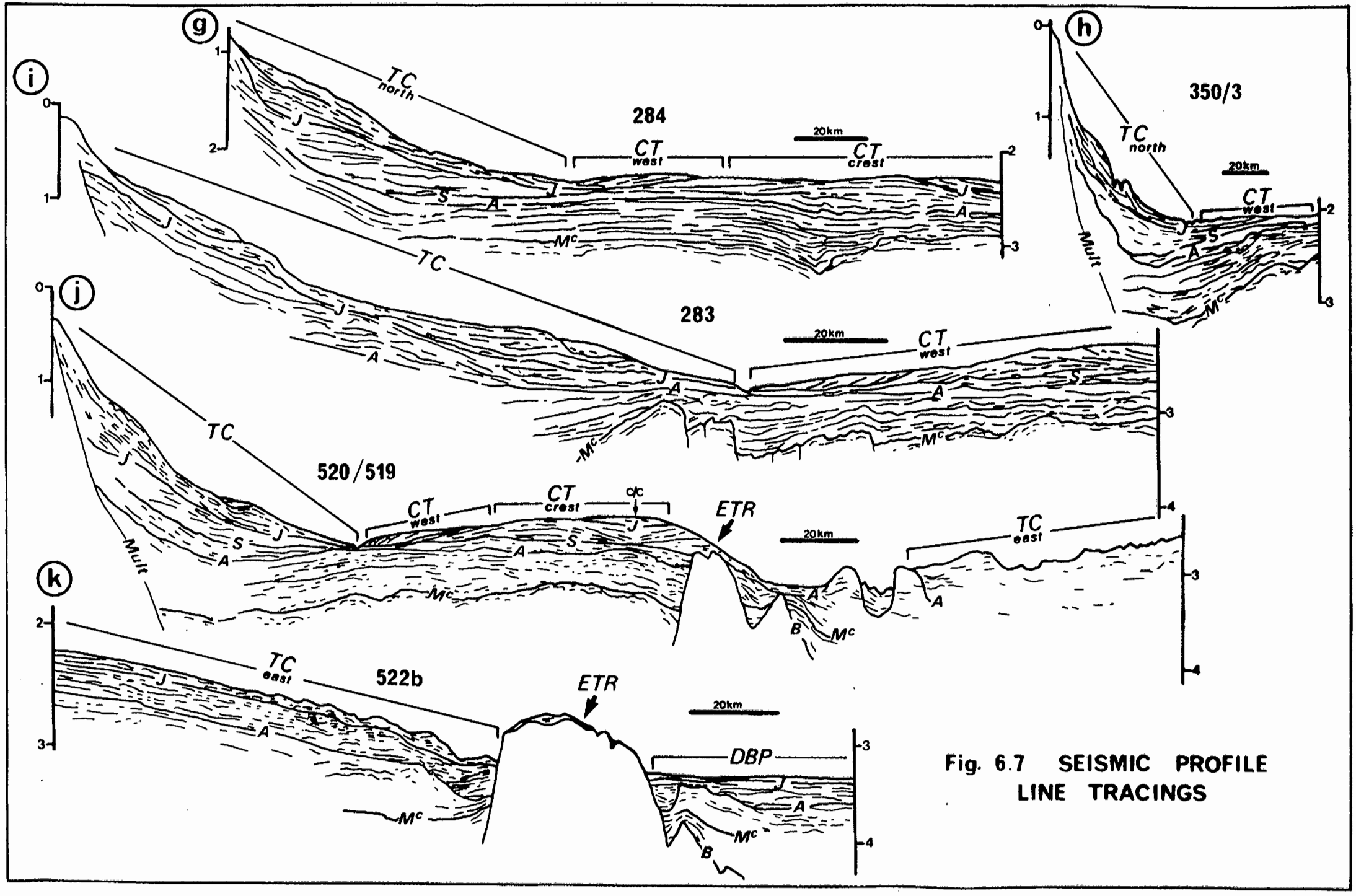

Fig. 6.7 SEISMIC PROFILE LINE TRACINGS

Fig. 6.8 SEISMIC PROFILE LINE TRACINGS

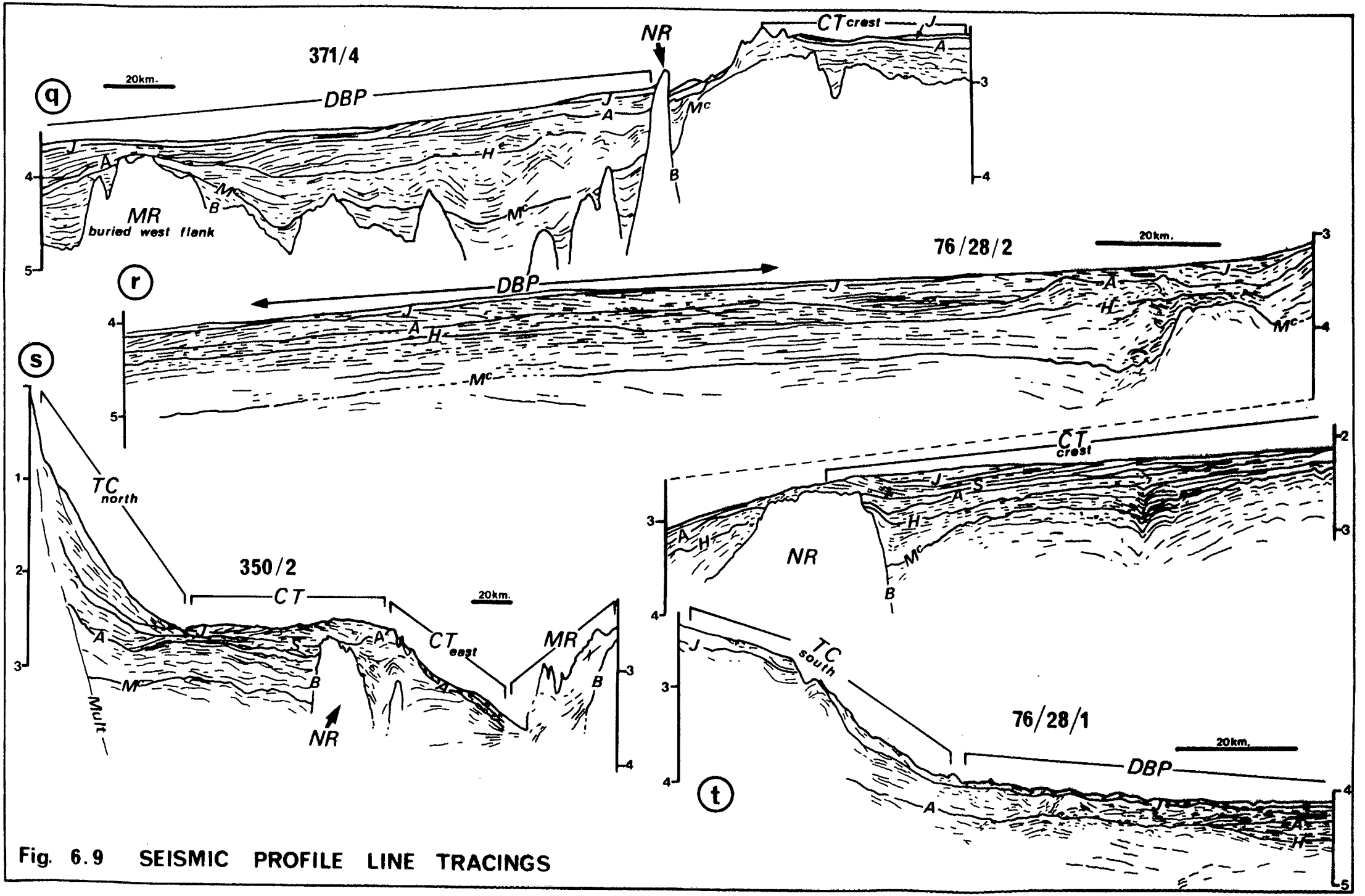

Fig. 6.9 SEISMIC PROFILE LINE TRACINGS

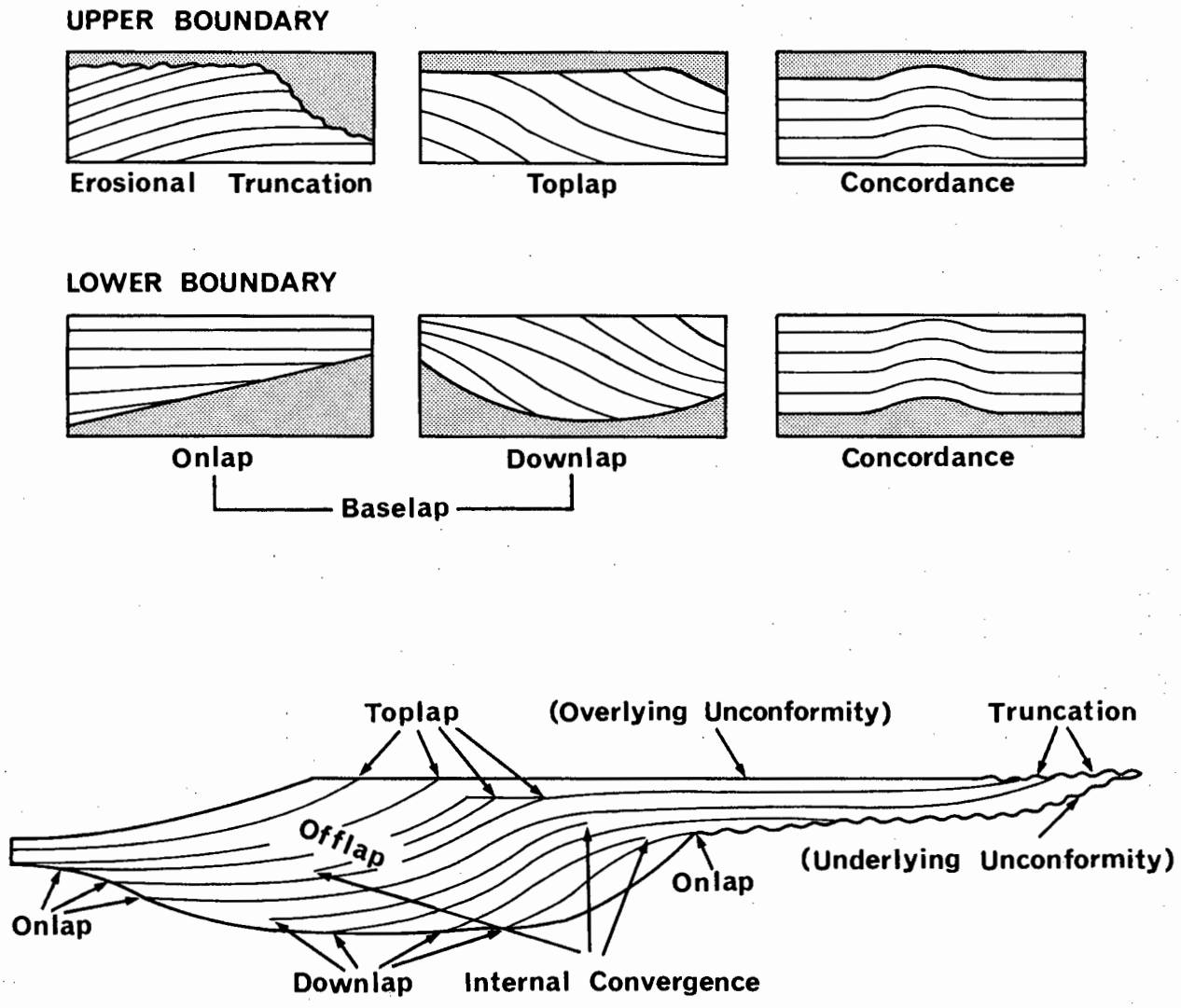

Fig.6.10 REFLECTOR GEOMETRY AT SEQUENCE BOUNDARIES AND MAJOR TYPES OF PROGRADING CLINOFORMS

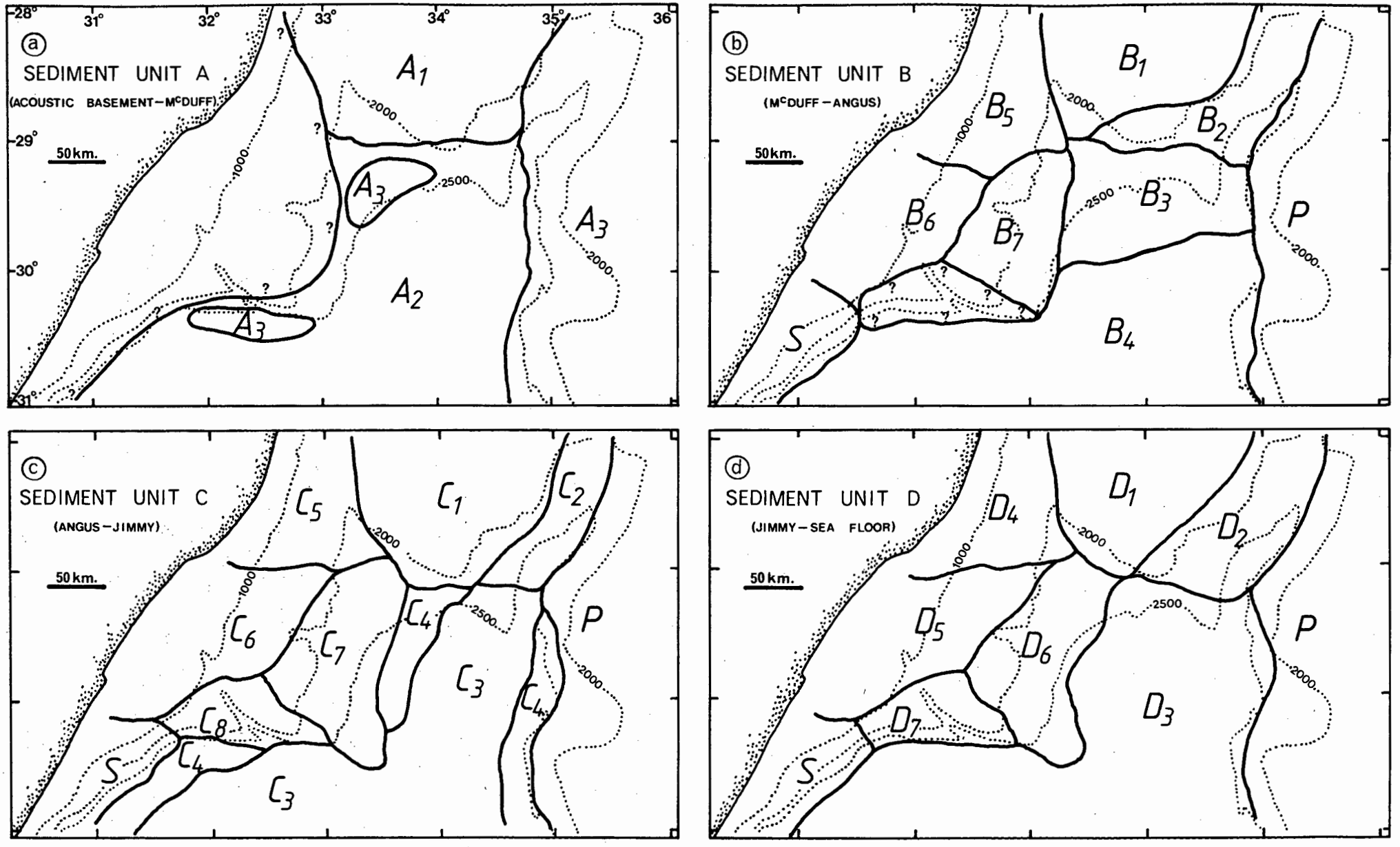

Fig. 6.11 DISTRIBUTION OF NATAL VALLEY SEISMIC SUB-FACIES

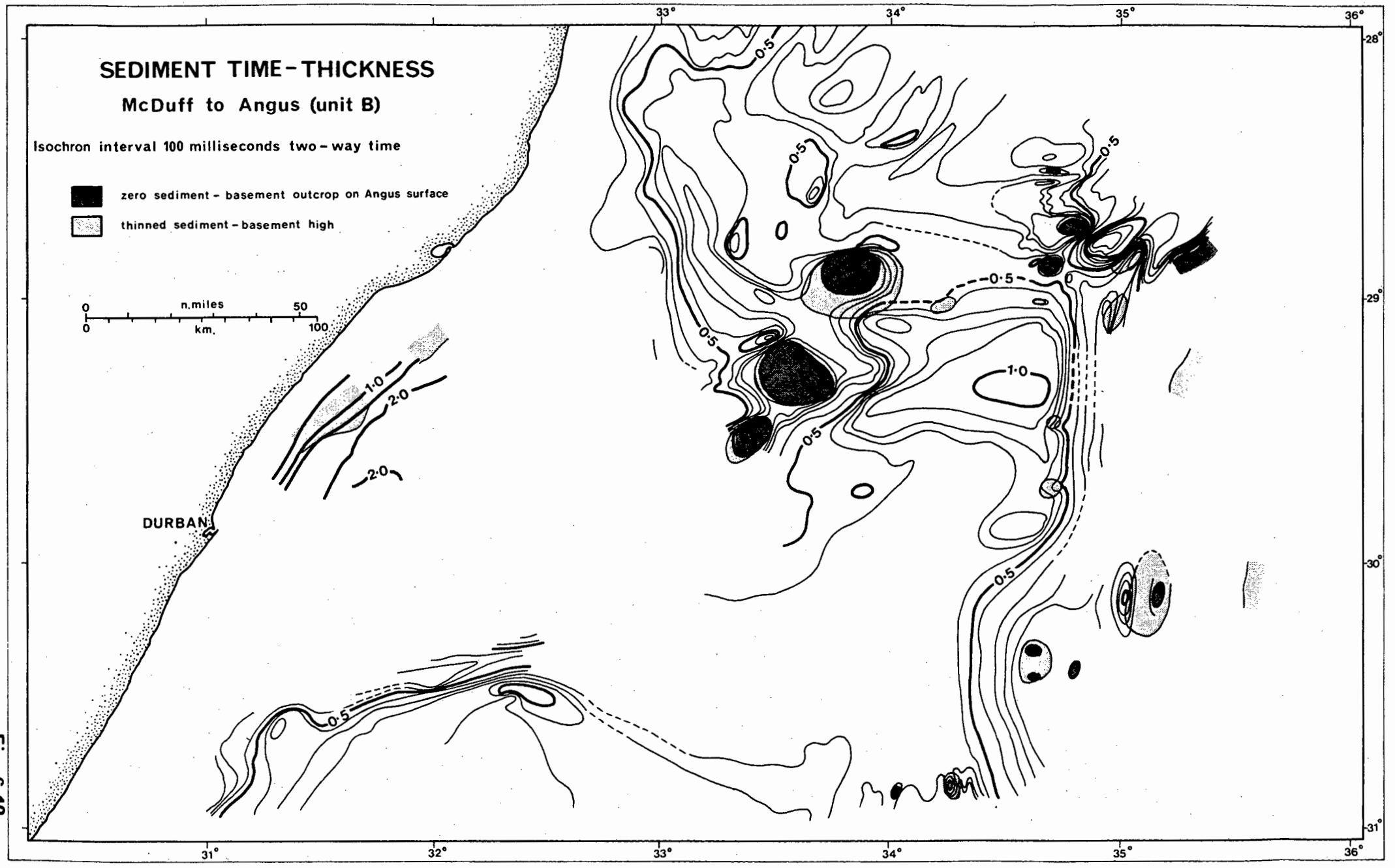
SEDIMENT TIME-THICKNESS
McDuff to Angus (unit B)
Isochron interval 100 milliseconds two-way time
zero sediment - basement outcrop on Angus surface
thinned sediment - basement high
0 n.miles 50
0 km. 100
DURBAN
0·5
1·0
2·0
33°
34°
35°
36°
28°
29°
30°
31°
32°

Fig. 6.12

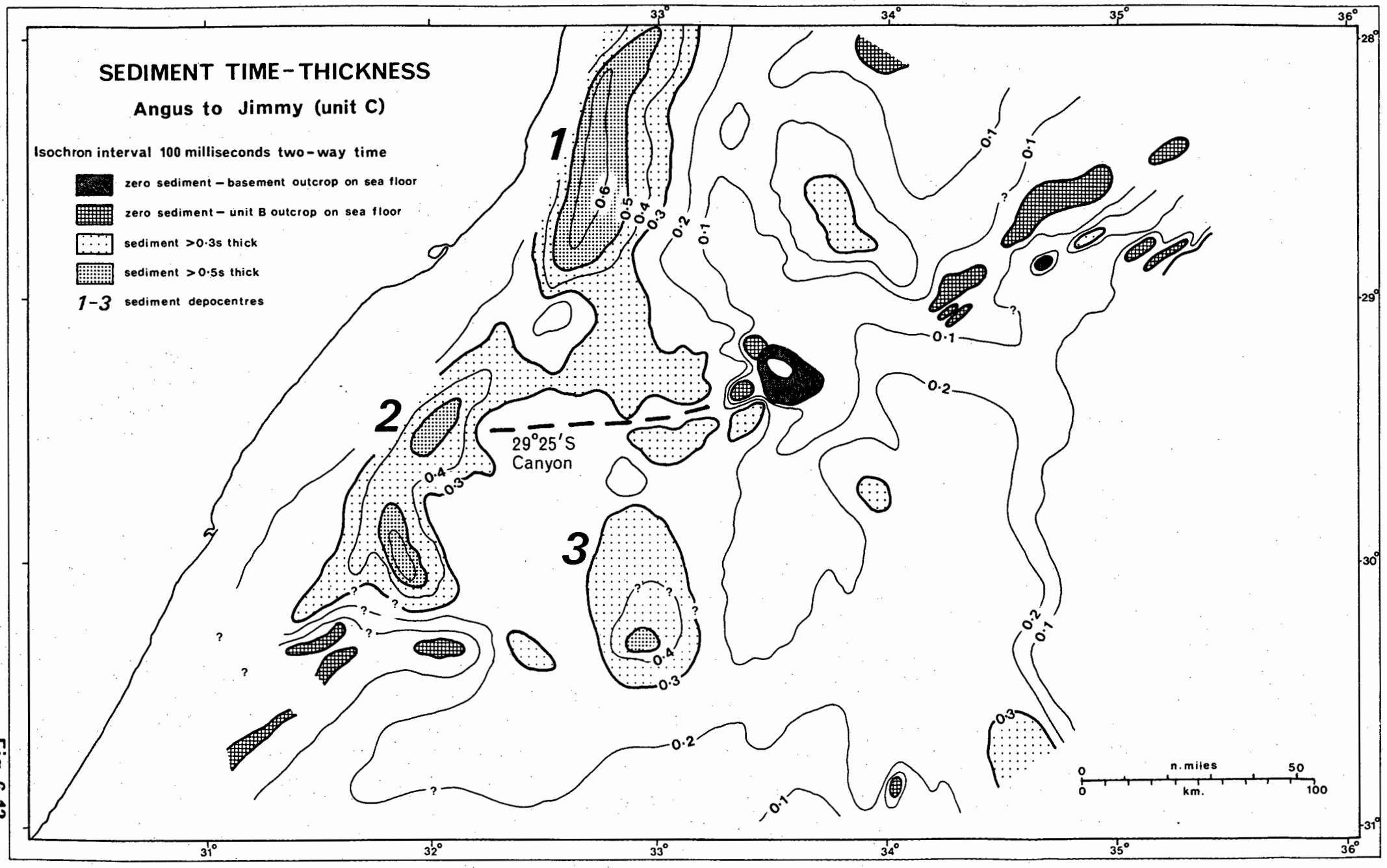
SEDIMENT TIME-THICKNESS
Angus to Jimmy (unit C)
Isochron interval 100 milliseconds two-way time
zero sediment – basement outcrop on sea floor
zero sediment – unit B outcrop on sea floor
sediment >0·3s thick
sediment >0·5s thick
1-3 sediment depocentres
1
2
3
29°25'S
Canyon
0·1
0·2
0·3
0·4
0·5
0·6
?
n. miles
km.
0
50
100
33°
34°
35°
36°
28°
29°
30°
31°
32°

Fig. 6.13

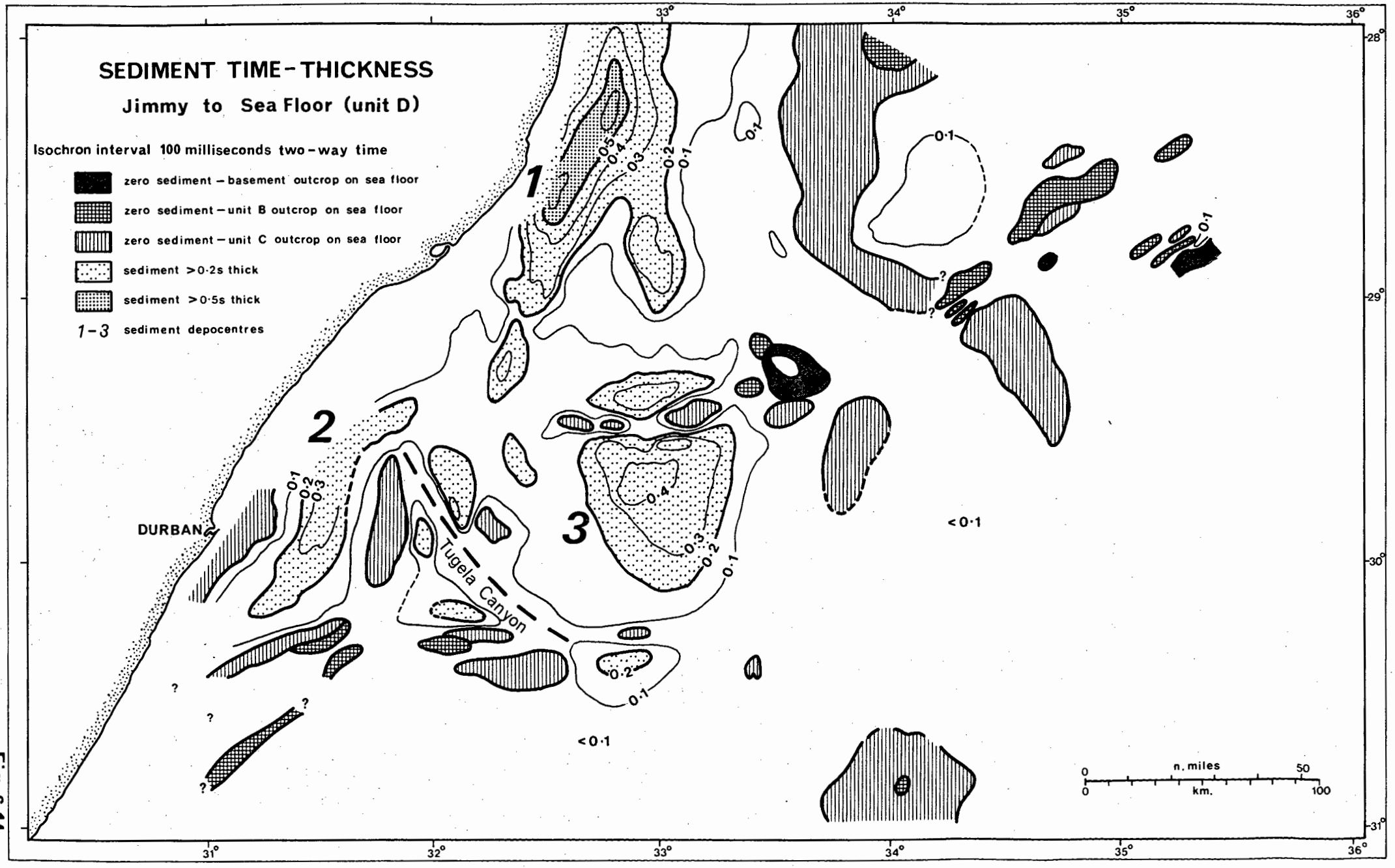
SEDIMENT TIME-THICKNESS
Jimmy to Sea Floor (unit D)
Isochron interval 100 milliseconds two-way time
zero sediment – basement outcrop on sea floor
zero sediment – unit B outcrop on sea floor
zero sediment – unit C outcrop on sea floor
sediment >0·2s thick
sediment >0·5s thick
1–3 sediment depocentres
1
2
3
DURBAN
Tugela Canyon
<0·1
<0·1
n. miles
km.
33°
34°
35°
36°
28°
29°
30°
31°
32°

Fig. 6.14

eastern Tugela Cone, perhaps with the B_6 delta acting as a sediment source. Minor onlap within sub-facies B_5 and B_7 is indicative of periodic reduction in sediment supply and possibly canyon erosion of the shelf/upper slope zone (Brown and Fisher, 1977).

On the Central Terrace, unit B is divided into sub-facies B_1 and B_2 (Fig.6.11b). Horizon H is strongly erosional over the central and west Central Terrace (Fig.6.6a; Plate B3.3a) splitting sub-facies B_1 into pre-H and post-H sequences (Table 6.1). Early unit B sedimentation on the Central Terrace comprises an onlap fill sequence infilling fault-generated McDuff topography. As the McDuff surface was smoothed, deep-sea fan complexes developed prograding westwards (sub-facies B_1; pre-H) and eastwards (sub-facies B_2) over the Central Terrace flanks (Figs.6.6a, 6.7j, 6.7h, 6.9s). Mixed offlap and onlap configuration in these fan complexes implies periodic progradational growth alternating with fan stagnation (reduced sediment supply). On the Central Terrace crest, an onlap fill facies modified by strong current activity (sub-facies B_1; post-H) overlies the fan complex. Current control is suggested by minor erosional surfaces, buried hummocks and a lenticular reflection configuration. Sub-facies B_2 locally outcrops over the SE Central Terrace (Fig.6.13).

Faulting is very common within unit B on the Central Terrace where pre-McDuff faults have been repeatedly reactivated. These growth faults (faulting contemporaneous with sedimentation) impart a regular, wavy configuration to the reflector package (Plates B3.3a, B3.4a and B3.4d).

Unit B sediments of the deep basin plain (sub-facies B_3 and B_4) have accumulated as an onlap fill sequence (Fig.6.9r; Plate B3.4a) with reflector convergence common along the basin margins (Figs.6.8m, 6.9q). Reflector configuration is more heterogeneous within sub-facies B_4 (Fig.6.8m) where horizon H is erosional and divides the sequence into pre-H and post-H depositional units (Table 6.1). Enhanced reflectivity and proximal onlap along the eastern basin margin suggests that the Mozambique Ridge was an important but diminishing detrital source zone until horizon Angus time.

During the latter stages of unit B sedimentation, immediately prior to the Angus hiatus, there is increased development of buried hummocks, erosional truncation and cross-cutting reflector relations in all sub-facies except B_6. These current-moulded and redistribution structures, particularly in sub-facies B_1, B_2, B_4 and B_7 (Plates B3.1a, B3.3b and B3.4b), indicate strengthening of bottom current flow during late-stage unit B deposition perhaps culminating in generation of the Angus hiatus and unconformity.

An isopachyte map (Fig.6.12) displays the highly variable time-thickness of unit B. Over the Central Terrace and adjacent basement ridge provinces, unit B thickness is strongly dependent on geometry of the McDuff and basement surfaces. Accumulation is minimal over basement highs and up-faulted McDuff blocks but in adjacent troughs, unit B onlap fill exceeds 0,4 secs reaching a maximum (>0,7 secs) north of the west Naude Ridge which locally acted as a dam to southerly sediment transport. Thickening on the Central Terrace flanks (up to 1,0 secs) is a response to fan complex development and contourite mounding. Little information

is available from the Tugela Cone (Fig.6.12) but under the upper slope, progradational sediments of sub-facies B_6 exceed 2,0 secs time-thickness. The deep basin plain is a major unit B depocentre with maximum development (>1,0 secs) in the northern (sub-facies B_3) and SW zones.

6.4.4 Sediment Unit C (Angus-Jimmy)

Unit C can be partitioned into eight gradational sub-facies (C_1-C_8). Sub-facies distribution is outlined in Figure 6.11c. Four sub-facies (C_5-C_8) are delineated over the Tugela Cone, each with some degree of offlap reflector configuration implying continued progradation with sediment input exceeding subsidence. Sub-facies C_6 (upper slope) has been constructed as both oblique tangential and oblique parallel prograding clinoforms (Figs.6.10, 6.6e; Plate B3.2e) downlapping onto horizon Angus. Bottomset reflectors are more parallel but fill a canyon feature (100 m deep; 1,5 km wide) on the Angus surface (Fig.6.6e; Plate B3.2e). From the progradational facies configuration and hinterland proximity, it is inferred that sub-facies C_6 developed on resumption of delta growth in post-Angus times.

Sub-facies C_5 (north Tugela Cone) and C_7 (east Tugela Cone) are characterised by a mixed offlap and onlap configuration (Fig.6.7g,i,j and k) with buried channels and cut and fill structure (Fig.6.9t). This implies alternation of progradational phases and upper slope/shelf erosional phases (downslope onlap) during fan complex construction. Onlap phases may be related to development of the 29° 25'S Canyon which eroded the upper slope to lay down levee and overbank deposits over the lower eastern slope (Fig.6.13). This canyon acted as a major sediment conduit

to foster growth of the sub-facies C_7 fan complex (northern zone). Horizon S is a prominent erosional unconformity within sub-facies C_5 dividing the sequence into two depositional units (Fig.6.7j). Bottom current flow has strongly modified the sub-facies C_7 seismic configuration immediately prior to horizon Jimmy with development of migratory sediment waves (Figs.7.3a, 6.7k; Plate B3.3d) and stationary sediment waves (Figs.7.5f, 6.8l; Plate B3.2a). Trough (? lag) laminae are generally most highly reflective within sub-facies C_7 (Fig.7.3a). Persistence of individual mounds in time and space emphasises the permanence of deep current control allied to sustained sediment input.

Mixed offlap and onlap within sub-facies C_8 (southern Tugela Cone) again suggests periodic progradational growth (Figs.6.8m and n). Chaotic and disrupted reflector attitude may be a result of penecontemporaneous instability and slumping on the steep slope (Table 3.1).

Over the Central Terrace, unit C is divided into sub-facies C_1 and C_2 (Fig.6.11c). Sub-facies C_1 onlap fill blankets the majority of the Central Terrace finally draping the Naude Ridge which no longer restricted southward sediment dispersal (Fig.6.7g,i and j; Plate B3.1a and b). Reflector attitude is concordant although minor offlap and chaotic configuration over the SW Central Terrace (Fig.6.7g and h) is probably indicative of local progradation and slumping. Pre-horizon S mounded bedforms (Plates B3.1b, B3.4d) are partly growth fault-controlled (? roll-over anticlines), but in the region of the Naude Ridge are almost certainly current-generated. Sub-facies C_1 strata extensively outcrop over the west and south Central Terrace (Fig.6.14). Mixed offlap and onlap in sub-facies C_2 (east Central Terrace)

indicates complex fan growth (Fig.6.6a and b; Plates B3.2c, B3.3a). Local reflectivity increases with bedding discordance adjacent to sediment unit B outcrops (Fig.6.13) may identify lag deposits resulting from current intensification.

Over the deep basin plain, sub-facies C_3 comprises an onlap fill sequence of high-continuity parallel reflectors showing local ponding (Figs.6.8p, 6.9r; Plates B3.2f, B3.4a). In N-S aligned marginal basin zones, sub-facies C_3 grades into the highly reflective and convergent onlap fill sequence of sub-facies C_4 (Fig.6.11c). Sub-facies C_4 is also characterised by mounding and bed discordance (Plate B3.4a) suggesting current influences during deposition.

Deep currents exercised strong local control during unit C deposition and their action is particularly evident over the eastern Tugela Cone (C_7), peripheral deep basin zones (C_4) and the flanks of the Central Terrace (C_1 and C_2).

Sediment unit C time-thickness is depicted in Figure 6.13. Three major depocentres (1-3; Fig.6.13) are recognised coincident with progradational growth (offlap) zones of the Tugela Cone. Thickest development (>0,6 secs) occurs in depocentres 1 (sub-facies C_5) and 2 (sub-facies C_6). Depocentre 3(sub-facies C_7) has prograded to a thickness of >0,5 secs over the SE Tugela Cone. Smaller depocentres are recorded in three areas: (1) levee and overbank deposits flanking the lower 29° 25'S Canyon; (2) sediments dammed north of the west Naude Ridge on prevention of southward sediment dispersal; (3) isolated patches over the eastern deep basin plain. Thin development (<0,2 secs) or absence of unit C sediments implies their non-deposition or erosion by vigorous curents (section 7.2). Affected areas

include the SW basin plain margin, SE Central Terrace and bordering zones of the East Tugela Ridge (Fig.6.13). Other thin unit C provinces (Mozambique Ridge and southern deep basin plain) probably result from low sediment supply.

6.4.5 Sediment Unit D (post -Jimmy)

Post-Jimmy sediments are divisable into seven gradational sub-facies (D_1-D_7). Sub-facies distribution is shown in Figure 6.11d. Unit D time-thickness is presented in isopachyte form (Fig.6.14). Surficial samples and cores provide some lithofacies data from which the seismic facies may be calibrated. However, available cores are short (<3 m) and vertical lithofacies changes within unit D are strongly suspected, probably as a response to provenance alteration during the major Pliocene/Pleistocene sea level fluctuations and climatic changes.

Sediment unit D on the Tugela Cone comprises four sub-facies (D_4-D_7). Sub-facies D_5 forms a progradational offlapping wedge along the upper slope which has developed in two major lobes (Fig.6.14; Fig.6.6e and f). Coast-parallel seismic tracks (e.g. traverse 287) indicate that the northern lobe has been constructed as a series of stacked progradational fan units. Each unit is elongate in a coast-normal direction and has been intermittently active as suggested by buried channels and switching levees. The southern lobe, west of the Tugela Canyon (Fig.6.14; 30°S, 31° 30'E), has developed as an oblique parallel prograding clinoform (Fig.6.6e and f; Plate B3.2e) as far east as 32° 10'E. Two major post-depositional events have eroded the southern lobe: (1) post-Jimmy formation of the Tugela Canyon (section 7.4.2) erosively cross-cuts its eastern margin

(Figs.6.6e, 6.13); (2) central sections of the lobe have been excavated (Fig.6.6e and f) by bottom currents causing pre-Jimmy strata to outcrop at the sea floor (Fig.6.14). Major growth of sub-facies D_5 depocentres probably occurred during Pliocene/Pleistocene sea level low stands when terrigenous clastic supply was at a maximum and erosional/winnowing processes of the Agulhas Current were at a minimum (Be and Duplessy, 1976; Hutson, 1980). Agulhas Current invigoration during intervening high sea level stands may have initiated erosion of the southern lobe of sub-facies D_5. Surficial sediments from sub-facies D_5 consist of terrigenous silty clays and sand-silt-clay (after Shepard, 1954) gradational eastwards to marly calcareous ooze with a significant terrigenous component. At drillsite Jc-1, terrigenous sands and sandy limestones were recovered from sub-facies D_5. These lithofacies are consistent with the progradational fan seismic configuration and hinterland proximity.

Sub-facies D_4 (northern Tugela Cone) comprises a slope front offlap wedge (Fig.6.7g,i and j). The offlap depositional style is locally modified by slumping and erosional processes. Four major slumps (Fig.6.7g-i; section 7.5) cause local depocentre thickening and underlying bed contortion. Post-depositional erosional canyons (topography IID-1, section 3.3.2; Fig.6.7h) dissect the northern extreme of the offlapping wedge. Surface samples 5727 and 5728 are reworked and winnowed foram sands (Appendices A5 and B1) but probably only retrieved material from recent current scoured lag deposits lying on top of the offlap series.

Sub-facies D_6 (Fig.6.11d; eastern Tugela Cone) displays a

mixed offlap and onlap acoustic configuration strongly modified by mounding (Figs.6.7k, 6.8l; Plate B3.3d). Both migrating and stationary mounds are recognised and interpreted to be a response to deep Agulhas Current geostrophic flow (section 7.2.5). Development of migratory mounds within an aggrading depocentre indicates high sedimentation rate allied to strong current control. Sediment cores 14-28 (Appendix B2), recovered from sub-facies D_6, comprise marly calcareous oozes becoming progressively more calcareous downslope towards the deep basin plain.

The seismic configuration of sub-facies D_7 (Fig.6.11d; southern Tugela Cone) is poorly resolved due to insufficient data control but appears to comprise a mixed offlap and onlap sequence cross-cut by the post-Jimmy Tugela Canyon (section 7.4). Mounded reflectors together with base-of-slope units B and C exposure (Fig.6.14) implies extant current scour. Recognition of glide plane scars (Fig.6.8l) with chaotic bedding suggests local slump tectonism. Cores 5115-5117 from sub-facies D_7 recovered carbonate-poor silty sand and sand-silt-clay confirming that the southern Tugela Cone is an active modern terrigenous depocentre.

Two unit D sub-facies (D_1 and D_2) are discriminated on the Central Terrace. Sub-facies D_1 on the west Central Terrace comprises a westward-prograding oblique parallel clinoform (Fig.6.7g,i and j; Plate B3.2b). This is separated from the onlap fill section of sub-facies D_1 by a wide outcrop of unit C sediments (Fig.6.14). Post-depositional erosion by vigorous bottom currents is inferred to explain the modification of the D_1 depositional unit. Cores 12 and 13 (Appendix B2) suggest that the prograding clinoform on the west Central Terrace is constructed of foram-rich marly calcareous oozes (hemipelagites).

Sub-facies D_2 is gradational from D_1 and forms a uniform sheet drape (Fig.6.6a) over the east and SE Central Terrace (Fig.6.11d). Foram ooze (cores 5 and 9) and winnowed coarse foram sand (samples 2 and 3) retrieved from sub-facies D_2 suggests that the drape is predominantly pelagic.

Sub-facies D_3 comprises an inhomogeneous sheet drape over the deep basin plain (Figs.6.8p, 6.9r; Plates B3.2f, B3.4a). Central basin cores (1 and 5751) recovered foram ooze or foram-rich marls indicating dominance of pelagite and hemipelagite sedimentation. Cores from the SW basin (5119 and 5753) are hemipelagic marls, but with a significant terrigenous component probably being introduced from the adjacent south Tugela Cone terrigenous depocentre.

The time-thickness isopachyte map (Fig.6.14) indicates that unit D sedimentation has been concentrated in three progradational (offlap) depocentres. Depocentre 1 (north Tugela Cone) locally contains >0,6 secs of sub-facies D_4 sediments. The detached lobes south and SE of the main offlap wedge demarcate the location of allochthonous sediment masses (section 7.5). Depocentre 2 (sub-facies D_5) over the Tugela Cone upper slope has developed to a time-thickness >0,3 secs although post-depositional erosion and formation of the Tugela Canyon has strongly modified its geometry. Depocentre 3 on the eastern Tugela Cone (sub-facies D_6) is locally thicker than 0,4 secs adjacent to the lower 29° 25'S Canyon suggesting aggradation of overbank and levee deposits. The small suprafan depocentre SE of the Tugela Canyon mouth has probably accreted by dumping of canyon-derived sediments. Extensive outcrop of unit B and C strata around the margins of the Central Terrace and Tugela Cone

(Fig.6.14) identify current-scoured areas (section 7.2). Thin development of unit D (<0,1 secs) over the deep basin plain is probably a function of low sediment supply.

6.4.6 Undifferentiated Post-McDuff Seismic Facies

Depositional sequence boundaries Angus and Jimmy cannot be discriminated over the Mozambique Ridge and SW continental slope. Honogeneous post-McDuff sediments in these physiographic zones are grouped as facies P (pelagic) and facies S (slump) respectively.

Facies P (Fig.6.11; Mozambique Ridge) is characterised by acoustic transparency (Fig.6.6d) but zones of low amplitude reflectors (Fig.6.6c) impart lateral heterogeneity. Widespread development of large sediment billows (Figs.6.6c, 6.8p), scour moats (Fig.6.6d), basement exposure (Figs.6.6a and b), units B and C outcrop (Fig.6.6d) and the strongly asymmetric sediment distribution (Fig.6.6a-d; 0-0,5 secs) confirms that deep current action has significantly affected facies P depositional processes. Acoustic transparency favours a pelagic origin for facies P and this is corroborated by DSDP 249 (Simpson, Schlich et al, 1974) which cored 287 m of nanno-ooze and nanno-chalk above horizon McDuff.

Facies S (Fig.6.11; SW continental slope) comprises a slope front wedge dominated by a low continuity chaotic reflection configuration. Shallow notches on the sea floor are interpreted to be slump scars. The chaotic reflection character of facies S has possibly resulted from penecontemporaneous gravitational slumping. Widespread slumping within facies S may be a response to: (1) the abnormally steep gradient (1:14); (2) high detrital

supply from youthful Natal rivers; and (3) base-of-slope current scour (unit B outcrop - Fig.6.8o) compounding slope instability. Over the upper slope where gradients are reduced, chaotic reflectors grade directly into an offlapping progradational sequence suggesting that slope steepness is important to slump generation in this area.

6.4.7 Total Sediment Thickness

Total sediment thickness data are incomplete because of the lack of deep penetration seismic profiles. Acoustic basement has been mapped in zones of relatively thin overburden (basement ridges and plateaux) or where multi-channel data are available (central continental margin). Total sediment time-thickness is presented in isopachyte form (Fig.6.15) while maximum thicknesses in several provinces have been depth-converted (Table 6.2). Compaction effects have not been assessed.

Thickest deposition has occurred over the upper Tugela Cone where a sediment pile of at least 7250 m (>4,5 secs) has accumulated. Basinward thinning is apparent and under the eastern Tugela Cone, the sedimentary column is only 2870 m thick. The Tugela Cone has remained a major depocentre from initiation of basin subsidence and significant growth has continued through post-McDuff times (Table 6.2; units B-D).

The Naude Ridge has acted as a dam to southward sediment dispersal and up to 2100 m (1,5 secs) of sediment has accumulated against its northern flank (Fig.6.15) while sediments are absent or thinly drape (<0,1 sec) its crest. Sediment distributions are equally irregular around the East Tugela Ridge (Fig.6.15). To the north, sediment thicknesses on the Central Terrace crest are

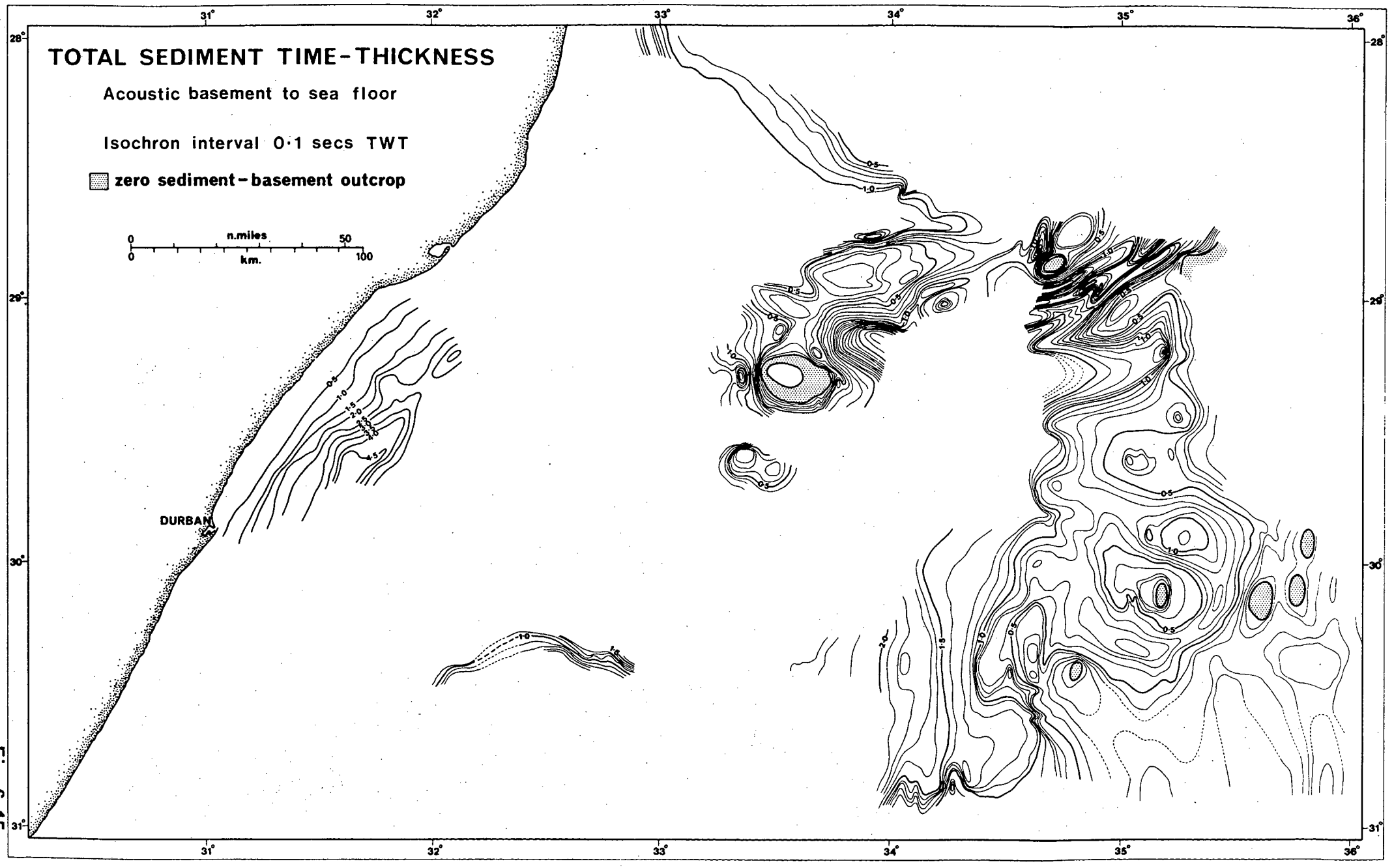
TOTAL SEDIMENT TIME-THICKNESS
Acoustic basement to sea floor
Isochron interval 0·1 secs TWT
zero sediment-basement outcrop
0
n.miles
50
0
km.
100
DURBAN
31°
32°
33°
34°
35°
36°
28°
29°
30°
31°

Fig.6.15

Table 6.2 Maximum Total Sediment Thickness

LOCATION	SEDIMENT UNIT A		SEDIMENT UNITS B-D		TOTAL THICKNESS
	(secs TWT)	(m)	(secs TWT)	(m)	(m)
Tugela Cone (upper)	1,6	3200[1]	3,0	4050[2]	7250
Tugela Cone (eastern)	-	1160	-	1710	2870[3]
Deep basin plain(30,5°S)	1,2	2400[1]	1,1	1100[4]	3500
Naude Ridge (north flank)	0,6	1200[1]	0,9	900[4]	2100
Central Terrace (crest)	?	?	0,6	600[4]	>600
Mozambique Ridge	1,0	1100[5]	0,5	410[6]	1510

In depth conversion, the following sonic velocities were used:
1 - 4,0 km/sec (Ludwig et al, 1968; site 160)
2 - 2,7 km/sec (du Toit and Leith, 1974; borehole Jc-1)
3 - thicknesses direct from site 160 of Ludwig et al (1968)
4 - 2,0 km/sec (Ludwig et al, 1968; site 160)
5 - 2,2 km/sec (Simpson, Schlich et al, 1974; DSDP 249)
6 - 1,65 km/sec (Simpson, Schlich et al, 1974; DSDP 249)

very variable dependent on faulted McDuff topography but may locally exceed 600 m (Table 6.2). On the Mozambique Ridge, basement configuration controls sediment thickness with up to 1,5 secs (1510 m) of accumulation in basement valleys (compare Figs.5.1 and 6.15).

In the deep basin plain, sediment thickness decreases southwards from 3500 m at 30,5°S (Table 6.2) to 1200 m at 35°S (Chetty and Green, 1977) where the southern Natal Valley merges with the Transkei Basin. Around the ridge provinces and in the deep basin plain, unit A (pre-McDuff) sediments comprise the major basin fill (Table 6.2).

6.5 DEPOSITIONAL STYLES AND SYSTEMS

6.5.1 Depositional Styles

Seismic-stratigraphic analysis of the Natal Valley basin fill (sections 6.3-6.4; Table 6.1) has defined six major depositional styles: offlap, onlap, mixed offlap/onlap, onlap fill, sheet drape and chaotic fill. Syn-sedimentary and post-depositional current action has strongly modified several of the seismic facies.

Offlap seismic configuration in the mid Natal Valley is restricted to the upper Tugela Cone during units B and C deposition spreading to the northern Tugela Cone during unit D deposition (Table 6.1). At borehole Jc-1, unit B and C offlap coincides with persistant deltaic progradation to the outer shelf and upper slope (du Toit and Leith, 1974) in response to sustained sediment supply exceeding the subsidence rate. During offlap, slope facies and fan-delta development shifts basinward and the basin is filled by slope deposition (Brown and Fisher,

1977). Oblique progradational offlap (Fig.6.10) is predominant within the Natal Valley succession (sub-facies B_6, C_6 and D_5; Table 6.1) suggestive of a high energy regime. Some combination of high sediment supply, minor basin subsidence and sea level stillstand permits rapid basin infill and bypass or scour of the upper depositional surface (?fan-delta plain). Terrigenous sandstone and claystone facies deposited by turbidite and slumping processes are common in oblique progradational units (Brown and Fisher, 1977) while calcareous slope deposits are important in sigmoidal units (Fig.6.10).

Onlap slope reflection patterns are common within units B-D of the basin fill but usually alternate with offlap units (Table 6.1). Onlap is inferred to be a response to sub-aerial or submarine erosion and downslope redeposition of shelf and upper slope sediments in the absence of a sustained sediment supply. Under conditions of slope erosional retreat, onlap slope environments gradually move landward as a result of a diminishing sediment source (Brown and Fisher, 1977). Lithofacies in onlap sequences are commonly fine-grained terrigenous sediments with interbedded hemipelagite units (Sangree and Widmier, 1977).

Mixed offlap and onlap seismic facies are widely developed within units B-D over deep-sea zones of the Tugela Cone and flanks of the Central Terrace (Table 6.1). Mixed offlap and onlap implies episodic fast progradational growth alternating with periods of slow sedimentation rate.

Onlap fill seismic facies is developed in valleys and fault-bound graben on the Central Terrace and Mozambique Ridge (units A and B) and along marginal zones of the deep basin plain (units A-C). The superposed arrangement of seismic reflectors requires balanced sediment supply and subsidence rate (Brown and Fisher,

1977). The onlap configuration and tendency to fill structural lows suggests that onlap fill facies is deposited by gravity-controlled flows interbedded with hemipelagites and pelagites (Sangree and Widmier, 1977).

Low-energy sheet drape facies are confined to the deep basin plain and the eastern Central Terrace within unit D. Uniform thickness sheet drape is typically indicative of hemipelagite and pelagite oozes but may be interbedded with mass-movement terrigenous deposits along basin margins (Sangree and Widmier, 1977).

Chaotic fill slope wedge development is limited to the SW continental slope (facies S). Continuous mass-transport slump and creep along with post-depositional mass-movement processes are probably responsible for generating the chaotic and discontinuous reflection character. Lithofacies is dependent on the sediment source and may be highly variable.

Syn-depositional and post-depositional current action has strongly modified the configuration of several seismic facies of units B,C and D. The influence of deep current flow (Agulhas Current and North Atlantic Deep Water) on sedimentation is fully discussed in section 7.2.

6.5.2 Depositional Systems

Progressive change in depositional style through time, as recognised in the Natal Valley basin fill (section 6.5.1), allows comparison to established seismic-stratigraphic models of basin development. The change from onlap fill (unit A) through mixed offlap, onlap and onlap fill (units B-C) to offlap and sheet drape (unit D) is equivalent to sequences mapped in Brazilian

rift and pull-apart basins (Brown and Fisher, 1977). The Brazilian sequences are considered typical of early rift basin fill and post-rift passive offlap fill.

Sediments are delivered to deep-water basins by three major sedimentary process models (Gorsline, 1978; 1980; Nardin et al, 1979b): (1) submarine canyon - fan - basin floor system (discontinuous growth); (2) slope and base-of-slope system (discontinuous growth); and (3) oceanic system dominated by pelagic and hemipelagic particle settling (continuous growth), with thermohaline current redistribution of sediments. Seismic stratigraphy together with sedimentological process studies (Chapters 7 and 8) suggests that all three models are applicable to the Natal Valley.

The post-McDuff Tugela Cone has developed through model (1) with discontinuous growth evidenced by alternation of offlap and onlap depositional styles within units B-D. Significant Tugela Cone progradational growth has taken place during unit D deposition judging by the dominance of offlap (sub-facies D_4-D_7) and the fast sedimentation rate (Table 6.3). Tugela Cone development is fully discussed in Chapter 9. Aggradation of the SW continental slope has followed model (2) with gravity mass transport processes inferred from the chaotic fill depositional style (Table 6.1; facies S). Post-Jimmy (unit D) development of the northern Tugela Cone grading into the Zululand continental slope may also have followed model (2) based on recognition of allochthonous sediment masses (section 7.5). Common sheet drape seismic facies over the deep basin plain, Central Terrace and Mozambique Ridge confirms the significance of model (3) during unit D aggradation. In these regions, relatively high carbonate

contents (Fig.8.3) prove the importance of biogenous input while abundant current-controlled features imply active remobilisation and moulding of sediments (section 7.2).

6.6 PALAEOBATHYMETRY

To evaluate morphologic development of the major physiographic provinces, time-depth maps of the depositional sequence boundaries have been constructed (Figs.6.16-6.18). Data control is summarised in section 6.1. Corrections for velocity contrasts (depth conversion), sediment loading and compaction effects and post-depositional subsidence have not been applied. As a result, the time-structure charts of horizons McDuff, Angus and Jimmy provide a distorted representation of the true palaeobathymetric surfaces.

6.6.1 Time-Depth to McDuff

A time-depth map of horizon McDuff is presented as Figure 6.16. Insufficient data (poor penetration) prevented map construction over the Tugela Cone and parts of the continental margin.

Although complete delineation of the proto-Tugela Cone is impossible, available data provides some indication of its early configuration. Unit A sediments aggraded as a wedge-shaped body (3200 m thick) at the base of the continental slope with horizon McDuff steeply onlapping onto basement. Eastward contour deflection north of the SW continental slope (Fig.6.16) may imply pre-McDuff progradation as far south as 30° 20'S. In contrast, NE-progradation must have been less extensive as evidenced by the

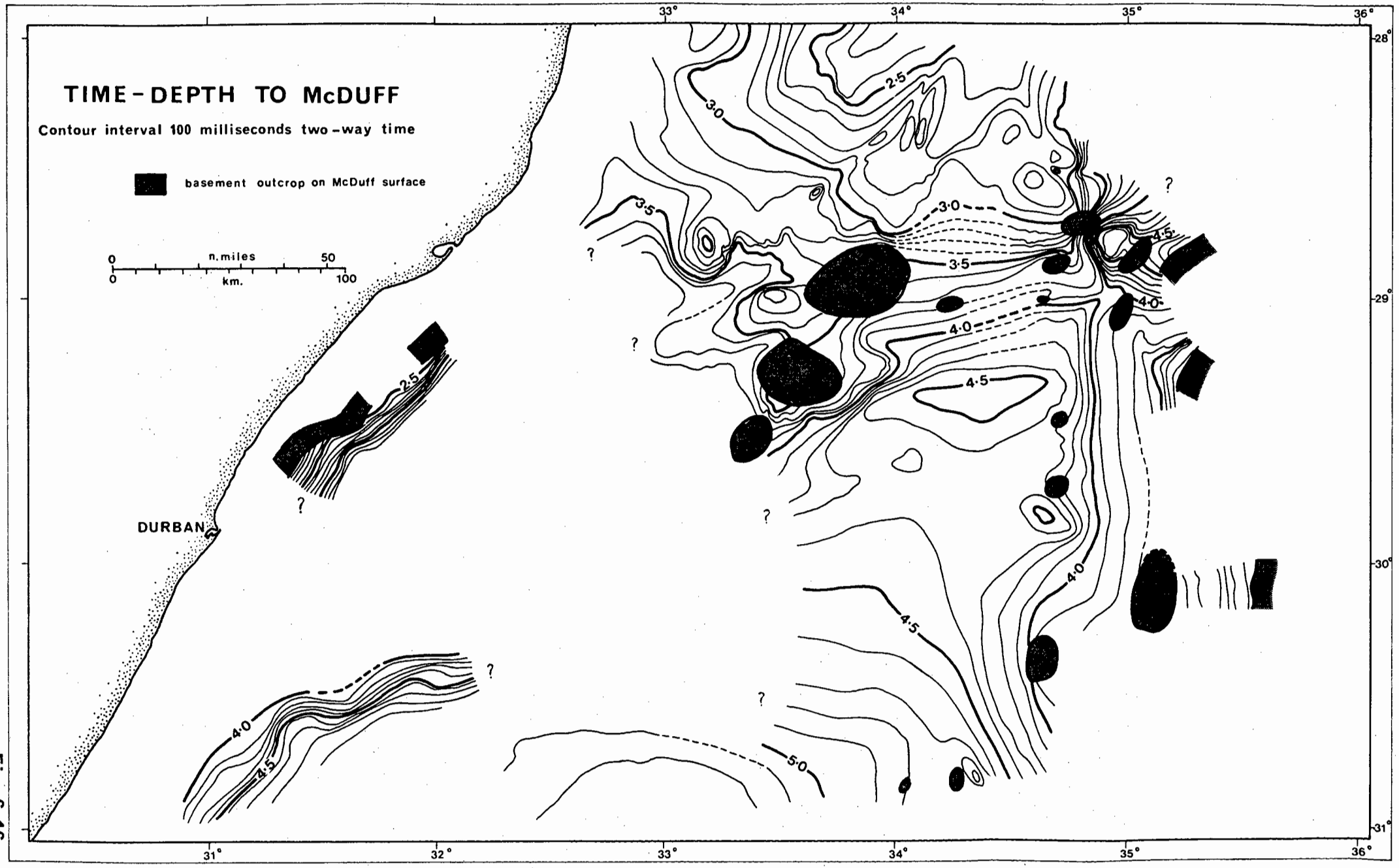
TIME - DEPTH TO McDUFF
Contour interval 100 milliseconds two-way time
basement outcrop on McDuff surface
0
n.miles
50
0
km.
100
DURBAN
2·5
3·0
3·5
4·0
4·5
5·0
?
33°
34°
35°
36°
28°
29°
30°
31°
31°
32°
33°
34°
35°
36°

Fig. 6.16

extent of the irregular and south-dipping McDuff surface SW of the Central Terrace.

The Central Terrace, cored by up-faulted basement blocks, is the shoalest (2,3-3,0 secs) horizon McDuff province. Horst, graben and half-graben structures (Fig.6.7i; Plate B3.1a) up to 50 by 10 km in size and 0,3 secs relief (Fig.6.16) disrupt the plateau crest. Similarly, horizon McDuff is elevated over the basement-cored Mozambique Ridge where pre-McDuff sediments (unit A) onlap fill the irregular basement topography (Fig.5.1).

From the Central Terrace and Mozambique Ridge, transition into the deep basin plain is delineated by a slope break at 4,2 secs (Fig.6.16). The smooth, low-gradient McDuff basin floor dips southwards to reach a maximum time-depth of 5,2 secs.

6.6.2 Time-Depth to Angus

Comparison of the present day bathymetry (Fig.3.2) and the horizon Angus time-depth map (Fig.6.17) indicates that the major physiographic elements of the Natal Valley (Tugela Cone, Mozambique Ridge, Central Terrace, deep basin and SW continental slope) have been in existence since at least Angus times.

The Tugela Cone is well developed as a large asymmetric sediment body with steep upper and southern slope zones. The relatively smooth eastern flanks exhibit lowest surface gradients. Isochrons have been omitted along the course of the Tugela Canyon which is suspected to be post-Jimmy in origin (section 7.4). The 29° 25'S Canyon is strongly defined on the Angus surface emerging from the Tugela Cone south of the East Tugela Ridge (Fig.6.17).

Central Terrace morphology is regular and smooth displaying

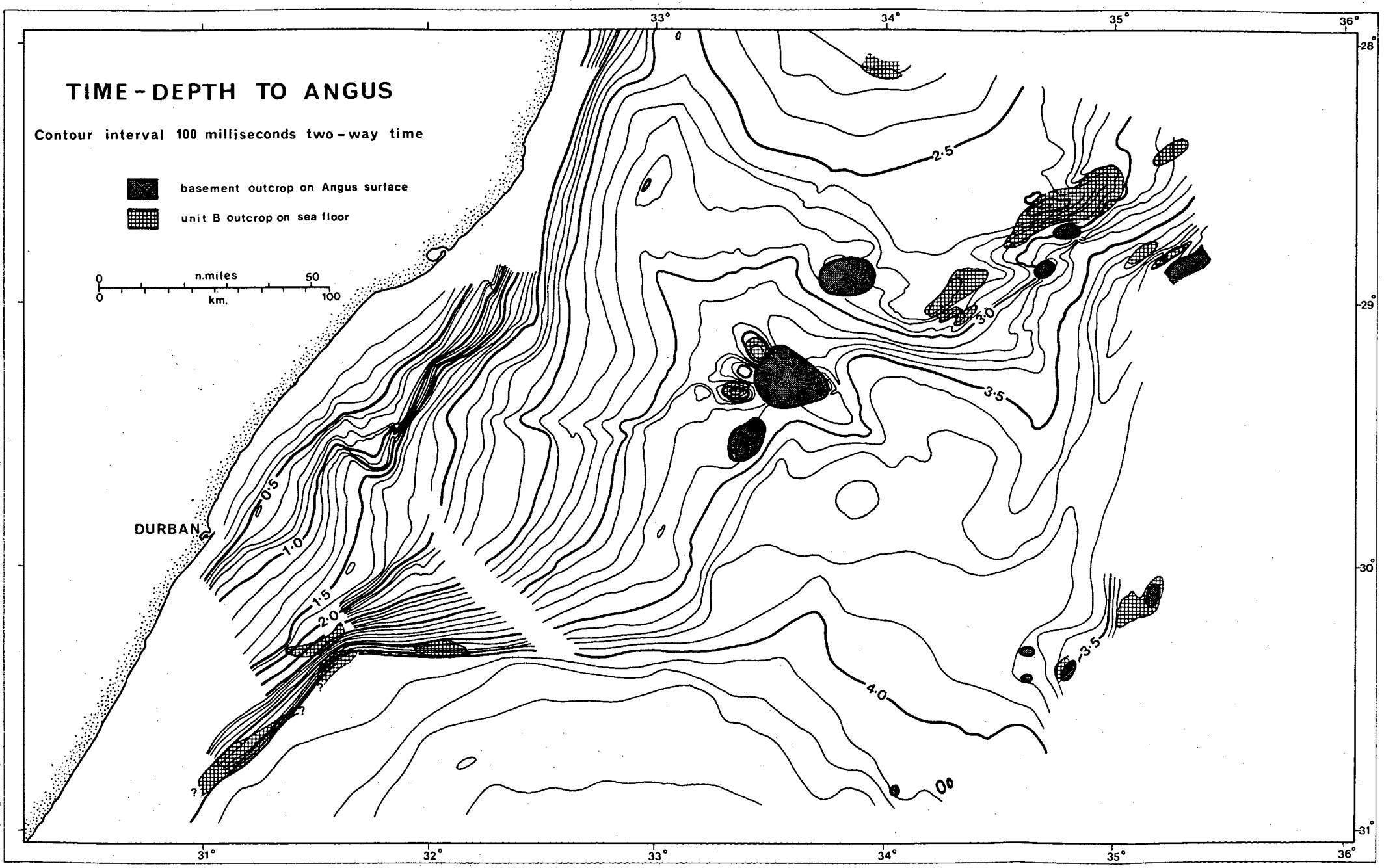
TIME - DEPTH TO ANGUS
Contour interval 100 milliseconds two - way time
basement outcrop on Angus surface
unit B outcrop on sea floor
0 n.miles 50
0 km. 100
DURBAN
0
0·5
1·0
1·5
2·0
2·5
3·0
3·5
4·0
?
33°
34°
35°
36°
28°
29°
30°
31°
31°
32°
33°
34°
35°
36°

Fig. 6.17

low gradients in all areas except its flanks. Rough surface topography is related to projected bottom current pathways (section 7.2) or basement outcrop (Fig.6.17) and thus the southern and SE flanks are most irregular with frequent ridges, mounds, valleys and moats. Horizon Angus cannot be traced within the acoustically-transparent seismic facies P of the Mozambique Ridge.

Resembling the present day morphology, the Angus deep basin plain is smooth and regular with a low gradient. Wide non-depositional and locally erosional moats are developed along the western and eastern basin margins (Figs.6.17, 6.8m and p) suggesting that deep thermohaline flow was firmly established by Angus times.

A shallow, wide curvilinear valley demarcates the eastern limit of the northern Tugela Cone and the western extent of the Central Terrace (Fig.6.17). As this valley deepens to merge with the northern deep basin, it becomes irregular with development of tributary valleys, mounds and troughs adjacent to the East Tugela Ridge.

6.6.3 Time-Depth to Jimmy

The time-depth map of horizon Jimmy (Fig.6.18) is morphologically similar to the present day sea floor (Fig.3.2) and is therefore only briefly described.

Tugela Cone morphology is almost identical to the modern configuration with steep upper slopes and southern flanks in contrast to the less steep and hummocky eastern flank. The 29° 25'S Canyon is evident as a major bathymetric feature with wide but poorly defined tributary valleys. Isochrons are omitted along site of the post-Jimmy Tugela Canyon (section 7.4).

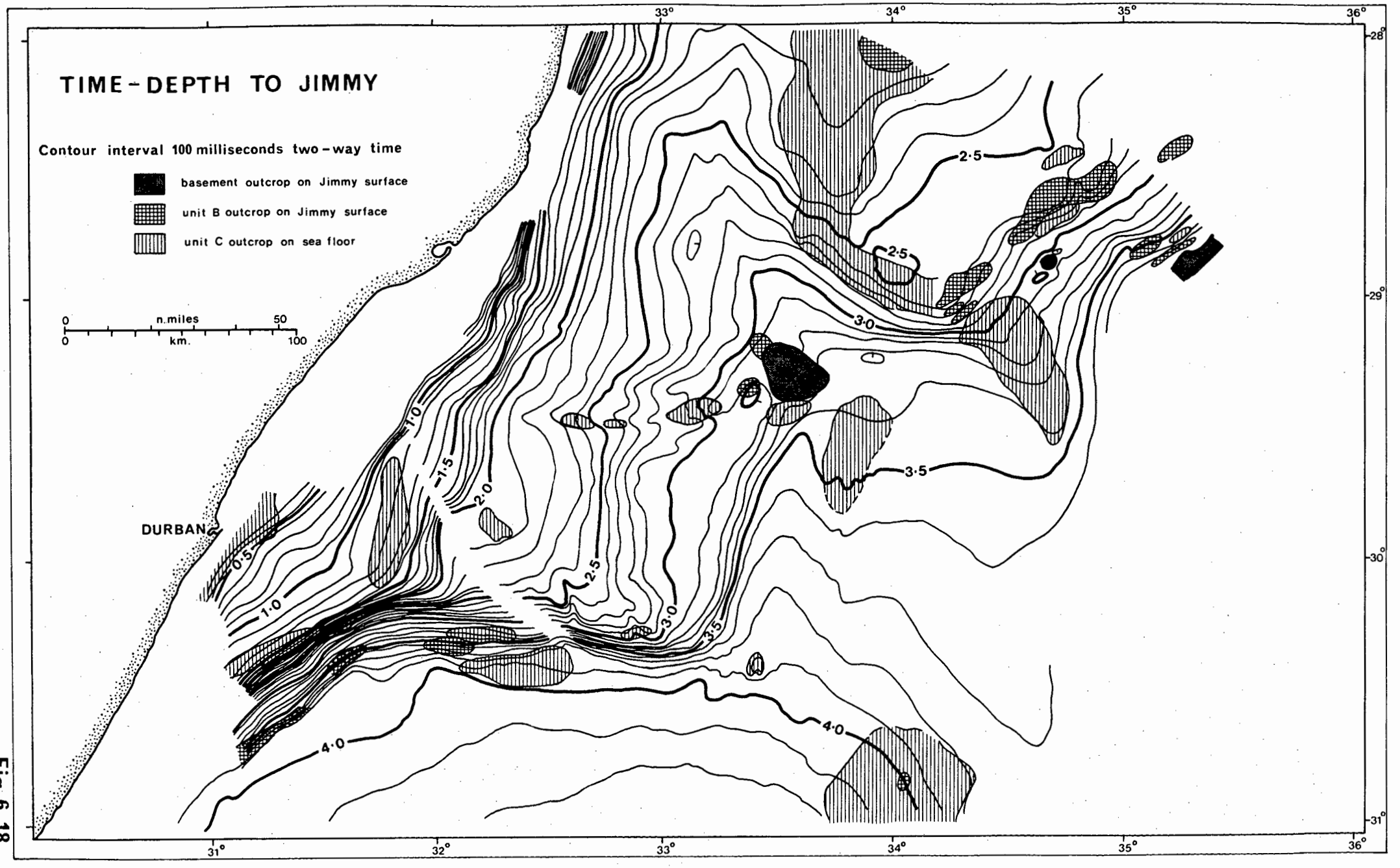
TIME-DEPTH TO JIMMY
Contour interval 100 milliseconds two-way time
basement outcrop on Jimmy surface
unit B outcrop on Jimmy surface
unit C outcrop on sea floor
0 n.miles 50
0 km. 100
DURBAN
0·5
1·0
1·5
2·0
2·5
3·0
3·5
4·0
33°
34°
35°
36°
28°
29°
30°
31°
32°

Fig. 6.18

With unit C sediments almost completely broaching the crest of the Naude Ridge basement complex, the surface expression of the Central Terrace is smooth and regular except adjacent to zones of pre-Angus strata (unit B) outcrop. The basin plain is smooth with gentle southward gradient excepting the Tugela Cone apex zone which is irregular and hummocky. Both east and west margins of the basin plain are sculpted into wide shallow moats. Trending SSE from the southeast Central Terrace, development of a low relief, elongate spur mirrors present day morphology.

6.6.4 Physiographic Development

Successive chronologic plots of several diagnostic contours and morphologic discontinuities reveals trends of net development of the major physiographic provinces. To aid graphic representation of net growth, the following parameters from McDuff, Angus, Jimmy and present day sea floors have been plotted: 1,0, 2,5, 3,2 and 3,7 sec TWT isochrons, Tugela Cone and Mozambique Ridge basal slope breaks and the valley axis separating the Tugela Cone and Central Terrace (Fig.6.19). Development of each province is briefly described.

Central Terrace Southward progression of both the 2,5 and 3,2 sec isochrons (Fig.6.19a and b) implies that the Central Terrace has steadily grown since the mid Cretaceous (McDuff) with maximum expansion towards the SE. Along the southern Central Terrace, Angus, Jimmy and present day 3,2 sec isochrons are almost superimposed (Fig.6.19a) indicating little morphologic change since the early Oligocene (Angus). Similarly, the SW Central Terrace flank has been static since the early Pliocene (Jimmy). In summary, uniform growth of the Central Terrace

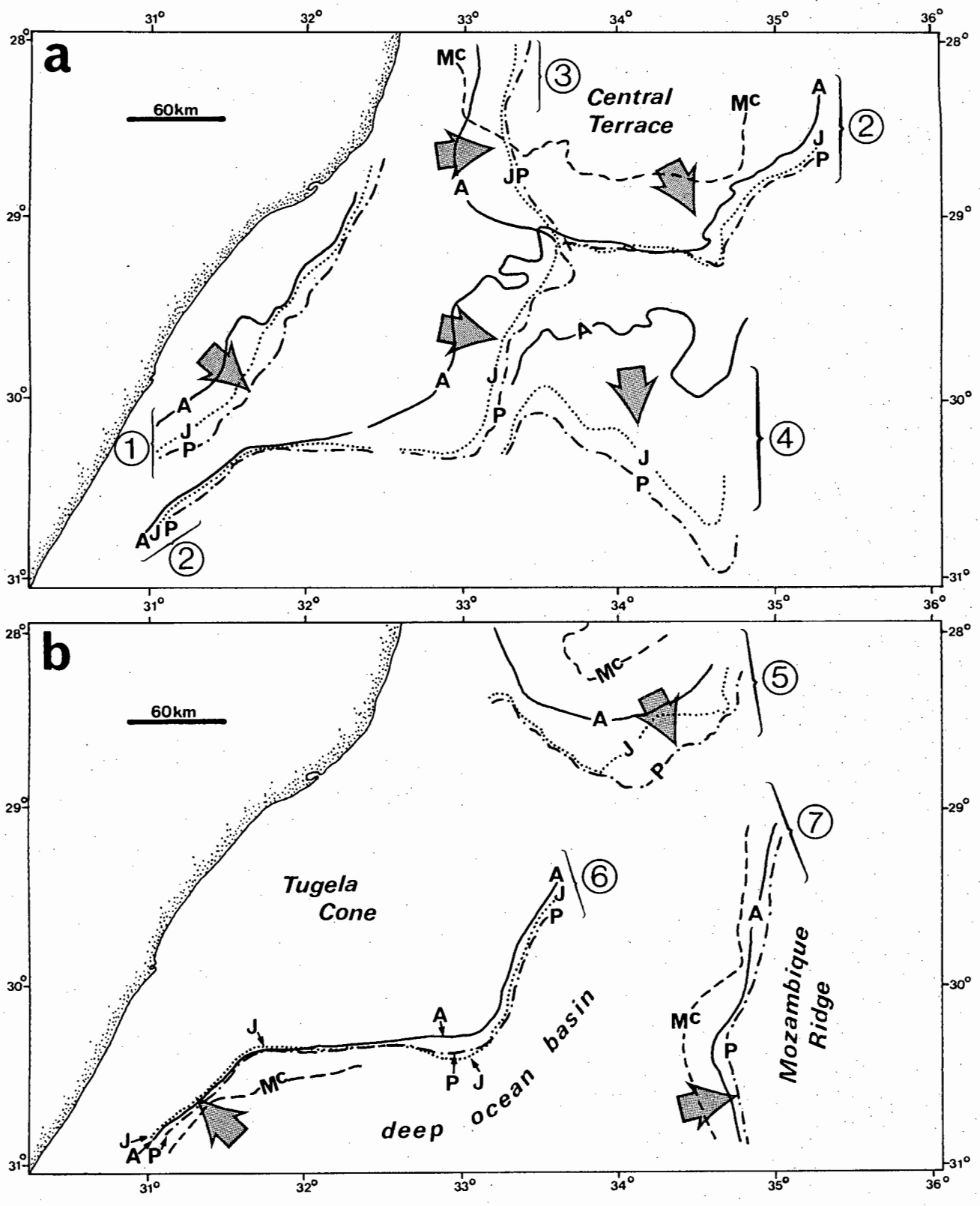

① 1.0 sec. depth contour
② 3.2 sec. depth contour
③ valley axis
④ 3.7 sec. depth contour
⑤ 2.5 sec. depth contour
⑥ Tugela Cone slope break
⑦ Mozambique Ridge slope break

--MC-- McDuff data
—A— Angus data
····J···· Jimmy data
–·P–· Present day data
Direction of net development

Data from Figs. 3.2 and 6.16 – 6.18

Fig. 6.19 MORPHOLOGIC DEVELOPMENT OF MAJOR PHYSIOGRAPHIC PROVINCES

proceeded until Angus time when asymmetric sedimentation emphasised development towards the SE while stagnating the southern margin.

Tugela Cone Progressive growth of the Tugela Cone since Angus is indicated by east and SE movement of the 1,0 and 3,2 sec isochrons (Fig.6.19a). However, a static position for the eastern cone slope break (Fig.6.19b) implies that post-Angus growth of the eastern Tugela Cone must have taken place through vertical aggradation. Along the southern Tugela Cone and SW continental slope, location of the Angus, Jimmy and present day 3,2 sec isochrons evidence only nominal growth (Fig.6.19a).

Deep Basin Plain Deep basin evolution is displayed by the sequential location of the 3,7 sec isochron (Fig.6.19a) and change in disposition of its marginal slope breaks (Fig.6.19b). Southward shift of the 3,7 sec isochron implies progressive infilling of the deep basin. Eastward movement of the Mozambique Ridge slope break (Fig.6.19b) suggests that the deep basin fill has progressively overlapped ridge sediments since McDuff times. Similarly, along the SW continental slope, basinal sediments encroach over slope sediments up to horizon Jimmy (Fig.6.19b). In this zone, however, slope sedimentation assumed dominance in post-Jimmy times as indicated by the present day slope break location.

6.7 SEDIMENTATION RATES AND BUDGET

6.7.1 Sedimentation Rates

Net accumulation rates reflect the interaction of several parameters including sea-level changes, climate (weathering,

precipitation and run-off), hinterland configuration and current action. High sedimentation rates are indicative of active hinterland denudation and high riverine sediment yield. Rapid biogenic carbonate accumulation reflects high influx of dissolved nutrients (Frakes, 1979). To sustain high run-off with abundant suspended and dissolved load, high precipitation rates are required. Diminished action of current-induced redispersal enhances the probability of local high accumulation rates. Rapid basin subsidence may also permit local rapid sedimentation.

Maximum sedimentation rates for each depositional sequence (sediment units A-D) have been calculated for selected physiographic provinces (Table 6.3 and Fig.6.20). Minimum rates for each sub-facies (Table 6.1; thickness range) primarily equate to areas of non-deposition or erosion (current scour or basement exposure) and low sediment supply. In general, within each depositional sequence, highest sedimentation rates are recorded over the Tugela Cone, particularly the northern and upper slopes. Reduced rates on the deep basin and Central Terrace provinces are a result of low detrital supply (distance from hinterland).

Accumulation rates for the depositional sequences of the Tugela Cone show a distinct trend through time (Table 6.3 and Fig.6.20). Using the upper Tugela Cone as an example, maximum rates for unit A are relatively high (119 m/my) declining through unit B (53 m/my) to unit C (40 m/my) before sharply increasing to 86 m/my in post-Jimmy times (unit D). The sedimentation rate jump for unit D is apparent in all Tugela Cone sub-facies (Fig.6.20). Proportionately-equivalent increases characterise the upper, south and east Tugela Cone whereas, over the northern

Table 6.3 Maximum Sedimentation Rates

SUB-FACIES[1]	LOCATION	SONIC[2] VELOCITY (km/sec)	MAXIMUM THICKNESS (secs TWT)	(m)	SEDIMENTATION[3] RATE (m/my)
A_2	deep basin (south)	4,0	1,2	2400	89
A_3	Moz. Ridge	2,2	1,0	1100	41
A	Tugela Cone (upper)	4,0	1,6	3200	119
B_1	Central Terrace	2,0	0,7	700	14
B_3	deep basin (north)	2,0	1,05	1050	21
B_6	Tugela Cone (upper)	2,7	~2,0	2700	53
C_1	Central Terrace	2,0	0,3	300	14
C_3	deep basin	2,0	0,3	300	14
C_5(dp1)	Tugela Cone (north)	2,7	0,65	878	42
C_6(dp2)	Tugela Cone (upper)	2,7	0,62	837	40
C_7(dp3)	Tugela Cone (east)	2,0	0,52	520	25
C_8	Tugela Cone (south)	2,0	0,3	300	14
D_1	Central Terrace	2,0	0,11	110	22
D_3	deep basin	2,0	0,09	90	18
D_4(dp1)	Tugela Cone (north)	2,2	0,6	660	132
D_5(dp2)	Tugela Cone (upper)	2,7	0,32	432	86
D_6(dp3)	Tugela Cone (east)	2,0	0,42	420	84
D_7	Tugela Cone (south)	2,0	0,3	300	60

1 - dp notation refers to depocentres 1-3 of units C and D (Figs.6.13 and 6.14)

2 - sonic velocity data from same sources as in Table 6.2

3 - basal unit A sediments dated as 125 Myr (start of post-drift subsidence and ?sedimentation); sequence boundary hiatus ranges or time (Fig.6.3) - McDuff (98-86 Myr), Angus (35-26 Myr), Jimmy (5 Myr); sediment unit time-span - unit A (27 my), unit B (51 my), unit C (21 my) and unit D (5 my).

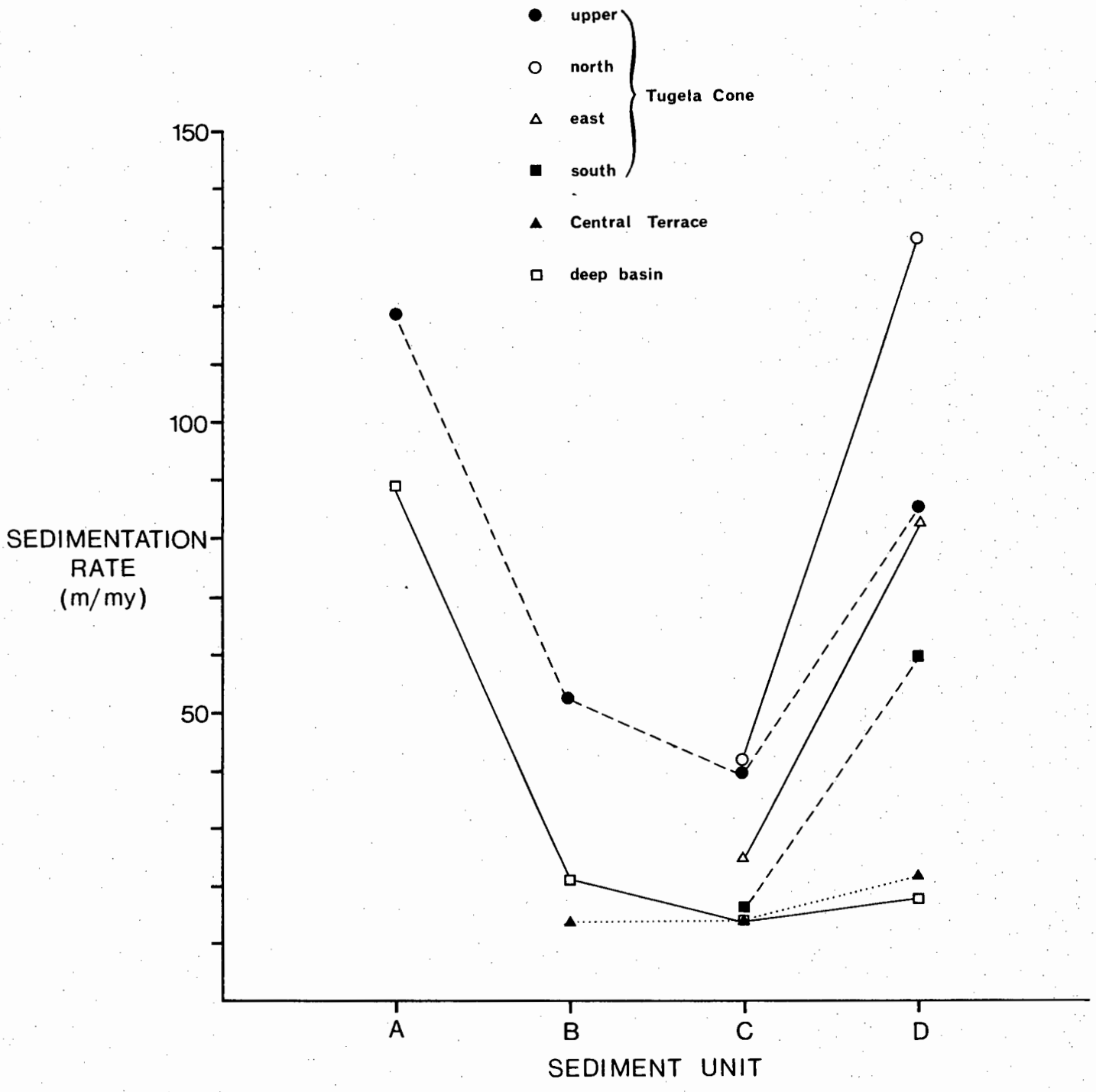

Fig. 6.20 COMPARISON OF SEDIMENTATION RATES BETWEEN DEPOSITIONAL SEQUENCES (SEDIMENT UNITS A-D)

Tugela Cone, unit D deposition rates are strongly exaggerated (Fig.6.20; 132 m/my). This emphasises the switching nature of deep-sea fan sedimentation. Similar trends are defined in the deep basin and Central Terrace provinces except that the unit D increases are not prominent (Fig.6.20). This implies that, since horizon Jimmy times, the Tugela Cone has been the major sediment sink with only minor aggradation taking place over the basin plain and Central Terrace. The major factors controlling these trends include: (1) terrigenous detritus supply rate; (2) basin subsidence rate; and (3) current influences.

High net sedimentation rates in unit A may be a result of two mechanisms. Firstly, continental fragmentation creates topographic relief adjacent to the newly-formed basin (Hay et al, 1981) encouraging development of a vigorous drainage system with resultant high sediment yield. Secondly, after the onset of drift, the high hinterland sediment yield is likely to be trapped in the newly-formed marginal basin. Rapid initial subsidence of the continental margin (Fig.5.17) may permit fast accumulation in proximal areas of the basin (proto-Tugela Cone).

Sedimentation rates decrease during units B and C and may indicate progressive hinterland peneplanation or climatic change leading to a reduction in sediment yield. Alternatively, declining subsidence rates (Fig.5.17) may induce sediment bypass of the proximal basin zones.

Acceleration of the sedimentation rate during unit D deposition has several possible explanations. Climatic deterioration in the last 5 my (Frakes, 1979; Donnelly, 1982), with dominance of cool or glacial episodes, fostered high run-off and erosion and hence high sediment yield to the offshore basin.

Late Tertiary hinterland uplift (Smith, 1982), if it took place, may also have increased erosional processes. In addition, low sea level stands (e.g. late Pliocene and Pleistocene; Dingle et al, 1983) allowed direct dumping into offshelf zones thus increasing the sedimentation rate. During glacial phases (e.g. Pleistocene), the Agulhas Current was reduced in vigour (Be and Duplessy, 1976; Hutson, 1980). With a decline in current-induced winnowing and sediment redistribution, general sedimentation rate increases may have resulted.

Gross Natal Valley sedimentation rate variations through time mirror local (Zululand), regional (SW Indian Ocean) and global rate changes (Table 6.4). In particular, the acceleration of sedimentation within unit D (post-early Pliocene) is paralleled by similar increases within regional and global data. Good correlation to regional and global data (Table 6.4) may imply that factors other than local conditions have been significant in defining Natal Valley sedimentation rates. Climatic changes (Davies et al, 1977a) and global sea-level changes (Shanmugam and Moiola, 1982) are considered to be the major controls on basinal sediment accumulation rates.

6.7.2 Sedimentation Budget

Volumetric data for the mid Natal Valley sediment fill (Tugela Cone and deep basin plain) may be combined with modern terrigenous supply to construct a preliminary sedimentation budget. Hinterland terrigenous sediment yields have been calculated by Flemming and Hay (1983) and are presented in Table 6.5. Biogenic supply rates are based on average calcium carbonate contents over the major terrigenous depocentres

Table 6.4 Comparison of Local, Regional and Global Sedimentation Rates[1]

SEDIMENT UNIT	SEQUENCE[2] AGE	NATAL[3] VALLEY	ZULULAND[4]	248[5]	250[5]	ATLANTIC/[6] INDIAN OCEANS
A	pre-Cenom.	20-81	15-70	-	-	-
B	Coniacian-Oligocene	8-45	16-53	2,5*	-	0-17
C	Oligocene-Miocene	5-32	-	14	25+	2-35
D	Pliocene-Recent	10-66	-	35	47	25-45

1 - rates in m/my
2 - sequence ages from Fig.6.3 and Table 6.3
3 - range of average sedimentation rates for all sub-facies of the Tugela Cone, Central Terrace and basin plain
4 - data from McLachlan and McMillan (1979)
5 - DSDP sites 248 and 250 (data from Simpson, Schlich et al, 1974; Davies, Luyendyk et al, 1974)
6 - data from Davies et al (1977a)
+ - Miocene only
* - Eocene only

Table 6.5 Annual Modern Sediment Supply to the Mid Natal Valley

DRAINAGE[1] REGION	TERRIGENOUS[2] INPUT ($10^6 m^3$)	BIOGENOUS[3] INPUT ($10^6 m^3$)	TOTAL INPUT ($10^6 m^3$)
I	4,845	-	
II (Tugela)	5,874	-	
III	4,243	-	
mid Natal Valley	14,962	2,236	17,198

1 - drainage regions (effective hinterland) from Fig.1.5
2 - data from Flemming and Hay (1983) - see Table 1.1
3 - biogenous input calculated by assuming it is equivalent to 13% of the total input - this average is taken from the upper and southern Tugela Cone terrigenous depocentres (cores 30-34 and 5115-5117) where the balance between modern terrigenous input and the carbonate flux should be reasonably established

combined with the terrigenous input (Table 6.5). The annual total sediment input to the mid Natal Valley is calculated at $17,2 \times 10^6 m^3$.

Volumes and volumetric sedimentation rates have been computed for post-Pleistocene sediments, post-Jimmy sediments (unit D) and the total sediment pile in the mid Natal Valley (Table 6.6). Sediment pile volumes for units A and B could not be estimated because of the poor data control over the Tugela Cone (e.g. Fig.6.12). Calculation methods are outlined in Table 6.6. Volumetric rates and modern inputs are compared in Table 6.6 and indicate a vast modern 'over-supply' of sediment. The modern input is 5-8 times greater than required to have constructed the calculated volumes of any of the three chronostratigraphic sequences. From past accumulation rates, it is inferred that past sediment input may only have been equivalent to 12-22% of the modern supply (Table 6.6). This disparity may be explained in three ways:

(1) A major proportion of the modern supply is exported from the mid Natal Valley. However, there are no identifiable dispersal routes suggestive of large-scale sediment export although some suspended fine fraction detritus must be lost through southward Agulhas Current and NADW flow;

(2) Sediment input has been over-estimated and the depocentre volumes under-estimated. Although errors of this nature are inevitable (e.g. wrong thickness assumptions, no correction for compaction, over-estimation of the carbonate flux and unknown effects of the Agulhas Current in supplying and removing detritus), they are unlikely to be of sufficient magnitude;

Table 6.6 Comparison of Past Sedimentation Rates and Modern Supply

	SEDIMENT[1] VOLUME($10^{12}m^3$)	DEPOSITIONAL[5] PERIOD (my)	SEDIMENTATION RATE($10^{12}m^3$/my)	% OF MODERN[6] SUPPLY
post-Pleistocene[2]	0,041	0,011	3,727	21,7
post-Jimmy[3]	10,98	5	2,196	12,8
total sed.[4] sequence	319,72	125	2,558	14,9

1 - excluding Central Terrace and Mozambique Ridge provinces

2 - volume calculated assuming an average thickness of 0,7 m over the Tugela Cone (cores 5117 and 5753; section 8.4.1.2) and 0,2 m over the basin plain (cores 361F and 361J; Vincent, 1970)

3 - volume calculated by integrating areas of the post-Jimmy (sediment unit D) isopachyte map (Fig.6.14). Sonic velocity assumed to be 2,0 km/sec

4 - volume calculated assuming an average thickness of 4,5 km for the Tugela Cone/SW continental slope and 2,5 km for the deep basin plain (Table 6.2)

5 - depositional periods from Table 6.3 and Broecker et al (1960)

6 - it is assumed that the major proportion of modern terrigenous input is deposited over the Tugela Cone and deep basin plain (Central Terrace and Mozambique Ridge excluded from volume calculations). Modern supply estimated at 17,2 x 10^6m^3 per annum (Table 6.5).

(3) Modern sediment input rates are significantly higher than in the geologic past. Accelerated erosional rates may be caused by environmental change or human activity, the latter being well-documented in USA (Toy, 1982). Modern erosion in the Tugela catchment has been estimated to be 28 times higher than in the geologic past, probably as a result of poor land management (Murgatroyd, 1979).

In conclusion, although all three options may contribute, modern agricultural malpractice in Natal and Zululand is the most likely explanation of the wide disparity between modern input and past accumulation rates.

CHAPTER 7 MAJOR SEDIMENTATION CONTROLS AND PROCESSES

7.1 INTRODUCTION

Major processes active in the modern Natal Valley or which have been operative in the geologic past include: (1) sediment redistribution by deep current flow; (2) hiatus formation; (3) canyon development; and (4) sediment mass movement. Effects of these processes, although well-documented in other continental margin and abyssal plain regions, have not been evaluated with respect to the mid Natal Valley. Goodlad (1979), however, presented some preliminary conclusions on current-controlled sediment dispersal and redistribution. To generate an overview model for Natal Valley sediment dynamics and dispersal, it is necessary to fully examine the influences of these four major processes.

Accordingly, the purpose of this chapter is four-fold. Firstly, the influence of deep geostrophic and thermohaline currents on sedimentation is outlined. Secondly, mechanisms of hiatus development in relation to local and global events are reviewed and assessed. Thirdly, major canyon evolution and the implications for sediment dispersal are briefly discussed. Finally, the role of sediment mass movement processes is appraised.

7.2 CURRENT-CONTROLLED SEDIMENTATION

7.2.1 Introduction

Abyssal contour current circulation as a primary influence over sedimentation dynamics has been well-documented within all

the major ocean basins (Hollister and Heezen, 1972; Kolla et al, 1980a; Mullins et al, 1980; Pinet and Popenoe, 1982; Scrutton and Stow, 1984). Recent studies have indicated that, within the SW Indian Ocean, both surface and deep components of the regional circulation system are locally major controls over sedimentation processes (Johnson and Damuth, 1979; Kolla et al, 1980a; Martin, 1981; Westall, 1984). Abundant evidence exists to prove the action of bottom currents in all water depths of the mid Natal Valley. Common occurrence of current-controlled bedforms, asymmetric sedimentation and erosional/non-depositional zones confirms active vigorous current scour. In addition, Flemming (1980; 1981) has verified the erosive competence of the Agulhas Current on the continental shelf zone.

Oceanographic and geologic evidence which verify the widespread action of bottom current flow within the mid Natal Valley are outlined in this section. Gross characteristics of the basin fill (thickness, sea floor topography and bedforms) are related to semi-permanent features of Agulhas Current and North Atlantic Deep Water (NADW) flow and to the shelf sediment compartment model of Flemming (1981). Finally, a conceptual model of deep basin flow is presented.

7.2.2 Major Current Pathways

Physical oceanography has been fully described in Chapter 2 and only a brief summary is presented here. Agulhas Current southward flow may alternatively follow either of two pathways (Fig.2.1) (Harris and van Foreest, 1977): (1) route X which traverses the northern Natal Valley following the 1000 m isobath to impinge on the continental margin south of 28°S; and (2) route

Y which meanders along the Mozambique Ridge crest before looping westward between 29°S and 32°S to conflux with route X south of Durban. North Atlantic Deep Water (NADW) flows beneath the ~2500 m lower limit of Agulhas Current deep water. NADW enters the mid Natal Valley in the SW and flows north constrained by adjacent bathymetric highs (continental slope and Tugela Cone). On encountering the Central Terrace, NADW flow is deflected to flow south along the west Mozambique Ridge flank (Fig.2.8).

7.2.3 Sediment Thickness and Current Circulation

From seismic-stratigraphic analysis (section 6.4), an upsurge in current-controlled sedimentation in post-Angus times is inferred. Comparison of units C and D time-thickness maps (Figs.6.13 and 6.14) reveals gross correspondence of thick and thin sediment zones suggesting stabilisation of major sedimentation controls. Accordingly, a post-Angus sediment (combined units C and D) isopachyte map (Fig.7.1) has been constructed. In general, areas of fast accumulation are associated with proximity to detrital supply and either sluggish currents or shear between opposing flow. Slow sedimentation areas and non-depositional/erosional zones are correlated with vigorous current flow and low sediment supply rates.

7.2.3.1 Zones of Thin Sediment

Areas of thin sedimentation (arbitrarily defined by the 0,2 sec isopach - Fig.7.1) are recognised over the Central Terrace, Mozambique Ridge and marginal zones of the deep basin plain. Assuming a velocity of 2 km/sec, the average accumulation rate is <8 m/my. Regions of pre-Angus (unit B) and pre-Jimmy (unit C)

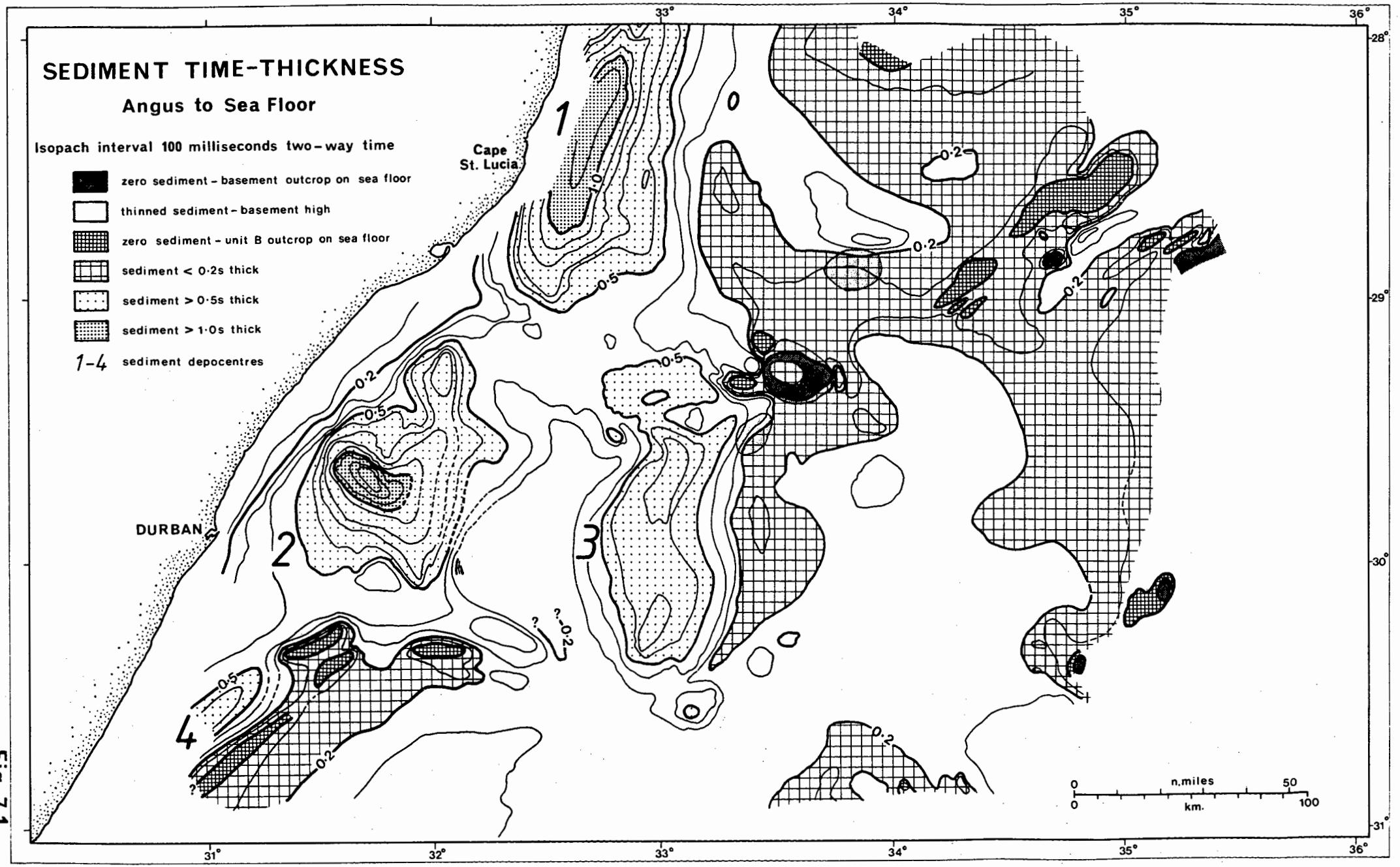
SEDIMENT TIME-THICKNESS
Angus to Sea Floor
Isopach interval 100 milliseconds two-way time
zero sediment - basement outcrop on sea floor
thinned sediment - basement high
zero sediment - unit B outcrop on sea floor
sediment < 0·2s thick
sediment > 0·5s thick
sediment > 1·0s thick
1-4 sediment depocentres
Cape St. Lucia
DURBAN
33°
34°
35°
36°
28°
29°
30°
31°
0
n.miles
50
0
km.
100

Fig. 7.1

strata outcrop are delineated in Figure 7.2 and are clearly associated with the thin sediment zones (compare Figs.7.1 and 7.2).

Above 2500 m, Agulhas Current deep water dominates the flow regime and, in conjunction with reduced sediment supply, can explain the disposition of the Central Terrace and Mozambique Ridge thin sediment provinces. These topographic highs are separated from the hinterland by flanking valleys and have probably had a history of low sediment supply, partially explaining the thin post-Angus drape. The high incidence of units B and C outcrop over the Central Terrace flanks (Fig.7.2) reflects vigorous current scour by components of the Agulhas Current. The extensive zone of unit C outcrop over the west Central Terrace is a result of erosive action of route X while exposure of units B and C strata over the SE Central Terrace is a response to intensive route Y scour. Over the western Central Terrace, unit C exposure is however coincident with a region of thick (0,2-0,4 secs) post-Angus sediment (Figs.7.1 and 7.2). Transformation from depocentre to erosive zone may imply post-Jimmy upsurge in route X activity.

Southward route Y flow over the Mozambique Ridge may be partly responsible for thin post-Angus accumulation together with low sediment supply. Current influences on the Mozambique Ridge crest is corroborated by recovery of an incomplete and condensed Pliocene and Quaternary sequence at DSDP 249 (Simpson, Schlich et al, 1974). Erosive zones on the Tugela Cone upper slope (Fig.7.2) are flanked by post-Jimmy depocentres which exhibit marginal truncation of reflectors. Initiation of upper slope erosion again suggests intensification of route X flow in post-

Fig.7.2

Distribution of Current-Control Indicators

1 - acoustic basement outcrop at sea floor; 2 - pre-Angus (unit B) strata outcrop at sea floor; 3 - pre-Jimmy (unit C) strata outcrop at sea floor; 4 - areas in which the sea floor topography is considered to be principally or occasionally generated by bottom currents; 5 - sea floor topography classification (see section 3.3.2); 6 - winnowed surficial samples; 7 - core barrel damage by ? hard sub-strate; 8 - sand fraction reworking; 9 - current-induced ripple lamination (traction flow); 10 - pre-Jimmy (unit C) strata recovered by coring; 11 - erosional and non-depositional moats; 12 - seismic profile location and number (see Figs.7.3-7.5); 13 - refers to seismic profile line drawings in Figs.7.3-7.5.

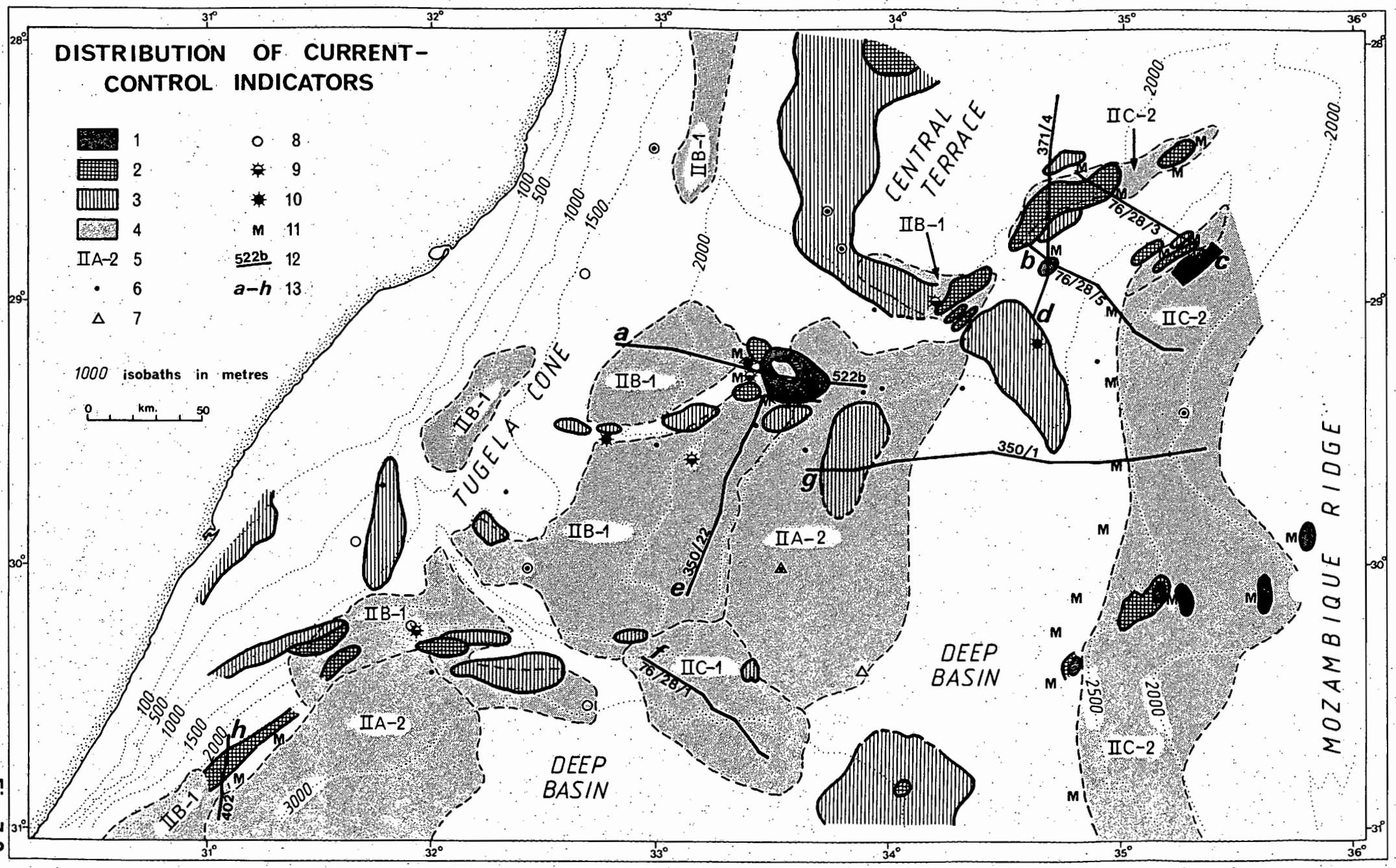
DISTRIBUTION OF CURRENT-CONTROL INDICATORS
1
2
3
4
IIA-2 5
6
7
8
9
10
M 11
522b 12
a–h 13
1000 isobaths in metres
0 km. 50
CENTRAL TERRACE
TUGELA CONE
DEEP BASIN
DEEP BASIN
MOZAMBIQUE RIDGE
IIB-1
IIA-2
IIC-1
IIC-2
522b
350/1
350/22
76/28/1
76/28/3
76/28/5
371/4
100
500
1000
1500
2000
2500
3000
28°
29°
30°
31°
31°
32°
33°
34°
35°
36°

Fig. 7.2

Jimmy times.

The basin-margin distribution of thin sediment accumulation zones is closely coincident with and therefore considered a response to the projected course of NADW flow. Within the deep basin, zero net sedimentation zones are most common along the western margins (Figs.7.1 and 7.2). However, the west margins probably receive relatively high detrital input on account of their proximity to the Tugela Cone. Over-riding the high input rate to cause extensive local non-deposition testifies that NADW scour is more powerful along the western basin margins, possibly due to Coriolis intensification.

7.2.3.2 Zones of Thick Sediment

Thick post-Angus sediment accumulation is restricted to four major depocentres on the Tugela Cone and SW continental slope (Fig.7.1; depocentres 1-4). Proximity to hinterland with resultant high detritus influx rate is the major control over their location while current flow is a secondary influence on their disposition. Several mechanisms may have individually or collectively influenced depocentre establishment:

(1) During low sea-level stands, the continental shelf is sub-aerially exposed. Increased hinterland gradient and enhanced denudation, caused by the sea-level drop, supplies large volumes of terrigenous detritus directly to the upper continental slope. Furthermore, during glaciation-induced low stands, Agulhas Current flow may be abated (Be and Duplessy, 1976; Hutson, 1980) reducing the potential for winnowing and removal of fine fraction detritus;

(2) The modern east coast shelf may be subdivided into four

independent sedimentary compartments (Flemming, 1981). The extent of separate compartments is governed by combination of structural and oceanographic controls: (a) bedload parting zones reflecting change from southward to northward flow; and (b) structural offsets where the shelf sand stream overshoots the shelf edge. This model demonstrates that bedload detritus is locally dumped within each compartment where the current-controlled sand stream overshoots the shelf. Flemming (1981) has estimated that >80% of Holocene bedload input has been transferred to off-shelf depocentres. Sedimentary compartment 2 (27,5°S-30,3°S) is the effective hinterland to depocentres 1 and 2 (Fig.7.1). Depocentre 4 is developed adjacent to the northern reaches of sedimentary compartment 3.

(3) During high sea-level phases with a powerful Agulhas Current, high velocity core flow of route X may become decoupled from more sluggish offshore waters creating a series of vortices within a slack water zone along its eastern margin. In an analogous situation, shear between coastal currents and the Agulhas Current core produces a vortex zone on the continental shelf (Fig.2.3). Sediment-laden water, becoming entrained in slack flow zones, should dump a proportion of its load in response to energy reduction. Sediment dumping along the eastern boundary of route X may have contributed to upper slope depocentre development.

Depocentre 2 has aggraded in the lee of a major structural offset at 29°S (Fig.7.1) where, during high sea-level stands, the shelf sand stream overshoots the shelf edge. This mechanism, in conjunction with direct upper slope dumping during low sea-level stands, has fostered growth of depocentre 2. Depocentre 1 has

developed adjacent to the narrow shelf north of Cape St. Lucia (Fig.7.1). During sea-level low stands, detritus supplied by a more extensive Zululand drainage system (Hill, 1975) would have been directly transferred to the upper slope depocentre. In modern times, canyon heads tap the shelf sand stream and thus channel detritus to depocentre 1. Depocentre 4 has aggraded on the SW continental slope (Fig.7.1). Direct upper slope dumping during low sea-level stands was probably the major process constructing depocentre 4. Two factors may have influenced growth of depocentre 3 on the Tugela Cone eastern flanks. Gravity-controlled flows in the 29° 25'S fan-valley, on encountering reduced gradients, probably deposited their sediment load in stacked levee systems (Chapter 9). Secondly, shear between SW flow of the Agulhas Current and NE contour circulation of NADW may result in settling of particles from sediment-laden waters.

7.2.4 Sea Floor Topography

Sea floor microrelief zones of the mid Natal Valley are classified and described in section 3.3. Backed up by seismic reflection profiles, correlation to previous echo character nomenclature (e.g. Damuth, 1980) has been attempted (Table 3.2). It is thus possible to define topographies generated in response to bottom current flow. On comparison to the investigations of Damuth (1978; 1980), a summary of categories interpreted as being principally or occasionally generated by bottom currents is presented below:

(IIA-1) - echoes of this type have been ascribed to bedforms created by gravity-controlled mass flows, turbidity current flow

and contour current activity and is thus not diagnostic of any one sedimentation process;

(IIA-2) - category IIA-2 is assumed to represent small erosional and/or non-depositional bedforms (ripples, sediment waves, erosional furrows) generated under the influence of bottom currents;

(IIB-1) - generation of these contourite mounds (broad, low-amplitude mounds with disconformable, migrating sub-bottoms) is attributable to contour current flow;

(IIC-1) - category IIC-1 (single, regular or irregular hyperbolae with conformable sub-bottom reflectors) may be related to turbidity current/mass flow and current-controlled deposition depending on the environmental setting. IIC-1 echoes are restricted to the Tugela Cone apex (Fig.3.5; zone 11) and the adjacent deep basin where current action is favoured as a major control. Initial influence of mass flow is however not entirely discounted;

(IIC-2) - topographies of this category denote zones of large, irregular, symmetric or asymmetric sediment billows, often with migrating and outcropping sub-bottoms. Similar billow morphologies have been delineated in the Agulhas Passage (Westall, 1984) and on the eastern Mozambique Ridge (Kolla et al, 1980a) and ascribed to bottom current flow.

From these interpretations, IIA-2, IIB-1, IIC-1 and IIC-2 topographies are indicative of permanent current control on sedimentation processes. Distributions of these four categories are presented in Figure 7.2 and indicate that regions dominated by current-controlled sedimentation include: the western Mozambique Ridge, south and SE Central Terrace, lower flanks of

the SW continental slope, southern and eastern Tugela Cone flanks and the western deep basin margins.

Type IIA-1 topographies, characterising the Tugela Cone upper slope and Central Terrace flanks, may partially be a response to current scour. This is particularly likely for the Central Terrace flanks where IIA-1 topographies are coincident with zones of unit C (pre-Jimmy) outcrop (compare Figs.3.9 and 7.2).

7.2.5 Current-Controlled Bedforms

Two styles of bedform, consistent with the microrelief zonation, are considered to be products of current-controlled sedimentation processes: (1) migrating sediment waves; and (2) sediment billows.

7.2.5.1 Migrating Sediment Waves

Sediment waves have been observed throughout the major oceanic basins and have been ascribed to sedimentation under control of both themohaline currents and downslope processes such as turbidity currents (Embley and Langseth, 1977; Bouma and Treadwell, 1975). Large fields of sediment waves are common to continental rises which are swept by fast undercurrents and which are characterised by high sedimentation rates (Embley and Langseth, 1977; Lonsdale and Smith, 1980). Measured dimensions of individual waveforms are very variable, characteristically ranging from 0,5 to >5 km in wavelength and from 10 to >100 m in amplitude. Along basin margins, sediment waves migrate almost exclusively in an upslope direction (Asquith, 1979; Lonsdale and Smith, 1980).

Within the Natal Valley, extensive fields of migrating waves have been delineated by recognition of topography type IIB-1 (Fig.7.2) and confirmed by seismic reflection profiles (Figs.7.3a, 7.4e and 7.5f). Profile locations are shown in Figure 7.2. The low eastern and southern flanks of the Tugela Cone are characterised by distinctive asymmetric migrating sediment waves (Figs.7.2, 7.3a and 7.4e). These waveforms are typically 10-40 m in amplitude with wavelengths ranging from 1-10 km. True orientation of the waves cannot be accurately determined on existing data but they appear to be preferentially oriented sub-parallel to the cone margin. Wave crests display upslope migration evidenced by the pattern of internal reflectors which show preferential deposition on their upslope flanks (Fig.7.3a). Current action is further corroborated by the common erosional truncation of reflectors inthe sediment wave zone (Fig.7.4e). Consistent thickening of sediments occurs on the upslope flank of each migrating wave. This suggests that the wave formation model of Lonsdale and Hollister (1979), developed on Rockall Trough data, may be applicable to the Natal Valley. In both cases, the sediment waves strike parallel to the regional flow route. The model relies on the isobar gradient being steeper on the downslope flank relative to the upslope flank. Under these conditions, there is a tendency for lower velocity geostrophic flow and hence faster deposition on the upslope flank thus maintaining upslope migration. Sub-bottom reflector configuration indicates that, on the Tugela Cone eastern flank, sediment wave formation has been active since at least Angus time (early Oligocene) within sub-facies C_7 and D_6, although only becoming dominant midway between the Angus and Jimmy

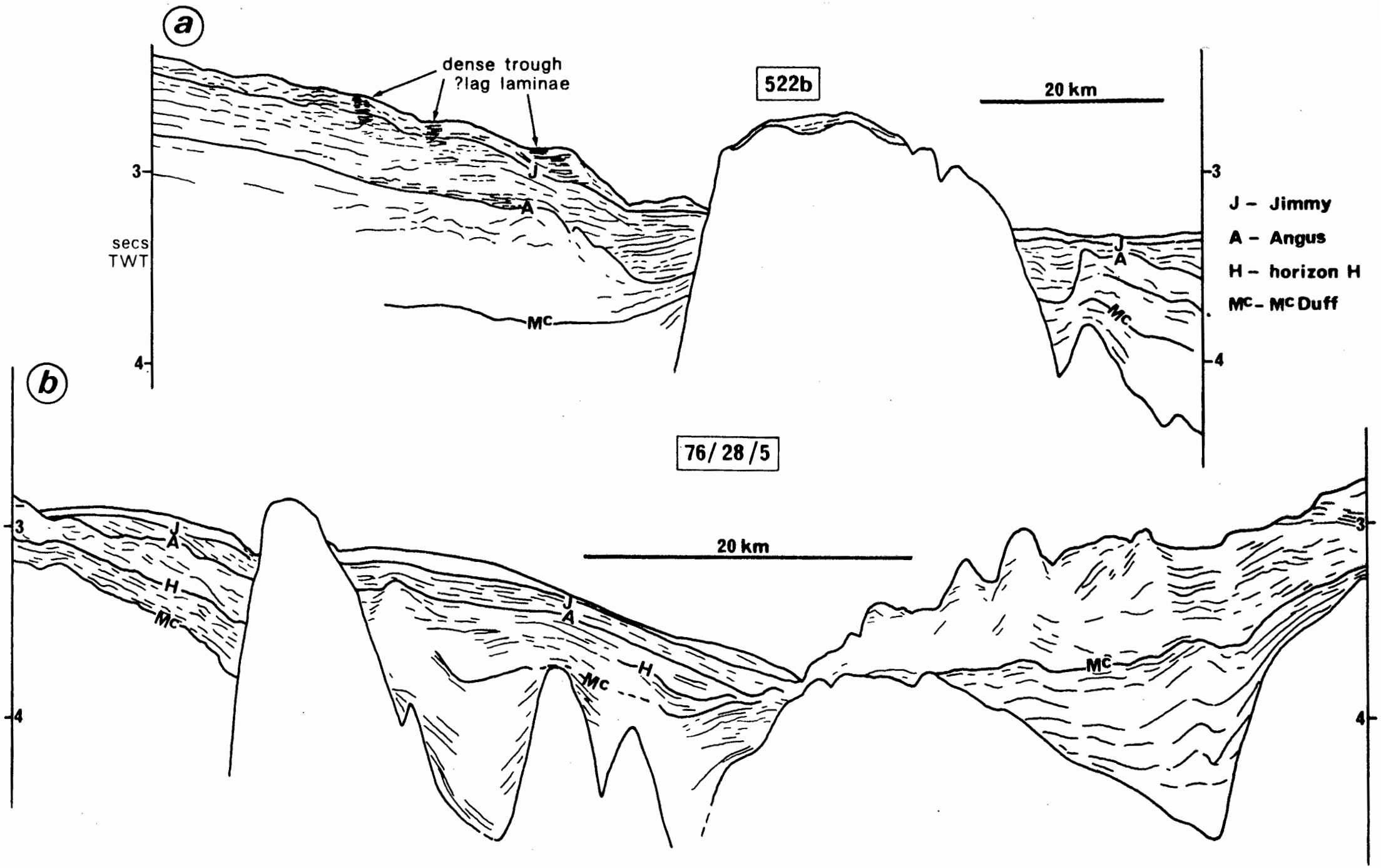

Fig. 7.3 CURRENT-CONTROLLED BEDFORMS AND MOATING

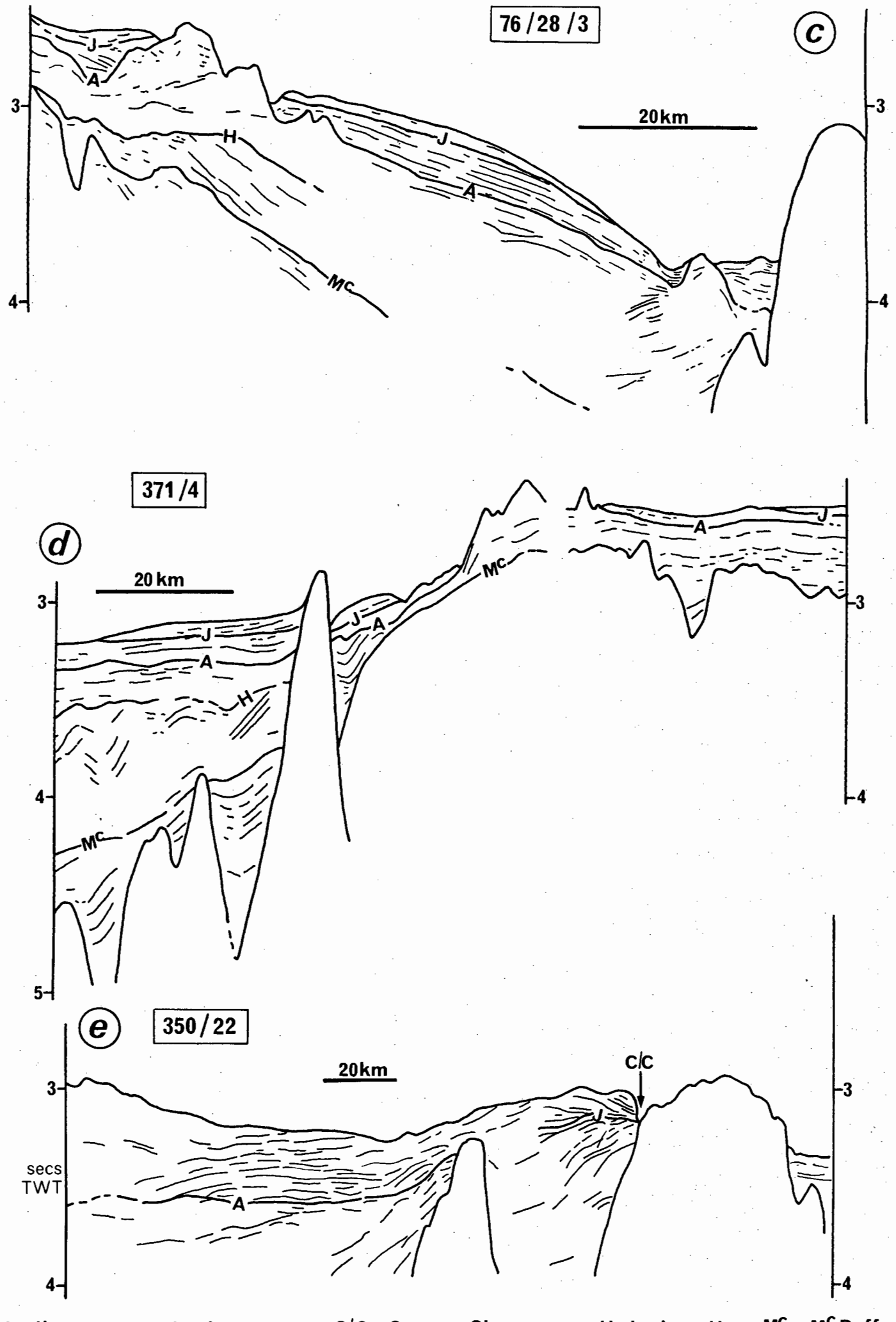

J – Jimmy A – Angus C/C – Course Change H – horizon H M^C – M^C Duff

Fig. 7.4 BEDFORMS, ASYMMETRIC SEDIMENTATION AND MOATING

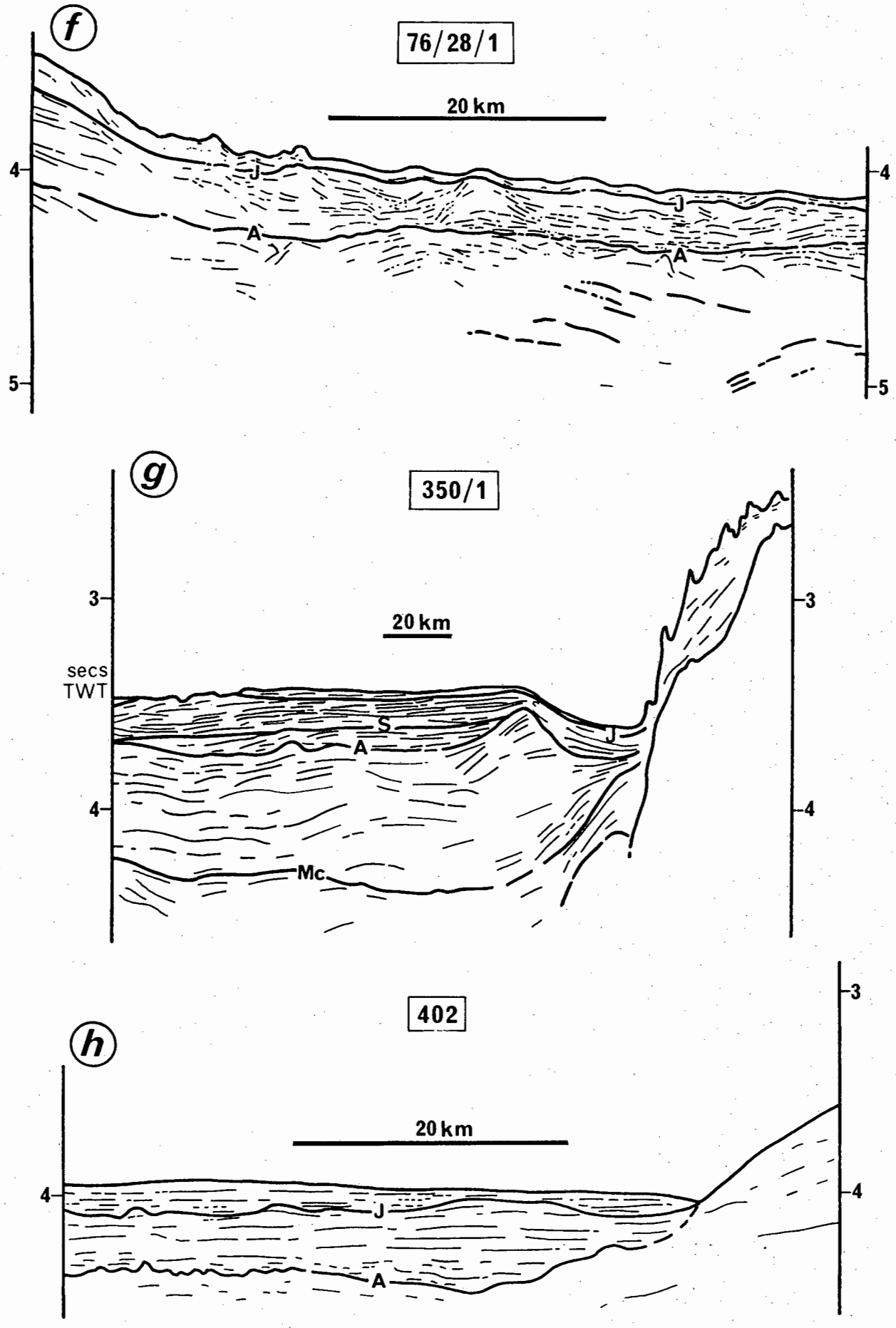

Fig. 7.5 BEDFORMS, ASYMMETRIC SEDIMENTATION AND MOATING

stratigraphic levels. Ripple cross-laminae, indicative of bedload traction, is identified in cores 9, 16 and 19 (Appendix B2) which were retrieved from zones of IIB-1 microrelief - migrating sediment waves (Fig.7.2). Ripple identification, as distinct from turbidite sequence ripple laminae, confirms that current-induced traction processes are operative in the migrating wave regions.

Type IIC-1 topography characterises the Tugela Cone apex zone (Figs.7.2 and 7.5f). IIC-1 waves are symmetric to slightly asymmetric, 1-4 km in wavelength, 40-80 m in height and may be either developed in fields or as solitary features. Sub-bottom reflectors show that IIC-1 waves are non-migrating (Fig.7.5f). Between isolated mounds the sea floor is corrugated. The non-migrating character may indicate that processes other than abyssal current circulation (e.g. gravity-controlled mass movement) were partly instrumental in wave generation. However, current action in this zone is clearly demonstrated. Several waves are flanked by narrow steep-sided moats (Plate 3.1g) suggesting that: (1) the waves are relict and semi-indurated; and (2) active, recent current flow is creating the scour moats.

Deep basin areas which border zones of sediment wave physiography (IIB-1) are characterised by IIA-2 microrelief (Fig.7.2). These corrugated morphologies correlate with zones of thin post-Angus sediment accumulation (Fig.7.1) and isolated zones of sediment unit C outcrop (Fig.7.2). In combination, these factors suggest that type IIA-2 is associated with low net sedimentation rate and relatively vigorous current flow. In contrast, generation of type IIB-1 requires substantially higher sedimentation rates and therefore a depositional regime. The

upslope change from IIA-2 (low/non-depositional regime) to IIB-1 (depositional regime) topographies may also be partly related to velocity gradients in the bottom current regime. Strongest currents are sited over IIA-2 zones with more sluggish currents localised to IIB-1 microtopographies. This velocity gradient may roughly correspond to change from NADW circulation (>2500 m depth; IIA-2 zones) to sluggish deep Agulhas flow (<2500 m depth; IIB-1 zones).

7.2.5.2 Sediment Billows

Sediment billows are characteristically very large, rarely symmetrical and may be locally crenulated on their flanks. Billows vary from 50-200 m in height and from 2-5 km in wavelength (Figs.7.3b and 7.5g). Delineated by topography type IIC-2, billows are restricted to the western flanks of the Mozambique Ridge (Fig.7.2).

Billow formation is probably a response to sharp velocity gradients in the bottom current regime. Billow deposition takes place beneath zones of slack water while non-depositional trough zones correlate with discrete bottom current flow-paths. Strong current influence is implied by the abundance of reflector erosional truncation in the billow facies (Fig.7.3b). Seismic profile coverage is insufficient to allow determination of billow crest attitude. Several of the billows appear to be relict being formed in pre-Angus time (Fig.6.6d; traverse 335) and may not be in equilibrium with the modern circulation scheme.

7.2.6 Asymmetric Sedimentation

Depositional asymmetry over basement topography, strongly indicative of bottom current activity (Purdy and Twichell, 1978;

Bowles, 1980), is evident over extensive areas within the Natal Valley. Asymmetry is particularly well-developed over the southern and SE flanks of the Central Terrace (Figs.7.3b, 7.4c and d) and western flanks of the Mozambique Ridge (Figs.7.3b and 7.5g). These zones are therefore considered to be under influence of vigorous bottom currents.

7.2.7 Erosional and Non-Depositional Moats

Large seamounts and steep slopes form major obstacles to the flow of bottom water and can therefore interfere with the transport of suspended sediment load (von Stackelberg et al, 1979). Bottom currents are compelled to accelerate around obstructing features (Bowles, 1980) causing sediment erosion (scouring) or at least inhibiting deposition (non-deposition). Both erosional and non-depositional processes will generate moats adjacent to flow obstructions. Both types of moat are recognised in the mid Natal Valley representing variations in the competency of bottom current flow.

Seismic profiles (Figs.7.3a, 7.4c and 7.5g) indicate that both erosional and non-depositional moats were first formed in post-Angus times and have remained active to the present day.

7.2.7.1 Erosional Moats

Moated seamounts are well-documented from many abyssal regions and are considered to be produced by current erosion and differential deposition (Roberts et al, 1974; Purdy and Twichell, 1978; Bowles, 1980). Erosional moats are typically narrow (<2 km), relatively deep (~50-70 m), steep-sided and often truncate sub-bottom reflectors.

Erosional moating is identified in three separate regional zones of the mid Natal Valley: (1) bordering basement outcrops on the Mozambique Ridge crest; (2) adjacent to Naude Ridge basement outcrop (Figs.7.3b and 7.4d) and unit B outcrop (Fig.7.10c and d) on the SE Central Terrace; and (3) bordering the East Tugela Ridge seamount (Figs.7.3a and 7.4e). Establishment of erosional moats beside unit B outcrops (Fig.7.2) implies that unit B is locally lithified. The surficial expression of these unit B outcrops may be comparable to modern oceanic 'hardgrounds' which are defined as surfaces of non-deposition on lithified sediments (Mullins et al, 1980; Malfait and van Andel, 1980). Several of the erosional moats are characterised by increased stratification and reflectivity (Fig.7.3a) suggesting they are bottomed by a coarse lag. Erosional moats are restricted to water depths less than 2500 m and have thus been generated by deep Agulhas Current flow. The existence of moats demonstrates relative stability in the regional current regime.

7.2.7.2 Non-Depositional Moats

Moats developed through non-deposition or at least differential sedimentation are relatively shallow (20-60 m) compared to their width (5-25 km). Beneath non-depositional moats, sediment units are thinned displaying reflector convergence and pinch-out. Non-depositional moats have evolved along the basin plain margins adjacent to two major physiographic provinces: (1) west flank of the Mozambique Ridge; and (2) SW continental slope.

Most impressive of this moat type is the wide (5-25 km) but

shallow (20-60 m) trench (Fig.7.5g) developed along the eastern deep basin margin adjacent to the Mozambique Ridge (Figs.3.2 and 7.2). Immediately to the west, an extensive sediment drift has been constructed sub-parallel to the moat (Fig.3.2). This drift (50 m high, 30 km wide and 200 km long) is considered to have been built in slack water conditions by sediments winnowed out during current excavation of the adjacent moat. Analogous smaller drifts, generated by sediment dumping adjacent to moats, have been described by Bornhold and Summerhayes (1977). Non-depositional moating is also developed along the base of the SW continental slope (Figs.7.2 and 7.5h). In this region, the moat is between 0,5-5 km wide and 15-40 m deep. Imperfect moat formation is evidenced by degradation into a series of closed depressions (Fig.3.2) which nevertheless confirms the action of stable deep thermohaline flow.

Non-depositional moats occur in water depths greater than 2500 m and have probably been generated by NADW thermohaline flow.

7.2.8 Sediment Reworking

Sediment reworking and post-depositional displacement of biogenous components is recognised by the admixture of non-contemporaneous (older) fauna into a younger faunal assemblage. Reworking implies mechanical erosion of sediment and component transport from an initial to final site of deposition (Thiede, 1981) by current action.

The locations of the nine sediment samples in which reworking has been identified are depicted in Figure 7.2. Foram species listings are presented in Appendix A5 (Table A5.1). The

faunal assemblage is essentially Quaternary but contains admixed (1-8% of the total) Miocene/Pliocene indicator species. The late Cretaceous species Globotruncana sp. is observed in samples 11 and 5748 (Table A5.1) retrieved from thin ? lag deposits patchily developed over unit C outcrop on the SW Central Terrace (Fig.7.2). Surficial sediment (cores 5117 and 5753) recovered from the southern Tugela Cone contain a typical Quaternary microfaunal assemblage but including non-coeval, reworked Tertiary discoasters.

Reworking sites (Fig.7.2) are correlatable with other indicators of deep current flow (sea floor topography, units B and C outcrop and scour moats) confirming an origin through bottom current scour.

7.2.9 Sediment Winnowing

Winnowing or selective sorting constitutes removal of fine particles to leave behind a coarse-grained lag. Coarsest lags can generally be correlated with highest velocity currents (Huang and Watkins, 1977). Winnowing can occur after deposition on the sea floor (post-depositional) or during settling through the water column (pre-depositional) with less energy being required (slower currents) for the latter (Prell, 1977). Within the Natal Valley, however, winnowing is the least satisfactory indicator of current scour since it cannot be entirely resolved whether the removal of fines is in part an artefact of the sampling technique. Spurious winnowing of the samples may have taken place during core winch-in procedure.

The areal distribution of winnowed surface samples is depicted in Figure 7.2. Like reworking, winnowing is confined to

zones of mounded/corrugated topography and thin lag deposits which overlie sediment unit C outcrops. This distribution suggests that winnowing is not a spurious effect and implies a close relationship with bottom current flow.

During coring operations, barrel damage is normally attributable to a hard sea floor which, in the absence of indurated sediment outcrop, may be caused by winnowing processes. At two sample stations (5122 and 5752) on the deep basin plain east of the Tugela Cone, extreme barrel damage was registered (Fig.7.2), suggesting that topography type IIA-2 may designate a hard, ? winnowed sea floor.

7.2.10 A Conceptual Model of Deep Current Flow

Characteristics and pathways of the major water bodies active within the Natal Valley have been summarised in Chapter 2 and section 7.2.2. Geostrophic calculations predict that Agulhas Current deep water flow may be competent to 2500 m depth. Physical properties of NADW prevent it from rising above ~2500 m in the Natal Valley.

Geologic responses to action of these water masses have been described in sections 7.2.3 - 7.2.9 and it only remains to consolidate this evidence and present an overview model of probable deep circulation pathways (Fig.7.6). Modelled free inertial jet tracks (van Foreest, 1977) have been added to Figure 7.6 in support of the Agulhas Current deep circulation model.

Deep flowpaths of the Agulhas Current are complex to define because of the alternating dominance of routes X and Y and the variable location (29-30°S) of route Y recurvature towards the Natal coast. Route X core flow is most strongly defined over the

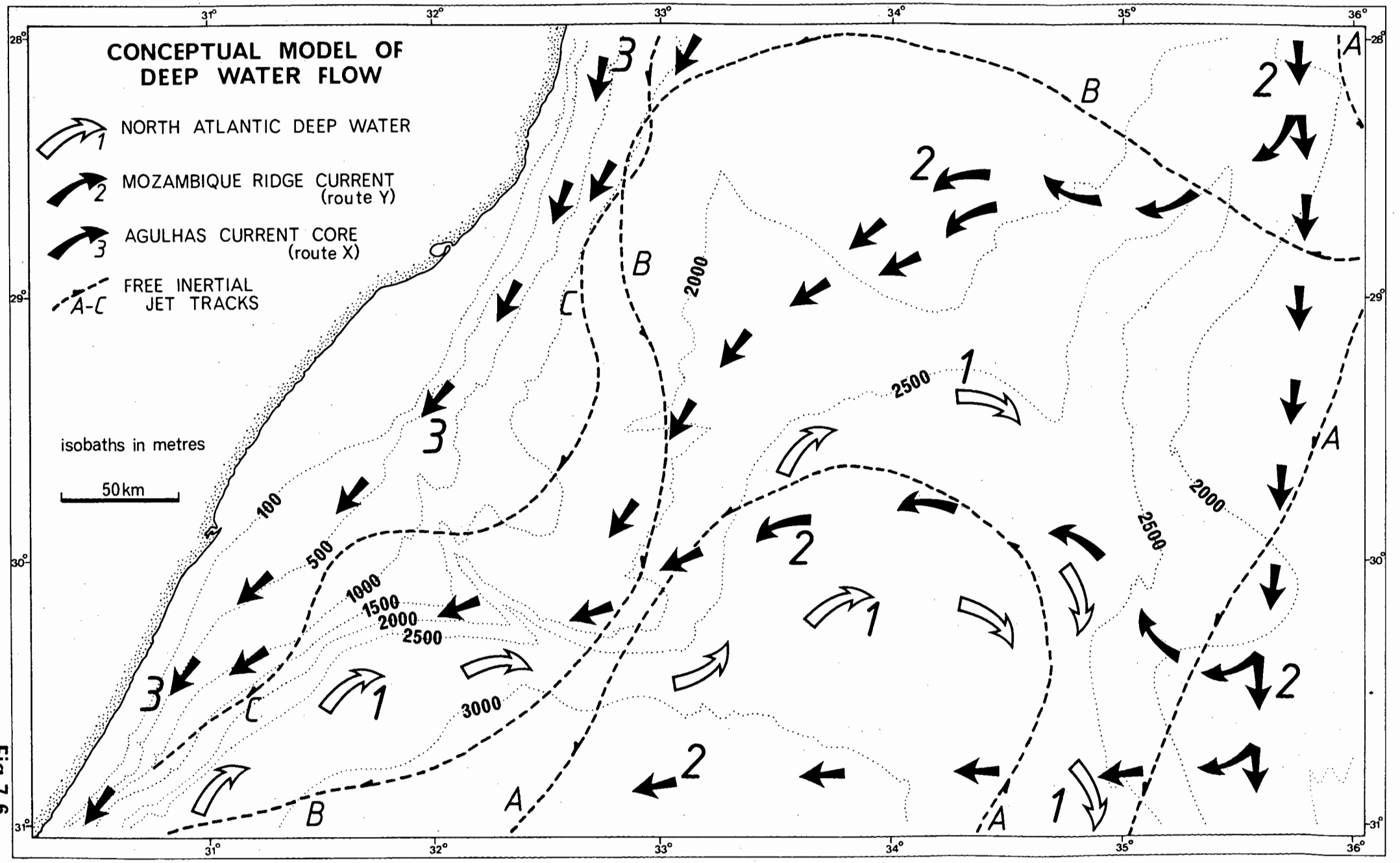
CONCEPTUAL MODEL OF DEEP WATER FLOW
NORTH ATLANTIC DEEP WATER
MOZAMBIQUE RIDGE CURRENT (route Y)
AGULHAS CURRENT CORE (route X)
FREE INERTIAL JET TRACKS
A-C
isobaths in metres
50km
100
500
1000
1500
2000
2500
3000
31°
32°
33°
34°
35°
36°
28°
29°
30°
31°

Fig. 7.6

upper continental slope. High sedimentation rates in this province (section 6.7.1) probably mask sedimentological responses to the vigorous current flow, although unit C outcrop and IIB-1 topography (Fig.7.2) may be ascribed to route X flow. Similarly, sediment wave fields in the shelf sand stream (Flemming, 1978; 1980) and unit C outcrop over the west Central Terrace are responses to route X flow. Inertial jet track C approximately parallels the route X pathway. To explain the remaining widespread distribution of current-controlled features above the 2500 m isobath (Figs.7.1 and 7.2), a complex system of presumably-intermittent flowpaths for westward recurvature of route Y water masses must be invoked (Fig.7.6). Inertial jet tracks A and B (Fig.7.6) afford theoretical support for the suggested route Y pathways.

The flowpath of NADW as defined on Figure 7.6 is clearly delineated by occurrence of several current-control indicators below 2500 m: thin post-Angus sediment accumulation (Fig.7.1), IIA-2 and IIC-1 topographies, unit C outcrop, non-depositional moats, sediment reworking and winnowing (compare Figs.7.2 and 7.6).

It can be concluded that a well-developed current regime, capable of redistributing sediment, has been operative within the Natal Valley since at least Angus times (early Oligocene). This current regime has significantly influenced sediment distribution and dispersal within the study area.

7.3 REGIONAL HIATUSES

7.3.1 Introduction

Hiatus development within an oceanic basin is a response to

both regional and global events. Numerous complexly-related variables including sea-level fluctuations, oceanic circulation, hinterland tectonism, climate, sediment supply, oceanic productivity and chemistry interact to generate regional hiatuses.

Significant gaps occur in the sedimentary record of the Indian Ocean and these hiatuses are often correlatable basin-wide (Kidd and Davies, 1978; Tucholke and Embley, 1984). Whether erosion, non-deposition or accumulation locally occurs is determined by the balance between sediment supply and removal rates (van Andel et al, 1975). Intensification of the circulation system in the geologic past has been proposed as a cause of the extensive hiatuses defined in Indian Ocean DSDP cores (e.g. Moore et al, 1978). Hiatuses have been delineated in abyssal environments and on bathymetric highs suggesting that both deep cold undercurrents and shallow tropical/sub-tropical circulation have been erosive.

In this section possible mechanisms for the development of SW Indian Ocean and Natal Valley hiatuses are reviewed and assessed. Several of the hypotheses proposed in sections 7.3.2.3 and 7.3.2.4 have already been published by Martin, Goodlad and Salmon (1982).

7.3.2 Hiatus Development Mechanisms

7.3.2.1 Sea-Level Fluctuations

Sea-level curves for southern Africa (Dingle et al, 1983) show reasonable correspondence to the global coastal onlap curve of Vail et al (1977) and the west Australian sea-level curve of

Quilty (1977)(compare Fig.7.7a,b and c). The correlation of southern African and global data (Fig.7.7) favours global eustatic sea-level change as the primary control over transgressive/regressive cycles around the Natal Valley basin rather than epeirogenesis of the African hinterland (Siesser and Dingle, 1981).

During low sea-level stands, terrigenous detritus is dumped directly on to the upper slope from river mouths near the shelf break. During high sea-level stands, terrigenous sediments are debouched on to the continental shelf. As a result, hiatuses may be generated over the shelf and uppermost slope during a low stand, while increased off-shelf sediment supply decreases the probability of a deep-sea hiatus (Vail et al, 1977). Conversely, during a high sea-level stand, terrigenous detritus is trapped on the continental shelf (Worsley and Davies, 1979a) increasing the likelihood of an abyssal hiatus. Continental erosion rates are however high enough to permit some by-passing of the shelf zone.

7.3.2.2 Hinterland Configuration

The tectonic and epeirogenic history of southern Africa remains controversial. King (1972) has suggested that all but one of the coastal regressions may be explained by hinterland uplift phases. Alternatively, de Swardt and Bennet (1974) postulate that the inland Drakensberg Escarpment (Fig.1.2) has been in a relatively elevated position since the break-up of Gondwanaland and did not evolve through a series of drastic uplifts. The correspondence of global and southern Africa sea-level curves (Fig.7.7) suggests that eustasy may explain the transgressive/regressive cycles without local epeirogenesis being required. Sedimentation rate calculations (section 6.7.1) imply

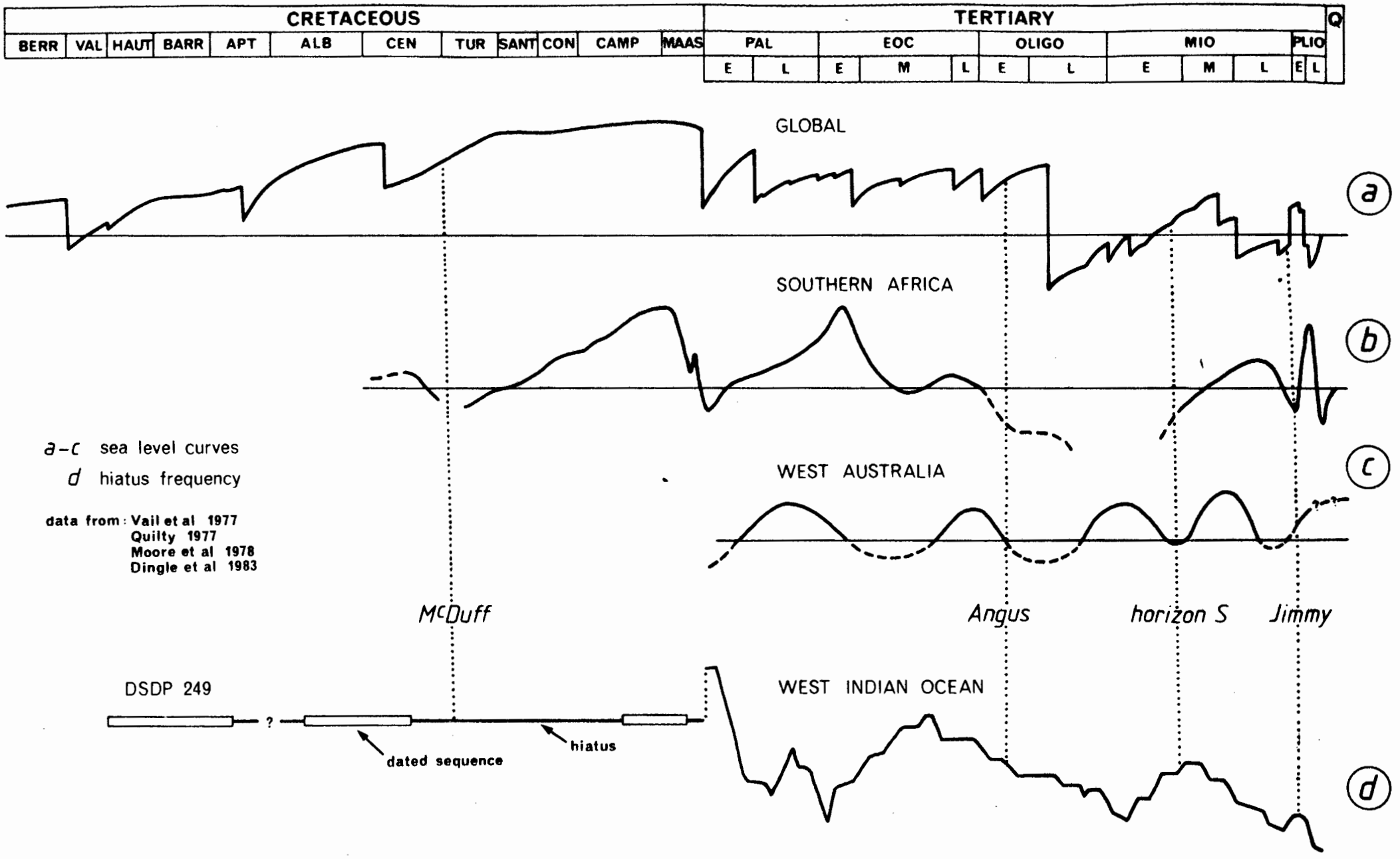

Fig.7.7 SEA LEVEL FLUCTUATION AND HIATUS ABUNDANCE

that, from the onset of continental drift through to the late Miocene, hinterland erosion steadily decreased possibly as a result of hinterland peneplanation. Climatic deterioration in the last 5 my (Donnelly, 1982) has dramatically increased the denudation rate (Table 6.3; Fig.7.8).

7.3.2.3 Oceanic Palaeo-Circulation

Indian Ocean DSDP data (Davies et al, 1975; Moore et al, 1978) indicates an increased abundance of hiatus development in five main periods: Cenomanian-Turonian, Cretaceous/Tertiary boundary, late Eocene-early Oligocene, early-middle Miocene and the Pliocene (Fig.7.7d). Most Indian Ocean hiatuses have been ascribed to current-induced erosion and non-deposition (Vincent, 1974; Davies and Kidd, 1977) because of the lack of evidence of tectonic influences. Tectonically-induced hiatuses have however been described (Leclaire, 1974). Hiatuses are generally more extensive in areas scoured by western boundary currents (Davies et al, 1975).

Cenomanian/Turonian

Changes in oceanic circulation may be linked to the formation of new sea-ways during continental fragmentation. Marine magnetic anomalies (Rabinowitz and LaBrecque, 1979; Simpson et al, 1979) date two major events crucial to establishment of open marine conditions in the SW Indian Ocean: (1) in the Albian (100-105 Myr), Antarctica cleared the southern tip of the Mozambique Ridge; and (2) in Albian/Cenomanian times

(~100 Myr), the Falkland Plateau separated from southern Africa. In addition, a change from euxinic to open-marine sedimentation in the western Indian Ocean occurred after the Cenomanian hiatus. Over the South Atlantic and Falkland Plateau, equivalent open marine sedimentation commenced in the Albian (Barker, Dalziel et al, 1976; Natland, 1978). Establishment of open marine conditions with enhanced flow through new sea-ways could therefore have caused hiatus generation and facies change. A lowering of the carbonate compensation level (Sclater et al, 1977) and the large differential between surface and abyssal temperatures (Margolis et al, 1977) suggests current intensification at this time. Global warming in the Coniacian/Santonian (Coplen and Schlanger, 1973) may have reduced current vigour allowing re-initiation of sedimentation.

Eocene/Oligocene

By the Eocene, western boundary currents equivalent to the modern Agulhas Current had formed off the east coast of southern Africa (Davies and Kidd, 1977; Frakes, 1979).

Formation of a near-complete circum-Antarctic sea-way near the Eocene/Oligocene boundary (Schnitker, 1980a) fostered climatic deterioration and initiated the psychrosphere (cold aggressive bottom water layer). Regional spread of Antarctic Bottom Water (AABW) can be correlated with sharp drops in sub-Antarctic temperatures (Kennett and Shackleton, 1976) and major reorganisations in benthic fauna (Benson, 1975; Corliss, 1979). Intensification in spread of AABW has been invoked as a major contributor to Eocene/Oligocene abyssal hiatus development (Davies et al, 1975; Moore et al, 1978) through both erosive and

dissolution processes. Climatic cooling also enhanced surface circulation (Davies et al, 1975) explaining the contemporaneous shallow and abyssal hiatus formation.

Erosion and hiatus formation may have been terminated by a combination of factors: (1) closure of Tethys at 18 Myr (Berggren and Hollister, 1974); (2) restriction of undercurrent flow by uplift of the SW Indian Ocean Ridge at 20 Myr (Sclater and Harrison, 1972); and (3) full development of circum-Antarctic circulation on opening of the Drake Passage at 22 Myr (Kennett, 1978).

Middle Miocene

Renewal of vigorous current activity in the middle Miocene has been correlated with two major tectonic events in the Northern Hemisphere (Schnitker, 1980b; Keller and Barron, 1983): (1) subsidence of the Iceland-Faeroe Ridge (Vogt, 1972); and (2) closure of the eastern Mediterranean interrupting global near-equatorial flow through Tethys (Berggren and Hollister, 1974). Resultant stimulation of North Atlantic Deep Water (NADW) flow by the later mid Miocene (Blanc et al, 1980; Schnitker, 1980a and b) probably induced hiatus initiation. Significant erosive NADW flow is delineated in the west Indian Ocean (section 7.2; Johnson and Damuth, 1979) and palaeo-NADW flow was probably similarly active and erosive.

Vast ice build-up in Antarctica during the middle Miocene and the resultant sea-level drop may have effectively shoaled the Iceland-Faeroe Ridge, moderating southward NADW flow (Schnitker, 1980b) and terminating the hiatus.

Pliocene

A Pliocene phase of world-wide circulation enhancement and

hiatus development is suggested (Moore et al, 1978) to be a direct consequence of Arctic ice cap growth starting at 4,5 Myr (Shackleton and Opdyke, 1977; Margolis and Herman, 1980). Sea-ice had been forming since the early Pliocene (Clark, 1971) allowing steady stimulation of NADW flow. Enhanced NADW and AABW flow probably significantly affected sedimentation patterns in the Indian Ocean. This phase of intensified current flow remains active to the present day although Pleistocene glacials are likely to have caused modifications.

7.3.2.4 Deep-Sea Sedimentation Rates

In all the major oceans, synchronous large variations in sedimentation rate occurred through the Cainozoic (Davies et al, 1977a; section 6.7.1). Correcting for compaction, Worsley and Davies (1979a and b) and Thiede et al (1980) correlated fast sedimentation rates with low sea-level stands (Fig.7.8) and direct sediment dumping on the upper slope. During high sea-level stands, eroded clastic detritus is trapped on the continental shelf although some sediment always reaches the adjacent deep-sea basins. In the modern Natal Valley, Flemming (1981) reports large scale flushing of sediment to the deep basin. During low sea-level stands, flushing of nutrients directly to the oceanic basins also fosters high biogenous sedimentation rates (Worsley and Davies, 1979a). Eocene to Recent Indian Ocean data support the link between low sea-level and high deep-sea sedimentation rates (low hiatus abundance) while Cretaceous and Palaeocene data do not (Fig.7.7b and d).

7.3.2.5 Conclusions on Hiatus Development Models

Intensified current circulation may create hiatuses by both

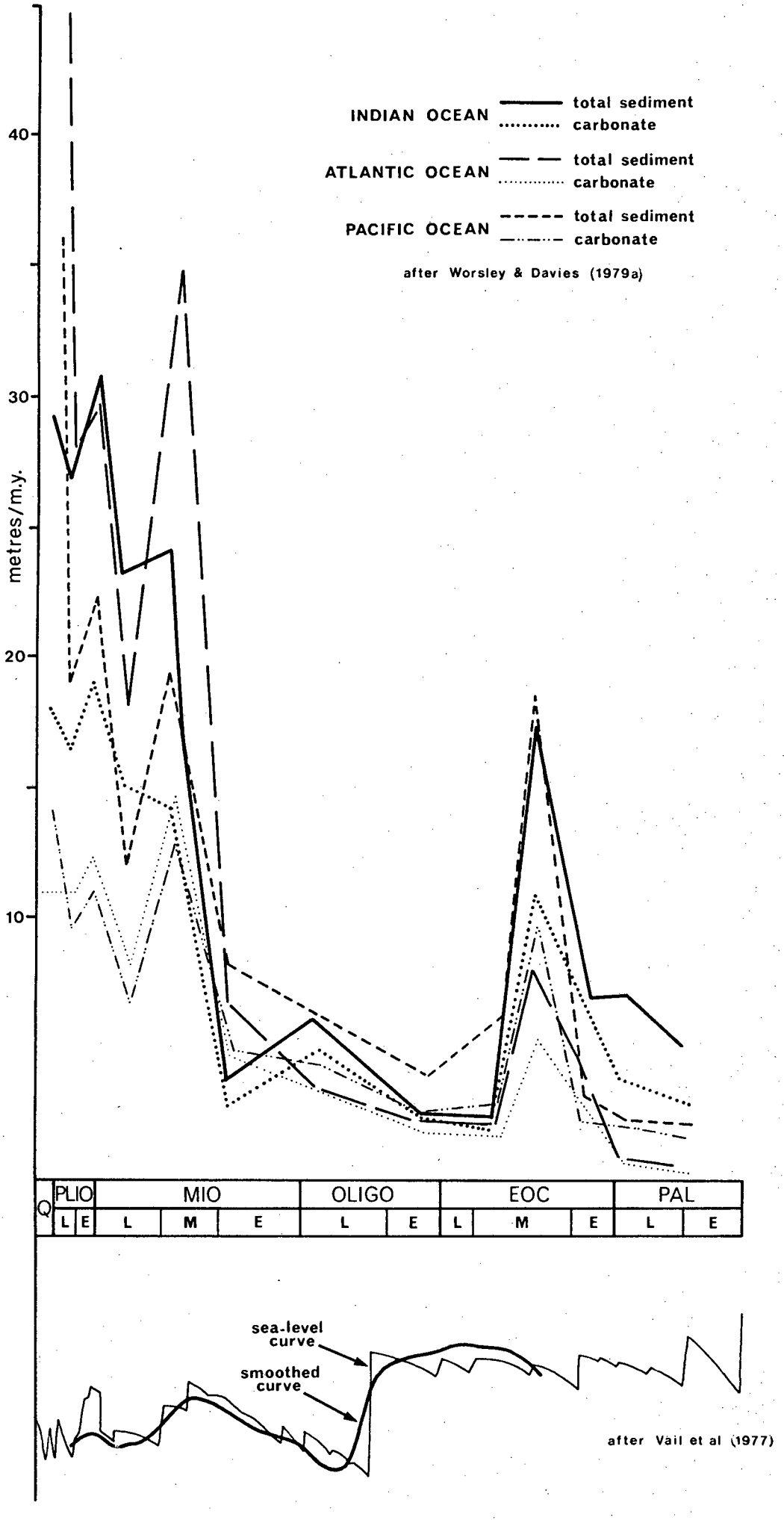

Fig 7.8 GLOBAL SEDIMENTATION RATES

dissolution and erosion/non-deposition processes. The possibility of precipitation decreases influencing detrital supply rate and hence hiatus development is partly supported by climatic evidence (Frakes, 1979). Assuming high off-shelf sedimentation rates to be associated with low sea-level (Vail et al, 1977; Worsley and Davies, 1979a), shelf hiatuses should alternate in time with deep-sea hiatuses. Basinal hiatuses in the Natal Valley correlate with both coastal regressions and phases of current intensification implying that both mechanisms have been simultaneously active. In Australia, an Oligocene shelf hiatus is the result of sea-level lowering while the contemporaneous basinal hiatuses are associated with current action (Carter, 1978).

In the case of glacio-eustatic sea-level low stands, climatic cooling may be linked to current stimulation (Kaneps, 1979) although the relationship between ice build-up and intensified currents has not been satisfactorily defined (Ledbetter, 1979). During glacial cycles, Be and Duplessy (1976) and Hutson (1980) have shown that Agulhas Current flow is greatly reduced in vigour. Contemporaneous deep undercurrents are typically intensified (Schnitker, 1980a). Conversely, during inter-glacial phases such as the Holocene, surface flow of the Agulhas current is vigorous while bottom current flow is more sluggish. From these two generalisations and assuming that Tertiary glacials invoked similar responses on current flow, idealised distributions of current-induced hiatuses can be postulated, presuming negligible influence of other factors:

(1) glacial phase - shelf zone hiatus (low sea-level), upper slope conformity (rapid sediment dumping on upper slope from

river mouths at the present day shelf break; minimal scour because of weak Agulhas Current), deep basin hiatus (intensified deep currents);

(2) interglacial phase - shelf zone hiatus or thin deposition (scour by competent Agulhas Current and removal of large amounts of suspended detritus to the Southern Oceans), upper slope reduced deposition or local hiatus (vigorous Agulhas Current scour and trapping of detritus on continental shelf), deep basin slow deposition (sluggish undercurrents) and ininterrupted deposition in current-free zones.

7.3.3 Natal Valley Hiatuses

7.3.3.1 McDuff (Cenomanian/Turonian Hiatus)

Open marine conditions were established in the Natal Valley during the Albian/Cenomanian following creation of new deep seaways around southern Africa. Upsurge of oxygenated conditions undoubtedly stimulated the major facies change of this time. Exposure to full oceanic circulation probably permitted fast development of thermohaline flow and may have contributed to McDuff formation. Seismic reflection profiles, however, show no indications of current control in generation of the non-depositional hiatus McDuff (section 6.3.2). Faulting of up to 0,3 secs throw disrupts horizon McDuff over the Central Terrace (Fig.6.7i) providing evidence of tectonism up to immediate post-McDuff times. Tectonism, therefore, may have provided impetus for hiatus development. McDuff also correlates with a low sea-level stand in the Cenomanian/Turonian (Fig.7.7a and b) which may have initiated hiatus development in the shallow proto-basin (~500m water depth; Martin, Goodlad and Salmon, 1982).

7.3.3.2 Angus (Oligocene Hiatus)

Reflection profiles exhibit a distinct increase in current-generated structures immediately below and above the Angus erosional unconformity and hiatus (section 6.3.3). This association with current-moulded features implies that circulation invigoration played a major role in Angus formation. Similarly, in abyssal basins around southern Africa, Tucholke and Embley (1984) ascribe development of an early Oligocene hiatus and unconformity to the onset of deep thermohaline flow. In addition, the Angus hiatus coincides with a drop in sea-level (Fig.7.7) perhaps explaining the coastal hiatus. Low regional sediment supply at this time (Fig.7.8) may also have contributed to non-deposition.

7.3.3.3 Horizon S (? early/middle Miocene Hiatus)

The position of horizon S in the sedimentary column suggests correlation with an early/middle Miocene stratigraphic level. DSDP columns indicate that this hiatus occurs in the NW Indian Ocean as a discrete event, while in the SW Indian Ocean it is compounded with an Oligocene hiatus. Changes in the north Indian Ocean circulation system affected the Mozambique Current (a source of the Agulhas Current) from the early Miocene perhaps initiating the horizon S hiatus. Furthermore, extensive NADW circulation is thought to have commenced at this time. Horizon S development in deep zones of the basin may be ascribed to NADW flow.

7.3.3.4 Jimmy (early Pliocene Hiatus)

The Miocene/Pliocene boundary sea-level low stand,

recognised globally and around southern Africa (Fig.7.7), may have initiated hiatus Jimmy in coastal areas. Intensification of NADW flow, primarily through Arctic glaciation, may explain the synchronous deep basin hiatus. Hiatus Jimmy development on the Tugela Cone is variable in extent and character (section 6.3.4) consistent with the model of hiatus development during glacio-eustatic regressions (section 7.3.2.5). In this model, the regression institutes a shelf zone hiatus while increased off-shelf sedimentation rates prevent non-sequences over the upper slope. Finally, bottom flow intensification locally creates an hiatus on the deep basin plain.

Natal Valley hiatuses correlate both with eustatic sea-level low stands and phases of invigorated current circulation. Assessment of hiatus development mechanisms suggests that variation in sediment supply (controlled by climate, hinterland configuration and sea-level) cannot fully explain the time correspondence of shelf and basinal hiatuses. Thus, current action is probably the major single control and in conjunction with sedimentation rate variation has defined non-sequence levels within the Natal Valley basin fill.

7.4 CANYONS AND VALLEYS

7.4.1 Introduction

Numerous investigations have focussed on the physiography of submarine canyons and the dynamic processes operating within these features (Shepard and Dill, 1966; Stanley and Kelling, 1978). Canyon systems of the SE African margin, however, have

not been extensively studied. Gully systems on the Zululand coast were described by Bang (1968) while Dingle and Robson (1985) have modelled canyon development off East London. In the mid Natal Valley, Dingle et al (1978) mapped both the major Tugela Canyon and the previously unknown 29° 25'S Canyon. New bathymetric data (Fig.3.2) has improved definition of individual canyons and gullies.

Submarine canyon formation has been ascribed to slope instability and failure (Farre et al, 1983), shelf/slope incision during low sea-level stands and erosive activity of turbidity currents. Once initiated, major processes responsible for development of canyon morphology include: (1) headward erosion; (2) lateral erosion causing side gullies, undercutting and slumping; (3) axial downcutting; and (4) rim upgrowth by levee construction (Andrews and Hurley, 1978; Farre et al, 1983). In this section the mode and age of origin of the major canyons and gullied zones are evaluated using seismic reflection data. Absence of synoptic in-canyon current data (e.g. Karl, 1980) and poor sample density has precluded discussion of canyon sedimentary processes. Key seismic profiles are presented in Figure 7.9 and their locations are depicted in Figure 7.10.

7.4.2 Canyon Formation

7.4.2.1 Tugela Canyon

A complete morphologic description of the Tugela Canyon is provided in section 3.2.4. Seismic reflection profiles (Fig.7.9a and b) indicate sharp truncation of reflectors at the canyon walls suggesting that erosional processes (axial downcutting)

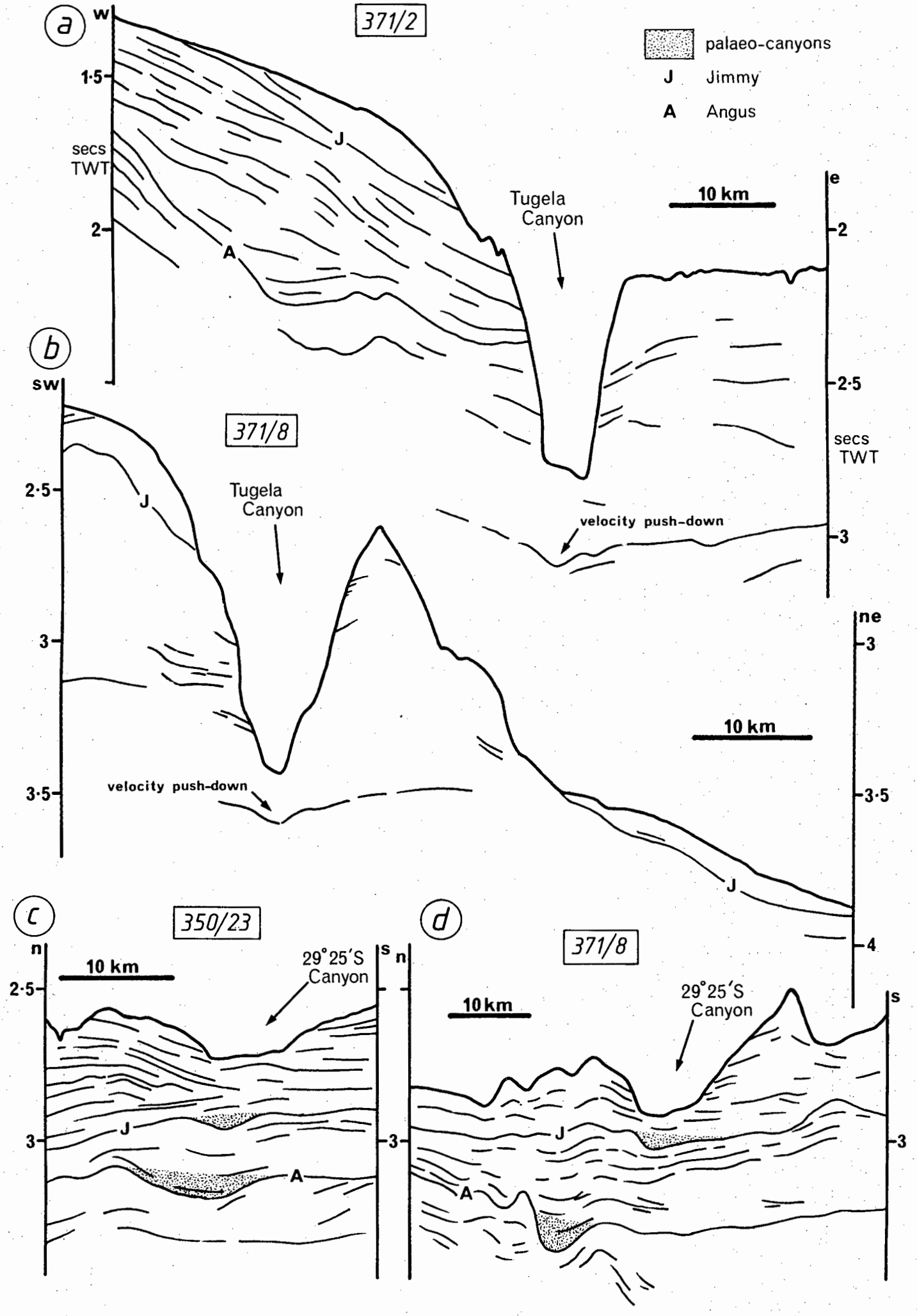

Fig.7.9 SEISMIC PROFILES (CANYONS)

have been dominant in canyon formation. Apparent dip of sub-bottom reflectors adjacent to the canyon (Fig.7.9a) is probably a spurious effect of water/sediment velocity contrasts. Rim upgrowth is not considered to be a significant process since no fossil levees are mappable below horizon Jimmy. However, stratigraphically above Jimmy, several profiles (Fig.3.7e and f) portray well-developed levees perched on almost horizontal bedding. This implies either of two possibe explanations: (1) overbank deposition was insignificant in pre-Jimmy times; or (2) canyon formation was only initiated in post-Jimmy times and proceeded through axial downcutting and rim upgrowth. Presence of near-horizontal reflectors beneath the canyon axis (Figs.7.9a and b) suggests the canyon has been in existence for a limited period. Reflector down-warp at this point probably represents a velocity push-down effect (Sheriff, 1976). High-angle erosional truncation in the canyon walls and restriction of levee development to post-Jimmy times supports canyon formation along the lines of explanation (2) of above. An erosional origin is also supported by the distinctive absence of distributary canyons (Fig.3.6). Depositional distributary systems typically bifurcate much more extensively. Canyon widening by oversteepening and slumping (Andrews and Hurley, 1978) has also shaped Tugela Canyon morphology with several slump scars recognisable on seismic profiles.

A possible model to explain the history of the Tugela Canyon is postulated as follows:

(1) during a low sea-level stand in post-Jimmy times (? Pleistocene glacials or late Pliocene regression - Dingle et al, 1983), riverine discharge may have been channelled directly to the shelf break;

(2) increased downslope sediment dispersal (turbidity currents and/or slumps) from the discharge zone may have concentrated along one route permitting axial downcutting and canyon formation;

(3) during this erosional phase, the canyon may have incised the shelf break to pirate shore-parallel sediment movement (e.g. Pegasus Canyon; Herzer and Lewis, 1979);

(4) with subsequent sea-level rise, re-initiation of vigorous Agulhas Current flow and establishment of a shelf zone sand stream, the direct conduit between the Tugela river and Tugela Canyon probably became inactive;

(5) drastic reduction in sediment supply to the canyon because of enhanced Agulhas Current flow may have instituted canyon stagnation as reflected by its modern morphology.

Tugela Canyon stagnation is evidenced by the water depth (~500 m) of its head zone, indicating that its upper reaches have been infilled. Several other east coast canyons have shelf zone extensions, incised during sea-level low stands, which are now infilled indicating stagnation (B. Flemming, pers.comm., 1981). The definite link between fossil onshore channels and offshore canyons has been outlined by Hill (1975). Canyon development thus progresses through a series of active and inactive phases primarily related to sea-level fluctuation (e.g. Hudson Canyon; Keller and Shepard, 1978).

7.4.2.2 29° 25'S Canyon

Canyon morphology has already been described in section 3.2.5. In contrast to the Tugela Canyon, the seismic configuration of this shallower, more irregular canyon can be

ascribed to a combination of both erosional and depositional processes. Cross-sections (Fig.7.9c and d) show both buried fossil and modern levees implying overbank deposition over a protracted period. Nevertheless, numerous reflectors are truncated in the valley flanks implying that competent erosive processes have also been active.

Spatial development of the 29° 25'S Canyon can be traced by the location of palaeo-channels (Fig.7.9c and d). Since Angus times, there has been progressive southward translation of the canyon axis possibly induced by Coriolis-intensified erosion of the southern wall or avulsion and fan-switching. The modern canyon is overdeep compared to palaeo-canyons (Fig.7.9c and d) perhaps implying that erosional/non-depositional processes have locally assumed dominance. This is corroborated by sampling (cores 15 and 24) and seismics which confirm that unit C strata outcrop within the lower reaches of the canyon (Fig.7.2). These local outcrops may have been exhumed by ? slump or erosional processes with modern in-canyon currents (Shepard, 1979) only being required to maintain non-deposition. In this situation, stagnation of valley floor aggradation allied to continued rim upgrowth by hemipelagite draping may explain the observed modern overdeepening. The upper reaches of the canyon have been infilled implying at least intermittent stagnation and the modern head zone is unusually deep at 1400 m below sea level (Fig.3.2).

The 29° 25'S Canyon has been in existence since Angus (early Oligocene) times at least (Fig.7.9c and d) yet there is no alignment with any major hinterland river. However, de Swardt and Bennet (1974) have suggested that the Tugela river formerly flowed along course of the modern Mhlatuzi river (Richards Bay).

Prior to river capture by the Tugela, a more powerful Mhlatuzi river may have aligned with and influenced formation of the 29° 25'S Canyon. It may be inferred that, prior to formation of the Tugela Canyon, the 29° 25'S Canyon had evolved as the major depositional fan valley system on the Tugela Cone.

Both the Tugela Canyon and 29° 25'S Canyon display left-handed curvature looking down-canyon (Figs.3.2 and 3.6) implying a regional rather than local cause. This phenomenon may be the result of Coriolis Force action on downslope flow of sediment-charged water packages within the two canyons. Similar structures on the Mozambique Fan (Zambesi Valley) have been ascribed to Coriolis effects (Kolla et al, 1980b). Cyclonic flow of NADW within the mid natal Valley may also be contributary to eastward deflection of the Tugela Canyon.

7.4.2.3 Erosional Gullies and Deep Basin Channels

Two gully provinces are defined over the north and south zones of the upper continental slope (Fig.3.2). Bang (1968) described the gullies of the north zone off Lake St. Lucia and ascribed their existence to erosion by persistent turbidity currents. These gullies have, however, been genetically linked with onland palaeo-river channels (Hill, 1975) suggesting they were formed by fluvial erosion and detrital discharge on to the upper slope during a low sea-level stand. This connection has been verified since interconnecting, infilled shelf valleys have been delineated by high resolution seismics (B. Flemming, pers.comm., 1981). The north zone gullies incise a smooth progradational sequence (sub-facies D_4) confirming an erosive origin. Canyons of the south zone (Fig.3.2) remain poorly known

but their formation is probably related to river incision (low sea-level stand) and/or slump tectonism. Whatever their origin, gullies of both provinces probably maintain their incised character by acting as conduits for downslope transport of detritus, even though their shelf zone extensions have now been infilled.

Sparse bathymetric control does not permit construction of a comprehensive map of deep basin channels although the recognition of shallow valleys (Fig.7.5g) implies that channelised processes are operational. Using GLORIA, a network of abyssal valleys have been outlined within the southern Natal Valley and Transkei Basin (R. Kidd, pers.comm., 1980) confirming the existence of a regional distributary system (Chapter 9). One major, 60 m deep channel is recognised SE off, and in alignment with the Tugela Canyon (Fig.3.2) suggesting some original genetic connection. Infilling and draping of an intervening zone of deep basin plain (Fig.3.2) argues that the Tugela Canyon and colinear basin valley are no longer dynamically connected.

7.5 ALLOCHTHONOUS PROCESSES

7.5.1 Introduction

Mass movement processes are principal agents of sediment mobilisation, deposition and transport in continental slope environments (Nardin et al, 1979a and b; Dingle, 1980b; Embley, 1980; Gorsline, 1980). Sediment slides have been delineated in a variety of settings along continental margin slopes (Embley, 1980; Saxov and Nieuwenhuis, 1982). Individual slide bodies may vary tremendously in volume ranging from <1 to several thousand

cubic kilometres (Knebel and Carson, 1979; Moore et al, 1976; Dingle, 1977; 1980b). Steep slopes are not essential for generation and propogation of slides (Lewis, 1971; Coleman and Garrison, 1977).

Impressive examples of submarine slides have been delineated on the south and west margins of southern Africa (Emery et al, 1975; Dingle, 1977; 1980b; Summerhayes et al, 1979), prompting examination of the east coast margin for similar structures. Four well-defined sediment slides (I-IV) are recognised on the northern Tugela Cone and it is the objective of this section to discuss the geometry, distribution and age of these products of mass movement. The areal distribution of the four slides is presented in Figure 7.10 while relevant seismic profiles are grouped as Figures 7.11 and 7.12. Terminology used in this section follows Dingle (1977) and Nardin et al (1979b).

7.5.2 Sediment Slides

7.5.2.1 Slide I

Slide I, on the upper slope of the northern Tugela Cone (Fig.7.10), exhibits diagnostic characteristics of a translational glide (Nardin et al, 1979b). The basal failure surface (glide plane) is planar, although locally irregular under the toe zone, and approximately parallels the surface slope (Fig.7.11a). The head region roughly follows the 800 m isobath (Fig.7.10). The slide has splayed out in radial fashion with maximum sediment translation (greatest length) directly downslope of the central head zone (Fig.7.10).

The main glide plane scar can be traced for ~15 km

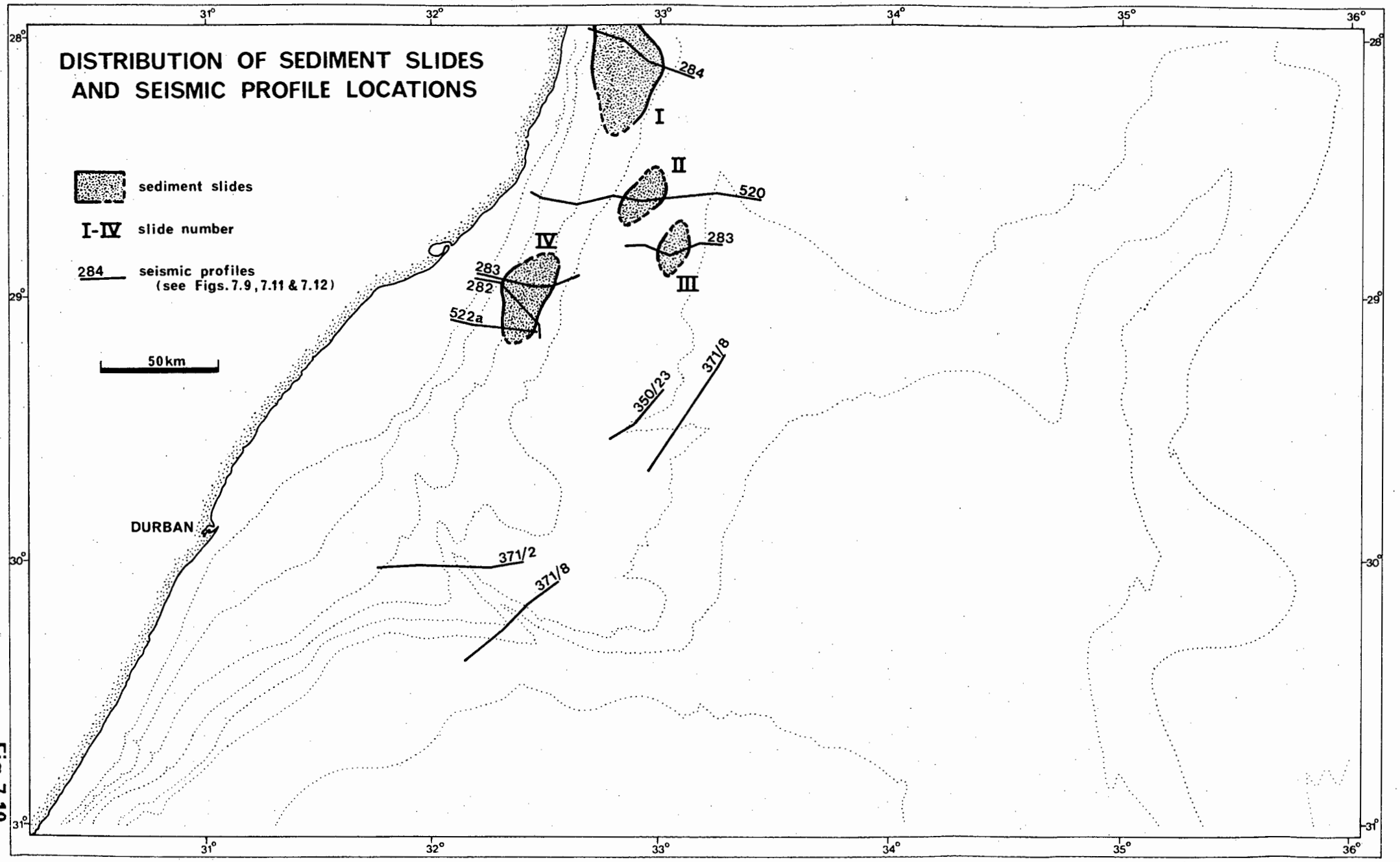
DISTRIBUTION OF SEDIMENT SLIDES
AND SEISMIC PROFILE LOCATIONS
sediment slides
I-IV slide number
284 seismic profiles
(see Figs. 7.9, 7.11 & 7.12)
50km
DURBAN
I
II
III
IV
284
520
283
283
282
522a
350/23
371/8
371/2
371/8
31°
32°
33°
34°
35°
36°
28°
29°
30°
31°

Fig. 7.10

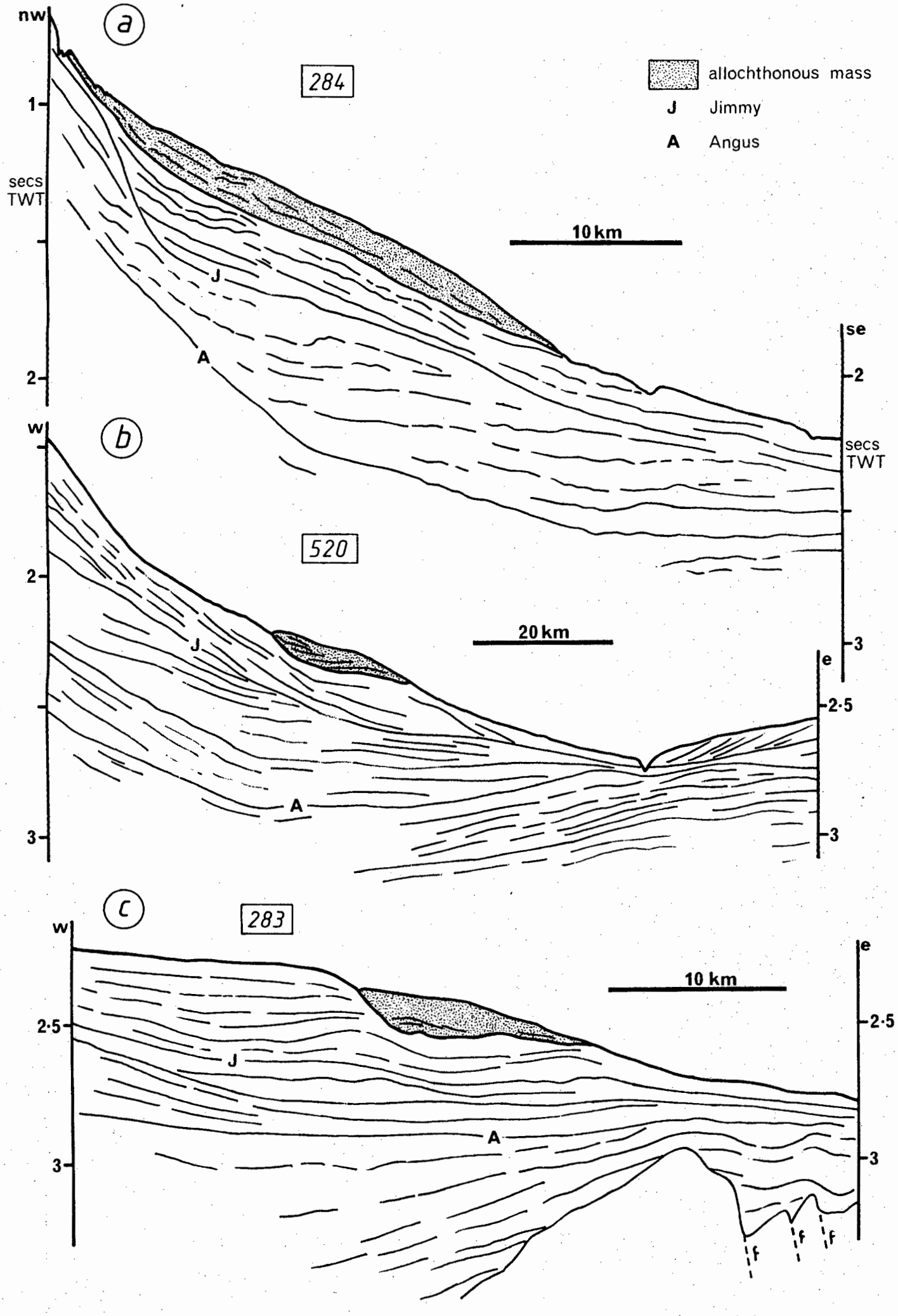

Fig.7.11 SEISMIC PROFILES (SEDIMENT SLIDES I-III)

delineating the intersection of the glide plane and sea floor. Tensional depression at this intersection (Dingle, 1977) has generated a 40 m deep bathymetric notch (Fig.7.11a). Downslope of the glide plane scar, several smaller sea floor notches may be surface manifestations of subsidiary glide plane scars. The main glide plane is essentially planar (Fig.7.11a) implying that rotational movement was therefore subordinate to downslope translation in slide generation. Nevertheless, the glide plane shows distinct curvature on the upslope margin of the detached sediment mass - a feature common to numerous sediment slides (Prior and Coleman, 1979).

Internal bedding is well preserved and coherent within the proximal region degrading to incoherent in the distal region (Fig.7.11a). Retention of primary internal bedding is again diagnostic of slide deposits (Nardin et al, 1979b) and indicates that plastic deformation was not significant except perhaps in the toe zone.

Slide I is relatively simple in structure comprising a single coherent block which is thickest (95 m) in its central zone (Fig.7.11a). The slide is approximately 25 by 45 km in size and thus extends over an area of 1125 km^2 (Table 7.1). Assuming an average thickness of 80 m, the displaced volume of sediment is calculated at 90 km^3 making it comparable in size to the Walvis Bay slide described by Summerhayes et al (1979). Slide I is the largest discrete product of mass movement delineated in the study area (Table 7.1), and perhaps extends northward onto the Zululand continental slope.

7.5.2.2 Slide II

This irregular slide has been demarcated on the northern

Table 7.1 Quantitative Parameters for Tugela Cone Slides

Slide	Seismic* Control	Mass Transport+ Process	Slope (o)	Average Length (km)	Average[1] Thickness (m)	Area (km^2)	Volume (km^3)	T/L[2] (%)
I	284,350/2,350/3	glide	1,5	25	80	1125	90	0,37
II	520	slump	8,9	14	75	~280	~21	1,0
III	283	slump	0,8	11	140	~190	~27	1,27
IV	282,283,522a	glide/slump	2,6	20	105	620	65	0,96

* - seismic traverses on which the slides are defined.

\+ - using nomenclature after Nardin et al (1979b). Note slide IV contains both slump and glide elements.

1 - calculated assuming a sound velocity of 2,0 km/sec within the slide sediment.

2 - maximum thickness to length ratio expressed as a percentage.

Tugela Cone between the 1590 and 1900 m isobaths (Figs.7.10 and 7.11b). The glide plane is distinctly curved (Fig.7.11b) suggesting significant rotational movement during mass transport. Slide II may thus be classified as a slump deposit (Nardin et al, 1979b). A shallow bathymetric notch (15 m deep) defines the intersection of the sea floor and main glide plane. Seismic profile coverage over this slump is very poor consisting of only one crossing (Fig.7.10) and thus its full areal extent remains unknown. Estimated dimensions are 14 by 20 km and with an average thickness of 75 m, the displaced sediment volume is approximately 21 km^3. The T/L ratio is higher than for slide I (Table 7.1) reflecting the rotational rather than translational character of this slump. Coherent reflectors dipping into the basal glide plane (Fig.7.11b) demonstrates both slump block rotation and the insignificance of internal deformation associated with slump processes. Along its downslope margin, the slump mass thickness decreases (Fig.7.11b) and may indicate local plastic debris flow.

7.5.2.3 Slide III

Sited 12 km SE of slide II on the northern Tugela Cone (Fig.7.10), slide III lies between the 1770 and 1910 m isobaths. The main glide plane of slide III is curved (Fig.7.11c) implying a degree of rotational movement during sediment displacement. Slide III is thus classified as a slump deposit. A 15 m deep notch delineates the zone of tensional depression immediately downslope of the glide plane scar. Seismic control is limited and thus the allochthonous mass size (Table 7.1) can only be estimated. Slump dimensions are approximately 14 by 13,5 km

(Fig.7.10) and the displaced volume is 27 km^3 (Table 7.1). Geometric and T/L ratio similarities between slides II and III (Table 7.1; Fig.7.11b and c) may imply a common mode of formation. Furthermore, the en-echelon arrangement of these two slides (Fig.7.10) favours an interconnected origin for their failure mechanisms (Prior and Coleman, 1979). Slide III is acoustically transparent relative to enclosing sub-facies D_4 sediments (Fig.7.11c) reflecting either internal reflector disruptance during slumping or poor seismic resolution. Nevertheless, some basal reflectors within the slump are recognised dipping into the glide plane confirming rotational movement.

7.5.2.4 Slide IV

Slide IV is sited on the Tugela Cone upper slope at about 29°S and lies between the 400 and 1420 m isobaths (Fig.7.10). The displaced mass is complex comprising intergradational slump and glide portions. In accord with this composite structure, the main glide plane exhibits two distinct configurations. Over the northern zone of the slide, the glide plane is planar although locally hummocky (Fig.7.12a and b) and approximately parallels the sea floor. This zone of the slide may be classified as a translational glide. In contrast, over southern zones of the slide, the glide plane shows distinct curvature (Fig.7.12c) suggesting predominance of rotational movement during mass transport. This southern zone is more correctly classified as a slump feature.

In the glide section of slide IV, primary reflectors are coherent and relatively undeformed (Fig.7.12a and b) verifying

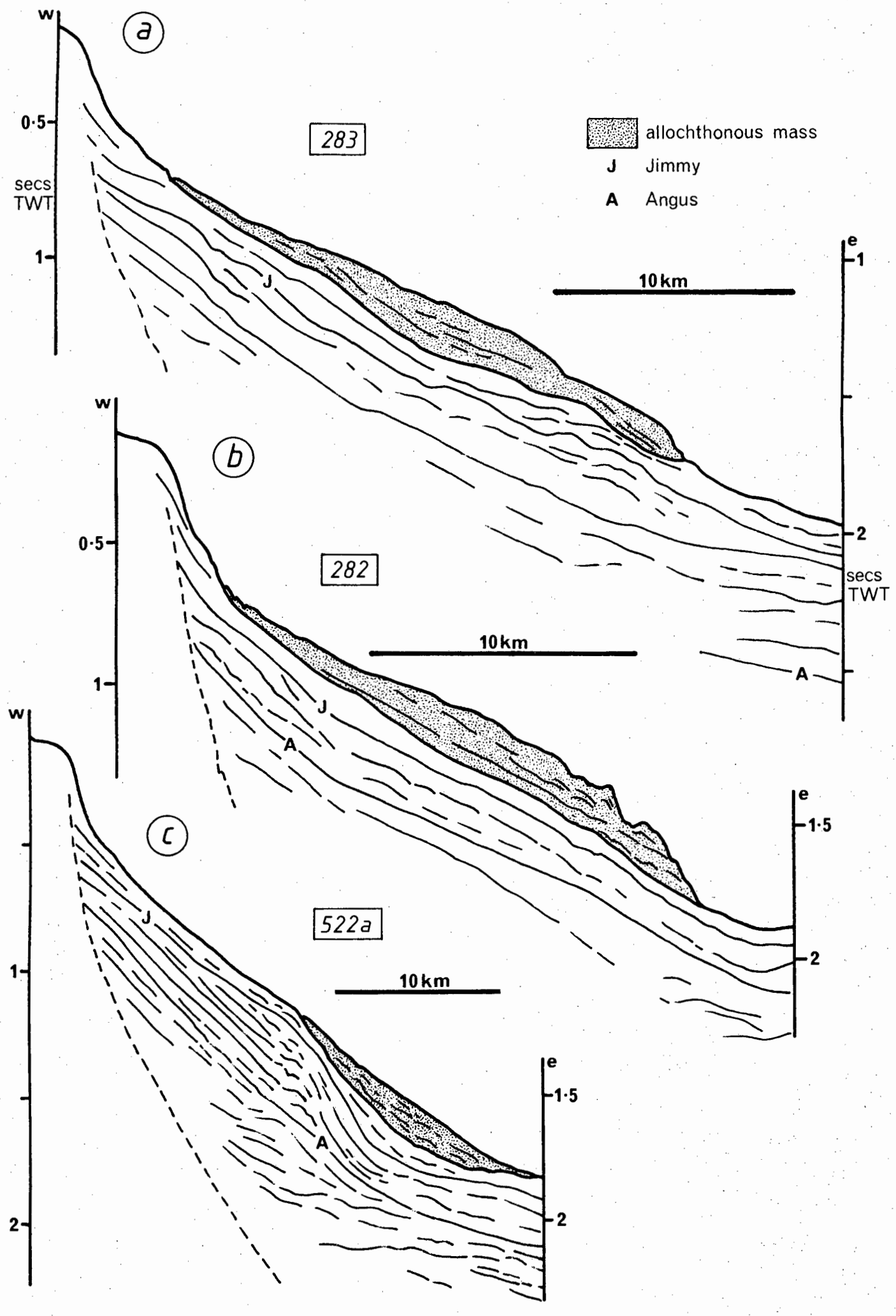

Fig.7.12 SEISMIC PROFILES (SEDIMENT SLIDE Ⅳ)

the expected elastic sediment behaviour (Nardin et al, 1979b). In this section however, the toe zone is demarcated by hummocky topography with local chaotic internal reflectors (Fig.7.12a and b). This disrupted structure probably represents the zone of downslope disintegration often associated with submarine landslides (Prior and Coleman, 1979). Reflectors are also coherent in the slump zone of slide IV but tend to be slightly deformed and folded above the glide plane (Fig.7.12c). Minor plastic deformation of this sort is often typical in slumping processes (Nardin et al, 1979b).

A 15 m deep glide plane scar and tensional depression is traced over a 25 km distance demarcating the upslope limit of the slide. The composite structure, including both glide and slump portions, covers a total area of 620 km^2. With an average thickness of 105 m, the allochthonous volume is estimated at 65 km^3. With limited seismic control and complete absence of geotechnical data, reasons for the complex structural style of slide IV cannot be evaluated. However, the glide portion of slide IV is confined to a steeper slope zone.

7.5.3 Trigger Mechanisms and Discussion

Downslope mass movement along a slip plane occurs when the shear strength of a sediment body is exceeded by the shear stress (Rupke, 1978). The failure threshold may be surpassed either through shear strength reduction or shear stress increase (Prior and Coleman, 1979). Sediment body disequilibrium (Rupke, 1978; Dingle, 1980b) may be initiated by: (1) slope oversteepening due to downslope excavation; (2) excessive deposition on the slope; (3) pore fluid pressure increases (biogenic gas production or

compaction); and (4) thixotropy or fluidisation caused by shock-induced strain (earthquakes or storm-waves). Low sea level stands may enhance mass-gravity transport processes (Dingle, 1980b) by: (1) inducing isostatic-correction instability; (2) changing sedimentation rates and patterns; and (3) bringing slope sediments within storm wave-base.

All of the above mechanisms may have influenced Natal Valley slide generation to a greater or lesser extent. Post-Jimmy slides are confined to the upper slope of the northern Tugela Cone (sub-facies D_4), a region characterised by very high sedimentation rates (132 m/my; Table 6.3). High accumulation rates in sub-facies D_4 was probably a response to climatic deterioration and direct upper slope deposition during low sea-level stands (section 6.7.1). Concomitantly, the Agulhas Current was reduced in vigour (Be and Duplessy, 1976). Resurgence of Agulhas Current flow during high sea-level phases (Hutson, 1980) may have caused local scour and slope oversteepening. Modern mid slope scour in this zone is indicated by reworking and winnowing in surface samples 5727 and 5728 (Fig.7.2). Several earthquakes have been recorded during historic times in SE Africa and the adjacent offshore basins (Fernandez, 1983). In particular, two shocks (>5 on Richter scale) had epicentres directly over the northern Tugela Cone slide zone (Oliver, 1956). Similar seismicity in the geologic past may have provided final triggering impetus.

No indications of mass transport are discerned below horizon Jimmy suggesting that the high sedimentation rate for sub-facies D_4 was the most important causal factor in slope failure. All four slides occur relatively recent within the D_4 sequence and in

all cases, the glide planes intersect the sea floor (Figs.7.11 and 7.12). Absence of significant post-glide draping and clear recognition of the glide plane scar suggests that slide formation is a relatively recent phenomenon and may have occurred during Pleistocene glacio-eustatic sea level low stands. It may be summarised that a combination of high sedimentation rate (? during low sea level stands), downslope undercutting and perhaps seismic activity culminated in slope failure over the northern Tugela Cone.

Slump and glide processes within the mid Natal Valley are confined to a province of low gradient ($0,8^{o}$-$2,6^{o}$; Table 7.1). The slump processes (slides II and III) are restricted to the gentlest slopes ($<1,0^{o}$) while the glide processes (slides I and IV) are common to marginally steeper slopes ($1,5^{o}$-$2,6^{o}$). Gorsline (1980) notes that, when slopes have such low gradients, instability will occur only when sedimentation rates are very high (e.g. sub-facies D_4) so that the water content is preserved. The T/L ratios (Table 7.1) of slides I-IV are extremely small (<1,3%) and are of similar magnitude to ratios of slides reviewed by Prior and Coleman (1979). The T/L ratio for Natal Valley slumps is greater than for glides (Table 7.1).

CHAPTER 8 SEDIMENTOLOGY

8.1 INTRODUCTION

The continental margin of SE Africa and the adjacent Natal Valley deep-water basin have to date remained largely unstudied in sedimentological terms (Nairn and Stehli, 1982). Previous work has been limited falling into one of two categories. Firstly, the Natal Valley has been incorporated in several regional studies (Leclaire, 1974; Kidd and Davies, 1978; Vincent, 1976; Kolla and Biscaye, 1977; Kolla et al, 1976a,b,c; 1980a,b) covering the entire SW Indian Ocean. In all these investigations, sample control is too scant to decipher extant local sedimentary processes within the Natal Valley. Other more localised studies (Moir, 1976; Flemming, 1978; 1980; 1981; Birch, in press a) have provided detailed process models but have concentrated on the continental shelf zone.

The results of a broad sedimentological investigation of the recent Natal Valley fill are presented in this chapter. Sample control and analytical procedures are outlined in section 8.2. Sediment chemistry, composition/mineralogy and grain-size/texture are described and discussed in sections 8.3-8.5. All aspects of sedimentology are collated to characterise depositional environments and finally, to construct a sediment dispersal model.

8.2 SAMPLE DISTRIBUTION AND ANALYTICAL METHODS

8.2.1 Sample Station Distribution

During three Natal Valley cruises (TBD 350, 371 and MN

76/28), a total of 58 sample stations were occupied. All sites were positioned by satellite navigation on existing seismic profiles thus providing some stratigraphic control to aid sedimentological interpretation. Dependent on sea floor conditions (topography and bottom competence), a variety of sampling devices were employed including piston corers, open-barrel gravity corers, grabs and dredges. Full details of location, water depth, sampling tool and recovery at each station are listed in Appendix B1.

The distribution of sample stations is depicted in Figure 8.1. Coverage is best over the Tugela Cone where upper slope control is improved by incorporation of existing data (Birch, in press a). In contrast, coverage is very poor over sections of the deep basin plain and Central Terrace. The Mozambique Ridge and SW continental slope were intentionally omitted from the survey because of insufficient cruise time. Conclusions regarding zones of sparse coverage must be weighed against the poor data base.

8.2.2 Laboratory Analysis

This section provides a condensed review of the major analytical techniques on which the sedimentology study is based. Full details of individual techniques are documented in Appendix A. The complementary flow-chart (Fig.8.2) depicts steps in the laboratory analysis in diagrammatic form.

Chemical Analysis

Calcimetry was performed using the 'Karbonat-Bombe' method (Birch, 1979a). In analysis, one gram of crushed sample is reacted with conc. HCl in a sealed perspex vessel. The pressure

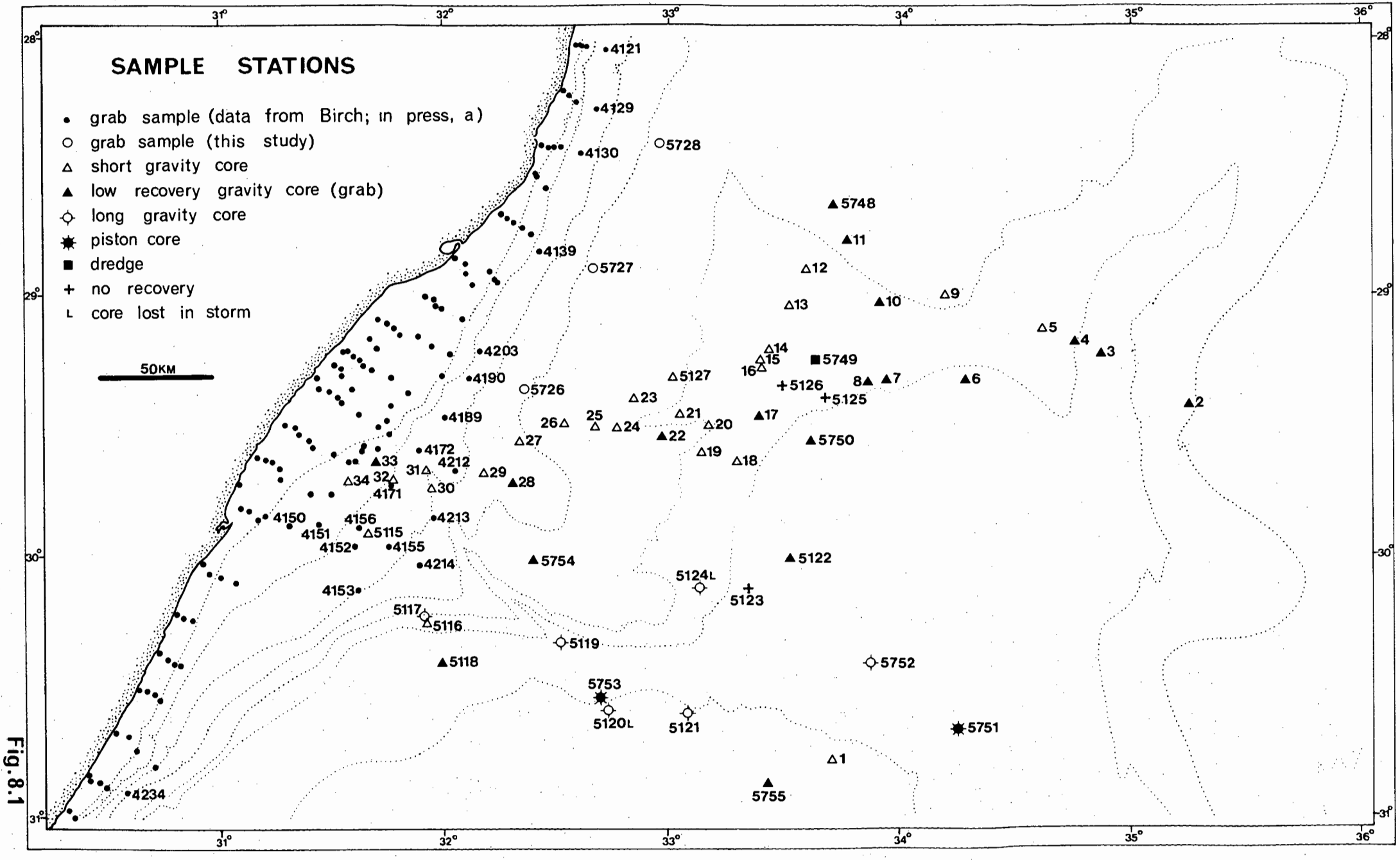
SAMPLE STATIONS
• grab sample (data from Birch; in press, a)
○ grab sample (this study)
△ short gravity core
▲ low recovery gravity core (grab)
long gravity core
piston core
■ dredge
+ no recovery
L core lost in storm
50KM
31°
32°
33°
34°
35°
36°
28°
29°
30°
31°
4121
4129
4130
5728
4139
5727
4203
4190
5726
4189
4172
4212
4171
4150
4156
4213
4151
5115
4152
4155
4214
4153
5117
5116
5119
5118
5753
5120L
5121
4234
5748
11
12
13
10
9
5
4
3
14
15
16
5749
5127
5126
5125
8
7
6
2
23
21
17
26
25
24
22
20
27
19
18
5750
33
34
32
31
29
28
30
5754
5122
5124L
5123
5752
5751
1
5755

Fig. 8.1

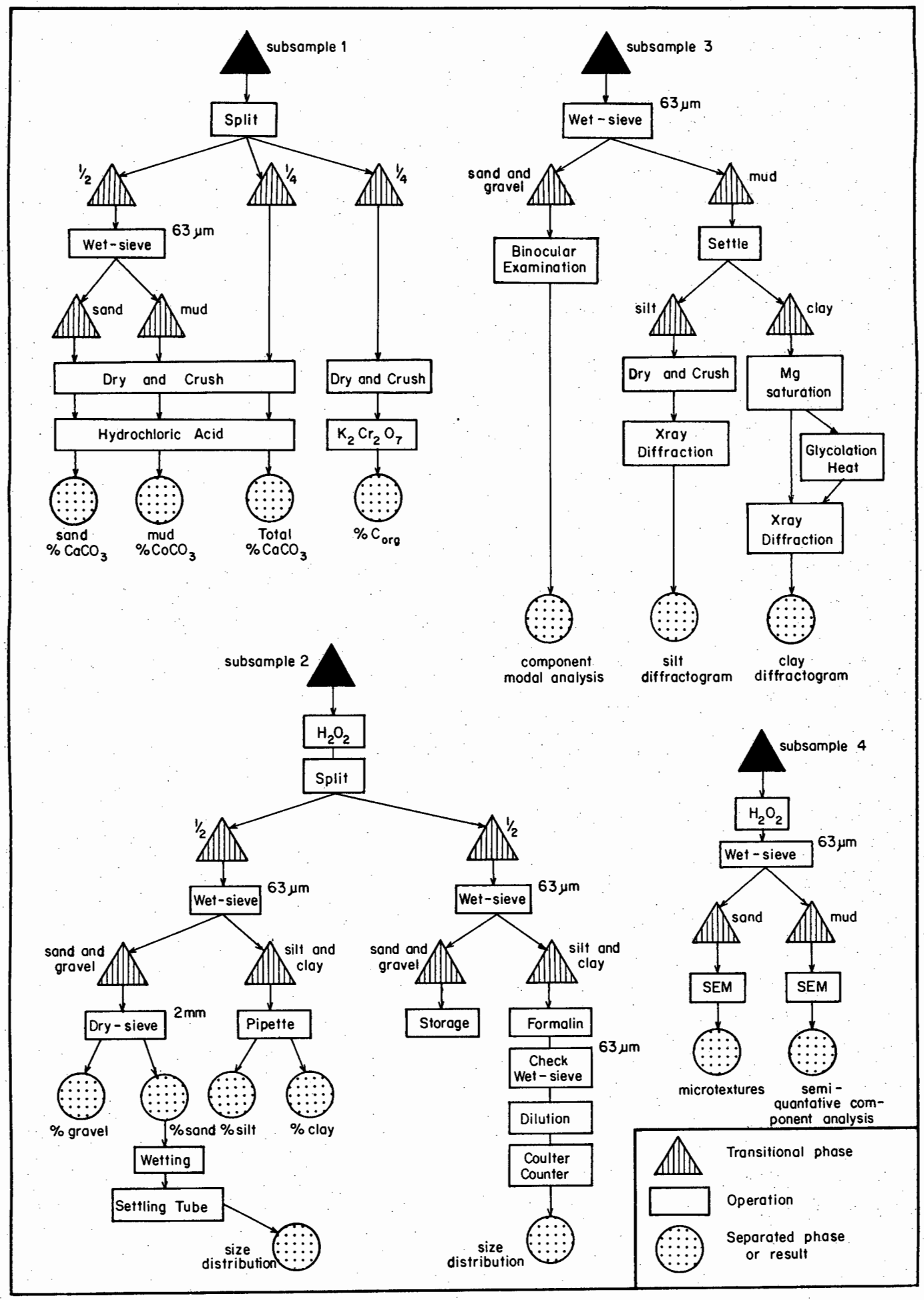

Fig 8.2 FLOWCHART OF ANALYTICAL OPERATIONS

of evolved CO_2, proportional to the $CaCO_3$ content, is registered on a graduated manometer. On calibration, the manometer reading provides a direct measure of the $CaCO_3$ content (Appendix A8).

Organic carbon contents were determined using the method of Morgans (1956) in which organic carbon is oxidised with excess chromic acid and back-titrated against ferrous sulphate (Appendix A9).

Mineralogy and Component Analysis

By wet-sieving and agitation/settling procedures, subsample 3 was partitioned into sand, silt and clay fractions (Fig.8.2). Modal component analyses of the sand fraction were derived using standard point-counting techniques under binocular microscope (Appendix A10). Semi-quantitative mineralogical analyses of the clay fraction (Appendix A11) and silt fraction (Appendix A12) were performed by X-ray diffraction techniques. The mud fractions (Fig.8.2; subsample 4) were scanned and point-counted (SEM) to provide semi-quantitative component analyses (Appendix A13). In addition, the sand fraction (subsample 4) was scanned to provide information on grain surficial microtextures.

Grain Size and Textural Analysis

Routine grain size analysis was performed on subsample 2 (Fig.8.2). After wet-sieving at 63 μm to separate out mud fractions, pipette analysis (Royse, 1970) was utilised to determine the proportions of silt and clay. Dry-sieving of the coarse fractions provided gravel to sand ratios (Appendix A14). The retained coarse fractions (>63 μm) were processed in a settling tube (Flemming, 1977; Flemming and Thum, 1978) to furnish hydraulic grain-size parameters (Appendix A15). Using sea-water as an electrolyte, silt fractions (63-8 μm) were

routinely analysed on a Coulter Counter TA-II to provide particle size data (Appendix A16).

8.3 SEDIMENT CHEMISTRY

The concentrations of both calcium carbonate and organic carbon are important basic parameters to the study of marine sediments. Existing data in the mid Natal Valley is very scant being restricted to shelf studies (Moir, 1976; Birch, in press a) and basin-wide investigations (Kolla et al, 1976c; 1980a) hampered by poor data control. Areal distributions of calcium carbonate and organic carbon in the surficial sediments are described and discussed in ths section. The new distribution maps (Figs.8.3, 8.4 and 8.6) are the most detailed yet published for the mid Natal Valley.

8.3.1 Calcium Carbonate

8.3.1.1 Introduction

Routine calcimetry was performed on 209 bulk sediment samples (35 surface; 174 sub-bottom) to provide an extensive regional data base. In addition, sand (>63 μm) and mud (<63 μm) fractions of 100 samples (35 surface; 65 sub-bottom) were analysed. Full details of the analytical technique ('Karbonat-Bombe') are contained in Appendix A8 while all calcimetry results are tabulated in Appendix B6. Modal analyses of winnowed surficial samples (Appendix B11) are included in the data base since these sands are suspected to be a true reflection of bottom sediments. Graphical representations of down-core trends in carbonate variation are presented in Appendix B2.

8.3.1.2 Distribution of Calcium Carbonate Bulk Sediment

Bulk calcimetry results are graphically depicted in the calcium carbonate distribution map (Fig.8.3). Lowest concentrations of $CaCO_3$ are registered over the continental shelf. The shelf may be divided into two carbonate provinces with a boundary approximately at 29° 30'S. To the north all sediments are depleted in carbonate (<25% $CaCO_3$), particularly in the northern 'Natal Bight' where concentrations drop to <5%. In contrast, the southern shelf zone is rich in carbonate (>75%) over the outer shelf and shelf break. In the south, low concentrations of $CaCO_3$ (<25%) are restricted to the nearshore sediment wedge illustrating its terrigenous origin.

Variable influences of the Agulhas Current explains the disparity between the north and south shelf zones. South of Durban, the Agulhas Current impinges onto the shelf, winnowing out all the fines (Flemming, 1980) to leave a biogenic gravel lag rich in $CaCO_3$ (Fig.8.3). In contrast, the wide shelf north of Durban (Natal Bight) is dominated by barotropically-driven eddy systems (section 2.2.4) and thus riverine terrigenous discharge escapes direct winnowing influences of the Agulhas Current. Since winnowing of terrigenous fines is ineffective, carbonate concentrations are low (Fig.8.3). Lowest $CaCO_3$ contents are registered in the lee of the coastal offset at 29°S suggesting that maximum shelter from oceanic currents is available in this area.

Based on variations in $CaCO_3$ concentration, surficial sediment of the Tugela Cone may be described relative to three

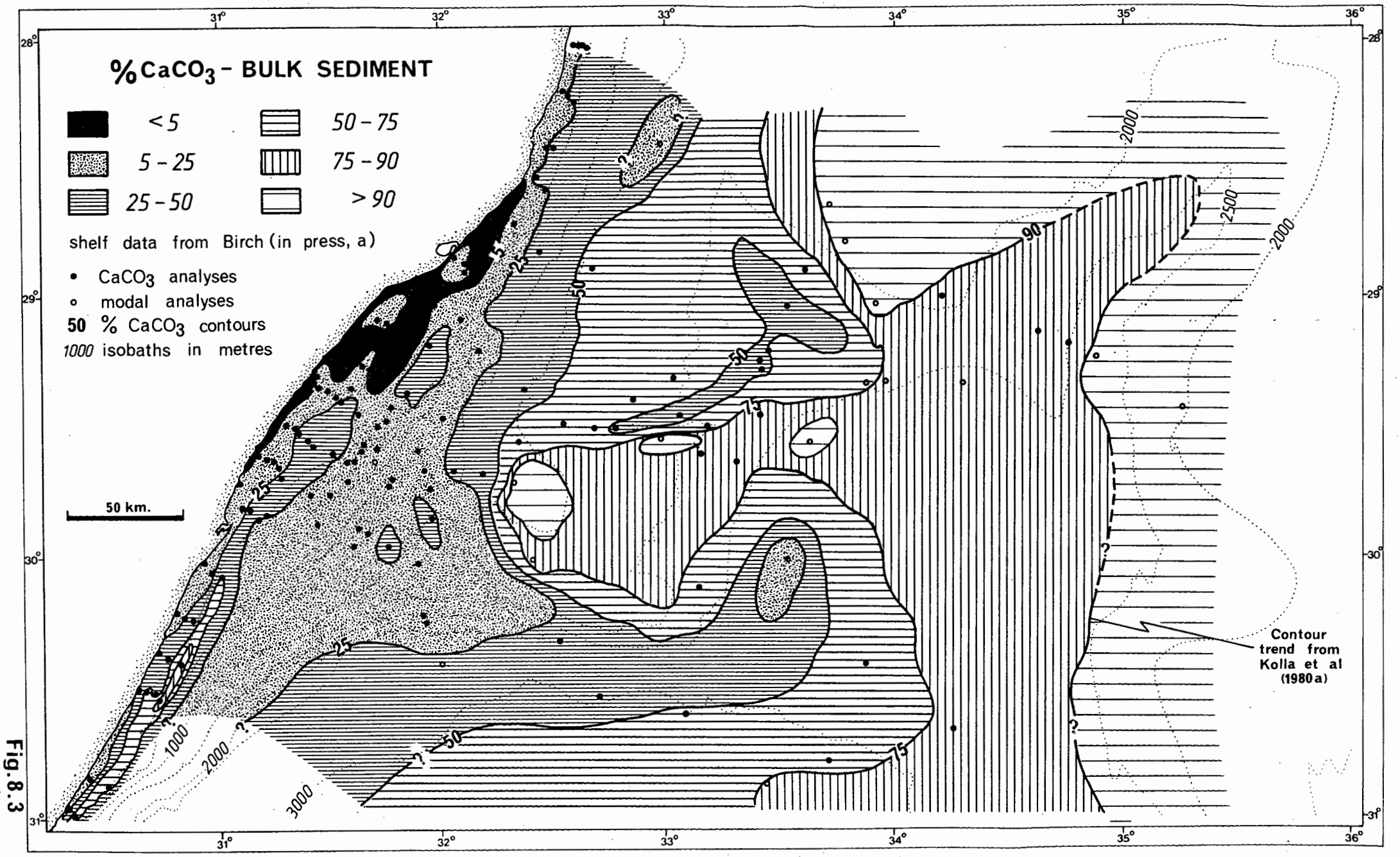
% $CaCO_3$ - BULK SEDIMENT
< 5
5 - 25
25 - 50
50 - 75
75 - 90
> 90
shelf data from Birch (in press, a)
• $CaCO_3$ analyses
∘ modal analyses
50 % $CaCO_3$ contours
1000 isobaths in metres
50 km.
Contour trend from Kolla et al (1980a)
31°
32°
33°
34°
35°
36°
28°
29°
30°
31°

Fig. 8.3

provinces:

(1) North of the 29° 25'S Canyon, the regular downslope $CaCO_3$ increase, from 25% at the shelf break to 50% at the base-of-slope valley, suggests a stabilised terrigenous sediment dilution system. Slope zones more remote from the hinterland receive less terrigenous detrital input and thus the $CaCO_3$ concentration is relatively high. The south of this province is demarcated by the 29° 25'S Canyon (Fig.8.3). This canyon stands out as an elongate zone of reduced carbonate concentration implying down-canyon transport of terrigenous detritus;

(2) The southern flanks and upper slope of the Tugela Cone are demarcated as the primary modern terrigenous depocentres by their low carbonate concentrations. The entire Tugela Cone southern flank west of the Tugela Canyon is depleted in carbonate (<25%) evidencing widespread terrigenous sediment dispersal. Carbonate concentrations are significantly increased east of the Tugela Canyon (32° 15'E) suggesting that eastward dispersal of terrigenous detritus is being suppressed by channelisation into the canyon;

(3) The east and SE flanks of the Tugela Cone are distinctive because of the extremely high carbonate content (>75%) of the modern sediments. Constructive fan growth processes have been operative in this zone in the geologic past. However, both morphological criteria and the high $\%CaCO_3$ point to present-day stagnation (Chapter 9).

The SW basin plain lies juxtaposed to the major modern terrigenous depocentre (south Tugela Cone) and thus must receive a significant input of continental detritus. This terrigenous influx dilutes the normal pelagic rain and adjacent to the cone

flank, $CaCO_3$ concentrations are <50% (Fig.8.3). Southward, away from the terrigenous source zone, concentrations exceed 50%. The base-of-cone region of carbonate-depleted sediment extends eastward to swing around the SE margin of the cone (Fig.8.3). It is surmised that Coriolis-intensified cyclonic flow of NADW (section 7.2.10) entrains fine terrigenous detritus at the base of the southern Tugela Cone and transports it eastwards along the cone base. Eastwards and SE from the Tugela Cone and adjacent carbonate-poor belt, $CaCO_3$ concentrations in modern sediments progressively climb to >75% as continental influence wanes. Data control in this pelagic province is however very poor.

The final two provinces are the Mozambique Ridge and Central Terrace. Biogenic sedimentation dominates these bathymetric highs and $CaCO_3$ concentrations in excess of 90% are registered. Reduced quantities of clastic detritus on the Mozambique Ridge is a response to remoteness from detrital supply. However, the Central Terrace must receive significant input of continental detritus from the Limpopo Cone to the north. Terrigenous input is probably fine-grained because of distance from source. Subsequent removal of the fines, maintaining a high $CaCO_3$ concentration, may be a result of scouring and winnowing action of the Agulhas Current (sections 7.2 and 8.4.1.2).

Sand Fraction

The distribution of % $CaCO_3$ in the sand fraction is presented in Figure 8.4a. Data control is reduced relative to Figure 8.3 being restricted to 35 analyses. No continental shelf data are available.

Carbonate distribution in the sand fraction roughly mirrors that of the bulk sediment with a general seaward increase in

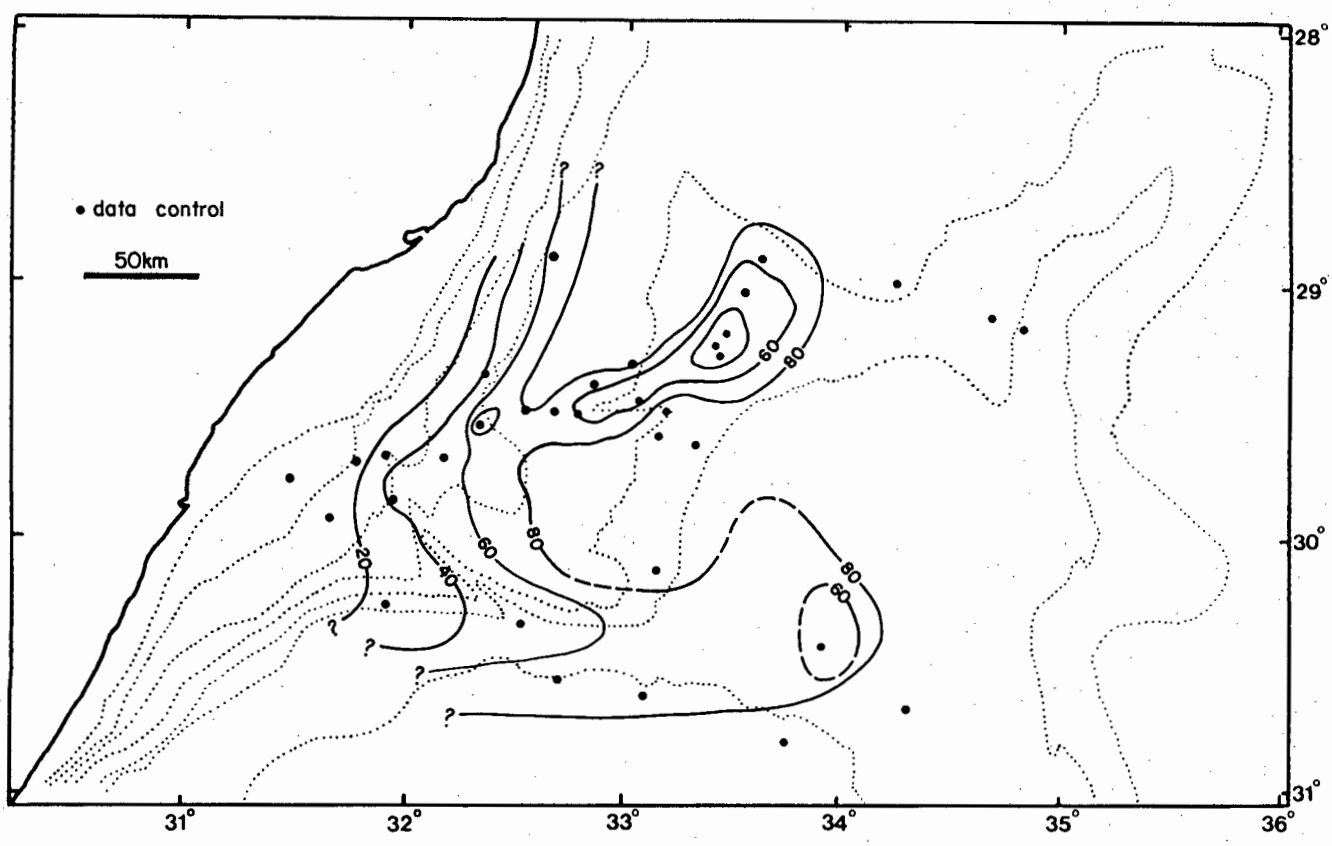

Fig. 8.4a % $CaCO_3$ – SAND FRACTION

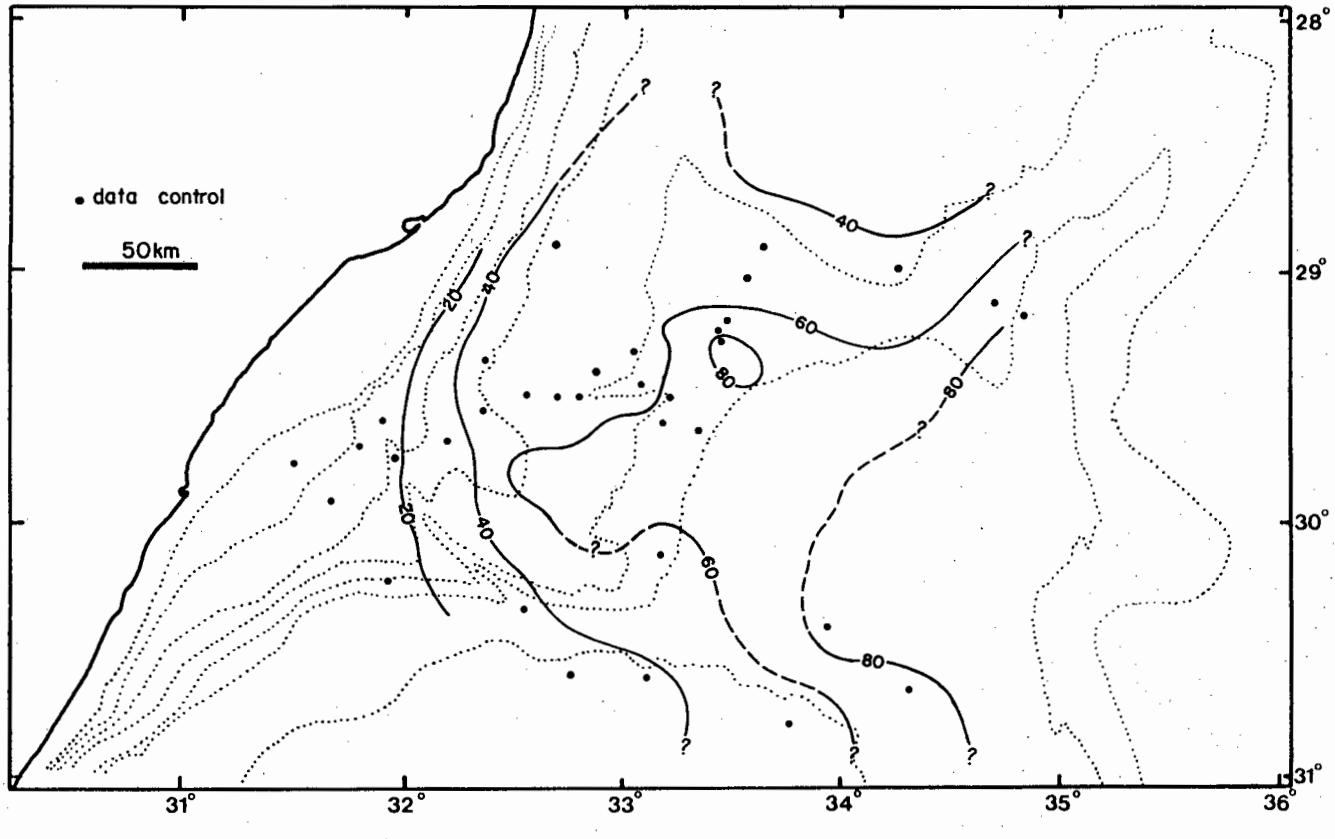

Fig. 8.4b % $CaCO_3$ – MUD FRACTION

$CaCO_3$ content reflecting the switch from terrigenous-dominant to pelagic-dominant sedimentation. Two anomalous zones of low carbonate concentration (29° 25'S Canyon and southern Tugela Cone) break this general pattern and delineate the major down-slope dispersal pathways for sand-grade clastic detritus. Other regions of the Tugela Cone are biogenic-rich and are effectively stagnant as terrigenous depocentres (Fig.8.4a). Sand fractions over the deep basin plain and elevated ridges (Mozambique Ridge and Central Terrace) are extremely rich in carbonate (>80%). Remoteness from hinterland prevents these areas from receiving significant coarse clastic input. As an exception, the basin plain adjacent to the south Tugela Cone receives terrigenous detritus from this cone depocentre. Redistribution of this detritus along the cone margin by deep undercurrents dilutes the pelagic component (Fig.8.4a).

Sand fraction carbonate detritus predominantly comprises whole and fragmented planktic foraminifera admixed with rarer mollusc fragments, benthic foraminifera and pteropod fragments (section 8.4). The prominence of planktic forams is reflected in the similarity of distribution patterns for $\%CaCO_3$ - sand fraction (Fig.8.4a) and % planktic forams (Fig.8.7a).

Mud Fraction

Carbonate concentrations in the mud fraction increase regularly seaward, regardless of water depth and sea-floor topography. Assuming regional equality in fine-grained carbonate input (see section 8.3.1.3), this distribution suggests that terrigenous fines are uniformly dispersed seawards by suspension processes. If bottom-process dispersal was dominant, significant physiographic control over the mud $\%CaCO_3$ should be evident.

Nevertheless, the mud fraction of the south Tugela Cone does appear to be slightly depleted in carbonate suggesting influx of terrigenous muds by bottom processes. The Central Terrace is considered to be an anomalous zone. The low carbonate concentration over this province implies significant input of terrigenous fines, presumably from the Limpopo Cone to the north. Severe winnowing in the area (sections 7.2.3.1 and 7.2.9) affects both terrigenous and biogenic fines equally and thus the carbonate-poor balance is preserved.

Down-Core Variations

Core density is sparse over large tracts of the study area (Fig.8.1). Low density restricts confident correlation between cores since lithofacies varies substantially between physiographic provinces. In addition, many of the cores are too short to provide definitive down-core variations in any sedimentological parameter. Although attempted using chemical, mineralogical and textural criteria, no effective basin-wide core correlation has been achieved. Only local correlation between adjacent cores is possible and without detailed isotope or micropalaeontological control these become relatively meaningless to the understanding of time-synchronous basinal processes. Localised chemical and component variations through time are therefore considered to be of insufficient use to warrant detailed discussion of individual cores. Within-core carbonate variations appear to be controlled by the textural and mineralogical character of individual units (Appendix B2).

8.3.1.3 Discussion

Four main factors combine to determine the calcium carbonate

content of marine sediments (Moore et al, 1973; Volat et al, 1980): (1) biological productivity of the overlying waters; (2) carbonate dissolution; (3) dilution by non-carbonate material; and (4) current-induced sediment winnowing and redistribution.

Productivity

The exact relationship between biological productivity and the carbonate content of underlying sediments remains controversial (see Volat et al, 1980 for review). Nevertheless, attempts to relate these parameters continue, commonly relying on measurements of the standing crop as an index of productivity. Only one survey of primary production (Ryther et al, 1966) is available from the study area (Fig.8.5). Poor data control allied to non-compensation for seasonal and annual productivity changes renders this distribution map to be of limited use in close correlation to Natal Valley carbonate gradients. The mid Natal Valley is however considered to be a zone of uniform high primary productivity implying that the carbonate supply to all physiographic provinces is relatively constant. Productivity may therefore only have limited control over sea floor carbonate gradients. The extremely high productivity levels offshore from Durban (Fig.8.5) are attributable to seasonally-high discharge from hinterland rivers.

Dissolution

Dissolution processes are suspected to have only marginal influence over the carbonate distribution in the study area for two main reasons. Firstly, previous studies (Kolla et al, 1976c) have determined that, in the SW Indian Ocean, the carbonate lysocline lies at a water depth of 4400 - 4450 m. Since the mid Natal Valley is shoaler than the regional lysocline, extensive

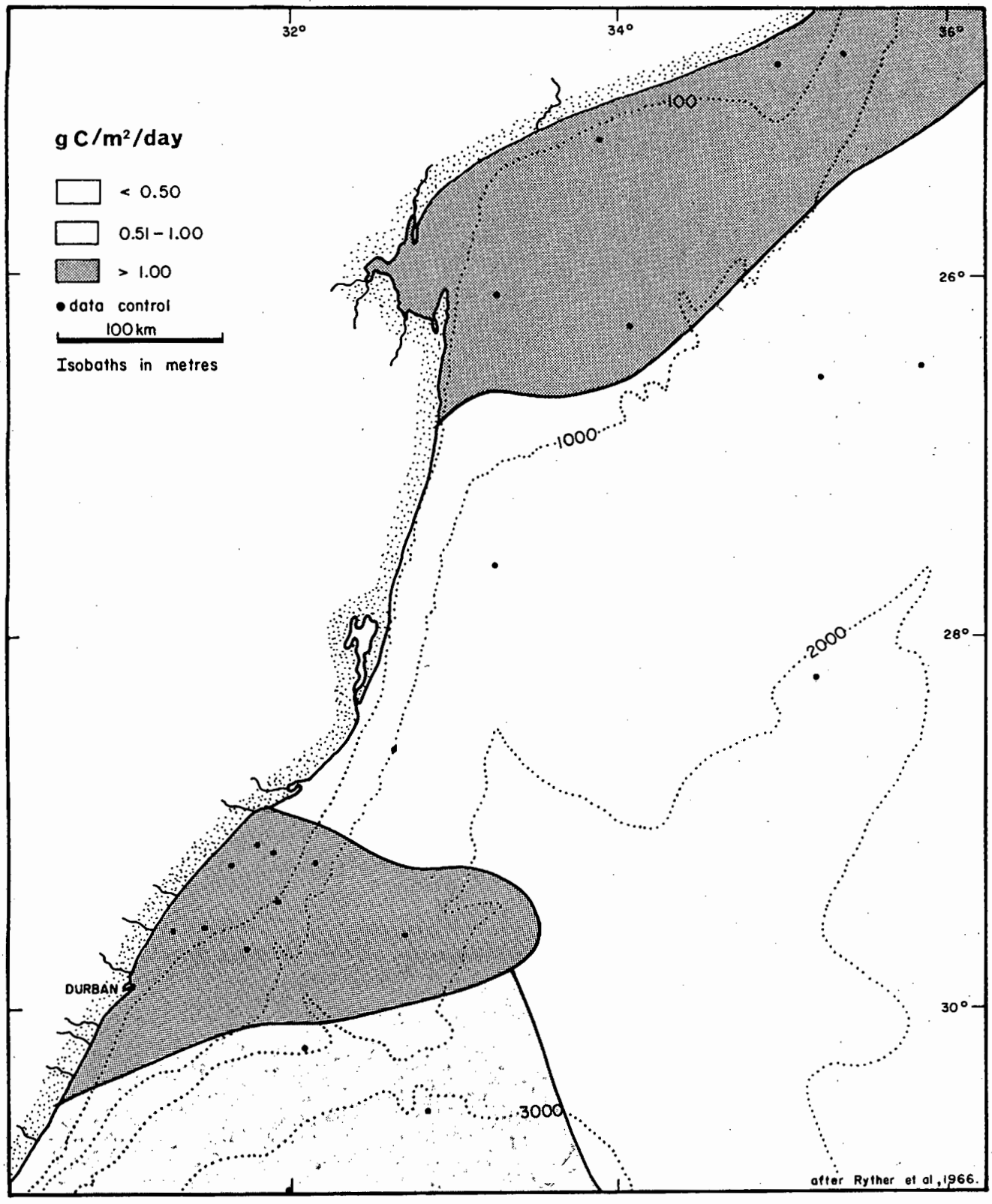

Fig. 8.5 PRIMARY ORGANIC PRODUCTIVITY

dissolution is an unlikely phenomenon. Secondly, if dissolution processes were strongly developed, the deep basin areas should be most affected. Examination of Figures 8.3, 8.4a and 8.7a show no trends of this nature. In fact, some of the highest carbonate concentrations are developed in the deep basin plain (cores 1 and 5751; Appendix B6). Thus dissolution cannot be considered as a dominant control over carbonate distribution.

Nevertheless, several studies (Berger, 1971; Kowsmann, 1973) have indicated that dissolution may be significantly advanced above the lysocline. SEM microscopy of planktic foraminifera (section 8.4.2.2; Table 8.2) verifies that dissolution is locally active with the Natal Valley basin. Rare influx of corrosive undersaturated waters can initiate widespread dissolution in deepest zones of the basin and may explain the poor preservational state (low $\%CaCO_3$, high ratio of fragmented to whole planktic forams; Thunell, 1982) of the lowermost 11 cm of core 1 (Appendices B2, B6 and B10).

With variance in the primary productivity and dissolution unable to account for the $\%CaCO_3$ distribution, it is necessary to invoke dilution and redistribution to explain the observed carbonate gradients.

Dilution

Dilution by non-carbonate sediment is recognised as an important variable governing carbonate distribution (Volat et al, 1980). Continental margins serve as sources of detrital material with decreasing influence towards more remote and deeper sites (Biscaye et al, 1976). Coupled with a constant areal carbonate productivity, this model results in low-carbonate sediments adjacent to the detrital source. The general situation over the

Tugela Cone illustrates this process with sediments over the entire upper slope being depleted in carbonate (Figs.8.3; 8.4a and b). In addition, dilution is enhanced over major zones of downslope transport (29° 25'S Canyon and southern Tugela Cone).

Winnowing and Redistribution

Current-induced winnowing and redistribution strongly influences the $CaCO_3$ distribution in two main areas:

In regions where a competent undercurrent impinges on an active terrigenous sediment dispersal route, detritus may be entrained and redeposited farther along the current pathway. The route of the current is recognised by a zone of depleted $CaCO_3$ in underlying sediments. This situation is active adjacent to the southern flanks of the Tugela Cone with deep NADW flow entraining detritus to redeposit it farther east around the Tugela Cone margin (Fig.8.3);

In zones of intermittent terrigenous supply, current scour may winnow out the fines thus maintaining a high carbonate concentration (foram tests). The winnowed fines dilute sediments down-current. This model is applicable to the Central Terrace which probably receives rare terrigenous input from the Limpopo Cone. Current scour maintains a high $\%CaCO_3$ in terrace crest sediments (Fig.8.3) and redeposits the winnowed clastic fines over the deep basin to the south (section 8.4.1.2).

8.3.2 Organic Carbon

8.3.2.1 Introduction

Duplicate organic carbon determinations were performed on 209 bulk sediment samples (35 surface; 174 sub-bottom). Full

details of the method and its accuracy are contained in Appendix A9. Analytical results are listed in Appendix B6. The off-shelf analyses have been assimilated with shelf data (Birch, in press a) to produce a composite map depicting the distribution of % organic carbon (Fig.8.6). Shelf and basin analyses are compatible since both studies utilised the wet chemical technique of Morgans (1956).

8.3.2.2 Distribution of Organic Carbon

The east coast shelf is greatly depleted in organic carbon relative to the world average of 0,5% (Emery, 1960). Very low concentrations (<0,1%) characterise the majority of the shelf zone (Fig.8.6) as a direct result of vigorous Agulhas Current flow which winnows out the fine fraction leaving a coarse lag (Flemming, 1981) hostile to C_{org} preservation. Anomalously high concentrations (>1,1%) occur in a restricted muddy depocentre adjacent to the Tugela fluvial system (Figs.8.6 and 8.19). Agulhas Current flow does not penetrate the wide shelf in this area (section 2.2.4) and thus the Tugela mud belt is hydrodynamically stable. Influenced by shelf currents and eddy systems, the mud belt is deflected northwards (Fig.8.6).

Slightly higher concentrations (0,1-0,3%) are registered over the Tugela Cone upper slope reflecting an increased mud content relative to the shelf. Two zones diverge from this general trend. A fan-shaped zone of increased concentration (0,3-1,1%) splays out from the Tugela mud belt (Fig.8.6) implying a terrigenous origin for the organic matter. A second upper slope zone of relatively high C_{org} concentration (>0,5%) is developed in mud-rich sediments of depocentre 1 on the northern


% ORGANIC CARBON
Contour Interval: 0.2 %
> 0.5
• data control
50 km
Shelf data from Birch
(in press, a)
31°
32°
33°
34°
35°
36°
28°
29°
30°
31°
0·1
0·3
0·5
0·7
0·9
?

Fig. 8.6

Tugela Cone/Zululand continental slope (Fig.6.14).

Farther offshore, trends become diffuse in step with reduced data control. In general, surficial sediments are depleted (<0,4%) in organic carbon with only two exceptions. Locally over the southern Tugela Cone, concentrations reach 1,0% while above-average values (0,5-0,6%) are recorded in the 29° 25'S Canyon. These regions are demonstrably the prevalent modern routes for downslope transport of terrigenous sediments (sections 8.3.1, 8.5 and 8.6.4) again implying that the organic matter is of continental origin. In addition, sediments of these zones are mud-enriched confirming a positive correlation between muds and high C_{org} concentrations.

8.3.2.3 Discussion

The accumulation and preservation of organic matter in marine sediments is governed by the complex interaction of several biological and physical factors. Biologic factors include the level of primary organic productivity in both the euphotic zone and adjacent hinterland. In addition, biochemical degradation initiated by scavenging metazoans and bacteria may greatly impede preservation. Physical factors include sediment particle size and sedimentation rates (Demaison and Moore, 1980).

Numerous studies (e.g. Bordovsky, 1965; Ibach, 1982) have subscribed to the traditional view that high surface productivity should promote organic enrichment of underlying sediments. In contrast, Demaison and Moore (1980) could not establish a systematic correlation between productivity and % C_{org} in sediments. Terrestrial organic matter transported seaward via rivers may also source marine sediments. Zones of highest

primary productivity (Fig.8.5) are considered to reflect extensive riverine discharge enriched in land-derived organic matter (Ryther et al, 1966). Maxima of C_{org} in the study area may therefore be of continental origin. These maxima generally coincide with the major recent terrigenous depocentres confirming that the C_{org} is terrestrially-derived. The correlation between terrigenous discharge and C_{org} is demonstrated by the bivariate plot of total carbonate versus organic matter (Fig.8.27c). Highest concentrations of organic matter are associated with carbonate depletion (terrigenous sediments). Conversely, low organic contents characterise pelagic sediments.

Under an oxygenated basin such as the Natal Valley, benthic fauna scavenge, rework and thus deplete the "organic rain" falling through the water column. In addition, although the sea floor muds may be anoxic, oxygen-respiring metazoans extensively bioturbate the top 30 cm of sediment (Peng et al, 1977), accelerating biochemical degradation and reducing the organic matter concentration. Bioturbation of this type is ubiquitous under oxic conditions including deep-sea environments (Turekian et al, 1978). Average sedimentation rates in post-Jimmy times (sediment unit D) vary from 10-66 m/my (Table 6.4). Residence time of sediment in the mixing zone (top 30 cm) may be up to 30 000 yrs. Over this time period, the metazoan biomass progressively consumes edible organic material thus reducing the C_{org} content. Below the bioturbation zone, sulphate reduction and bacterial CO_2 reduction in an anaerobic environment further diminishes the organic content (Demaison and Moore, 1980). With the onset of additional reactions on burial, highest concentrations of C_{org} should exist in the surficial sediments.

Downcore variations in C_{org} content (Appendix B6) confirm common sea floor enrichment (cores 9, 14, 19, 27 and 5121). Alternatively, the C_{org} content within several environments may be controlled by grain size and texture. For example, in turbidite-graded sequences, organic matter is concentrated in the finer-grained sequence tops perhaps explaining the sea floor C_{org} enrichment in cores 30, 34 and 5115 (Appendixes B2 and B6).

There is a positive correlation between the organic carbon and mud content in Natal Valley sediments (compare Figs.8.6 and 8.19). This is illustrated by a bivariate plot (Fig.8.27d) in which high % organic matter equates with high mud content. This relationship is however strongly influenced by physiographic setting with different groups of samples showing different trends (section 8.5.3.3). Fine-grained sediments are typically characterised by reduced permeabilities preventing free diffusion of oxidants. Combined with lower levels of bacterial activity (Bordovsky, 1965), this may explain the broad correlation between grain size and organic carbon content.

The overall rate of accumulation of organic carbon is related to the bulk sedimentation rate (Heath et al, 1977). Under oxygenated waters, fluctuations in C_{org} content may be correlated to sedimentation rate changes (Demaison and Moore, 1980). This correlation is demonstrated in the mid Natal Valley by considering three sediment unit D sub-facies (Table 8.1). Rapid burial with consequent reduction in residence time within the zones of C_{org} consumption near to the sediment-water interface accounts for this positive correlation.

Table 8.1 Comparison of Sedimentation Rates and Organic Carbon Content

SUB-FACIES*	PHYSIOGRAPHIC* PROVINCE	SEDIMENTATION* RATE RANGE (m/my)	AVERAGE C_{org} (%)
D_3	deep basin	0-18	0,33+
D_7	south Tugela Cone	0-60	0,6&
D_5	Tugela Cone - central upper slope	0-86	0,7**

* - data from Tables 6.1 and 6.3
\+ - cores 1, 5121, 5751 and 5753 (Appendix B6)
& - cores 5117 and 5119 (Appendix B6)
** - cores 30, 31, 32, 34 and 5115 (Appendix B6)

8.4 SEDIMENT COMPOSITION AND MINERALOGY

A thorough knowledge of sediment composition and mineralogy is essential if full understanding of regional sediment dispersal processes is to be achieved. Regional variations in sediment composition may be used to evaluate provenance, transport agents and routes, and environments of deposition.

In broad structure, this section comprises compositional evaluations of the sand, clay and silt fractions with subsidiary SEM studies of the sand and mud fractions. Details of the data base and analytical methods are contained within the relevant appendices. Analytical steps as performed on subsample 3 (components and mineralogy) are summarised in Figure 8.2.

8.4.1 Sand Fraction Mineralogy and Components

8.4.1.1 Introduction

An investigation of the variations in mineralogy and

component assemblages is an integral part of any comprehensive regional sedimentological study. In particular, the sand fraction lends itself to component studies since discrete grains are large enough to facilitate identification. In addition, sand grade material is hydrodynamically coarse enough to escape most processes of regional homogenisation unlike the mud fraction. Thus the distribution of individual components may be indicative of provenance, transport routes and local depositional and erosional processes (e.g. Kowsmann, 1973; Moore et al, 1973).

Component and mineralogy studies along the SE African continental margin have previously been restricted to the shelf zone (Moir, 1976; Flemming, 1978; Birch, in press a). This section presents the first comparable data from the adjacent off-shelf zone. Component modal analyses of 118 sand fraction samples (53 surface; 65 sub-bottom) provides an extensive data base. Standard point-counting techniques were employed (Appendix A10) to obtain the modal analyses listed in Appendices B10 and B11.

8.4.1.2 Distribution of Sand Grade Components

Using the modal analyses, distribution maps for each component have been constructed. Only components showing significant local or regional variations are presented and discussed in this section.

Planktic Foraminifera

The relative abundance of pelagic components such as planktic foraminifera tests is primarily a reflection of the balance between the rates of supply and removal (Kowsmann, 1973) and the effects of dilution and redistribution. The importance

of these processes has been outlined in section 8.3.1.3. In summary, processes of sediment dilution, redistribution and dispersal are judged to exert major control over the distribution of planktic forams while variance in productivity and dissolution is suspected only of minor influence.

Whole planktic forams comprise the most abundant sand grade component within the study area (Fig.8.7a). Whole tests are very abundant (>80%) over five main zones: the Central Terrace crest, Mozambique Ridge, eastern deep basin plain, east/SE Tugela Cone and the lower slopes of the NE Tugela Cone. Intermediate concentrations (40-70%) characterise three physiographic areas: the 29° 25'S Canyon, south and SW Central Terrace and the deep basin plain adjacent to the south Tugela Cone. Zones of lowest planktic test concentration (<20%) are conspicuous along the upper continental margin and indicate dilution by terrigenous detritus debouched from hinterland rivers. This nearshore "dilution zone" extends into deeper water over the southern Tugela Cone (Fig.8.7a) implying that this region is a major terrigenous detritus depocentre.

Major routes of continental detritus dispersal are outlined as zones of intermediate planktic concentration splaying out from the major terrigenous depocentres. Low axial percentages of planktic forams (<40%) illustrates that the 29° 25'S Canyon is a conduit for downslope dispersal of continental detritus. A major redistribution zone borders the southern Tugela Cone receiving detrital input directly from the adjacent terrigenous depocentre. Sediment entrainment and eastwards redistribution in this deep water province is achieved by cyclonic NADW flow (section 2.3.2) and thus the concentration of planktic forams is effectively

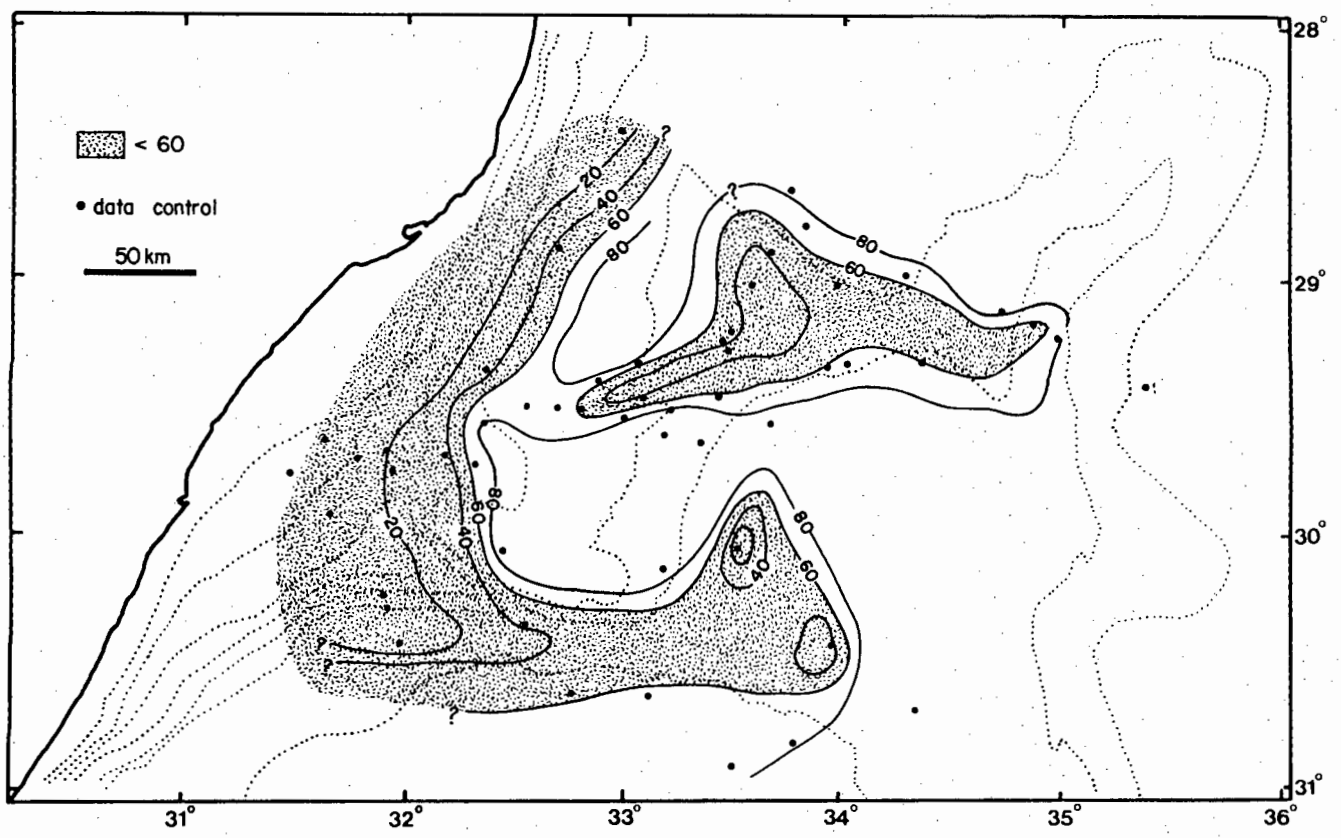

Fig. 8.7a % PLANKTIC FORAMINIFERA - SAND FRACTION

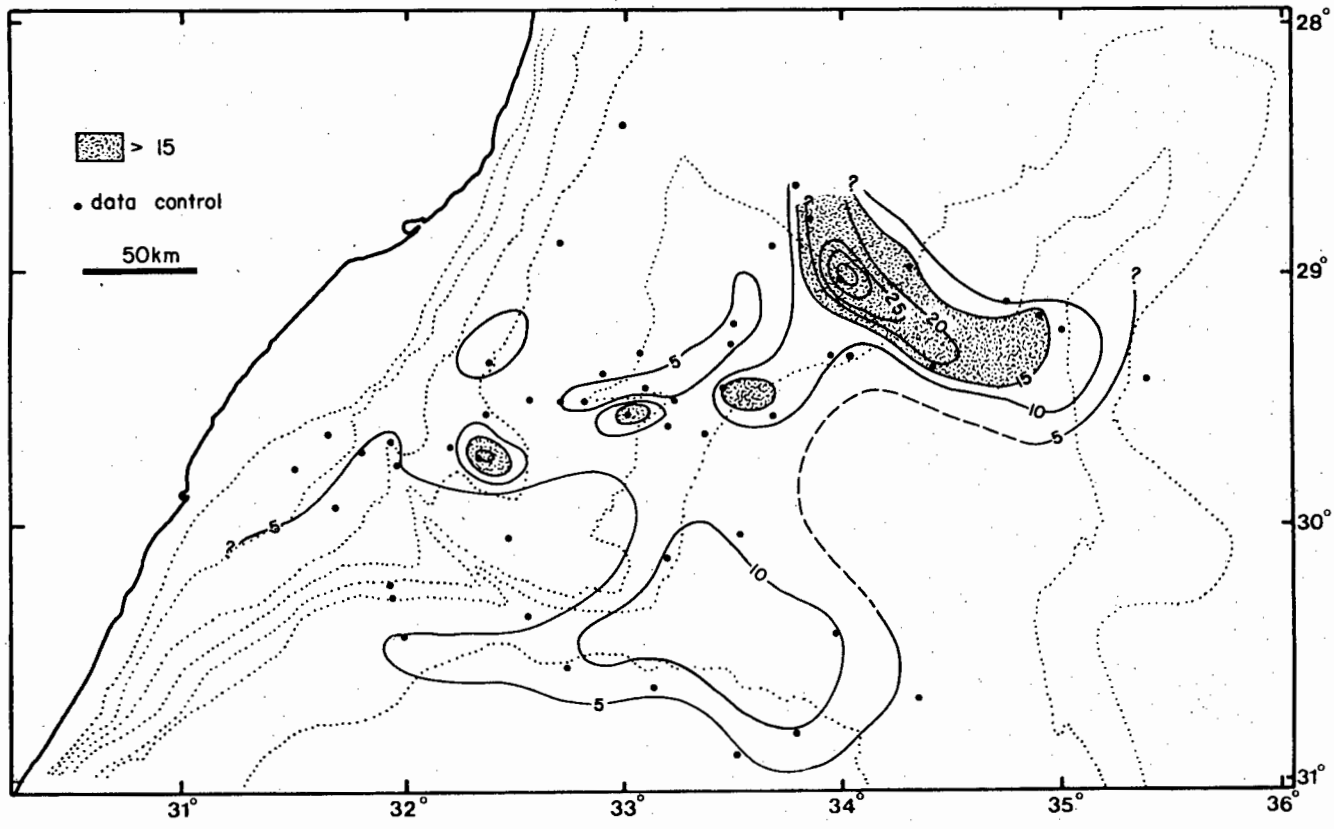

Fig. 8.7b % PLANKTIC FORAM FRAGMENTS - SAND FRACTION

reduced.

Excluding the southern Tugela Cone and the 29° 25'S Canyon zone, all deep water provinces are characterised by high concentrations of planktics (>80%; Fig.8.7a) implying a waning of terrigenous input and influence. Extensive scouring and winnowing over the Central Terrace (sections 7.2.3 and 7.2.8) removes the fine fractions maintaining a relatively high concentration of hydrodynamically-stable sand-grade planktic tests.

Planktic Foraminifera Fragments

Planktic foram fragments are a minor component, regionally averaging from 5-10% of the total sand fraction (Fig.8.7b). The distributions of whole and fragmented planktic forams are closely inter-related with the former introducing bias to the latter. By removing this bias, real distribution trends are observed and these reflect the incidence of high energy bottom processes such as sea-floor scouring and winnowing. Local bias is removed by considering the distribution of fragments as a percentage of the total planktic foram population rather than the total sand fraction (Fig.8.8a). From examination of Figures 8.7b and 8.8a, six distinctive foram fragment provinces are identified.

Relative to whole foraminifera, the concentration of fragments is low over the Central Terrace crest. However, vigorous current activity over this zone (section 7.2.3) must initiate widespread test breakage. The resultant fragments must be removed to maintain the high relative concentration of whole tests. As in the Panama Basin (Kowsmann, 1973), the current causing the fragmentation is of sufficient competence to then remove the hydrodynamically-finer fragments.

A second province encompasses the south and SW Central

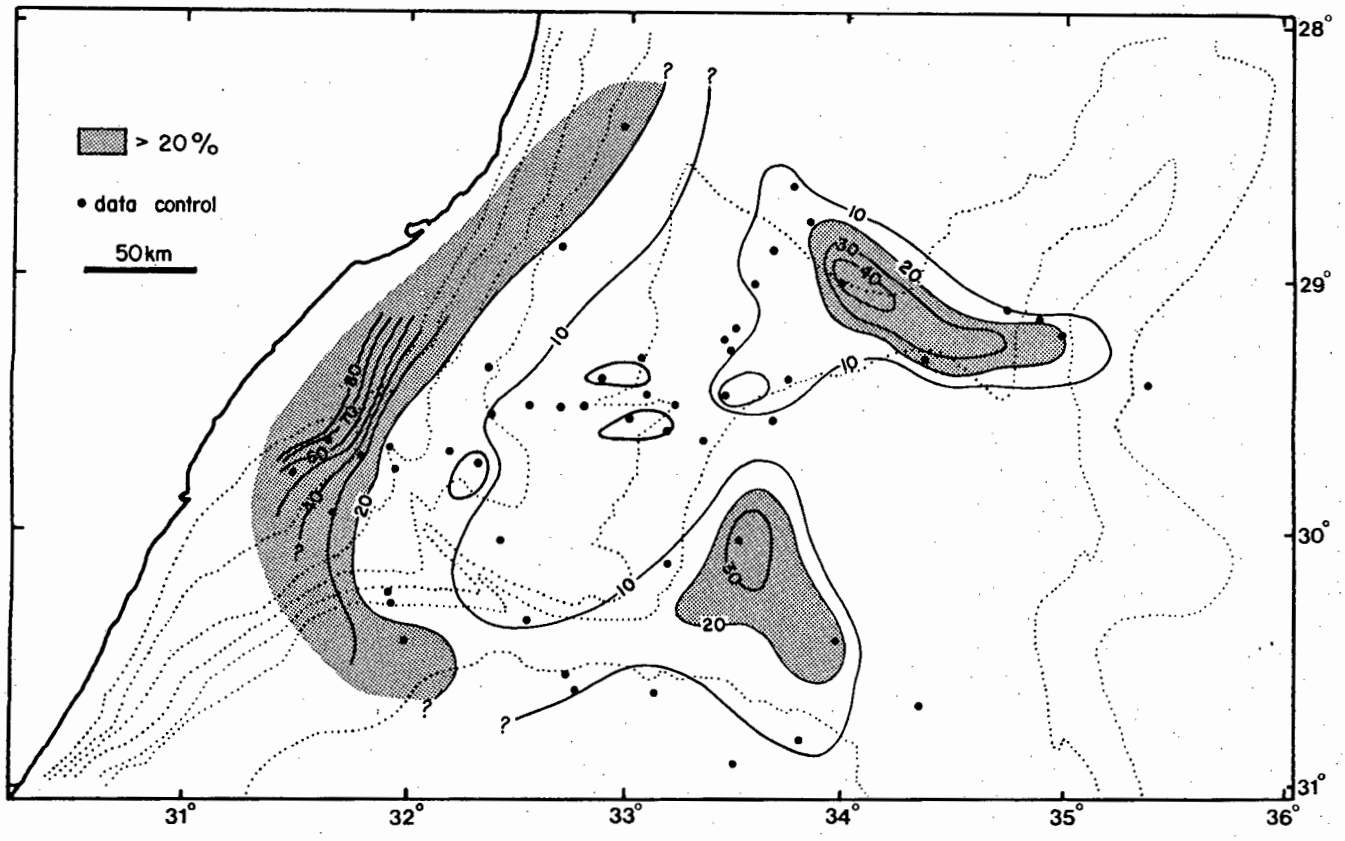

Fig. 8.8a PERCENTAGE RATIO OF FRAGMENTED TO TOTAL PLANKTIC FORAMINIFERA POPULATION

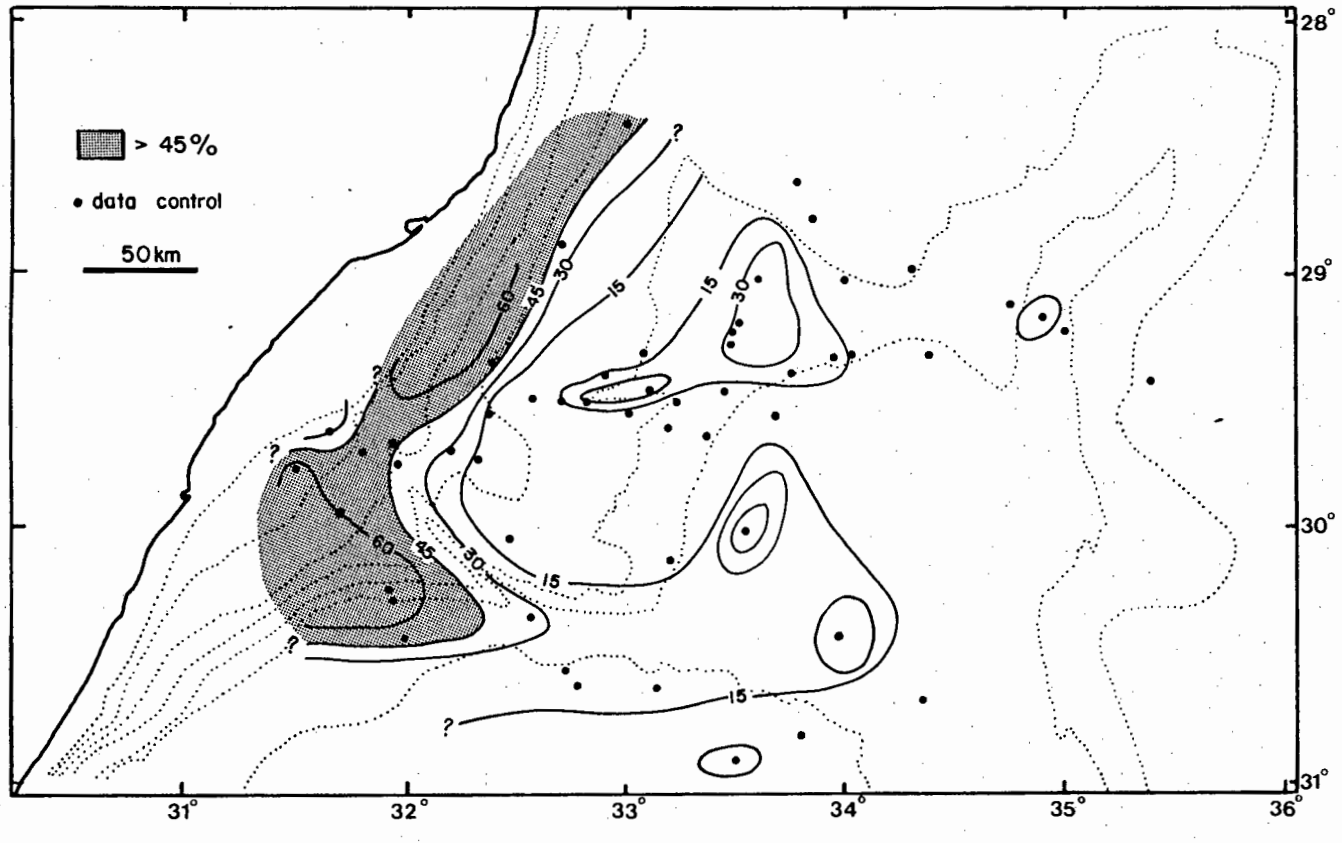

Fig. 8.8b % QUARTZ - SAND FRACTION

Terrace. In this region the concentration of fragments is greatly increased (Figs.8.7b and 8.8a) to comprise over 40% of the total sand fraction. Downstream along the Agulhas Current flow path, these areas are depocentres for the majority of fragments generated over the terrace crest.

The east and NE Tugela Cone together with a major proportion of the deep basin plain are outlined as zones of minimal foram breakage (Figs.8.7b and 8.8a). Since these deep water regions are also characterised by an abundance of whole tests, the low concentration of fragments must indicate relatively tranquil bottom conditions.

Upslope towards the continental shelf, numbers of fragmented tests increase markedly relative to whole tests (Fig.8.8a) although the absolute number of fragments remains static (Fig.8.7b). The largest increase occurs above the 750 m isobath where fragments comprise >80% of the total foram component (Fig.8.8a). This trend is probably a result of an upslope increase in Agulhas Current vigour. Greatest current core competence has been documented shallower than the 750 m isobath (Lutjeharms, 1971).

Low absolute concentrations of fragments characterise the southern Tugela Cone in response to terrigenous dilution. However, relative to whole tests, the fragment concentration is high (Fig.8.8a). This may be an inherited feature since these sediments are partially sourced from the shelf and upper slope areas where forams are subjected to scour breakage. In addition, processes of downslope dispersal probably initiate further abrasion and breakage.

The final province roughly corresponds to the scour and

redistribution pathway adjacent to the southern Tugela Cone. Whole planktic forams are depleted over this zone (Fig.8.7a) confirming dilution by redistributed terrigenous detritus. In contrast, fragmented tests are relatively enriched (Fig.8.8a) suggesting that the bottom currents responsible for redistribution are vigorous enough to initiate test breakage.

Quartz

The distribution of sand fraction quartz (Fig.8.8b) is almost antithetic to whole planktic foraminifera and demarcates the major depocentres for sand-grade continental detritus. Quartzose detritus is most concentrated (>60%) over the upper continental margin and the southern Tugela Cone where it strongly dilutes all other sand-grade components. In the uppermost slope region, however, the quartz component is diminished to <30% (sample 33) because of additional dilution by rock fragments, coarse mollusc debris and glauconite (Appendix B11).

In response to waning continental influence, the quartz concentration declines over the eastern Tugela Cone (Fig.8.8b). However, the 29° 25'S Canyon and adjacent areas stand out as a downslope dispersal route as indicated by the local increase in quartz concentration. Much of the terrigenous material transported down this canyon is dumped around the canyon mouth area beside the East Tugela Ridge (Fig.8.8b).

The final quartz depocentre encompasses the sediment redistribution zone adjacent to the south and SE margins of the Tugela Cone. In this region, continental detritus transported down the southern Tugela Cone is entrained by cyclonic NADW flow to be redispersed along the Tugela Cone margin. This is the only

section of the deep basin plain over which the quartz concentration exceeds 15%. Being remote from terrigenous supply, major areas of the deep basin plain and Central Terrace are very depleted in quartz detritus.

Feldspar and Heavy/Opaque Minerals

The distribution patterns of feldspar (Fig.8.9a) and heavy/opaque minerals (Fig.8.9b) show close similarities to the distribution of quartz (Fig.8.8b) and also delineate the major terrigenous depocentres. The models applicable to quartz dispersal are applicable to these subordinate terrigenous fractions.

Down-Core Variations

Regional correlation of cores is impossible because of the low sample density and absence of detailed micro-palaeontological information. Within each core, component variability is lithofacies-controlled (Appendices B2 and B10) and thus no regional patterns are discerned. In zones which have received recent continental debris input, core-top sediments are generally enriched in quartz, feldspar and heavy minerals (e.g. core 5117). Elsewhere, fluctuations in terrigenous versus biogenic material reflects periodic waxing and waning of continental detritus input and probably, to a lesser extent, surface water productivity.

Pleistocene/Holocene Boundary

Biostratigraphic information is available for cores 5117 and 5753 (Salmon, 1979a). The results of this study, in which the Pleistocene/Holocene boundary is locally defined, are summarised in this section and the inferred climatic changes may be equated to concomitant alterations in the sand-grade components.

Based on criteria established by Vincent (1970) but with

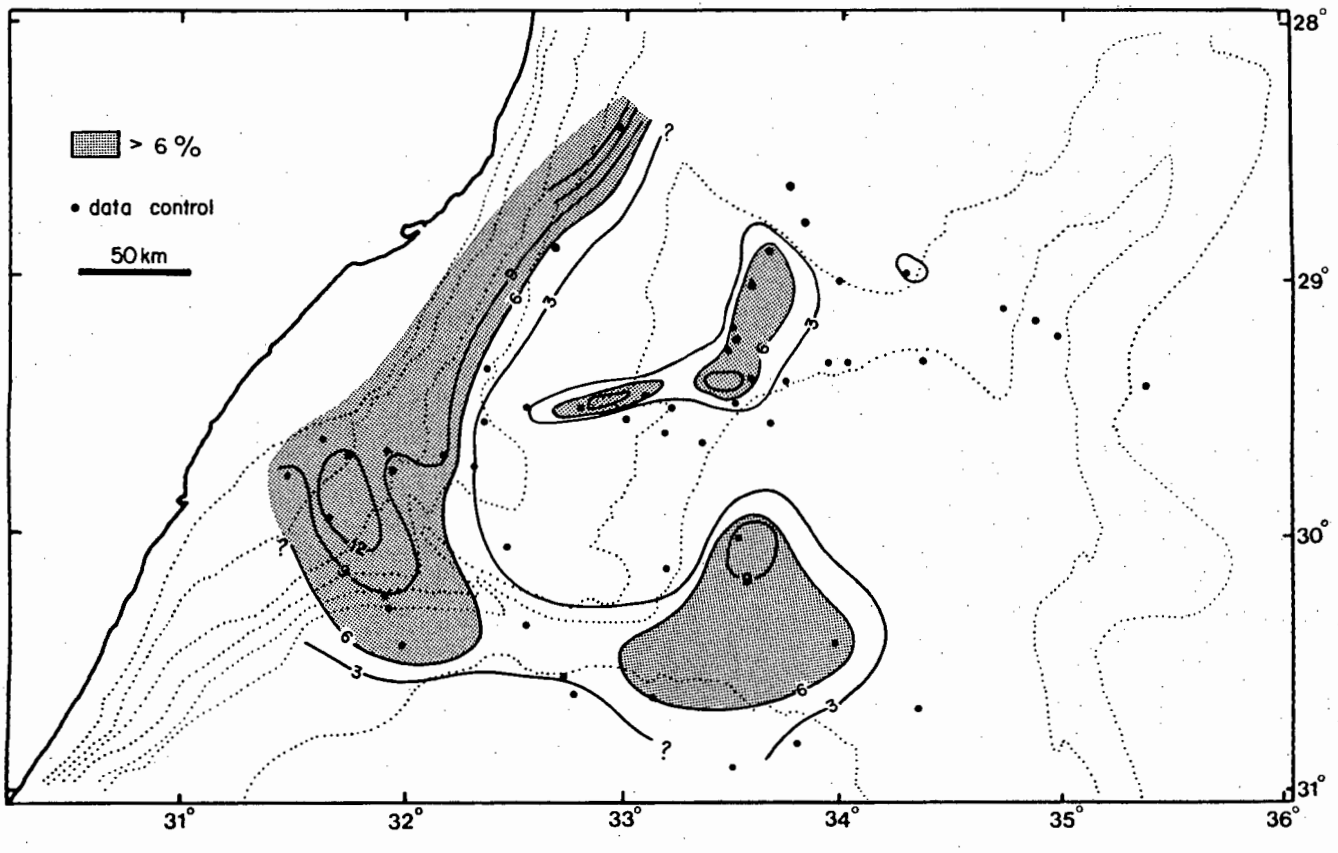

Fig. 8.9a % FELDSPAR – SAND FRACTION

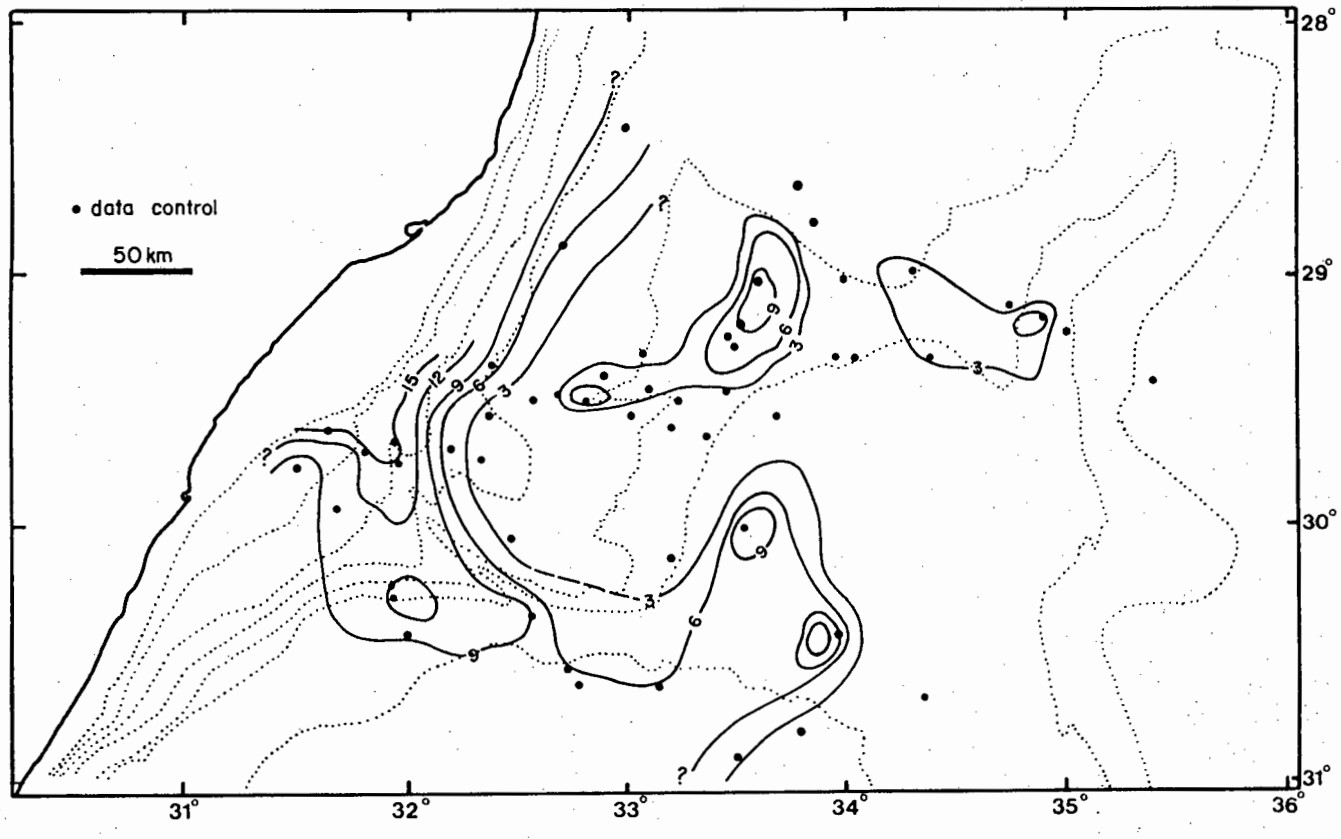

Fig. 8.9b % HEAVY / OPAQUE MINERALS – SAND FRACTION

some modifications, Salmon (1979a) uses the following parameters to define the Pleisocene/Holocene boundary:

(1) The warm/total ratio (warm water species to the total planktic foram count) increases into the Holocene;

(2) The % of Globorotalia inflata (transitional species) relative to the total planktic count decreases into the Holocene;

(3) The % of Pulleniatina obliquiloculata (warm water species) relative to the total planktic count increases into the Holocene.

Plots of these three parameters versus depth are displayed in Figure 8.10. In core 5117, the warm/total ratio indicates a cool interval below 75 cm. This cooling is reflected by P. obliquiloculata which decreases in abundance below the same depth. However, increased proportions of G. inflata, discriminating the cooler interval, are only registered below 90 cm (Fig.8.10). The Pleistocene/Holocene boundary is therefore picked at between 75 and 90 cm (Salmon, 1979a). Using the same criteria in core 5753, the Pleistocene/Holocene boundary is inferred to lie between 45 and 80 cm depth.

Down-core plots of the quartz plus feldspar % (sand fraction) and the $CaCO_3$ content of the total sediment are appended to Figure 8.10. In both cores, the quartz plus feldspar trends indicate that terrigenous components were relatively more abundant during the Pleistocene glacials. Cooler climate and intensified precipitation in the Pleistocene (Frakes, 1979) probably increased the continental detritus supply (Kolla and Biscaye, 1977), while a low sea level stand (Fig.7.7) allowed direct off-shelf sediment dumping. Increased terrigenous sediment supply to basinal areas and retarded Agulhas Current flow during the glacial phase (Hutson, 1980) may have intensified

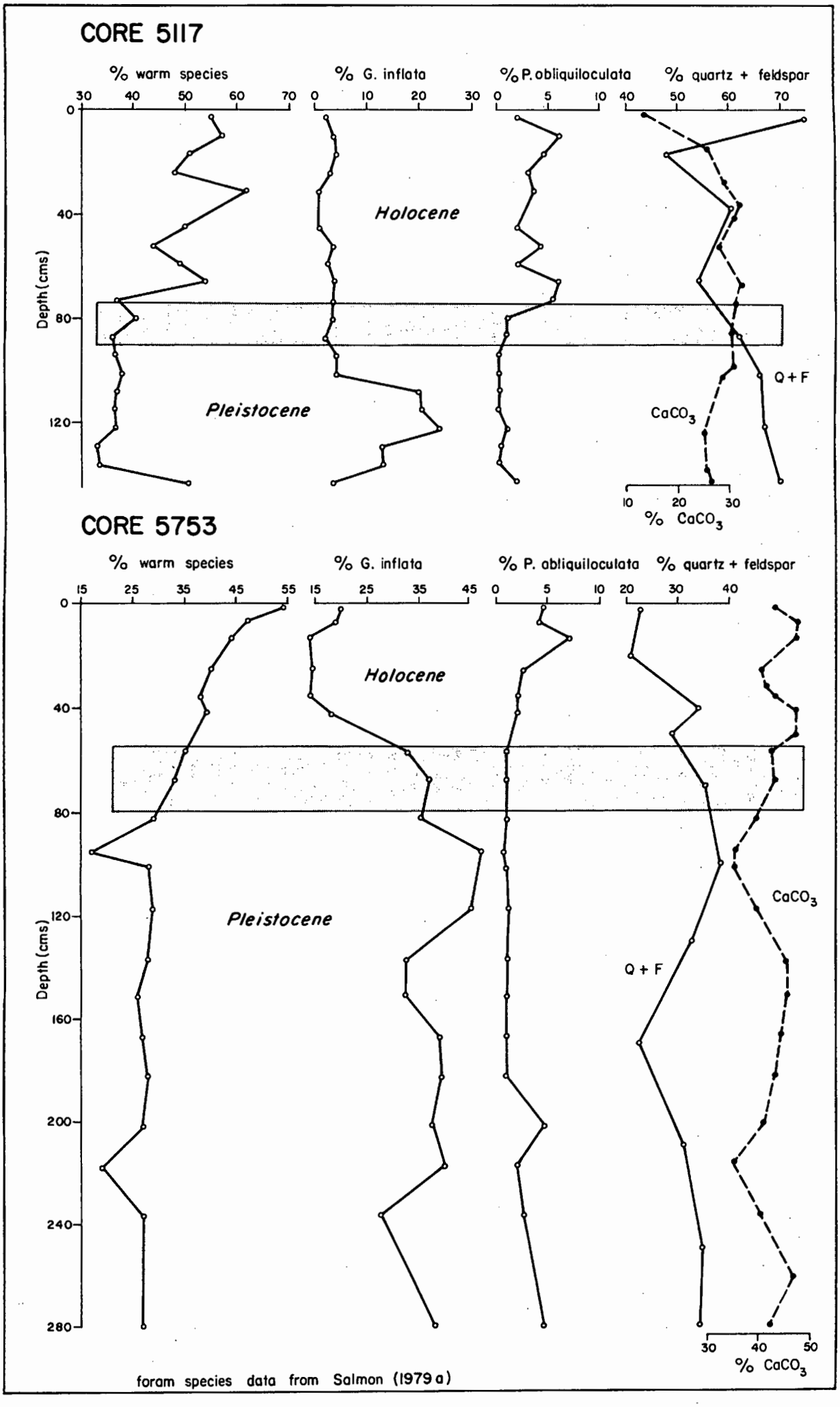

Fig. 8.10 PLEISTOCENE / HOLOCENE BOUNDARY IN TWO NATAL VALLEY CORES

downslope transport of sand-grade quartz and feldspar.

In contrast, the $CaCO_3$ content of the total sediment displays no obvious trend change at the Pleistocene/Holocene boundary (Fig.8.10). However, after basin-wide investigations in the Indian Ocean, Kolla et al (1976c) concluded that carbonate variations through time are controlled by several variables. Complex and unknown interactions of controlling factors may explain the absence of clear $CaCO_3$ trends in cores 5117 and 5753.

8.4.2 Scanning Electron Microscopy of the Sand Fraction

Scanning electron microscope (SEM) investigations have been undertaken to augment the component and mineralogy results derived from modal analyses (section 8.4.1). Quartz grain microtextures and planktic foram abrasion/breakage patterns have been evaluated at selected sites throughout the Natal Valley to provide additional information concerning physical and chemical processes operative at the sea floor. Seventeen samples, representative of all the major physiographic provinces, were chosen for SEM study. Grain selection, and scanning procedures are fully described in Appendix A13.

8.4.2.1 Quartz Grain Microtextures

The study of surface irregularities on coarse (200-500 μm) quartz grains using SEM techniques has evolved into a major tool for interpreting sedimentary environment and transport mechanisms (Krinsley and McCoy, 1977; Georgiev and Stoffers, 1980). Over thirty distinct surface features have previously been documented (Higgs, 1979; Culver et al, 1983) and the recognition of suites of these microtextures may furnish important environmental

information (Krinsley and Doornkamp, 1973).

A minimum of twenty quartz grains, considered sufficiently representative of within-sample variability (Krinsley and Doornkamp, 1973), were picked from each sample. Up to fourteen diagnostic surface features, often co-existent, are recognisable in the scanned samples (Table 8.2). The environmental significance of these surficial irregularities has been fully documented in the literature (Krinsley and Margolis, 1969; Krinsley and Doornkamp, 1973; Higgs, 1979). Photomicrographs presented in Plates 8.1 and 8.2 show the salient features of each microtexture category. The presence or absence and relative abundance of diagnostic microtextures are listed in Table 8.2.

The majority of scanned grains display composite features containing surfaces attributable to a combination of source breakage, subaqueous chemical and mechanical activity. Composite microtextures from any one physiographic province confuses environmental interpretation and only the following concluding observations may be made:

Sub-aqueous indicators (Krinsley and Doornkamp, 1973; Higgs 1979) such as mechanical V-shaped indentations (Plate 8.1a, b, d and l), straight and curved grooves (Plate 8.1b, e and f), grain rounding (Plate 8.1a) with more infrequent oriented chemical etch (Plate 8.1a, c and m) are characteristic of samples from all physiographic provinces (Table 8.2). It is inferred that, at some stage during their depositional history, the great majority of quartz sand grains passed through a sub-aqueous environment of high enough tubulent energy to initiate grain rounding and abundant impact pitting. Sub-aqueous abrasion textures (Table 8.2) are more predominant on the Tugela Cone compared to the

Table 8.2 Sand Fraction (>63μm) Grain (Quartz and Planktic Foraminifera) Surface Features

Core/ Grab No.	Sample Depth	Physiographic Setting	Quartz Grain Surface Textures: A	B	C	D	E	F	G	H	I	J	K	L	M	N	Planktic Foraminifera Surface Features: Abrasion	Solution	Boring
11		Central Terrace - scoured western flank	▼	+	+	+	+	+	+		+	▼			+		□	▼	
9	0cm	Central Terrace - scoured southern flank	+	▼	▼	+	+	+	+			▼				+	□	+	
5	0cm	Central Terrace - scoured southeast flank (QUATERNARY)	▼	▼	▼	+	+	+	+		+						▼	+	
5	29cm	Central Terrace - scoured southeast flank (MIOCENE/PLIOCENE)	▼	▼	▼	+	▼	+	+		+						▼	+	
2		Mozambique Ridge - western flank	▼	▼	▼		+			+	+	+					▼	+	+
5728		Tugela Cone - northern upper slope	+	▼	+					+	+	+	+				▼	+	
34	0cm	Tugela Cone - central upper slope	+	▼	▼	+	▼	+	+			+				+	▼		+
27	0cm	Tugela Cone - mid slope	▼	+	▼	+	+					▼	+	▼		+			
18	0cm	Tugela Cone - eastern margin	□	+	▼	+	+	▼	▼			▼					▼		
5117	0cm	Tugela Cone - southern flank	+	▼	▼	+	▼					+				+	+		
30	0cm	Tugela Canyon - upper zone axis	▼	▼	▼	+	+	+	+		+	▼					□		+
5753	0cm	Tugela Canyon - lowermost zone suprafan	+	▼	▼	▼	▼				+	+					□		
24	0cm	29°25'S Canyon - upper zone axis	+	▼	□	▼				+	+	+					+		
15	0cm	29°25'S Canyon - lower zone axis (QUATERNARY)	+	▼	▼	+	+			+	+			▼			▼	+	
15	15½cm	29°25'S Canyon - lower zone axis (MIOCENE/PLIOCENE)	▼	▼	▼	▼	▼	+	+	+		+		▼		+	▼	+	
5750		Deep basin - northwest margin	▼	+	▼	▼	+	+	+		+	+					+	+	+
5751	0cm	Deep basin - south central	+		+		+	+	+	+		+						▼	

A - conchoidal fracture
B - relict conchoidal fracture
C - mechanical V-forms
D - straight/slightly-curved grooves
E - mechanical upturned plates
F - flat cleavage face
G - cleavage planes (semi-parallel)
H - smooth precipitation surface
I - chemically-etched V-forms
J - irregular solution-precipitation surface
K - deep surface solution
L - precipitated upturned silica plates
M - silica plastering
N - capping layer

□ - dominant
▼ - common
+ - present

Plate 8.1 SEM Photomicrographs - Sand(>63μm) Fraction

a - Core 5, 29cm: sub-aqueous mechanical V-forms indenting a rounded, smooth grain surface which also features large irregular depressions and infrequent chemical etching. Scale divisions = 10μm.

b - Core 5753, 0cm: complex grain with abundant sub-aqueous textures (mechanical V-forms, curved grooves) but also mechanically-formed upturned plates. Grain irregularity is enhanced by silica solution and precipitation. Scale divisions = 10μm.

c - Core 2: intense oriented chemical etching with rare mechanical impact V-forms and straight grooves. Scale divisions = 3μm.

d - Core 30, 0cm: composite grain with relict conchoidal fracture and stepped cleavage planes modified by abundant mechanical percussion V-forms and scarce upturned plates. Scale divisions = 10μm.

e - Core 5, 29cm: straight to slightly-curved grooves, V-forms and irregular depressions indicating sub-aqueous mechanical abrasion together with rare chemical etching. Scale divisions = 3μm.

f - Core 5753, 0cm: admixture of mechanical (V-forms, curved grooves and upturned plates) and more infrequent chemical (etching) microtextures. Scale divisions = 3μm.

g - Core 5750: fresh conchoidal fracture with minor development of upturned plates. Scale divisions = 10μm.

h - Core 5, 29cm: conchoidal fracture accentuated by mechanically upturned plates and cleavage planes. Scale divisions = 3μm.

i - Core 18, 0cm: fresh conchoidal fracture with cleavage planes displaying straight and arcuate steps. Scale divisions = 10μm.

j - Core 15, 15,5cm: relict and fresh conchoidal fracture with the former (extreme left) displaying severe mechanical abrasion (V-forms) and the latter showing development of cleavage planes and precipitated silica plates. Scale divisions = 3μm.

k - Core 5751, 0cm: well-developed flat cleavage faces and semi-parallel cleavage planes. Scale divisions = 3μm.

l - Core 9, 0cm: cleavage planes with semi-parallel steps heavily impacted by sub-aqueous mechanical V-forms. Scale divisions = 3μm.

m - Grab 5728: complex grain with smooth silica precipitation over a relict cleavage plane. Subsequent mechanical abrasion (V-forms) and chemical etching has modified the composite surface. Scale divisions = 10μm.

n - Core 5750: conchoidal fracture surface with ? semi-parallel cleavage planes modified by en-echelon chemical etch. Scale divisions = 3μm.

o - Core 30, 0cm: irregular solution/precipitation surface further modified by en-echelon chemically-etched V-forms and elongate depressions. Scale divisions = 3μm.

Plate 8.1 SEM PHOTOMICROGRAPHS —— SAND (>63μm) FRACTION

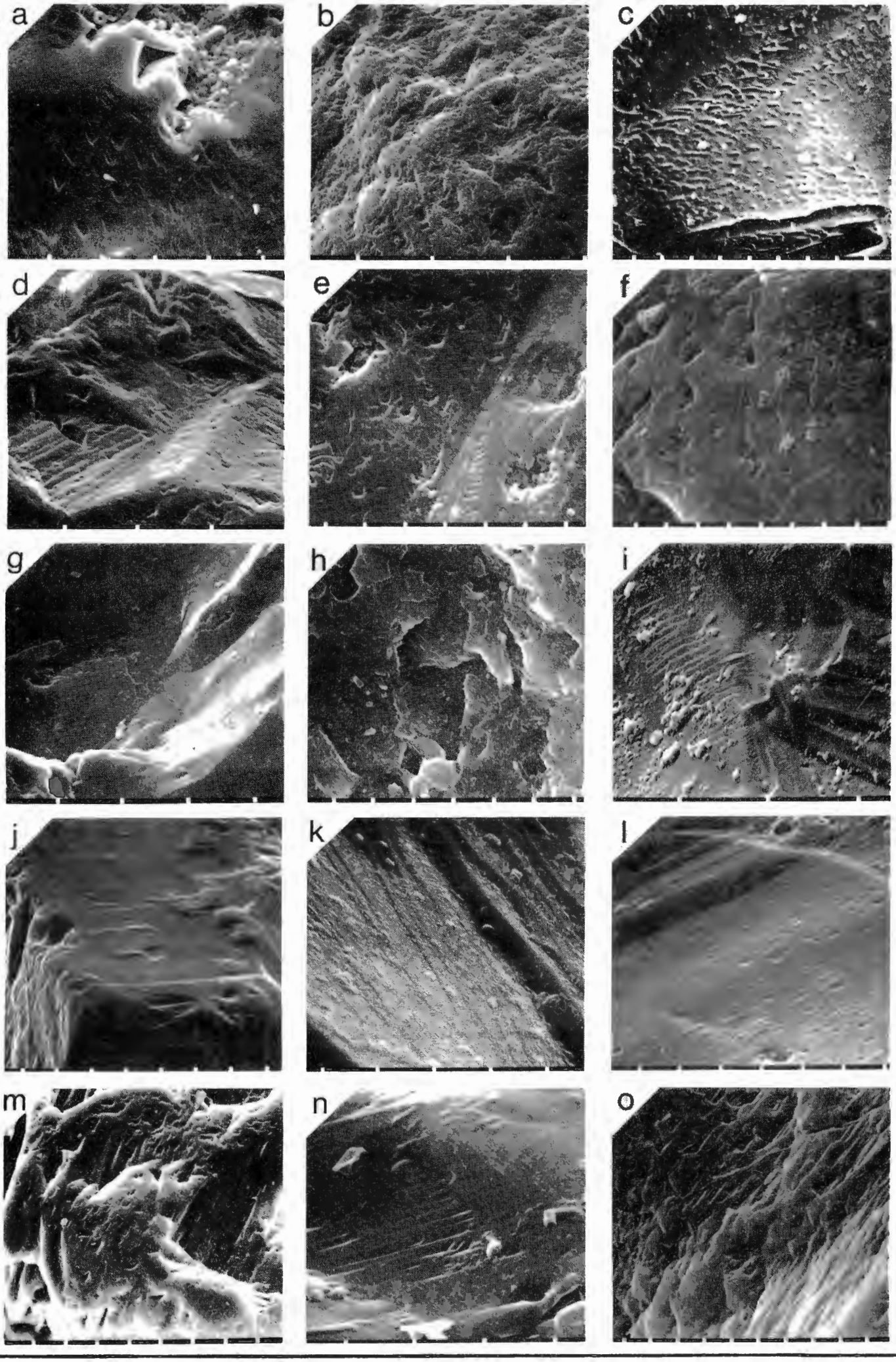

Plate 8.2 SEM Photomicrographs - Sand (>63μm) Fraction

a - Core 15, 0cm: combination of smooth precipitation surface and precipitated upturned silica plates superimposed by mechanically-abraded V-forms and chemically-etched V-forms. Scale divisions = 10μm.

b - Core 15, 15,5cm: relict conchoidal cleavage face pitted by abundant mechanical V-forms and later overgrown by precipitated upturned silica plates. Scale divisions = 10μm.

c - Core 9, 0cm: capping layer strongly modified by subsequent irregular solution and precipitation. Scale divisions = 3μm.

d - Core 5, 0cm: advanced nucleated dissolution etch on test of Pulleniatina obliquiloculata. Scale divisions = 100μm.

e - Core 5, 0cm: close-up of corrosion etch marks from previous photomicrograph (d). Scale divisions = 10μm.

f - Core 5751, 0cm: pore widening and coalescence in Globorotalia menardii defining minor dissolution. Scale divisions = 100μm.

g - Core 11: reworked and severely abraded test of Globotruncana sp. (? coronata) also showing evidence of minor dissolution. Scale divisions = 100μm.

h - Core 9, 0cm: combined dissolution etch and large scale breakage of ? Candeina nitida. Scale divisions = 100μm.

i - Grab 5728: destruction of the normal test morphology of Globorotalia menardii by severe mechanical abrasion and minor dissolution. Scale divisions = 100μm.

j - Core 5, 29cm: complete chamber destruction and smoothing of the resultant jagged test walls by mechanical attrition. Scale divisions = 30μm.

k - Core 5753, 0cm: peeling-off of test layers in response to mechanical abrasion. Scale divisions = 30μm.

l - Core 34, 0cm: severe mechanical breakage of Globigerina ?falconensis causing several chamber walls to be breached. Scale divisions = 30μm.

m - Core 15, 0cm: breakage of keel and chamber walls in Globorotalia menardii indicating mechanical attrition. Scale divisions = 30μm.

n - Core 27, 0cm: well-preserved Globigerinoides ruber juvenile with majority of delicate spines intact indicating that the test has not been subjected to dissolution or mechanical abrasion. Scale divisions = 30μm.

o - Core 34, 0cm: planktic foraminifera test almost completely broken away to reveal a glauconite internal mould. Scale divisions = 30μm.

Plate 8.2 SEM PHOTOMICROGRAPHS — SAND (>63μm) FRACTION

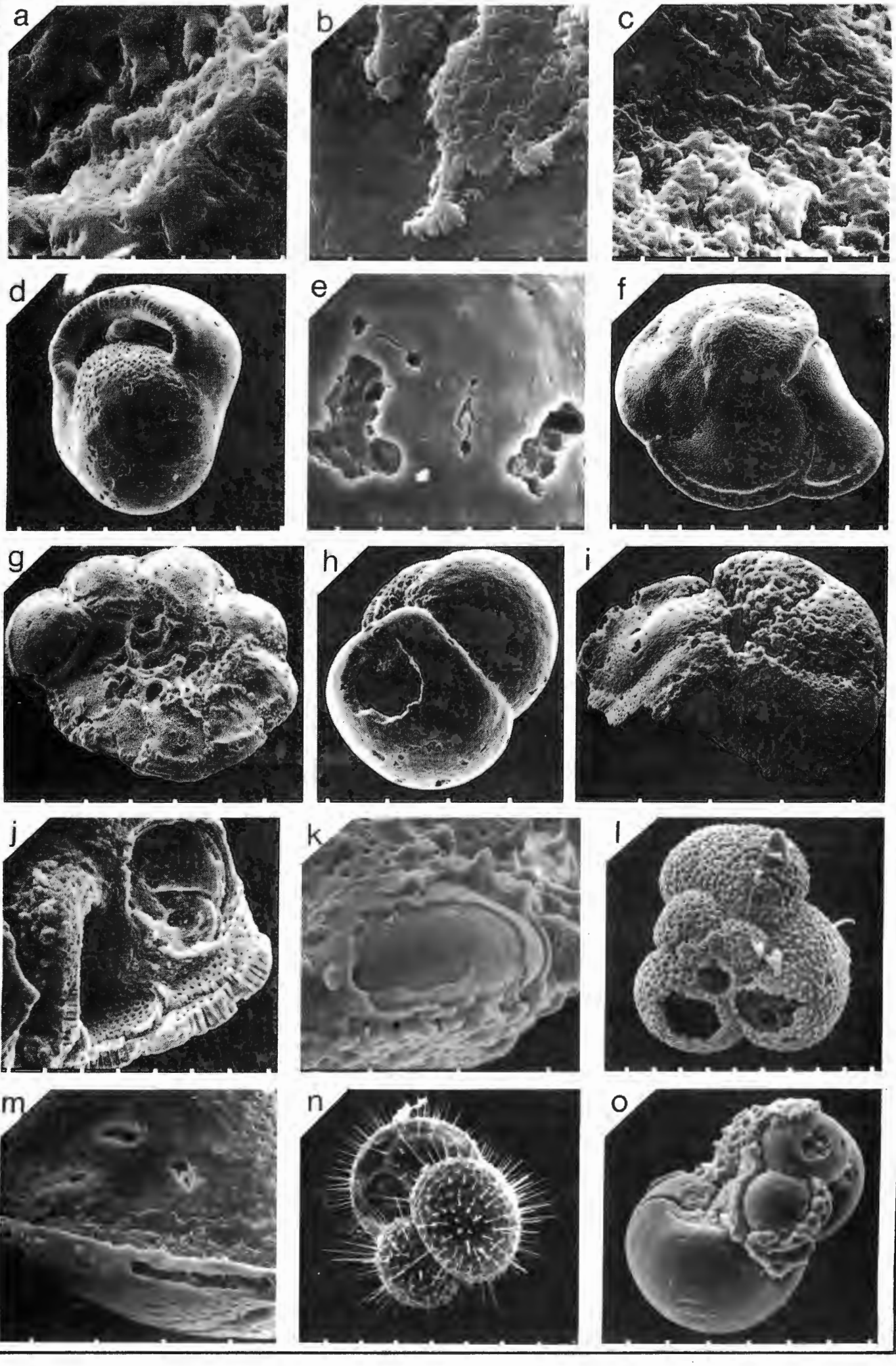

Central Terrace, even though the latter area is a known zone of bottom scouring (section 7.2).

It is envisaged that the bulk of sub-aqueous abrasion takes place either in the littoral zone or in the Agulhas Current-entrained shelf sand stream. The terrigenous sand fraction of the Central Terrace is probably sourced from the Limpopo Cone to the north. In the northernmost Natal Valley, the Agulhas Current core diverges from the continental shelf to flow in deeper water (Martin, 1981). In this source zone, therefore, there is no shelf sand stream and the incidence of mechanical abrasion may be reduced.

By comparison, the sand stream is strongly developed on the east coast shelf which is the transit zone for sediment transported to the Tugela Cone. High energy conditions within this shelf sand stream may explain the abundance of mechanical abrasion microtextures on the Tugela Cone relative to the Central Terrace.

Known bottom current scour zones (Central Terrace - cores 5, 9 and 11; eastern deep basin plain - core 5750) display no obvious concentration of mechanical abrasion textures (Table 8.2). Although sediment winnowing takes place in these zones (Fig.7.2), the bottom currents must be of insufficient power to abrade individual quartz grains.

Chemical dissolution of quartz also generates a distinctive set of microtextures including en-echelon etch pits (Plate 8.1c, n and o; Plate 8.2a) and solution surfaces (Plate 8.1b and o; Plate 8.2c). Crystallographic etching of this type is restricted to a marine environment where the degree of chemical dissolution exceeds that of mechanical abrasion (Strass, 1978). To achieve

effective chemical etching, quartz detritus must be exposed to waters undersaturated with respect to silica (alkaline) for a significant length of time (Strass, 1978; Higgs, 1979).

In contrast, silica precipitation is evidenced by smooth overgrowths (Plate 8.1m; Plate 8.2a), irregular precipitation-solution surfaces (Plate 8.1o; Plate 8.2c), precipitated upturned silica plates (Plate 8.1j; Plate 8.2b) and capping layers (Plate 8.2c). Grains exhibiting these features have been primarily exposed to acidic (silica-oversaturated) conditions (Higgs, 1979).

No definitive areal distribution patterns are evident for either chemical dissolution or chemical precipitation indicators (Table 8.2) suggesting that widespread mixing may have destroyed any original regional segregation. Many grains showing solution/precipitation surfaces are modified by subsequent abrasion microtextures of sub-aqueous origin (Plate 8.1m and o; Plate 8.2a) while the reverse (precipitation over abrasion surface) is extremely rare. This implies that the chemical microtextures were predominantly generated prior to entering the marine environment. Effective mixing could have taken place in the fluvial or littoral environments prior to final deposition in deep-water zones of the Natal Valley.

Conchoidal fractures (fresh and relict) and related cleavage steps (Plate 8.1i, k and l) are ubiquitous to all physiographic zones (Table 8.2). It is most likely that these distinctive microtextures were created at source (Krinsley and Doornkamp, 1973) with liberation of grains from crystalline hinterland rocks. The preservation of fresh conchoidal fracture (Plate 8.1g, h and i) reflects short transport and rapid deposition

(Georgiev and Stoffers, 1980). However, many grains exhibit relict conchoidal fracture (Plate 8.1e, j and l) implying significant residence time within subsequent environments. Grains which develop conchoidal fracture at source must be transported in the fluvial environment to pass through the high energy littoral zone before being available for marine deposition. Residence within these high energy regimes could modify the original texture to develop relict conchoidal surfaces (Table 8.2).

Previous authors (Krinsley and McCoy, 1977; Georgiev and Stoffers, 1980) have suggested that high energy marine conditions (littoral zone; turbidity currents) may initiate conchoidal grain breakage. Processes in these zones, in addition to traction transport in the shelf sand stream, may have contributed to the common occurrence of conchoidal fracture. Breakage in the marine environment may explain the existence of fresh conchoidal microtextures since, in this situation, the broken grains are available for rapid transport and deposition without re-entering the high energy near-shore regime.

8.4.2.2 Planktic Foraminifera Dissolution and Abrasion .

Component analyses of the sand fraction (binocular microscope) indicated that many forams had been subjected to corrosion or breakage and often both. Accordingly, a pilot study was undertaken to provide information concerning two aspects of foram surficial microtextures: (1) the distribution of dissolution microtextures; and (2) the areal segregation of common abrasion breakage and correlation to zones of bottom current scour. A minimum of fifteen tests from each sample were

randomly selected for study. Common dissolution and breakage microtextures are displayed in Plate 8.2 while the distribution and relative abundance of these features are detailed in Table 8.2. Surficial microtextures may be adjudged relative to a well-preserved test (Plate 8.2n) which has escaped the destructive effects of both abrasion and dissolution.

Dissolution of planktic forams results in progressive structural breakdown of the test (Bé et al, 1975) and in severe cases, chamber walls may be completely dissolved. However, only minor solution phenomena are recorded in any of the Natal Valley samples. Commonest examples of dissolution include nucleated breakdown (Plate 8.2d, e and h) and pore widening/coalescence (Plate 8.2f). In all cases dissolution weight losses are probably <5% (comparison to Bé et al, 1975).

Although many variables influence and regulate carbonate dissolution (Takahashi and Broecker, 1977; Honjo, 1977), as a general rule, solution increases with water depth (Berger, 1970; Kolla et al, 1976c; Volat et al, 1980). This effect is verified in the study area with deepest samples (core 5751; water depth - 2778 m) exhibiting more common solution phenomena (Table 8.2; Plate 8.2f). However, deepest zones of the mid Natal Valley are much shoaler than the foram lysocline (4400-4500 m) for comparable latitudinal zones of the Indian Ocean (Kolla et al, 1976c) and thus no dramatic dissolution should be expected. This is verified by the overall deficit of solution textures within the study area (Table 8.2).

The Central Terrace and Mozambique Ridge (sample depth range 1886-2395 m) are considered as anomalous zones with all forams displaying distinct surface solution (Table 8.2). Calcium

carbonate dissolution is not confined to deep water beneath the lysocline but will occur in any environment in which the water column is undersaturated with respect to calcite (Alexandersson, 1975). Sediments of these two regions must, at least periodically, be in contact with carbonate-depleted waters.

Mechanical attrition of planktic foraminifera produces two distinguishable surface textures: (1) sharp angular breakage resulting from high energy collisions (Plate 8.2h,k,l and m); (2) worn abraded appearance as a result of lower energy collisions and rolling (Plate 8.2g, i and j).

Although these two types of abrasion indicator are not segregated in Table 8.2, the incidence of high energy breakage appears to be areally-controlled. Samples displaying severe breakage are restricted to the Central Terrace (cores 5, 9 and 11), the upper slope of the Tugela Cone (cores 30 and 34; grab 5728) and canyon axes (cores 15 and 5753). The former two are confirmed zones of strong, deep Agulhas Current flow (section 7.2) illustrating the positive correlation between foram test breakage and sea floor scour. Breakage in the Tugela and 29° 25'S Canyons may be caused by downslope sediment movement or may be relict from source material which is current-scoured over the upper slope of the Tugela Cone.

The action of boring organisms such as sponges, algae and fungi is evident in four samples (Table 8.2), but from this small data base no regional distribution patterns can be discerned.

8.4.3 Clay Mineralogy and Sedimentation

8.4.3.1 Introduction

The origin of the non-biogenic clay fraction (<2 μm) in

marine sediments along with its modes of transport to and within oceanic basins remains a problem in the understanding of deep-sea sedimentation (Biscaye, 1965). The relative abundance of this size grade within Natal Valley sediments mitigates for an extensive regional study of clay group distributions. Compositionally, the clay fraction is complex, mainly comprising terrigenous clay minerals but with subordinate amounts of quartz, feldspar, comminuted foram tests, calcareous nannofossils and organic matter. Only the non-biogenic fraction and in particular the major clay mineral groups are considered in this section.

Previous campaigns have studied clay mineral distributions within the SW Indian Ocean (Biscaye, 1965; Rateev et al, 1969; Kolla et al, 1976b; 1980a). These investigations were however based on a restricted data base and thus their conclusions can only be considered as preliminary. In the present project, analyses of 80 samples (37 surface, 25 sub-bottom, 18 riverine) provides a basis for a more detailed regional evaluation of clay mineral distribution in the Natal Valley.

Separation, pre-treatment, mounting and X-ray analysis procedures and the criteria for mineral identification are described in Appendix A11. Relative abundances of the major clay mineral groups are presented in Appendices B9 and B13. No attempt has been made to quantify the abundance of non-clay mineral constituents although their presence is verified by recognition of diagnostic basal reflection maxima (Fig.8.11). The proportions of illite, kaolinite and smectite have been normalised to 100%.

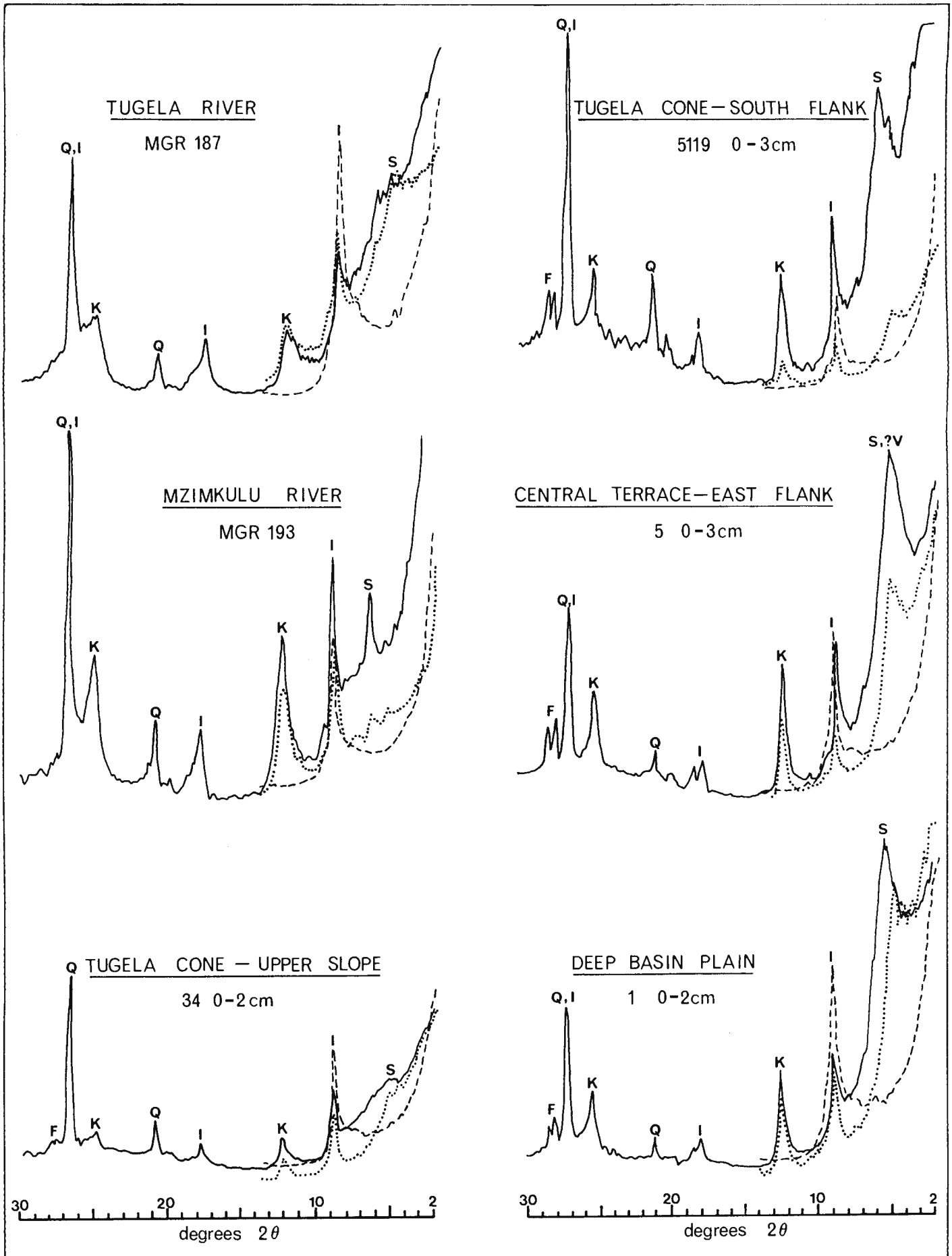

Fig. 8.11 SPECIMEN CLAY FRACTION (<2μm) X-RAY DIFFRACTOGRAMS

8.4.3.2 Origin of Clay Minerals

Clay mineral formation results either directly or indirectly from the hydrolytic decomposition of primary aluminosilicates (Singer, 1980). The decomposition processes are strongly influenced by the rate of leaching. A high leaching rate leads to increased clay generation and produces clay minerals that are in an advanced state of weathering (Jackson, 1969). Climate, particularly the rainfall rate, is of prime importance in production of a characteristic clay mineral suite from any source area. Hinterland geology exerts control over clay mineral generation (Johnson, 1970). Clays in the marine environment may differ little from those of the source zone of weathering (Savin and Epstein, 1970). Clay mineral formation may occur in situ within oceanic basins. Biscaye (1965) concluded that small amounts of illite form diagenetically in the marine environment. In addition, Kolla et al (1976b) point out the strong correlation between smectite and the incidence of submarine basalts in the Indian Ocean.

Illite is sourced almost exclusively from continental hinterlands and its marine distribution is closely related to the location of major fluvial sediment systems (Jacobs and Hays, 1972). Illites are primarily generated through decomposition of layer silicates under acid conditions (Keller, 1970). Disaggregation of illitic argillaceous rocks may also yield abundant illite for transportation to the marine environment. In general, South African soils are considered to be rich in illite (Rateev et al, 1969).

Kaolinite group minerals in the marine environment are sourced entirely from continental landmasses (Biscaye, 1965).

Tropical climates with strong leaching (precipitation > evaporation) and chemical weathering provide ideal conditions for kaolinite production from a variety of parent rock types (Jacobs and Hayes, 1972). Tropical and sub-tropical zones of Africa as far south as 30°S, and in particular Madagascar, contribute high amounts of kaolinite to the adjacent oceanic basins. However, local deposition of kaolinite may be influenced by surface and bottom currents (Kolla et al, 1976b).

Smectites are composite in origin (Biscaye, 1965) and may be hinterland-sourced or form in situ in the marine environment. Smectites of continental origin are derived from a range of parent rock types under a variety of climatic and latitude regimes (Biscaye, 1965). Smectites are also minor products of in situ alteration of submarine basalts (Griffin and Goldberg, 1963). Recently Marchig and Rosch (1983) have equated deep-marine smectite formation to diagenesis and dissolution of calcareous oozes. Continental smectite formation requires ineffective leaching (Singer, 1980) and these conditions are present in semi-arid areas and stagnant lakes. As with kaolinite, Madagascar provides extensive quantities of smectite to the SW Indian Ocean (Kolla et al, 1976b). Surface and abyssal currents play important roles in its oceanwide dispersal.

Although the hinterland geology of Natal and Zululand is diverse (section 1.2.2), major formation boundaries are aligned approximately coast-parallel (Fig.1.3). As a result, each major river erodes through several different lithologies along its seaward course. Since relatively equivalent bedrock-types are cross-cut by the major rivers, hinterland geology is unlikely to have introduced significant variation, in clay mineral assemblage between different source regions.

8.4.3.3 Distribution of Clay Minerals

RIVERINE CLAYS

A suite of 18 sediment samples from the major Natal and Zululand rivers were analysed to characterise gross variations in the hinterland clay mineral assemblage. Specimen diffractograms of the riverine clay fraction are presented in Figure 8.11. Analytical results (Appendix B13) suggest that climate exerts a stronger influence on the overall clay composition than bedrock geology. The progressive south to north change in clay assemblage reflects an aridity increase towards the north (Zululand and northern Natal).

Illitic clays comprise a major proportion of the clay mineral assemblage in all regions of the hinterland (Fig.8.12a) accounting for 28-65% of the total (average 48%) and confirms that Natal soils are illite-rich (Rateev et al, 1969). There are no obvious regional variations in the relative amount of illite discharged by hinterland rivers.

Kaolinite clay, typical of zones of strong leaching (Henson, 1973), is more abundant towards the southern hinterland (Fig.8.12b). For example, the average kaolinite abundance north of Richards Bay is 23% increasing to 42% to the south. High kaolinite proportions in the southern hinterland is a response to higher rainfall levels conducive to leaching (section 1.2.3).

Smectite clays portray a reciprocal distribution to that of kaolinite with greatest abundances over the northern hinterland (Fig.8.13a). North of Durban the average abundance of smectite is 25% dropping to 2% south of Durban. Smectite formation is enhanced by ineffective leaching (Singer, 1980) and the higher

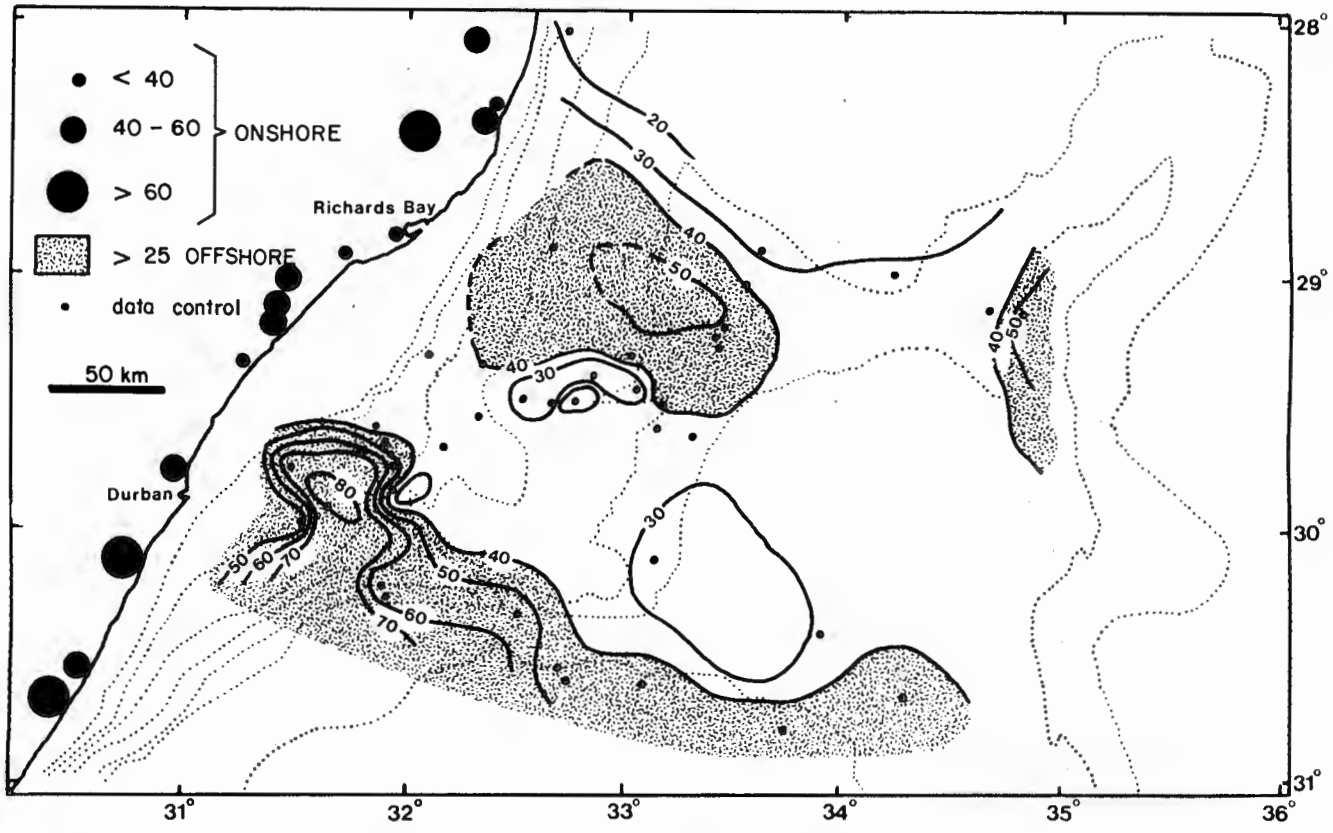

Fig. 8.12 a % ILLITE - CLAY FRACTION

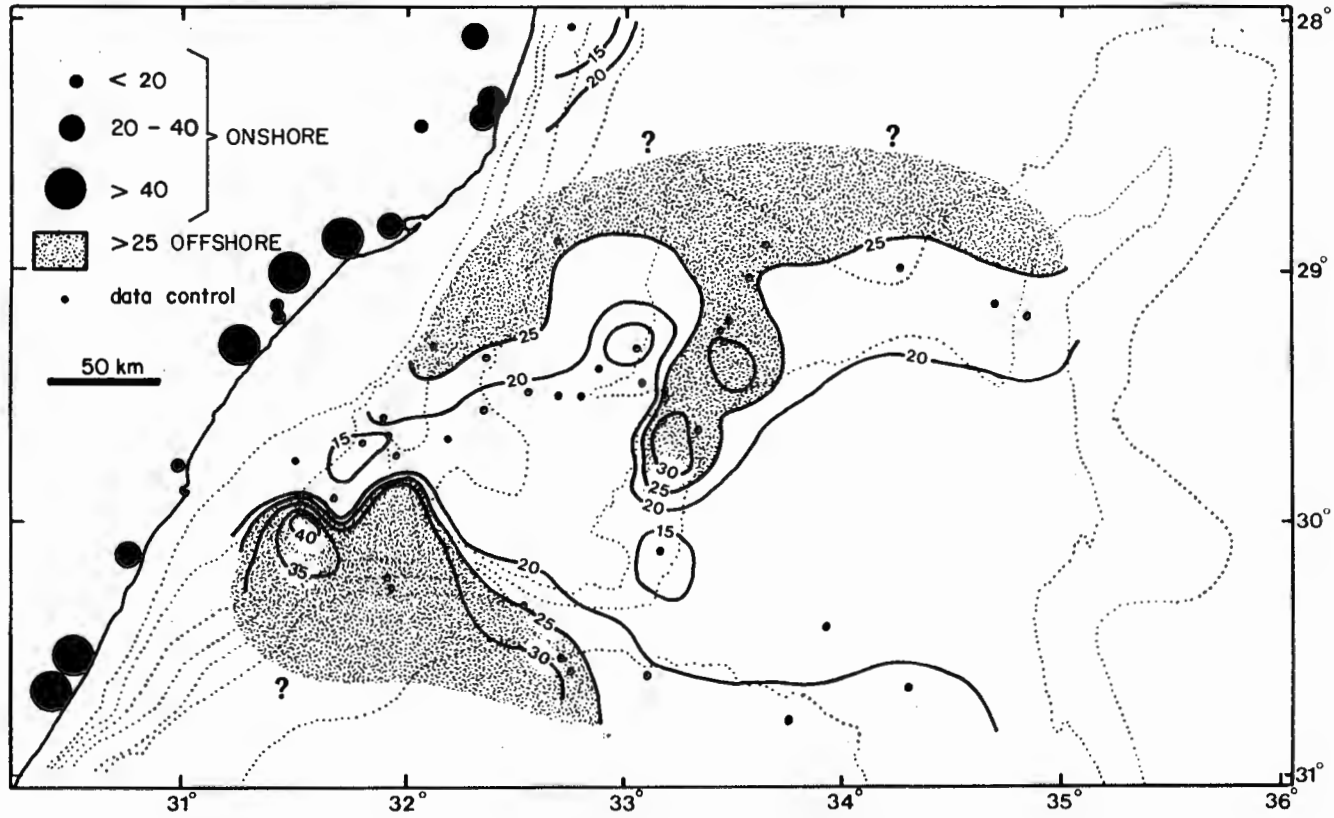

Fig. 8.12b % KAOLINITE - CLAY FRACTION

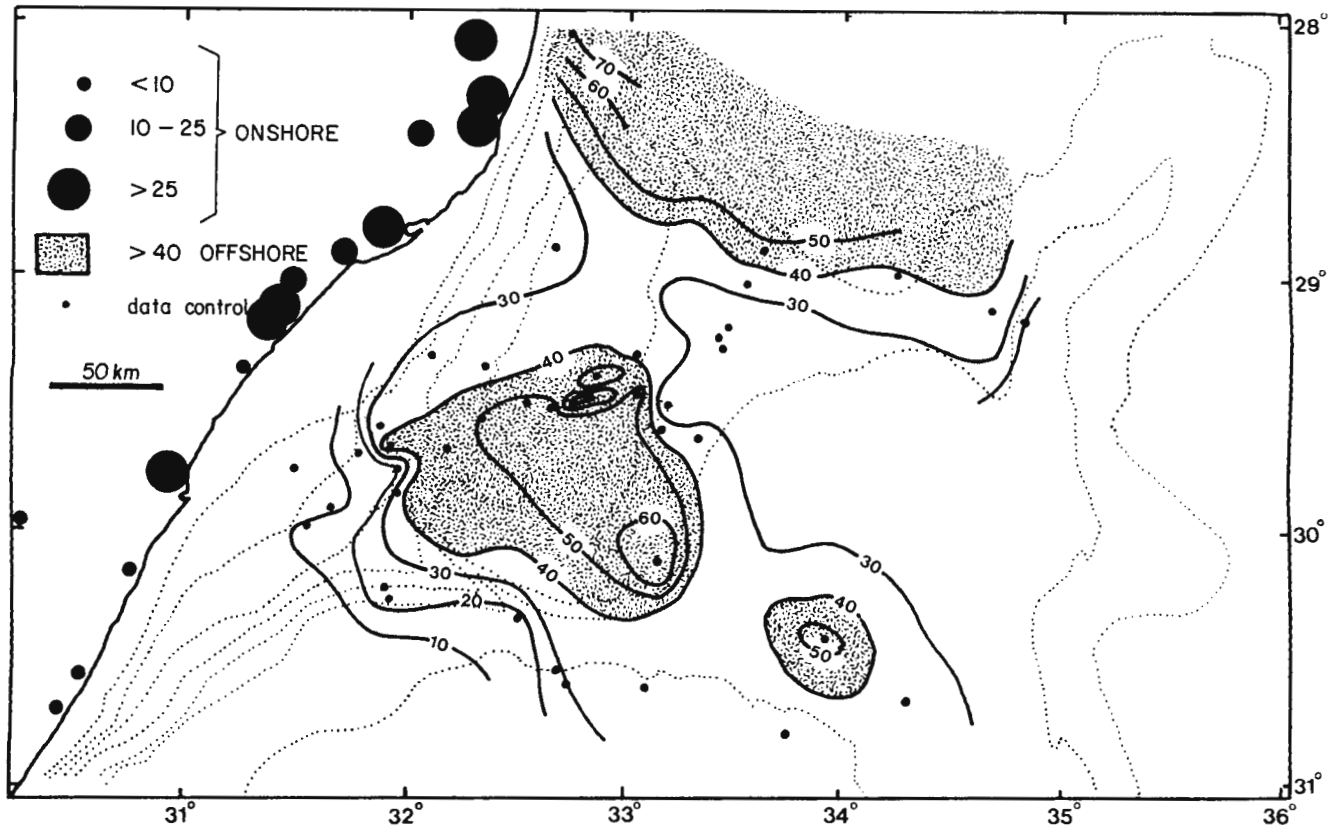

Fig. 8.13a % SMECTITE – CLAY FRACTION

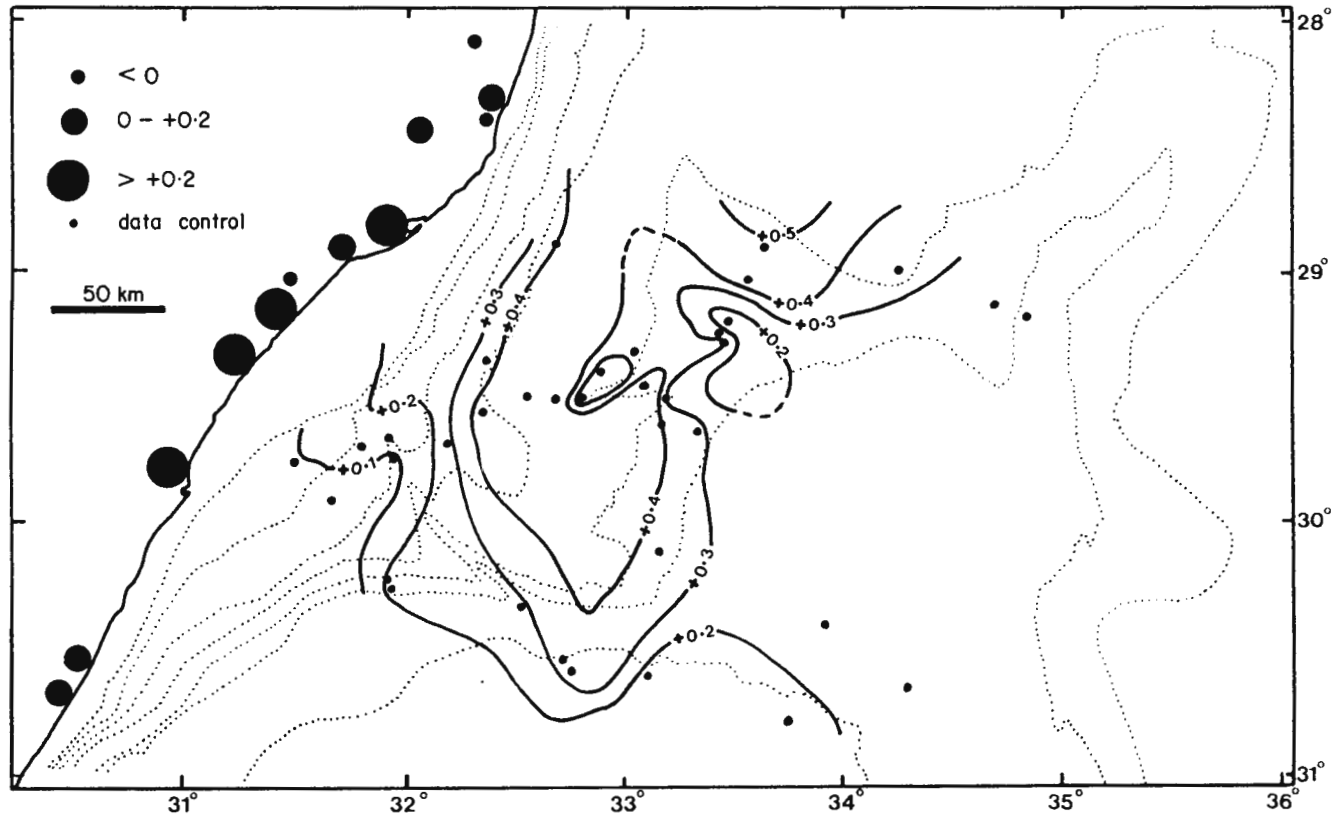

Fig. 8.13b SMECTITE CRYSTALLINITY (V/P RATIO)

proportion in the northern hinterland is a reflection of the semi-arid climatic conditions.

Smectite crystallinity indices, as measured by the v/p ratio (Fig.8.13b), corroborate the findings of Biscaye (1965) who concluded that higher latitude source zones produce more crystalline smectites. Within the Natal/Zululand hinterland, v/p ratios range from -0,18 to +0,33 generally becoming more positive (more crystalline) towards the south.

MARINE CLAYS

Illite

Illite is the dominant clay mineral group (average 44%) within the study area (Fig.8.12a) in agreement with the conclusions of Kolla et al (1976b). Maximum illite concentrations (up to 80%) are recorded over the southern Tugela Cone decreasing southwards to average 40-50% in the southern deep basin plain. A secondary illite depocentre, demarcated by the 40% contour, encompasses the NE Tugela Cone north of the 29° 25'S Canyon. Lowest illite concentrations are associated with the Central Terrace and sections of the deep basin plain, both averaging <30% illite (Fig.8.12a).

Kaolinite

Kaolinitic clays are least abundant (average 22%) of the major clay groups in the study area (Fig.8.12b). Small amounts of chlorite may have been included in the kaolinite total. The most prominent kaolinite depocentre is developed over the southern Tugela Cone where abundances >40% are locally registered. This province splays out onto the deep basin plain. Subsidiary kaolinite depocentres are developed over the Central

Terrace crest and upper slope zones of the central/northern Tugela Cone. Kaolinite is also concentrated southwards from the wide valley separating the Central Terrace and NE Tugela Cone (Fig.8.12b). Large proportions of the eastern Tugela Cone and deep basin plain are depleted in kaolinite averaging <20% of the total clay assemblage.

Smectite

The distribution of smectite (Fig.8.13a) exhibits an approximately reciprocal trend to that of illite. Major smectite concentrations (locally >60%) occur over the eastern Tugela Cone. Within this province there is a general seaward increase in the smectite proportion. High smectite percentages are also registered over the SE basin plain (30-50%), Central Terrace and northern Tugela Cone (40-70%). Zones of low smectite abundance are demarcated along the upper slope of the Tugela Cone (<30%), the northern deep basin plain (<30%) and the southern Tugela Cone and adjacent SW basin plain (<20%). Within the Natal Valley, the range of smectite abundances and the regional average of 34% is consistent with results released by Kolla et al (1976b).

Smectite Crystallinity

The distribution of the smectite crystallinity index (v/p ratio of Biscaye, 1965) is presented in Figure 8.13b. Highest crystallinities are recorded over the eastern Tugela Cone and the crest of the Central Terrace (v/p> +0,40). The Tugela Cone upper slope and deep basin plain all display poor crystallinity (v/p< +0,30), particularly the southern Tugela Cone where the v/p index drops to < +0,10. In contrast to the riverine clay analyses, no negative crystallinities are registered in the marine clays.

Down-Core Variations

Down-core samples selected from piston and gravity cores

were analysed in an attempt to define sub-bottom variations in the clay fraction mineralogy. Results from the 25 analyses are tabulated in Appendix B13. In most cores, the smectite proportion decreases up-core while illite shows an antithetic relationship. The opposite trend is only observed in cores 19 and 23. Towards the core tops, % kaolinite consistently exhibits a marginal increase or remains constant. No trends are discernible from the smectite crystallinity index.

8.4.3.4 Discussion

Based on Figures 8.12 and 8.13, six regional clay mineral assemblages are distinguished. Although the assemblages are transitional into one another and their limits are arbitrary, their distinction summarises the salient features of the clay mineral distribution pattern (Table 8.3). Consequently, understanding of the sources and dispersal of the clay mineral groups is facilitated.

The distribution of the various clay mineral groups within the Natal Valley basin may be discussed in terms of the inter-relationship of four major factors:

1) regional differences in the clay mineral input from the hinterland;
2) influx of suspended clay minerals in the south-flowing Agulhas Current;
3) differentials in settling velocity and potential flocculation between the various clay mineral groups; and
4) redistribution and scour effects of the strong basin-wide circulation system (Agulhas Current).

Although there is no obvious regional variation in the

illite supply from the hinterland, sedimentation of this clay mineral has not been uniform within the marine basin. Illite concentrations are highest in two major depocentres: the southern Tugela Cone/adjacent SW basin plain and the NE Tugela Cone. Outside these provinces, the illite proportion is reduced to below the basin average. These two illite depocentres are associated with the major recent Tugela Cone terrigenous depositional sites (section 8.3.1.2). Although hinterland-derived illite is being supplied to the marine basin by all rivers (Fig.8.12a), with the largest volume coming from the Tugela (section 1.2.5), its seaward dispersal is focussed into two main routes supplying assemblages 1,4 and 5 (Table 8.3).

Table 8.3 Marine Clay Provinces*

ASSEMBLAGE	LOCATION	ILLITE (%)	KAOLINITE (%)	SMECTITE (%)	SMECTITE (v/p)
1	southern Tugela Cone	50-80	25-40	<20	<+0.2
2	Central Terrace	<30	>25	>50	>+0,4
3	eastern Tugela Cone	30-40	<20	40-60	>+0,3
4	NE Tugela Cone	40-50	20-25	30-40	?
5	SW basin plain	50-70	20-30	<20	<+0.2
6	northern basin plain	<40	20-25	30-40	<+0.3

* - data from Appendices B9 and B13 and Figures 8.12 and 8.13.

The marine distribution of kaolinite is too complex to explain in simple terms of hinterland sourcing. The hinterland output of kaolinite increases southward and is partly reflected by the offshore distribution. The maximum concentration of kaolinite (25-40%) is localised to the southern Tugela Cone which probably receives the majority of hinterland discharge. One surface sample (4121) from the Zululand continental slope is kaolinite-poor (11%) matching the low source potential of the adjacent northern hinterland (Fig.8.12b). However, relatively high amounts of kaolinite are registered over the Central Terrace and adjacent to the eastern Tugela Cone (Fig.8.12b). The Agulhas Current, which flows srongly to the SW, must prevent kaolinite sourced in the southern hinterland from being transported to the northern basin. Alternative supplies must be invoked to explain the high % kaolinite in assemblages 2 and 6.

Denudation of Madagascar and the Zambesi drainage basin contributes high amounts of kaolinite to the SW Indian Ocean (Biscaye, 1965; Kolla et al, 1976b). Significant volumes of these clays should be transported south by the Mozambique Current and other Agulhas Current source waters. Influx of clays from the north may be diluting the local clay regime of assemblages 2 and 6 thus increasing their kaolinite content. More specifically, the zone of high kaolinite (>30%) in assemblage 6 splays out south from the wide valley separating the Central Terrace and northern Tugela Cone (Fig.8.12b). This valley may be acting as a conduit for southward transport of kaolinitic clays from the northern Natal Valley.

The smectite distribution within the marine basin is

reciprocal to that of illite (compare Figs.8.12a and 8.13a). Highest concentrations of smectite are found in assemblage 2 (>50%) and assemblage 3 (40-60%) while very low amounts (<20%) are recorded in assemblage 5 (Table 8.3). Although this distribution partially mirrors the smectite source potential of the hinterland (Fig.8.13a), it is too complex to explain without invoking additional controls. The low proportion of smectite in the SW basin plain corresponds to the low output from the adjacent hinterland. Likewise, the large smectite output from northern hinterland can be equated with the high % smectite over the eastern Tugela Cone, Central Terrace and Zululand continental slope. However, in these latter depocentres, the % smectite may be too high to correlate to local sources alone.

Madagascar has been noted as an excellent source zone for smectite clays (Kolla et al, 1976b). In addition, Biscaye (1965) considered smectite to be a principal mineral within the SW Indian Ocean, mostly sourced from in situ alteration of volcanic rocks in the Madagascar-Mascarene area. Alteration of volcanic rocks from the northern Natal Valley (Almirante Leite Bank - Dingle et al, 1978) and the Mozambique Ridge may provide additional quantities of smectite to the regional system. As with kaolinite, it is probable that significant amounts of smectite are carried south suspended in the Agulhas Current system to be deposited in the mid Natal Valley.

Smectite crystallinity is relatively good in assemblages 2 and 3 (Table 8.3) and bears little relation to the poorly crystalline smectites characteristic of the hinterland (Fig.8.13b). Biscaye (1965) concluded that smectite

crystallinity changes little on entering the marine environment, further emphasising the disparity between hinterland and marine clays. In general, smectites derived from tropical environments tend to be poorly crystalline. As an exception however, smectites generated in the Madagascar/Mascarene area are anomalously well-crystallised (Biscaye, 1965). The southward transport of smectites from these source areas with deposition in the Natal Valley may explain the high v/p ratios in assemblages 2 and 3 as compared to hinterland-supplied smectite.

Lateral changes in the clay mineralogy of marine sediments have been ascribed to three mechanisms: chemical alteration, differential flocculation and size segregation. Chemical alteration is now considered to be an insignificant process (Gibbs, 1977). Differential flocculation causing separation of the major clay mineral groups was demonstrated by Whitehouse et al (1960). However, the effectiveness of differential segregation of clay flocs is complex and strongly dependent on floc diameter (Gibbs, 1985) although smectite characteristically has a low floc settling velocity. Hyne et al (1979) have demonstrated that electrolytic flocculation is quickest to affect kaolinite perhaps influencing its segregation. Areal differentiation of clays may also be caused by the natural variations in grain size distributions (Gibbs, 1977). Illites have the largest particle size followed by kaolinite and smectite. With size sorting therefore, illite will be deposited first and smectite last. Clay minerals may also be deposited in the form of faecal pellets behaving hydraulically as silt-sand size particles.

Controls over the distribution of each clay mineral group in the Natal Valley are complex unlike the west coast of southern Africa where a simple model of physical size segregation (Birch, 1978) is operative. Nevertheless, within individual Natal Valley depocentres seaward changes are recognised. In assemblage 1 (southern Tugela Cone), a model of size segregation may explain the illite dominance over the upper slope grading to kaolinite-dominant on the mid slope (Fig.8.12a and b). With increasing water depth into assemblage 3 (eastern Tugela Cone), a distinctive increase in the proportion of smectite may be interpreted in terms of size segregation perhaps enhanced by poor flocculation (Hyne et al, 1979). Trends within other assemblages are inconclusive possibly due to dilution effects induced by clay influx from the north.

Clay mineral redistribution by competent currents is an effective process in the Natal Valley as indicated by the suspected large influx of kaolinite and smectite from the north. The total clay distribution map (Fig.8.18) portrays the influence of deep currents, showing low clay proportions in defined scour zones (Central Terrace, basin plain margins). Similar patterns cannot be discerned in the individual clay mineral plots (Figs.8.12 and 8.13a), probably because the deep currents are too variable to selectively remove one or more of the clay members. Under conditions of scour, smectite should be preferentially removed. However, in the most likely scour zone (Central Terrace), smectites are added to the system from the north masking any possible scour removal trends. The high proportion of illite and low proportion of smectite on the Mozambique Ridge

(sample 2) may indicate local winnowing conditions.

Down-core clay mineralogy data (Appendix B13) indicates that illite is most abundant in core-top sediments while smectite is dominant in older core sections. Smectites are predominantly sourced from the northern hinterland (section 8.4.3.3). Holocene choking of the Zululand drainage system (section 1.2.4) has reduced smectite supplies to the marine basin thus diminishing the smectite concentration in the most recent sediments.

8.4.4 Silt Fraction Mineralogy

8.4.4.1 Introduction

Sediments from all physiographic provinces within the Natal Valley contain significant proportions (locally >40%) of silt-grade (2-63 μm) detritus. In this section, areal variations in the mineralogy of recent silts are described and the implications are briefly discussed. Both terrigenous-rich silts (Fig.8.15a) and carbonate-rich silts (Fig.8.15b) are recognised and the delineation of these types is emphasised. X-ray diffraction techniques were employed as the principal tool in the silt component studies producing a data base of 57 diffractograms (32 surface; 25 sub-bottom).

Full details of the sample preparation, mounting and diffraction techniques are listed in Appendix A12. After X-ray analysis, diffractograms (Fig.8.14) were interpreted in a qualitative mode using a ranked abundance scale modified after Matti et al (1974). Results are tabulated in Appendix B12.

The general reliability of the X-ray mineralogy results have

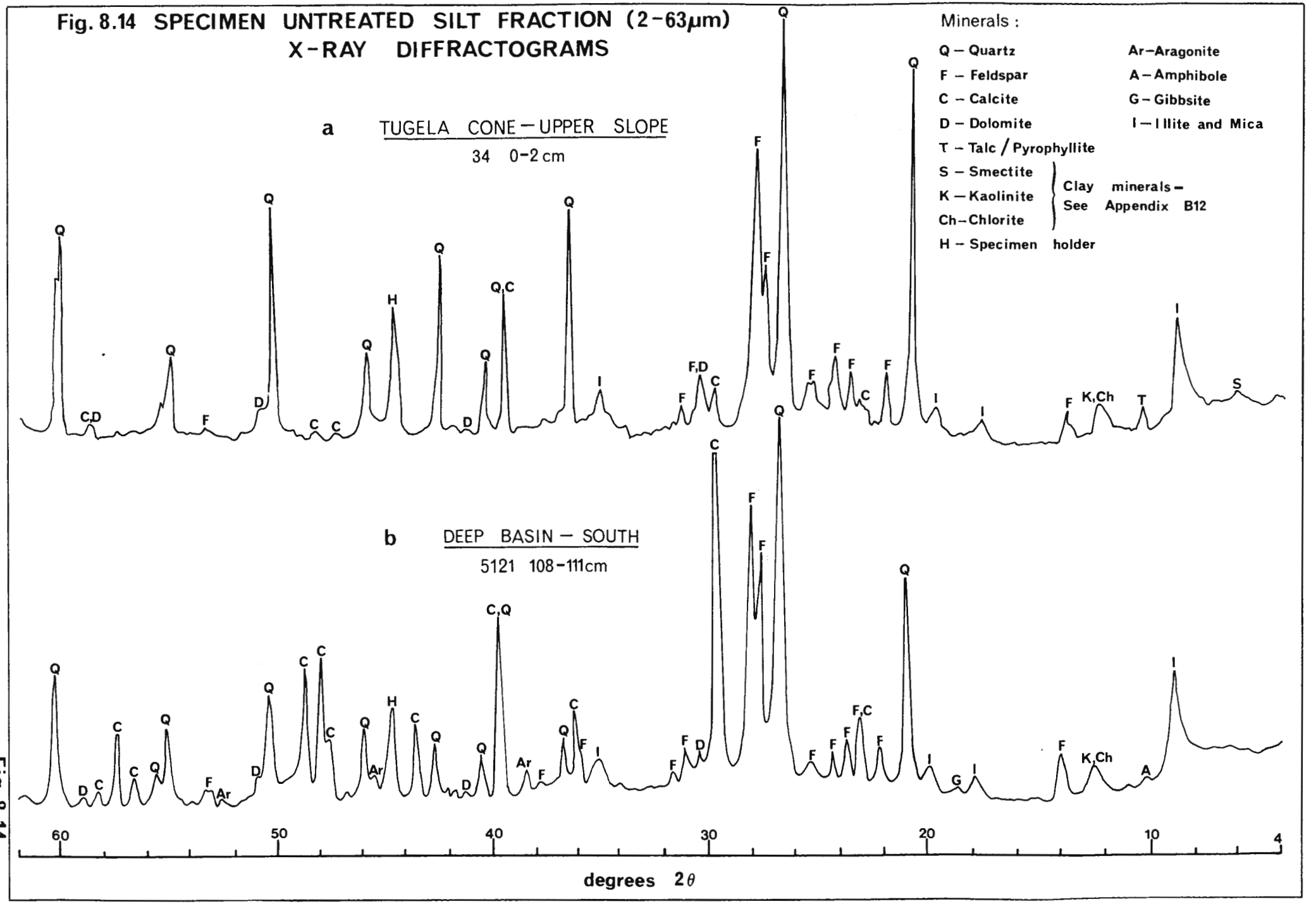
Fig. 8.14 SPECIMEN UNTREATED SILT FRACTION (2-63μm)
X-RAY DIFFRACTOGRAMS
Minerals :
Q – Quartz
F – Feldspar
C – Calcite
D – Dolomite
T – Talc / Pyrophyllite
S – Smectite
K – Kaolinite
Ch – Chlorite
H – Specimen holder
Ar – Aragonite
A – Amphibole
G – Gibbsite
I – Illite and Mica
Clay minerals – See Appendix B12
a TUGELA CONE – UPPER SLOPE
34 0-2 cm
b DEEP BASIN – SOUTH
5121 108-111cm
60
50
40
30
20
10
4
degrees 2θ
Fig. 8.14

been subjectively checked by use of SEM techniques (section 8.4.5). Twelve mud samples were routinely scanned on the SEM (Appendix A13) and their compositions semi-quantitatively estimated. Although the X-ray diffraction study provides basic bulk mineralogy data and helps resolve certain components not readily identifiable by optical methods (e.g. zeolites), the SEM method is much more useful for distinguishing between the many types of calcareous and siliceous faunal components.

8.4.4.2 Distribution of Silt Fraction Minerals

The distribution of silt-grade quartz is presented in Figure 8.15a. Quartz is the major silt fraction component over the Tugela Cone upper slope and southern flanks confirming hinterland detrital supply to these terrigenous depocentres. Excessive deposition of quartz on the upper slope may be related to sudden reduction of current vigour seaward of the shelf-break. In addition, the abundance of quartz over the south Tugela Cone depocentre identifies the predominant pathway for basinward dispersal of silt-grade terrigenous detritus by bottom processes. Silt-size quartz remains an "abundant" component over the entire basin declining to "common" only over the southern deep basin plain and adjacent to the 29^{o} 25'S Canyon. Other terrigenous silt minerals (plagioclase, K-feldspar) define a relatively homogeneous basin-wide distribution (see Appendix B12).

The proportions of mica-illite and clay (smectite, kaolinite and chlorite combined) in the silt fraction show basin-wide equality (Appendix B12) except for two major zones. Micas and clays are depleted over areas of the eastern Tugela Cone (cores 4

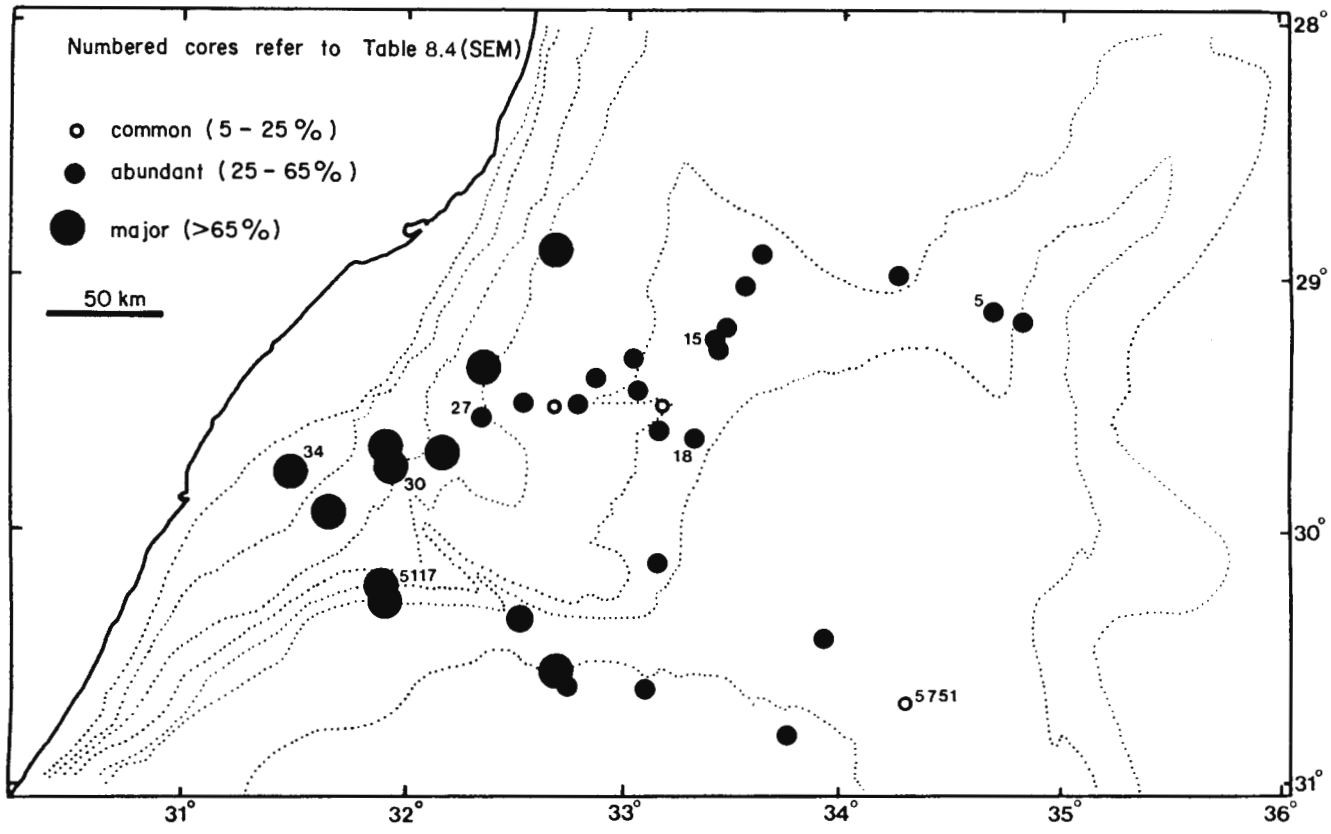

Fig. 8.15a QUARTZ CONTENT - SILT FRACTION

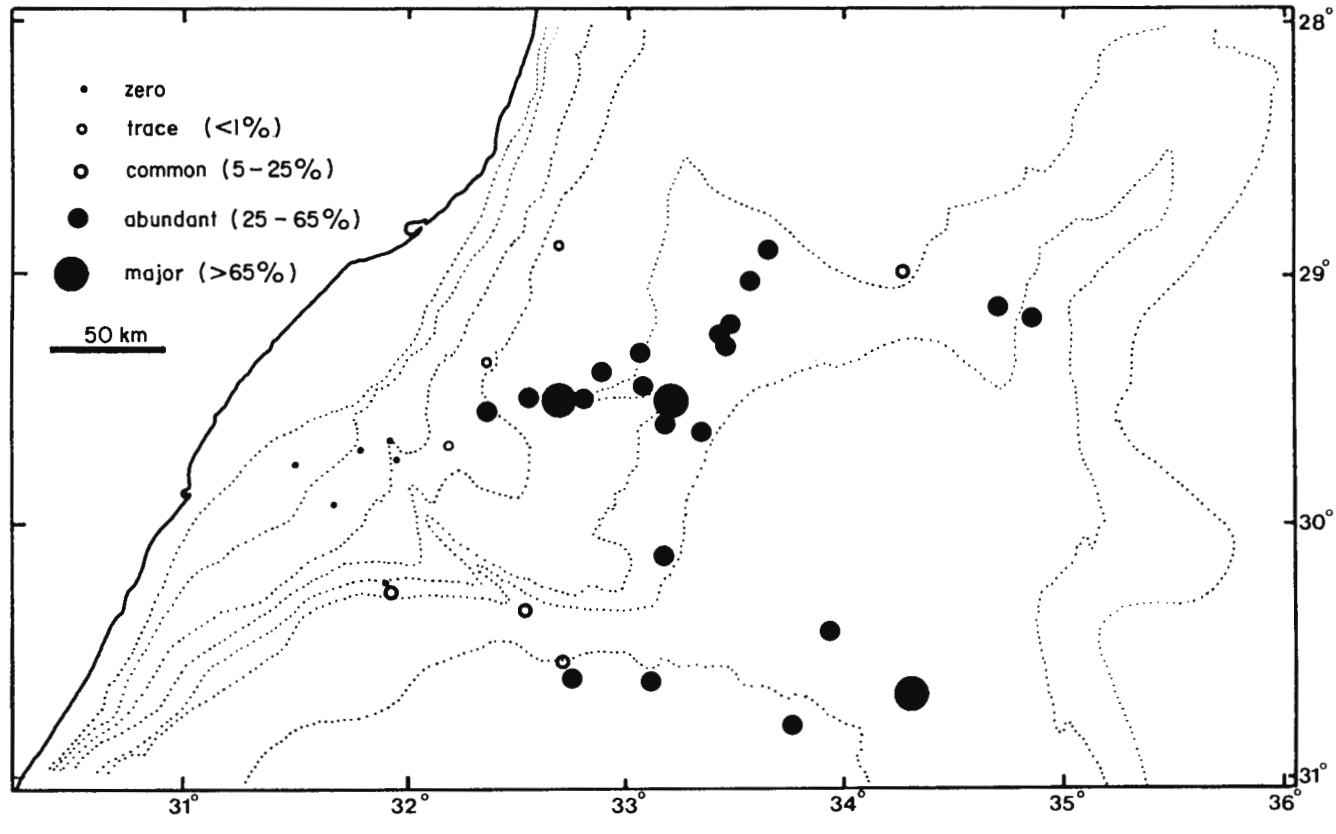

Fig. 8.15b CALCITE CONTENT - SILT FRACTION

and 5) and the mid-upper slope of the northern Tugela Cone (samples 5726 and 5727). These regions have been delineated as pathways of enhanced bottom water flow (section 7.2) perhaps maintaining partial winnowing of the mica-illite and clay components. Clays and micas are thus the only silt-grade minerals which show a response to deep current action, possibly as a result of two factors. Both micas and clays have platey morphologies and may hydrodynamically behave as a finer size fraction. In addition, the clay minerals, although within the silt-grade fraction, are most typically of sizes <20 μm (Birch, 1978) and would therefore be the first component of the silt fraction to be influenced by deep current flow.

The distribution of calcite within the silt fraction (Fig.8.15b) is almost reciprocal to quartz. Over the eastern Tugela Cone, Central Terrace and deep basin plain, calcite proportions are "abundant" or occasionally "major". In contrast, towards the upper slope of the Tugela Cone, calcite is completely absent from the silt fraction (Fig.8.15b). Similarly, over the south Tugela Cone terrigenous depocentre, dominance of detrital silt is implied by the low calcite abundances. In conclusion, over the major terrigenous depocentres, calcite abundances are low because of terrigenous silt (quartz) dilution effects. The abundances of the minerals talc/pyrophyllite, aragonite, dolomite, gibbsite and phillipsite (Appendix B12) are regionally insignificant and little meaning can be attached to their distribution patterns.

Silt fraction quartz, K-feldspar and calcite portray consistent vertical compositional within-core trends (Appendix

B12). In the detrital depocentres (e.g. south Tugela Cone), quartz and K-feldspar increase in proportion up-core (cores 5117, 5119 and 5753) in response to growing continental influence. Conversely, in the same depocentre, calcite concentrations decrease up-core through dilution by continental detritus.

8.4.5 Scanning Electron Microscopy of the Mud Fraction

8.4.5.1 Introduction

Electron microscopy of the mud fraction was peformed with two objectives in mind:

(1) to subjectively evaluate the reliability of the silt mineralogy results (section 8.4.4);

(2) to acquire additional information concerning the diversity of calcareous and siliceous nannofossils and continental detritus within the sediment.

Twelve samples were selected for SEM study.

Semi-quantitative compositional analyses were obtained by standard point-counting techniques adapted for SEM use. After preparation and mounting (Appendix A13), the sample stub was traversed in a pre-determined but random grid beneath the electron beam. Counting of particles central to the scanner screen proceeded till a minimum of 100 grains were identified. The resultant component analyses are presented in Table 8.4 with particles being assigned to thirteen categories. Most particles, particularly biogenic forms, were readily distinguishable on morphology alone. Use of the EDAX facility (energy dispersive X-ray analysis) helped in identification of ambiguous grains,

Table 8.4 Semi-Quantitative Compositional Analysis of the Mud Fraction

core	1	2	3	4	5	6	7	8	9	10	11	12	13	Mud %$CaCO_3$
5751	8	-	tr	16	tr	6	3	45	tr	-	tr	20	2	73,5
2	8	8	4	27	3	tr	2	25	-	-	-	19	4	+
5	7	5	5	22	4	2	4	29	1	-	-	19	2	63,8
5(29cm)	8	19	7	20	6	-	1	13	2	-	-	22	2	41,2
11	6	1	tr	11	-	12	40	16	-	-	-	13	1	+
15	4	3	1	11	2	2	10	42	tr	tr	-	22	3	75,2
15(15,5cm)	8	8	1	12	2	7	13	36	2	-	-	9	2	62,0
18	4	1	tr	25	3	12	8	40	tr	-	tr	5	2	61,2
27	16	10	4	16	5	-	1	11	-	2	1	34	-	56,4
5117	14	10	12	48	2	-	-	3	-	-	-	11	-	11,5
30	30	25	3	22	4	-	-	1	-	-	tr	14	1	18,9
34	30	10	10	45	tr	-	tr	1	-	-	tr	4	-	4,4

Category key: 1 - quartz (<10μm), 2 - quartz (>10μm), 3 - feldspar, 4 - clay minerals, 5 - undifferentiated terrigenous particles, 6 - juvenile forams, 7 - planktic foram fragments, 8 - coccoliths, 9 - discoasters, 10 - diatoms, 11 - radiolaria, 12 - calcareous detritus (<4μm), 13 - undifferentiated biogenic particles, + - no data available. Results based on a minimum of 100 point-counts (SEM). Mud % $CaCO_3$ data from Appendix B6.

especially clay-size material and feldspars. The mud fraction %$CaCO_3$ is appended to Table 8.4 acting as a yardstick of reliability against the SEM point-counts. The % $CaCO_3$ should equate to the total of all calcareous material wihin any sample. Comparison of the two parameters (Table 8.4) confirms this general correspondence suggesting that the semi-quantitative point-count data are reliable.

8.4.5.2 Results

Correspondence of Table 8.4 to the XRD data presented in Appendix B12 cannot be precise since the latter data are qualitative only. Nevertheless, comparability between the two data sets is satisfactory. There is however, no correspondence between clay mineral proportions since all clays (<2 μm) were removed from the silt fraction prior to diffraction.

The SEM study emphasises the large regional variation in mud fraction composition and clearly distinguishes between zones dominated by pelagic and terrigenous sedimentation. Calcium carbonate contents vary from <5% (core 34) to >75% (core 15 0cm). Individual components of the carbonate fraction also vary greatly in proportion between samples. For example, coccoliths are dominant in core 15 0cm while calcareous detritus (<4 μm) is the major carbonate phase in core 27 (Table 8.4).

Muds from the Tugela Cone upper and southern slopes (cores 30, 34 and 5117) are continental in origin as indicated by low $CaCO_3$ contents (Table 8.4). Outside these areas, on the eastern Tugela Cone (core 18), Central Terrace (cores 5, 11 and 15), Mozambique Ridge (core 2) and deep basin plain (core 5751),

skeletal carbonate detritus dominates the mud fraction (Table 8.4) verifying the importance of pelagic sedimentation. Within these pelagic provinces, however, there are strong regional variations in the major carbonate detrital type.

Over the eastern Tugela Cone and deep basin plain, coccoliths are the most abundant individual component comprising from 36-45% of the total mud fraction (Table 8.4; Plate 8.3a, d, e, k and l). This category also includes more exotic members of the sub-order COCCOLITHINEAE such as Thoracosphaera (Plate 8.3h and l), Rhabdosphaera (Plate 8.3a and l) and well-preserved coccospheres (Plate 8.3j). Subsidiary carbonate constituents include calcareous detritus (<4 μm) and planktic foram juveniles and fragments (Plate 8.3b). The terrigenous fraction of these pelagic muds is dominated by clay-grade material (Table 8.4) while quartz is an important clastic phase (Plate 8.3c and g).

Terrigenous minerals (quartz, feldspar and clays) assume greater importance over the Central Terrace (cores 5 and 11) and Mozambique Ridge (core 2) constituting up to 50% of the total mud fraction (Table 8.4). Increased proportions of continental detritus may indicate that the Limpopo catchment zone is acting as a source for terrigenous fines dispersed southwards by the Agulhas Current. This supply may not have been constant in the geologic past as evidenced by the higher porportion of continental detritus in the MIOCENE/PLIOCENE of the Central Terrace (core 5 29cm). Over the Central Terrace and Mozambique Ridge, coccoliths are reduced in abundance and are equal in proportion to calcareous detritus (<4 μm).

Planktic foram fragments comrpise an anomalously high 40% of

Plate 8.3 SEM Photomicrographs - Mud (<63μm) Fraction

a - Core 15, 15,5cm: groundmass comprising abundant assorted coccolithids including Helicopontosphaera (bottom right) and rhabdosphaerids (left central). Subordinate portion of the fine fraction comprises angular terrigenous detritus (top right) with poorly crystalline clay minerals and calcareous detritus (<4μm). Scale divisions = 3μm.

b - Core 15, 15,5cm: large angular foram fragment within the fine fraction. Major proportion of the matrix comprises various coccolithids and discoasterids. Scale divisions = 10μm.

c - Core 15, 15,5cm: large angular quartz clast included in calcareous-rich matrix of coccolithids, discoasterids, undifferentiated calcareous detritus (<4μm) and clay minerals. Scale divisions = 10μm.

d - Core 15, 15,5cm: coccolithid-rich groundmass. Scale divisions = 10μm.

e - Core 15, 15,5cm: blow-up of central section of micrograph d showing well-preserved coccolith (?Cyclococcolithina macintyrei). Scale divisions = 3μm.

f - Core 15, 15,5cm: well-preserved discoaster (?Discoaster brouweri). Scale divisions = 3μm.

g - Core 15, 0cm: quartz fragment in diverse matrix of platey clay minerals, calcareous nannoplankton, comminuted foram fragments and calcareous detritus (<4μm). Scale divisions = 3μm.

h - Core 15, 0cm: various nannoplankton including coccolithids, thoracospaerid fragments (mid left) and diatom frustules draped by clay minerals and calcareous detritus (<4μm). Scale divisions = 3μm.

i - Core 15, 0cm: angular bryozoan fragment and unidentified detrital debris within a matrix of calcareous nannoplankton, clay minerals and calcareous detritus (<4μm). Scale divisions = 10μm.

j - Core 15, 0cm: preserved coccosphere. Scale divisions = 3μm.

k - Core 5751, 0cm: abundant varied calcareous nannoplankton with rare comminuted foram fragments draped by biogenic and terrigenous clays. Scale divisions = 10μm.

l - Core 18, 0cm: thoracosphaerid within groundmass of assorted coccolithids and rhabdosphaerids (mid right), angular detrital fragments and partially-crystalline detrital clays. Scale divisions = 3μm.

m - Core 27, 0cm: diatom frustule. Scale divisions = 30μm.

n - Core 27, 0cm: diatom (?Nitzschia sp.) frustule. Scale divisions = 30μm.

o - Core 34, 0cm: abraded detrital quartz (max. dimension 30μm) within a groundmass comprising poorly-crystalline terrigenous clays and minor amounts of finely-comminuted detrital minerals (max. dimension <10μm). Note complete absence of calcareous nannoplankton. Scale divisions = 10μm.

Plate 8.3 SEM PHOTOMICROGRAPHS —— MUD (<63μm) FRACTION

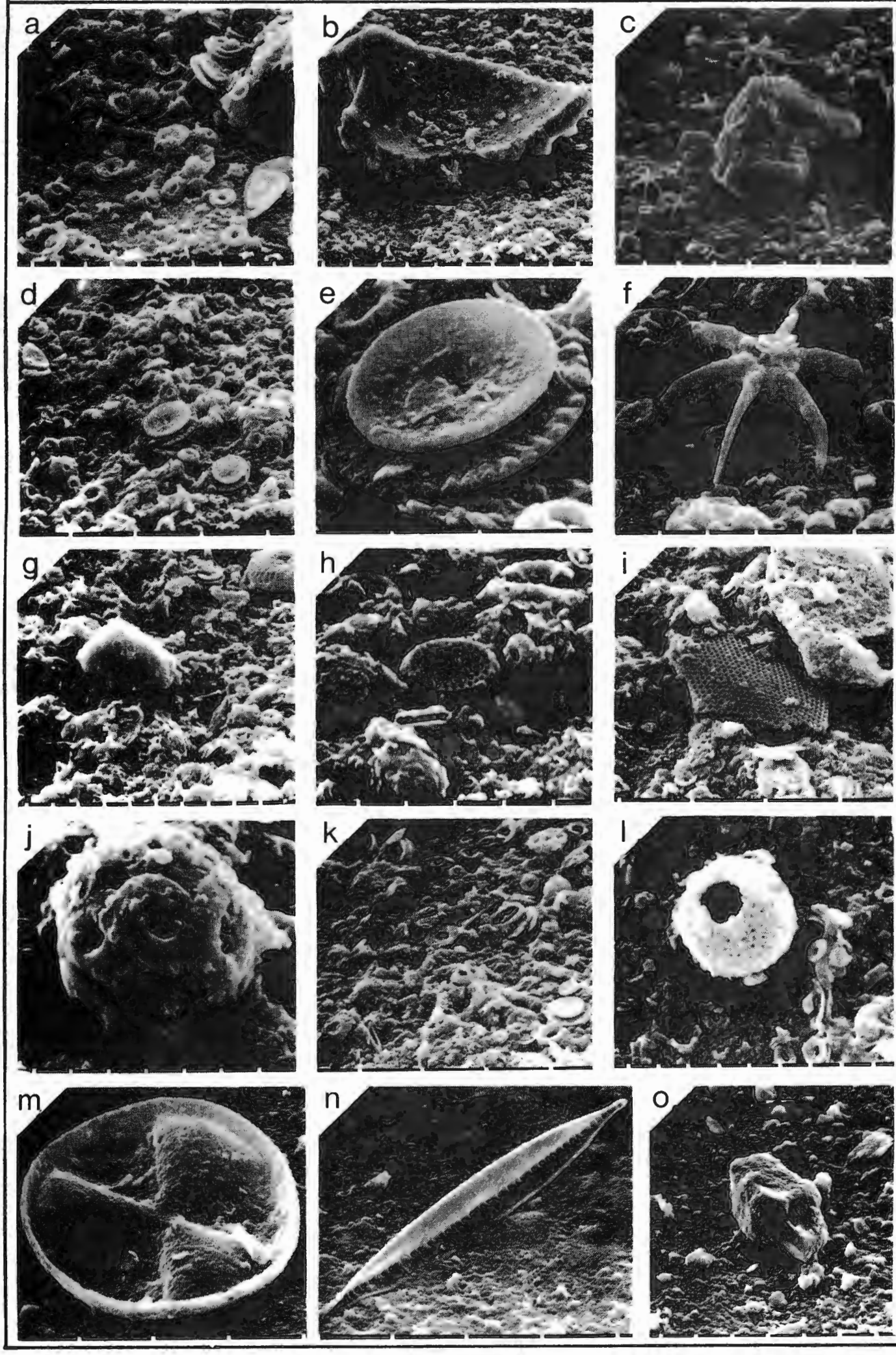

the total mud fraction in core 11 (Table 8.4). The core site lies within the zone of vigorous Agulhas Current flow over the western Central Terrace flanks (section 7.2). Under strong scour conditions, breakage of foram tests must be enhanced. Discoasters constitute an important accessory component at several of the Central Terrace and eastern Tugela Cone sites (Table 8.4). In the MIOCENE/PLIOCENE samples (cores 5 29cm and 15 15,5 cm), discoasters comprise approximately 2% of the total mud fraction (Plate 8.3c and f). Surface sediments at these sites contain lesser amounts of discoasters arguing that local reworking has been operative.

A final grouping of samples encompasses the upper and southern Tugela Cone (cores 30, 34 and 5117). Mud fraction samples from these areas are depleted in carbonate (Table 8.4) implying a dominantly terrigenous origin. Quartz, feldspar and clays are the most important detrital minerals (Plate 8.3o) while calcareous detritus (<4 μm) is the dominant carbonate phase. In transect from the upper slope (cores 30 and 34) to the southern slope (core 5117), the SEM mineralogy indicates a change from being quartz and feldspar dominant (silt-size) to clay mineral dominant. This gradation emphasises the validity of similar grain-size trends demonstrated by the silt and clay distributions (Figs.8.17 and 8.18).

Muds from the mid slope of the Tugela Cone (core 27) are hemipelagic in character but are unusual in that they contain abnormally-high percentages of diatom frustules (Plate 8.3h, m and n) and radiolaria. This may be a result of local high nutrient supply.

Several mud samples contain fragments of more exotic flora and fauna including algae, mollusca and bryozoa (Plate 8.3i). Exotic biogenic grains have been classified as undifferentiated in Table 8.4.

8.5 GRAIN-SIZE ANALYSIS

8.5.1 Introduction

Grain-size distributions within sedimentary depocentres may be controlled by several factors (Taira and Scholle, 1979b) including: a) local processes of transportation and deposition; b) inherited characteristics from previously-active processes; and c) controls on the availability and type of sediment. Textural analysis is therefore fundamental to the understanding of processes and responses in any sedimentary environment. With this premise in mind, textural analysis has been performed at two levels of precision:

1) Gross textural characteristics (gravel, sand, silt and clay) were determined by sieve and pipette analysis;
2) Detailed hydraulic grain-size parameters of the sand fraction were resolved by settling tube analysis; and
3) Detailed size analysis of the coarse to fine silt fraction (63-8 μm) was performed on an electronic particle-size counter.

Previous textural work in the Natal Valley has focussed on the shelf zone. Moir (1976) and Birch (in press, a) have presented isopleth maps of the gravel, sand, silt and clay fractions for the shelf area. More detailed hydraulic analyses of shelf sands have been published by Flemming (1978). Off-shelf zones have to date remained totally unstudied in sedimentological

terms. Distribution patterns for all textural parameters derived from the gross and detailed grain-size analyses are presented and discussed in this section. This provides a basis for development of the process-response and sediment dispersal models discussed in this section and section 8.6. Methodology is briefly outlined in section 8.2 while full analytical details are presented in Appendices A14-A16.

8.5.2 Surficial Sediment Distribution Patterns

8.5.2.1 Introduction

The general textural characteristics of sea floor sediments within the mid Natal Valley are illustrated by percentage isopleth maps of the individual grain-size components. The relative percentage data for each component (gravel, sand, silt and clay) were derived by standard sieve and pipette analysis (Royce, 1970; Appendix A14). Data control for the surficial sediment study was limited to 35 samples (Appendix B6). The limitations of sieve/pipette analysis have been well-documented (Royce, 1970; Shideler, 1976b). However, gross analysis of this type is practical in evaluation of sedimentological processes in a poorly-known basin such as the Natal Valley. Other regional investigations around the South African margin (e.g. Birch, 1975) have relied heavily on sieve/pipette methodology. This technique has been retained to provide regionally-compatible data.

Because of the great difficulty in core correlation (non-availability of detailed palaeontological and palaeomagnetic data), the exercise of comparing textural distributions through time was not attempted. Nevertheless, textural analysis was

performed on 173 sub-bottom samples. This data base is utilised in the discussion of lithofacies and sedimentation processes (section 8.6). The few samples containing gravel are depicted on the sand isopleth map (Fig.8.16). Shelf data supplied by Birch (in press, a) are incorporated to provide complete nearshore coverage.

8.5.2.2 Sand Fraction

Areal variations in sand fraction (2 mm - 63 μm) concentrations are illustrated by the sand isopleth map (Fig.8.16). At off-shelf stations, sand contents range from <10% (core 5117) to >80% (grab 5726) but average around 50%. On the shelf zone, sand concentrations approach 100%. The sand distribution pattern displays distinct regional trends with several sand-rich and sand-poor zones. Three sand-rich provinces may be delineated: the shelf zone, lower slope of the northern Tugela Cone and the Central Terrace/deep basin plain.

The continental shelf zone is extremely rich in sand-grade detritus (Fig.8.16) and with the exception of the Tugela mud belt (section 8.3.2), concentrations typically exceed 70%. High sand concentrations may be equated to the high energy flow regime caused by impingement of the vigorous Agulhas Current onto the shelf (Flemming, 1978; 1980). Over the central shelf zone (Natal Bight), sand concentrations are reduced and the presence of the hydraulically-stable Tugela mud belt demonstrates the inability of the Agulhas Current to penetrate this region.

The lower slope of the northern Tugela Cone and the Central Terrace are characterised by high sand concentrations (>70%). Comparison to Figure 8.4a indicates that this sand component is


% SAND (2mm - 63µm)
Contour interval 20%
< 30%
Significant gravel (>1%)
data control
50 km
Shelf data from Birch (in press, a)
31°
32°
33°
34°
35°
36°
28°
29°
30°
31°

Fig. 8.16

primarily biogenic (planktic forams). However, terrigenous mud and very fine sand input into these areas is probably large, being sourced from the Tugela and Limpopo Cones. The observed high biogenic sand contents must be equated to deep Agulhas Current winnowing action which sifts out the terrigenous and biogenic fines (section 8.4.1.2 and 8.4.2.2).

Sand concentrations over the eastern deep basin plain are above average (50-70%) reflecting high pelagic fall-out of foram tests. This zone, like the Central Terrace, probably receives significant mud (terrigenous and biogenic) input. However, bottom currents are of insufficient competence to reduce this mud proportion by winnowing action.

In off-shelf basinal areas, two sand-depleted zones (<30%) are not delineated: the southern Tugela Cone and the upper slope of the northern Tugela Cone. Both zones have been outlined as major terrigenous depocentres (section 8.3.1) with low sand concentrations (Fig.8.16) implying a mud sink status in equilibrium with the prevailing hydraulic regime. Southward dispersal of mud over the southern Tugela Cone in turn influences the SW deep basin plain which is sand-depleted relative to the eastern deep basin (Fig.8.16). Reduced sand contents are locally apparent along the axis of the 29° 25'S Canyon (Fig.8.16) implying canyon stagnation or mud transport.

A small biogenic gravel component (abraded mollusca debris) is registered at three off-shelf stations (Fig.8.16, section 8.6.4). These gravels, sourced from relict biogenic gravel lags on the shelf zone (Flemming, 1978), now appear to be associated with the modern terrigenous dispersal routes and depocentres. It is suggested that the gravels are entrained and transported from

the shelf zone during periods of increased hydraulic energy (? storms). Deposition occurred on re-entering a lower energy environment. Within the southern Tugela Cone depocentre, gross texture reflects the relative energy gradient with downslope decrease in energy level. At the top-of-slope, sediments contain a small gravel fraction. Towards the base-of-slope, sand concentrations decrease and sediments become greatly mud-enriched (Fig.8.16).

8.5.2.3 Silt Fraction

The areal distribution of silt-grade (63-4 μm) detritus in the sea-floor sediments is illustrated by the silt isopleth map (Fig.8.17). This fraction comprises variable admixtures of biogenic (calcareous nannofossils and fragmented forams) and terrigenous (quartz, feldspar and large clay-mineral aggregates) detritus. Silt proportions at individual off-shelf stations range from <5% (core 13) and >40% (core 5753) averaging out at approximately 20%. Relative to the regional average, only two zones are markedly silt-deficient: the continental shelf and as one contiguous zone, the lower slope of the northern Tugela Cone and Central Terrace.

On the shelf zone, silt is extremely depleted often comprising <1% of the total sediment (Birch, in press a). One exception is the Tugela mud belt where the silt proportion locally exceeds 50% (Fig.8.17). Existence of this mud belt illustrates the combination of high mud discharge from the Tugela river and lower energy regime in the central shelf zone. Southward deflection of the mud belt over the outer shelf evidences increased Agulhas Current influence. Depletion to <10%


% SILT (63 - 4 µm)
Contour Interval: 10%
> 30%
• data control
50 km
Shelf data from Birch (in press, a)
31°
32°
33°
34°
35°
36°
28°
29°
30°
31°

Fig. 8.17

over the Central Terrace and adjacent zones of the Tugela Cone is a response to pervasive scouring by deep Agulhas flow which continually winnows out the fine fractions causing sand grade enrichment.

Silt enrichment occurs in two distinct zones: the southern Tugela Cone and the upper slope of the northern Tugela Cone. In the former province, the silt fraction locally exceeds 40% (Fig.8.17), and is rich in quartz and feldspar but poor in biogenic material (sections 8.4.4 and 8.4.5). The south Tugela Cone is thus an effective modern terrigenous silt depocentre. Within this depocentre, the silt isopleth trends are approximately inverse to the sand trend with maximum silt deposition at the base-of-slope. Continuity of the Tugela mud belt apex and the up-slope limit of the slope depocentre (Fig.8.17) suggests a close inter-relationship. It is possible that a large proportion of the silt detritus supplied to the south Tugela Cone may be traversing the shelf as bedload via this stable mud belt.

The second silt depocentre encompasses the upper slope of the northern Tugela Cone and corresponds to a sand depletion zone (Figs.8.16 and 8.17). Increased % silt in this zone reflects the dominance of mud deposition in this terrigenous depocentre. Isolated small concentrations of silt detritus are developed along the course of the 29° 25'S Canyon, endorsing its status as a downslope conduit for muddy detritus.

8.5.2.4 Clay Fraction

The areal variability of clay-size (<4 μm) detritus is illustrated by the clay isopleth map (Fig.8.18). Clay percentages at individual off-shelf stations range from <10% to a


% CLAY (<4μm)
Contour Interval : 10%
> 40%
• data control
50 km
Shelf data from Birch
(in press, a)
31°
32°
33°
34°
35°
36°
28°
29°
30°
31°

Fig. 8.18

maximum of >70% (core 30) illustrating that clay is quantitatively greater than silt within the modern mud depocentres. The regional clay distribution is inversely related to the sand distribution pattern. Local areas of high clay content equate to silt-enriched zones.

Clay-deficient provinces are delineated on the shelf zone, the Central Terrace/adjacent northern Tugela Cone and the deep basin plain. Factors establishing sand-enrichment in these zones may also be invoked to explain the clay deficiency.

Agulhas Current scour on the shelf zone is responsible for the almost complete absence of clay (Fig.8.18). However, weakened current strength allied to excessive riverine input of fines (Tugela river) in the central shelf zone has allowed construction of the clay-rich Tugela mud belt. Deep-current winnowing and reduced terrigenous input (remoteness from the hinterland) may, in combination, explain the clay-grade deficiency over the Central Terrace and adjacent Tugela Cone. In contrast, predominance of sand-grade biogenic material over the deep basin plain is interpreted as indicating dilution by pelagic fall-out of large forams.

Relatively high clay contents are registered in two off-shelf depocentres. Clay concentrations locally exceed 70% over the south Tugela Cone which is the primary modern terrigenous depocentre and seaward dispersal route. Concentration of clay and silt in this depocentre suggests that a major proportion of the fines must be transported by bottom process rather than by suspension.

A second concentration of clay-grade detritus is demarcated over the upper slope of the northern Tugela Cone (Fig.8.18).

This province is also characterised by silt-enrichment and sand-depletion and thus constitutes a modern mud depocentre.

8.5.2.5 Gross Textural Provinces

General textural characteristics of the sea floor sediments (section 8.5.2) may be combined with morphologic data to delineate textural provinces. To define these provinces, mud contents and textural type distributions have been mapped (Figs.8.19-8.21).

Mud Content

The areal distribution of mud (silt + clay) in the surficial sediment is illustrated by the mud isopleth map (Fig.8.19). Close similarity to the clay and, to a lesser extent, silt isopleth maps is maintained and thus no detailed description of the mud distribution is provided. In general, mud-depleted zones include the continental shelf excepting the Tugela mud belt, the Central Terrace and adjacent lower slope of the northern Tugela Cone and the eastern basin plain. Mud-enriched sectors encompass the eastern and particularly the southern Tugela Cone. A subsidiary depocentre is sited over the upper slope of the northern Tugela Cone.

Textural Classification and Distribution

The textural variability of Natal Valley surficial sediments has been evaluated in terms of sand, silt and clay components. Sediment classification, after Shepard (1954), is illustrated in ternary diagram form (Fig.8.20) and indicates a definite regional segregation of texture. Although some superimposition of provinces is apparent (e.g. Central Terrace and eastern basin

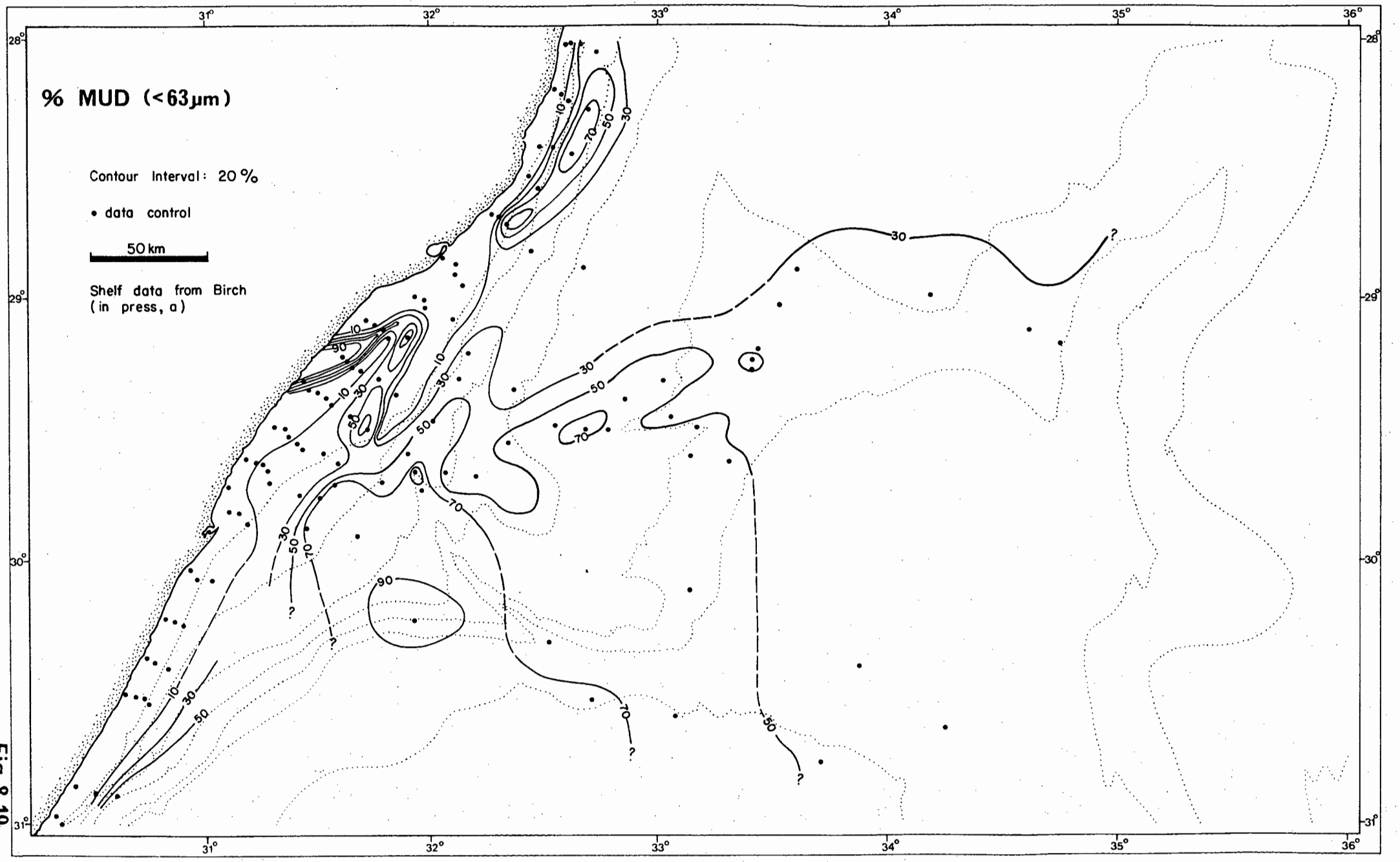
% MUD (<63μm)
Contour Interval: 20 %
• data control
50 km
Shelf data from Birch
(in press, a)
31°
32°
33°
34°
35°
36°
28°
29°
30°
31°

Fig. 8.19

plain), five textural groups (I-V) are distinguishable (Fig.8.20). The five groups have distinct physiographic connotation reflecting the variation in hydrodynamic processes between provinces. Texture and group designation have also been mapped to show their areal segregation within the mid Natal Valley (Fig.8.21). Each group, which may correspond to one or more physiographic zones, is briefly described in turn:

Group I: This group encompasses the southern flanks and central upper slope of the Tugela Cone (Fig.8.21). Sediments are classified as silty clays (Fig.8.20) confirming that equilibrium mud deposition is taking place in this modern terrigenous depocentre.

Group II: Incorporating the eastern flanks of the Tugela Cone, group II sediments are texturally classified as sand-silt-clay (Figs.8.20 and 8.21). A combination of high $CaCO_3$ content (Fig.8.3) and a foram-rich sand fraction (Fig.8.7a) implies that this hemipelagic province receives infrequent terrigenous supply.

Group III: Group III sediments are delineated over the deep basin plain south of the Tugela Cone (Fig.8.21). Texturally, sediments of this group are classified as sand-silt-clay and thus there is overlap with group II (Fig.8.20). Significant differences in the $CaCO_3$ content (Fig.8.3) necessitates discrimination of the groups.

Group IV: Of large areal extent, group IV clayey sands (Fig.8.20) are delineated over the Central Terrace and eastern basin plain. High input of foram tests with little terrigenous mud dilution preserves the sand-rich character of this group. Central Terrace samples (cores 5, 12 and 13) plot nearest to the sand apex in Figure 8.20 reflecting the importance of winnowing.

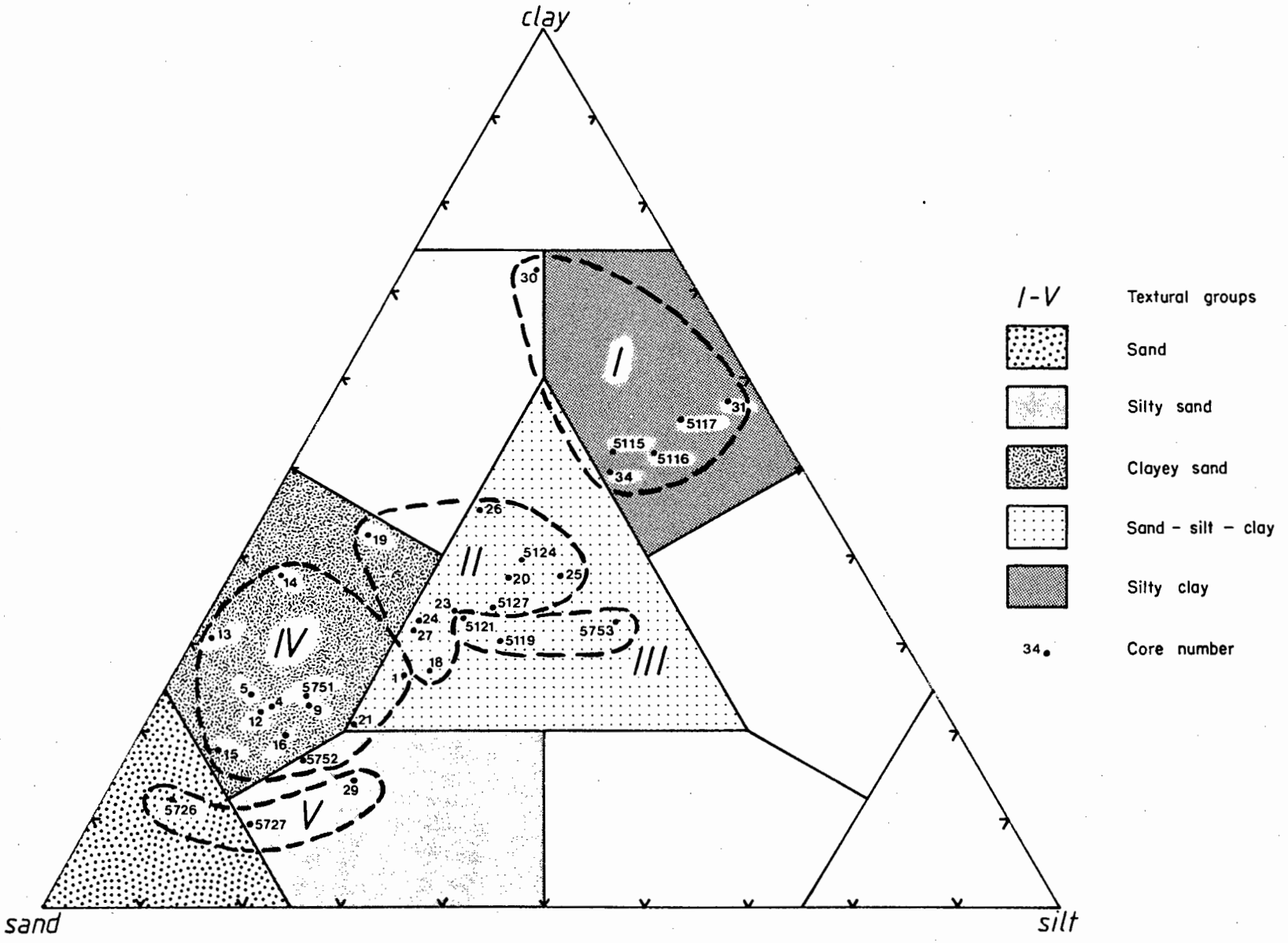

Fig. 8.20 TEXTURAL TERNARY PLOT

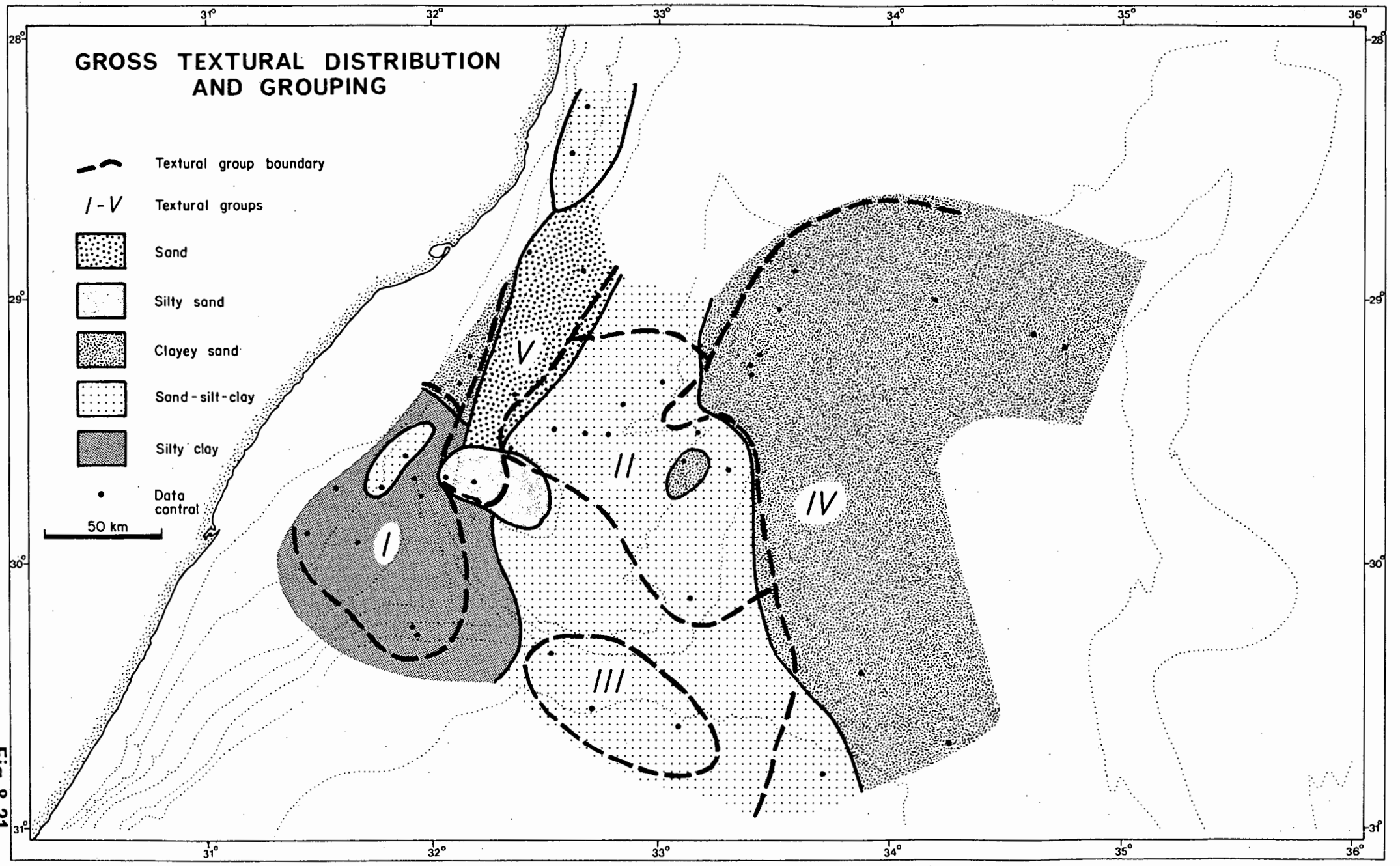
GROSS TEXTURAL DISTRIBUTION
AND GROUPING
Textural group boundary
I - V
Textural groups
Sand
Silty sand
Clayey sand
Sand - silt - clay
Silty clay
Data control
50 km
I
II
III
IV
V
31°
32°
33°
34°
35°
36°
28°
29°
30°
31°

Fig. 8.21

Group V: This sediment group, areally located over the mid slope of the northern Tugela Cone parallel to the shelf break (Fig.8.21), may be texturally classified as sands and silty sands (Fig.8.20). Mud depletion in this zone suggests high energy levels, possibly related to Agulhas Current scour and winnowing action.

This textural grouping system is used in sections 8.6.2 and 8.6.3 where it is incorporated with other sedimentological data to establish a facies assemblage classification.

8.5.3 Hydraulic Grain-Size Analysis of the Sand Fraction

8.5.3.1 Introduction

In spite of good statistical reproducibility, sieve size analysis is time-consuming and often inaccurately reflects the true size distribution of a sediment (Sengupta and Veenstra, 1968; Flemming, 1977). In recent times, therefore, an increasing number of sedimentologists have switched to settling techniques for the detailed size analysis of sand grade detritus (e.g. Gibbs, 1974; Flemming, 1977). Since most natural sediments are deposited during processes of hydraulic transport (Bagnold, 1968), settling analysis, which provides hydraulically-related size data, may be more meaningful in the study of depositional processes than sieve analysis which relies solely on particle dimensions (Taira and Scholle, 1979a and b).

The hydraulic approach, in which settling velocities of individual particles are measured in a water medium, has been adopted in this study. Computerised data reduction of these velocities provides the "settling diameter" as a resultant grain-

size parameter. All particles of identical settling velocity relative to the calibration material are regarded as being hydraulically-equivalent, irrespective of grain density and shape. The sand fraction is treated as an ideal hydraulic population and the mud (<63 μm) component has been excluded from computation of statistical grain-size parameters. Although numerous studies (Shideler, 1976a; 1978) have computed textural statistics on the total sediment, this approach is regarded as partially invalid since it averages parameters from several sub-populations. Each sub-population is generated by an unique process-response system and must thus be considered hydraulically-discrete. Evaluation of the sand grade alone may alleviate but cannot entirely eradicate this problem since the sand fraction alone may constitute several mixed sub-populations.

The spatial distribution patterns for various grain-size parameters of the sand fraction are described and discussed within this section. Inter-relationships between these parameters are examined in terms of depositional processes. Using sub-sample 2 (Fig.8.2), settling tube analysis of 35 sea-floor samples serves as a limited data base for this investigation. Sample preparation, operational procedures and data reduction are fully outlined in Appendix A15. Reduced data are tabulated in Appendix A15. Reduced data are tabulated in Appendices B2 and B7. Sub-bottom data (173 analyses) are included in these appendices but are only discussed in section 8.6.

8.5.3.2 Grain-Size Parameter Distribution Patterns

Grain-size and statistical parameters have been derived

using the total sand fraction data. Distribution patterns therefore reflect a combination of mechanisms controlling biogenic and terrigenous detritus deposition. Restriction of sample size (Appendix A7) precluded separation of the terrigenous and biogenic fractions and thus no differentiated size data are available. Following widespread general acceptance by sedimentologists, grain diameters and statistical parameters have been computed in phi (ϕ) notation (Krumbein, 1934). Percentage abundances of hydraulically-equivalent coarse and very coarse sand are insignificant in the great majority of samples (Appendix B7) and thus no distribution patterns for these fractions have been mapped.

Medium Sand (1-2ϕ)

The areal variability of medium sand as a percentage of the total sand fraction is illustrated by an isopleth map (Fig.8.22a). Highest concentrations of medium sand (>25%) are restricted to the Central Terrace crest being associated with high bottom energy levels (Agulhas Current scour). In contrast, lowest concentrations (<10%) are registered over the southern Tugela Cone and adjacent to the lower 29° 25'S Canyon. The majority of the Tugela Cone is characterised by a medium sand proportion from 10-20%. Concentrations >20% typify the eastern basin plain.

Comparison to the distributions of sand fraction % carbonate (Fig.8.4a) and sand grade components (Figs.8.7 - 8.9) verifies that individual components have a definite size control. Over zones rich in medium sand (Central Terrace), the sand fraction is very calcareous and dominated by planktic forams. Regions depleted in medium sand (south Tugela Cone and lower 29° 25'S

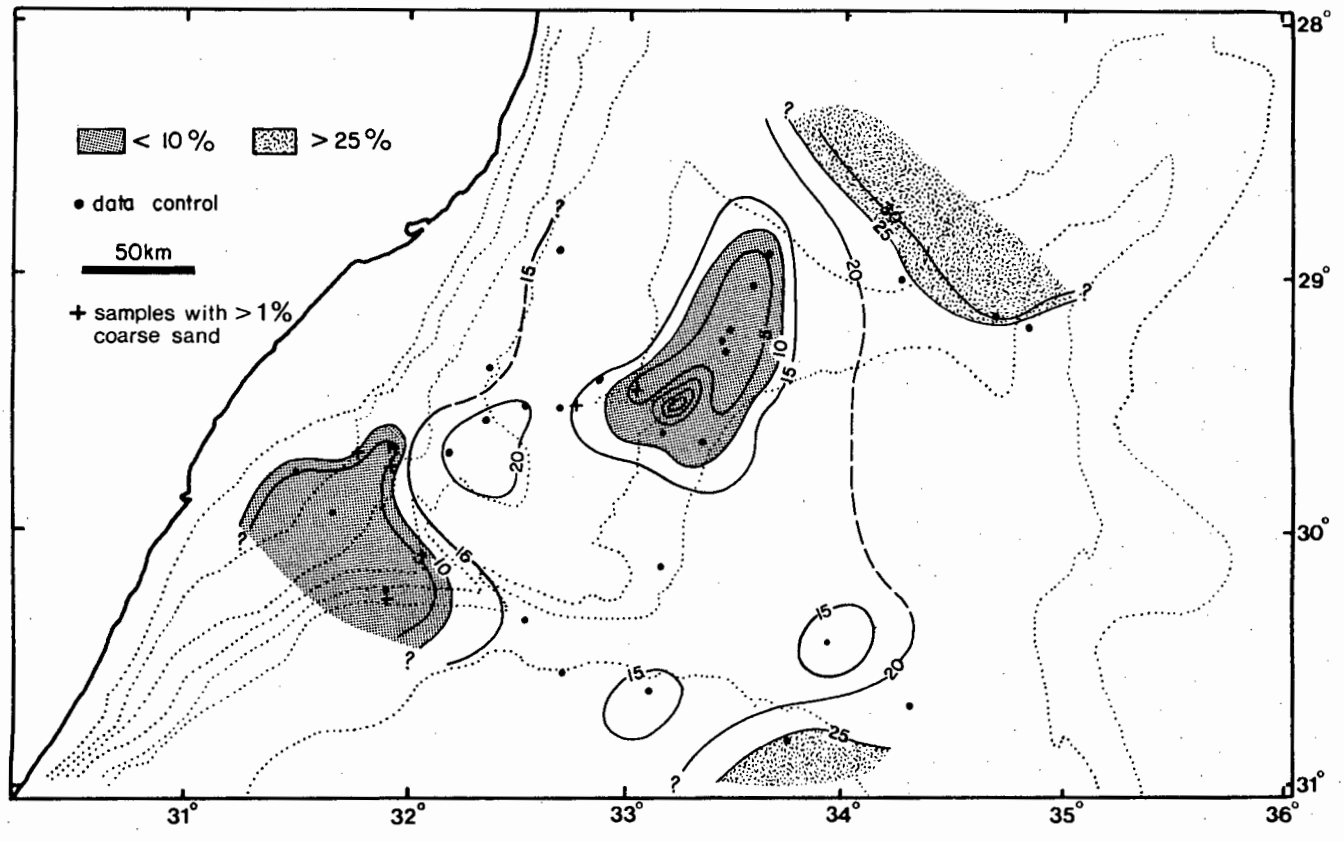

Fig. 8.22 a % MEDIUM SAND

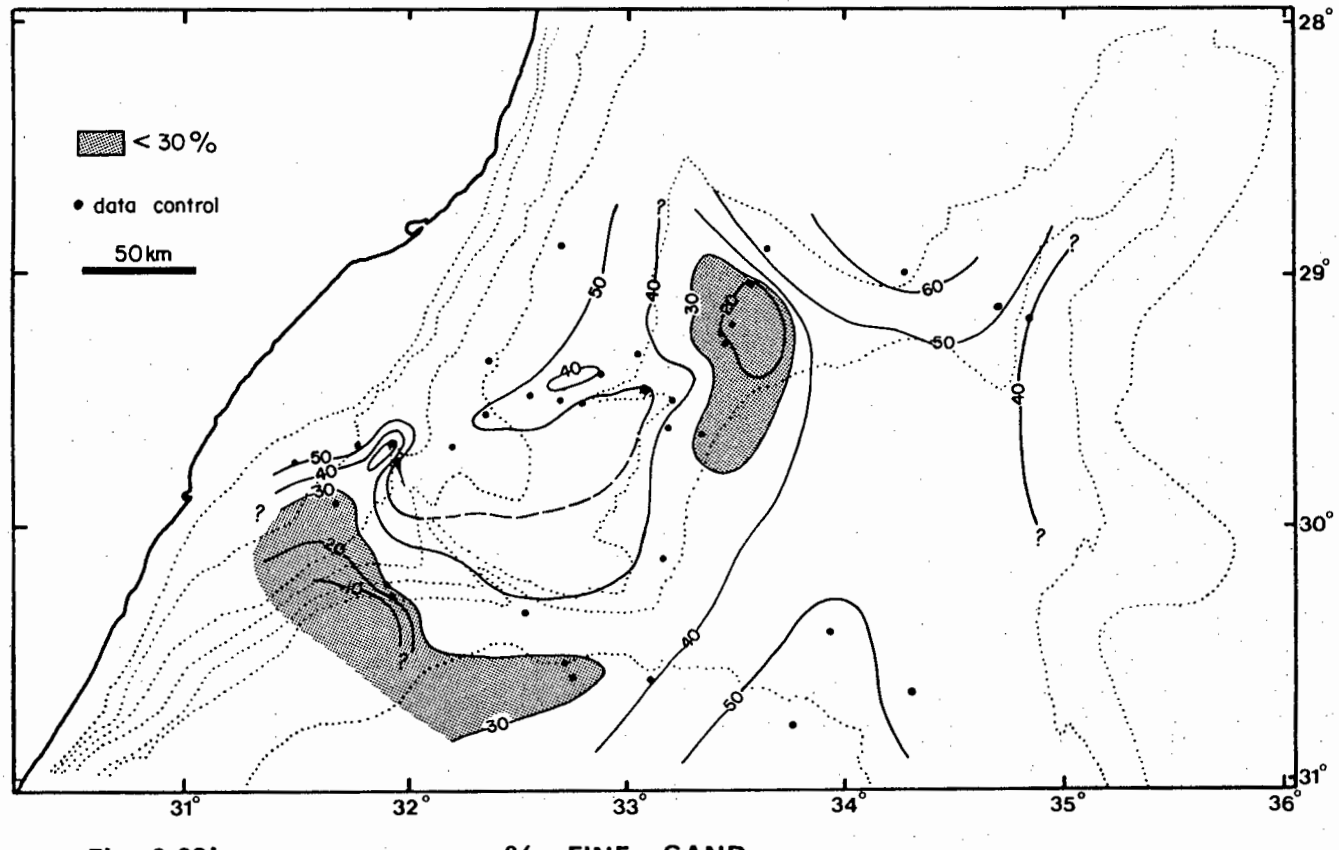

Fig. 8.22b % FINE SAND

Canyon) correlate to low sand carbonate levels (Fig.8.4a) and enrichment of terrigenous detritus (Figs.8.8b and 8.9).

It may be concluded that planktic forams account for almost the entire medium sand fraction. Medium sand depocentres correlate to zones of high pelagic input, low terrigenous dilution and/or high bottom energy levels (current scour).

Although the medium sand fraction is almost exclusively biogenic, the few samples containing coarse sand (Fig.8.22a) correlate to terrigenous depocentres (south Tugela Cone and the 29° 25'S Canyon). This small proportion of coarse detrital sand is transported from the shelf area in the bedload.

Fine Sand (2-3ϕ)

The distribution of fine sand (Fig.8.22b) is clearly related to medium sand. Zones of enrichment and depletion of these two size grades show close correspondence. Highest concentrations of fine sand (locally >60%) are documented over the Central Terrace. In contrast, extreme fine sand deficiency (locally <10%) is coincident with the major modern terrigenous depocentres (upper and southern Tugela Cone and the lower 29° 25'S Canyon). Intermediate percentages (30-50%) characterise the remainder of the Tugela Cone and deep basin with no definitive trends being displayed.

Comparison to chemical and mineralogical data evidences the strong component control over size distribution. As with medium sand, greatest abundances of fine sand correlate to biogenic provinces remote from terrigenous dilution processes and particularly those scoured by bottom currents (Central Terrace). Inactive zones of the Tugela Cone (eastern flanks) and the basin plain are classified as hemipelagic or pelagic provinces and are

relatively enriched in fine sand. In contrast, terrigenous provinces are consistently characterised by low fine sand concentrations.

A belt of low fine sand concentration fringes the lower flanks of the Tugela Cone and connects the two fine sand-depleted terrigenous depocentres (Fig.8.22b). Other sedimentological parameters mimic this trend (e.g. Figs.8.7a, 8.8b and 8.9a) as a response to detritus entrainment and hydraulic size sorting by NADW flow (section 2.3.2). Dilution by argillaceous sediments and very fine sand explains the depletion of fine sand along this zone.

Very Fine Sand (3-4ϕ)

The very fine sand fraction shows a reciprocal distribution pattern when compared to the coarser sand grades (Fig.8.23a). Very fine sand deposition is closely associated with the major terrigenous depocentres with highest concentrations being recorded over the southern Tugela Cone and lower 29° 25'S Canyon. Detritus in this latter depocentre probably utilises the canyon as a transport conduit. Immediately north of the canyon, an elongate zone of slight very fine sand enrichment (Fig.8.23a) corresponds to levee development (section 7.4.2.2). The levee is finer-grained than the surrounding slope and thus the canyon must, at least periodically, be a conduit for mud and very fine sand transport.

The relatively low concentration (20-30%) of very fine sand over the eastern basin plain and Central Terrace probably reflects the remoteness from terrigenous input. Extra depletion (<20%) over the Central Terrace crest may be due to local winnowing.

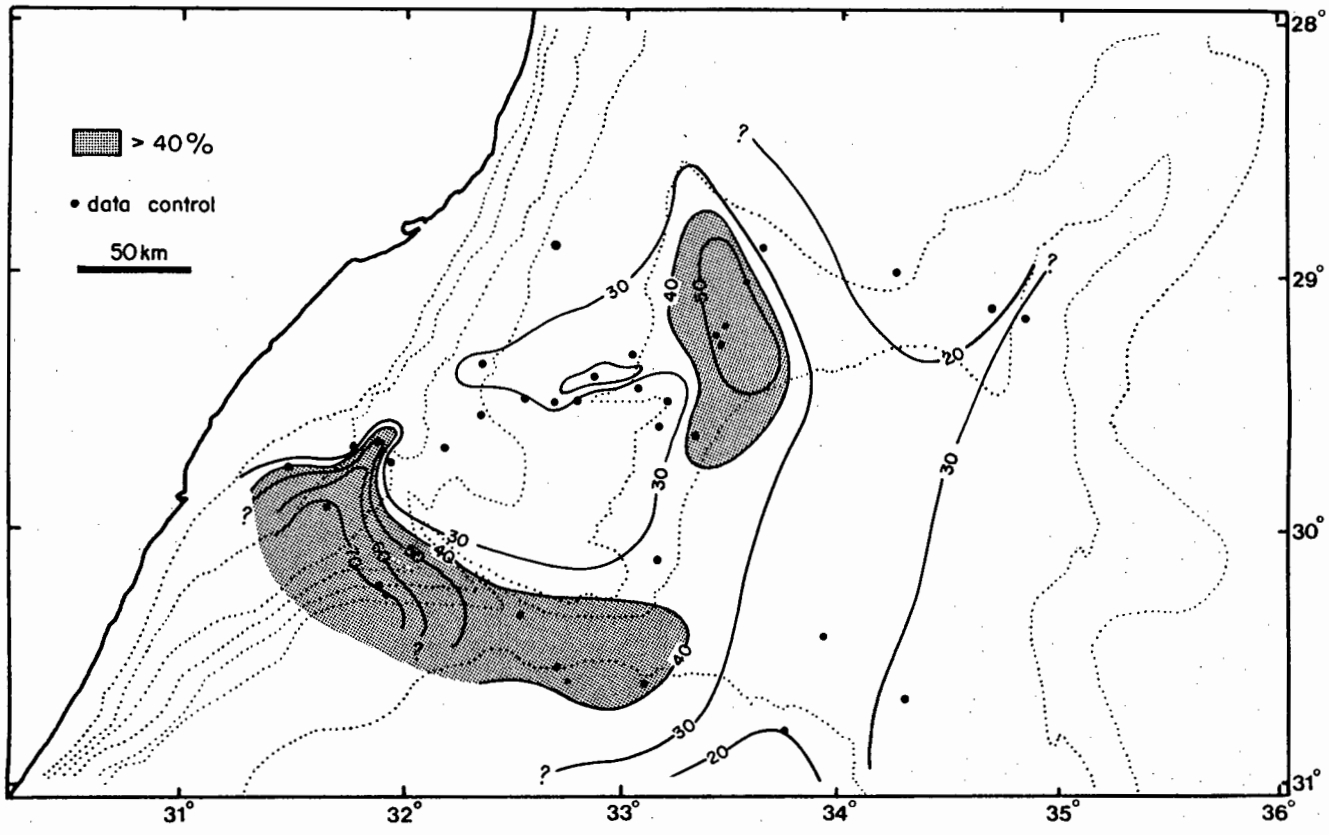

Fig. 8.23a % VERY FINE SAND

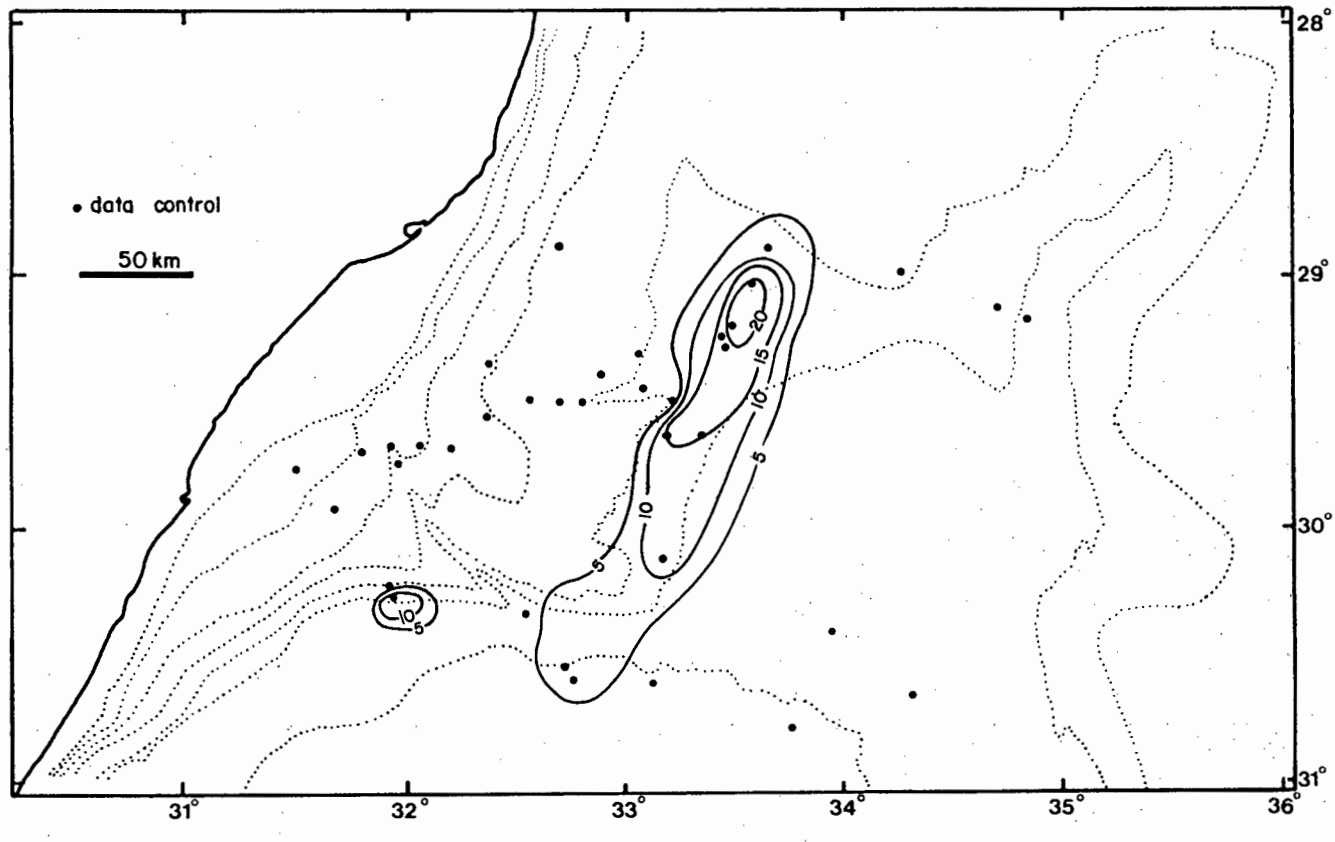

Fig. 8.23b % COARSE SILT (HYDRAULIC) IN THE SAND FRACTION (SIEVE)

Comparison to the sand carbonate and component data confirms that the very fine sand fraction is predominantly terrigenous. Depocentres for carbonate-poor sand (Fig.8.4a), quartz (Fig.8.8b), feldspar (Fig.8.9a) and heavy/opaque minerals (Fig.8.9b) exhibit good areal correspondence to the major very fine sand concentrations illustrating a terrigenous clastic origin. Intermediate to low concentrations of very fine sand over the eastern Tugela Cone confirms that this area is relatively stagnant as a terrigenous depocentre (Chapter 9).

Coarse Silt (4-5ϕ)

The presence of measurable amounts of hydraulically-equivalent silt (Appendix B7 and Fig.8.23b) within the sieved sand fraction illustrates the systematic error in sieving techniques. Many particles with sieve diameters in the sand fraction range are hydraulically-equivalent to silt-sized material. In terms of hydraulic equivalence, sieve results typically over-estimate the average grain-size towards a coarser size class (Flemming, 1977).

Although most samples contain some hydraulically-equivalent silt (Appendix B7), excessive proportions (5-20%) are only registered in a wide belt along the lower eastern margin of the Tugela Cone (Fig.8.23b). Highest concentrations of coarse silt (15-20%) are recorded around the outflow area of the 29° 25'S Canyon. Isolated pockets are developed over the southern Tugela Cone.

It is apparent that high proportions of hydraulically-equivalent silt in the sieved sand fraction areally correlate to distal terrigenous depocentres or to redistribution pathways for fine-grained terrigenous detritus. Although biogenic detritus is

predominant in the sand fraction at several sites (e.g. cores 18 and 19) within this belt, it is suspected that irregularly-shaped terrigenous particles comprise the hydraulically-equivalent silt component.

To check this hypothesis, several sand fraction samples from the anomalous area were leached with 5% HCl to remove the biogenic fraction prior to settling tube analysis. Reduced data together with comparative analyses are presented in Table 8.5. Examination of the results indicate that at all sites the mean settling diameter is significantly finer for the terrigenous sand as compared to the bulk sand. In addition, in samples from the "silt province" (core 5753), the terrigenous-only fraction mean falls within the coarse silt size grade (Table 8.5). Furthermore, the terrigenous-only fraction contains an extremely large hydraulically-equivalent silt proportion (>50%) within the sieved sand fraction (Table 8.5). Outside the "silt province" (cores 12, 32 and grab 5726), this feature is less pronounced. It may be concluded that a large proportion of the terrigenous very fine sand as defined by sieve diameter actually behaves hydraulically as coarse silt.

Disregarding localised complexities, the sand distribution patterns within the mid Natal Valley suggest the presence of two overlapping hydraulic populations. The coarser population consists of medium to fine sand grade biogenic detritus primarily supplied by pelagic fall-out. The finer population comprises very fine sand and hydraulically-equivalent coarse silt of terrigenous origin supplied by the hinterland drainage systems. The overlapping nature of the two hydraulic populations indicates

that they have been mixed in varying proportions in different physiographic provinces. Localised influences such as deep current scour have imprinted their effects on the mixed populations. Further discussion on sediment mixing is contained in section 8.5.3.4.

Table 8.5 Comparison of Grain Size Parameters for the Bulk and Terrigenous Sand Fraction

Core	Sample interval	Mean	% CS	% MS	% FS	% VFS	% CSi
5753*	200-203B	3,01	-	12,5	32,5	50,0	5,0
	200-203T	4,05	-	0,9	1,8	37,2	62,8
5753*	235-238B	2,98	0,1	11,6	33,8	51,1	3,3
	235-238T	4,01	-	2,0	2,4	41,2	54,5
21	3,5-7B	2,78	0,2	5,1	63,5	29,9	1,3
	3,5-7T	3,38	-	4,0	17,0	57,4	21,6
32	2-4B	1,85	15,1	18,4	37,9	16,2	1,0
	2-4T	3,21	6,0	9,0	19,4	40,8	24,8
5726	B	2.71	0,1	11,4	56,3	31,0	1,1
	T	3,75	-	-	1,5	64,8	33,7

Mean - mean settling diameter in phi
%CS - proportion of coarse sand
%MS - proportion of medium sand
%FS - proportion of fine sand
%VFS - proportion of very fine sand
%CSi - proportion of coarse silt
B - bulk sand fraction
T - terrigenous sand fraction only (acid-leached)
* - samples from province with enriched proportions of hydraulically-equivalent silt (Fig.8.23b).

Mean Diameter

The dominant features of the sand sub-fraction distributions are summarised by the mean diameter isopleth map (Fig.8.24a). Both major terrigenous depocentres (south Tugela Cone and the lower 29° 25'S Canyon) are clearly outlined by mean diameters finer than 3ø. Within these depocentres, upslope higher energy

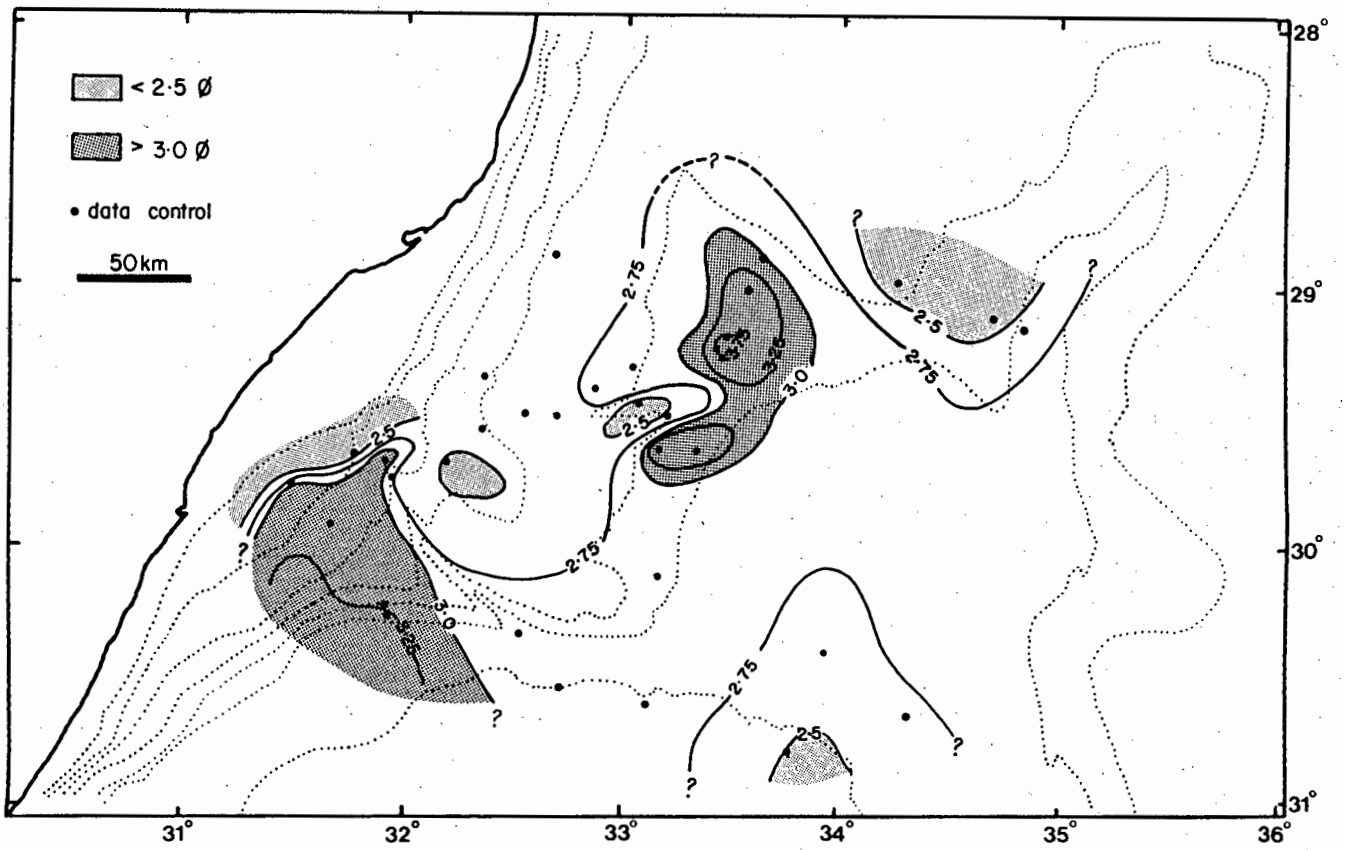

Fig. 8.24a MEAN DIAMETER (ø) – SAND FRACTION

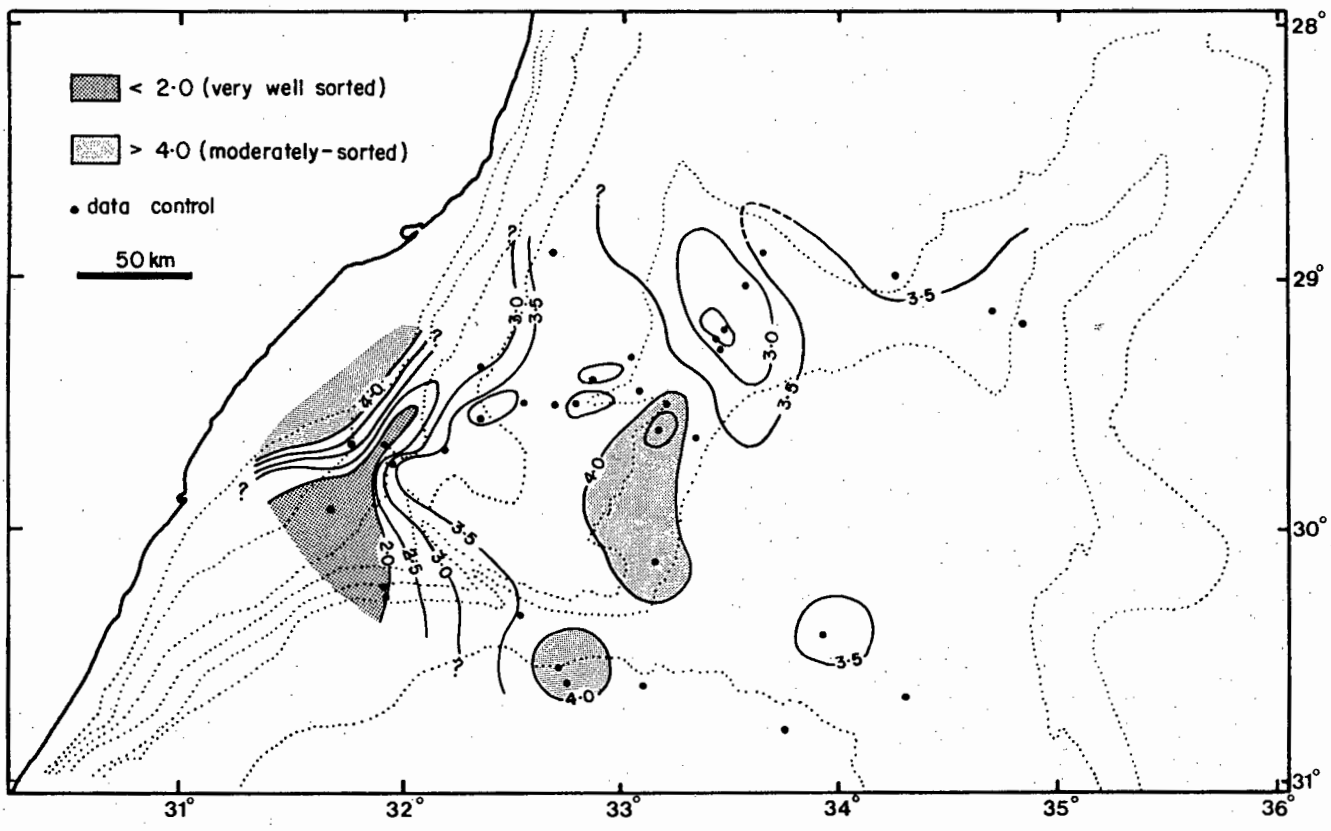

Fig. 8.24b RELATIVE SORTING (QH) – SAND FRACTION

conditions are represented by increasing mean grain size in the sand fraction. Coarsest mean diameters are registered over the predominantly pelagic provinces (Central Terrace, deep basin plain and stagnant zones of the Tugela Cone). Where scour action has concentrated the hydraulically-coarsest forams (e.g. Central Terrace), mean diameters are locally coarser than 2,5ϕ (Fig.8.24a). The mean diameter distribution pattern supports the trends displayed by the individual sand sub-fractions and reinforces the argument that the sand fraction comprises a mixture of at least two distinct hydraulic populations.

Sorting

To provide information regarding control processes in sedimentary environments, usage of the genetically-related parameter "relative sorting" (Walger, 1962) is preferred to the standard sorting parameter in discussion of the standard deviation of grain-size distributions. Relative sorting is considered superior since it is independent of the average grain-size of the sediment. Dimensionless relative sorting coefficients (QH) have been calculated from the standard deviation (second moment) after the method of Flemming (1977). Both relative and standard sorting coefficients are tabulated in Appendix B7. The relative sorting variability of the sea floor sand fraction is illustrated by an isopleth map (Fig.8.24b). Relative sorting values at individual stations range from a minimum of 1,68 (very well-sorted) to a maximum of 4,72 (moderately-sorted).

Best sorting is associated with the major terrigenous depocentre (south Tugela Cone). In this province, mixing of hydraulically-distinct populations (terrigenous and pelagic) is

minimised and thus the sand fraction is well to very well-sorted. The sand fraction is also relatively well-sorted in the subsidiary terrigenous depocentre over the lower 29° 25'S Canyon.

Poorest relative sorting coefficients are registered within the uppermost slope of the south Tugela Cone where the presence of a coarse biogenic fraction within the fine terrigenous sands greatly influences the sorting parameter. Moderate sorting characterises sediments of the SE and east Tugela Cone lower flanks. In these relatively stagnant zones, depleted influx of terrigenous clastics are admixed with the hydraulically-distinct pelagic fall-out to reduce the level of sorting.

Over the remainder of the Tugela Cone, basin plain and Central Terrace, sands may be classified as well-sorted. However, in scour zones such as the Central Terrace crest, sorting is unexpectedly poorer than in the major terrigenous depocentre. Although scouring must remove a high proportion of the very fine sand, winnowing is obviously insufficient to significantly improve the sorting coefficient.

Skewness

The regional variation in the skewness measure of the sand fraction is illustrated in Figure 8.25. Sand fractions at individual stations range from strongly positive skewed (+0,6) to strongly negative skewed (-0,59), and may be divided into two skewness provinces. A major proportion of the deep water zones (Central Terrace, basin plain and the NE Tugela Cone) are positively skewed. Towards the south, central and upper slope zones of the Tugela Cone, the size-frequency distribution asymmetry progressively changes and the sand fraction becomes negatively skewed.

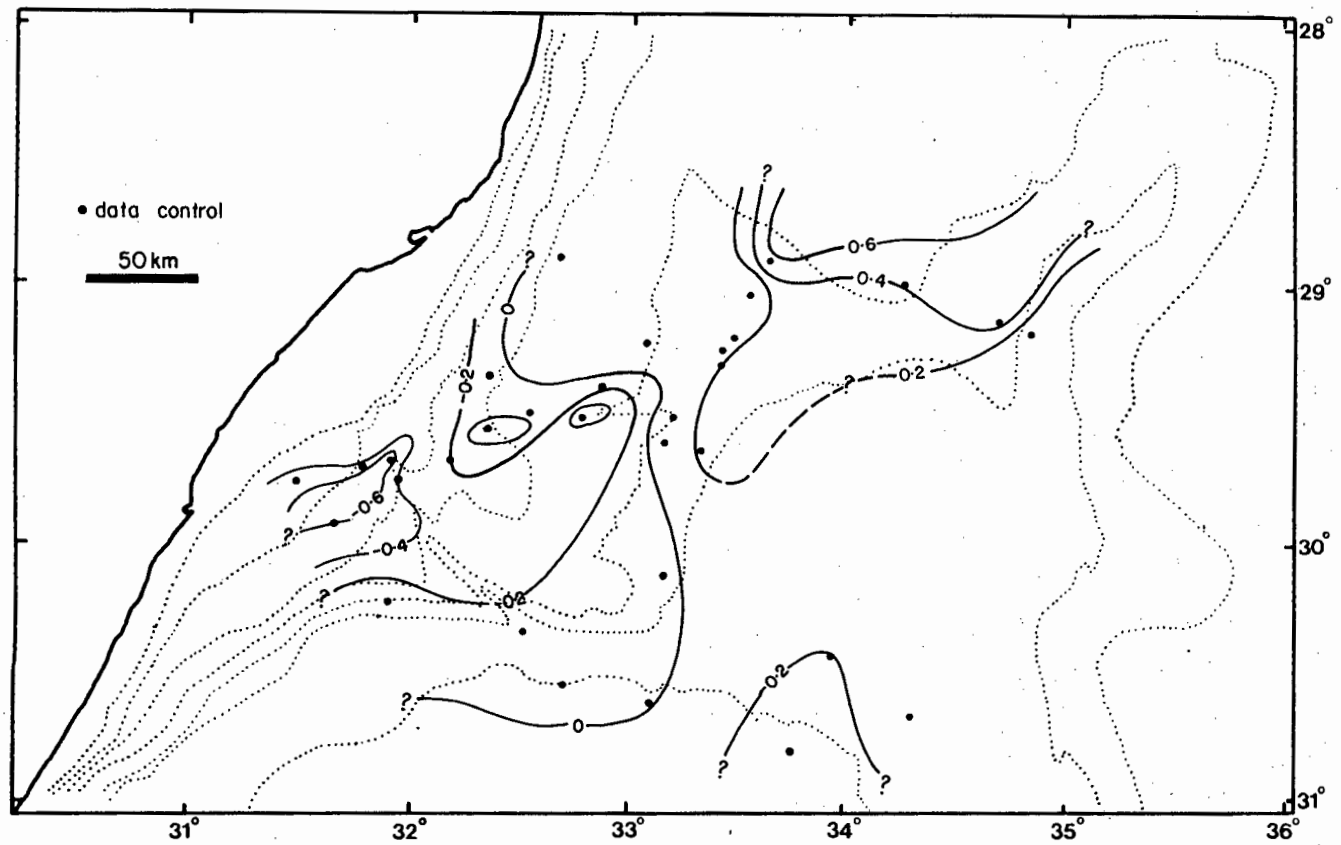

Fig. 8.25 SKEWNESS – SAND FRACTION

Skewness of size-frequency distributions is recognised as a useful tool in characterising sedimentary environments (Valia and Cameron, 1977; Huang and Watkins, 1977) but several, often contradictory interpretations of skewness response have been published (see Valia and Cameron, 1977 for brief review). In addition, Friedman (1967) has cautioned on the unpredictable nature of grain-size distribution parameters within polymodal sediments such as those of the Natal Valley.

Skewness relationships may be satisfactorily explained in terms of variable mixing of distinct hydraulic populations. The two prime populations have previously been described as a very fine terrigenous population and a fine to medium-grained biogenic population. Over the southern Tugela Cone, the terrigenous population predominates and thus the size-frequency distribution is negatively skewed. Strongest negative skewness correlates to the upper slope (core 34) resulting from the presence of a coarse tail to the size-frequency distribution. In contrast, positive skewness over deep water zones suggests dominance of the pelagic population as corroborated by the high % $CaCO_3$ in the sand fraction (Fig.8.4a). Strongest positive skewness over the Central Terrace is related to current scour since foram test breakage will continuously generate a fine tail in the sand fraction.

Near-zero skewness indicates a symmetrical size-frequency distribution or approximately-equal mix of the two populations. Over the eastern Tugela Cone, balanced input of terrigenous and pelagic material has resulted in a symmetrical size-frequency distribution with near-zero skewness (Fig.8.25).

8.5.3.3 Sand Fraction Groups

Construction of bivariate scatter plots for a full range of sedimentological parameters has provided graphical confirmation that there is a fundamental geographic control over sediment type. Depocentre geography and sea floor physiography must exert a significant influence on the depositional processes and responses and thus sediment type (Taira and Scholle, 1979b). The scatter plots verify that sediments from any one distinct province show similar recognisable characteristics. This premise has already been crudely outlined by definition of the gross textural provinces (section 8.5.2.5). However, utilisation of the sand fraction in isolation provides the basis for a more refined grouping.

With the aid of a full suite of bivariate plots (Figs.8.26 and 8.27 for eight examples) but using the sand % $CaCO_3$ versus mean (Fig.8.26a) as the principal instrument, at least seven distinct groups (A-G) may be discerned. This grouping system concerns the hydraulic sand fraction alone and discounts any reference to the mud fraction. Integration with mud fraction data to provide an overall lithofacies classification is reserved for section 8.6. Pertinent data relating to the cores categorised in each group are summarised in Table 8.6, while the areal extent of each group is shown in Figure 8.28. The five parameters listed in Table 8.6 are sufficient to individually define the seven groups although several samples do not conform to the grouping system either in the scatter plots (Figs.8.26 and 8.27) or the location map (Fig.8.28). In general, however, the seven groups are consistently apparent in the separate bivariate

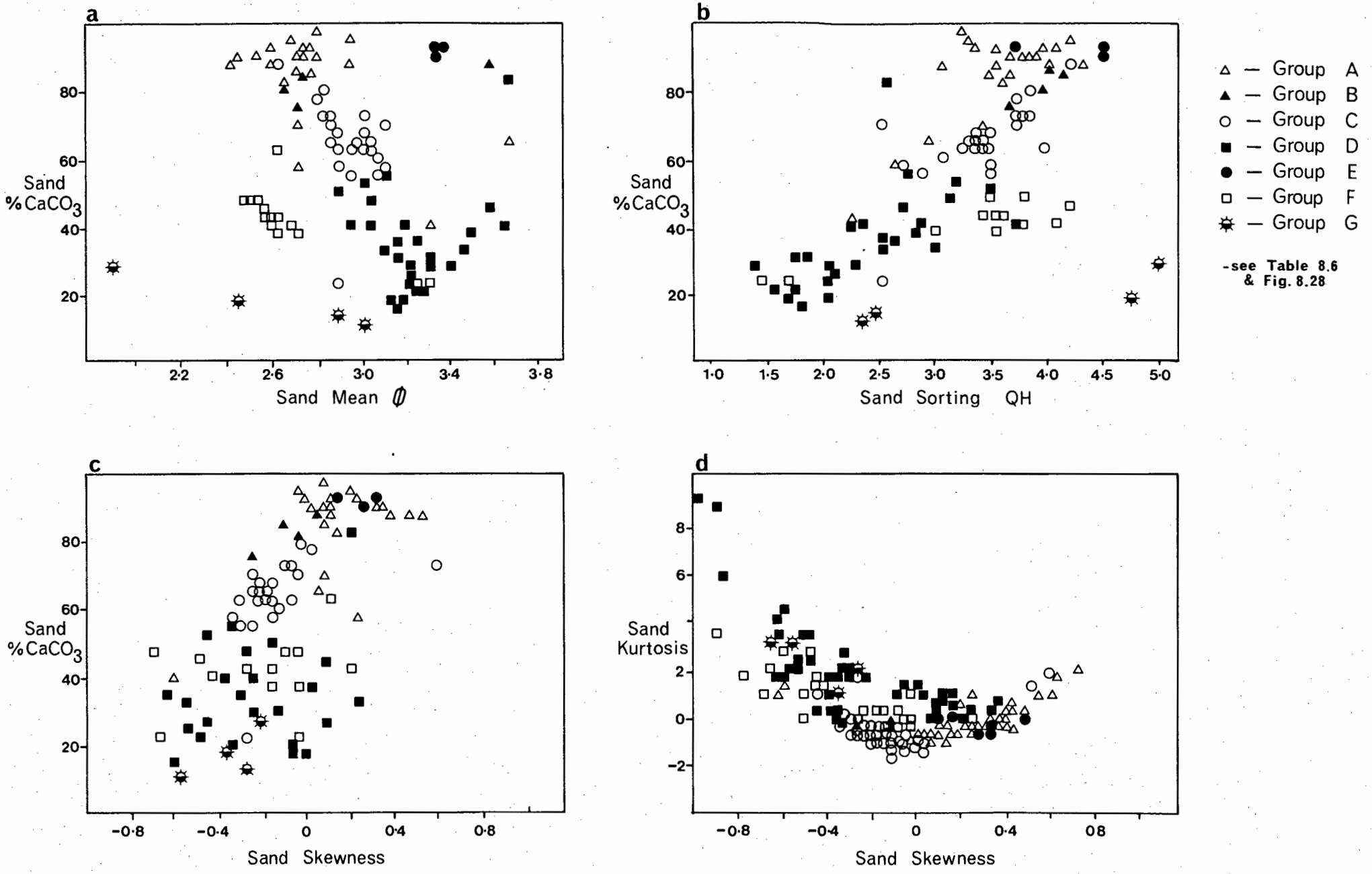

Fig. 8.26 BIVARIATE PLOTS OF KEY GRAIN-SIZE AND CHEMICAL PARAMETERS

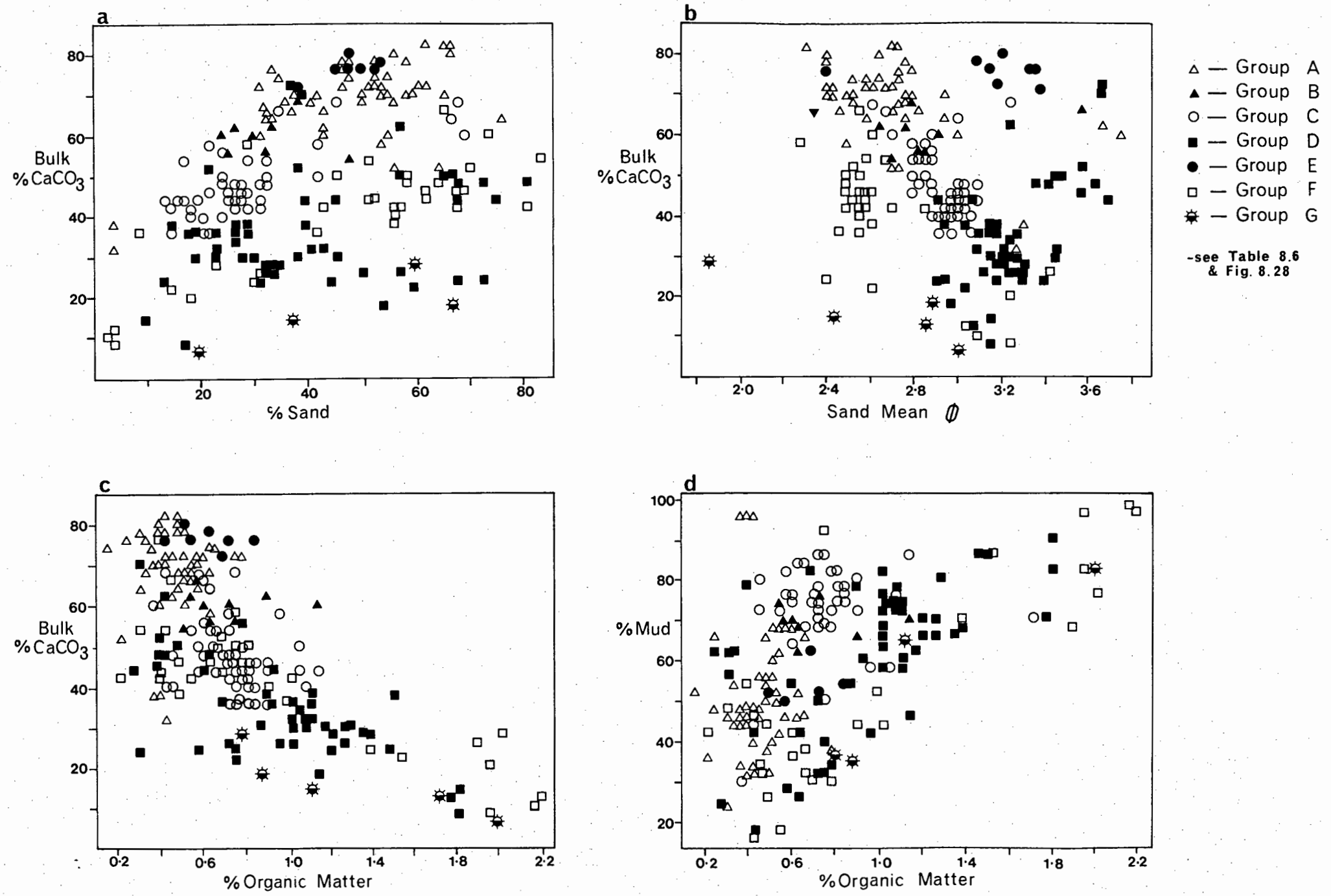

Fig. 8.27 BIVARIATE PLOTS OF KEY GRAIN-SIZE AND CHEMICAL PARAMETERS

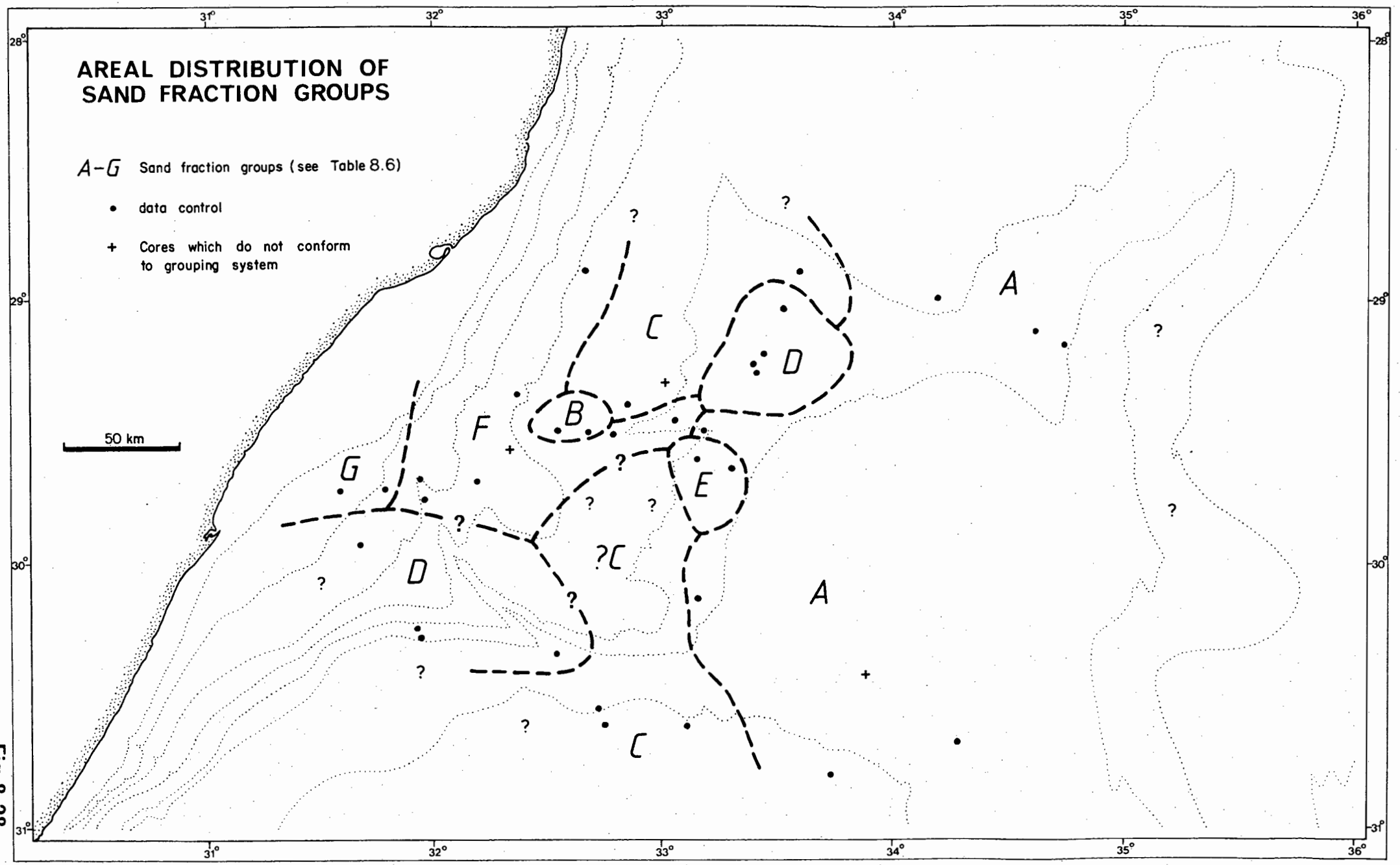
AREAL DISTRIBUTION OF SAND FRACTION GROUPS
A–G Sand fraction groups (see Table 8.6)
• data control
+ Cores which do not conform to grouping system
50 km
31°
32°
33°
34°
35°
36°
28°
29°
30°
31°
A
B
C
D
E
F
G
?C

Fig. 8.28

Table 8.6 Sand Fraction Groups (Hydraulic and Chemical Parameters)

GROUP	CORES	%$CaCO_3$	%ORG[1] MATTER	MEAN (ϕ)	RELATIVE SORTING(QH)	SKEWNESS	PRINCIPAL[+] COMPONENTS
A	1,4,5,9,20,27 5124,5127,5751	80-100	0,15-0,65	2,4-2,9	3,2-4,2	0,0 to +0,6	P>>T
B	25,26	80-87	0,5-0,65	2,6-2,75	3,7-4,2	-0,3 to 0,0	P>>T
C	12,23,5121,5753	55-75	0,45-0,9	2,8-3,1	3,0-3,9	-0,3 to 0,0	P>T
D	13-16,5115-5117,5119,5120	15-50	0,3-1,8	2,9-3,45	1,5-3,0	-0,6 to +0,1	T>or=P
E	18,19	90-95	0,45-0,8	3,3-3,45	4,3-4,5	+0,1 to +0,3	P>>T
F	21,24,29-31 5752,5726,5727	35-50	0,2-2,0	2,4-2,7	3,4-4,2	-0,2 to +0,2	T>P
G	32,34	10-30	0,9-1,95	1,85-3,0	2,4-5,0	-0,6 to -0,2	T>>P

1 - % organic matter (C_{org} x 1,82) in bulk sediment

\+ - principal components (see Appendix B10);
T = terrigenous (quartz, feldspar, heavy and opaque minerals)
P = pelagic (whole and broken planktic foram tests)

plots suggesting that the system is indeed valid. Recognition of these groups as responses to sedimentary environmental conditions is basic to the understanding of processes of hydraulic mixing and as such will be discussed in the following section.

8.5.3.4 A Model Approach to Textural Response

The interaction of environmental conditions and the sediment during transport is reflected in the resultant size distribution parameters. Graphic display of these parameters provides a tool to facilitate rationalisation of the overall system. Bivariate plots of mean diameter against skewness, mean diameter versus sorting and sorting versus skewness for all data points have been constructed as Figures 8.29a, 8.29b and 8.30 respectively. These three two-dimensional plots combine to represent the overall system in three-dimensional form. However, complexity of the sedimentary regime with several inter-mixed populations masks any obvious three-dimensional trend. This model does no more than verify that the grouping system (Table 8.6) is valid with good definition of most of the seven groups. Nevertheless, by selecting discrete physiographic provinces (southern Tugela Cone and adjacent deep basin) in which sediment mixing is suspected, application of this method yields conclusive results.

Sediment Mixing

In recent years, size distribution phenomena in a wide variety of environmental settings have been explained in terms of sediment mixing (Flemming, 1977; Bein and Sass, 1978; Taira and Scholle, 1979a; Walton et al, 1980). Strict control over textural response is typically maintained during mixing of two

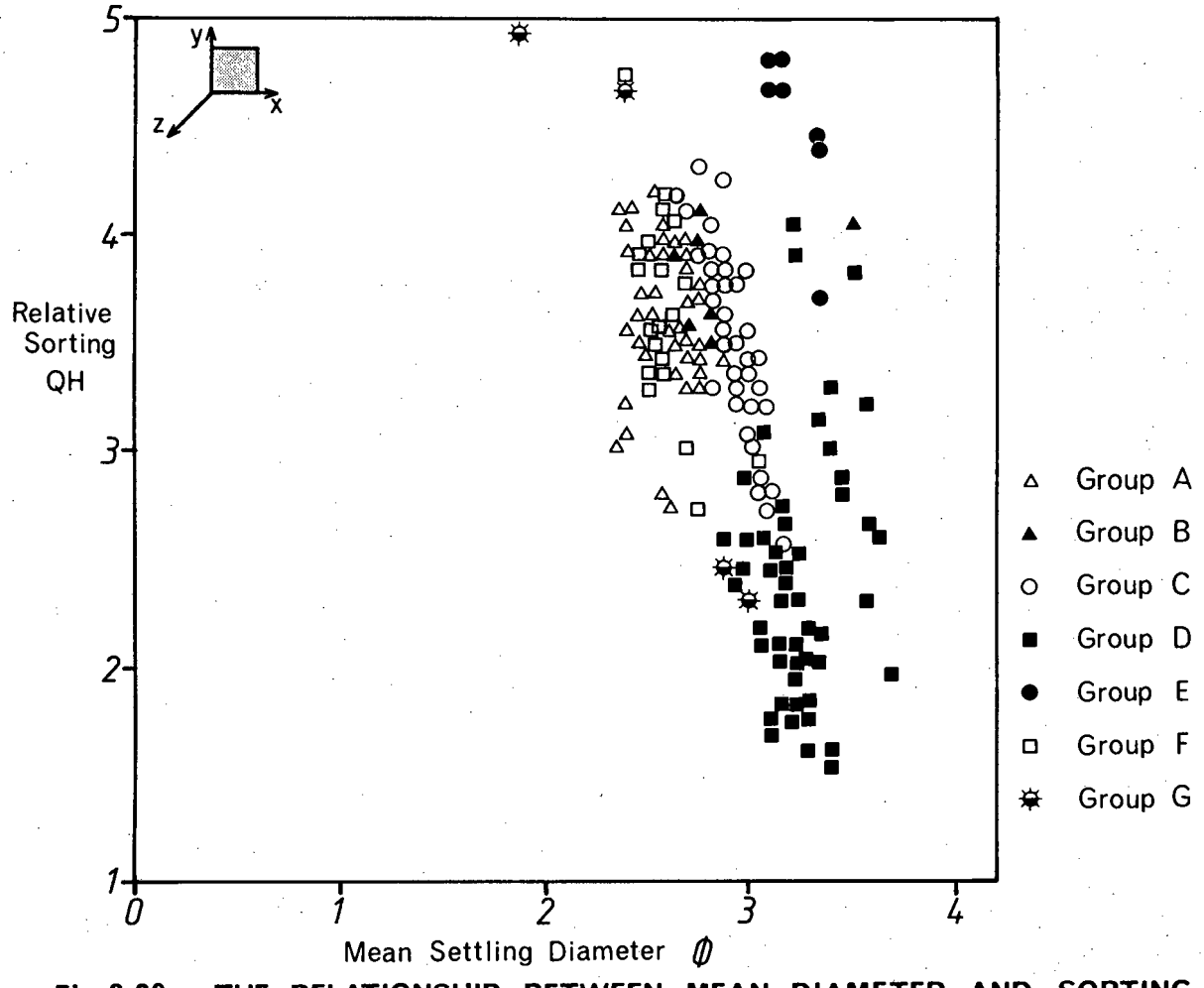

Fig.8.29a THE RELATIONSHIP BETWEEN MEAN DIAMETER AND SORTING

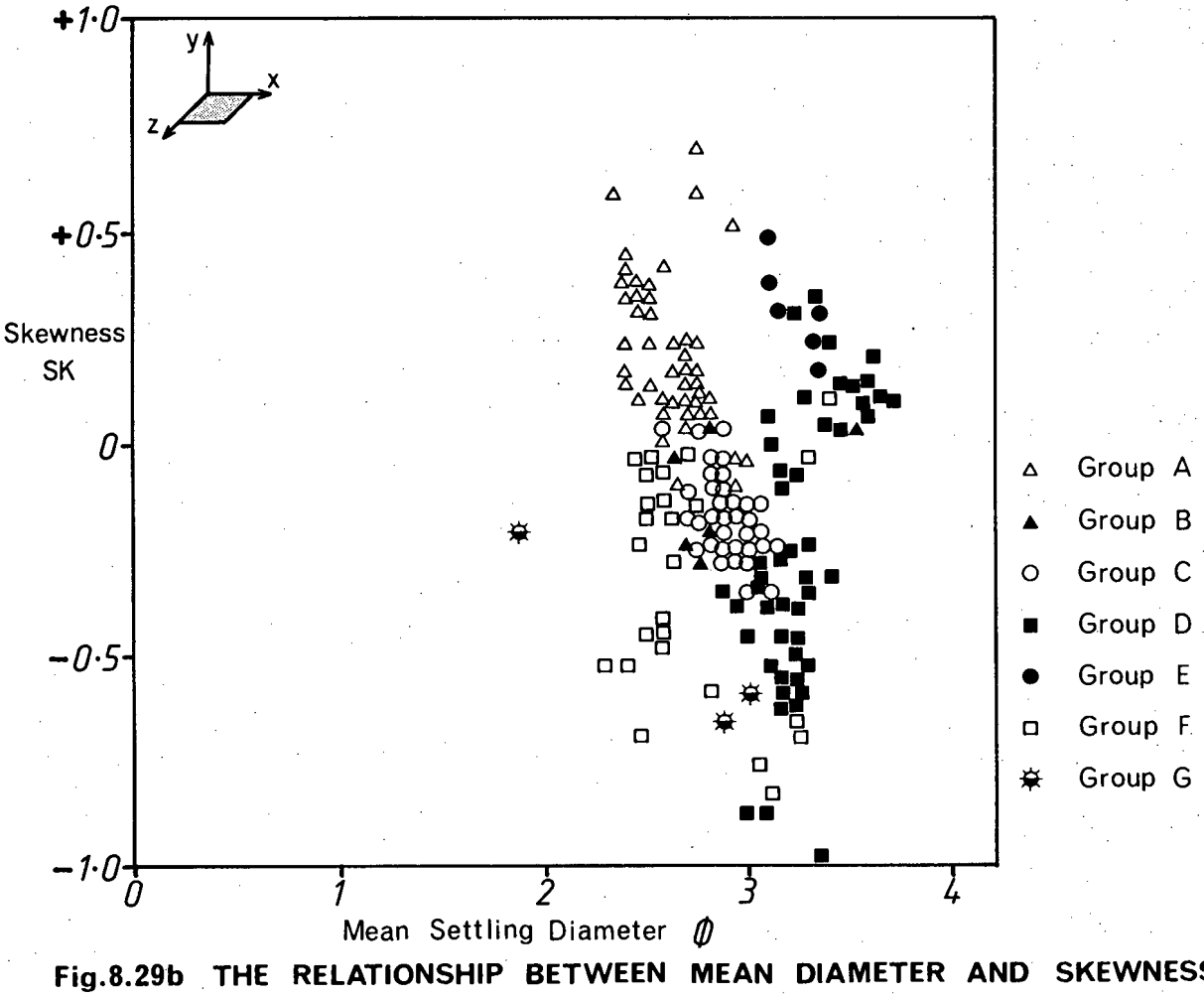

Fig.8.29b THE RELATIONSHIP BETWEEN MEAN DIAMETER AND SKEWNESS

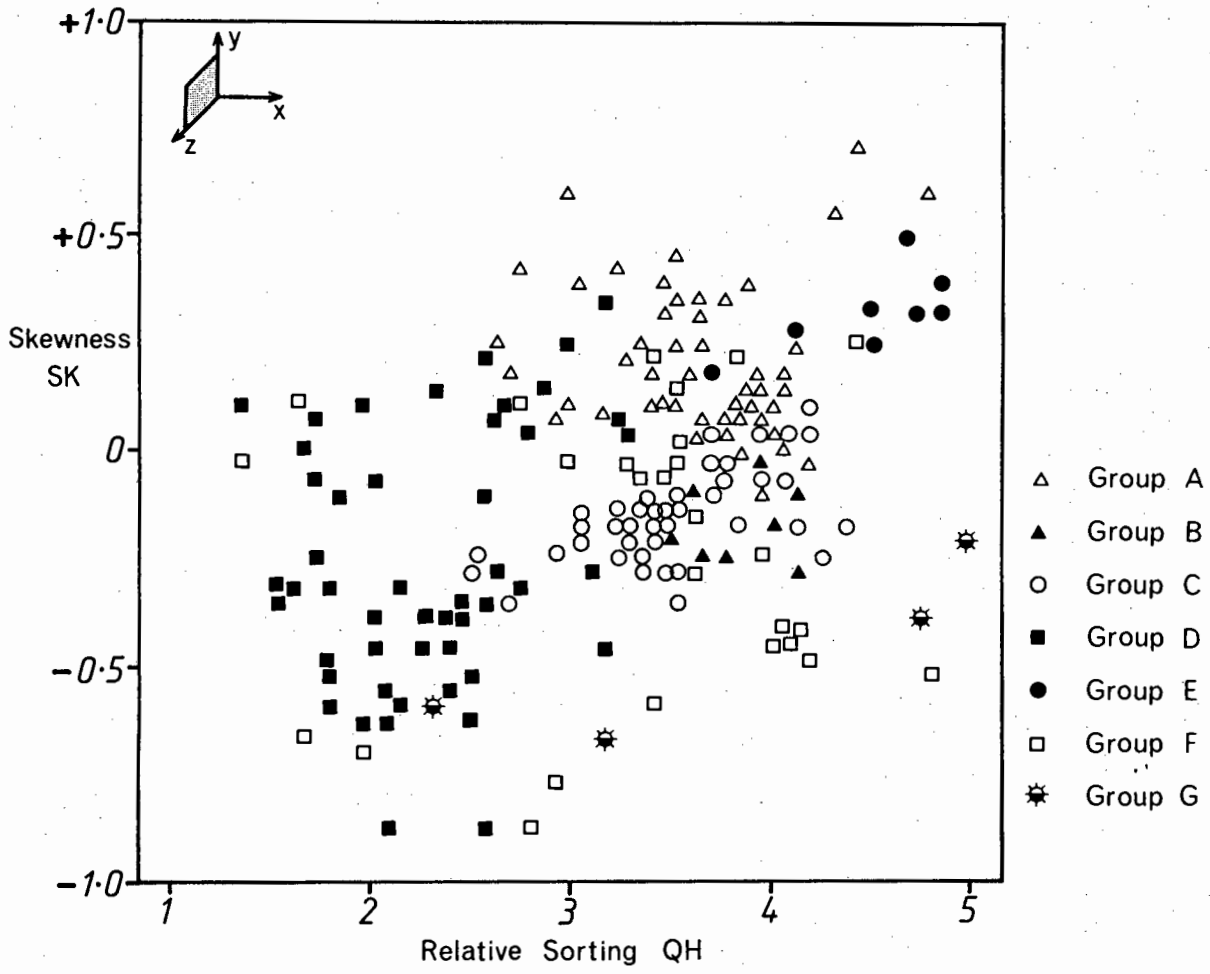

Fig.8.30 THE RELATIONSHIP BETWEEN SORTING AND SKEWNESS

lognormal populations of different mean size. In the Natal Valley, spatial relationships of sorting, skewness and grouping between adjacent provinces are best explained in terms of progressive mixing of distinct hydraulic populations.

In simplistic form, the relationship between mean diameter, sorting and skewness during the mixing process is illustrated in Figure 8.31 after Flemming (1977). As the degree of mixing increases, the relative sorting index (QH) progressively decreases reaching a low when the populations are equally mixed. In parallel, as mixing progresses the finer population initially becomes negatively skewed while the coarser population develops positive skewness. The distribution re-achieves symmetry at the point of equal mixing (Flemming, 1977).

The same relationship may be displayed in three-dimensional form (Fig.8.32). In this model, a regression line through the point cluster describes a helix with the central axis paralleling the mean diameter coordinate (X - axis). By projecting the helix perpendicularly on to the three axial planes, the three-dimensional plot may be displayed as three two-dimensional images (Fig.8.32): (1) mean diameter versus skewness (XZ plane); (2) mean diameter versus sorting (XY plane); and (3) sorting versus skewness (YZ plane).

Attempts to model sedimentation dynamics by this model fail in most physiographic regions of the Natal Valley because data control is insufficient. However, applicability of the model may be checked in a terrigenous detritus dispersal route with reasonable sample control. On this consideration, the south Tugela Cone and adjacent basin plain was selected as a potential mixing zone on which to test the model.

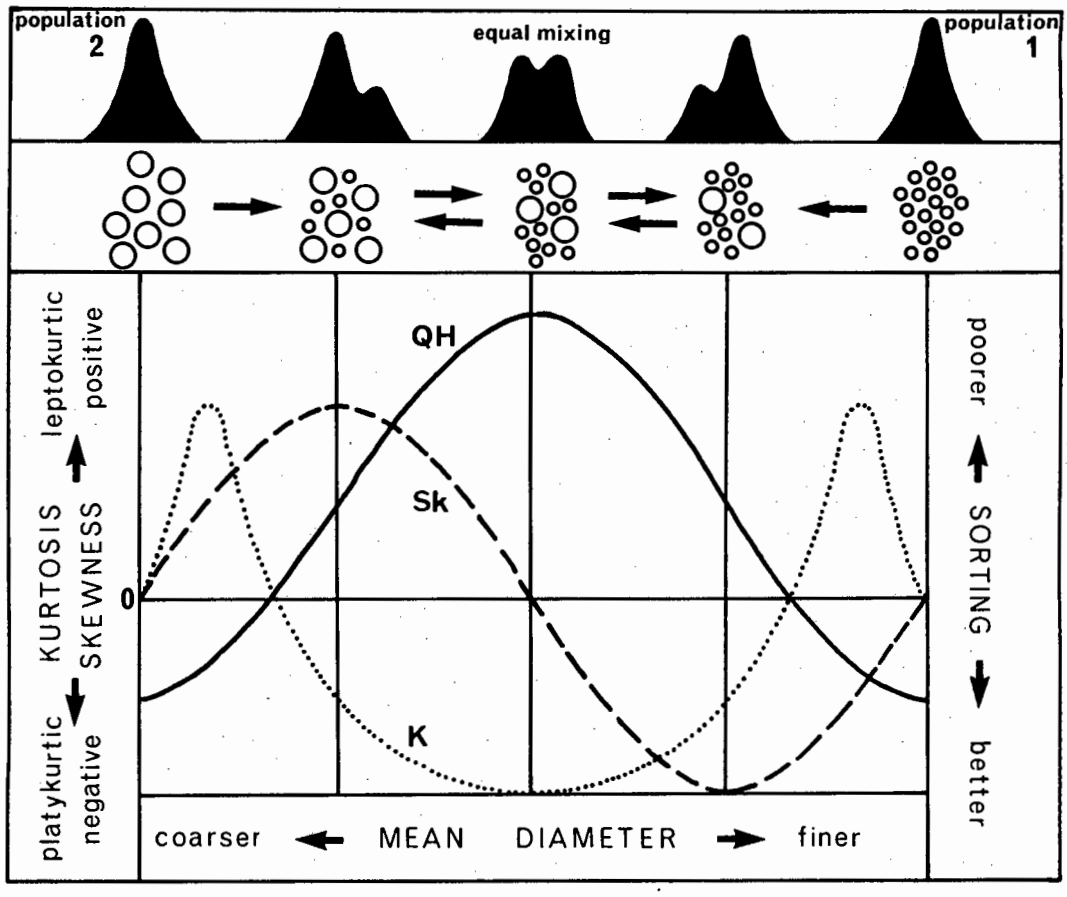

Fig.8.31 THE RELATIONSHIP BETWEEN TEXTURAL PARAMETERS IN PROGRESSIVELY MIXING LOGNORMAL POPULATIONS

after Flemming (1977)

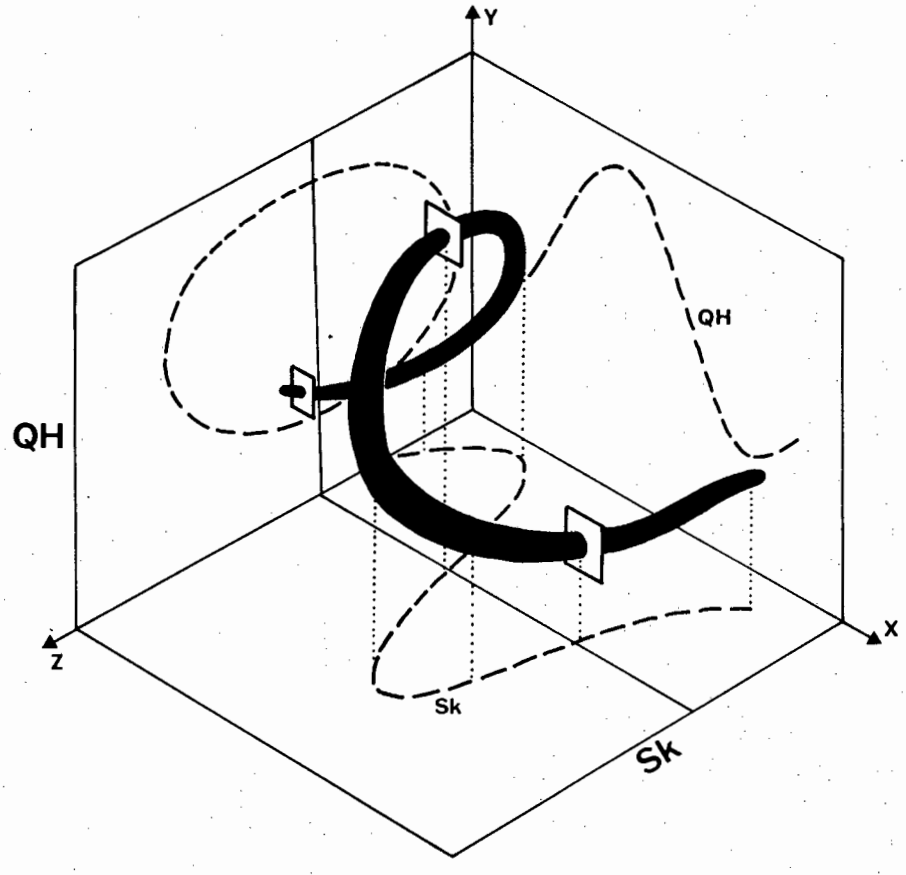

Fig.8.32 THE SAME RELATIONSHIP IN 3-D FORM

after Folk and Ward (1957)

Quick-look sedimentological parameters indicate that sediment mixing is probably active over this zone based on the following:

(1) The areal distribution of sand fraction groups suggest that groups D and A may be mixed to form group C (Fig.8.28);

(2) Bivariate plots of several parameters (Figs.8.26 and 8.27) show group C sediments to be positioned intermediate to groups A and D suggesting a mixed derivation;

(3) Component data (Appendix B10) likewise implies that group C sediments (cores 5121 and 5753) are mixtures of pelagic group A sediments (cores 1 and 5751) and terrigenous group D sediments (cores 5115 and 5119).

(4) Size-frequency distributions of the sand fraction for groups A, D and C are displayed in Figure 8.33. The principal mode of group D (terrigenous) sands approximates to 3,1ϕ. In contrast, although group A may be locally bimodal, the principal settling diameter mode is close to 2ϕ. Group C sediments are strongly bimodal with main modes at 2ϕ and 3,1ϕ demonstrating a mixed source from group A and D parent populations. The size-frequency distributions plotted in Figure 8.33 also illustrate the concept of progressive mixing. With distance from the hinterland, the 3,1ϕ mode (terrigenous) progressively decreases to become minimal in group A sands. In reciprocal, the 2ϕ mode (pelagic) assumes prominence seawards after first becoming conspicuous in core 5119 (Fig.8.33).

The foregoing interpretation that population mixing is operative over the southern Tugela Cone and adjacent deep basin relies entirely on spatial relationships between grain-size parameters. It is necessary to view the data graphically in the

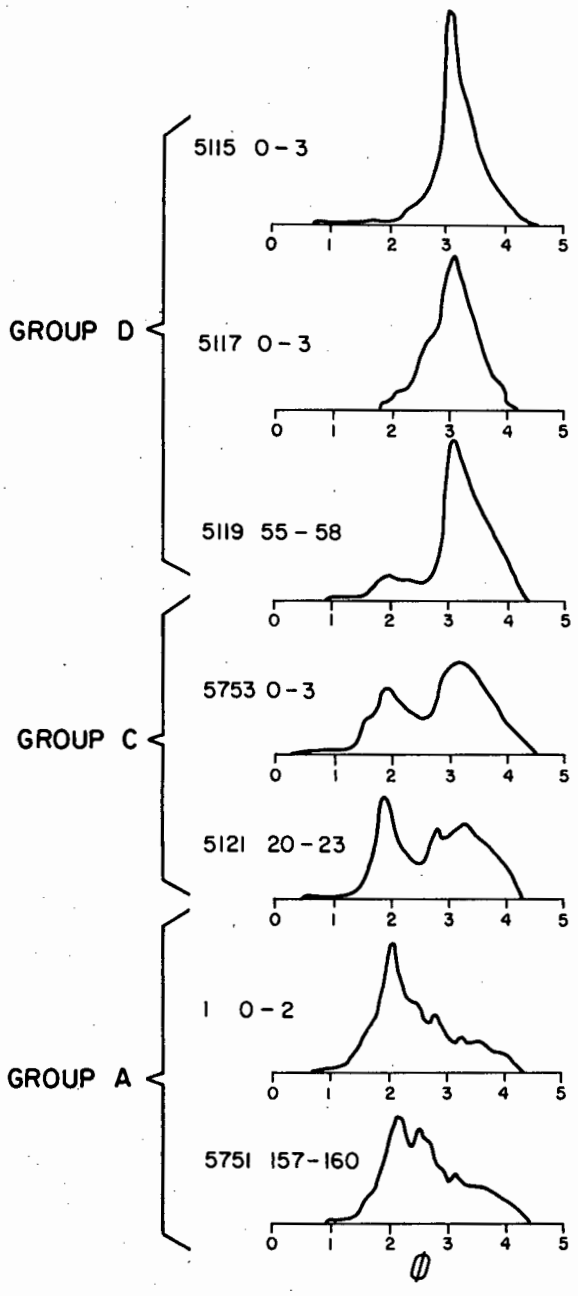

$\%CaCO_3$ = 14.3 ; QH = 1.79 ; SK = -0.59

$\%CaCO_3$ = 30.0 ; QH = 1.83 ; SK = -0.11

$\%CaCO_3$ = 39.2 ; QH = 2.29 ; SK = -0.37

$\%CaCO_3$ = 61.7 ; QH = 3.95 ; SK = -0.07

$\%CaCO_3$ = 79.5 ; QH = 3.84 ; SK = -0.02

$\%CaCO_3$ = 89.2 ; QH = 3.78 ; SK = 0.34

$\%CaCO_3$ = 91.3 ; QH = 3.53 ; SK = 0.24

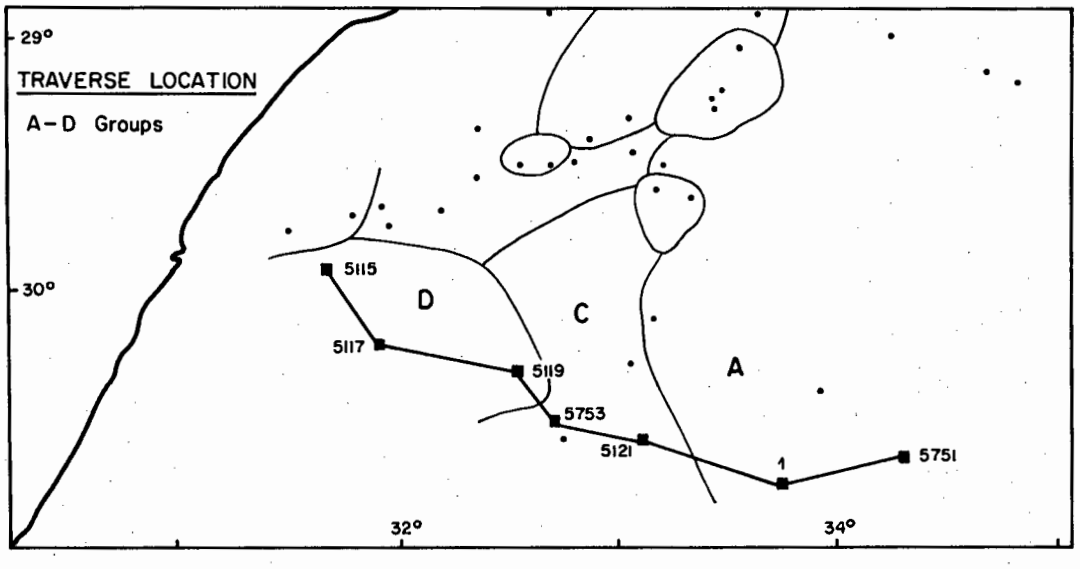

Fig. 8.33 SIZE - FREQUENCY DISTRIBUTIONS THROUGH MIXING ZONE

form of scatter plots to provide support for the interpretation. The three scatter plots presented in Figures 8.34 and 8.35 are reduced versions of Figures 8.29 and 8.30 only containing information from groups A, C and D.

The relationship between mean diameter and relative sorting is investigated in Figure 8.34a. There is clear distinction of the two hydraulic end-member populations (groups A and D) in accord with the size distribution patterns. Progressive mixing is illustrated by the upward-converging arms of the point cluster. Mixing culminates in group C sands characterised by decreased levels of sorting and an intermediate mean diameter. As mixing progresses, the finer terrigenous population (group D) decreases rapidly in sorting while becoming coarser. In parallel, the coarser biogenic population (group A) gradually fines on mixing but there is little change in the level of relative sorting. This suggests that the group A parent population is not log-normal and may already be a product of mixing or winnowing unrecognisable in the scope of this study. In group C, the degree of mixing is such that the original size characteristics of the parent populations (particularly group D) are almost entirely obscured.

In Figure 8.34b, the groups A, D and C point cluster is projected on to the mean diameter - skewness plane. Group D sands are generally negative-skewed and very fine-grained while the group A sediments are positive-skewed and fine-grained. Mixing of these oppositely-skewed parent populations produces a symmetrical (near-zero skewness) bimodal population with an intermediate mean diameter (group C). This bivariate plot illustrates a three-dimensional point configuration stretched out

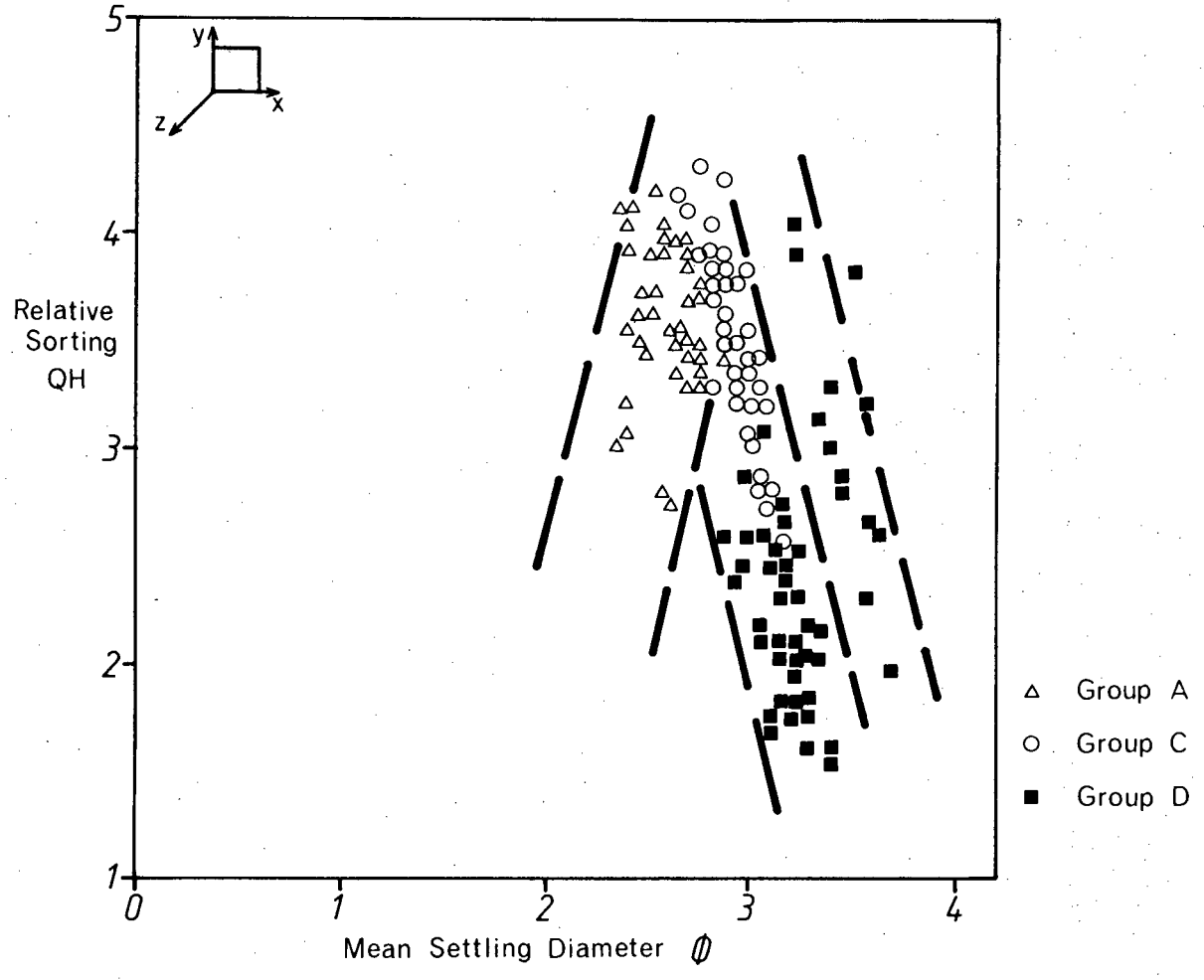

Fig.8.34a MEAN DIAMETER VERSUS SORTING (MIXING ZONE)

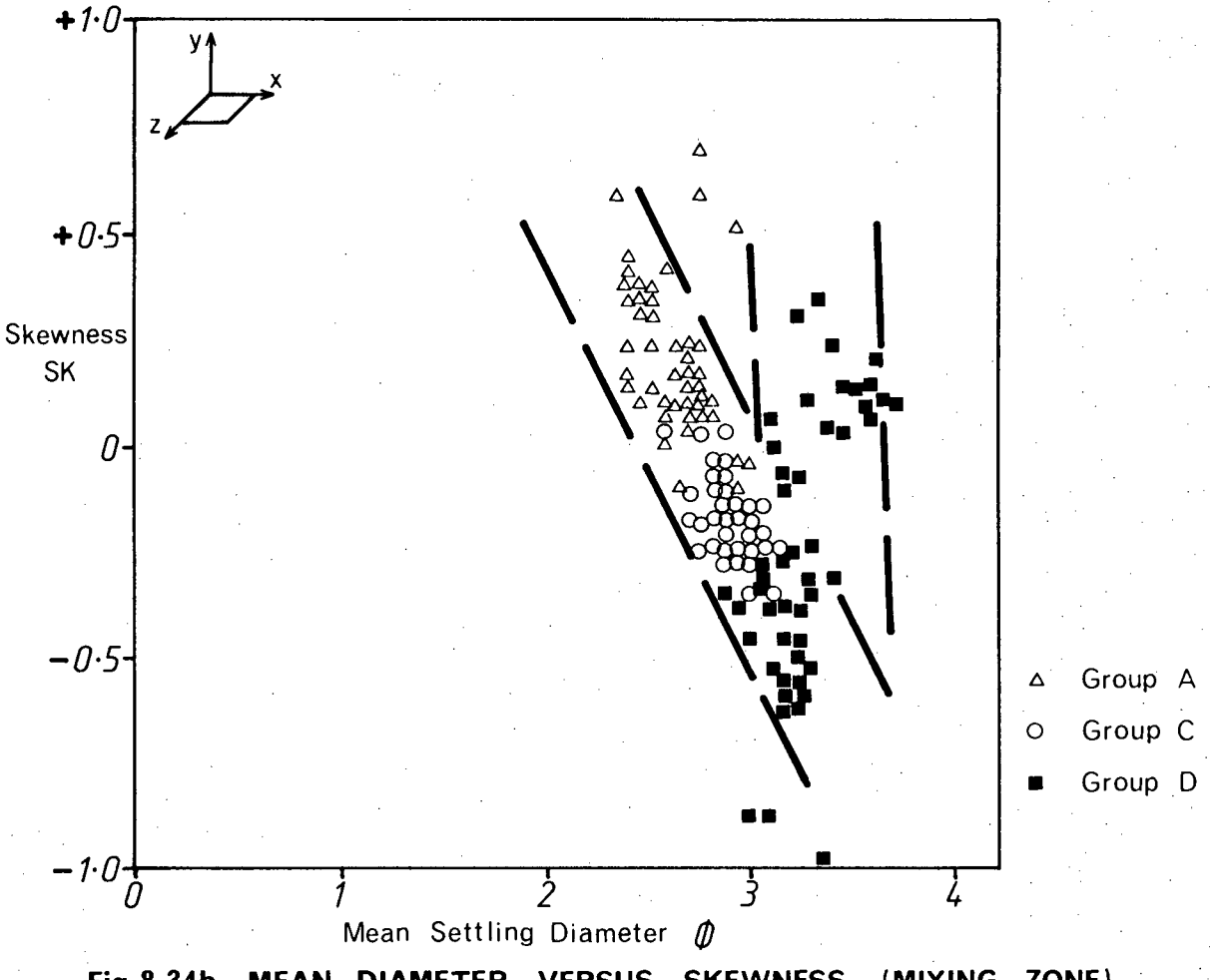

Fig.8.34b MEAN DIAMETER VERSUS SKEWNESS (MIXING ZONE)

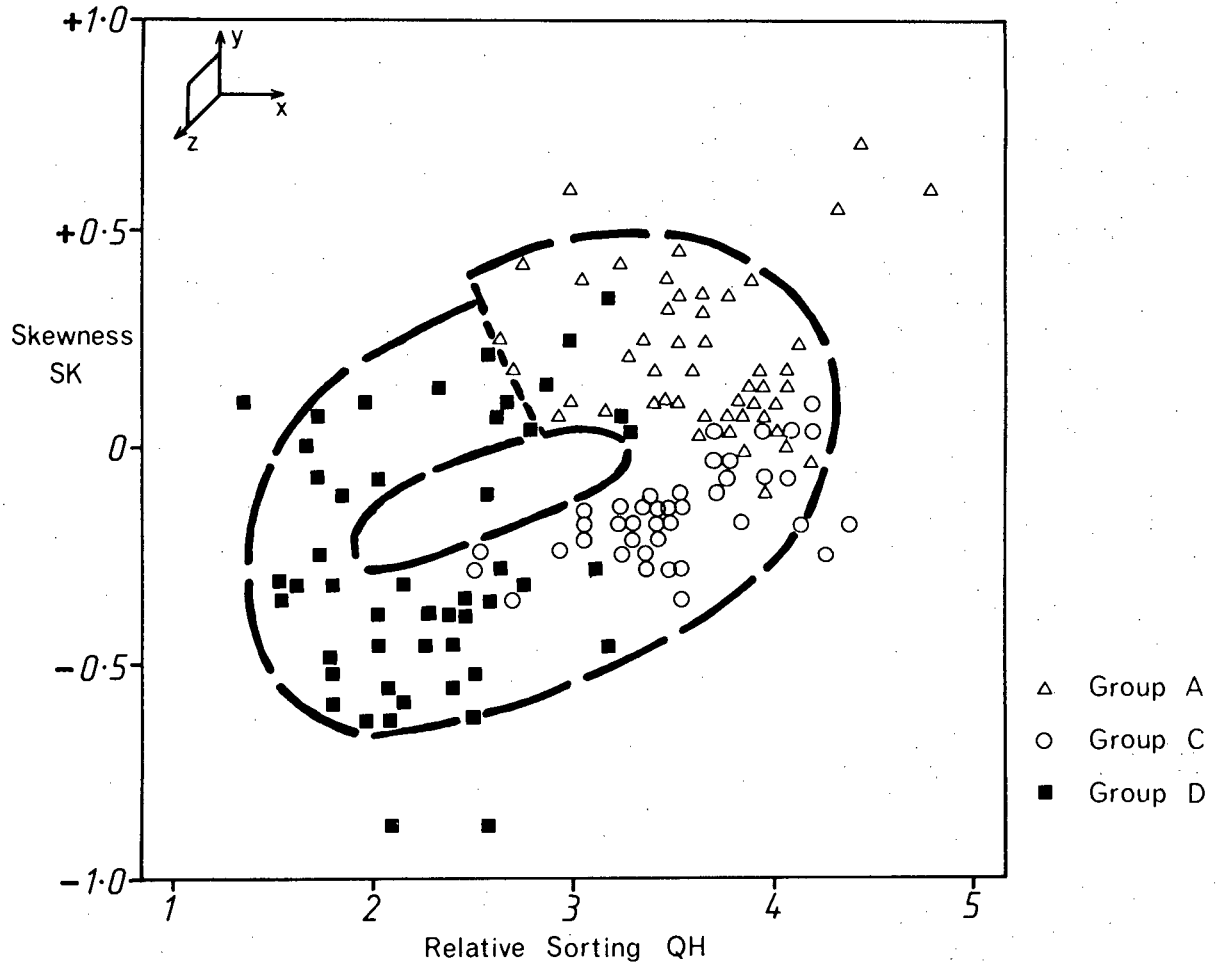

Fig.8.35 SORTING VERSUS SKEWNESS (MIXING ZONE)

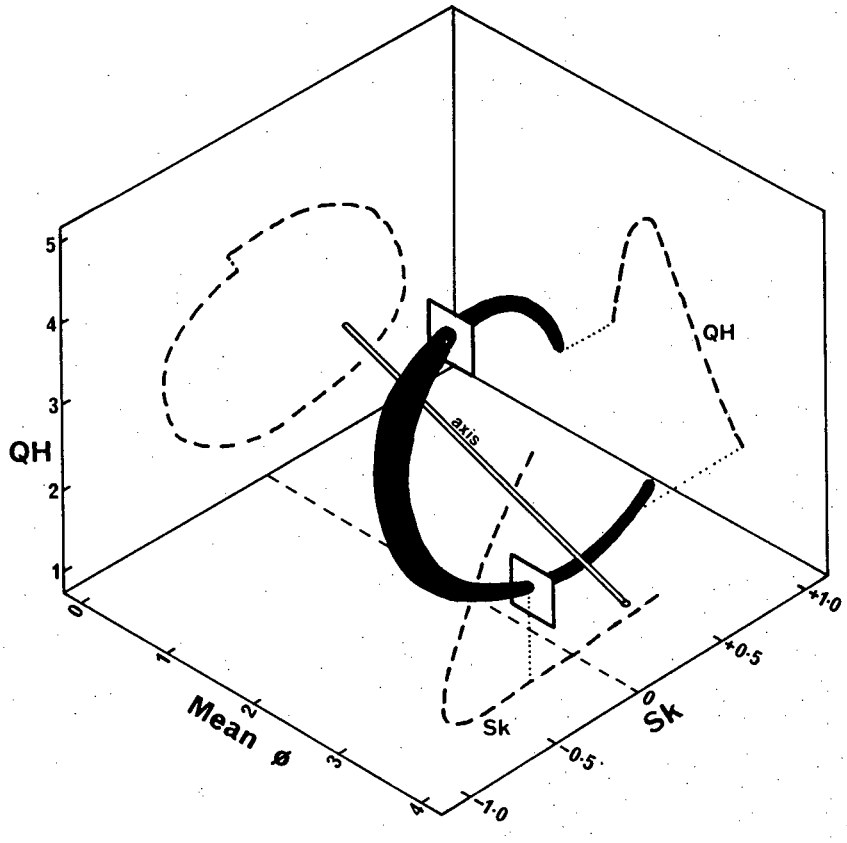

Fig.8.36 HELICAL 3-D RELATIONSHIP BETWEEN TEXTURAL PARAMETERS (MIXING ZONE)

in a helical structure similar to that described by Folk and Ward (1957) - see Figures 8.31 and 8.32. Unlike the model case, however, the axial trend of the helix is not aligned parallel to the mean diameter coordinate but is inclined at an oblique angle. Non-log-normality of the parent populations (Fig.8.33) offers the most likely explanation for this deviation from the idealised model (Flemming, 1977).

The relationship between relative sorting and skewness is presented in Figure 8.35. The helix model of Folk and Ward (1957) predicts that data projected onto this plane should generate a circular point distribution with a central void. The system outlined in Figure 8.35 is more ellipsoidal and the void is displaced to the left-central demonstrating that the helix axial trend does not parallel the mean diameter coordinate. This obliqueness effectively obscures the overall trend since, in the two-dimensional projections, successive sections of the helix tend to overlap.

The idealised helix described by the three two-dimensional plots (Figs.8.34 and 8.35) has been sketched in Figure 8.36 to show its general position and orientation. Poor definition of parts of the helix, particularly in the coarser biogenic-rich arm, is explained through inadequate sample control over the basin plain. The preceding graphical analysis of mean diameter, relative sorting and skewness trends reinforces the quick-look interpretation using sedimentological parameters and thus confirms that progressive mixing is operative over the southern Tugela Cone and adjacent basin plain.

After discussion of textural distributions and mixing

models, the natural progression should be the consideration of modes of sediment transport with aims to categorize energy levels at the time of deposition. Studies of this type were introduced by Passega (1957) who, by cross-plotting the coarsest 1% of the size-frequency distribution against the median diameter, distinguished between several transport modes of varying competence. Validity of this approach was proven by Flemming (1977) who successfully modelled marine sediment transport in a coastal embayment using the Passega method.

Unfortunately, this approach is of limited use in the Natal Valley because the great majority of samples contain significant proportions of biogenic detritus not transported with the bulk sediment but rather deposited via a pelagic rain. Destructive leaching of large sample volumes to eliminate carbonates was rejected leading to a reduced data base. Data control was deemed insufficient to warrant presentation of a graphic plot of the first percentile against the mean. However, several terrigenous-dominant samples from the upper and southern Tugela Cone were plotted (raw data in Appendix B7) to judge future application of the method. Using terminology from Flemming (1977), it is generally observed that turbidites (cores 5115 and 5117) fall in the "graded suspension" mode of transport. In contrast, upper slope samples (cores 29, 30, 32 and 34) plot in the "saltation" and "traction" transport fields.

A greatly increased data base with sufficient sample to allow carbonate leaching is required before a meaningful basin-wide study of transport modes can be attempted.

8.5.4 Electronic Particle Size Analysis of the Silt Fraction

8.5.4.1 Introduction

Detailed particle size analysis of the fine fraction is of equal importance to the study of the sand fraction. This is particularly relevant in quiet sedimentary environments where the sand fraction may be severely depleted or show little local textural variation. Unfortunately, fine-grained sediments are least amenable to size analysis because of the great difficulty in preserving the naturally-occurring size distribution throughout sampling and analysis. Water-mud systems are dynamic with the degree of flocculation being governed by clay mineralogy, salinity, sediment concentration and fluid shear (Whitehouse et al, 1960). Physical conditions prevailing at the time of deposition cannot be estimated in the laboratory. The ultimate size distribution, obtained by maximum dispersion of the suspension using peptizing agents, provides little diagnostic value in the interpretation of sedimentary processes. It is therefore very difficult to achieve meaningful particle size analysis of mud fractions, particularly fine silt and clay.

A wide variety of operational methods have been designed to size-analyse fine-grained sediments (Swift et al, 1972). Of those methods available to this investigation, pipette analysis was considered to be too time-consuming to provide high resolution results. Instead, electronic analysis using a Coulter Counter TA II was adopted for routine use. Electronic particle counting is well-documented as a reliable fast technique for size analysis of fine sediments (Swift et al, 1972; Blaeser and Ledbetter, 1982). Particles suspended in a weak electrolyte are

sucked through an aperture of known diameter flanked by immersed electrodes. As particles pass through the aperture, electrolyte is displaced and a resistance change between the electrodes is registered. These resistance changes are converted to equivalent unit volumes (i.e. counts). Counts are accumulated in specific channels dependent on size thus providing a size-frequency distribution plot.

Size-frequency distribution plots for the very fine silt and clay grades may be easily obtained but whether the results can be meaningfully interpreted is open to doubt. Unlike the sand and coarse silt fractions, size analysis of finer sediments are influenced to an unknown extent by electrostatic charges, surface area, viscosity and flocculation. In view of the uncertainty in obtaining valid results it was decided to omit all size grades finer than 8 μm (7ϕ) from analysis. In doing so, operational procedures were greatly simplified since a one-tube analytical method could be used. Each analytical tube can effectively measure a particle size range from 2-40% of the tube-aperture diameter (Shideler, 1976b). The desired size range of 4-7ϕ (63-8 μm) was conveniently analysed using one tube with a 280 μm aperture. The system was calibrated to measure particle diameters between 4 and 7ϕ with a ten channel resolution, each channel representing a size increment of 0,33ϕ. However, electronic truncation at 8 μm in addition to sieve truncation at 63 μm introduces a major analytical artefact to the size distribution data. Accordingly, the calculation of statistical parameters was not attempted on the truncated populations. The primary tools remaining available for general discussion of silt-grade ditribution patterns are sub-fraction percentages.

A full review and criticism of electronic particle size analysis has been published by Swift et al (1972) and Shideler (1976b). Rigorous analytical technique is critical to achieving quality results and thus full details of methodology are provided in Appendix A16. Raw data are tabulated in Appendix B8 while size-frequency distribution curves are plotted down-core in Appendix B2.

8.5.4.2 Distribution of Silt Sub-Fractions

As with the sand fraction (section 8.5.3), silt is considered as an independent hydraulic population governed by unique processes. In evaluation of the silt fraction distribution patterns, concentrations of coarse silt (4-5ϕ), medium silt (5-6ϕ) and fine silt (6-7ϕ) have been normalised to 100%. The distribution of each of these sub-fractions is briefly outlined in this section.

Coarse Silt

The regional distribution of coarse silt is illustrated in Figure 8.37a. Highest concentrations are recorded along the upper continental slope as a direct result of dumping of terrigenous load (compare with Fig.8.15a) although winnowing may be locally operative. Down-slope onto the Tugela Cone, general reduction in concentration (locally <20%) reflects the regional energy gradient and diminished terrigenous supply. However, deviations from this general trend are noted in several areas.

In the south Tugela Cone terrigenous depocentre (Fig.8.15a), increased supply of clastic detritus is recognised by the persistence of coarse silt (>40%) to the middle slope zone. Likewise, in the lower Tugela Canyon, high concentrations

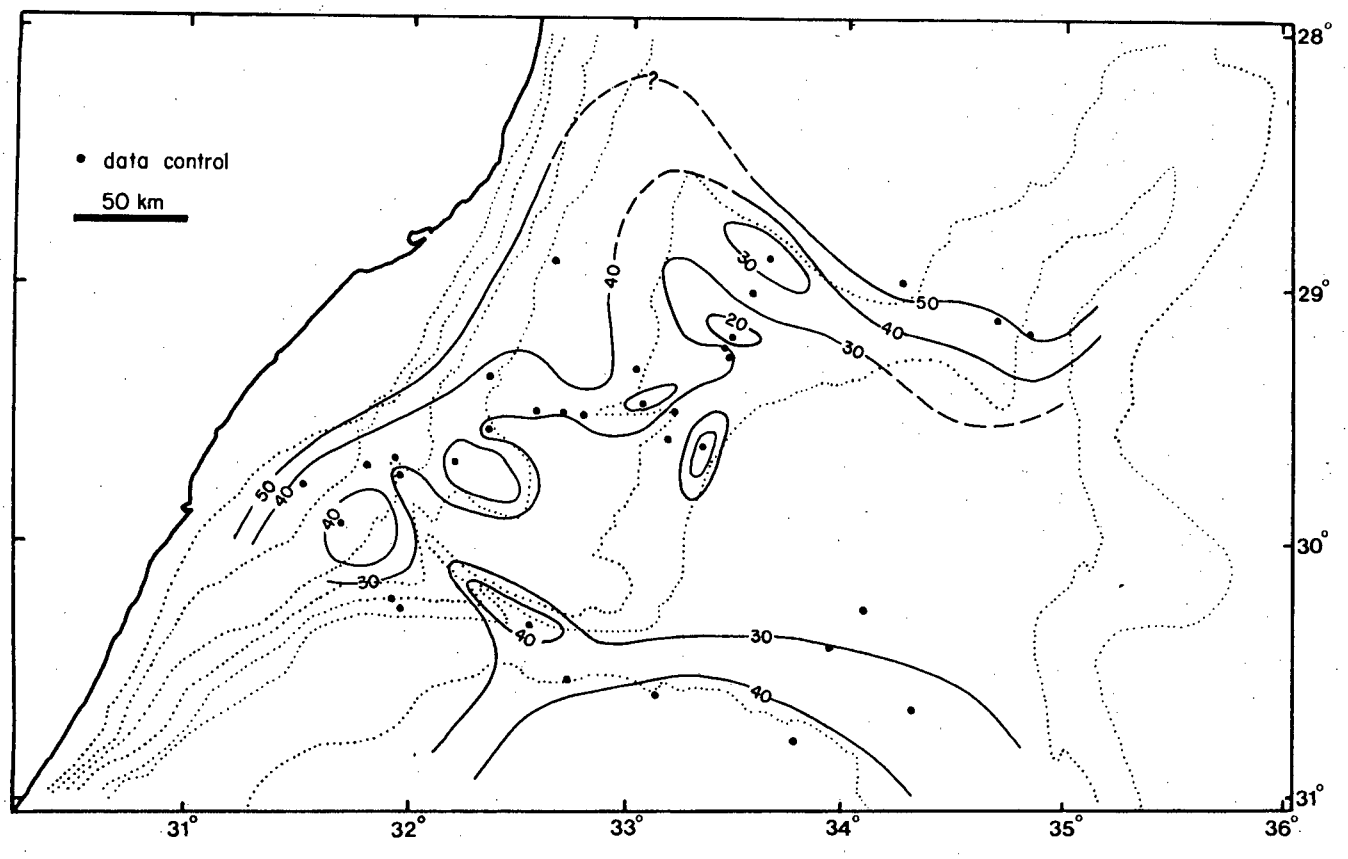

Fig. 8.37a % COARSE SILT

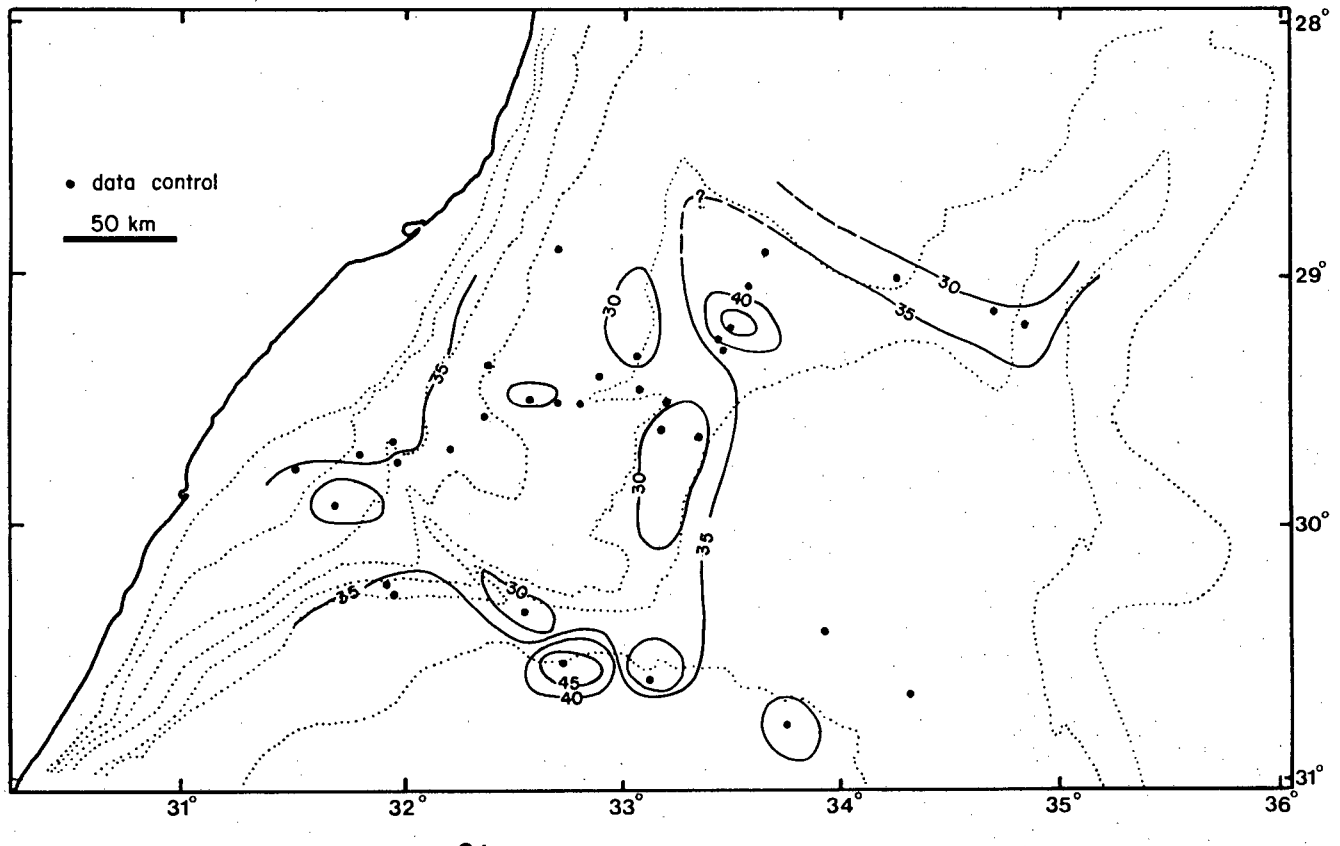

Fig. 8.37b % MEDIUM SILT

indicate that the canyon, at least periodically, funnels coarse silt detritus to the basin plain. Dumping of the coarse silt occurs immediately on encountering the flat basin plain.

Immediately north of the Tugela Canyon, coarse silt proportions >40% are recorded on the local terrace outlined by the 1500 m isobath. Likewise, the Central Terrace is dominated by coarse silt (>50%) relative to medium and fine silts, corroborating previous interpretations that these areas are current-scoured (section 7.2.2; Fig.7.2). The basin plain is characterised by intermediate amounts (30-40%) of coarse silt of both terrigenous and pelagic (juvenile forams) origin.

Medium Silt

Medium silts show little variation in concentration over the entire study area (Fig.8.37b). The upper Tugela Cone is characterised by a medium silt concentration of 35-40% decreasing to <30% over the lower slopes reflecting the regional depositional energy gradient. On the adjacent basin plain pelagic province, proportions rise to >35% in line with increased concentrations of $CaCO_3$ (Fig.8.4b and Table 8.4). This is a response to waning terrigenous influence and enhancement of the proportion of medium silt-size coccoliths (Table 8.4).

The Central Terrace shows mild depletion of medium silt (<30%) relative to the adjacent pelagic provinces. While coarse silt is concentrated by scouring in this area, medium silt is partially winnowed out to be deposited in slack water over the terrace flanks, locally in proportions >50% (Fig.8.37b).

Anomalies around the Tugela Canyon mouth suggest that medium silt concentrations are affected by down-canyon transport. In this area, medium silts are enriched down-slope of the coarser

silt (Figs.8.37a and b) perhaps as a result of sudden dumping of detritus on encountering the low gradient basin floor.

Fine Silt

The areal distribution of fine silt detritus is illustrated in Figure 8.38a and shows an almost reciprocal pattern to the coarse silt fraction. Highest proportions of fine silt (35-40%) characterise low energy environments which also receive significant fine terrigenous input (middle to lower slope of the Tugela Cone). The basin plain is primarily a pelagic province and receives abundant coccolith and juvenile foram input of medium-coarse silt grade. Accordingly, the fine silt proportion is relatively depleted (20-30%). Higher energy regions are fine silt-poor (<20%) irrespective of whether they are terrigenous-dominant (Tugela Cone upper slope) or pelagic-dominant (Central Terrace) provinces.

In summary, relative concentrations of the silt sub-fractions may be outlined as follows:

a) Coarse silts predominate over the upper continental slope and the Central Terrace crest; in the former area due to combination of terrigenous dumping and localised winnowing and in the latter area primarily because of current scouring.

b) Over the southern Tugela Cone a relative energy gradient is evident with coarse silt predominant over the top-of-slope grading to fine silt over the base-of-slope.

c) The basin plain and eastern Tugela Cone are approximately equi-proportional in coarse, medium and fine silt concentration although strong local variations adjacent to the major canyons are noted.

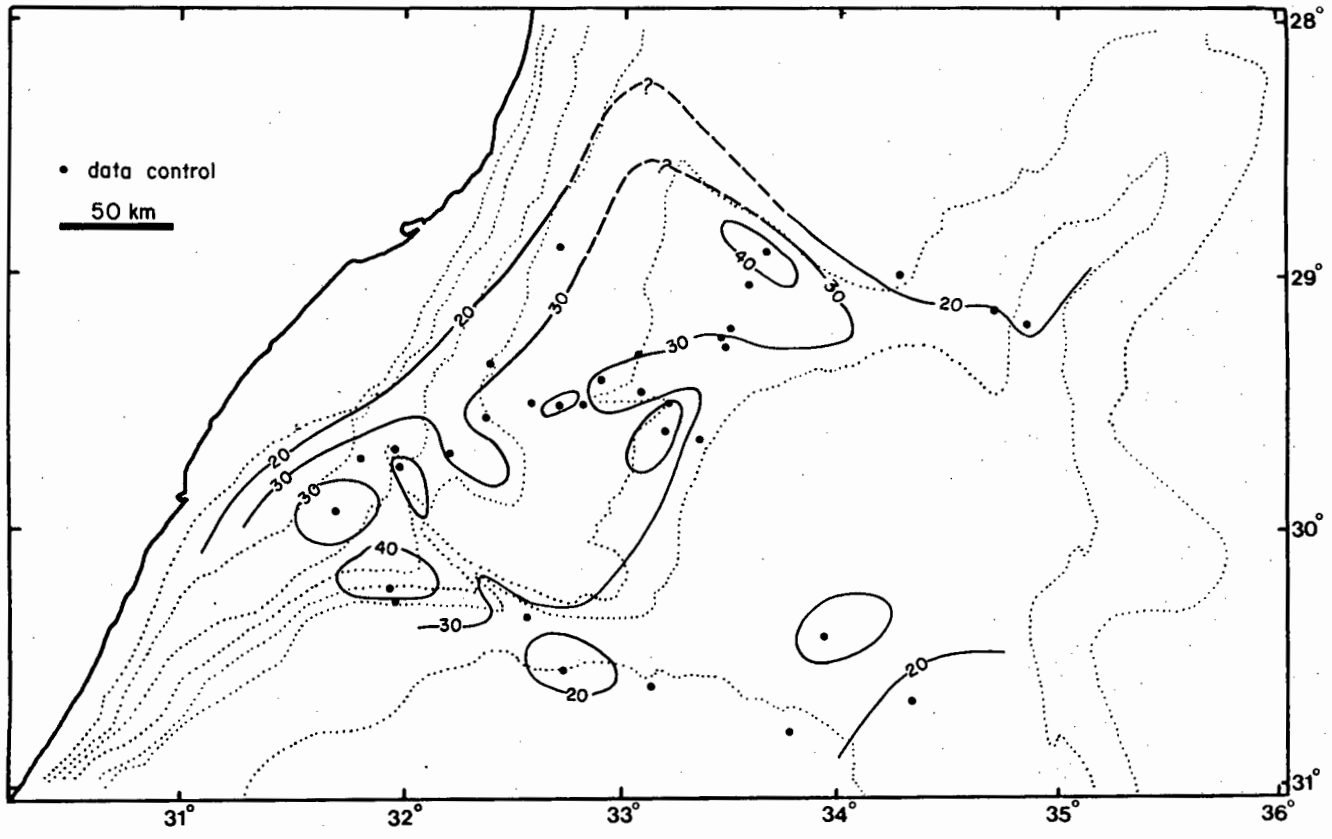

Fig. 8.38 % FINE SILT

8.6 MODERN DEPOSITIONAL ENVIRONMENTS AND SEDIMENT DISPERSAL

8.6.1 Introduction

The large sedimentological data base, including discussions on sediment chemistry, composition, mineralogy and texture, has been presented in sections 8.2-8.5. Detailed core descriptions are listed in Appendix B2. It remains to rationalise and synthesise all sedimentological data with pertinent bathymetric, seismic and oceanographic data to provide an overall integrated approach.

This section is directed towards identification of lithofacies and depositional environments which in turn furnishes information regarding transport and depositional processes. Following on from a discussion of downslope transport, all aspects of sediment provenance, transport, erosion and deposition are combined to construct a schematic sediment dispersal model for the mid Natal Valley. Development of the Tugela Cone is outlined in Chapter 9.

8.6.2 Lithofacies and Depositional Processes

Fine-grained sediments volumetrically comprise the predominant fill of modern oceanic basins (Piper, 1978; Stow and Bowen, 1980) and this generalisation is applicable to the mid Natal Valley. Several mechanisms transport fine sediments into deep-water basins and these generate distinct depositional lithofacies. By evaluating process systems, three broad facies groups may be discriminated: turbidites, contourites and pelagites/hemipelagites. Processes responsible for their deposition are, respectively, gravity-controlled turbidity

currents, semi-permanent bottom currents and settling out through the water column (Stow, 1985). Contourites may be discussed in terms of sandy and muddy end-members. These distinct processes form part of a continuum of mechanical behaviour, flow concentration and flow velocity and thus the resultant depositional lithofacies are intergradational (Stow, 1985) and not always easy to discriminate. Lithofacies notation can be assigned on the basis of the major structural, textural and compositional attributes of a sedimentary sequence but taking note of complementary oceanographic, bathymetric and seismic data. Abbreviated core descriptions collating the most important sedimentological characteristics are appended as Table 8.7. In the Natal Valley, turbidites and sandy contourites are most easily recognised while the distinctions between muddy contourites and hemipelagites are more subtle and difficult to evaluate. Full reviews of processes, responses and diagnostic criteria for the recognition of the major deep-water, fine-grained lithofacies groups are outside the scope of his study but are available in the literature (e.g. Stow and Lovell, 1979; Stow and Shanmugam, 1980; Allen, 1984; Nelson and Nilsen, 1984; Stow, 1985). Only factors directly influencing classification of mid Natal Valley modern lithofacies are discussed in this section. Salient features of each lithofacies are briefly described:

Turbidite

Turbidity currents are documented worldwide as important processes in the transportation of muddy terrigenous sediments to continental slope regions (Piper, 1978). Although turbidite processes may have been important in Tugela Cone construction in the geologic past, modern stagnation of cone growth (Chapter 9)

Table 8.7 Abbreviated Core Descriptions and Lithofacies Interpretation[1]

FACIES[2] ASSEMBLAGE	CORE	SEDIMENTARY[3] STRUCTURE	LITHOLOGICAL[4] CLASSIFICATION	TEXTURE[5]	LITHOFACIES
I	30	Upward-fining; distribution and composition-graded; T_1-T_6 lamination sequence; rare burrows	Silty clay over marly calcareous ooze	Silty clay over clayey sand	TURBIDITE
I	31	Upward-fining; distribution and composition-graded; T_0-T_8 lamination sequence; rare burrows and mottles	Silty clay over sand-silt-clay	Silty clay over sand-silt-clay	TURBIDITE
I	34	Upward-fining; distribution and composition-graded; T_1-T_4 lamination sequence; rare burrows and mottles	Silty clay over sand-silt-clay and clayey sand	Silty clay over sand-silt-clay and clayey sand	TURBIDITE
I	5115	Upward-fining; T_0-T_4 lamination sequence over semi-indurated basal unit; distribution and composition-graded; erosive base; no bioturbation	Silty clay over silty sand	Silty clay over silty sand	TURBIDITE
I	5116	Upward-fining; distribution-graded; T_0-T_3 lamination sequence; rare mottles	Silty clay over sand-silt-clay	Silty clay over sand-silt-clay	TURBIDITE
I	5117	Two upward-fining, distribution-graded units with T_2-T_6 lamination sequence separated by more calcareous poorly-laminated and ungraded unit; sharp base and gradational top to fining-upward units; rare burrows and mottles	Silty clay to sand-silt-clay	Graded units – silty clay over sand-silt-clay Ungraded unit – sand-silt-clay	TURBIDITES + interbedded HEMIPELAGITE
IIa	18	Very poorly laminated; ungraded; strongly burrowed and mottled	Calcareous ooze	Clayey sand to sand-silt-clay	PELAGITE
IIa	19	Poorly laminated; ? ripple lamination; ungraded; strongly burrowed and mottled	Calcareous ooze	Clayey sand to sand-silt-clay	PELAGITE
IIa	20	Unlaminated; fining-upward sequence; strongly mottled	Calcareous ooze	Sand-silt-clay	PELAGITE
IIa	5124	Structureless; ungraded; moderately mottled	Marly calcareous ooze	Sand-silt-clay	HEMIPELAGITE
IIb	1	Stacked unlaminated to faintly bedded units; ungraded; minor burrows and mottles	Marly calcareous ooze	Sand-silt-clay	HEMIPELAGITES
IIb	5751	Unlaminated to poorly-bedded, ungraded units; local strong burrowing and mottling	Foraminiferal ooze	Clayey sand to sand-silt-clay	PELAGITES + HEMIPELAGITES
IIb	5753	Unlaminated to poorly-bedded, ungraded units; minor to moderate burrowing and mottling	Marly calcareous ooze	Sand-silt-clay	HEMIPELAGITE
IIIa	5119	Unlaminated to poorly-parallel laminated unit with coarse biogenic lags gradational into an unlaminated to coarse-bedded sequence; both units locally graded and slightly mottled	Marly calcareous ooze	Sand-silt-clay	MUDDY CONTOURITE over HEMIPELAGITE
IIIa	5121	Alternating inter-gradational unlaminated and poorly-laminated units locally strongly mottled and burrowed. Local normal grading but reverse-graded at top	Marly calcareous ooze	Sand-silt-clay to silty clay	MUDDY CONTOURITES + interbedded HEMIPELAGITES
IIIb	27	Poorly-laminated, ungraded sequence with coarse lags gradational into a strongly mottled, structureless unit	Marly calcareous ooze	Sand-silt-clay	MUDDY CONTOURITE over HEMIPELAGITE
IIIb	23	Fining-upward, distribution and composition-graded unit with T_3-T_8 lamination sequence and sharp, erosive base overlying more calcareous, poorly-laminated, ungraded unit; basal unit strongly bioturbated	Marly calcareous ooze	Silty sand to sand-silt-clay	TURBIDITE over HEMIPELAGITES
IIIb	24	Poorly-laminated, ungraded, mottled unit with basal biogenic lag overlying semi-indurated biosparitic wackestone	Marly calcareous ooze	Sand-silt-clay	MUDDY CONTOURITE over 'hardground'

Table 8.7 continued

FACIES[2] ASSEMBLAGE	CORE	SEDIMENTARY[3] STRUCTURE	LITHOLOGICAL[4] CLASSIFICATION	TEXTURE[5]	LITHOFACIES
IIIb	25	Structureless, ungraded ; moderately mottled	Marly calcareous ooze	Sand-silt-clay	HEMIPELAGITE
IIIb	26	Upward-fining, distribution-graded unit with T_3-T_5 lamination sequence and sharp base overlying more calcareous, poorly-laminated, ungraded and moderately mottled unit	Marly calcareous ooze	Sand-silt-clay	TURBIDITE over HEMIPELAGITE
IIIb	5127	Poorly-laminated sequence overlying parallel-laminated unit with distinctive sandy lags ; both sequences ungraded and slightly mottled ; lower unit has sharp top	Marly calcareous ooze	Sand-silt-clay	HEMIPELAGITES over MUDDY CONTOURITE
IVa	5	Unlaminated, ungraded and slightly mottled unit with sharp base over semi-indurated MIOCENE/PLIOCENE basal sequence	Foraminiferal ooze	Clayey sand	SANDY CONTOURITE over 'hardground'
IVa	9	Poorly to strongly-laminated ; parallel to ripple lamination ; coarse biogenic lag in ripple laminated zone ; slightly mottled	Foraminiferal ooze	Clayey sand	SANDY CONTOURITE
IVa	12	Poorly-parallel laminated, ungraded ; slightly mottled	Marly calcareous ooze	Clayey sand	SANDY CONTOURITE
IVa	13	Poorly-laminated, slightly-graded unit containing large intraclast gradational into a poorly-laminated, mottled basal unit	Marly calcareous ooze	Clayey sand over sand-silt-clay	SANDY CONTOURITE over HEMIPELAGITE
IVa	14	Two poorly-laminated, ungraded units ; slightly mottled and burrowed	Marly calcareous ooze	Clayey sand	SANDY CONTOURITES
IVa	15	Unlaminated to poorly-laminated, ungraded unit with slight mottling and sharp base overlying semi-indurated basal MIOCENE/PLIOCENE unit	Marly calcareous ooze	Clayey sand to sand	SANDY CONTOURITE over 'hardground'
IVa	16	Moderately-laminated, ungraded unit with parallel and ? ripple laminae ; rare mottles	Marly calcareous ooze	Clayey sand to sand	SANDY CONTOURITE
IVa	21	Poorly-laminated, ungraded sequence ; slightly mottled	Marly calcareous ooze	Clayey sand to sand	SANDY CONTOURITE
IVb	29	Poorly to strongly-laminated units ; sharp top to reverse distribution-graded sequence ; locally strongly mottled and burrowed	Marly calcareous ooze	Silty sand	HEMIPELAGITES + interbedded SANDY CONTOURITE

1 Lithofacies interpretation aided by full suite of textural, mineralogical and chemical parameters (Appendices B2-B13) and the geographic location of cores

2 Facies assemblages (see Fig. 8.39 and Table 8.8)

3 Brief description of primary and secondary sedimentary structures ; T lamination sequence refers to terminology of Stow and Shanmugam (1980)

4 Lithological classification as described in Appendix A7

5 Textural classification, independent of the $CaCO_3$ content, based on the method of Shepard (1954) - see Figure 8.20

has limited terrigenous turbidite deposition to the southern Tugela Cone (Fig.8.39). Infrequent biogenic-enriched turbidites also characterise the eastern Tugela Cone adjacent to the 29° 25'S Canyon (Fig.8.39).

An assemblage of structural, textural and compositional properties distinguish sediments of turbidity current origin. Turbidites recognised in the mid Natal Valley are thin-bedded (Nelson et al, 1978) with an average thickness of 20-30 cm. Texturally, they are classified as silty clays to clayey sands. Assignment of a turbidity current origin relies on the recognition of two major criteria: the sequence of sedimentary structures and indications of rapid autoburial.

(1) Structural Sequence - the muddy texture of Natal Valley turbidites restricts the use of the 'Bouma' lamination sequence which is more suited to thicker sandy turbidites. Instead, a standard structural sequence for fine-grained turbidites (Stow and Shanmugam, 1980) is utilised. Typically, each turbidite displays a sharp basal contact which may or may not be erosive. Most turbidites can be correlated to the ideal sequence of Stow and Shanmugam (1980) but the complete sequence (T_0-T_8) is rarely found. In most cores only a partial or interrupted sequence is developed (Table 8.7). All the turbidites fine-upwards by distribution grading (Middleton and Hampton, 1976) reflected by the absence of a significant coarse fraction in the upper section. Compositional parameters display progressive vertical changes associated with this distribution grading. If overlain by interbedded hemipelagites, the upper turbidite contact is usually gradational.

(2) Rapid Autoburial - evidence of rapid deposition is an

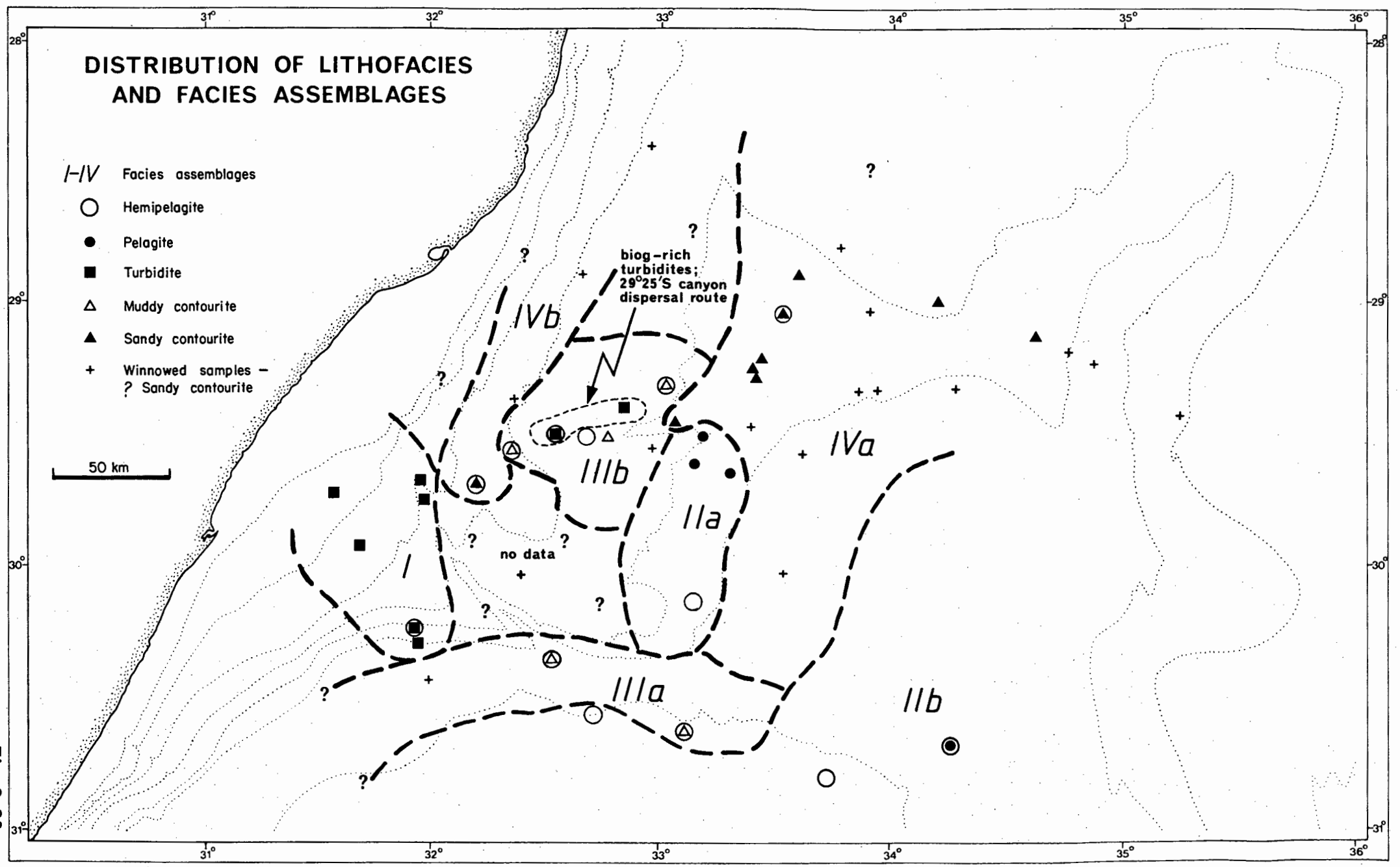
DISTRIBUTION OF LITHOFACIES
AND FACIES ASSEMBLAGES
I–IV Facies assemblages
Hemipelagite
Pelagite
Turbidite
Muddy contourite
Sandy contourite
+ Winnowed samples – ? Sandy contourite
50 km
biog–rich turbidites; 29°25'S canyon dispersal route
IVb
IVa
IIIb
IIa
I
IIIa
IIb
no data
31°
32°
33°
34°
35°
36°
28°
29°
30°
31°

Fig. 8.39

important criterion in establishing the validity of the turbidite depositional process. Indicators of rapid deposition and burial in the Natal Valley turbidites include restriction of bioturbation to the tops of units, occasional non-erosional ripples, and relatively high organic carbon content although the latter may only reflect a particular source area.

Each sedimentation unit displaying normal grading, a standard stratification sequence and evidence of rapid autoburial represents deposition from a single fine-grained turbidity current. Turbidite coarse fractions are compositionally distinct from the interbedded hemipelagites. Quartz and heavy mineral enrichment (Appendix B10) and pelagic detritus depletion suggests introduction from a continental provenance area. In addition, turbidites display relatively high benthic/planktic foram ratios (section 8.6.4; Fig.8.41) indicating downslope sediment dispersal. The turbidite lithofacies zone (south Tugela Cone; Fig.8.39) shows definite downslope textural and grain-size trends (section 8.5.2.2). In contrast, textural trends in contourite lithofacies are developed along the slope (contour currents) allowing their mutual distinction.

Hemipelagite

Hemipelagic muds are the most common modern Natal Valley lithofacies draping large areas of the eastern and northern Tugela Cone and the basin plain (Fig.8.39). Hemipelagites result from admixture of the pelagic detrital rain and suspended terrigenous fines with deposition occurring on settling-out from the water column. Hemipelagite classification is dependent on the biogenous proportion comprising 30-70% of the sediment volume. An arbitrary boundary at 70% $CaCO_3$ artificially

separates the gradational hemipelagite and pelagite lithofacies.

Hemipelagite muds of the Natal Valley are typically homogeneous and structureless although local grading (core 5119) and indistinct lamination are recognised (Table 8.7). Occasional lag concentrations of pelagic micro-skeletons in conjunction with local grading may imply an intermittent current influence and hence gradation to the contourite lithofacies. Hemipelagite units are highly variable in thickness (10-100 cm) and are lithologically classified as marly calcareous oozes. Texturally, they are relatively coarse (up to 40% sand) being categorised as sand-silt-clay (Shepard, 1954). The dispersed sand fraction is almost exclusively biogenic and is composed of foram tests with minor pteropod debris. Since the sand fraction is biogenic, the sandier hemipelagites are more calcareous. An important feature of the hemipelagite muds is the strong degree of bioturbation (burrowing and mottling) which may be partly responsible for the homogeneity and poor preservation of primary stratification.

Pelagite

Pelagite lithofacies classification is dependent on recognition of two major criteria: (a) $CaCO_3$ content is >70% reflecting the dominance of a biogenic source; and (b) evidence for deposition by settling from suspension in the water column.

The high biogenous content implies general remoteness from continental influence and heavy dilution of the small terrigenous component. Zones presently dominated by pelagites include restricted areas of the eastern Tugela Cone and basin plain (Fig.8.39). Pelagite deposition over the eastern Tugela Cone confirms the modern stagnation of this zone as an active terrigenous depocentre.

On sedimentary structure, pelagites show close similarity to hemipelagites and are typically homogeneous to very poorly laminated and ungraded. Very restricted evidence of ripple lamination (core 19) and normal grading (core 20) indicates occasional current influence. Texturally, the pelagites are classified as clayey sand or sand-silt-clay on account of the large (<60%) biogenic sand-size component. Lithologically, they are categorised as calcareous or foraminiferal oozes. Like the hemipelagite lithofacies, strong bioturbation (burrowing and mottling) is characteristic and thus primary sedimentary structures are rarely preserved.

Although it is generally accepted that bottom contour currents play an important role in construction of deep-water continental margins, the criteria available for distinguishing between contourites and turbidites remain inconclusive. This problem has been reviewed by Stow and Lovell (1979) and Stow (1985) and their revised criteria are used here to distinguish between contourites and turbidites.

Dependent on the competence of the contour currents, two distinct contourite facies may be developed. Muddy contourites are deposited from nepheloid layers associated with sluggish contour currents. More vigorous currents, however, tend to winnow away the fine fraction of turbidites and related deposits to produce reworked sandy contourites (Lovell and Stow, 1981). Both muddy and sandy contourite lithofacies are recognised in the mid Natal Valley.

Muddy Contourite

Muddy contourites (Table 8.7) are localised to the basin

plain south of the southern Tugela Cone and adjacent to the lower 29° 25'S Canyon (Fig.8.39). Both regions are demonstrably influenced by bottom current flow (Fig.7.2) while a nepheloid layer has been mapped in the mid Natal Valley (Fig.2.5) by Kolla et al (1976a). Combined development of a nepheloid layer and bottom water flow in the Natal Valley is favourable for deposition of muddy contourites.

Muddy contourites of the eastern and southern Tugela Cone are dominantly homogeneous with sporadic poorly-defined lamination. No grading is evident although occasional well-sorted lag concentrations of coarse foram tests are discriminated. These intercalations probably result from short-lived surges of increased current competence. Texturally, the muddy contourites are classified as sand-silt-clay and more rarely silty clay. The frequently high sand content (<45%), comprising foram tests, is atypical for normal muddy contourites (Stow and Lovell, 1979) suggesting that a continuum may exist between muddy and sandy contourites. Bioturbational mottling and burrowing is common to the muddy contourites resulting in homogeneity of texture and composition excepting lag concentrations.

Sandy Contourite

The sandy contourite lithofacies is localised to regions where deep Agulhas Current flow impinges on the sea floor instituting winnowing processes. Sandy contourites are therefore well-developed over the Central Terrace crest and flanks (cores 5, 9, 12 and 13). In addition, current acceleration and eddy formation around basement seamounts (section 7.2.7) causes local winnowing and sandy contourite formation (Fig.8.39; cores 14, 15

and 16). Development of this lithofacies on the Tugela Cone coincides with independent indications of current influence. For example, sandy contourites have been identified in core 21 (Table 8.7) retrieved from a zone of sediment waves (section 7.2.5).

Natal Valley sandy contourites are commonly disturbed and bioturbated (burrowed and mottled) and thus show little primary structure except irregular coarse lag layers. Where undisturbed, poor horizontal lamination and occasional cross lamination is developed but without a regular stratification sequence. Grading is uncommon although both normal and reverse grading are locally recognised, probably denoting waning and waxing of current strength. Winnowing action has reduced the mud content of the sandy contourites and they are texturally classified as sands or clayey sands. Since the sand fraction in the current-swept areas is predominantly biogenic, the sandy contourites are lithologically described as marly calcareous oozes or foram oozes.

Coring operations at several sites on the Central Terrace crest and flanks met with limited success and only sandy surficial samples were retrieved (Appendix B1). Poor coring success at these sites (Fig.7.2) may reflect sub-strate conditions with the presence of hard, compact lag deposits preventing penetration (section 7.2.9). If this explanation is correct, then these lag deposits may be classified as sandy contourites with extremely low mud contents. Outside the sandy contourite lithofacies region, core success was much improved implying a softer sub-strate.

8.6.3 Facies Assemblages

The distribution of lithofacies types as described in Table

8.7 is presented in Figure 8.39. Taking cognizance of complementary seismic, oceanographic and sedimentologic data, four distinct facies assemblages may be defined (Fig.8.39; I-IV). Diagnostic characteristics and major controlling factors for each facies assemblage are listed in Table 8.8. Facies assemblage zones have been superimposed on a 3D structural plot of the Tugela Cone, Central Terrace and basin plain (Fig.8.40) to show their relationship to sediment dispersal routes and deep undercurrent routes. Although facies assemblage boundaries have been delineated on Figure 8.39, their positions must only be regarded as first appraisals due to the shortage of core data. Regions with insufficient core data have been omitted from the facies assemblage classification (Figs.8.39 and 8.40).

Facies Assemblage I

Cores attributed to assemblage I are dominated by thin-bedded turbidites of terrigenous origin with occasional interbedded hemipelagites. Assemblage I is developed over the southern flanks and central upper slope of the Tugela Cone and delineates the primary modern terrigenous depocentre and down slope dispersal route in the mid Natal Valley (Fig.8.40). The thin-bedded and fine-grained character of assemblage I terrigenous sediments prompts classification as distal mud turbidites (Stow, 1985). The absence of sandy beds may be a sampling density artefact with no channelised turbidite facies having been intersected. Alternatively, the low sand content may be an indicator of the turbidite provenance. If detrital sands are restricted from bypassing the shelf sand stream (Flemming, 1981), then potential sand input to the south Tugela Cone is reduced, resulting in an excessive proportion of fine-grained

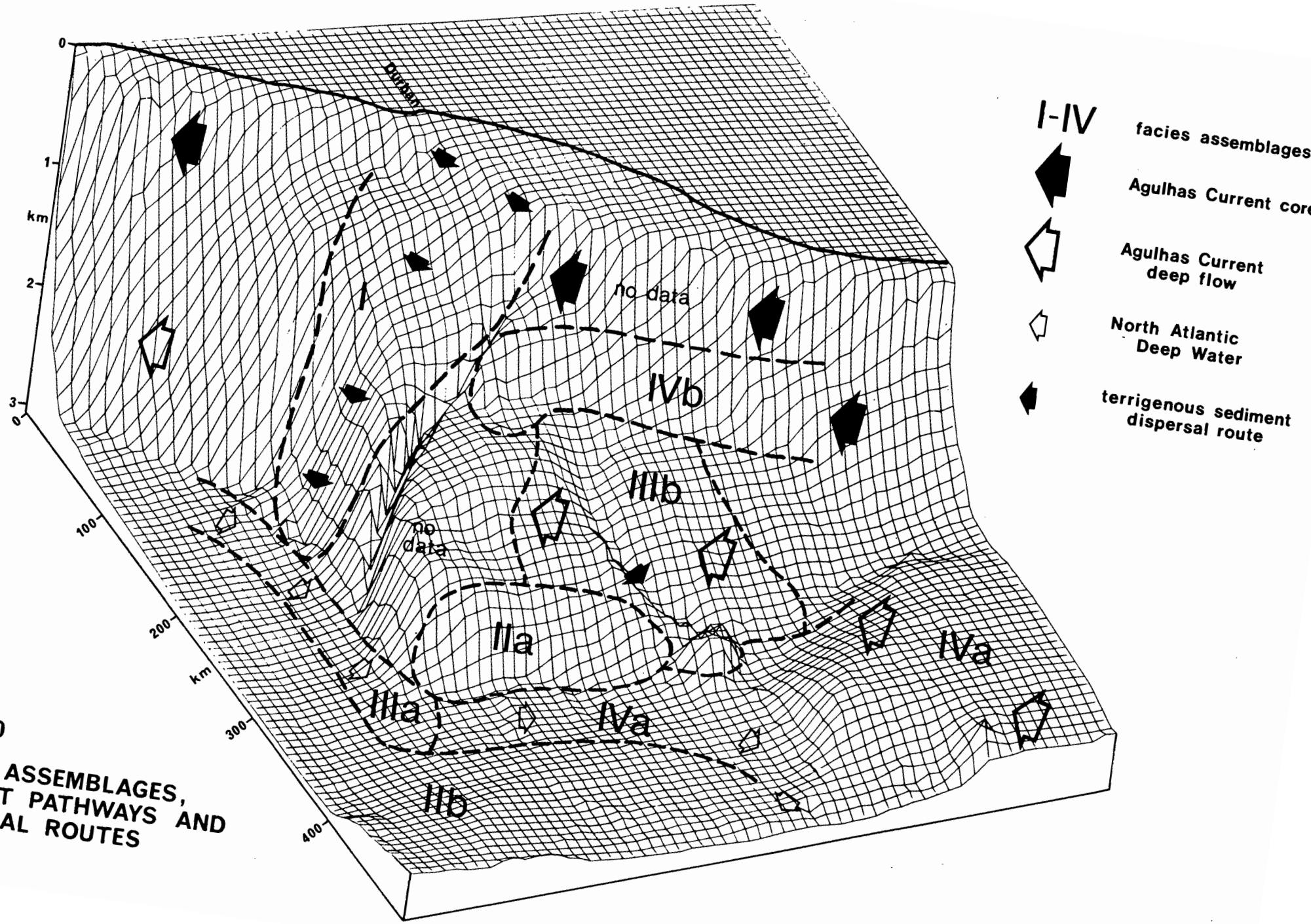

Fig. 8.40

FACIES ASSEMBLAGES, CURRENT PATHWAYS AND DISPERSAL ROUTES

Table 8.8 Facies Assemblage Characteristics

FACIES ASSEMBLAGE	LOCATION	LITHOFACIES TYPE	MAJOR CONTROLLING FACTORS
I	southern Tugela Cone	turbidite/minor hemipelagite	major modern terrigenous depocentre and downslope dispersal route
IIa	lower eastern Tugela Cone	mixed pelagite/ hemipelagite	stagnant region of cone receiving minor modern terrigenous input; sediment bypassing via Tugela and 29° 25'S Canyons
IIb	basin plain	mixed pelagite/ hemipelagite	remoteness from terrigenous sediment supply
IIIa	basin plain adjacent to south Tugela Cone	mixed hemipelagite/muddy contourite	pathway of NADW flow; remoteness from terrigenous sediment supply
IIIb	eastern Tugela Cone adjacent to 29° 25'S Canyon	mixed hemipelagite/muddy contourite (local turbidite)	migrating sediment wave field (Fig.7.2) associated with deep Agulhas Current flow; local biogenic-rich turbidite deposition along the 29° 25'S Canyon dispersal route
IVa	Central Terrace and basin plain margins	sandy contourite	zones of strong bottom current scouring; Central Terrace (deep Agulhas Current flow) and basin margins (NADW)
IVb	northern Tugela Cone mid-upper slope	sandy contourite/minor hemipelagite	Agulhas Current core flow impingement on the sea floor

turbidites. In general, fine-grained turbidites are deposited from low-density turbidite incursions, channel overbank flow and from the tails of turbidity current flows. The frequent development of distribution-grading (Appendix B2 and Table 8.7) indicates transport in the form of low concentration flows (Middleton, 1976). Infrequent interbeds of hemipelagite imply local breaks in turbidite deposition. Hemipelagites are a proportionately minor constituent of facies assemblage I.

Facies Assemblage II

Facies assemblage II is recognised in two discrete areas and is thus divided into assemblages IIa and IIb (Fig.8.39 and Table 8.8). Assemblage II is dominated by pelagites and hemipelagites implying that settling from suspension is the major depositional process.

Assemblage IIa pelagites/hemipelagites are restricted to the lowermost eastern Tugela Cone (Figs.8.39 and 8.40) where stagnation of cone development and cessation of terrigenous influence is most advanced (Chapter 9). Assemblage IIa is flanked by both the Tugela and 29° 25'S Canyons (Fig.8.40) both of which probably pirate the majority of potential bottom-process terrigenous input to the eastern Tugela Cone. Only suspended terrigenous detritus reaches this region of the cone contributing to the hemipelagite lithofacies of assemblage IIa.

Assemblage IIb pelagites/hemipelagites characterise the basin plain excluding the current-influenced marginal areas adjacent to the Tugela Cone and Central Terrace. Remoteness from terrigenous detritus supply is the major control over lithofacies type (Table 8.8) although variations in the terrigenous supply are indicated by the development of either hemipelagite or

pelagite.

Facies Assemblage III

Facies assemblage III comprises interbedded muddy contourites and hemipelagite muds deposited under conditions of variable current flow in zones of reduced terrigenous detritus input (suspended and bedload). Assemblage III is developed in two areas and is thus split into assemblages IIIa and IIIb (Fig.8.39 and Table 8.8).

Assemblage IIIa is recognised over the deep basin margin adjacent to the south Tugela Cone (Figs.8.39 and 8.40) where the development of biogenic-rich contourite and hemipelagite lithofacies (Table 8.8) confirms the drop in terrigenous influence. The absence of turbidites implies that gravity-controlled depositional processes diminish in importance away from the Tugela Cone apron being replaced by settling from suspension. Development of muddy contourites attest to deep current influence on assemblage IIIa sedimentation processes and this is corroborated by local erosion of unit D sediments (section 7.2.3.1), sediment reworking and redistribution (sections 7.2 and 8.4.1.2). Assemblage IIIa approximately delineates the pathway for deep NADW flow (Fig.8.40). Interbedding of muddy contourites and hemipelagites suggests that NADW flow along the basin margin has been inconsistent occurring as waxing and waning pulses of unknown duration.

Assemblage IIIb is delineated over the eastern Tugela Cone flanking the 29° 25'S Canyon (Figs.8.39 and 8.40) where terrigenous input is limited to far-travelled suspended fines within the hemipelagite and muddy contourite lithofacies. Muddy contourites indicate current influence and this is confirmed by

coincident recognition of migrating sediment waves and IIB-1 topography (sections 7.2.4 and 7.2.5.1; Fig.7.2). Current-control on depositional processes as indicated by bedform and lithofacies type is a response to bottom impingement of deep Agulhas Current flow (section 7.2; Fig.7.2).

Turbidite deposition is also recognised in facies assemblage IIIb suggesting that gravity-controlled processes are locally important adjacent to the 29° 25'S Canyon (Fig.8.39). Their fine-grained and thin-bedded character (Table 8.7) indicates deposition in an overbank, interchannel environment while evidence of distribution-grading may imply supply from a low-density turbidity flow. Assemblage IIIb turbidites are more calcareous than assemblage I turbidites distinguishing two dissimilar source areas. While the provenance for assemblage I turbidites is almost entirely continental, biogenic fall-out has strongly diluted the terrigenous fraction in the assemblage IIIb turbidite source region (upper 29° 25'S Canyon).

Facies Assemblage IV

Facies assemblage IV is dominated by sandy contourites and assumed sandy contourites (winnowed surface samples) implying strong current-control on sedimentation processes. Assemblage IV is recognised in two regions and is thus subdivided into assemblages IVa and IVb (Fig.8.39; Table 8.8).

Assemblage IVa is delineated over the Central Terrace and basin margin adjacent to the east Tugela Cone and Central Terrace (Figs.8.39 and 8.40). Dominance of sandy contourites in these regions is consistent with the recognition of other current-control indicators (Fig.7.2) including sediment unit D thinning

and erosion (section 7.2.3.1), asymmetric sedimentation (section 7.2.6) and moat development (section 7.2.7). Over the Central Terrace, deep Agulhas Current flow (route Y) is the major control over sedimentation processes. In contrast, along the deep basin marginal areas, cyclonic NADW flow is responsible for sandy contourite generation (Figs.8.39 and 8.40; Table 8.8).

Assemblage IVb is demarcated as an elongate zone along the mid-upper slope of the central to northern Tugela Cone (Figs.8.39 and 8.40). The recognition of sandy contourites implies strong current influences which may be equated to impingement of Agulhas Current core flow (route X) on the sea floor (compare Figs.7.6 and 8.39). The development of local interbedded hemipelagites may indicate variation in current competence or switching of the flow route.

It may be concluded that there is a strong relationship between lithofacies and dominant modern depositional/erosional process within the mid Natal Valley. Facies assemblage zonation is primarily controlled by the composite effects of: (a) sediment dispersal routes; (b) proximity to hinterland terrigenous source; (c) deep current scour and winnowing; (d) water depth; and (e) productivity of the water mass.

8.6.4 Downslope Transport

Several biological, chemical and sedimentological criteria may be collectively used to confirm the major pathways of downslope transport in the mid Natal Valley. Each criterion is briefly reviewed before the conclusions are summarised.

Benthic/Total Foraminifera Ratio

Excluding anomalies created by benthos fertility variations and dissolution, the ratio of benthic/planktic forams is primarily controlled by water depth (Diester-Haass, 1982) with the ratio typically decreasing towards abyssal depths. High ratios in deep water may therefore be related to downslope transport (Lutze et al, 1979) with injection of shallow-water sediment and fauna into abyssal zones. Using component data (Appendix B10), a distribution map of the benthic/total foram ratio (Fig.8.41) has been constructed. Atypical benthic foram enrichment is localised to the northern basin plain adjacent to the lower 29° 25'S Canyon and over large areas of the southern Tugela Cone. In both these areas the ratio locally exceeds 5% which is more typical of the upper slope (Fig.8.41). The benthos-enriched regions are coincident with major canyons or major terrigenous depocentres which are undoubtedly sites of downslope transport. However, high benthic foram counts over the northern basin plain may partially be sourced from the northern Natal Valley, being swept in from the Central Terrace by strong Agulhas Current bottom scour (Fig.7.6).

Benthic foram identification (D. Salmon, pers. comm., 1980) confirms the probability of downslope transportation since numerous shallow water fauna (e.g. Ammonia beccarii, Quinqueloculina spp., Cibicides spp., and Elphidium crispum) have been recognised in the deep water zones. Furthermore, several of the shallow-water benthics are partially abraded and often glauconite-infilled suggesting a relict shelf origin followed by transportation to deep water. Although the anomalous zones are sited in relatively deep water (1500-3000 m), lack of evidence of

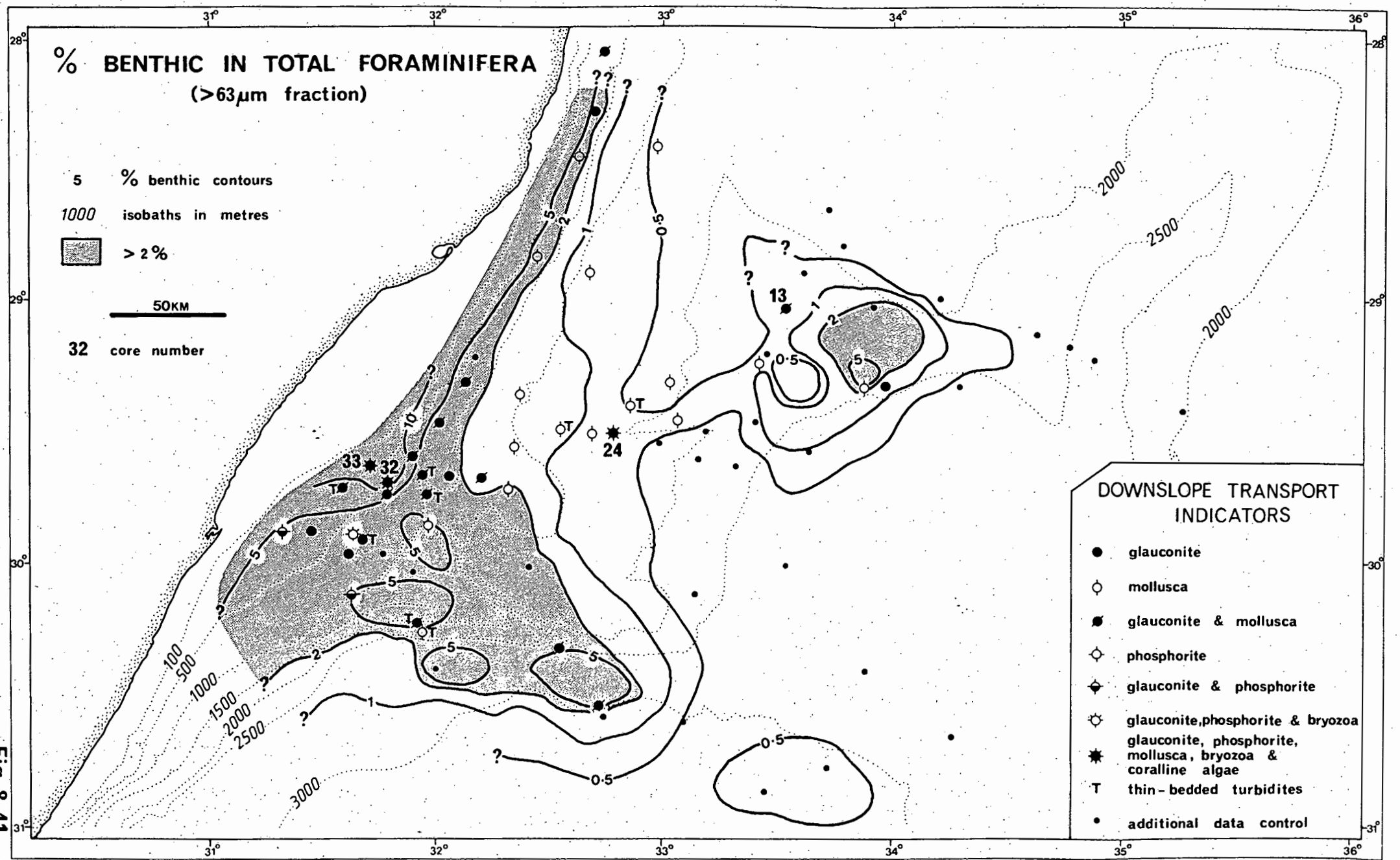
% BENTHIC IN TOTAL FORAMINIFERA
(>63μm fraction)
5 % benthic contours
1000 isobaths in metres
> 2 %
50KM
32 core number
DOWNSLOPE TRANSPORT INDICATORS
glauconite
mollusca
glauconite & mollusca
phosphorite
glauconite & phosphorite
glauconite,phosphorite & bryozoa
glauconite, phosphorite, mollusca, bryozoa & coralline algae
T thin-bedded turbidites
additional data control
31°
32°
33°
34°
35°
36°
28°
29°
30°
31°
100
500
1000
1500
2000
2500
3000
2000
2500
2000
13
24
33
32

Fig. 8.41

advanced planktic foram corrosion (section 8.4.2.2) implies that dissolution is unlikely to have contributed significantly to benthos enrichment.

Distribution of Calcium Carbonate

The $CaCO_3$ content of surficial sediments (Fig.8.3) has been fully described in section 8.3.1. Assuming relatively uniform primary productivity over the mid Natal Valley (section 8.3.1.3), influx of terrigenous detritus from the hinterland results in carbonate dilution over the continental margin. Decreasing terrigenous influence down the continental slope should be mirrored by an increase in carbonate content. This model may be satisfactorily applied to the mid Natal Valley although two anomalous zones are apparent. Sediments depleted in $CaCO_3$ persist into water depths of 2500 m over large tracts of the southern Tugela Cone. Prominent dilution in this area confirms that it is a modern terrigenous depocentre and therefore a zone of downslope transport of continental detritus. Similarly, $CaCO_3$ concentrations are reduced over an elongate zone coincident with the 29° 25'S Canyon. It is argued that carbonate depletion along this canyon reflects channelised downslope transport of terrigenous detritus.

Thin-Bedded Turbidites

Turbidity currents are gravity-controlled bottom flows and can be generally considered to transport sediment in a downslope direction. Although high energy turbidites may flow upslope for short distances (Damuth and Embley, 1979), the recognition of turbidites almost certainly confirms downslope sediment dispersal.

The criteria for identification of turbidites have been

fully described in section 8.6.2. The locations of cores with identifiable turbidites are depicted in Figure 8.41 with abbreviated lithofacies descriptions being listed in Table 8.7. Thin-bedded turbidites are areally concentrated over the southern Tugela Cone and the upper 29° 25'S Canyon suggesting prevalence of downslope transport in these regions.

Glauconite and Phosphorite

Sediments rich in glauconite and phosphorite have been mapped over the south and west continental shelves of southern Africa (Birch, 1979b). These deposits originated by disaggregation of partially-lithified authigenic-rich bottom sediments during Tertiary regressive/transgressive erosional cycles. Although only minor quantities of glauconite and phosphorite have been recorded on the east coast continental shelf (Birch, 1979b), a similar origin may be postulated. Over the Tugela Cone upper slope, glauconite is commonly developed in close association with and frequently infilling abraded and/or fragmented benthic and planktic foram tests (Plate 8.2o). Similarly, the phosphorite has nucleated around abraded shallow-water flora, fauna and clastic detritus (Plate 8.4 a-e). These associations suggest that the authigenic minerals are relict. However, it cannot be totally discounted that the mild upwelling associated with Agulhas Current flow (section 2.2.4) is promoting modern authigenic phosphorite growth as described off eastern Australia (O'Brien and Veeh, 1980). Glauconite and phosphorite concentration linked to both upwelling processes and sea level change-induced disaggregation of authigenic mineral-rich bedrock should primarily affect shelf and upper slope zones. It follows that recognition of glauconite and phosphorite in deep water

Plate 8.4 Sedimentary Clast Photomicrographs

a-c - Core 32, 2-4cm: PHOSPHATISED BIOMICRITIC WACKESTONE. Mud-supported admixture of detrital terrigenous and biogenous clasts in a strongly-phosphatised and iron-stained micrite matrix. Clasts include: a - quartz, plagioclase, altered alkali feldspars, planktic forams, gastropods and undefined mollusc fragments; b - feldspar, quartz, glauconite, planktic forams and unidentifiable biogenic debris; c - quartz, feldspar, coralline algae, bryozoa, mollusc and planktic foram fragments.

d-e - Grab 33: BIOMICRITIC WACKESTONE. Matrix-supported bioclastic and detrital grains. The micrite matrix is patchily phosphatised and iron-stained. Clasts include: d - quartz, rare feldspar, planktic and benthic forams, bryozoa and bivalve fragments and pelletal glauconite; e - bryozoa, coralline algae, corroded bivalve fragments, benthic forams, pelletal glauconite and quartz.

f-g - Core 24, 8,5-10,5cm: BIOSPARITIC WACKESTONE. Mud-supported mixture of bioclastic and terrigenous grains. The matrix is primarily recrystallised micrite or microspar. Clasts include: f - quartz, feldspar, minor hornblende, bivalve and gastropod fragments; g - quartz, feldspar, igneous lithic clasts, bivalve fragments, coralline algae, benthic forams and pelletal glauconite.

h - Core 13, 1cm: MICRITIC MUDSTONE. Silt-sized detrital grains of quartz and feldspar with accessory biotite and magnetite supported in a weakly-phosphatised and iron-stained micrite matrix. Detrital grains constitute only 10% of the rock.

Plate 8.4 SEDIMENTARY CLAST PHOTOMICROGRAPHS

a

1mm

b

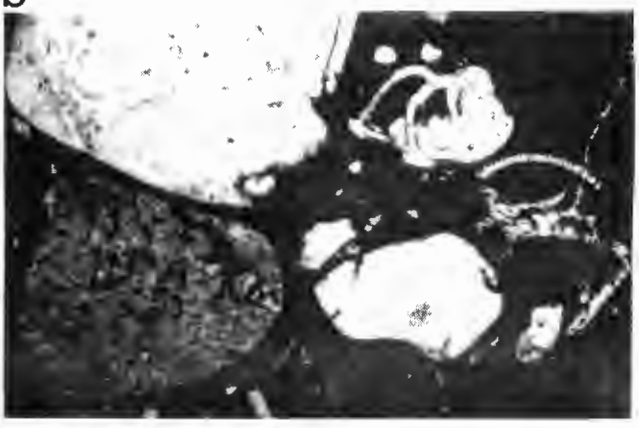

0.5mm

c

1mm

d

1mm

e

1mm

f

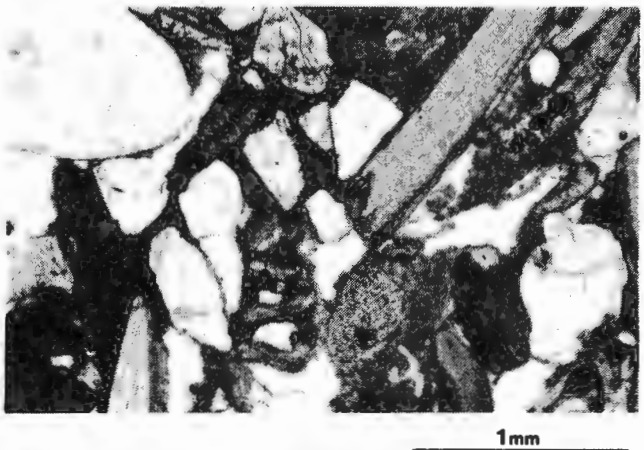

1mm

g

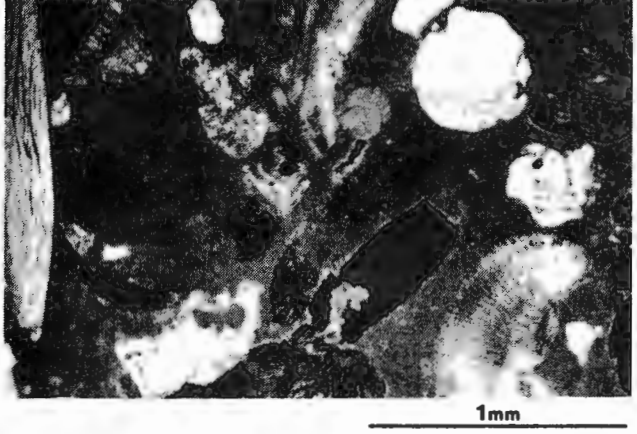

1mm

h

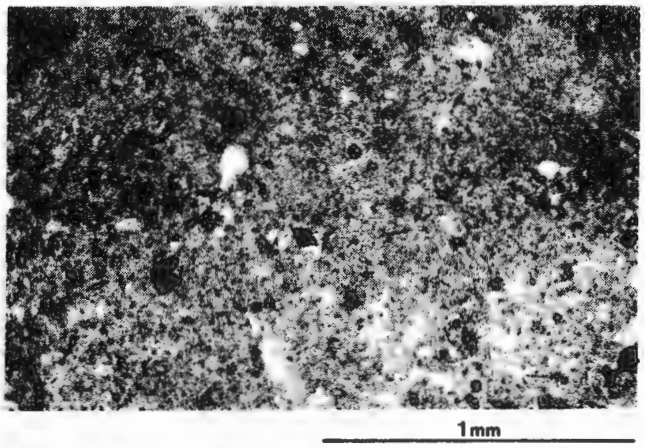

1mm

zones of the Tugela Cone is indicative of downslope transport rather than in situ authigenesis.

Surficial sediment samples containing authigenic components are identified in Figure 8.41. Glauconite and phosphorite concentration along the upper slope suggests a localised origin. Downslope occurrences of glauconite and phosphorite are restricted to the southern Tugela Cone and the 29° 25'S Canyon (Fig.8.41). These two regions have previously been described as active conduits for downslope sediment movement.

Bedload Material

In physiographic regions outside storm wave base and the influence of vigorous currents, bedload material under tractional transport will be channelled in a downslope direction under gravitational influence. Large intraclasts of gravel size have been retrieved in four off-shelf cores. Thin section photomicrographs and descriptions of these intraclasts are presented in Plate 8.4.

The intraclasts from grab 33 and cores 32 and 24 (Fig.8.41) are classified as biomicritic or biosparitic wackestones (Plate 8.4) comprising an admixture of bioclastic and terrigenous detritus cemented by phosphatised and iron-stained micrite and/or microspar. The abundance of shelf to nearshore flora and fauna (coralline algae and bryozoa; Wray, 1977) within these intraclasts (Plate 8.4 a-f) denotes a shallow-water origin. It is probable that the iron-staining and phosphatisation processes were operative during residence time on the shelf zone. Intraclast deposition at sites 32 and 33 represents short-distance transport over the shelf break onto the upper slope. More significantly, large intraclast deposition at site 24 in the

axis of the 29° 25'S Canyon implies long distance downslope transport (Fig.8.41).

The intraclast of micritic mudstone described in core 13 (SW Central Terrace) shows no features diagnostic of a shallow-water origin (Plate 8.4h). This clast may be a product of local substrate erosion on the Central Terrace crest.

Displaced Continental Shelf Fauna and Flora

The distribution of mollusca and mollusca fragments is depicted in Figure 8.41. Thin-shelled bivalves are predominant but these cannot be considered diagnostic of a high energy source environment such as the east coast shelf. In addition, the absence of significant valve abrasion or breakage implies a minimum of transport. Thin-shelled bivalves cannot therefore be used as indicators of downslope transport. In contrast, the deep-water occurrence of thick-shelled mollusca (bored, corroded and occasionally phosphatised) is best interpreted as the result of downslope transport of relict continental shelf biogenic debris. Relict or abraded mollusc debris is recognised over small sections of the southern Tugela Cone and in the axis of the 29° 25'S Canyon confirming downslope transport.

Coralline algae and bryozoa typically inhabit nearshore to outer shelf environments (Wray, 1977) and their presence in deep-water environments must be indicative of transport. Coralline algae and bryozoa have been identified at three sites on the upper slope of the southern Tugela Cone (Fig.8.41) implying off-shelf transport. Similar recognition at 1950 m in the 29° 25'S Canyon proves long distance canyon axial transport.

The combined evidence presented in this section confirms

that downslope transport of clastic detritus is restricted to two regions of the Tugela Cone: (1) primary dispersal route - southern Tugela Cone; (2) subsidiary and ? intermittently active dispersal route - 29° 25'S Canyon. Other areas of the Tugela Cone are relatively stagnant as modern depocentres with suspended terrigenous input being severely diluted by the pelagic rain. Although gravity-controlled processes are probably active in these zones, downslope transport within the biogenous sediments cannot be proven with the available data base.

8.6.5 Modern Sediment Dispersal

The object of this section is to construct a conceptual framework describing the general sediment dispersal system within the mid Natal Valley. This model has been inferred from observed sediment distribution patterns (grain size, texture and composition), lithofacies, facies assemblages, physiography and oceanography. The model briefly summarises the distribution and interaction of the major sedimentary processes active within the study area. Major controlling elements of the schematic model are graphically depicted in Figure 8.42.

8.6.5.1 Sediment Sources

Modern sediment input to the mid Natal Valley is sourced primarily from four major provenance zones: (1) terrigenous coarse fraction bedload detritus derived from the hinterland (Fig.8.42; 1); (2) terrigenous fine fraction suspended detritus from the hinterland (Fig.8.42; 2); (3) ? bedload and suspended detritus (terrigenous and biogenic) transported south by Agulhas Current flow (Fig.8.42; 1N and 2N); and (4) pelagic rain

Fig.8.42

Schematic Illustration of Major Processes Controlling Sediment Dispersal

Sediment Sources: 1 - hinterland coarse fraction bedload input (riverine discharge and coastal erosion) supplying the nearshore sand wedge; 2 - hinterland fine fraction suspended input (riverine discharge); 1N and 2N - ? bedload and suspended detritus (terrigenous and biogenic) transported south by Agulhas Current flow; 3 - pelagic rain.

Transport and Dispersal Processes: 4 - shelf sand stream; 5 - shelf edge overshoot; 6 - grain flow and creep; 7 - debris flow; 8 - turbidite; 9 - slumps and glides; 10 - scour redispersal (AC - Agulhas Current; NADW - North Atlantic Deep Water); 11 - suspended sediment dispersal.

12 - facies assemblage boundaries (see Figs.8.39 and 8.40). Basemap is computer-drawn 3D structural image of the Tugela Cone, Central Terrace and basin plain viewed from E30^{o}S at an elevation of 30^{o} above horizontal (vertical exaggeration 80x).

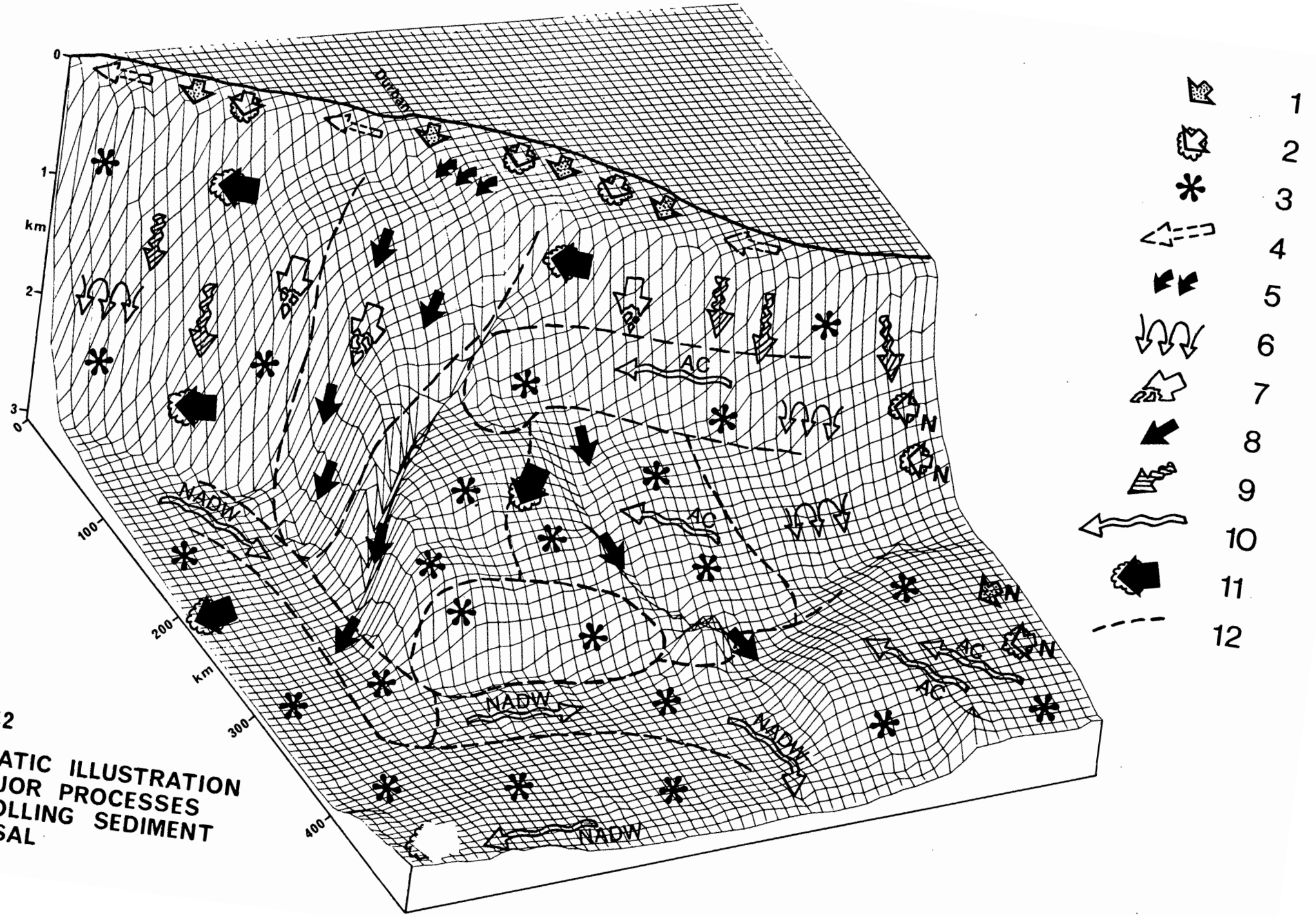

Fig. 8.42

SCHEMATIC ILLUSTRATION OF MAJOR PROCESSES CONTROLLING SEDIMENT DISPERSAL

(Fig.8.42; 3).

Coarse fraction shelf sediments comprise an admixture of terrigenous detritus derived from riverine discharge and coastal erosion together with biogenic detritus sourced from local benthic and pelagic communities. Along the inner shelf these populations are transported by wave action, longshore drift, rip currents and inshore counter currents but are commonly locked in the nearshore sand wedge. In contrast, outer shelf sediments are strongly influenced by Agulhas Current core flow. In this zone, current strengths are sufficient to entrain sand-grade detritus into a southerly-flowing shelf sand stream (Fig.8.42) travelling over a relict gravel pavement. The sand stream is continuously replenished from erosion of the nearshore sandy prism by lateral migration of the Agulhas Current flow-path (Flemming, 1981). Muddy detritus is hydrodynamically too fine to remain stable in this high energy environment. Transferal of the coarse bedload detritus onto the upper Tugela Cone is strongly restricted by shelf dynamics and is only prominent where Agulhas Current flow overshoots the shelf break at shelf zone structural offsets (Flemming, 1981). A major offset occurs at 29° 40'S (Fig.8.39) where the shelf sand stream partially overshoots the shelf break thus supplying bedload detritus to the upper slope (Fig.8.42). In addition, in such a high energy shelf environment, it is likely that there is slow local transferal of coarse detritus onto the upper Tugela Cone along the entire shelf break, perhaps via a process such as cascade feeding (Ferentinos et al, 1985). Sediment budget calculations (Flemming, 1981) suggest that at least 80% of Holocene bedload shelf sediments are ultimately deposited in upper slope sediment sinks, primarily in the lee of

structural offsets.

Seasonal discharge by the hinterland rivers provides large volumes of suspended detritus to the Natal Valley system (Fig.8.42). These muds are unstable under high energy shelf conditions and virtually the entire terrigenous mud fraction is transported in suspension to off-shelf zones of the basin (Flemming, 1981). Small amounts of terrigenous mud may be deposited in local low energy shelf environments (e.g. Tugela mud belt). Muds carried in suspension over the shelf break settle out in slacker water conditions over the upper slope of the Tugela Cone diluting the carbonate fraction (Fig.8.3). Mud deposition is probably enhanced by floc formation and faecal pellet production. Reduced amounts of the suspended terrigenous mud are available for transportation to and deposition in more remote deep basin environments. In addition, significant volumes of suspended mud must be entrained in the Agulhas Current system to be transported south to the Transkei Basin.

Oceanic circulation off SE Africa is dominated by the Agulhas Current system and this competent current is capable of transporting significant amounts of suspended detritus (pelagic and terrigenous) into the mid Natal Valley (Fig.8.42). Detritus debouched by the rivers of Mozambique and Madagascar may ultimately be deposited in the Natal Valley. Sand-grade detritus may also be introduced from the shoaler northern Natal Valley by tractional bedload transport under Agulhas Current influences. Sand input from the north should largely comprise foram tests but could include terrigenous material remobilised from the margins of the Limpopo Cone.

Skeletal carbonate debris produced by the pelagic and

benthic biomass comprises the final major sediment source. The relatively high productivity (Ryther et al, 1966) ensures a prolific and widespread pelagic rain although the effect of this source is often masked by terrigenous dilution. In regions remote from the hinterland, skeletal components form 90% of the bulk sediment. In contrast, severe dilution of the carbonate fraction occurs in the major terrigenous depocentres where biogenic components comprise only 10% of the total.

8.6.5.2 Downslope Transport and Dispersal

Detritus deposited over the upper Tugela Cone is available for downslope transport depending on local stability of the sediment mass. Downslope dispersal of unstable detritus may proceed by a variety of gravity-controlled processes including turbidity currents, slumps/glides and debris flows. Local conditions probably determines which mass flow process is predominant although debris flows have not been recognised in the core or seismic data base.

Turbidite deposition is prevalent over the two major downslope dispersal routes (southern Tugela Cone and 29° 25'S Canyon) based on core lithofacies data (Figs.8.41 and 8.42). Well-defined channels are not observed over the southern Tugela Cone suggesting that the turbidity currents move downslope as broad-fronted, unconfined sheet flows rather than in the channelised mode (facies assemblage I). However, down-canyon turbidity current flow must be operative in the major Tugela and 29° 25'S Canyons. These major conduits supply terrigenous detritus to the basin plain as evidenced by the suprafan construction at the mouth of the Tugela Canyon (Fig.9.3).

Hemipelagic sedimentation dominates zones of reduced terrigenous supply. Over the eastern Tugela Cone canyon-bypassing pirates a large proportion of potential sediment input while the slope north of the 29° 25'S Canyon features inherent low detrital supply. In these regions, slow hemipelagite deposition (facies assemblages IIa and IIb) continues over the entire slope rather than unstable terrigenous build-up along the upper slope. The incidence of turbidity current flow is accordingly reduced probably at the expense of slow gravitational creep.

Allochthonous sediment movement as a result of local oversteepening and high sedimentation rates is noted over the northern continental slope (Fig.8.42). Here, four slides have transported a large volume of sediment downslope (section 7.5) in post-Jimmy times. Similarly, seismic facies over the SW continental slope suggests that slumping has been a prime transport agent in this area. Recognition of narrow canyons in the south of this area implies slope bypassing with sediment being conduited directly to the lower continental slope.

Over the basin plain, terrigenous sedimentation is confined to the slow influx of suspended fines and perhaps occasional turbidite incursions south of the Tugela Cone. Biogenic-rich sedimentation is therefore prevalent in these areas (facies assemblage IIb). Similarly, the Mozambique Ridge and Central Terrace provinces are dominated by pelagite sedimentation although post-depositional modification of Central Terrace sediments by current winnowing may be masking the original composition.

8.6.5.3 Winnowing and Redistribution

Current scour in the Natal Valley significantly influences sediment distribution patterns by initiating winnowing and redistribution processes. In this respect, both deep Agulhas Current flow and North Atlantic Deep Water (NADW) are active.

The Agulhas Current exerts a very strong influence on shelf dynamics by formation of the shelf sand stream. This southward-flowing series of dune trains (Flemming, 1981) is continuously recharged by erosion of the nearshore sand prism by the meandering Agulhas Current. Almost all fines are winnowed out from this high energy mobile belt. Along the outer shelf, current velocities are so high that only gravel lags are in hydraulic equilibrium (Flemming, 1981).

Downslope, on the upper Tugela Cone, current influences are less severe but are sufficient to generate a microtopography style (section 7.2.4) and lithofacies type (facies assemblage IVb) indicative of current action. Winnowing and redistribution are locally confirmed by the delineation of pre-Jimmy strata (sediment unit C) outcrops (Fig.7.2).

In deeper water zones, the Central Terrace (Figs.7.2 and 8.42) provides the most visible evidence confirming current scour. In this physiographic zone, sea floor outcrops of sediment units B and C, erosional moating and development of sandy contourite lithofacies (facies assemblage IVa) attests to current vigour. In terms of sediment dispersal, these strong currents winnow out a major proportion of the fine-grained detritus and fragmented or juvenile biogenic debris. Coarse foram sands remain in equilibrium on the scoured terrace crest.

Resuspended detritus is finally dumped over the south and SW flanks of the Central Terrace or over the northern basin plain.

Deep Agulhas Current flow also locally influences sedimentation over the Mozambique Ridge by moulding large current-controlled sediment billows and scour moats. Similar influences over the NE Tugela Cone adjacent to the 29° 25'S Canyon have resulted in construction of a large field of sediment waves confirming active redistribution processes.

Cyclonic NADW flow around the basin plain margin (Fig.8.42) fosters processes of sediment redistribution. Indicators of current flow include abnormal thinning of sediment unit D, local mound and moat formation, microfossil reworking, eastward dispersal of terrigenous muds south of the Tugela Cone and development of both muddy and sandy contourite lithofacies (facies assemblages IIIa and IVa; Fig.8.40). NADW flow probably only influences the mud fraction during sediment redistribution. In contrast, the more vigorous Agulhas Current is competent enough to entrain and redistribute sand-grade detritus.

8.6.5.4 Sediment Export

Under influence of the high flow competence of the Agulhas Current, significant volumes of fine-grained detritus (terrigenous and biogenic) must be carried south in suspension (Fig.8.42) to be deposited in the southern Natal Valley and Transkei Basin. Some detritus in suspension, introduced from the north by Agulhas Current flow, may completely bypass the mid Natal Valley being transported south to abyssal depocentres. Unavailability of suspended load data for Agulhas Current waters prevents construction of a detailed modern sediment budget

(section 6.7.2). It is therefore impossible to estimate the proportion of the mud input transported south to abyssal depocentres.

Fine-grained detritus may also be escaping from the mid Natal Valley under influence of NADW flow. Along the basin margin adjacent to the Mozambique Ridge, southward cyclonic NADW flow, exiting from the mid Natal Valley, has sculptured an elongate non-depositional moat (section 7.2.7.2). Along this pathway (Fig.8.42), suspended muds may be exported south to Transkei Basin depocentres.

To a lesser extent, sand-grade detritus may be exported from the mid Natal Valley system by being entrained in the shelf sand stream. This mechanism only affects the SW continental shelf area (Fig.8.42) since, to the north, the bedload is either retained within individual shelf compartments or transported into the basin at shelf offsets (Flemming, 1981). In basinal areas, bedload losses from the mid Natal Valley must be minor being restricted to occasional mass flows or turbidites of sufficient kinetic energy to traverse the flat basin plain.

Other than the above mechanisms, absence of demonstrable sediment dispersal export routes implies that a major proportion of detritus supplied to the mid Natal Valley is retained within the basin.

CHAPTER 9 TUGELA FAN DEVELOPMENT

9.1 INTRODUCTION

Numerous modern deep-sea fans have been studied over the last 15 years leading to the establishment of several descriptive models characterising fan morphology, facies and development (see Nelson and Nilsen, 1984 for review). These models have been derived from conventional seismic-stratigraphic and sedimentological data analysis while the recent use of long-range side-scan sonar (GLORIA) has revealed detailed information about channel morphology and relative age relationships (Damuth and Flood, 1983/1984; Masson et al, 1985).

In this chapter, generalised models of morphology, depositional patterns and development of deep-sea fans are described. Using seismic, bathymetric and sedimentologic data, the development and modern status of the Tugela Cone is compared to conceptual models of deep-sea fan evolution.

9.2 MODEL OF DEEP-SEA FAN DEVELOPMENT

9.2.1 Major Depositional Pattern Controls

Major factors influencing deep-sea fan development have been fully discussed by Stow et al (1983/1984) who identify three primary controls: (1) sediment type and supply; (2) tectonic setting and activity; and (3) sea-level fluctuations.

The volume of sediment supplied to a marine basin strongly influences the dimensions of the resultant fan while sediment grain size helps determine the extent and efficiency of the fan channel systems. Tectonic setting of a depositional basin

controls basin size, shape and gradients and thus influences fan shape, channel growth patterns and facies distributions. Relative sea-level is a major control over fan development. During high sea-level stands, sediment transport across the shelf is retarded and fans enter a relatively inactive phase. In contrast, during low sea-level stands, sediments are funnelled directly to slope canyons resulting in higher sedimentation rates and enhancement of fan growth. Low sea-level stands probably correlate with increased frequency of turbidity current activity and greater supply of coarse detritus to deep-sea fans (Shanmugam and Moiola, 1982). Sea-level fluctuations may instigate highly contrasting styles of fan growth (Stow et al, 1983/1984): (1) low sea-level - progradational sequences, fan rejuvenation and channel incisement; (2) high sea-level - regradational sequences, channel and lobe abandonment.

9.2.2 Deep-Sea Fan Classification and Morphology

Stow et al (1983/1984) identify two end-member submarine fan types (elongate and radial fans) and a third end-member non-fan system (slope debris apron) resulting from variations in sediment type and supply. Elongate fans (>100 km diameter) are mud-dominated with high input rates and the sediment source is usually a major river or delta. Radial fans are sand-dominated with medium input rates and are supplied via a single canyon system from a local river or littoral drift cell (Stow et al, 1983/1984). Most fans are hybrid in character showing mixed features of both end-member types.

Fans commonly develop with asymmetric shapes because of confining basin morphologies, disruptive tectonic features

(seamounts or basement high plateaux) and variable channel growth patterns (Nelson and Nilsen, 1984). Most fans have recognisable morphologic divisions (e.g. Fig.9.1) that may be related to distinct facies associations (e.g. Fig.9.2).

The rugged concave-upward (Damuth and Kumar, 1975) upper fan is characterised by a single, active, leveed, distributary channel continuous with the supply canyon (assuming restriction of sediment supply to one submarine canyon). The depositional channel is commonly distinguished by a sinuous meandering thalweg flanked by relatively flat terraces which grade into prominent levee systems (e.g. Fig.9.2). Upper fan ruggedness is a result of levee development and remnants of abandoned fan channels. Steepest gradients occur in the upper fan area. During active periods of fan growth, the major active submarine canyon usually directly feeds into the main leveed upper fan valley. Canyons are morphologically distinct from upper fan valleys and are recognised by deep erosive V-shaped profiles, high wall relief, absence of levees and the presence of tributaries (Nelson and Kulm, 1973). Canyon character may bear little relation to fan dimensions. Sizes of upper fan distributary channel complexes are highly variable. Axial depths may range from 8 m (Navy Fan - Normark, 1978) to 225 m (Amazon Fan - Damuth and Kumar, 1975) while widths of levee/channel systems may vary from 10-100 km (Normark, 1978; Curray and Moore, 1971). The main upper fan channel is the depositional site for the coarsest fraction of sediment supplied to the fan. Coarsest detritus is restricted to the channel thalweg, occasionally spilling onto flanking levees. Upper fan levee, overbank and crevasse splay successions predominantly comprise thin-bedded turbidite facies (Fig.9.2;

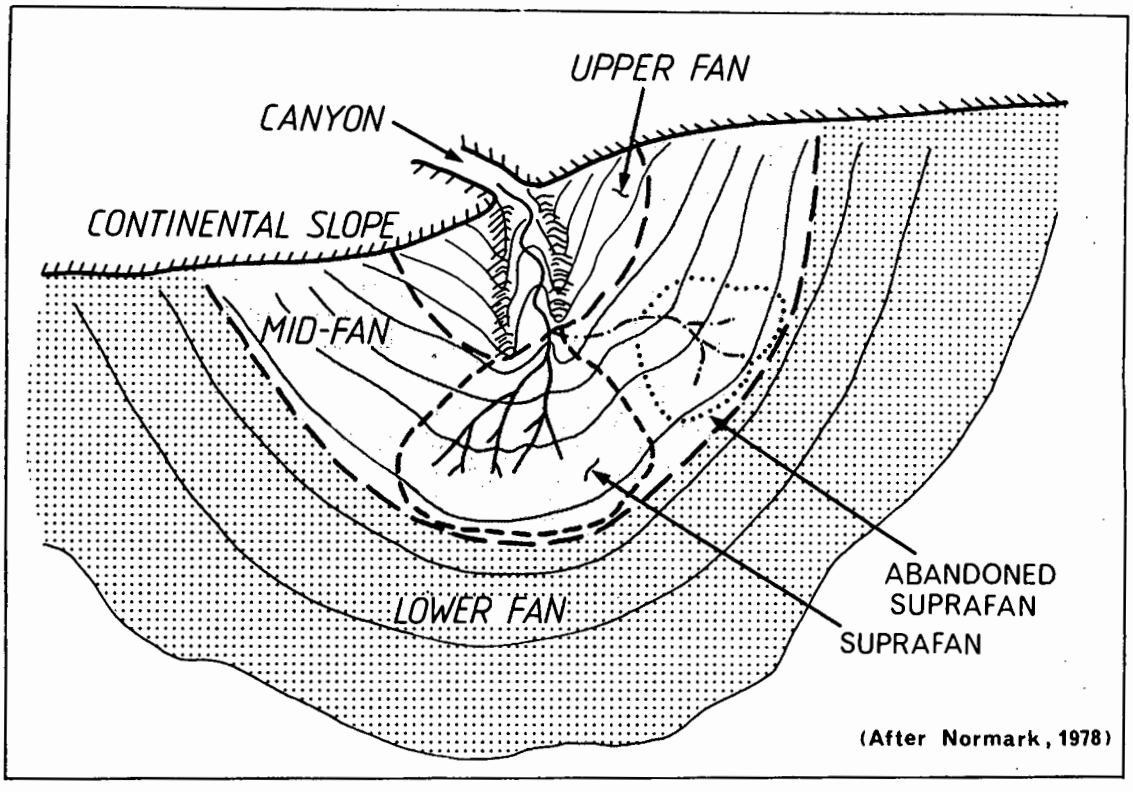

Fig. 9.1 GROWTH MODEL FOR SUBMARINE FAN (RADIAL)

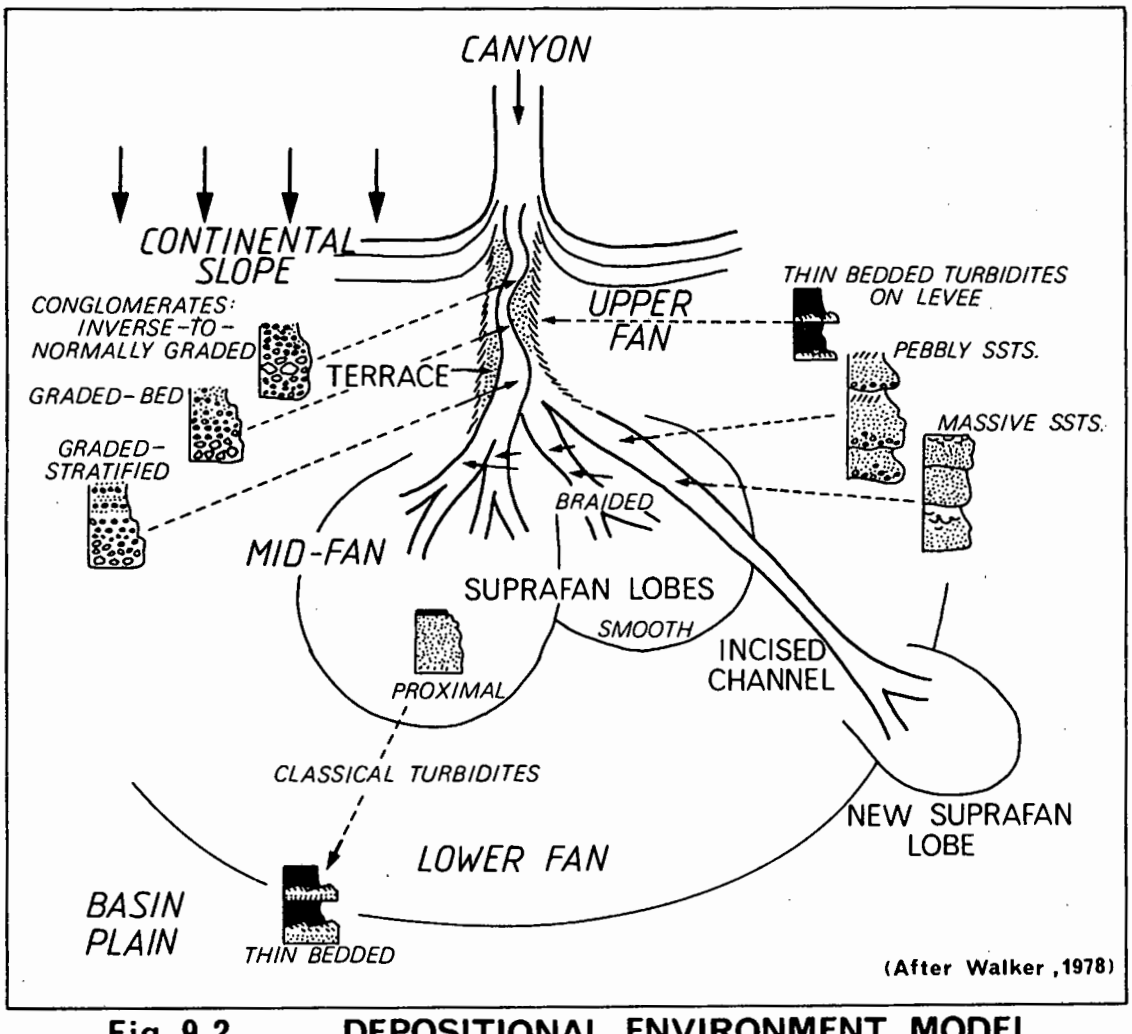

Fig. 9.2 DEPOSITIONAL ENVIRONMENT MODEL FOR SUBMARINE FAN (RADIAL)

Walker, 1978). Not all upper fan valleys are depositional. Erosional canyons may be incised into the upper fan region dissecting the fan surface and resulting in sediment bypassing much of the fan area (e.g. La Jolla fan valley - Shepard and Buffington, 1968).

The middle fan region is characterised by a convex-upward bathymetric profile. On radial fans these depositional bulges have been termed 'suprafans' (Normark, 1978) and the mid-fan zone is constructed of several coalescing suprafan lobes (e.g. Figs.9.1 and 9.2). Middle fan valley morphology is determined by fan type. On smaller radial fans, mid-fan valleys rapidly lose their levees and develop a braided character (Nelson and Nilsen, 1984). In contrast, on large mud-rich elongate fans, mid-fan valleys develop high-sinuousity meanders with local bifurcations perched on top of a wide levee systems (Damuth and Flood, 1983/1984). The mid-fan depositional bulge probably comprises a series of overlapping and stacked levee complexes. Meander development is proportional to fan steepness being most poorly formed on steep fans (e.g. Rhone Fan - Droz and Bellaiche, 1985). Middle fan deposition is dependent on fan type, fan steepness and sediment supply. Lithofacies may vary from massive or pebbly sand in braided distributary channels to thin-bedded, fine-grained turbidites over the levee complexes (Walker, 1978). Suprafans may also be constructed at the termination of erosional fan valleys (Fig.9.2).

The lower fan and basin plain display a smooth concave-upward topography with low gradients (Damuth and Flood, 1983/1984). Numerous small distributary channels may cross the lower fan but these are not associated with levee development.

Slow hemipelagite deposition interrupted by turbidites are characteristic of the lower fan zone resulting in a uniform stratified succession.

Application of these generalised models of fan processes and depositional patterns to modern evolution of the Tugela Cone is dependent on retrieval of accurate geophysical and sedimentological data. Conventional echo-sounding and single-channel seismic reflection profiling techniques are noted for lack of resolution thus hampering the recognition of diagnostic morphological and seismic facies characteristics. Piston and gravity coring methods allow only shallow penetration into fan sediments rarely reaching the shallowest sub-bottom reflectors and often only retrieving Holocene sediments (Normark, 1978). The distribution and character of Holocene sediments on numerous modern fans may not be in equilibrium with gross fan morphology and structure. In general, short core samples from modern fans may only reflect Holocene conditions (high sea-level stand), probably significantly different from preceding Tertiary conditions.

9.3 TUGELA FAN DEVELOPMENT

9.3.1 Modern Status

In this section the Tugela Cone and deep basin plain are considered as integral zones of a deep-sea fan and are thus collectively referred to as the Tugela Fan. It is emphasised that this study does not examine the full extent of the Tugela Fan since southern margins of the lower fan (deep basin plain) merge into the abyssal Transkei Basin at a depth of ~4000 m close

to 34°S (Dingle and Camden-Smith, 1979).

9.3.1.1 Tugela Fan Morphology

The Tugela Fan (Tugela Cone and deep basin plain) is divided into three morphologic divisions (Fig.9.3) based on acoustic characteristics and general morphology. The upper fan extends from the shelf break to approximately 1500 m where there is a prominent slope break (Fig.9.3). The rugged, concave-upward upper fan zone corresponds to the upper slope physiographic unit (Fig.3.5; unit 5). Gradients average around 1:33 (1,7°) reaching a maximum of 1:13 (3,8°) beneath the shelf break. The major morphologic feature of the upper fan is the Tugela Canyon and associated levee on its NE flank. The middle fan extends from 1500 m to 2500-2900 m (Fig.9.3) where another gradient change marks the transition into the lower fan (deep basin plain). The middle fan is hummocky and convex-upward corresponding to physiographic units 6 and 7 (Fig.3.5). Mid fan gradients range from 1:27 (2,1°) to 1:125 (0,5°). Major morphologic features of this fan zone include the erosional Tugela Canyon (section 7.4.2.1) and the more sinuous 29° 25'S Canyon which shows features of both depositional and erosional processes (section 7.4.2.2). Stacked overlapping levee complexes border the 29° 25'S Canyon. The lower fan extends southwards and eastwards from about 2500-2900 m (Fig.9.3) and corresponds to the deep basin plain (Fig.3.5; units 14-16). Gradients are low ranging from 1:200 (0,3°) to 1:600 (0,1°) over the smooth, concave-upward lower fan (basin plain). Narrow, shallow unleveed channels are infrequently developed over the lower fan zone (Fig.9.3).

The upper and middle fan zones together comprise the Tugela

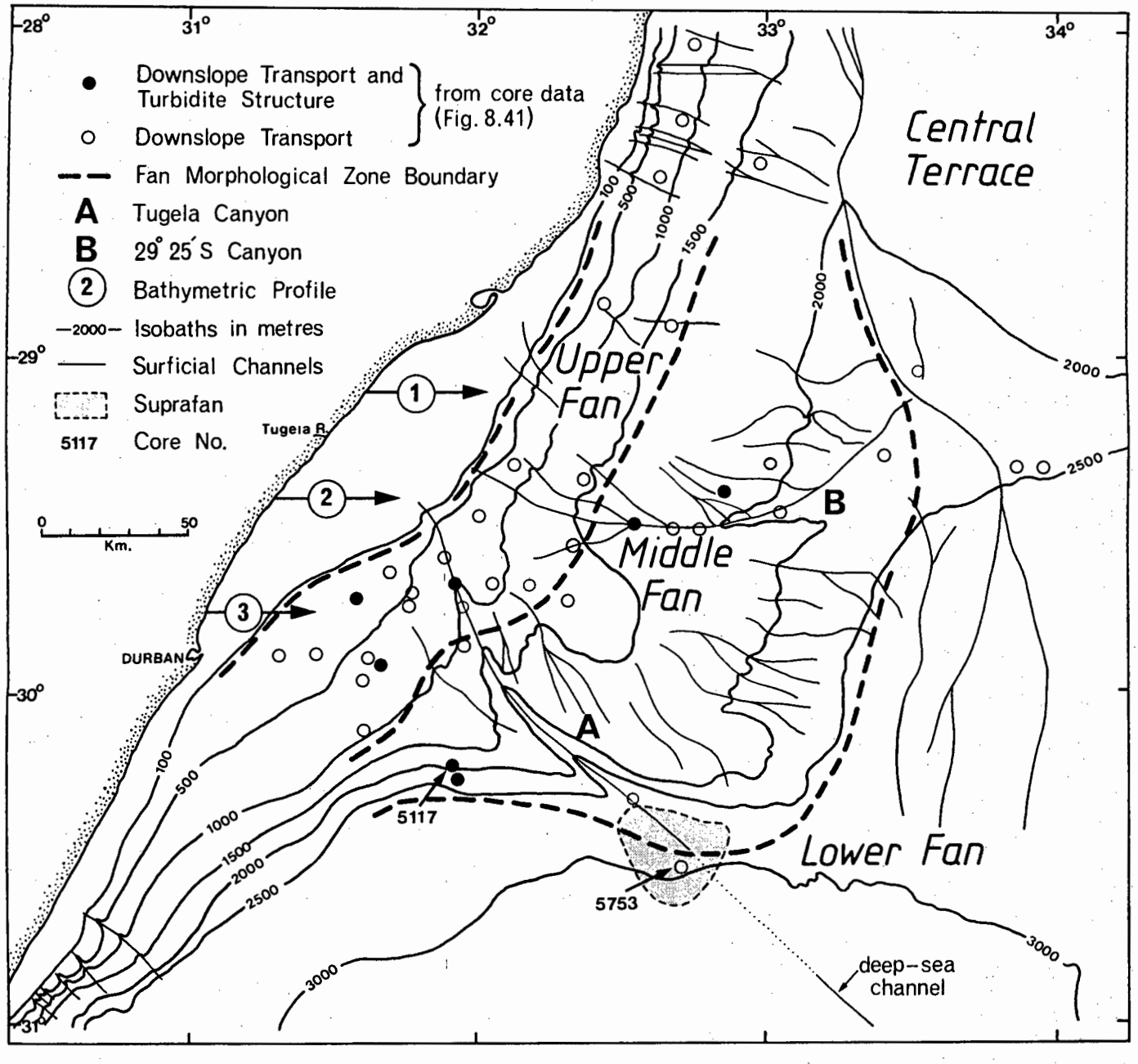

PROFILES

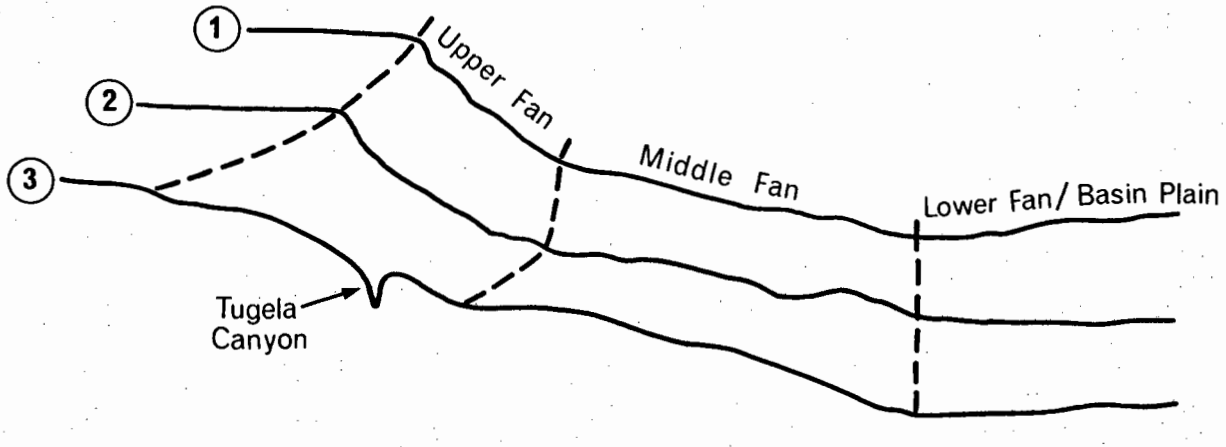

Fig. 9.3 TUGELA CONE MORPHOLOGY AND DISTRIBUTION OF SURFICIAL CHANNELS

Cone which exhibits asymmetric 'triangular' geometry and is approximately 230 x 170 km in dimension (Fig.9.3). The large lower fan region extends approximately 400 km south of the mid/lower fan boundary. Tugela Fan development has been strongly influenced by basinal confinement and obstructing tectonic features. Elongation of the Natal Valley in a N-S direction, with the Mozambique Ridge forming an eastern boundary, has constrained the lower Tugela Fan to prograde southwards in a coast-parallel direction. Sediment input along the east coast margin south of Durban (e.g. Dingle and Robson, 1985) and resultant debris apron development must have interfered with and modified lower Tugela Fan development. The Central Terrace (Fig.9.3) and East Tugela Ridge basement highs have also disrupted fan growth by preventing progradation in a NE direction. Deep current action has modified physiography over two mid fan regions (section 7.2). Oversteepening of the Tugela Cone southern flanks and the presence of mounded facies over the eastern flanks (section 7.2.5.1) are atypical of standard fan morphologies (Normark, 1978) but may be attributed to deep current activity.

9.3.1.2 Canyon and Valley Systems

A striking feature of the Tugela Fan is the poor development of surficial depositional channels (Figs.3.2 and 9.3) compared to other active modern fans (e.g. Amazon deep-sea fan; Damuth and Flood, 1983/1984). The series of coalescing but discontinuous channels over the mid fan (Fig.9.3) probably represent abandoned and partly-infilled distributaries. Infrequent wide shallow channels can be traced N-S over the lower fan (Fig.9.3). Two

large canyons have been formed on the upper and middle fan zones: Tugela Canyon and 29° 25'S Canyon.

The Tugela Canyon slices obliquely across the upper and middle fan (southern Tugela Cone) and was probably initiated during a post-Jimmy (early Pliocene) sea-level low stand (section 7.4.2). Morphological and seismic criteria (V-shaped profile, high wall relief, absence of significant levee systems, development of tributaries and reflector truncation - section 7.4.2 and Fig.9.3) indicate that the Tugela Canyon was essentially erosional in origin. However, levee construction on the NE canyon margin (Fig.3.7) implies local overbank deposition in the upper fan region. The Tugela Canyon is oversized relative to standard fan canyons retaining an erosional character across both the upper and middle fan zones. Oversized canyons are typically formed by the action of large mass failure processes or through excessive drainage during low sea-level stands (Nelson and Nilsen, 1984). Although apparently ending at the base of the mid fan (Fig.9.3), the Tugela Canyon may extend into the parallel-aligned, 60 m deep channel on the lower fan (Fig.9.3). Infilling of an intervening zone of the lower fan (suprafan development - Fig.9.3) argues for the modern stagnation of this valley connection.

The 29° 25'S Canyon cross-cuts the middle fan (eastern cone) also losing its identity on merging with the lower fan. Morphology and seismic criteria suggest that the 29° 25'S Canyon was formed by combined depositional and erosional processes (section 7.4.2.2). Canyon sinuousity, extensive levee system development and a U-shaped cross section indicates dominance of depositional processes. Since at least Angus (early Oligocene)

time, the 29° 25'S Canyon has functioned as the major middle fan distributary valley resulting in significant levee system aggradational growth. Low sinuousity of this fan valley may be a function of fan steepness (Nelson and Nilsen, 1984). In the modern 29° 25'S Canyon, erosional processes have assumed dominance as indicated by canyon overdeepening (axial depths - 250 m), axial outcrop of pre-Jimmy strata (Fig.6.18) and abundant reflector truncation (section 7.4.2.2). The infilling of the 29° 25'S head zone suggests modern inactivity and stagnation as a major sediment dispersal conduit. Head zone infilling may have commenced with post-Jimmy formation of the Tugela Canyon which could have pirated potential input to the 29° 25'S Canyon. With reduction in sedment supply, dispersal processes may have stagnated leaving the head zone to slowly fill by draping and gravitational creep processes.

The modern distribution and character of fan valleys and channels is atypical of an active deep-sea fan. Anomalous situations include: (1) the Tugela Canyon is oversized and dominantly erosional through the upper and middle fan regions; (2) there is no active mid fan distributary valley. The 29° 25'S Canyon, although an active distributary system through the geologic past, is presently in a stagnant or erosional phase and levee development has temporarily ceased; and (3) minor distributary channels on the mid and lower fan lack definition and are probably being infilled in an abandonment phase.

9.3.1.3 Sediments and Lithofacies

Sediment cores provide textural and component information allowing definition of the modern terrigenous depocentres and

dispersal routes on the Tugela Fan. Depositional processes, facies assemblages and sediment dispersal have been fully discussed in section 8.6 and only a brief summary is presented in this section. The major modern terrigenous depocentre and dispersal route corresponds to the facies assemblage I turbidite province which is delineated over the upper and southern slopes of the Tugela Cone (section 8.6.3; Figs.8.39 and 8.40). In fan terminology, facies assemblage I encompasses the southern upper and mid fan zones. In this province, greyish-green to olive green fine-grained and thin-bedded turbidites (Fig.9.3 for location) are the dominant Holocene lithofacies. The absence of well-defined channels suggests that the Holocene turbidites have moved downslope as broad-fronted unconfined sheet flows. Although the 29° 25'S Canyon has assumed a stagnant or erosive status in modern times, minor downslope dispersal of biogenic-rich turbidites is operative in the canyon area (Table 8.8 and Fig.8.39; facies assemblage IIIb).

Outside the terrigenous depocentres, over the eastern Tugela Cone (mid fan) and basin plain (lower fan), Holocene sediments are predominantly light yellowish-brown calcareous marls or foram oozes (section 8.6.3; facies assemblages II-IV). Dominance of hemipelagite and pelagite lithofacies indicates cessation of significant terrigenous input and temporary inactivity of fan growth.

9.3.1.4 Sedimentation Rates

The Holocene/Pleistocene boundary has been delineated in cores 5117 and 5753 retrieved from the mid fan region (Fig.9.3). This 11 000 yr BP datum (Broecker et al, 1960) is recognised at

sub-sea floor depths of 45-80 cm in core 5753 and 75-90 cm in core 5117 (section 8.4.1.2; Salmon, 1979a). Using these data, average Holocene accumulation rates range from 4,1 - 8,2 $cm/10^3yr$. These rates are derived from the major terrigenous depocentre and should represent maximum Holocene accumulation rates on the Tugela Fan. Similar Holocene growth rates (4-6 $cm/10^3yr$) have been computed for the Amazon deep-sea fan (Damuth and Kumar, 1975).

Maximum post-Jimmy (early Pliocene) sedimentation rates are presented in Table 6.3. Accumulation rates for the major post-Jimmy depocentres (Table 6.3; sub-facies D_5-D_7) vary from 8,4-13,2 $cm/10^3yr$ and are thus higher than the Holocene rates. The post-Jimmy rates are averages of high rates associated with low sea-level stands and low rates correlatable to high sea-level stands. Thus, although no empirical sedimentation rates are available for the Pleistocene (sea-level low stand), they are inferred to be significantly greater than calculated Holocene rates.

9.3.1.5 Holocene Stagnation

Low Holocene accumulation rates confirm that large zones of the Tugela Fan, including the modern terrigenous depocentres (facies assemblage I; core 5117), are presently in an inactive phase. Reduced Holocene terrigenous detrital supply to the mid fan channel system has caused its temporary abandonment and draping by hemipelagites. Holocene stagnation of the eastern Tugela Cone (middle fan) may also have been a response to changes in fan canyon status and resultant canyon-induced sediment bypassing processes. In post-Jimmy times, formation of the

erosive oversized Tugela Canyon and cessation of large scale depositional processes in the 29° 25'S Canyon marked a major reorganisation of the Tugela Fan valley system. Bedload detritus subsequently supplied to the upper fan was probably funnelled into these non-depositional canyons to be transported past the mid fan region directly onto the lower fan. Similar bypass processes have been documented in the La Jolla and Monterey fan valleys with resultant stagnation of the upper and middle fan areas (Piper, 1970; Hess and Normark, 1976). Sediment bypassing via the Tugela Canyon is identified by the development of a suprafan at its termination (Fig.9.3) conforming to the incised channel suprafan model (Fig.9.2) of Walker (1978). Calcareous marls retrieved in core 5753 (Fig.9.3; Appendix B2) confirm that this suprafan has not been active during the Holocene and was probably constructed during a low sea-level stand.

During low sea-level phases, the overall sediment supply rate was probably high enough to sustain extensive fan growth and rejuvenate the 29° 25'S distributary fan valley system. In contrast, reduced terrigenous sediment supply during high sea-level stands (e.g. Holocene) has resulted in stagnation of large sections of the Tugela Fan.

Several other studies have emphasised the widespread Holocene stagnation in modern fans (Normark, 1978; Damuth and Flood, 1983/1984; Stow et al, 1983/1984). Present day relative inactivity of large zones of the Tugela Fan conforms to this worldwide pattern.

9.3.2 Cretaceous and Tertiary Development

In the absence of borehole data, the geological history of

the Tugela Fan cannot be accurately established. Total fan thickness is at least 7250 m (Table 6.2). Depositional sequence boundary mapping indicates that the Tugela Fan was well established by the mid Cretaceous as delineated by the horizon McDuff time-depth map (section 6.6.1) and had already aggraded to a thickness of 3200 m (Table 6.2). Seismic-stratigraphic analysis of the fan sediment pile identifies offlapping progradational fan complexes within sediment units B, C and D (Table 6.1). Maximum fan growth equates to these progradational episodes denoting a high sedimentation rate in excess of the subsidence rate. Deltaic build-out to the outer shelf (borehole Jc-1; du Toit and Leith, 1974) during deposition of units B and C would have provided an abundant sediment source to foster Tugela Fan offlap growth. Active fan growth often takes place during sea-level low stands (Stow et al, 1983/1984). Unit D high sedimentation rates (Fig.6.20) and offlap fan growth (Table 6.1) may be equated to low sea-level stands (Late Pliocene and Pleistocene glacials) and general late Tertiary climatic deterioration (Donnelly, 1982) fostering higher hinterland sediment erosional yields.

Limitations in seismic profile coverage and resolution prevent comprehensive mapping of palaeo-valley and levee systems. However, the 29° 25'S Canyon has been operational since at least the early Oligocene (Figs.6.17 and 6.18) and is the primary distributary channel system on the Tugela Fan. This canyon shows characteristics of both depositional and erosional processes and these may speculatively be linked to periods of low and high sea-level respectively. The 29° 25'S Canyon is flanked by thick fossil levee systems (section 7.4.2.2; Fig.7.9d). It is probable

that the depositional bulge over the eastern mid fan (Fig.9.3) has been constructed by stacking of overlapping levee systems associated with this fan valley. In contrast, the Tugela Canyon is post-Jimmy in age and erosional in origin and has thus not enhanced upper and mid fan growth.

9.3.3 Summary

Seismic and sedimentological studies indicate that development of the Tugela Fan (comprising the Tugela Cone and basin plain) has followed standard models of deep-sea fan evolution (section 9.2). The characteristic threefold fan morphological zonation (upper, middle and lower fan) is recognised (Fig.9.3) although the overall physiographic structure is atypical of deep-sea fans. Structural modification is a response to growth confinement and interference by the Mozambique Ridge and Central Terrace tectonic highs.

The 29° 25'S Canyon has acted as the major mid fan distributary channel/levee system since at least the early Oligocene. The mid fan depositional bulge has been constructed of overlapping and stacked levee systems associated with this canyon. Major fan growth has probably taken place during low sea-level stands and/or phases of deltaic progradation to the outer shelf. Under these conditions terrigenous detritus is directly conduited into the slope canyon systems. Thick sequences with offlap reflector configuration identify zones of maximum fan aggradation. Since the early Oligocene (post-Angus), maximum aggradation (Figs.6.13 and 6.14) has taken place over the Tugela Cone upper slope (upper fan) and the eastern Tugela Cone (mid fan).

Formation of the erosive Tugela Canyon in post-Jimmy times has disrupted standard fan growth patterns. Major effects of the Tugela Canyon formation include: (1) inducing sediment channelisation into the canyon with resultant bypassing of the upper and mid fan zones; and (2) ? relative abandonment and head zone infilling of the 29° 25'S Canyon through pirating of potential bedload supply. Changes in canyon status and reduced Holocene terrigenous sediment supply to the deep basin have together induced temporary stagnation of fan growth over the eastern Tugela Cone (mid fan) and the basin plain (lower fan). Cessation of bedload supply to the mid fan distributary system has resulted in abandonment and channels are presently being infilled by hemipelagite/pelagite drape lithofacies.

Muddy turbidites identified over the southern upper and mid fan zones (Fig.9.3) define the only major active Holocene terrigenous depocentre although sedimentation rates in this area are still relatively low (4-8 cm/10^3yr).

The large size but atypical morphology of the Tugela Fan prompts its classification as an hybrid fan type (Stow et al, 1983/1984) but with close affinities to the elongate fan type end-member.

CHAPTER 10 SUMMARY OF MAJOR CONCLUSIONS

10.1 TECTONIC AND CRUSTAL ELEMENTS

10.1.1 Basement Elements

Regional mapping of acoustic basement has defined the major structural elements within the Natal Valley (Figs.5.1 and 5.14). The continental margin and Mozambique Ridge are the major basement structural high zones and thus define general basin configuration. Subsidiary ridge and pinnacle complexes (South Tugela, East Tugela and Naude Ridges) are demarcated coring the southern and eastern Tugela Cone and southernmost Central Terrace respectively. Palaeo-physiographies of the Central Terrace and proto-Tugela Cone were probably strongly influenced by these barriers to free sediment dispersal. North of the Naude Ridge on the Central Terrace, relatively elevated basement is postulated to satisfy both seismic and magnetic model data constraints. South of the ridge complexes and west of the Mozambique Ridge, oceanic crust floors the deep basin plain.

10.1.2 Crustal Types

Four basement crustal types are distinguished in the mid Natal Valley: continental crust; subsided thinned continental or transitional crust; marginal ridges; and oceanic crust (Fig.5.14).

The eastern limit of normal elevated continental crust is defined by three contiguous geological lineaments: (1) the Agulhas Fracture Zone; (2) the cross-shelf trending basement scarp from 31°S to 29°S; and (3) the Lebombo Line.

The proposed distribution of thinned continental or transitional crust is more speculative. Gravimetric (Darracott, 1974), refraction (Ludwig et al, 1968), magnetic and seismic reflection data suggest that a southern limit may be demarcated by alignment of the marginal ridges (Naude, East Tugela and South Tugela Ridges) and a colinear non-magnetic fracture ridge east of the Naude Ridge. To the north and west, the Central Terrace and Tugela Cone are floored by subsided thinned continental crust. Heavy sediment loading over the Tugela Cone has induced greater subsidence relative to the Central Terrace. Crustal structure of the Mozambique Ridge remains unresolved although its morphology together with refraction (Hales and Nation, 1973) and gravimetric (Scrutton, 1976) data favour genesis as a thinned, subsided continental fragment.

The marginal ridges (Naude, East Tugela and South Tugela Ridges) are considered as a composite crustal type group on account of their similar tectonic settings. Geochemical analyses of basalts from the East Tugela Ridge suggest a 'transitional' character but with continental affinities (Fig.5.13). It is postulated that these marginal ridges were constructed by extensive volcanism during initial sundering of South America (Falkland Plateau) and Africa. Attitude of the basement ridges may reflect gross geometry of the continental/oceanic crust boundary (COB) in the mid Natal Valley (Fig.5.14).

The deep basin plain is underlain by normal oceanic crust as indicated by refraction studies (Hales and Nation, 1973) and recognition of Mesozoic sea-floor spreading magnetic anomalies.

Morphological development of the Natal Valley basin throughout its history has been strongly influenced by the

disposition of basement-high zones: the Mozambique Ridge (east); foundered, thinned continental basement (north and NE); and the African continental margin (west). This basement configuration was primarily delineated during the pre-drift taphrogenic phase of basin development and during fragmentation of West Gondwana. Later modifications were induced by post-drift epeirogenic subsidence and sediment loading.

10.1.3 Basement Subsidence

Subsidence rates for several Natal Valley basement provinces have been calculated and compared to generalised subsidence models. Rates for the East Tugela and Mozambique Ridges are 18,5 m/my implying that basement is thinned continental crust (after model of Kinsman, 1975) in agreement with refraction and gravimetric data. A subsidence rate of 17 m/my over a 95 my period suggests that continental crust under the shelf zone (borehole Jc-1) is of normal (30 km) thickness. Oceanic crust in the Natal Valley is 1500 m shoaler than subsidence curves predict, perhaps as a result of incomplete decoupling from the surrounding relatively buoyant continental blocks (Table 5.5).

Juxtaposition of the northern Natal Valley, Mozambique Ridge, Agulhas Bank and Falkland Plateau in a Gondwana reconstruction composes an elongate zone (1500 x 500 km) cored by subsided thinned continental and/or transitional crust. These areas were subjected to a protracted phase (~80 my) of heating, uplift and erosional cycles primarily associated with axial uplift along incipient rifts created during East/West Gondwana and West Gondwana continental fragmentation. Subsidence-related crustal thinning, post-drift cooling and local sediment loading

provides an explanation for the abnormally-large zone of subsided continental crust bordering SE Africa and including the Falkland Plateau (Fig.4.8).

10.1.4 Mesozoic Magnetic Anomalies

The recognition of Mesozoic magnetic anomalies M0-M12 within the southern Natal Valley (Fig.5.9) provides constraint on the motion of South America (Falkland Plateau) relative to Africa during the early opening phase of West Gondwana. Delineation of the M0-M12 sequence also provides support for the revised SW Gondwana reconstruction of Martin, Hartnady and Goodlad (1981). Colinear with M12, magnetic anomaly G (Rabinowitz and LaBrecque, 1979) is recognised north of the South Tugela Ridge, an acoustic basement ridge suspected to have been emplaced within continental crust immediately north of the COB during the initial rifting phase. Starting from a revised West Gondwana reconstruction (Martin et al, 1981), the Falkland Plateau can be rotated into the Natal Valley superposing corresponding Georgia Basin and Natal Valley magnetic anomalies. This achieves optimum continuity of inter-continental structural lineaments (section 5.3.4) by overlapping of an anomaly intermediate to M10 and M11 ($\sim$M10N after Larson and Hilde, 1975). It is inferred that the Natal Valley COB is located between anomalies M10 and M11, implying that in this zone of SW Gondwana, sea floor spreading commenced at $\sim$125 Myr.

10.1.5 Mozambique Ridge Micro-Plate Movement

With improvement in definition of the major crustal type boundaries in the Natal Valley, it is speculated that the

Mozambique Ridge is presently situated 160 km east of its pre-drift palaeo-position (Fig.5.21). Back-rotation (160 km) of the Mozambique Ridge relative to Africa along the S72°W fracture zone trend achieves a best morphological fit of the conjugate west Mozambique Ridge and east Tugela Cone/Falkland Plateau continental block margins. This reconstruction removes the untenable gap between these opposing margins as apparent in all other SW Gondwana reconstructions (e.g. Martin et al, 1981). Fracture zone trends are identified by acoustic basement morphology, magnetic lineaments, bathymetric offsets and the non-magnetic fracture ridge SE of the Naude Ridge (Fig.5.18). The non-magnetic fracture ridge is considered to be the major Mozambique Ridge translation domain and may be analogous to the Agulhas marginal fracture ridge being constructed through volcanic eruption contemporaneous with transform motion. Additional movement along subsidiary fracture zones (Fig.5.20) could improve the morphological fit.

10.1.6 Northern Natal Valley Tectonic Status

In a new reconstruction of Antarctica/Africa, Martin and Hartnady (1983) abut East Antarctica against the Lebombo Mts, thus implying that the northern Natal Valley (NNV) is underlain by oceanic crust. An oceanic crustal status for the NNV is in opposition to the distribution of tectonic elements presented in this thesis (e.g. Fig.5.14). However, Martin and Hartnady (1983) are not able to provide any evidence supporting an oceanic origin for NNV crust. Major points of contention not addressed in their hypothesis include: (1) absence of demonstrable transform faults and sea floor spreading magnetic lineations; (2) 'transitional'

nature, with strong continental affinities, of East Tugela Ridge basalts; (3) major crustal thickness and structural style change at the Naude Ridge; (4) time and space problem in generating oceanic crust 145 my old when the NNV is draped by 190-137 my old Lebombo Group volcanics; (5) the Lebombo region is recognised as a tensional regime.

These points taken together strongly argue against an oceanic crustal status for the NNV, severely weakening the case for a refit of East Antarctica against the Lebombo Mts as proposed by Martin and Hartnady (1983). All points are resolved if it is assumed that the NNV and Mozambique Ridge (north of 35°S) are underlain by attenuated continental crust (sections 5.5.3 and 5.5.8).

10.2 SEISMIC STRATIGRAPHY OF THE BASIN IN-FILL

Six physiographic provinces are recognised in the mid Natal Valley: continental shelf, continental slope, Tugela Cone, Central Terrace, Mozambique Ridge and deep basin plain. Seismic stratigraphy of the basin fill is summarised relative to these major morphologic provinces.

10.2.1 Reference Reflectors

Seismic-stratigraphic analysis of the basin fill is established with respect to three prominent regional reflectors (McDuff, Angus and Jimmy) and acoustic basement. Age relationships of the three reference reflectors have been assigned on correlation to borehole data (Jc-1 and DSDP 249), refraction site data and chronostratigraphic columns for SE African sedimentary basins (Fig.6.3). On this basis, reflector

McDuff equates to a Cenomanian-Turonian hiatus, reflector Angus correlates to an early Oligocene hiatus and reflector Jimmy is correlative to an early Pliocene hiatus. The widespread distribution of hiatuses throughout the east coast sedimentary basins corresponding in age to the major reference reflectors confirms their importance as regional sedimentation breaks often heralding seismic facies changes.

Horizon McDuff demonstrates both toplap and concordant stratigraphic relationships with pre-McDuff strata and represents a non-depositional hiatus and major seismic facies change. Numerous normal and growth faults (<300 m throw) disrupt the McDuff surface, particularly over the Central Terrace. Horizon Angus is smoother but the high incidence of truncation and mounding confirms its association with strong erosive activity. Horizon Jimmy displays erosional truncation, toplap and concordant relations with pre-Jimmy strata. Neither Angus nor Jimmy are associated with major seismic facies change.

10.2.2 Depositional Sequences

The three reference reflectors and acoustic basement define four major depositional sequences within the basin fill (sediment units A-D). These sediment units may be partitioned into sub-facies (A_1-A_3; B_1-B_7; C_1-C_8; D_1-D_7) dependent on seismic character and reflector package geometry (Table 6.1; Fig.6.11). Time-thickness maps have been constructed for each sediment unit allowing depocentre delineation and sedimentation rate calculation.

Sediment unit A (basement - McDuff) comprises a reflective onlap fill sequence within basement graben over the Central

Terrace and Mozambique Ridge locally exceeding 1,0 secs time-thickness. In the southern deep basin plain, a low reflectivity onlap fill sequence has aggraded to 1,2 secs time-thickness. Common faulting and volcanogenic sedimentation (Simpson, Schlich et al, 1974) over the basement-high provinces implies active syn-sedimentary tectonic instability and volcanism during unit A deposition.

During unit B (McDuff - Angus) deposition, active Tugela Cone progradational growth is implied from the dominance of offlap reflector configuration in sub-facies B_5-B_7. Deltaic development over the subsiding upper slope zone (B_6) locally exceeds 2,0 secs time-thickness and probably supplied abundant detritus sustaining deep-sea fan complex growth over the eastern (B_7) and northern (B_5) Tugela Cone. Early unit B onlap fill over the Central Terrace later developed into deep-sea fan complexes periodically prograding both east and west to a time-thickness of 1,0 secs. Growth faulting implies continued instability while 'contourite' mounding indicates strong current control during deposition of uppermost unit B sediments over the east Central Terrace. In the deep basin, unit B onlap fill is locally >1,0 secs time-thick.

Renewed Tugela Cone progradation and fan complex growth during unit C deposition is suggested by recognition of offlapping sequences developed to >0,6 secs time-thickness. Intermittent deep-sea fan growth (mixed offlap/onlap) continued over the east Central Terrace while onlap fill dominated the deep basin and Central Terrace crest areas. Contourite mounds within the uppermost section of unit C over the eastern Tugela Cone (sub-facies C_7) and around the Naude Ridge confirm active deep

current control on sedimentation.

Unit D offlap and mixed offlap/onlap corroborates reactivation of Tugela Cone progradational growth although with intermittent phases of stagnation (onlap). Major offlap growth occurred over the northern Tugela Cone (>0,6 secs). The Central Terrace is characterised by onlap fill/sheet drape although prograding clinoforms in the west indicate deep-sea fan growth. A thin (<0,1 secs) sheet drape is developed over the deep basin. Deep Agulhas Current flow has strongly modified unit D sedimentation causing widespread erosion over the west and south Central Terrace and upper Tugela Cone and generating contourite mounds over the eastern Tugela Cone.

Total sediment thickness reaches a maximum of 7,25 km under the upper Tugela Cone declining to vary between 2,8 and 3,5 km under the eastern Tugela Cone and deep basin. By damming southward sediment dispersal, 2,1 km of sediment has aggraded north of the Naude Ridge.

Dominant depositional styles vary through time evolving from onlap fill (unit A) through mixed offlap, onlap and onlap fill (units B-C) to offlap and sheet drape (unit D). Similar sequences mapped in Brazil are considered typical of early rift basin fill and post-rift passive offlap fill (Brown and Fisher, 1977).

10.2.3 Palaeobathymetry

Construction of time-depth maps for the depositional sequence boundaries (McDuff, Angus and Jimmy) has enabled assessment of physiographic development in the mid Natal Valley. The major physiographic provinces have been established since at

least McDuff time (Cenomanian-Turonian). Configurations of the Central Terrace and proto-Tugela Cone in pre-McDuff times were however markedly dissimilar to the present day (Fig.6.16). Structural shapes of the major physiographic elements have changed little since the early Oligocene (Angus)(Figs.6.17 and 6.18). It is inferred that the major dispersal processes and oceanographic parameters controlling sediment distribution have remained relatively constant in space during deposition of Neogene sediments.

10.2.4 Sedimentation Rates and Budget

Sedimentation rates show a distinct trend through time in parallel to global variations (Tables 6.3 and 6.4). Rates are high in unit A (41-119 m/my) dropping through units B (14-53 m/my) and C (14-42 m/my) before dramatically increasing in unit D (18-132 m/my). This trend is apparent in all physiographic zones although Tugela Cone growth is exaggerated within unit D (Fig.6.20). Major controls on sedimentation rate include: the balance between terrigenous supply and basin subsidence, relative sea-level and climatic change.

Sediment budget calculations suggest that the present hinterland erosional yield is 5-8 times higher than required to have constructed the major depositional sequences of the mid Natal Valley. Agricultural malpractice is the most favoured explanation for the excessive modern terrigenous supply rate.

10.2.5 Current-Controlled Erosion and Deposition

A combined time-thickness map of sediment units C and D

(Fig.7.1) confirms that deep currents have strongly affected basinal sedimentation patterns in post-Angus (post-early Oligocene) times. In general, thick sediment depocentres are associated with abundant detrital supply and sluggish currents. In contrast, erosional and non-depositional zones are associated with vigorous current flow.

Prominent regions of post-early Oligocene slow sediment accumulation (<8 m/my) include the deep basin margins and crest and flanks of the Central Terrace and Mozambique Ridge. Local outcrop of pre-Jimmy strata is closely coincident with these thin sediment zones. Below 2500 m, thin net sediment accumulation along the basin margins is a response to North Atlantic Deep Water (NADW) cyclonic circulation. Shallower than 2500 m, thin post-Angus sediments and outcrop of units B and C strata are results of Agulhas Current deep water flow (routes X and Y).

Other major indicators of current-control on sedimentation include: current-generated bedforms and microtopographies, asymmetric sedimentation, erosional and non-depositional moating, reworking and winnowing. The distribution of these parameters are typically concurrent and coincide with zones of thin post-Angus sediment and units B and C outcrop (Figs.7.1 and 7.2). Their recognition confirms that deep scour and winnowing processes are active over the Central Terrace/Mozambique Ridge (Agulhas Current deep water) and deep basin margins (NADW). A well-developed current regime (Fig.7.6) capable of redistributing sediment has been operative in the mid Natal Valley from at least the early Oligocene (Angus) to the present day.

Thick post-Angus sediment accumulations are restricted to four major depocentres on the Tugela Cone and SW continental

slope (Fig.7.1). Major aggradation of these depocentres probably coincided with sea-level low stands when increased hinterland erosional yield was directly debouched over the upper slope or into canyon-fan valley systems supplying the eastern Tugela Cone (Chapter 9). During glacial sea-level low stands, a weak Agulhas Current (Hutson, 1980) with resultant reduction in scour and winnowing processes would have enhanced depocentre growth. Location of the upper slope depocentres is partially controlled by the extent of shelf sedimentary compartments as defined by Flemming (1981).

10.2.6 Hiatuses

A review of hiatus development mechanisms relevant to the SW Indian Ocean provides models applicable to mid Natal Valley hiatuses. Seismic profiles show no evidence of current control in generation of horizon McDuff (Cenomanian-Turonian hiatus) although abundant faulting implies contemporaneous tectonism. Regional tectonism together with the Cenomanian/Turonian low sea-level stand may have provided impetus for hiatus development. Initiation of full oceanic circulation and upsurge in oxygenated conditions probably stimulated the major seismic facies change coincident with McDuff. Abundant current-generated mound structures associated with horizon Angus implies that current invigoration generated this major early Oligocene hiatus. An Oligocene low sea-level stand may explain the equivalent coastal hiatus (Fig.7.7). A Miocene/Pliocene boundary global sea-level low stand initiated horizon Jimmy (early Pliocene) in shelf and coastal areas (Fig.7.7). Concomitantly, intensification of deep-sea currents related to global cooling probably induced the synchronous deep basin hiatus.

10.2.7 Canyons

The 29° 25'S Canyon, traversing the eastern Tugela Cone, has been in existence since at least early Oligocene (Angus) times. Thick stacked coalescing levees are associated with the canyon confirming that it has acted as the major distributary fan-valley system on the Tugela Cone. However, modern overdeepening, side-wall reflector truncation and head zone infilling implies that the canyon is temporarily in an inactive or erosional phase.

In contrast, the Tugela Canyon which cross-cuts the southern Tugela Cone is totally erosional in origin (Fig.7.9) being formed in post-early Pliocene (post-Jimmy) times. The Tugela Canyon formed during a post-Jimmy low sea-level stand when Tugela riverine discharge was dumped directly over the shelf break. Concentration of downslope mass transport (slumps/turbidites) into one route may have initiated axial downcutting thus forming the canyon. During the modern high sea-level stand, canyon relative inactivity is inferred from infilling of its head zone and a colinear deep basin valley.

10.2.8 Allochthonous Processes

Four allochthonous sediment masses are recognised on the northernmost upper slope of the Tugela Cone within sub-facies D_5 sediments. Both translational glides and slumps are delineated. Internal bedding is well-preserved and coherent in both types confirming elastic sediment behaviour, although degrading towards the toe zone in the glides. Basal failure surfaces in the glides are approximately planar and parallel to the sea floor. In the slumps, however, failure surfaces are distinctly curved implying rotational movement. Areal dimensions of the four slides vary

from approximately 200-1100 km^2 while allochthonous sediment volumes range from 20-90 km^3. Translational glides are restricted to steeper slopes (>1°) and have lower thickness to length ratios than the slumps. A combination of high sedimentation rate (sub-fácies D_5) and downslope scour probably culminated in general slope instability. Seismic shocks may have provided the final trigger to start mass movement.

10.3 SEDIMENTOLOGY

10.3.1 Sediment Chemistry

The calcium carbonate content of surficial sediments (Fig.8.3) increases basinward ranging from <5% (continental shelf) to >90% (deep basin). This general pattern is broken over terrigenous detritus dispersal routes (south Tugela Cone and 29° 25'S Canyon) which are characterised by reduced $CaCO_3$ contents. Inactive growth areas of the Tugela Cone (eastern flanks) are enriched in $CaCO_3$. Dilution by terrigenous detritus is the major controlling factor over the modern carbonate distribution although winnowing and redistribution processes locally exert strong influences. Variation in primary productivity and carbonate dissolution have little noticeable effect.

Average basinal organic carbon contents are <0,4% although high concentrations (0,3-1,1%) characterise the Tugela mud belt, a fan-shaped mud depocentre splaying from the Tugela river estuary. Above average concentrations are also recorded over the south Tugela Cone and 29° 25'S Canyon terrigenous dispersal routes. The positive correlation between C_{org} and muddy terrigenous sediment confirms that the bulk of organic matter in modern basinal sediments is terrestrially-derived.

10.3.2 Sand and Silt Fraction Composition

Distributions of sand fraction components delineate the major terrigenous depocentres and hence zones of maximum dilution of the biogenous fraction. Over regions remote from modern terrigenous detrital supply (eastern Tugela Cone, Central Terrace, deep basin plain), whole and fragmented foram tests comprise >80% of the sand fraction. In contrast, quartz, feldspar and heavy minerals are dominant over the upper continental slope and Tugela Cone dispersal routes. The silt fraction displays similar mineralogical trends to the sand fraction. Down-core plots of sand-grade quartz and feldspar indicate an increased influx of terrigenous detritus during the Pleistocene glacials, probably in response to enhanced hinterland erosional yield and detrital supply to the deep basin.

10.3.3 Sand Fraction Surficial Microtextures

The majority of quartz grains show composite surface microtextures resulting from a combination of source breakage and subaqueous chemical and mechanical activity. All quartz grains exhibit mechanical abrasion features, probably generated during transit in the fluvial environment, littoral zone or shelf sand stream. Chemical microtextures predate mechanical abrasion and may relate to fluvial residence. Conchoidal fracture is typically relict suggesting it is a source breakage feature. Rare fresh conchoidal fracture may be a result of breakage during marine transport (shelf sand stream or mass transport processes).

Dissolution phenomena in planktic forams are rare being restricted to very minor nucleated breakdown and pore

widening/coalescence in the deep basin. Severe mechanical attrition of planktic tests is common in areas of strong bottom current scour (Central Terrace and upper Tugela Cone) and in conduits for rapid sediment transport (major canyons).

10.3.4 Clay Mineralogy

Illites are the dominant clay mineral group in modern surficial sediments followed by smectite and kaolinite. Their distributions are complex and do not solely reflect the areal variability of hinterland output (Figs.8.12 and 8.13).

The illite source potential is uniform throughout the major hinterland rivers although the greatest volume is debouched by the Tugela river. The major basinal illite concentration coincides with the south Tugela Cone terrigenous depocentre confirming that illites are hinterland-sourced. Kaolinite clays sourced from the southern hinterland are also transported to the south Tugela Cone depocentre. Above-average concentrations of kaolinite clays over the Central Terrace are probably sourced from the Mozambique-Madagascar area being transported south by the Agulhas Current. The offshore distribution of smectite is reciprocal to illite with maximum concentrations recorded over the north and east Tugela Cone partially matching the increased source potential of the northern hinterland. Like kaolinite, smectites are predominantly introduced from the north by Agulhas Current flow.

10.3.5 Textural Analysis

Sieve and pipette analysis has defined five surficial sediment textural groups in the mid Natal Valley. Silty clays

over the southern and upper Tugela Cone (group I) confirm that equilibrium mud deposition is taking place in this modern terrigenous depocentre. Group II sand-silt-clays (east Tugela Cone) are characterised by a high $CaCO_3$ content and a foram-rich sand fraction implying modern inactivity as a terrigenous depocentre. Group III sand-silt-clays (basin plain south of Tugela Cone) are more depleted in $CaCO_3$ suggesting terrigenous input from the south Tugela Cone. Clayey sands over the Central Terrace and eastern basin plain (group IV) are a response to high input of foram tests and low terrigenous mud dilution preserving the sand-rich and $CaCO_3$-rich group character. Central Terrace sediments are particularly sand-enriched reflecting the importance of winnowing. Sands and silty sands over the northern Tugela Cone (group V) are also a response to high energy Agulhas Current winnowing.

10.3.6 Sand Populations and Mixing

Hydraulically-equivalent grain size parameters for the sand fraction have been computed using settling tube analysis. Size-frequency distribution patterns identify two prominent hydraulic populations in the basin: (1) medium to fine sand (biogenic) dominating the major pelagic provinces (deep basin, Central Terrace and inactive zones of the Tugela Cone); and (2) very fine sand and hydraulically-equivalent coarse silt (terrigenous) characterising the major terrigenous depocentres (south and upper Tugela Cone and lower 29° 25'S Canyon). These two populations are mixed in varying proportions within the basinal provinces. Sorting and skewness trends within the sand fraction are definable in terms of a mixing model.

Construction of bivariate plots for sand fraction sedimentological parameters clearly defines seven groups (A-G), each geographically-distinct, confirming a basic geographic and physiographic control over sand fraction processes and responses. The grouping system is used to confirm mixing over the southern Tugela Cone.

Mixing of the two major hydraulic populations is best demonstrated over the southern Tugela Cone and adjacent deep basin. Quick-look sedimentological parameters including component data, size-frequency distributions, bivariate plots and geographic location suggest that group D (terrigenous; mode 3,1ϕ) and group A (pelagic; mode 2ϕ) are mixed in variable proportions to form group C (bimodal; 2ϕ and 3,1ϕ). Graphic 3D analysis of mean diameter, sorting and skewness (Folk and Ward, 1957) confirms that progressive mixing of the terrigenous and pelagic end-members is operative over the southern Tugela Cone.

10.3.7 Silt Fraction Size Analysis

Electronic particle size analysis (Coulter Counter) has provided size-frequency data for the silt sub-fractions. Coarse silts predominate over the upper continental slope (terrigenous-dominant) and Central Terrace crest (current scouring). A relative energy gradient is apparent within the southern Tugela Cone terrigenous depocentre with coarse silt predominant over the upper slope grading to fine silt over the slope-base. Concentrations of coarse, medium and fine silt are approximately equal over the major biogenic provinces not affected by current scour.

10.3.8 Lithofacies and Facies Assemblages

Five major modern lithofacies (turbidite, hemipelagite, pelagite, muddy contourite and sandy contourite), each representative of a discrete depositional process, are discriminated in basinal sediments. Their definition is dependent on recognition of an assemblage of structural, textural and compositional properties within the correct geographic location. In many cases the lithofacies are intergradational.

Four facies assemblages defined by lithofacies distributions are distinguished in the basin (Fig.8.39). Three of these assemblages are areally subdivided (Table 8.8). Facies assemblage I over the southern Tugela Cone and adjacent upper slope is dominated by thin-bedded muddy terrigenous turbidites and delineates the major modern terrigenous depocentre. Facies assemblage II comprises mixed hemipelagites and pelagites. Assemblage IIa on the lower eastern Tugela Cone is a response to modern cone stagnation while assemblage IIb is remote from terrigenous sediment supply. Facies assemblage III is characterised by mixed muddy contourites and hemipelagites. Over the basin plain adjacent to the south Tugela Cone, assemblage IIIa has developed under the influence of North Atlantic Deep Water (NADW) flow and low modern terrigenous supply. On the eastern Tugela Cone adjacent to the 29° 25'S Canyon, assemblage IIIb is a response to Agulhas Current deep water flow and contourite mound generation. Facies assemblage IV is dominated by sandy contourites and thus indicates vigorous bottom current scour. Assemblage IVa is mapped over the Central Terrace (Agulhas Current deep water) and the deep basin margins (NADW)

while assemblage IVb is developed along the mid-upper slope of the northern Tugela Cone (Agulhas Current core flow).

In the mid Natal Valley, variable textures and lithofacies are responses to different syn-depositional and post-depositional environments and processes. Facies assemblages are strongly controlled by proximity to terrigenous detritus supply, dispersal routes and the strength of current influences (Fig.8.40).

10.3.9 Modern Sediment Dispersal

Modern sediment input to basinal areas of the mid Natal Valley is derived from four main sources: (1) off-shelf transport of terrigenous bedload driven by Agulhas Current flow; (2) suspended muds debouched by hinterland rivers; (3) bedload and suspensates transported in from the north by the Agulhas Current; and (4) the pelagic rain (Fig.8.42).

Terrigenous detritus supplied to the upper Tugela Cone is ?intermittently funnelled as bedload to the southern Tugela Cone and, to a lesser extent, the 29° 25'S Canyon. Biological, chemical and sedimentological criteria confirm downslope transport in these zones (Fig.8.41). Suspended terrigenous muds are more widely available for dispersal and mix with the pelagic rain to generate widespread hemipelagites. Remote regions receive little input of continental suspensates and are dominated by pelagite lithofacies.

Deep current scour causing sediment redistribution is widely active in the mid Natal Valley. Regions strongly affected by winnowing and redistribution include the Central Terrace and upper Tugela Cone (deep Agulhas Current flow) and the deep basin margins (cyclonic NADW flow).

The absence of active distributary routes implies that modern bedload detrital supply is retained within the Natal Valley basin. In contrast, under the influence of vigorous Agulhas Current and NADW flow, significant amounts of suspended muds are potentially exported from the basin.

10.4 TUGELA FAN DEVELOPMENT

Development of the Tugela Fan (Tugela Cone and deep basin) has followed standard models of deep-sea fan evolution despite its atypical morphology (Fig.9.3). The 29° 25'S Canyon has acted as the major mid fan distributary channel/levee system since at least the early Oligocene. This fan valley system has constructed the eastern mid fan depositional bulge through stacking of overlapping levee depositional units. Major fan growth has probably taken place during low sea-level stands and/or phases of deltaic progradation to the outer shelf. Formation of the erosive Tugela Canyon in post-early Pliocene times disrupted upper and mid fan growth and may have induced stagnation of the 29° 25'S fan valley. Changes in canyon status and reduced Holocene terrigenous sediment supply to the deep basin (high sea-level stand) may have together induced temporary fan growth stagnation over the eastern Tugela Cone (mid fan) and basin plain (lower fan). The large size (upper-mid fan is 230 x 170 km in dimension) but atypical morphology of the Tugela Fan prompts its classification as an hybrid fan type but with close affinity to the elongate fan type end-member.

REFERENCES

Adie,R.J. 1972. Evolution of volcanism in the Antarctic peninsula. In: R.J.Adie (ed.). Antarctic geology and geophysics. Universitetsforslaget, Oslo: 137-142.

Alexandersson,E.T. 1975. Etch patterns of calcareous sediment grains: petrographic evidence of marine dissolution of carbonate minerals. Science 189: 47-48.

Allen,J.R.L. 1984. Sedimentary structures, their character and physical basis. Developments in Sedimentology,30 (V.I and II), Elsevier, Amsterdam: 1256pp.

Andrews,J.E. and Hurley,R.J. 1978. Sedimentary processes in the formation of a submarine canyon. Mar. Geol. 26: M47-M50.

Andrews,P.B. 1977. Depositional facies and the early phase of ocean basin evolution in the circum-Antarctic region. Mar. Geol. 25: 1-13.

Asquith,S.M. 1979. Nature and origin of the lower continental rise hills off the east coast of the United State. Mar. Geol. 32: 165-190.

Bagnold,R.A. 1968. Deposition in the process of hydraulic transport. Sedimentology 10: 45-56.

Bailey,D.K. 1977. Continental rifting and mantle degassing. In: E.R.Neuman and I.B.Ramberg (eds.). Petrology and geochemistry of continental rifts. Riedel, Dordrecht: 1-13.

Bang,N.D. 1968. Submarine canyons off the Natal coast. S.Afr. Geog. J. 50: 45-54.

Bang,N.D. and Pearce,A.F. 1978. Water Circulation. In: A.E.F.Heydorn (ed.). Ecology of the Agulhas Current region: an assessment of biological responses to environmental parameters in the south-west Indian Ocean. Trans. Roy. Soc. S. Afr. 43(2): 151-190.

Barker,P.F. 1976. Correlation between sites on the eastern Falkland Plateau by means of seismic reflection profiles. In: P.F.Barker, I.W.D.Dalziel et al. Init. Rept. Deep-Sea Drill. Proj. 36. U.S.Govt. Print. Off., Washington: 971-990.

Barker,P.F. 1979. The history of ridge-crest off-set at the Falkland-Agulhas Fracture Zone from a small circle geophysical profile. Geophys. J. Roy. Astr. Soc. 59: 131-145.

Barker,P.F., Dalziel,I.W.D. et al. 1976. Init. Rept. Deep-Sea Drill. Proj. 36. U.S.Govt. Print. Off., Washington: 1080 pp.

Barron,E.J., Harrison,C.G.A. and Hay,W.W. 1978. A revised reconstruction of the southern continents. EOS. Trans. Am. Geophys. Union 59: 436-449.

Bé,A.W.H. and Duplessy,J-C. 1976. Subtropical convergence fluctuations and Quaternary climates in the middle latitudes of the Indian Ocean. Science 194: 419-421.

Bé,A.W.H., Morse,J.W. and Harrison,S.M. 1975. Progressive dissolution and ultrastructural breakdown of planktonic foraminifera. Cushman Found. Foram. Res. Spec. Publ. 13: 27-55.

Beaumont,C. 1978. The evolution of sedimentary basins on a visco-elastic lithosphere: theory and examples. Geophys. J. Roy. Astr. Soc. 55: 471-497.

Beck,R.H. and Lehner,P. 1974. Oceans, new frontiers in exploration. Am. Assoc. Pet. Geol. Bull. 58: 376-395.

Bein,A. and Sass,E. 1978. Analysis of log-probability plots of recent Atlantic sediments and its analogy with simulated mixtures. Sedimentology 25: 575-581.

Benson,R.A. 1975. The origin of the psychrosphere as recorded in changes of deep-sea ostracode assemblages. Lethaia 8: 69-83.

Berger,W.H. 1970. Planktonic foraminifera: selective solution and the lysocline. Mar. Geol. 8: 111-138.

Berger,W.H. 1971. Sedimentation of planktonic foraminifera. Mar. Geol. 11: 325-358.

Berggren,W.A. and Hollister,C.D. 1974. Palaeogeography, palaeobiogeography and the history of circulation in the Atlantic Ocean. SEPM Spec. Publ. 20: 127-186.

Bergh,H.W. 1977. Mesozoic sea floor off Dronning Maud Land, Antarctica. Nature 269: 686-687.

Bezrukov,P.L., Yemel'yanov,Y.M., Lisitsyn,A.P. and Romankevich,Y.A. 1977. Organic carbon in the upper sediment layer of the world ocean. Oceanology 17: 561-564.

Birch,G.F. 1975. Sediments on the continental margin off the west coast of South Africa. Ph.D. thesis. Joint GSO/UCT Mar. Geosc. Bull. 6: 142pp.

Birch,G.F. 1978. The distribution of clay minerals on the continental margin off the west coast of South Africa. Trans. Geol. Soc. S. Afr. 81: 23-34.

Birch,G.F. 1979a. The Karbonat-Bombe: A precise, rapid and cheap instrument for determining calcium carbonate in sediment and rocks. Joint GSO/UCT Mar. Geosc. Tech. Rept. 11: 122-126.

Birch,G.F. 1979b. The nature and origin of mixed apatite/glauconite pellets from the continental shelf off South Africa. Mar. Geol. 29: 313-334.

Birch,G.F. 1981. Nearshore Quaternary sedimentation off the south coast of South Africa. Bull. Geol. Surv. S. Afr. 67: 20pp.

Birch,G.F. (in press a). Unconsolidated sediments on the eastern margin of South Africa (Cape Padrone to Cape Vidal). Bull. Geol. Surv. S. Afr.

Birch,G.F. (in press b). Clay mineralogy of fine sediment from South African rivers and the adjacent continental shelf. Bull. Geol. Surv. S. Afr.

Biscaye,P.E. 1965. Mineralogy and sedimentation of recent deep-sea clay in the Atlantic Ocean and adjacent seas and oceans. Geol. Soc. Am. Bull. 76: 803-832.

Biscaye,P.E., Kolla,V. and Turekian,K.K. 1976. Distribution of calcium carbonate in the surface sediments of the Atlantic Ocean. J. Geophys. Res. 81: 2595-2602.

Blaeser,C.R. and Ledbetter,M.T. 1982. Deep-sea bottom currents differentiated from texture of underlying sediment. J. Sediment. Petrol. 52: 755-768.

Blanc,P.L., Rabussier,D., Vergnaud-Grazzini,C. and Duplessy,J-C. 1980. North Atlantic Deep Water formed by the later middle Miocene. Nature 283: 553-555.

Bolli,H.M. and Ryan,W.B.F. et al. 1978. Init. Rept. Deep-Sea Drill. Proj. 40. U.S.Govt. Print. Off., Washington: 1079pp.

Bordovsky,O.K. 1965. Accumulation and transformation of organic substance in marine sediments. Mar. Geol. 3: 3-114.

Bornhold,B.D. and Summerhayes,C. 1977. Scour and deposition at the foot of the Walvis Ridge in the northernmost Cape Basin, South Atlantic. Deep-Sea Res. 24: 743-752.

Bott,M.H.P. 1976. Formation of sedimentary basins of graben type by extension of the continental crust. Tectonophysics 36: 77-86.

Bott,M.H.P. 1979. Subsidence mechanisms at passive continental margins. Am. Assoc. Pet. Geol. Mem. 29: 3-10.

Bouma,A.H. and Treadwell,T.K. 1975. Deep-sea dune-like features. Mar. Geol. 19: M53-M59.

Bowles,F.A. 1980. Stratigraphy and sedimentation of the archipelagic apron and adjoining area southeast of Bermuda. Mar. Geol. 37: 267-294.

Bristow,J.W. 1976. The geology and geochemistry of the southern Lebombo. M.Sc.thesis. Univ. Natal, Durban (unpubl.): 331pp.

Bristow,J.W. 1980. Karoo volcanics of the Lebombo Monocline: a geological and geochemical appraisal. Ph.D.thesis. Univ. Cape Town (unpubl.).

Broecker,W.S., Ewing,M. and Heezen,B.C. 1960. Evidence for an abrupt change in climate close to 11000 years ago. Am. J. Sci. 258: 429-448.

Brown,L.F. and Fisher,W.L. 1977. Seismic-stratigraphic interpretations of depositional systems: examples from Brazilian rift and pull-apart basins. Am. Assoc. Pet. Geol. Mem. 26: 213-248.

Bryan,W.B. 1974. Fe-Mg relationships in sector zoned submarine basalt plagioclase. Earth Planet. Sci. Letts. 24: 157-165.

Bullard,E., Everrett,J.E. and Smith,A.G. 1965. The fit of the continents around the Atlantic. Phil. Trans. Roy. Soc. Lond. 258: 41-51.

Carlson,R.L., Christensen,N.I. and Moore,R.P. 1980. Anomalous crustal structures in ocean basins: continental fragments and oceanic plateaux. Earth Planet. Sci. Letts. 51: 171-180.

Carter,A.N. 1978. Contrasts between oceanic and continental 'unconformities' in the Oligocene of the Australian region. Nature 274: 152-154.

Cassidy,D.S., Ciesielski,P.F., Kaharoeddin,F.A., Wise,S.W. and Zemmels,I. 1977. ARA Islas Orcadas cruise 07.75 sediment descriptions. Sediment. Res. Lab. Rept. Florida State Univ. 45: 76pp.

Chetty,P. and Green,R.W.E. 1977. Seismic refraction observations in the Transkei Basin and adjacent areas. Mar. Geophys. Res. 3: 197-208.

Ciesielski,P.F. and Wise,S.W. 1977. Geologic history of the Maurice Ewing Bank of the Falkland Plateau (south-west Atlantic sector of the southern ocean) based on piston and drill cores. Mar. Geol. 25: 175-205.

Clark,D.L. 1971. Arctic Ocean ice cover and its Late Cenozoic history. Geol. Soc. Am. Bull. 82: 3313-3324.

Cleverly,R.W. 1979. The volcanic geology of the Lebombo Monocline in Swaziland. Trans. Geol. Soc. S. Afr. 82: 343-348.

Cleverly,R.W. and Bristow,J.W. 1979. A revised volcanic stratigraphy for the Lebombo Monocline. Trans. Geol. Soc. S. Afr. 82: 227-230.

Clowes,A.J. and Deacon,G.E.R. 1935. The deep water circulation of the Indian Ocean. Nature 136: 936-938.

Coleman,J.M. and Garrison,L.E. 1977. Geological aspects of marine slope stability, N.W. Gulf of Mexico. Mar. Geotechnol. 2: 9-44.

Coplen,T.B. and Schlanger,S.O. 1973. Oxygen and carbon isotope studies of carbonate sediments from site 167, Magellan Rise, Leg 17. In: E.L.Winterer, J.I.Ewing et al. Init. Rept. Deep-Sea Drill. Proj. 17. U.S.Govt. Print. Off., Washington: 505-509.

Corliss,B.H. 1979. Response of deep-sea benthonic foraminifera to the development of the psychrosphere near the Eocene/Oligocene boundary. Nature 282: 63-65.

Cox,K.G. 1978. Flood basalts, subduction and the break-up of Gondwanaland. Nature 274: 47-49.

Cox,K.G., MacDonald,R. and Hornung,G. 1967. Geochemical and petrographic provinces in the Karoo basalts of southern Africa. Am. Mineral. 52: 1451-1474.

Creer,K.M. 1973. A discussion of the arrangement of palaeomagnetic poles on the map of Pangaea for epochs in the Phanerozoic. In: D.H.Tarling and S.K.Runcorn (eds.). Implications of continental drift to the earth sciences. Academic Press, London: 47-76.

Culver,S.J., Bull,P.A., Campbell,S., Shakesby,R.A. and Whalley,W.B. 1983. Environmental discrimination based on quartz grain surface textures: a statistical investigation. Sedimentology 30: 129-136.

Curray,J.R. and Moore,D.G. 1971. Growth of the Bengal deep-sea fan and denudation in the Himalayas. Geol. Soc. Am. Bull. 82: 563-572.

Dalziel,I.W.D. and Elliot,D.H. 1971. The evolution of the Scotia Arc. Nature 233: 246-252.

Damuth,J.E. 1975. Echo character of the western Equatorial Atlantic floor and its relationship to the dispersal and distribution of terrigenous sediments. Mar. Geol. 18: 17-45.

Damuth,J.E. 1978. Echo character of the Norwegian-Greenland Sea: relationship to Quaternary sedimentation. Mar. Geol. 28: 1-36

Damuth,J.E. 1980. Use of high-frequency (3.5-12kHz) echograms in the study of near-bottom sedimentation processes in the deep-sea: a review. Mar. Geol. 38: 51-75.

Damuth,J.E. and Embley,R.W. 1979. Upslope flow of turbidity currents on the northwest flank of the Ceara Rise: western Equatorial Atlantic. Sedimentology 26: 825-834.

Damuth,J.E. and Flood,R.D. 1983/1984. Morphology, sedimentation processes and growth pattern of the Amazon deep-sea fan. Geo-Marine Letts. 3: 109-117.

Damuth,J.E. and Hayes,D.E. 1977. Echo character of the East Brazilian continental margin and its relationship to sedimentary processes. Mar. Geol. 24: 73-95.

Damuth,J.E. and Kumar,N. 1975. Amazon Cone: morphology, sediments, age, and growth pattern. Geol. Soc. Am. Bull. 86: 863-878.

Darbyshire,J. 1964. A hydrological investigation of the Agulhas Current area. Deep-Sea Res. 11: 781-815.

Darracott,B.W. 1974. On the crustal structure of southeastern Africa and the adjacent Indian Ocean. Earth Planet. Sci. Letts. 24: 282-290.

Darracott,B.W. and Kleywegt,R.J. 1974. The structure of the southern portion of the Lebombo volcanic belt deduced from gravity data. Trans. Geol. Soc. S. Afr. 77: 301-308.

Davies,T.A., Hay,W.W., Southam,J.R. and Worsley,T.R. 1977a. Estimates of Cenozoic oceanic sedimentation rates. Science 197: 53-55.

Davies,T.A., Musich,L.F. and Woodbury,P.B. 1977b. Automated classification of deep-sea sediments. J. Sediment. Petrol. 47: 650-656.

Davies,T.A. and Kidd,R.B. 1977. Sedimentation in the Indian Ocean through time. In: J.R.Heirtzler et al. (eds.). Indian Ocean Geology and Biostratigraphy. Am. Geophys. Union, Washington: 61-85.

Davies,T.A., Luyendyk,B.P. et al. 1974. Init. Rept. Deep-Sea Drill. Proj. 26. U.S.Govt. Print. Off., Washington: 1129pp.

Davies,T.A., Weser,O.E., Luyendyk,B.P. and Kidd,R.B. 1975. Unconformities in the sediments of the Indian Ocean. Nature 253: 15-19.

Demaison,G.J. and Moore,G.T. 1980. Anoxic environments and oil source bed genesis. Am. Assoc. Pet. Geol. Bull. 64: 1179-1209.

De Swardt,A.M.J. and Bennet,G. 1974. Structural and physiographic development of Natal since the late Jurassic. Trans. Geol. Soc. S. Afr. 77: 309-322.

Detrick,R.S., Sclater,J.G. and Thiede,J. 1977. The subsidence of aseismic ridges. Earth Planet. Sci. Letts. 34: 185-196.

Dewey,J.F. and Burke,K. 1974. Hot spots and continental break-up. Geology 2: 57-60.

De Wit,M.J. 1977. The evolution of the Scotia Arc as a key to the reconstruction of south-western Gondwanaland. Tectonophysics 37: 53-81.

Diester-Haass,L. 1982. Indicators of water depth in bottom sediments of the continental margin off West Africa. Mar. Geol. 49: 311-326.

Dietrich,V.J. and Jones,E.J.W. 1980. Volcanic rocks from Rosemary Bank (Rockall Trough, NE Atlantic). Mar. Geol. 35: 287-297.

Dingle,R.V. 1973. Post-Palaeozoic stratigraphy of the eastern Agulhas Bank, South African continental margin. Mar. Geol. 15: 1-23.

Dingle,R.V. 1977. The anatomy of a large submarine slump on a sheared continental margin (S.E. Africa). J. Geol. Soc. Lond. 134: 293-310.

Dingle,R.V. 1978. South Africa. In: M.Moullade and A.E.M.Nairn (eds.). The Phanerozoic geology of the world 2. The Mesozoic A. Elsevier, Amsterdam: 401-433.

Dingle,R.V. 1979. Sedimentary basins and basement structures on the continental margin of southern Africa. Bull. Geol. Surv. S. Afr. 63: 29-46.

Dingle,R.V. 1980a. Sedimentary basins on the continental margins of southern Africa - an assessment of their hydrocarbon potential. Erdol und Kohle 33(10): 457-463.

Dingle,R.V. 1980b. Large allochthonous sediment masses and their role in the construction of the continental slope and rise off southwestern Africa. Mar. Geol. 37: 333-354.

Dingle,R.V. and Camden-Smith,F. 1979. Acoustic stratigraphy and current-generated bedforms in deep ocean basins off southeastern Africa. Mar. Geol. 33: 239-260.

Dingle,R.V., Goodlad,S.W. and Martin,A.K. 1978. Bathymetry and stratigraphy of the northern Natal Valley (SW Indian Ocean): a preliminary account. Mar. Geol. 28: 89-106.

Dingle,R.V. and Robson,S. 1985. Slumps, canyons and related features on the continental margin off East London, SE Africa (SW Indian Ocean). Mar. Geol. 67: 37-54.

Dingle,R.V. and Scrutton,R.A. 1974. Continental break-up and the development of post-Palaeozoic sedimentary basins around southern Africa. Geol. Soc. Am. Bull. 85: 1467-1474.

Dingle,R.V., Siesser,W.G. and Newton,A.R. 1983. Mesozoic and Tertiary Geology of Southern Africa. Balkema, Rotterdam: 375pp.

Donnelly,T.W. 1982. Worldwide continental denudation and climatic deterioration during the late Tertiary: evidence from deep-sea sediments. Geology 10: 451-454.

Droz,L. and Bellaiche,G. 1985. Rhone deep-sea fan: morphostructure and growth pattern. Am. Assoc. Pet. Geol. Bull. 69: 460-479.

Duncan,C.P. 1970. The Agulhas Current. Ph.D.thesis. Univ. Hawaii (unpubl.).

Dunn,D.A. 1980. Revised techniques for calcium carbonate analysis using the "Karbonat-Bombe", and comparisons to other quantitative carbon analysis methods. J. Sediment. Petrol. 50: 631-636.

Du Plessis,A. 1967. Total magnetic field measurements. Agulhas Bank Geophys. Surv. Prog. Rept. Dept. Geology, Univ. Cape Town: 11-23.

Du Plessis,A. 1977. Sea Floor spreading south of the Agulhas Fracture Zone. Nature 270: 719-721.

Du Plessis,A. 1978. Magnetic anomalies associated with the Agulhas Fracture Zone in the area of the Cape Rise. Joint GSO/UCT Mar. Geosc. Tech. Rept. 10: 85-95.

Du Plessis,A. and Simpson,E.S.W. 1974. Magnetic anomalies associated with the southeastern continental margin of South Africa. Mar. Geophys. Res. 2: 99-110.

Du Toit,S.R. 1979. The Mesozoic history of the Agulhas Bank in terms of plate tectonic theory. Geol. Soc. S. Afr. Spec. Publ. 6: 197-203.

Du Toit,S.R. and Leith,M.J. 1974. The J(c)-1 borehole on the continental shelf near Stanger, Natal. Trans. Geol. Soc. S. Afr. 77: 247-252.

Ellwood,B.B., Ledbetter,M.T. and Johnson,D.A. 1979. Sedimentary fabric: a tool to delineate a high-velocity zone within a deep western Indian Ocean bottom current. Mar. Geol. 33: M51-M55.

Embley,R.W. 1980. The role of mass transport in the distribution and character of deep-ocean sediments with special reference to the North Atlantic. Mar. Geol. 38: 23-50.

Embley,R.W. and Langseth,M.G. 1977. Sedimentation processes on the continental rise of north eastern South America. Mar. Geol. 25: 279-297.

Embley,R.W., Rabinowitz,P.D. and Jacobi,R.D. 1978. Hyperbolic echo zones in the eastern Atlantic and the structure of the southern Madeira Rise. Earth Planet. Sci. Letts. 41: 419-433.

Emery,K.O. 1960. The sea off south California. Wiley, New York: 366pp.

Emery,K.O., Uchupi,E., Bowin,C.O., Phillips,J. and Simpson,E.S.W. 1975. Continental margin off western Africa: Cape St Francis (South Africa) to Walvis Ridge (South West Africa). Am. Assoc. Pet. Geol. Bull. 59: 3-59.

Engel,C.G. and Fisher,R.L. 1975. Granitic to ultramafic rock complexes of the Indian Ocean ridge system, western Indian Ocean. Geol. Soc. Am. Bull. 86: 1553-1578.

Erlank,A.J. and Reid,D.L. 1974. Geochemistry, mineralogy and petrology of basalts, Leg 25 Deep-Sea Drilling Project. In: E.S.W.Simpson, R.Schlich et al. Init. Rept. Deep-Sea Drill. Proj. 25. U.S.Govt. Print. Off., Washington: 543-552.

Ewing,J.I., Ludwig,W.J., Ewing,M. and Eittreim,S.C. 1971. Structure of the Scotia Sea and Falkland Plateau. J. Geophys. Res. 76: 7118-7137.

Fainstein,R., Milliman,J.D. and Jost,H. 1975. Magnetic character of the Brazilian continental shelf and upper slope. Rev. Brazil. Geociencias 5: 198-211.

Falvey,D.A. 1974. The development of continental margins in plate tectonic theory. J. Aust. Pet. Expl. Assoc. 14: 95-106.

Farre,J.A., McGregor,B.A., Ryan,W.B.F. and Robb,J.M. 1983. Breaching the shelf-break: passage from youthful to mature phase in submarine canyon evolution. SEPM Spec. Publ. 33: 25-39.

Ferentinos,G., Collins,M.B., Pattiaratchi,C.B. and Taylor,P.G. 1985. Mechanisms of sediment transport and dispersion in a tectonically active submarine valley/canyon system: Zakynthos straits, NW Hellenic Trench. Mar. Geol. 65: 243-269.

Fernandez,L.M. 1983. Catalogue of earthquakes in southern Africa and surrounding oceans for 1979. Geol. Surv. S. Afr. Seism. Ser. 13: 1-22.

Flemming,B.W. 1977. Depositional processes in Saldanha Bay and Langebaan Lagoon. Ph.D.thesis. Joint GSO/UCT Mar. Geosc. Bull. 8: 215pp.

Flemming,B.W. 1978. Underwater sand dunes along the southeast African continental margin - observations and implications. Mar. Geol. 26: 177-198.

Flemming,B.W. 1980. Sand transport and bedform patterns on the continental shelf between Durban and Port Elizabeth (south east African continental margin). Sediment. Geol. 26: 179-205.

Flemming,B.W. 1981. Factors controlling shelf sediment dispersal along the south-east African continental margin. Mar. Geol. 42: 259-277.

Flemming,B.W. and Hay,R. 1983. On the bulk density of South African marine sands. Joint GSO/UCT Mar. Geosc. Tech. Rept. 14: 171-176.

Flemming,B.W. and Thum,A.B. 1978. The Settling Tube - a hydraulic method for grain size analysis of sands. Kieler Meeresforschungen 4: 82-95.

Flores,G. 1973. The Cretaceous and Tertiary sedimentary basins of Mozambique and Zululand. In: G.Blant (ed.). Sedimentary basins of the African coasts, part 2, south and east coasts. Paris Assoc. Afr. Geol. Surv.: 81-111.

Floyd,P.A. and Winchester,J.A. 1975. Magma type and tectonic setting discrimination using immobile elements. Earth Planet. Sci. Letts. 27: 211-218.

Folk,R.L. and Ward,W.C. 1957. Brazos River bar: a study in the significance of grain size parameters. J. Sediment. Petrol. 27: 3-26.

Forster,R. 1975. Geological history of the sedimentary basin of southern Mozambique and some aspects of the origin of the Mozambique Channel. Palaeogeog. Palaeoclim. Palaeoecol. 17: 267-287.

Frakes,L.A. 1979. Climates through Geologic Time. Elsevier, Amsterdam: 310pp.

Francheteau,J. and Le Pichon,X. 1972. Marginal fracture zones as structural framework of South Atlantic continental margins. Am. Assoc. Pet. Geol. Bull. 56: 991-1007.

Friedman,G.M. 1967. Dynamic processes and statistical parameters compared for size frequency distribution of beach and river sands. J. Sediment. Petrol. 37: 327-354.

Georgiev,V.M. and Stoffers,P. 1980. Surface textures of quartz grains from Late Pleistocene to Holocene sediments of the Persian Gulf/Gulf of Oman - an application of the scanning electron microscope. Mar. Geol. 36: 85-96.

Gerrard,I. and Smith,G.C. 1983. The post-Palaeozoic succession and structure of the south-western African continental margin. Am. Assoc. Pet. Geol. Mem. 34: 49-74.

Gibbs,R.J. 1974. A settling tube system for sand size analysis. J. Sediment. Petrol. 44: 583-588.

Gibbs,R.J. 1977. Clay mineral segregation in the marine environment. J. Sediment. Petrol. 47: 237-243.

Gibbs,R.J. 1985. Settling velocity, diameter, and density for flocs of illite, kaolinite, and montmorillonite. J. Sediment. Petrol. 55: 65-68.

Girdley,W.A., Leclaire,L., Moore,T.C., Vallier,T.L. and White,S.M. 1974. Lithologic summary, Leg 25, DSDP. In: E.S.W.Simpson, R.Schlich et al. Init. Rept. Deep-Sea Drill. Proj. 25. U.S.Govt. Print. Off., Washington: 725-742.

Goodlad,S.W. 1979. Some aspects of deep current activity in the mid Natal Valley. Joint GSO/UCT Mar. Geosc. Tech. Rept. 11: 91-98.

Goodlad,S.W., Martin,A.K. and Hartnady,C.J.H. 1982. Mesozoic magnetic anomalies in the southern Natal Valley. Nature 295: 686-688.

Gorsline,D.S. 1978. Anatomy of margin basins. J. Sediment. Petrol. 48: 1055-1068.

Gorsline,D.S. 1980. Deep-water sedimentologic conditions and models. Mar. Geol. 38: 1-21.

Griffin,J.J. and Goldberg,E.D. 1963. Clay mineral distributions in the Pacific Ocean. In: M.N.Hill (ed.). The Sea. V.3. Interscience, New York: 728-741.

Grundlingh,M.L. 1977. Drift observations from Nimbus VI satellite-tracked buoys in the southwestern Indian Ocean. Deep-Sea Res. 24: 903-913.

Grundlingh,M.L. and Lutjeharms,J.R.E. 1979. Large-scale flow patterns of the Agulhas Current system. S. Afr. J. Sci. 75: 269-271.

Guidish,T.M., Lerche,I., Kendall,C.G. and O'Brien,J.J. 1984. Relationship between eustatic sea level changes and basement subsidence. Am. Assoc. Pet. Geol. Bull. 68: 164-177.

Hales,A.L. and Nation,J.B. 1972. A crustal structure profile on the Agulhas Bank. Bull. Seism. Soc. Am. 62: 1029-1051.

Hales,A.L. and Nation,J.B. 1973. A seismic refraction study in the southern Indian Ocean. Bull. Seism. Soc. Am. 63: 1951-1966.

Hallam,A. and Bradshaw,M.J. 1979. Bituminous shales and oolitic ironstones as indicators of transgressions and regressions. J. Geol. Soc. Lond. 136: 157-164.

Harris,T.F.W. 1972. Sources of the Agulhas Current in the Spring of 1964. Deep-Sea Res. 19: 633-650.

Harris,T.F.W. 1978. Review of coastal currents in southern African waters. S. Afr. Nat. Sci. Prog. Rept. 30: 103pp.

Harris,T.F.W., Legeckis,R. and Van Foreest,D. 1978. Satellite infra-red images in the Agulhas Current system. Deep-Sea Res. 25: 543-548.

Harris,T.F.W. and Van Foreest,D. 1977. The Agulhas Current system. Int. Rept. Dept. Oceanog. Univ. Cape Town: 34pp.

Harrison,C.G.A. 1976. Magnetization of the oceanic crust. Geophys. J. Roy. Astr. Soc. 47: 257-283.

Harrison,C.G.A., Barron,E.J. and Hay,W.W. 1979. Mesozoic evolution of the Antarctic Peninsula and the southern Andes. Geology 7: 374-378.

Hart,S.R., Erlank,A.J. and Kable,E.J.D. 1974. Sea Floor basalt alteration: some chemical and Sr isotopic effects. Contr. Mineral. Petrol. 44: 219-230.

Hay,W.W., Barron,E.J., Sloan,J.L. and Southam,J.R. 1981. Continental drift and the global pattern of sedimentation. Geol. Rundschau 70: 302-315.

Heath,G.R., Moore,T.C. and Dauphin,J.P. 1977. Organic carbon in deep-sea sediments. In: N.R.Andersen and A.Malahoff (eds.). The fate of fossil fuel CO_2 in the oceans. Plenum Press, New York: 605-626.

Heezen,B.C. 1974. Atlantic type continental margins. In: C.A.Burke and C.L.Drake (eds.). The geology of continental margins. Springer-Verlag, New York: 13-24.

Henson,M.R. 1973. Clay minerals from the Lower New Red Sandstone of South Devon. Proc. Geol. Assoc. 84: 429-445.

Herzer,R.H. and Lewis,D.W. 1979. Growth and burial of a submarine canyon off Motunau, North Canterbury, New Zealand. Sediment. Geol. 24: 69-83.

Hess,G.R. and Normark,W.R. 1976. Holocene sedimentation history of the major fan valleys of Monterey Fan. Mar. Geol. 22: 233-251.

Higgs,R. 1979. Quartz grain surface features of Mesozoic-Cenozoic sands from the Labrador and western Greenland continental margins. J. Sediment. Petrol. 49: 599-610.

Hill,B.J. 1975. The origin of southern African coastal lakes. Trans. Roy. Soc. S. Afr. 41: 225-239.

Hollister,C.D. and Heezen,B.C. 1972. Geologic effects of ocean bottom currents: western North Atlantic. In: A.L.Gordon (ed.). Studies in physical oceanography. Gordon and Breach, New York: 37-66.

Honjo,S. 1977. Biogenic carbonate particles in the ocean: do they dissolve in the water column? In: N.R.Andersen and A.Malahoff (eds.). The fate of fossil fuel CO_2 in the oceans. Plenum Press, New York: 269-294.

Huang,T.C. and Watkins,N.D. 1977. Contrasts between the Brunhes and Matuyama sedimentary records of bottom water activity in the South Pacific. Mar. Geol. 23: 113-132.

Hutson,W.H. 1980. The Agulhas Current during the Late Pleistocene: analysis of modern faunal analogs. Science 207: 64-66.

Hyne,N.J., Laidig,L.W. and Cooper,W.A. 1979. Prodelta sedimentation on a lacustrine delta by clay mineral flocculation. J. Sediment. Petrol. 49: 1209-1216.

Ibach,L.E.J. 1982. Relationship between sedimentation rate and total organic carbon content in ancient marine sediments. Am. Assoc. Pet. Geol. Bull. 66: 170-188.

Jackson,M.L. 1969. Weathering of primary and secondary minerals in soil. Trans. 9th Int. Cong. Soil Sci. 4: 281-292.

Jacobs,M.B. and Hays,J.D. 1972. Palaeoclimatic events indicated by mineralogical changes in deep-sea sediments. J. Sediment. Petrol. 42: 889-898.

Jacobs,S.S. and Georgi,D.T. 1977. Observations on the southwest Indian/Antarctic Ocean. Deep-Sea Res. 24 (supplement): 43-84.

Jenkyns,H.C. 1980. Cretaceous anoxic events: from continents to oceans. J. Geol. Soc. Lond. 137: 171-188.

Johns,W.D., Grim,R.E. and Bradley,W.F. 1954. Quantitative estimations of clay minerals by diffraction methods. J. Sediment. Petrol. 24: 242-251.

Johnson,D.A. and Damuth,J.E. 1979. Deep thermohaline flow and current-controlled sedimentation in the Almirante Passage: Western Indian ocean. Mar. Geol. 33: 1-44.

Johnson,L.J. 1970. Clay minerals in Pennsylvania soils. Relation of lithology of the parent rock and other factors - I. Clays and Clay Mins. 18: 247-260.

Kaneps,A.G. 1979. Gulf Stream: velocity fluctuations during the late Cenozoic. Science 204: 297-301.

Karl,H.A. 1980. Influence of San Gabriel submarine canyon on narrow-shelf sediment dynamics, southern California. Mar. Geol. 34: 61-78.

Keller,G.H. and Barron,J.A. 1983. Paleoceanographic implications of Miocene deep-sea hiatuses. Am. Assoc. Pet. Geol. Bull. 94: 590-613.

Keller,G.H. and Shepard,F.P. 1978. Currents and sedimentary processes in submarine canyons off the northeast United States. In: G.Kelling and D.J.Stanley (eds.). Sedimentation in submarine canyons, fans and trenches. Dowden, Hutchinson and Ross, Stroudsburg, Pa.: 15-32.

Keller,W.D. 1970. Environmental aspects of clay minerals. J. Sediment. Petrol. 40: 788-813.

Kennedy,W.J. and Klinger,H.C. 1971. A major intra-Cretaceous unconformity in eastern South Africa. J. Geol. Soc. Lond. 127: 183-186.

Kennedy,W.J. and Klinger,H.C. 1975. Cretaceous faunas from Zululand and Natal, South Africa. Bull. Brit. Mus. Nat. Hist. Geol. 25: 265-315.

Kennett,J.P. 1978. The development of planktonic biogeography in the Southern Ocean during the Cenozoic. Mar. Micropalaeontol. 3: 301-345.

Kennett,J.P. and Shackleton,N.J. 1976. Oxygen isotopic evidence for the development of the psychrosphere 38 myr ago. Nature 260: 513-515.

Kent,P.E. 1974a. Continental margin of East Africa - a region of vertical movement. In: C.A.Burke and C.L.Drake (eds.). The geology of continental margins. Springer-Verlag, New York: 313-320.

Kent,P.E. 1974b. Leg 25 results in relation to East African coastal stratigraphy. In: E.S.W.Simpson, R.Schlich et al. Init. Rept. Deep-Sea Drill. Proj. 25. U.S.Govt. Print. Off. Washington: 679-684.

Kidd,R.B. and Davies,T.A. 1978. Indian Ocean sediment distribution since the Late Jurassic. Mar. Geol. 26: 49-70.

King,L.C. 1967. Scenery of South Africa. Oliver and Boyd, Edinburgh: 308pp.

King,L.C. 1972. The Natal Monocline: explaining the origin and scenery of Natal, South Africa. Univ. Natal, Durban: 113pp.

Kinsman,D.J.J. 1975. Rift valley basins and sedimentary history of trailing continental margins. In: A.G.Fischer and S.Judson (eds.). Petroleum and global tectonics. Princeton Univ. Press: 83-126.

Knebel,H.J. and Carson,B. 1979. Small scale slump deposits, middle Atlantic continental slope off eastern United States. Mar. Geol. 29: 221-236.

Kolla,V., Sullivan,L., Streeter,S.S. and Langseth,M.G. 1976a. Spreading of Antarctic Bottom Water and its effects on the floor of the Indian Ocean inferred from bottom-water potential temperature, turbidity and sea-floor photography. Mar. Geol. 21: 171-189.

Kolla,V., Henderson,L. and Biscaye,P.E. 1976b. Clay mineralogy and sedimentation in the western Indian Ocean. Deep-Sea Res. 23: 949-961.

Kolla,V., Be,A.W.H. and Biscaye,P.E. 1976c. Calcium carbonate distribution in the surface sediments of the Indian Ocean. J. Geophys. Res. 81: 2605-2616.

Kolla,V. and Biscaye,P.E. 1977. Distribution and origin of quartz in the sediments of the Indian Ocean. J. Sediment. Petrol. 47: 642-649.

Kolla,V., Eittreim,S., Sullivan,L., Kostecki,J.A. and Burckle,L.H. 1980a. Current-controlled, abyssal microtopography and sedimentation in Mozambique Basin, southwest Indian Ocean. Mar. Geol. 34: 171-206.

Kolla,V., Kostecki,J.A., Henderson,L. and Hess,L. 1980b. Morphology and Quaternary sedimentation of the Mozambique Fan and environs, southwestern Indian Ocean. Sedimentology 27: 357-378.

Kowsmann,R.O. 1973. Coarse components in surface sediments of the Panama Basin. J. Geol. 81: 473-494.

Krinsley,D.H. and Doornkamp,J.C. 1973. Atlas of quartz sand surface textures. University Press, Cambridge: 91pp.

Krinsley,D.H. and Margolis,S. 1969. A study of quartz sand grain surface textures with the scanning electron microscope. Trans. N.Y. Acad. Sci. 31: 457-475.

Krinsley,D.H. and McCoy,F.W. 1977. Significance and origin of surface textures on broken sand grains in deep-sea sediments. Sedimentology 24: 857-862.

Krumbein,W.C. 1934. Size frequency distributions of sediments. J. Sediment. Petrol. 4: 65-77.

Ladd,J.W. 1976. Relative motion of South America with respect to North America and Caribbean tectonics. Geol. Soc. Am. Bull. 87: 969-976.

Lamb,J.L. and Beard,J.H. 1972. Late Neogene planktonic foraminifers in the Caribbean, Gulf of Mexico, and Italian stratotypes. Kansas Univ. Palaeontol. Contr. 57: 67pp.

Larson,R.L. and Hilde,T.W.C. 1975. A revised time-scale of magnetic reversals for the Early Cretaceous and Late Jurassic. J. Geophys. Res. 80: 2586-2594.

Larson,R.L. and Ladd,J.W. 1973. Evidence for the opening of the South Atlantic in the Early Cretaceous. Nature 246: 209-212.

Laughton,A.S., Matthews,D.H. and Fisher,R.L. 1971. The structure of the Indian Ocean. In: A.E.Maxwell (ed.). The Sea. V.4. Wiley, New York: 543-586.

Leclaire,L. 1974. Late Cretaceous and Cenozoic pelagic deposits - palaeoenvironment and palaeoceanography of the central western Indian Ocean. In: E.S.W.Simpson, R.Schlich et al. Init. Rept. Deep-Sea Drill. Proj. 25. U.S.Govt. Print. Off. Washington: 481-505.

Ledbetter,M.T. 1979. Fluctuations of Antarctic Bottom Water velocity in the Vema Channel during the last 160,000 years. Mar. Geol. 33: 71-89.

Le Pichon,X. 1960. The deep water circulation in the south west Indian Ocean. J. Geophys. Res. 65: 4061-4074.

Lewis,K.B. 1971. Slumping on a continental slope inclined at 1°-4°. Sedimentology 16: 97-110.

Lonardi,A.G. and Ewing,M. 1971. Sediment transport and distribution in the Argentine Basin 4: Bathymetry of the continental margin, Argentine Basin and related provinces, canyons and sources of sediment. Physics & Chemistry of the Earth 8: 79-121.

Lonsdale,P. and Hollister,C.D. 1979. A near-bottom traverse of Rockall Trough: hydrographic and geologic inferences. Oceanol. Acta. 2: 91-105.

Lonsdale,P. and Smith,S.M. 1980. 'Lower insular rise hills' shaped by a bottom boundary current in the mid-Pacific. Mar. Geol. 34: M19-M25.

Lovell,J.P.B. and Stow,D.A.V. 1981. Identification of ancient sandy contourites. Geology 9: 347-349.

Ludwig,W.J., Krasheninnikov,V. et al. 1980. Tertiary and Cretaceous palaeoenvironments in the southwest Atlantic Ocean: preliminary results of Deep-Sea Drilling Project Leg 71. Geol. Soc. Am. Bull. 91: 655-664.

Ludwig,W.J., Krasheninnikov,V. et al. 1983. Init. Rept. Deep-Sea Drill. Proj. 71(1). U.S. Govt. Print. Off. Washington: 477pp.

Ludwig,W.J., Nafe,J.E., Simpson,E.S.W. and Sacks,S. 1968. Seismic refraction measurements on the southeast African continental margin. J. Geophys. Res. 73: 3707-3719.

Lutjeharms,J.R.E. 1971. A descriptive physical analysis of water movement in the south-west Indian Ocean during the north-east monsoon season. M.Sc.thesis, Univ. Cape Town (unpubl.).

Lutjeharms,J.R.E., Bang,N.D. and Duncan,C.P. 1981. Characteristics of the currents east and south of Madagascar. Deep-Sea Res. 28: 879-899.

Lutze,G., Sarnthein,M., Koopman,B., Pflaumann,U., Erlenkeuser,H. and Thiede,J. 1979. Meteor cores 12309: Late Pleistocene reference section for interpretation of the Neogene of site 397. In: U.von Rad, W.B.F.Ryan et al. Init. Rept. Deep-Sea Drill. Proj. 47. U.S.Govt. Print. Off. Washington: 727-739.

Malan,O.G. and Schumann,E.H. 1979. Natal shelf circulation revealed by Landsat Imagery. S. Afr. J. Sci. 75: 136-137.

Malfait,B.T. and Van Andel,Tj.H. 1980. A modern oceanic hardground on the Carnegie Ridge in the eastern Equatorial Pacific. Sedimentology 27: 467-497.

Marchig,V. and Rosch,H. 1983. Formation of clay minerals during early diagenesis of calcareous ooze. Sediment. Geol. 34: 283-299.

Margolis,S.V. and Herman,Y. 1980. Northern Hemisphere sea-ice and glacial development in the Late Cenozoic. Nature 286: 145-149.

Margolis,S.V., Kroopnick,P.M. and Goodney,D.E. 1977. Cenozoic and Late Mesozoic palaeoceanographic and palaeoglacial history recorded in circum-Antarctic deep-sea sediments. Mar. Geol. 25: 131-147.

Martin,A.K. 1981. The influence of the Agulhas Current on the physiographic development of the northernmost Natal Valley (S.W. Indian Ocean). Mar. Geol. 39: 259-276.

Martin,A.K. 1984. Plate tectonic status and sedimentary basin infill of the Natal Valley (S.W. Indian Ocean). Ph.D. thesis. Joint GSO/UCT Mar. Geosc. Bull. 14: 209pp.

Martin,A.K., Goodlad,S.W., Hartnady,C.J.H. and du Plessis,A. 1982. Cretaceous palaeopositions of the Falkland Plateau relative to southern Africa using Mesozoic seafloor spreading anomalies. Geophys. J. Roy. Astr. Soc. 71: 567-579.

Martin,A.K., Goodlad,S.W. and Salmon,D.A. 1982. Sedimentary basin in-fill in the northernmost Natal Valley, hiatus development and Agulhas Current palaeo-oceanography. J. Geol. Soc. Lond. 139: 183-201.

Martin,A.K. and Hartnady,C.J.H. 1983. A revised reconstruction of East Antarctica and Africa: plate tectonic status of the northern Natal Valley and Mozambique Ridge. Joint GSO/UCT Mar. Geosc. Tech. Rept. 14: 215-234.

Martin,A.K., Hartnady,C.J.H. and Goodlad,S.W. 1981. A revised fit of South America and South Central Africa. Earth Planet. Sci. Letts. 54: 293-305.

Marsh,J.S. 1973. Relationships between transform directions and alkaline igneous rock lineaments in Africa and South America. Earth Planet. Sci. Letts. 18: 317-323.

Masson,D.G., Gardner,J.V., Parson,L.M. and Field,M.E. 1985. Morphology of Upper Laurentian Fan using GLORIA side-scan sonar. Am. Assoc. Pet. Geol. Bull. 69: 950-959.

Matti,J.C., Zemmels,I. and Cook,H.E. 1974. X-ray mineralogy data, Arabian and Red Sea. In: R.B.Whitmarsh,O.E.Weser et al. Init. Rept. Deep-Sea Drill. Proj. 23. U.S.Govt. Print. Off. Washington: 1137-1156.

Maud,R.R. 1961. A preliminary review of the structure of coastal Natal. Trans. Geol. Soc. S. Afr. 64: 247-256.

McCoy,F.W. 1980. Photographic analysis of coring. Mar. Geol. 38: 263-282.

McElhinny,M.W. 1973. Palaeomagnetism and plate tectonics. Cambridge Univ. Press, New York: 357pp.

McKenzie,D. 1978. Some remarks on the development of sedimentary basins. Earth Planet. Sci. Letts. 40: 25-32.

McLachlan,I.R. and McMillan,I.K. 1979. Microfaunal biostratigraphy, chronostratigraphy and history of Mesozoic and Cenozoic deposits of the coastal margin of South Africa. Geol. Soc. S. Afr. Spec. Publ. 6: 161-181.

Melson,W.G. and Thompson,G. 1971. Petrology of a transform fault zone and adjacent ridge sediments. Phil. Trans. Roy. Soc. Lond. 268: p423.

Middleton,G.V. 1976. Hydraulic interpretation of sand size distributions. J. Geol. 84: 405-426.

Middleton,G.V. and Hampton,M.A. 1976. Subaqueous sediment transport and deposition by sediment gravity flows. In: D.J.Stanley and D.J.P.Swift (eds.). Marine sediment transport and environmental management. Wiley, New York: 197-218.

Milliman,J.D. and Meade,R.H. 1983. World-wide delivery of river sediment to the oceans. J. Geol. 91: 1-21.

Mitchell,C., Taylor,G.K., Cox,K.G. and Shaw,J. 1986. Are the Falkland Islands a rotated microplate? Nature 319: 131-134.

Mitchum,R.M., Vail,P.R. and Thompson,S.III. 1977a. Seismic stratigraphy and global changes of sea level, part 2: the depositional sequence as a basic unit for stratigraphic analysis. Am. Assoc. Pet. Geol. Mem. 26: 53-62.

Mitchum,R.M., Vail,P.R. and Sangree,J.B. 1977b. Seismic stratigraphy and global changes of sea level, part 6: stratigraphic interpretation of seismic reflection patterns in depositional sequences. Am. Assoc. Pet. Geol. Mem. 26: 117-133.

Moir,G.J. 1975. Bathymetry of the upper continental margin between Cape Recife (34°S) and Ponta do Ouro (27°S), South Africa. Joint GSO/UCT Mar. Geosc. Tech. Rept. 7: 68-78.

Moir,G.J. 1976. Preliminary textural and compositional analyses of surficial sediments from the upper continental margin between Cape Recife (34°S) and Ponto do Ouro (27°S), South Africa. Joint GSO/UCT Mar. Geosc. Tech. Rept. 8: 68-75.

Moore,D.G., Curray,J.R. and Emmel,F.J. 1976. Large submarine slide (olistostrome) associated with Sunda Arc subduction zone, North East Indian Ocean. Mar. Geol. 21: 211-227.

Moore,J.G. and Fabbi,B.P. 1971. An estimate of the juvenile sulphur content of basalt. Contr. Mineral. Petrol. 33: 118-127.

Moore,J.G. and Schilling,J-G. 1973. Vesicles, water, and sulfur in Reykjanes Ridge basalts. Contr. Mineral. Petrol. 41: 105-118.

Moore,T.C., Heath,G.R. and Kowsmann,R.O. 1973. Biogenic sediments of the Panama Basin. J. Geol. 81: 458-472.

Moore,T.C., Van Andel,Tj.H., Sancetta,C. and Pisias,N. 1978. Cenozoic hiatuses in pelagic sediments. Micropalaeontol. 24: 113-138.

Morgans,J.F.C. 1956. Notes on the analysis of shallow-water soft substrata. J. Anim. Ecol. 25: 367-387.

Muller,G. and Gastner,M. 1971. The "Karbonat-Bombe", a simple device for the determination of the carbonate content in sediments, soils and other materials. Neues Jahrb. Miner. Mh. 10: 466-469.

Mullins,H.T., Neumann,A.C., Wilber,R.J., Hine,A.C. and Chinburg,S.J. 1980. Carbonate sediment drifts in the northern Straits of Florida. Am. Assoc. Pet. Geol. Bull. 64: 1701-1717.

Murgatroyd,A.L. 1979. Geologically normal and accelerated rates of erosion in Natal. S. Afr. J. Sci. 75: 395-396.

Nairn,A.E.M. and Stehli,F.S. 1982. The ocean basins and margins 6: the Indian Ocean. Plenum Press, New York: 776pp.

Nardin,T.R., Edwards,B.D. and Gorsline,D.S. 1979a. Santa Cruz Basin, California Borderland: dominance of slope processes in basin sedimentation. SEPM Spec. Publ. 27: 209-221.

Nardin,T.R., Hein,F.J., Gorsline,D.S., and Edwards,B.D. 1979b. A review of mass movement processes, sediment and acoustic characteristics, and contrasts in slope and base-of-slope systems versus canyon-fan-basin floor systems. SEPM Spec. Publ. 27: 61-73.

Natland,J.H. 1978. Composition, provenance and diagenesis of Cretaceous clastic sediments drilled on the Atlantic continental rise off southern Africa, DSDP site 361 - implications for the early circulation of the South Atlantic. In: H.M.Bolli, W.B.F.Ryan et al. Init. Rept. Deep-Sea Drill. Proj. 40. U.S.Govt. Print. Off. Washington: 1025-1061.

Nelson,C.H.and Kulm,L.D. 1973. Submarine fans and channels. In: G.V.Middleton and A.H.Bouma (eds.). Turbidites and deep water sedimentation. SEPM Pacific Sect., Short Course Notes, Anaheim: 39-78.

Nelson,C.H. and Nilsen,T.C. 1984. Modern and ancient deep-sea fan sedimentation. SEPM Short Course 14: 404pp.

Nelson,C.H., Normark,W.R., Bouma,A.H. and Carlson,P.R. 1978. Thin-bedded turbidites in modern submarine canyons and fans. In: G.Kelling and D.J.Stanley (eds.). Sedimentation in submarine canyons, fans and trenches. Dowden, Hutchinson and Ross, Stroudsburg, Pa.: 177-189.

Newton,A.R. 1976. Was there an Agulhas triple junction? Nature 260: 767-768.

Nicolas,A., Bouchez,J.L., Blaise,J. and Poirier,J.P. 1977. Geological aspects of deformation in continental shear zones. Tectonophysics 42: 55-73.

Nicolaysen,L.O. 1973. Progress in marine geology and geophysics in South Africa during the past three years. S. Afr. Nat. Ocean. Symp. Div. Sea Fisheries, Cape Town: 8-9.

Normark,W.R. 1978. Fan valleys, channels and depositional lobes on modern submarine fans: characters for recognition of sandy turbidite environments. Am. Assoc. Pet. Geol. Bull. 62: 912-931.

Normark,W.R., Hess,G.R., Stow,D.A.V. and Bowen,A.J. 1980. Sedimentary waves on the Monterey Fan levee: a preliminary physical interpretation. Mar. Geol. 37: 1-18.

Norton,I.O. and Sclater,J.G. 1979. A model for the evolution of the Indian Ocean and break-up of Gondwanaland. J. Geophys. Res. 84: 6803-6830.

O'Brien,G.W. and Veeh,H.H. 1980. Holocene phosphorite on the east Australian continental margin. Nature 288: 690-693.

Oliver,H.O. 1956. South African earthquakes, Jan. 1953 - Dec. 1955. Trans. Geol. Soc. S. Afr. 59: 123-133.

Orme,A.R. 1974. Estuarine sedimentation along the Natal coast, South Africa. Tech. Rept. 5. Office of Naval Research, Virginia, U.S.A.: 54pp.

Parsons,B. and Sclater,J.G. 1977. An analysis of the variation of ocean floor bathymetry and heat flow with age. J. Geophys. Res. 82: 803-827.

Passega,R. 1957. Texture as characteristic of clastic deposits. Am. Assoc. Pet. Geol. Bull. 41: 1952-1984.

Pearce,A.F. 1977. The shelf circulation on the east coast of South Africa. NRIO Prof. Res. Series 1. Stellenbosch, South Africa: 220pp.

Pearce,J.A. 1975. Basalt geochemistry used to investigate past environments on Cyprus. Tectonophysics 25: 41-67.

Pearce,J.A. and Cann,J.R. 1973. Tectonic setting of basic volcanic rocks determined using trace element analyses. Earth Planet. Sci. Letts. 19: 290-300.

Peng,T.H. et al. 1977. Benthic mixing in deep-sea cores as determined by C^{14} dating and its implication regarding climate, stratigraphy and the fate of fossil fuel CO_2. In: N.R.Anderson and A.Malahoff (eds.). The fate of fossil fuel CO_2 in the oceans. Plenum Press, New York: 355-373.

Pinet,P.R. and Popenoe,P. 1982. Blake Plateau: control of Miocene sedimentation patterns by large-scale shifts of the Gulf Stream axis. Geology 10: 257-259.

Piper,D.J.W. 1970. Transport and deposition of Holocene sediment on La Jolla deep-sea fan, California. Mar. Geol. 8: 211-227.

Piper,D.J.W. 1978. Turbidite muds and silts on deep-sea fans and abyssal plains. In: G.Kelling and D.J.Stanley (eds.). Sedimentation in submarine canyons, fans and trenches. Dowden, Hutchinson and Ross, Stroudsburg, Pa.: 163-176.

Powell,C.McA., Johnson,B.D. and Veevers,J.J. 1980. A revised fit of east and west Gondwanaland. Tectonophysics 63: 13-29.

Prell,W.L. 1977. Winnowing of Recent and Late Quaternary deep-sea sediments: Colombia Basin, Caribbean Sea. J. Sediment. Petrol. 47: 1583-1592.

Prior,D.B. and Coleman,J.M. 1979. Submarine landslides - geometry and nomenclature. Z. Geomorph. N.F. 23: 415-426.

Purdy,G.M. and Twichell,D.C. 1978. Sediment distribution around the Bouvet triple junction. Mar. Geol. 28: M53-M57.

Quilty,P.G. 1977. Cenozoic sedimentation cycles in Western Australia. Geology 5: 336-340.

Rabinowitz,P.D. 1976. Geophysical study of the continental margin of southern Africa. Geol. Soc. Am. Bull. 87: 1643-1653.

Rabinowitz,P.D., Cande,S.C. and LaBrecque,J.L. 1976. The Falkland Escarpment and Agulhas Fracture Zone: the boundary between oceanic and continental basement at conjugate continental margins. Ann. Brazil Acad. Sci. 48 (supplement): 241-251.

Rabinowitz,P.D. and LaBrecque,J.L. 1979. The Mesozoic South Atlantic Ocean and evolution of its continental margin. J. Geophys. Res. 84: 5973-6002.

Raitt,R.W. 1963. The crustal rocks. In: M.N.Hill (ed.). The Sea. V.3. Interscience, New York: 175-217.

Rateev,M.A., Gorbunova,Z.N., Lisitzin,A.P. and Nosov,G.L. 1969. The distribution of clay minerals in the ocean. Sedimentology 13: 21-43.

Roberts,D.G., Hogg,N.G., Bishop,D.G. and Flewellen,C.G. 1974. Sediment distribution around moated seamounts in the Rockall Trough. Deep-Sea Res. 21: 175-184.

Rooseboom,A. 1978. Sedimentafvoer in Suider-Afrikaanse riviere. Water S. Afr. 4: 14-17.

Rowley,D.B. and Sahagian,D. 1986. Depth-dependent stretching : a different approach. Geology 14: 32-35.

Royse,C.F. 1970. An introduction to sediment analysis. Arizona State Univ.: 180pp.

Rupke,N.A. 1978. Deep clastic seas. In: H.G.Reading (ed.). Sedimentary environments and facies. Blackwell, Oxford: 372-415.

Ryther,J.H., Hall,J.R., Pease,A.K., Bakun,A. and Jones,M.M. 1966. Primary organic production in relation to the chemistry and hydrography of the western Indian Ocean. Limnol. Oceanogr. 11: 371-380.

Salmon,D.A. 1979a. Micropalaeontological investigations of piston cores from the SW Indian Ocean: some preliminary results and implications. Joint GSO/UCT Mar. Geosc. Tech. Rept. 11: 63-71.

Salmon,D.A. 1979b. Quaternary foraminifers in piston cores from the SW Indian Ocean. Joint GSO/UCT Mar. Geosc. Tech. Rept. 11: 72-79.

Sangree,J.B. and Widmier,J.M. 1977. Seismic stratigraphy and global changes of sea level, part 9: seismic interpretation of clastic depositional facies. Am. Assoc. Pet. Geol. Mem. 26: 165-184.

Savin,S.M. and Epstein,S. 1970. The oxygen and hydrogen isotope geochemistry of ocean sediments and shales. Geochim. Cosmochim. Acta 34: 43-63.

Saxov,S. and Nieuwenhuis,J.K. 1982. Marine slides and other mass movements. Plenum Press, New York: 353pp.

Schlanger,S.O. and Jenkyns,H.C. 1976. Cretaceous oceanic anoxic events: causes and consequences. Geol. en. Mijn. 55: 179-185.

Schnitker,D. 1980a. Global palaeoceanography and its deep water linkage to the Antarctic glaciation. Earth Sci. Rev. 16: 1-20.

Schnitker,D. 1980b. North Atlantic oceanography as possible cause of Antarctic glaciation and eutrophication. Nature 284: 615-616.

Schulze,B.R. 1965. Climate of South Africa (part 8, general survey). Weather Bureau, S. Afr. Dept. Transport: 330pp.

Sclater,J.G., Abbot,D. and Thiede,J. 1977. Palaeobathymetry and sediments of the Indian Ocean. In: J.R.Heirtzler et al (eds.). Indian Ocean Geology and Biostratigraphy. Am. Geophys. Union. Washington: 25-59.

Sclater,J.G. and Christie,P.A.F. 1980. Continental stretching: an explanation of the post-Mid-Cretaceous subsidence of the Central North Sea Basin. J. Geophys. Res. 85: 3711-3739.

Sclater,J.G. and Harrison,C.G.A. 1972. Elevation of mid-ocean ridges and the evolution of the south-west Indian Ocean Ridge. Nature 230: 175-177.

Scrutton,R.A. 1973a. The age relationship of igneous activity and continental break-up. Geol. Mag. 110: 227-234.

Scrutton,R.A. 1973b. Structure and evolution of the sea floor south of South Africa. Earth Planet. Sci. Letts. 19: 250-256.

Scrutton,R.A. 1976. Continental break-up and deep crustal structure at the margins of southern Africa. Ann. Brazil Acad. Sci. 48 (supplement): 101-120.

Scrutton,R.A. 1979. On sheared passive continental margins. Tectonophysics 59: 293-305.

Scrutton,R.A. and du Plessis,A. 1973. Possible marginal fracture ridge south of South Africa. Nature 242: 180-182.

Scrutton,R.A. and Stow,D.A.V. 1984. Seismic evidence for Early Tertiary bottom-current controlled deposition in the Charlie Gibbs Fracture Zone. Mar. Geol. 56: 325-334.

Segoufin,J. 1978. Anomalies magnetiques Mesozoiques dans le bassin de Mozambique. C.R. Acad. Sci. Paris 287D: 109-112.

Sengupta,S. and Veenstra,H.J. 1968. On sieving and settling techniques for sand analysis. Sedimentology 11: 83-98.

Shackleton,N.J. and Opdyke,N.D. 1977. Oxygen isotope and palaeomagnetic evidence for early Northern Hemisphere glaciation. Nature 270: 216-219.

Shanmugam,G. and Moiola,R.J. 1982. Prediction of deep-sea reservoir facies. Gulf Coast Assoc. Geol. Soc. Trans. 32: 275-281.

Sheldon,R.W. and Parsons,T.R. 1967. A practical manual on the use of the Coulter Counter in marine science. Coulter Electronics, Toronto: 66pp.

Shepard,F.P. 1954. Nomenclature based on sand-silt-clay ratios. J. Sediment. Petrol. 24: 151-158.

Shepard,F.P. 1963. Submarine geology. Harper and Row, New York: 557pp.

Shepard,F.P. 1979. Currents in submarine canyons and other types of sea-valleys. SEPM Spec. Publ. 27: 85-94.

Shepard,F.P. and Buffington,E.C. 1968. La Jolla submarine fan-valley. Mar. Geol. 6: 107-143.

Shepard,F.P. and Dill,R. 1966. Submarine canyons and other sea valleys. Rand-McNally, Chicago: 381pp.

Sheriff,R.E. 1976. Inferring stratigraphy from seismic data. Am. Assoc. Pet. Geol. Bull. 60: 528-542.

Shideler,G.L. 1976a. Textural distribution of sea-floor sediments, South Texas outer continental shelf. J. Res. U.S. Geol. Surv. 4: 703-713.

Shideler,G.L. 1976b. A comparison of electronic particle counting and pipette techniques in routine mud analysis. J. Sediment. Petrol. 46: 1017-1025.

Shideler,G.L. 1978. A sediment-dispersal model for the south Texas continental shelf, northwest Gulf of Mexico. Mar. Geol. 26: 289-313.

Siedner,G. and Mitchell,J.G. 1976. Episodic Mesozoic volcanism in Namibia and Brazil: a potassium-argon isochron study with bearing on the opening of the South Atlantic. Earth Planet. Sci. Letts. 30: 292-302.

Siesser,W.G. and Dingle,R.V. 1981. Tertiary sea-level movements around southern Africa. J. Geol. 89: 83-96.

Siesser,W.G. and Miles,G.A. 1979. Calcareous nannofossils and planktic foraminifers in Tertiary limestones, Natal and eastern Cape, South Africa. Ann. S. Afr. Mus. 79: 139-158.

Simpson,E.S.W. 1974. Chart 125A, NRIO. Stellenbosch, South Africa.

Simpson,E.S.W. 1977. Evolution of the South Atlantic. Geol. Soc. S. Afr. Annex. 80: 1-15.

Simpson,E.S.W., Schlich,R. et al. 1974. Init. Rept. Deep-Sea Drill. Proj. 25. U.S.Govt. Print. Off. Washington: 884pp.

Simpson,E.S.W., Sclater,J.G., Parsons,B., Norton,I. and Meinke,L. 1979. Mesozoic magnetic lineations in the Mozambique Basin. Earth Planet. Sci. Letts. 43: 260-264.

Singer,A. 1980. The paleoclimatic interpretation of clay minerals in soils and weathering profiles. Earth Sci. Rev. 15: 303-326.

Sleep,N.H. 1971. Thermal effects of the formation of Atlantic continental margins by continental breakup. Geophys. J. Roy. Astr. Soc. 24: 325-350.

Smith,A.G. 1982. Late Cenozoic uplift of stable continents in a reference frame fixed to South America. Nature 296: 400-404.

Smith,A.G. and Hallam,A. 1970. The fit of the southern continents. Nature 225: 139-144.

Sowerbutts,W.T.C. 1972. Rifting in eastern Africa and the fragmentation of Gondwanaland. Nature Phys. Sci. 235: 435-437.

Stainforth,R.M., Lamb,J.L., Luterbacher,H., Beard,J.H. and Jeffords,R.M. 1975. Cenozoic planktonic foraminiferal zonation and characteristics of index forms. Kansas Univ. Palaeontol. Contr. 62: 425pp.

Stanley,D.J. and Kelling,G. 1978. Sedimentation in submarine canyons, fans and trenches. Dowden,Hutchinson and Ross, Stroudsburg, Pa.: 395pp.

Stavropoulos,C.C. and Duncan,C.P. 1974. A satellite-tracked buoy in the Agulhas Current. J. Geophys. Res. 27: 2744-2746.

Steckler,M.S. and Watts,A.B. 1978. Subsidence of the Atlantic-type continental margin off New York. Earth Planet. Sci. Letts. 41: 1-13.

Stow,D.A.V. 1985. Fine-grained sediments in deep water: an overview of processes and facies models. Geo-Marine Letts. 5: 17-23.

Stow,D.A.V. and Aksu,A.E. 1978. Disturbances in soft sediments due to piston coring. Mar. Geol. 28: 135-144.

Stow,D.A.V. and Bowen,A.J. 1980. A physical model for the transport and sorting of fine-grained sediment by turbidity currents. Sedimentology 27: 31-46.

Stow,D.A.V., Howell,D.G. and Nelson,C.H. 1983/1984. Sedimentary, tectonic, and sea-level controls on submarine fan and slope-apron turbidite systems. Geo-Marine Letts. 3: 57-64.

Stow,D.A.V. and Lovell,J.P.B. 1979. Contourites: their recognition in modern and ancient sediments. Earth Sci. Rev. 14: 251-291.

Stow,D.A.V. and Shanmugam,G. 1980. Sequence of structures in fine-grained turbidites: comparison of recent deep-sea and ancient flysch sediments. Sediment. Geol. 25: 23-42.

Strass,I.F. 1978. Microtextures of quartz sand grains in coastal and shelf sediments, More, western Norway. Mar. Geol. 28: 107-134.

Sudo,T., Oinuma,K. and Kobayashi,K. 1961. Mineralogical problems concerning rapid clay mineral analysis of sedimentary rocks. Acta Univ. Carolinae Geol. Supp. 1: 189-219.

Summerhayes,C.P., Bornhold,B.D. and Embley,R.W. 1979. Surficial slides and slumps on the continental slope and rise of south-west Africa. Mar. Geol. 31: 265-277.

Swift,D.J.P., Schubel,J.R. and Sheldon,R.W. 1972. Size analysis of fine-grained suspended sediments: a review. J. Sediment. Petrol. 42: 122-134.

Taira,A. and Scholle,P.A. 1979a. Origin of bimodal sands in some modern environments. J. Sediment. Petrol. 49: 777-786.

Taira,A. and Scholle,P.A. 1979b. Discrimination of depositional environments using settling tube data. J. Sediment. Petrol. 49: 787-800.

Takahashi,T. and Broecker,W.S. 1977. Mechanisms for calcite dissolution on the sea floor. In: N.R.Andersen and A.Malahoff (eds.). The fate of fossil fuel CO_2 in the oceans. Plenum Press, New York: 429-454.

Thiede,J. 1981. Reworking in Upper Mesozoic and Cenozoic central Pacific deep-sea sediments. Nature 289: 667-670.

Thiede,J., Agdestein,T. and Strand,J.E. 1980. Depth distribution of calcareous sediments in the Mesozoic and Cenozoic North Atlantic Ocean. Earth Planet. Sci. Letts. 47: 416-422.

Thiede,J., Chriss,T., Clauson,M. and Swift,S.A. 1976. Settling tubes for size analysis of fine and coarse fractions of oceanic sediments. Oregon State Univ.: 87pp.

Thompson,G., Bryan,W.B., Frey,F.A. and Dickey,J.S. 1978. Basalts and related rocks from deep-sea drilling sites in the central and eastern Indian Ocean. Mar. Geol. 26: 119-138.

Thompson,G., Bryan,W.B., Frey,F.A., Dickey,J.S. and Davies,H. 1982. Petrology, geochemistry and original tectonic setting of basalts from the Mozambique Basin and Ridge (DSDP Sites 248, 249 and 250), and from the Southwest Indian Ocean Ridge (DSDP Site 251). Mar. Geol. 48: 175-195.

Thompson,R.W. 1976. Mesozoic sedimentation on the eastern Falkland Plateau. In: P.F.Barker, I.W.D.Dalziel et al. Init. Rept. Deep-Sea Drill. Proj. 36. U.S.Govt. Print. Off. Washington: 877-891.

Thunell,R.C. 1982. Carbonate dissolution and abyssal hydrography in the Atlantic Ocean. Mar. Geol. 47: 165-180.

Toy,T.J. 1982. Accelerated erosion: process, problems and prognosis. Geology 10: 524-529.

Tripp,R.T. 1967. An atlas of coastal surface drifts, Cape Town to Durban. Dept. Oceanog., Univ. Cape Town: 10pp.

Truswell,J.F. 1970. An introduction to the historical geology of South Africa. Purnell, Cape Town: 167pp.

Tucholke,B.E. and Embley,R.W. 1984. Cenozoic regional erosion of the abyssal sea floor off South Africa. Am. Assoc. Pet. Geol. Mem. 36: 145-164.

Tucholke,B.E., Houtz,R.E. and Barrett,D.M. 1981. Continental crust beneath Agulhas Plateau, southwest Indian Ocean. J. Geophys. Res. 86: 3791-3806.

Turekian,K.K., Cochran,J.K. and De Master,D.J. 1978. Bioturbation in deep-sea deposits: rates and consequences. Oceanus 21: 34-41.

Uchupi,E. and Austin,J.A. 1981. The continent-ocean transition off southwest Africa. EOS. Trans. Am. Geophys. Union 62: 407.

Vail,P.R., Mitchum,R.M. and Thompson,S. 1977. Seismic stratigraphy and global changes of sea level, part 4: global cycles of relative changes of sea level. Am. Assoc. Pet. Geol. Mem. 26: 83-97.

Valia,H.S. and Cameron,B. 1977. Skewness as a palaeoenvironmental indicator. J. Sediment. Petrol. 47: 784-793.

Van Andel,Tj.H., Heath,G.R. and Moore,T.C. 1975. Cenozoic history and paleo-oceanography of the central equatorial Pacific Ocean. Geol. Soc. Am. Mem. 143: 134pp.

Van der Plas,L. and Tobi,A.C. 1965. A chart for judging the reliability of point counting results. Am. J. Sci. 263: 87-90.

Van Foreest,D. 1977. The Agulhas Current above the intermediate level. M.Sc.thesis, Univ. Cape Town (unpubl.).

Van Wijk,A.M. and Scheepers,G.L. 1966. Geomagnetic secular variation observations in southern Africa, 1961. Hermanus Mag. Obs., Geophys. Ser. 1 (C4). Govt. Printer, Pretoria: 67pp.

Van Zinderen Bakker,E.M. 1976. The evolution of Late Quaternary palaeoclimates of southern Africa. In: E.M.van Zinderen Bakker (ed.). Palaeoecology of Africa 9. Balkema, Cape Town: 160-202.

Veevers,J.J., Powell,C.McA. and Johnson,B.D. 1980. Seafloor constraints on the reconstruction of Gondwanaland. Earth Planet. Sci. Letts. 51: 435-444.

Vincent,E. 1970. Climatic change at the Pleistocene-Holocene boundary in the southwestern Indian Ocean. Am. Assoc. Pet. Geol. Bull. 54: 558-567.

Vincent,E. 1974. Cenozoic planktonic biostratigraphy and palaeo-oceanography of the tropical western Indian Ocean. In: R.L.Fisher, E.T.Bunce et al. Init. Rept. Deep-Sea Drill. Proj. 24. U.S.Govt. Print. Off. Washington: 1111-1150.

Vincent,E. 1976. Planktonic foraminifera, sediments and oceanography of the Late Quaternary, SW Indian Ocean. Allen Hancock Monograph Mar. Biol. 9: 235pp.

Vine,F.J. 1965. Interpretation of magnetic anomalies observed at sea. Ph.D.thesis, Univ. Cambridge (unpubl.).

Viswanatha Reddy,V., Subbarao,K.V., Reddy,G.R., Matsuda,J. and Hekinian,R. 1978. Geochemistry of volcanoes from the Ninetyeast Ridge and its vicinity in the Indian Ocean. Mar. Geol. 26: 99-117.

Vogt,P.R. 1972. The Faeroe-Iceland-Greenland aseismic ridge and the western boundary undercurrent. Nature 239: 79-81.

Volat,J., Pastouret,L. and Vergnaud-Grazzini,C. 1980. Dissolution and carbonate fluctuations in Pleistocene deep-sea cores: a review. Mar. Geol. 34: 1-28.

Von Stackelberg,U., Von Rad,U. and Zobel,B. 1979. Asymmetric sedimentation around Great Meteor Seamount (North Atlantic). Mar. Geol. 33: 117-132.

Walger,E. 1962. Die Korngrossenverteilung von Einzellagen sandiger Sedimente und ihre genetische Bedeutung. Geol. Rundschau 51: 494-507.

Walker,R.G. 1978. Deep-water sandstone facies and ancient submarine fans: models for exploration for stratigraphic traps. Am. Assoc. Pet. Geol. Bull. 62: 932-966.

Walton,E.K., Stephens,W.E. and Shawa,M.S. 1980. Reading segmented grain-size curves. Geol. Mag. 117: 517-524.

Warren,B.A. 1974. Deep flow in the Madagascar and Mascarene Basins. Deep-Sea Res. 21: 1-21.

Watts,A.B. and Thorne,J. 1984. Tectonics, global changes in sea level and their relationship to stratigraphical sequences at the US Atlantic continental margin. Mar. Pet. Geol. 1: 319-339.

Weissel,J.K., Hayes,D.G. and Herron,E. 1977. Plate tectonic synthesis: the displacements between Australia, New Zealand and Antarctica since the Late Cretaceous. Mar. Geol. 25: 231-277.

Westall,F. 1984. Current-controlled sedimentation in the Agulhas Passage, SW Indian Ocean. Ph.D.thesis. Joint GSO/UCT Mar. Geosc. Bull. 12: 276pp.

Whitehouse,G., Jeffrey,L.M. and Debbrecht,J.D. 1960. Differential settling tendencies of clay minerals in saline waters. Clays and Clay Mins. 7: 1-79.

Willis,J.P., Ahrens,L.H. et al. 1971. Some inter-element relationships between lunar rocks and fines and stoney meteorites. Geochim. Cosmochim. Acta (Supp. 1) 2: 1123-1138.

Winter,H. de la R. 1973. Geology of the Algoa Basin. In: G.Blant (ed.). Sedimentary basins of the African coasts, part 2, south and east coasts. Paris Assoc. Afr. Geol. Surv.: 17-48.

Worsley,T.R. and Davies,T.A. 1979a. Sea level fluctuations and deep-sea sedimentation rates. Science 203: 455-456.

Worsley,T.R. and Davies,T.A. 1979b. Cenozoic sedimentation in the Pacific Ocean: steps towards a quantitative evaluation. J. Sediment. Petrol. 49: 1131-1146.

Wray,J.L. 1977. Calcareous Algae. Developments in Palaeontology and Stratigraphy 4. Elsevier, Amsterdam: 185pp.

Wyrtki,K., Bennet,E.B. and Rochford,D.J. 1971. Oceanographic atlas of the international Indian Ocean expedition. Nat. Sci. Found. Washington D.C.

APPENDIX A DATA REDUCTION AND ANALYTICAL TECHNIQUES

This appendix includes brief reports on instrumentation and methodology utilised during the data collection, analysis and compilation phases of the investigation. Appendix A contents are structured as follows:

Appendix A1 Bathymetric Profile Data

Bathymetric data were collected on R/V Thomas B. Davie cruises 157, 246, 258, 267, 277, 290, 291, 350, 371 and R/V Meiring Naude cruises 76/6 and 76/28 using a conventional hull-mounted 12kHz ELAC PDR. Additional data sources are listed on the 20 m bathymetry map (Fig.3.2). In fair-chart construction, depth-plotting highlighted the often large discrepancies in track cross-over correlations. These problems were minimised by adjusting older tracks with unreliable navigation to fit a framework of traverses (cruises TBD 350, 371 and MN 76/28) with satellite navigation accuracy ($\pm$400 m; Fainstein et al, 1975). Both bathymetry and seismic profile data were used as controls during track navigational re-alignment. A nominal velocity of 1500 m/sec has been used in sea floor depth computations.

Appendix A2 Seismic Reflection Profile Data

Continuous seismic reflection profiles used in this study were collected during the 1970-1977 period. Single channel systems used are detailed in Table A2.1. The multitude of systems used during different surveys have generated a wide variety of records, both in type and quality. Penetration varied from about 1 sec TWT (40in^3 airgun) to >2 secs TWT (300in^3 airgun). During cruise TBD 371, 10in^3 and 300in^3 airguns were triggered in tandem and the reflected signal was recorded on two different band-passes: 25-150 Hz (deep penetration, low resolution) and 150-500 Hz (high resolution). This optimum available system generated good-quality records from parts of the deep basin plain and Central Terrace. In conjunction with bathymetric data, traverse intersection discrepancies were rectified by adjusting old tracks to the satellite-navigated track framework (see Appendix A1).

Appendix A3 Magnetic Profile Data

Continuous magnetic profiles were routinely retrieved during all cruises listed in Table A2.1 using ELSEC, VARIAN and GEOMETRICS proton magnetometers. As a standard, the sensor fish was towed 10-15 m below the sea surface and approximately 100 m astern the ship.

Table A2.1 Natal Valley Cruises - Seismic Reflection Profiling Systems

CRUISE	DATE	NAVIGATION	ENERGY SOURCE	HYDROPHONES	RECORDER	FREQUENCY(Hz)
TBD 246	Oct 1970	Omega	10kJ sparker	single; 48 element	Alden	200-800
TBD 267	Oct-Nov 1971	Omega	40in^3 airgun	*	EPC4100	*
TBD 277	Oct-Nov 1972	Omega	40in^3 airgun	*	EPC4100	*
TBD 291	Oct-Nov 1973	Omega	40in^3 airgun; 10kJ sparker	single; 24 element	EPC4100	*
AII93-5+	Feb-Mar 1976	Satellite	40,300in^3 airgun	double; 200 element	HP	10-100
MN 76/6	Mar-Apr 1976	Satellite	40in^3 airgun	*	EPC4100	*
TBD 350+	May-Jun 1976	Satellite	40+40in^3 airgun	double; 24 element	EPC4100	60-150
MN 76/28+	Dec 1976	Satellite	40+40in^3 airgun	double; 24 element	EPC4100	50-180
TBD 371+	Oct-Nov 1977	Satellite	40+40 or 10+300 in^3 airgun	double; 24 element	EPC4100 EPC4600	25-150; 150-500

+ cruises in which S W Goodlad participated

* information not available

In removal of the regional geomagnetic reference field, all profiles were reduced to a common epoch (August 1966) by applying secular variation corrections (van Wijk and Scheepers, 1966). Reference field removal at intervals along traverses, with intervening linear interpolation, provided zero-datum magnetic anomaly data over the study area. The many factors limiting the accuracy of reduced magnetic measurements have been outlined by du Plessis (1967) and accordingly, no great stress is placed on anomalies of <100γ amplitude.

Appendix A4 Whole Rock Geochemical Analysis

Whole rock chemical analysis of dredge 5749 basalts were conducted in the Dept of Geochemistry, University of Cape Town using standard XRF techniques (Willis et al, 1971). Both SIEMENS SRS-1 and PHILLIPS PW 1220 spectrometers were used. Calibration was accomplished using both 'in-house' and international standards. Analytical procedures are documented in Bristow (1980). Rock samples were thoroughly cleaned and photographed. Before sub-sampling, the altered rind was cut away to leave a relatively fresh sample.

Sub-splits of 5749 D1-D3 were also analysed by the GSO, Pretoria and by Dr J Bristow (Cape Town) to assess inter-institution and intra-department analytical variance (Table A4.1). Reproducibility between institutions is relatively good excepting the trace elements Cr and V which were measured at significantly lower concentrations in the GSO laboratory. More disturbing is the poor correspondence between the Cape Town analyses, particularly for abundances of Fe_2O_3, Cu, Zn, Sr and Rb.

Appendix A5 Routine Micropalaeontology

Routine examination of all surficial and selected down-core samples was performed by Mr D Salmon. Using standard micropalaeontological techniques, 300-500 foram tests in the >150 μm size fraction were picked and identified for each sample. Three distinctive age assemblages are identified from species listings: (1) Quaternary; (2) undifferentiated Late Miocene/Pliocene; and (3) Quaternary containing reworked Tertiary

Table A4.1 Replicate Geochemical Analysis of Dredge Sample 5749

	5749 D1			5749 D2		5749 D3	
	1	2	3	1	3	1	3
SiO_2	43,44	44,28	43,45	49,04	50,54	35,08	36,10
TiO_2	1,35	1,36	1,41	1,96	2,06	1,21	1,27
Al_2O_3	15,99	16,40	17,39	17,27	17,36	11,30	11,92
Fe_2O_3*	11,75	10,50	11,12	13,23	12,71	9,73	9,23
MnO	0,12	0,06	0,13	0,10	0,12	0,13	0,14
MgO	5,13	5,25	5,05	3,95	3,90	3,01	2,72
CaO	12,18	12,15	12,33	5,00	5,25	19,02	20,06
Na_2O	2,05	2,40	1,59	2,10	1,78	1,24	0,64
K_2O	1,19	0,99	0,85	2,76	2,47	2,46	1,61
P_2O_5	0,18	0,16	0,33	0,40	0,50	0,39	0,54
H_2O^+	3,11	2,80	3,28	3,98	3,11	3,37	5,33
CO_2	3,52	3,65	3,07	0,22	0,21	13,06	10,44
TOTAL	100,01	100,00	100,00	100,01	100,01	100,00	100,00
Co	69	-	53	80	63	49	46
Cr	355	-	47	330	83	252	66
Cu	77	56	80	149	146	66	61
Ga	17	-	19	19	20	12	16
Nb	4	2	10	11	15	9	13
Ni	219	221	204	197	205	160	145
Rb	21	16	28	33	33	34	36
Sr	198	186	196	190	180	142	144
V	372	-	60	145	61	131	71
Y	21	19	16	31	29	26	20
Zn	157	135	144	162	147	105	92
Zr	76	72	87	132	136	82	86

Major elements normalised to 100%; trace element data in ppm

* total Fe presented as Fe_2O_3

1 Analyst S W Goodlad (Cape Town)

2 Analyst J Bristow (Cape Town)

3 Analysed in GSO, Pretoria

Table A5.1 Foram Species List for Neogene and Reworked Samples

[1]SPECIES \ SAMPLE NO.	NEOGENE SAMPLES				REWORKED SAMPLES							
	5	15	24		2	11	5115	5727	5728	5748	5754	4234+
	27-29	12½-15½	13-15	4212+			16½-19½					
Globigerina ciperoensis			*									
G. digitata								*				
G. nepenthes		*									*	*
G. pachyderma			*			*						
G. quinqueloba									*			
G. rubescens					*		*		*	*		
G. venezuelana	*	*	*	*					*			
Globigerinella adamsi					*		*			*		
G. siphonifera	*	*	*		*	*	*	*	*	*	*	*
Globigerinatella insueta							*					
Globigerinita glutinata	*	*	*		*		*		*	*		
Orbulina bilobata					*		*				*	
O. suturalis	*	*							*		*	
O. universa	*	*	*		*	*	*	*	*	*	*	*
Globigerinoides conglobatus			*			*	*	*	*		*	
G. extremus	*	*	*								*	
G. fistulosus	*	*						*			*	
G. quadrilobatus sacculifer	*	*	*		*	*	*	*	*	*	*	*
G. cf. trilobus	*	*	*		*	*	*	*		*	*	*
G. ruber	*	*	*		*	*	*	*	*	*	*	*
G. sicanus	*	*	*									
G. transitoria	*	*	*									
Sphaeroidinellopsis seminulina	*	*	*				*				*	*
Sph. sphaeroides		*	*									
Sph. subdehiscens	*	*										
Sphaeroidinella dehiscens		*			*		*		*	*	*	
Globoquadrina altispira altispira	*	*	*	*	*		*		*		*	*
G. altispira globosa	*	*	*								*	
G. dehiscens											*	
G. dutertrei	*				*	*	*	*	*	*	*	
Pulleniatina obliquiloculata	*	*	*	*	*	*	*	*	*	*	*	*
Pull. finalis					*		*				*	
Globorotalia acostaensis	*	*	*									
G. bullbrooki						*						
G. crassaformis	*	*	*		*		*				*	*
G. flexuosa									*		*	
G. hirsuta		*	*			*	*	*	*		*	*
G. humerosa	*	*	*									
G. inflata	*	*		*	*	*	*	*	*	*	*	*
G. menardii	*	*			*	*	*	*	*	*	*	
G. menardii gibberula					*		*					
G. multicamerata	*	*	*		*	*	*			*	*	
G. pertenuis		*										
G. pleiotumida			*									
G. prachirsuta	*										*	
G. praemiocenica	*	*	*								*	
G. quetra	*											
G. scitula	*	*	*						*			
G. tosaensis	*	*	*								*	
G. truncatulinoides					*	*	*	*	*	*	*	*
G. tumida	*			*	*	*	*	*			*	*
G. ungulata									*		*	
G. sp. (Palaeocene-Cretaceous type)						*						
Candeina nitida	*									*		
Globotruncana sp.	*					*				*		
[2]					1%	1%	3%	1%	3%	1%	8%	4%

1 Identification of species by D.A. Salmon.

2 Percentage estimate of number of reworked foraminifers.

\+ Grab samples collected on TBD Cruise 290 by C. Moir.

and Cretaceous microfauna. All core-top samples are assigned a Quaternary age using the species listing of Salmon (1979b). Four down-core samples are assigned a Neogene age and in view of their importance in dating horizon Jimmy, complete species listings are contained in Table A5.1. Using this species list, a Late Miocene/Pliocene age is established for all four samples. Several cores, retrieved from current-scoured zones, are characterised by a Quaternary assemblage (Salmon, 1979b) but contain up to 8% admixed Tertiary and Cretaceous microfauna (Table A5.1).

Appendix A6 Sample Recovery and Core Handling Procedures

In total, 57 sedimentological stations were occupied during cruises TBD 350, 371 and MN 76/28. At each station an appropriate sample device (Shipek grab; gravity corer; piston corer-TBD 371 only) was selected dependent on sea floor microtopography. Sample recovery was not achieved at all stations (Appendix B1). All coring devices employed a plastic liner system. On core recovery, the sediment-filled liners were extracted from the barrel to be capped and sealed. Sealed cores were stored vertically but unfrozen during transportation to the laboratory. Grab samples were stored in air-tight plastic containers.

All cores were X-rayed, unsplit within their plastic liners, by the SABS on a 150 kV machine (Cu filter) using AGFA D5 film. The source-to-film distance was maintained at 1 m. Exposure parameters for different diameter cores were selected as follows: (1) large diameter - 4 mins at 5 mA (tube voltage 75 kV); (2) medium diameter - 3 mins at 5 mA (tube voltage 75 kV); and (3) small diameter - 2,7 mins at 4,75 mA (tube voltage 70 kV). Core X-radiographs were used as an aid in core description (Appendix B2) and several positive prints are presented in Appendix B5.

Photographic plates of all cores were shot immediately after splitting in both black/white and colour mediums. Smeared sediment on the sliced core face was carefully removed before photography. Several plates have been compiled in Appendix B4. As with the X-radiographs, the printing process has reduced resolution and may have introduced relative shifts in the density

and grey level between cores. True colours are described in Appendix B2.

Appendix A7 Core Description and Sampling

Core description procedures adopted in this investigation are based on a combination of the methods employed by Cassidy et al (1977) and Davies et al (1977b). Core descriptions are presented in Appendix B2 and these include a verbal account of sediment characteristics together with a graphic log illustrating lithology, structures and intraclasts. Each core log also includes a detailed down-core analysis of the grain size distribution (sand-silt-clay ratio; settling tube analysis - sand; electronic particle size analysis - silt) and calcium carbonate content. Lithologic units are defined on the basis of composition, texture and sedimentary structure data (visual and X-ray). Sediment classification follows the system presented by Cassidy et al (1977) using both microscopic and megascopic information. Colours were recorded (Geol. Soc. Am. colour chart) immediately after core splitting. Core shortening effects (e.g. Stow and Aksu, 1978) could not be assessed.

All cores were sampled at regular down-core intervals with extra samples being taken at significant lithological or structural interfaces. Care was taken to remove streaked and disturbed core margins before sampling (McCoy, 1980). In total, 209 samples were selected for sedimentological analysis. Sample size was determined by degree of core lamination and core diameter, typically varying from 1-3 cm core length (30-50g). Using semi-permeable membrane, all samples were dialysed in tap water (24 hours) to remove soluble interstitial salts.

Sub-splitting of these bulk samples was achieved by the following method: (a) samples agitated in tap water to produce a uniform suspension; (b) suspension split into two representative sub-samples via a glass funnel with Y-shaped double outlet; (c) additional sub-splits derived by repeating the process. In most cases samples were split into three and assigned as follows (Fig.8.2): (1) sub-sample 1 - quarter split for chemical analysis; (2) sub-sample 2 - half split for textural analysis; and (3) sub-sample 3 - quarter split for component studies.

Seventeen additional small aliquots (sub-sample 4) were selected for SEM study.

Appendix A8 Calcium Carbonate Analysis

Routine calcium carbonate determinations were performed using the 'Karbonat-Bombe' method (Muller and Gastner, 1971; Birch, 1979a). This gasometric method measures the pressure of evolved CO_2 on reacting 1 gram of crushed sample with 5 ml of conc. HCl in a sealed perspex vessel (Karbonat-Bombe) fitted with a pressure gauge. After calibration and daily drift checks, the manometer reading is proportional to the $CaCO_3$ concentration in the sample. Full details of the methodology are available in Birch (1979a) while some cautions are listed by Dunn (1980).

Precision and accuracy of the method has been tested by Birch (1979a) who concluded that precision is better than 3%. More conservative accuracies of 1-5% are suggested by Dunn (1980). Only 2% of samples analysed in this study have $CaCO_3$ contents <10% where accuracy is less reliable. The calcimetry flow-chart is displayed in Figure 8.2. In total, 409 $CaCO_3$ analyses were performed (209 bulk sediment; 100 sand fraction only; 100 mud fraction only)(Appendix B6).

Appendix A9 Organic Carbon Analysis

Organic carbon content was determined employing the wet chemical method of Morgans (1956) in which non-oxidised organic carbon in the sample is oxidised with excess chromic acid and back-titrated against ferrous sulphate. All 209 analyses were duplicated or triplicated to ensure low standard deviation of results (Appendix B6). The majority of sediments contain <1% organic carbon and at these concentrations, Birch (1975) concluded that accuracy of the method is $\pm$30% (95% confidence level). In conversion of organic carbon to organic matter content, a multiplier of 1,82 has been used (Bezrukov et al, 1977).

Appendix 10 Sand Fraction Composition

Standard point-counting techniques under binocular microscope were employed to provide modal compositional analyses of the sand fraction (63μm-2mm). Small representative sub-

samples of dried sand were obtained using a microsplitter and these were sprinkled on a grided tray. A minimum of 300 grains were identified and counted from randomly chosen squares on the tray. All grains within any square were counted. Component categories and results are listed in Appendices B10 and B11. Unidentified grains were counted under the category 'other'. Accuracy of the results may be estimated by use of the nomogram of Van der Plas and Tobi (1965) and is dependent on total number of grains counted and the percentage of individual components. For example, counting 300 grains the accuracy of a 20% component mode is 4,5% at the 95% confidence level.

Appendix A11 Clay Fraction Mineralogy

Semi-quantitative clay mineralogy studies were performed using procedures (see Fig.8.2) outlined by (Birch, 1975). Clay fractions were isolated from the bulk sediment by process of repeated agitation, dispersion, settling and siphoning. Based on Stoke's Law, supernatants containing only <2μm equivalent diameter particles were siphoned off, concentrated and retained for clay mineralogy studies.

Calcium carbonate was dissolved out by treatment with unbuffered 25% acetic acid and organic matter was oxidised on addition of 30% hydrogen peroxide. Each sample was treated with 3N $MgCl_2$ solution to ensure equal expansion of the clay layers and finally triple-washed (distilled water) to remove excess $MgCl_2$ solution. For each sample, two glass slides were prepared by the pipette method. Approximately 0,5-0,8 mg of pre-treated clay suspension was evenly pipetted onto each slide creating a clay layer of optimum thickness (Sudo et al, 1961). Quick drying at a maximum temperature of 50°C prevented any differential settling.

Slide 1 was diffracted at room temperature, heated to 550°C (1 hour) and re-diffracted. Slide 2 was carefully painted with ethylene glycol before X-ray diffraction. Analyses were conducted on a PHILLIPS PW1130 diffractometer. Untreated slides were scanned from 2-30° 2θ (1°2θ per minute) while heated and glycolated slides were diffracted from 2-14° 2θ at the same speed.

Clay mineral groups may be identified by their characteristic basal X-ray diffraction maxima (Fig.8.11).

Illites are recognised by their 10 Å and 5 Å peaks (Biscaye, 1965), both unaffected by heating or glycolation. Smectites are detected by a 14 Å basal reflection which expands to 17 Å on glycolation but collapses to 10 Å on heating. Kaolinites are distinguished by a 7 Å peak, unaffected by glycolation but which vanishes on heating to 550°C. Trace amounts of vermiculite (e.g. core 5 0-3 cm; Fig.8.11) are recognised by a 14 Å peak collapsing to 10 Å on heating but showing no expansion with glycolation. Chlorites are completely absent from Natal Valley marine and riverine samples. Smectite crystallinites are estimated by the empirical measure of Biscaye (1965) using the v/p ratio of the 17 Å basal reflection.

The method of Johns et al (1954), in which peak areas on glycolated diffractograms are integrated and weighted, has been used in semi-quantitative analysis. Peaks and weighting factors used are as follows: illite - 4 x 10 Å peak area; smectite - 17 Å peak area; kaolinite - 2 x 7 Å peak area. Analytical results are tabulated in Appendix B13. Birch (1981) concluded that the above methodology provided precision better than 3% for all concentrations of illite, kaolinite and smectite.

Appendix A12 Silt Fraction Mineralogy

Qualitative silt fraction (2-63μm) mineralogical determinations were performed using X-ray diffraction techniques. After removal of the <2μm fraction (Appendix A11), the 2-63μm residues were dried at 50°C and crushed in an automatic agate pestle and mortar. For each sample, approximately 2 grams of crushed sediment was carefully mounted in an aluminium holder by powder-press technique. Using a PHILLIPS PW1130 diffractometer, powder-press mounts of the silt fraction were scanned from 4-62° 2θ ($2°2\theta$ per minute). Mineral identification was achieved by comparison of diffraction maxima with the comprehensive ASTM reference index system. Abundances were estimated on a qualitative basis using a ranked scale modified after Matti et al (1974): (1) TRACE (<1%) - one weak diagnostic peak; (2) PRESENT (1-5%) - two weakly developed diagnostic peaks; (3) COMMON (5-25%) - several characteristic peaks developed but subordinate to peaks of other minerals; (4) ABUNDANT (25-65%) - diffraction

peaks prominent and of equal intensity to peaks of other minerals; (5) MAJOR (>65%) - diffraction maxima completely dominant. Using this qualitative scale, ranked abundances of silt fraction minerals are tabulated in Appendix B12.

Appendix A13 Scanning Electron Microscopy

SEM techniques were used to provide information on three topics: (1) quartz grain surface microtextures; (2) planktic foram abrasion, breakage and solution patterns; and (3) mud fraction composition. SEM examination was performed on a CAMBRIDGE S180 operated at 30 kV. All sample stubs were coated with gold-palladium. Micrographs were obtained as secondary electron images and recorded on ILFORD 120 film using a 60 sec frame period (800 lines per frame).

To study quartz grain microtextures, 17 sediment samples (sub-sample 4; Fig.8.2) were selected from 15 core and grab stations (Table 8.2). Twenty mono-crystalline quartz grains 200-500μm in diameter (Higgs, 1979), considered to be sufficiently representative of within-sample variability (Krinsley and Doornkamp, 1973), were randomly picked from each sample. All grains were treated with 25% HCl to digest $CaCO_3$, rinsed, dried and mounted on aluminium stubs. SEM viewing magnifications ranged from 100-4000 times. Individual microtextures were only recorded (Table 8.2) if they covered >5% of the grain surface area. Representative photomicrographs are contained in Plates 8.1 and 8.2.

To study foram abrasion and dissolution, 20 tests were randomly picked from the same 17 samples as above. Sample sieving, washing and drying was performed with utmost care to prevent any spurious breakage of delicate tests. Abrasion and solution phenomena are recorded in Table 8.2 and photomicrographs are presented in Plate 8.2.

Twelve samples (sub-sample 4; Fig.8.2) were selected for SEM scanning to furnish mud composition data. Muds were treated with 30% H_2O_2 to oxidise organic matter. Addition of 0,5% Calgon ensured complete disaggregation before mud slurries were pipetted onto stubs. Ethanol was added to the stub slurry to minimise

unwanted mud aggregation during drying. General scanning was performed at magnifications of between 1000 and 10 000 times. Representative photomicrographs are collated in Plate 8.3. Mud compositions were semi-quantitatively estimated by point-counting on the SEM scan screen. A minimum of 100 particles were randomly selected for identification by shifting the SEM stage in regular increments over a series of parallel traverses. Identification was based on morphological criteria but the EDAX facility was used qualitatively in ambiguous cases (e.g. high Ca peak count differentiates between clay-size calcareous detritus and clay minerals). Compositional analyses are listed in Table 8.4.

Appendix A14 Grain Size Analysis

Routine grain size analysis of 208 bulk sediment samples (sub-sample 2; Fig.8.2) was carried out to furnish basic textural information. All samples were treated with 30% H_2O_2 to oxidise organic matter and were then dispersed in Calgon (sodium hexametaphosphate) solution (5 grams/litre). Wet-sieving at 63μm and dry-sieving at 2mm provided quantitative data for the gravel (>2mm), sand (63μm-2mm) and mud (>63μm) fractions. Silt and clay contents were determined by pipette analysis of the mud fraction (Royse, 1970). Analytical results are listed in Appendix B6. Sand fractions were retained for hydraulic grain size analysis (Appendix A15).

Appendix A15 Hydraulic Grain Size Analysis (Sand Fraction)

In relating grain size to depositional environments, settling velocity may be a more significant parameter than other dimensional measures (Taira and Scholle, 1979b). Accordingly, hydraulic size analysis (settling tube) was adopted to provide sand fraction grain size parameters. A detailed critique of the method and theory of settling tube analysis is provided by Flemming (1977) while the basic tube design has been described by Flemming and Thum (1978).

Using sub-sample 2 (Fig.8.2), a 2-4 gram split of the sand fraction was taken using a microsplitter. To remove air trapped in foram test cavities, a 'wetting' procedure after Thiede et al (1976) was applied to all samples as follows: (1) samples dried

at 80°C (24 hours); (2) 5 ml acetone added in a vacuum desiccator; (3) desiccator evacuated to 300 torr six times in three minutes; (4) 4 ml 95% ethanol added; (5) evacuation procedure repeated; (6) 5 ml 2% Calgon solution added; (7) evacuation procedure repeated; (8) excess supernatant decanted. Samples were stored wet in air-tight containers to prevent any desiccation.

After settling tube analysis, raw data (cumulative mass %) were converted to settling velocities and then to hydraulically-equivalent grain size diameters (ϕ notation) using computerised software packages (Flemming, 1977). Grain size data were computed at increments of 0,1ϕ. In addition, normal moment statistical measures (mean, sorting, skewness and kurtosis) were routinely calculated. Numerical data and moment statistics are tabulated in Appendix B7. Size-frequency distribution curves are plotted in Appendix B2.

Appendix A16 Electronic Particle Size Analysis (Silt Fraction)

In recent years, size analysis of fine-grained sediments using electronic particle counters has received increasing support. Efficiency of the rapid electronic technique is much superior compared to the alternative pipette method. Standardisation of operational procedures must be implemented to achieve high quality analyses.

Electronic particle counting and sizing techniques have been used on a routine basis to provide size distribution data for the silt fraction (sub-sample 2; Fig.8.2). Analyses were performed on a COULTER COUNTER TA-II adhering to operational procedures described by Sheldon and Parsons (1967). In Coulter Counter analysis a small aliquot of sample (0,01g), obtained by representative sub-sampling (Shideler, 1976b), is diluted with 350 ml of electrolyte and continuously agitated by a stirrer in a round-bottomed, baffled beaker. An analytical tube with an aperture of fixed diameter is introduced into the resultant uniform suspension. The suspension is drawn through the aperture under vacuum pressure. Electrodes on either side of the aperture generate an electrical field. Passage of particles through this field induces electrical resistance which is measured and converted to volumetric diameter. Particles are counted in size

groups (channels) during analysis providing size-frequency distribution curves.

Sample preparation techniques closely followed the methodology of Shideler (1976b) except that sea water was selected as the electrolyte in preference to Calgon which creates a totally dispersed and thus artificial suspension. Continual problems with algal growth in Calgon electrolytes also prompted use of sea water. Salinities were maintained at 35°/oo (Duncan, 1970) and addition of sodium azide (0,1 g/l) ensured sterility.

A one-tube analytical technique was utilised following the calibration method of Sheldon and Parsons (1967). Each tube is capable of measuring a particle size range from 2-40% of the aperture diameter. Usage of a single 280μm tube allowed accurate measurement in the desired size range of 8-63μm (7-4ϕ). After analysis, volume data from channels 4-14 were normalised to reflect a 100% distribution (Appendix B8).

Replicate analysis of one sample (1 0-3 cm) was performed to gauge reproducibility and precision of the method. Results are summarised in Table A16.1. Low values obtained for the coefficient of variation in each size group (channel) indicates a high analytical precision.

Table A16.1 Replicate Electronic Particle Size Analysis

	CHANNEL*										
	4	5	6	7	8	9	10	11	12	13	14
	6069	10176	12870	7512	1823	864	376	203	86	20	1
	6128	10278	12941	7321	1836	821	368	214	74	18	1
	6177	10105	12876	7368	1890	868	418	197	80	20	1
	6224	10348	12592	7389	1891	837	416	199	83	20	1
	6103	10243	12746	7503	1838	842	422	204	78	20	1
	6163	10264	12697	7472	1841	833	428	202	79	20	1
	6180	10205	12806	7407	1857	832	401	208	84	19	1
	6171	10257	12753	7412	1880	836	392	198	81	19	1
	6096	10282	12798	7472	1812	842	396	200	81	20	1
	6200	10191	12815	7392	1862	839	399	199	82	20	1
$\bar{X}$	6151	10235	12789	7425	1853	841	402	202	81	20	1
s	49,9	67,9	99,3	62,4	27,6	14,3	19,7	5,2	3,4	0,7	0,0
CoV	0,81	0,66	0,78	0,84	1,49	1,70	4,91	2,58	4,16	3,57	0,0

* - channels 4-14; see Appendix B8 for size range.
$\bar{X}$ - mean of counts in each channel.
s - standard deviation of counts in each channel.
CoV - coefficient of variation ($s/\bar{X}$ in per cent) for each channel.

APPENDIX B DATA BASE

Appendix B presents a comprehensive listing of raw and reduced geophysical and sedimentological data as generated during the course of this investigation. Appendix B contents are structured as follows:

APPENDIX B1 Sample Location and General Description

SAMPLE No.	LAT. (S)	LONG. (E)	WATER DEPTH (m)	SAMPLING[1] DEVICE	RECOVERY[2]	GENERAL[3] DESCRIPTION
CRUISE MN 76/28 (December 1977)						
1	30°46.1'	33°43.6'	3014	sC	57½	B2
2	29°26.4'	35°16.3'	1980	sC	ss	coarse foram sand
3	29°15.1'	34°53.2'	2680	sC	ss	muddy foram sand
4	29°11.5'	34°46.2'	2510	sC	ss	calcareous sandy clay
5	29°08.8'	34°38.4'	2395	sC	29	B2
6	29°20.3'	34°19.0'	2535	sC	ss	coarse foram sand
7	29°20.2'	33°57.9'	2494	sC	ss	coarse foram sand
8	29°20.5'	33°52.7'	2500	sC	ss	coarse foram sand
9	29°00.0'	34°13.8'	1910	sC	49	B2
10	29°03.0'	33°56.3'	2148	sC	ss	coarse foram sand
11	29°48.0'	33°48.8'	1886	sC	ss	coarse foram sand
12	29°54.3'	33°38.1'	2164	sC	13½	B2
13	29°02.6'	33°33.6'	2325	sC	17	B2
14	29°12.0'	33°29.0'	2150	sC	20½	B2
15	29°15.2'	33°26.8'	2280	sC	15½	B2
16	29°16.7'	33°27.0'	2362	sC	12½	B2
17	29°26.7'	33°25.8'	2210	sC	ss	coarse foram sand
18	29°38.4'	33°20.5'	2400	sC	22½	B2
19	29°36.0'	33°10.7'	2088	sC	28½	B2
20	29°29.7'	33°13.0'	2018	sC	23	B2
21	29°27.4'	33°04.6'	2125	sC	7	B2
22	29°32.1'	32°57.9'	1950	sC	ss	coarse foram sand
23	29°23.7'	32°51.3'	1850	sC	50	B2
24	29°30.1'	32°46.9'	1950	sC	15	B2
25	29°30.3'	32°40.7'	1840	sC	12½	B2
26	29°28.8'	32°32.8'	1680	sC	44	B2
27	29°33.4'	32°27.1'	1577	sC	41	B2
28	29°42.4'	32°19.7'	1450	sC	ss	coarse foram sand
29	29°40.9'	32°13.0'	1320	sC	43½	B2
30	29°44.2'	31°58.2'	1340	sC	54	B2
31	29°40.3'	31°54.8'	1100	sC	48½	B2
32	29°42.7'	31°46.9'	657	sC	4	B2
33	29°39.0'	31°41.6'	305	sC	ss	glauconitic quartz sand
34	29°42.3'	31°35.0'	304	sC	22	B2
CRUISE TBD 350 (May-June 1976)						
5115	29°54.7'	30°40.5'	765	C	19½	B2
5116	30°14.7'	31°54.9'	2010	C	13	B2
5117	30°13.6'	31°54.7'	1705	C	145	B2
5118	30°24.2'	31°59.6'	2985	C	ss	foraminiferal quartz sand
5119	30°18.9'	32°32.7'	2813	C	200	B2
5120	30°34.2'	32°44.3'	3000	C	~200+	marly calcareous ooze
5121	30°35.8'	33°07.6'	3030	C	184	B2
5122	30°00.7'	33°34.0'	2760	C	ss	foraminiferal quartz sand
5123	30°08.2'	33°23.0'	2850	C	-	-
5124	30°07.8'	33°10.0'	2221	C	205+	B2
5125	29°24.0'	33°42.9'	2490	sC	-	-
5126	29°21.3'	33°32.0'	2210	sC	-	-
5127	29°19.1'	33°02.0'	1940	sC	50½	B2

APPENDIX B1 (contd.)

SAMPLE No.	LAT. (S)	LONG. (E)	WATER DEPTH (m)	SAMPLING[1] DEVICE	RECOVERY[2]	GENERAL[3] DESCRIPTION
CRUISE TBD 371 (October-November 1977)						
5726	29°21.6'	32°23.2'	1420	G	ss	muddy foram sand
5727	28°53.2'	32°39.8'	1535	G	ss	foram sand
5728	28°23.8'	32°58.9'	1611	G	ss	foram sand
5748	28°39.9'	33°43.9'	1826	G	ss	coarse foram sand
5749	29°14.8'; 33°40.9'E to 29°15.0'S; 33°38.8'E		2480-2100	D	4kg	weathered igneous rocks
5750	29°33.4'	33°39.2'	2577	G	ss	coarse foram sand
5751	30°38.7'	34°17.4'	2778	P	249	B2
5752	30°24.1'	33°54.7'	2804	P	35*	marly calcareous ooze
5753	30°31.9'	32°42.6'	2992	P	282	B2
5754	30°01.3'	32°25.2'	1630	P	ss	coarse foram sand
5755	30°52.0'	33°29.2'	3120	P	ss	mud

LEGEND:

1 - sC : short open-barrel gravity corer
C : long open-barrel gravity corer
G : Shipek grab
D : dredge
P : piston corer (modified Alpine corer)

2 - 43 : core length in centimetres
4 kg : weight of dredge recovery
ss : surface sample only
- : no recovery
+ : main length of core washed overboard in storm; core catcher/cutting edge samples only available for study
* : core barrel severely bent during operation; suspected homogenisation of core sample during removal from bent core barrel

3 - B2 : comprehensive description presented in Appendix B2

APPENDIX B2 Core Descriptions

This appendix contains a compilation of Natal Valley core logs. Descriptions include graphic logs and a verbal account of the main lithologic and sedimentary structure characteristics. Each log also contains a detailed down-core analysis of the grain-size distribution (sand-silt-clay ratio; settling tube and Coulter Counter analysis) and calcium carbonate distribution. Lithofacies interpretations are discussed in section 8.6. The core log legend is appended below:

LITHOLOGY LEGEND:

- Foraminiferal ooze
- Calcareous ooze
- Marly calcareous ooze
- Biosparite wackestone
- Mottling
- Bioturbation
- --- Gradational contact
- —— Sharp contact
- Silty clay
- Sand-silt-clay
- Silty sand, clayey sand
- **M** Mollusc fragments
- **E** Echinoid fragments
- **B** Bryozoa fragments
- **G** Glauconite
- **P** Phosphatic nodules

GRAIN SIZE DISTRIBUTION LEGEND:

- Sand
- Silt
- Clay
- Sampled intervals

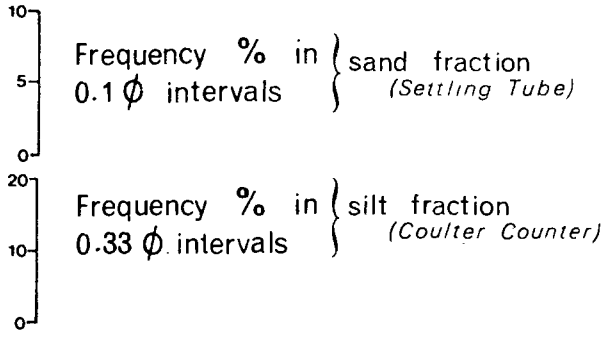

CORE NO. 1 POSITION: 30° 46.1'S 33° 43.6'E WATER DEPTH: 3014m.

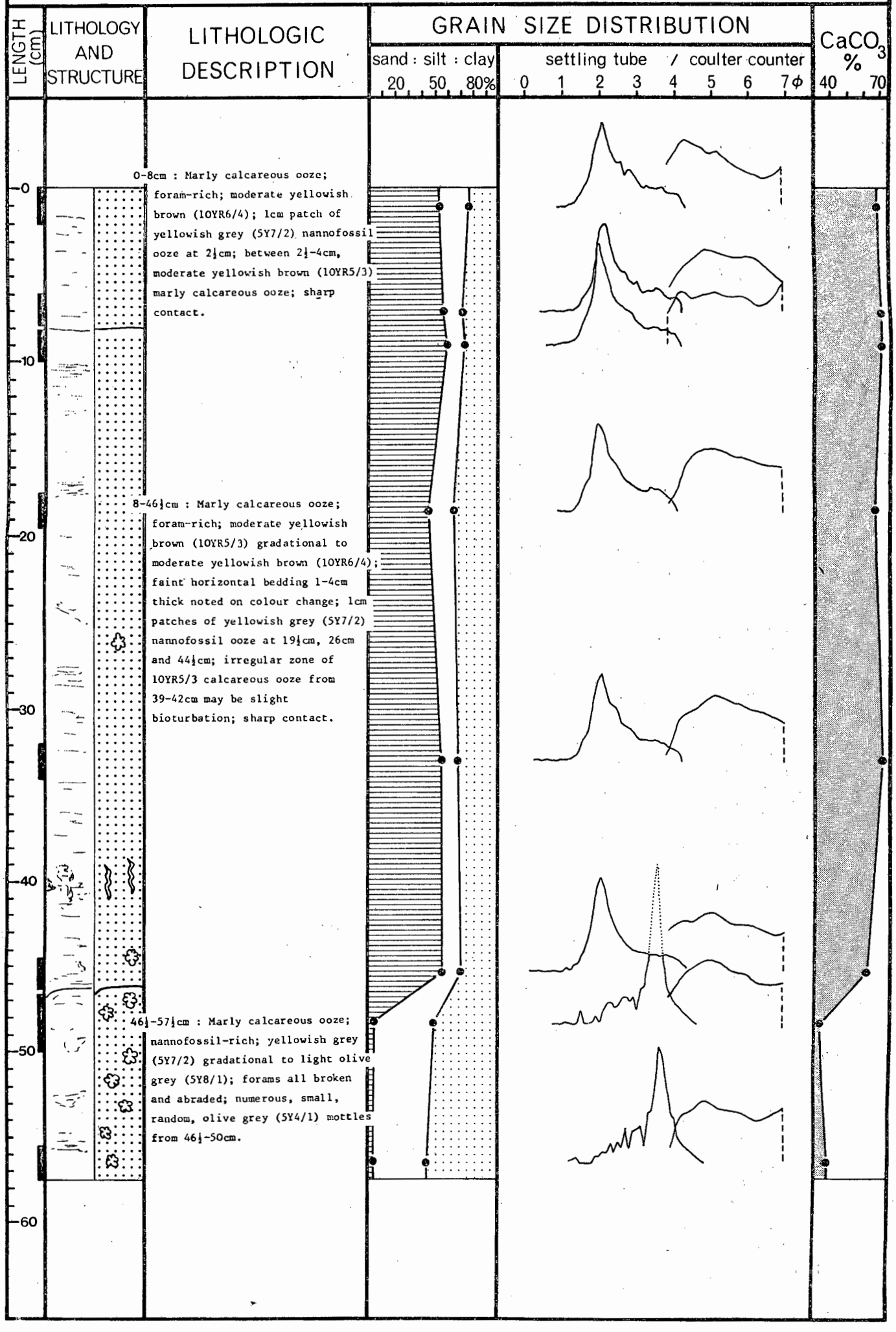

CORE NO. 5 POSITION: 29° 08.8′S 34° 38.4′E WATER DEPTH: 2395m.

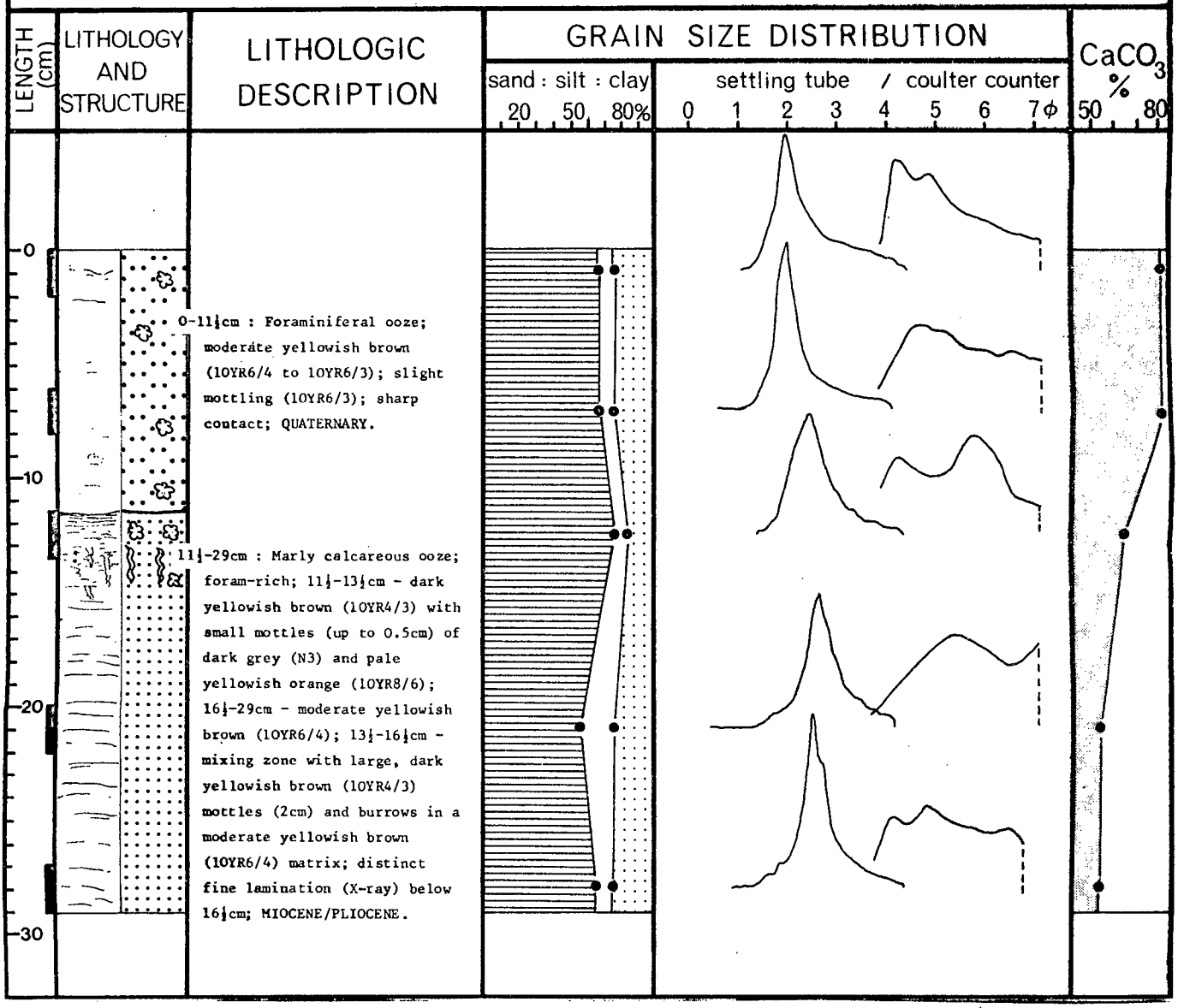

CORE NO. 12 POSITION: 28° 54.3′S 33° 38.1′E WATER DEPTH: 2164m.

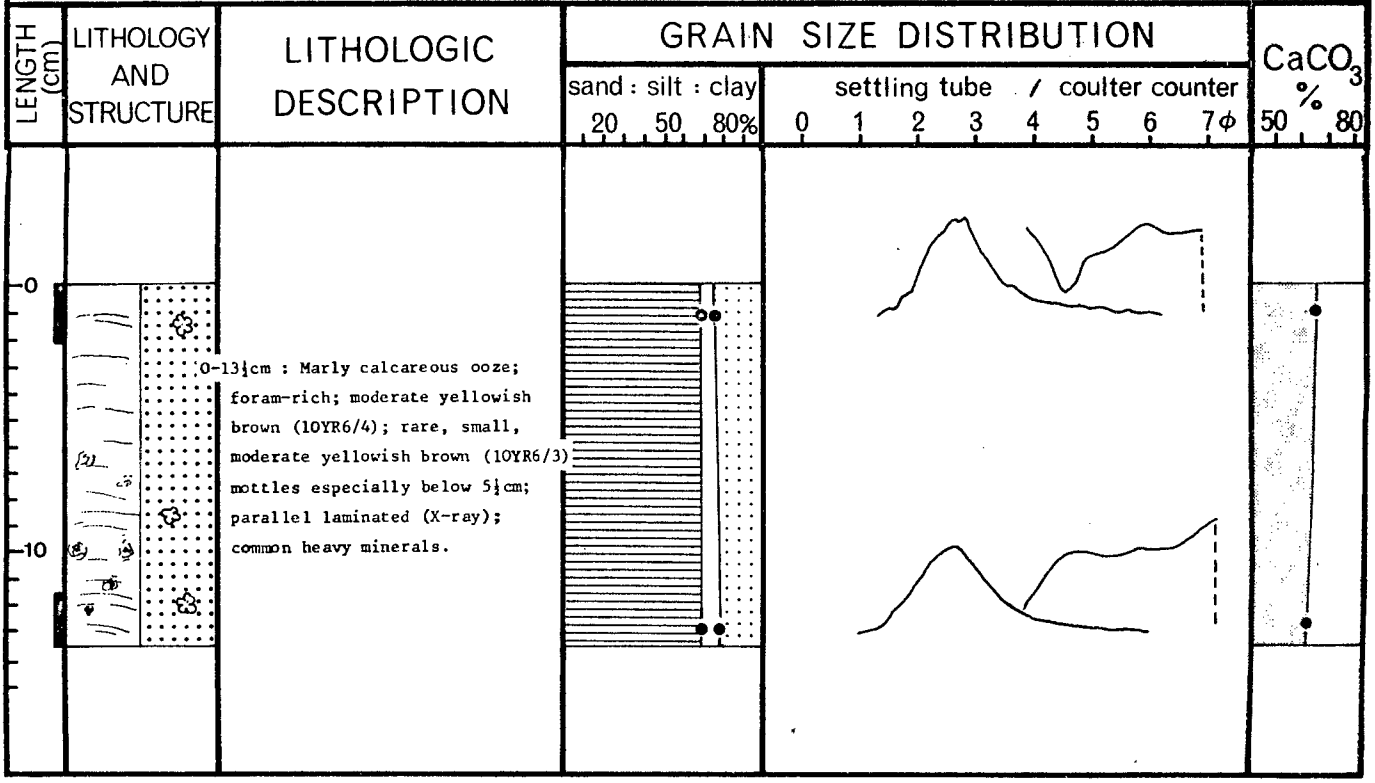

CORE NO. 9 POSITION: 29° 00.0'S 34° 13.8'E WATER DEPTH: 1910m.

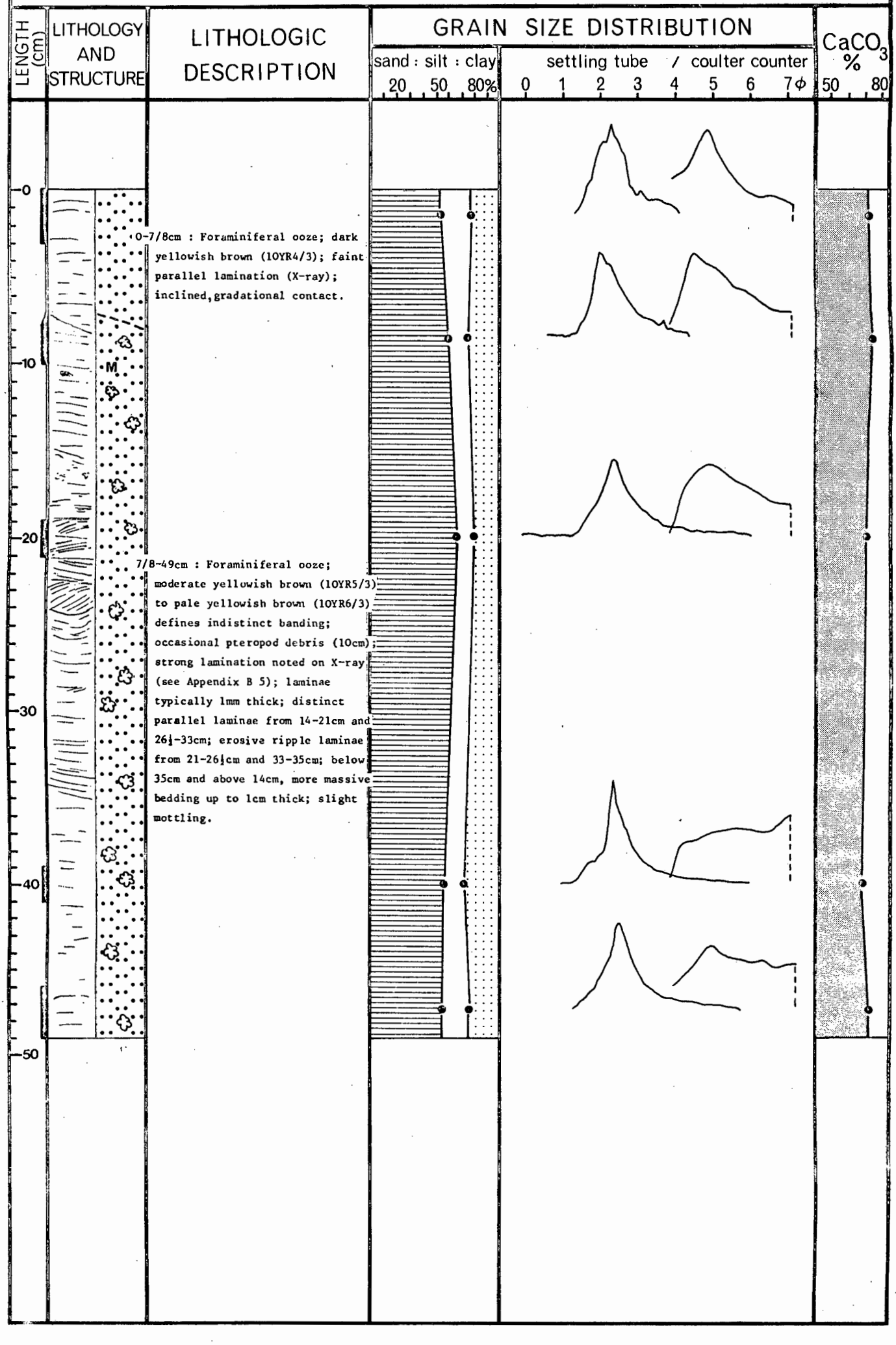

CORE NO. 13 POSITION: 29° 02.6′S 33° 33.6′E WATER DEPTH: 2325m.

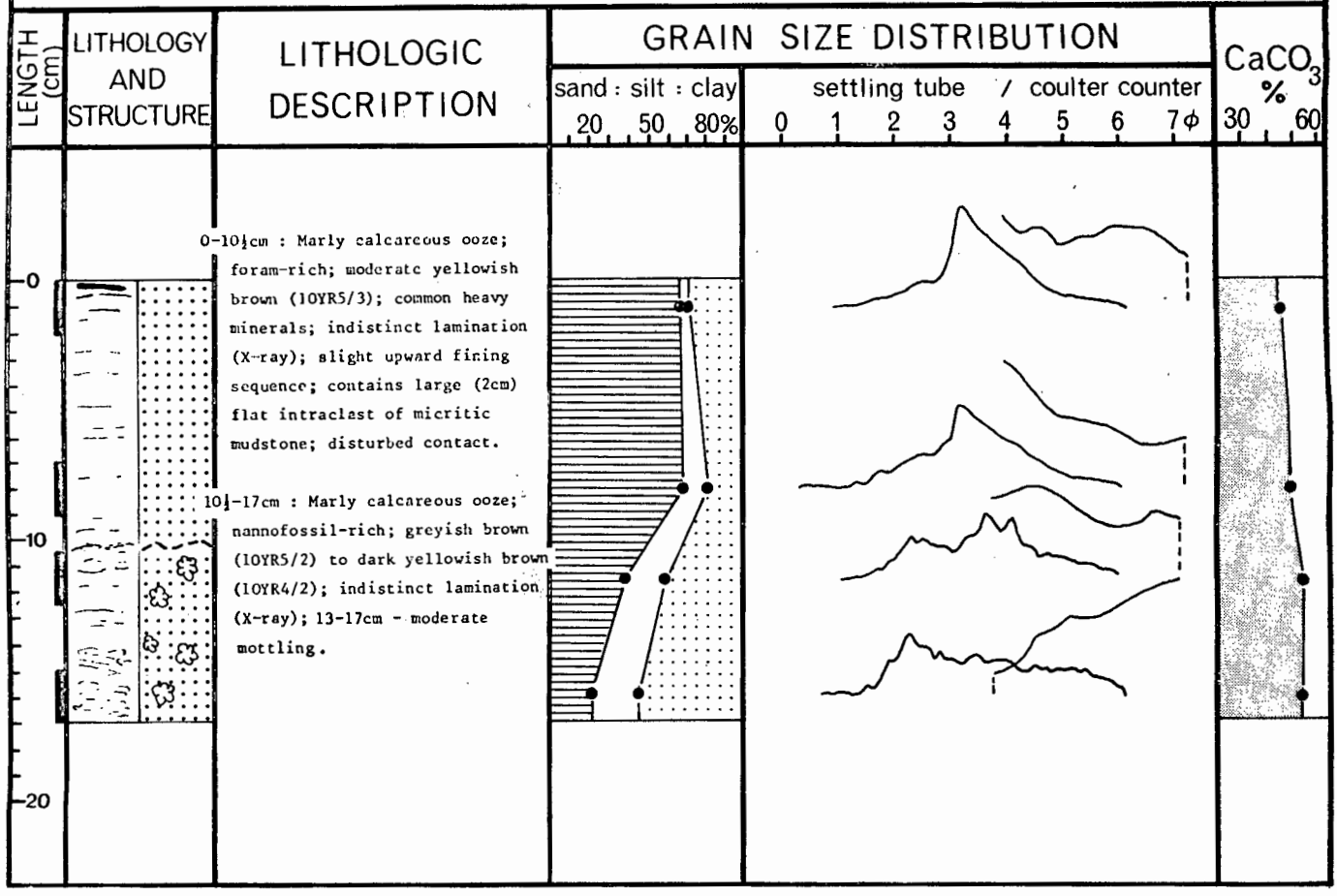

CORE NO. 14 POSITION: 29° 12.0′S 33° 29.0′E WATER DEPTH: 2150m.

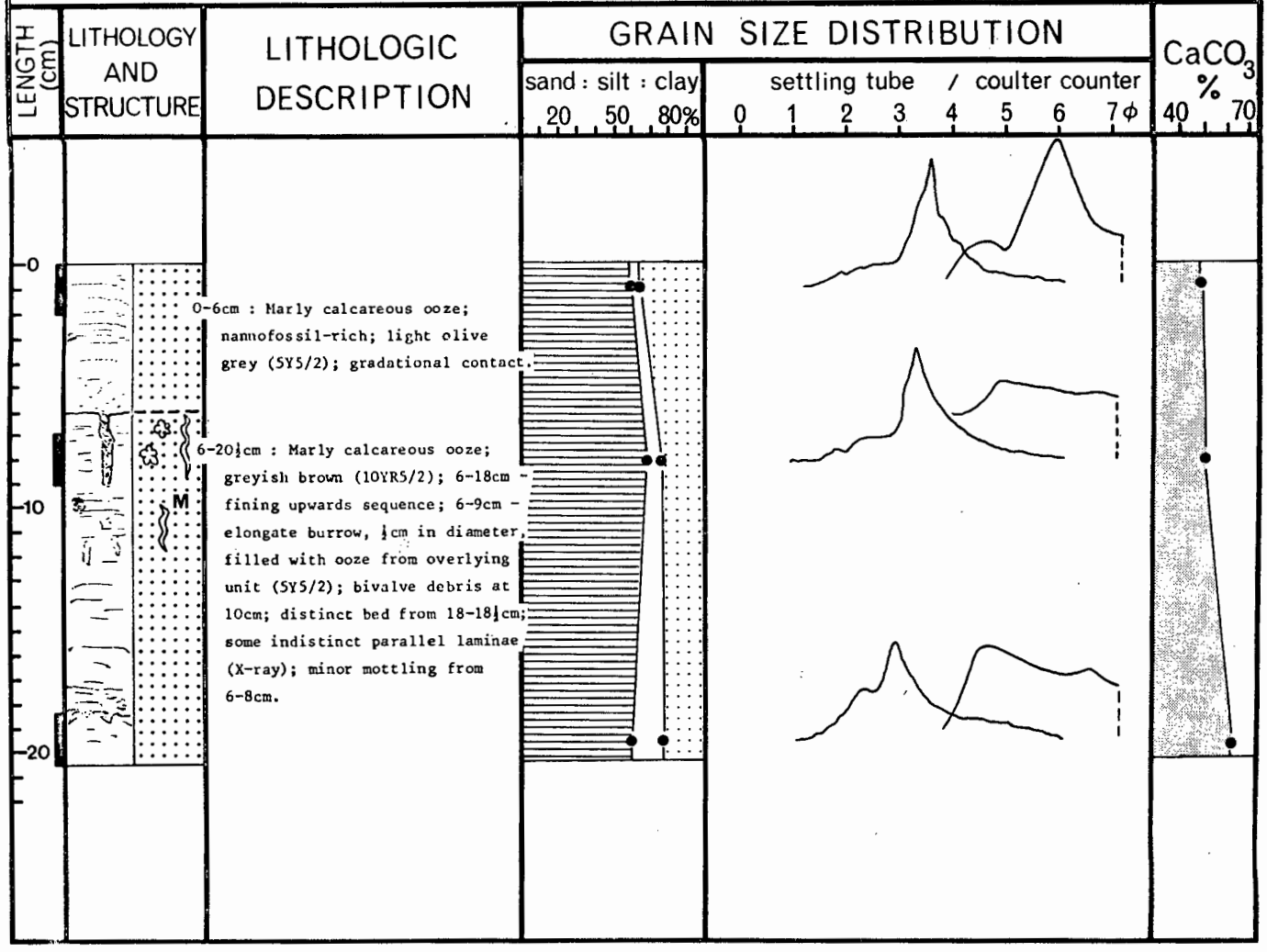

CORE NO. 15 — POSITION: 29° 15.2′S 33° 26.8′E — WATER DEPTH: 2280m.

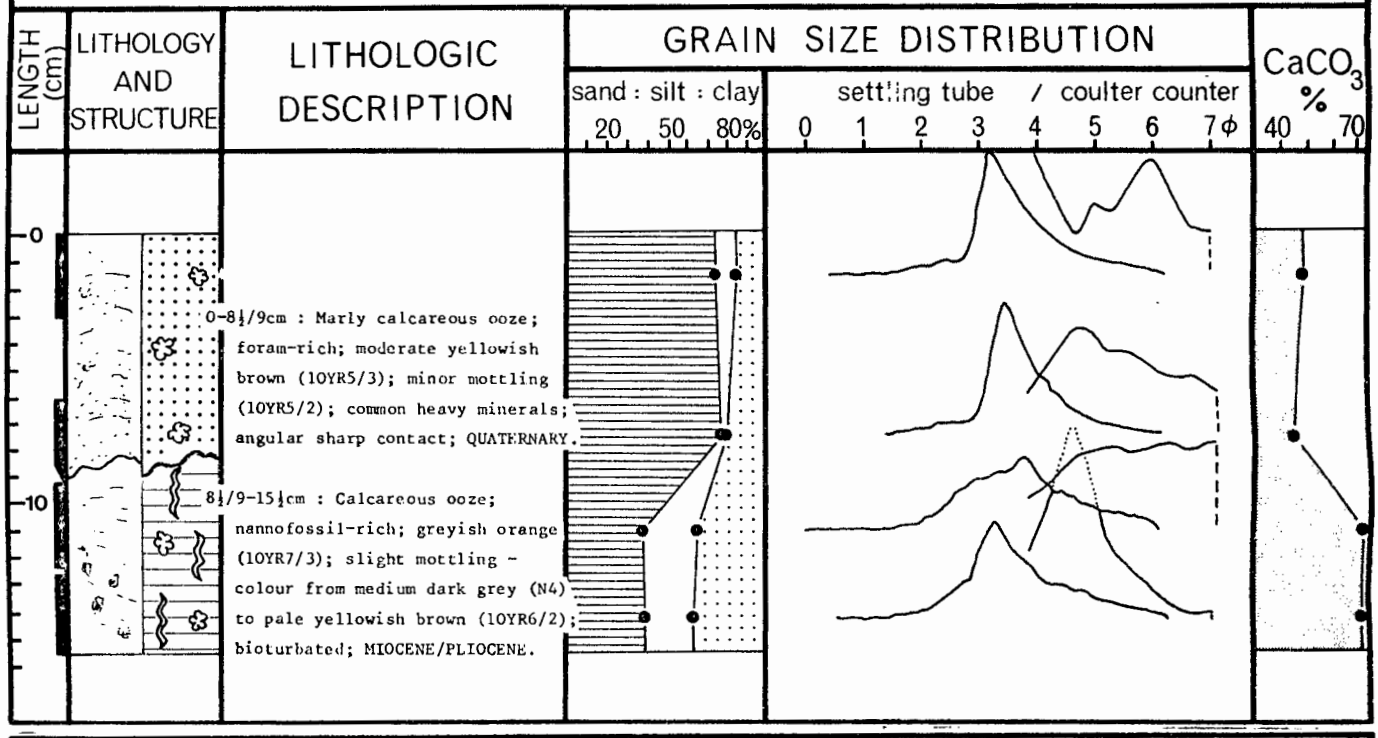

CORE NO. 16 — POSITION: 29° 16.2′S 33° 27.0′E — WATER DEPTH: 2362m.

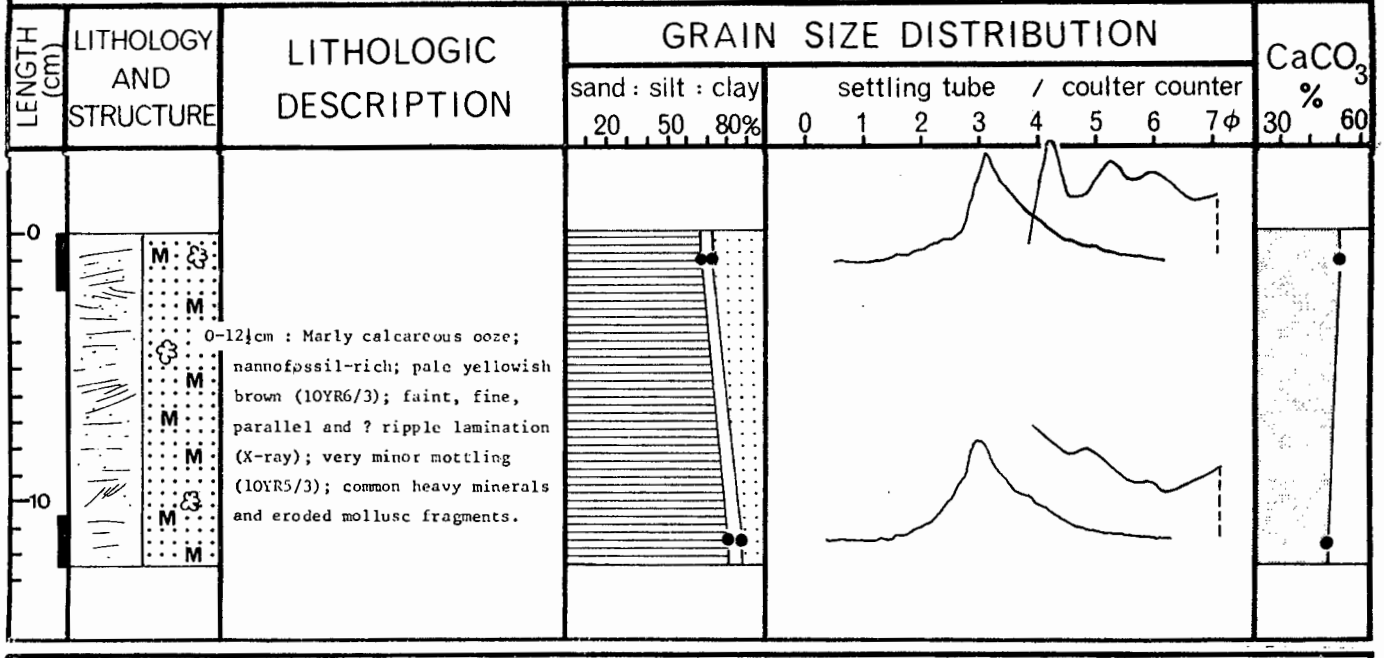

CORE NO. 21 — POSITION: 29° 27.4′S 33° 04.6′E WATER DEPTH: 2125m.

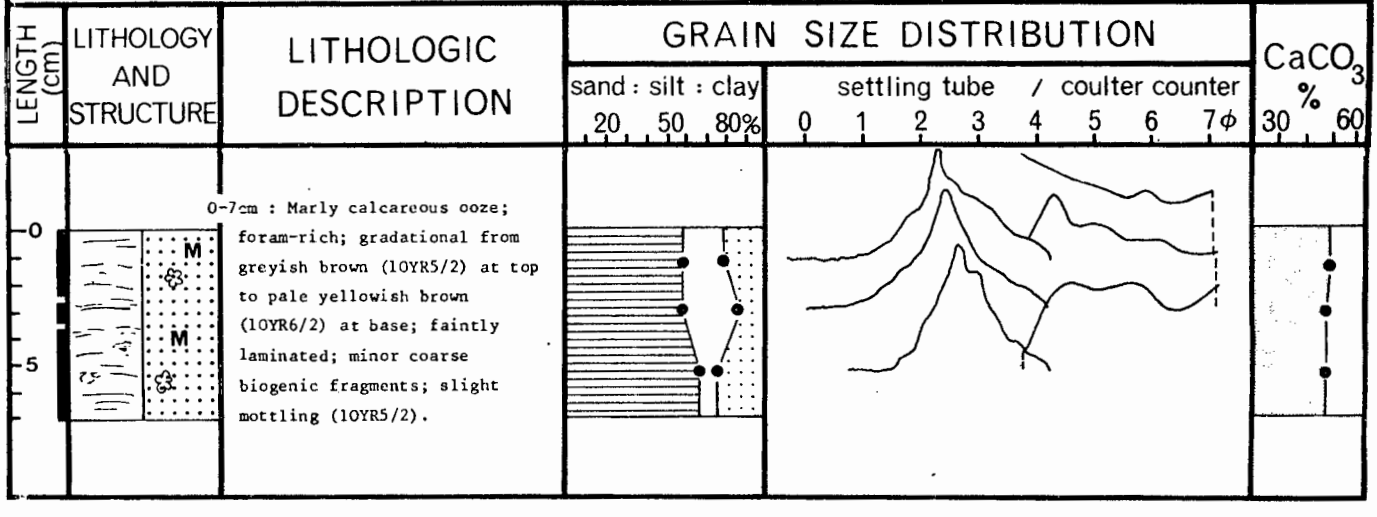

CORE NO. 18 POSITION: 29° 38.4′S 33° 20.5′E WATER DEPTH: 2400m.

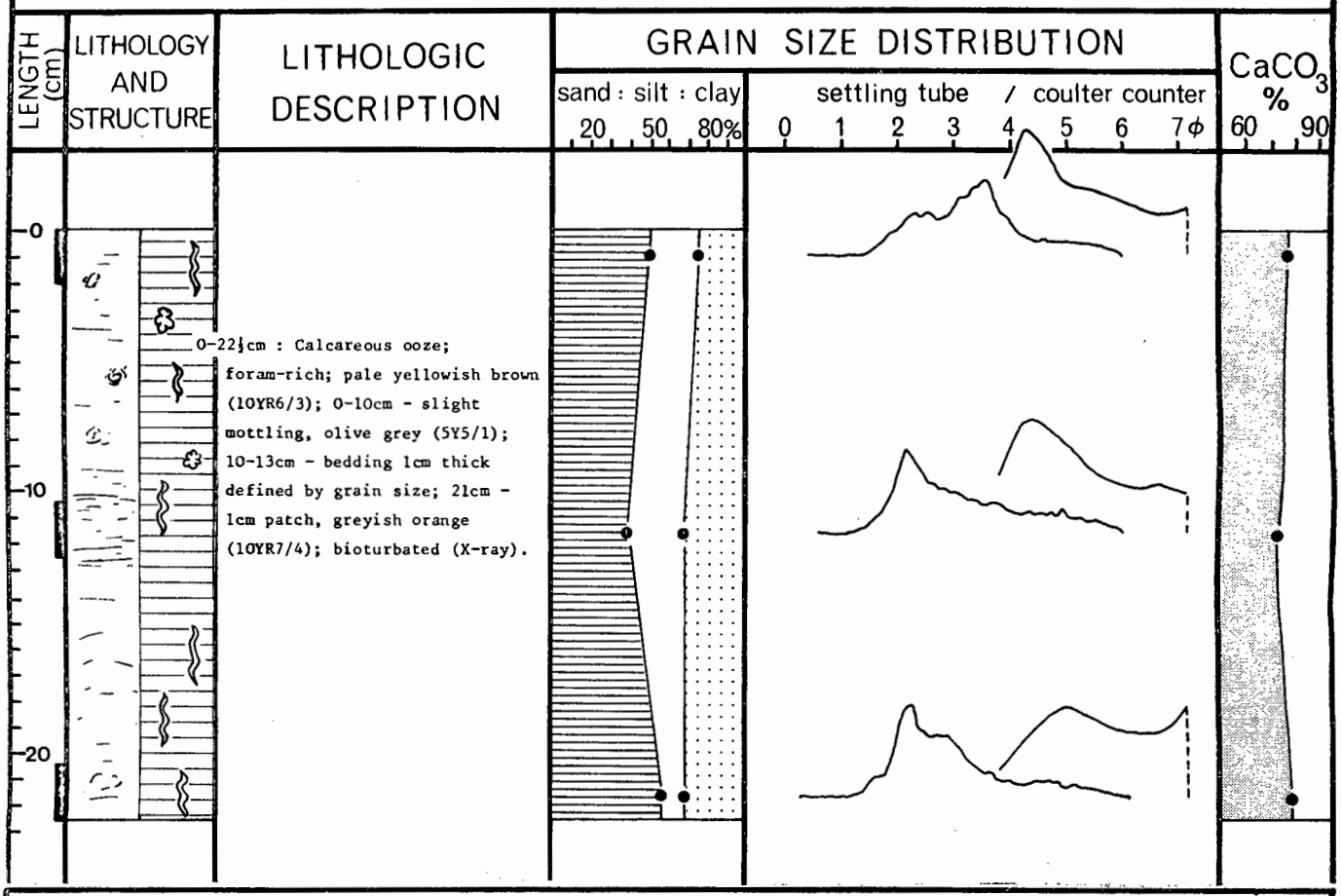

CORE NO. 19 POSITION: 29° 36.0′S 33° 10.7′E WATER DEPTH: 2088m.

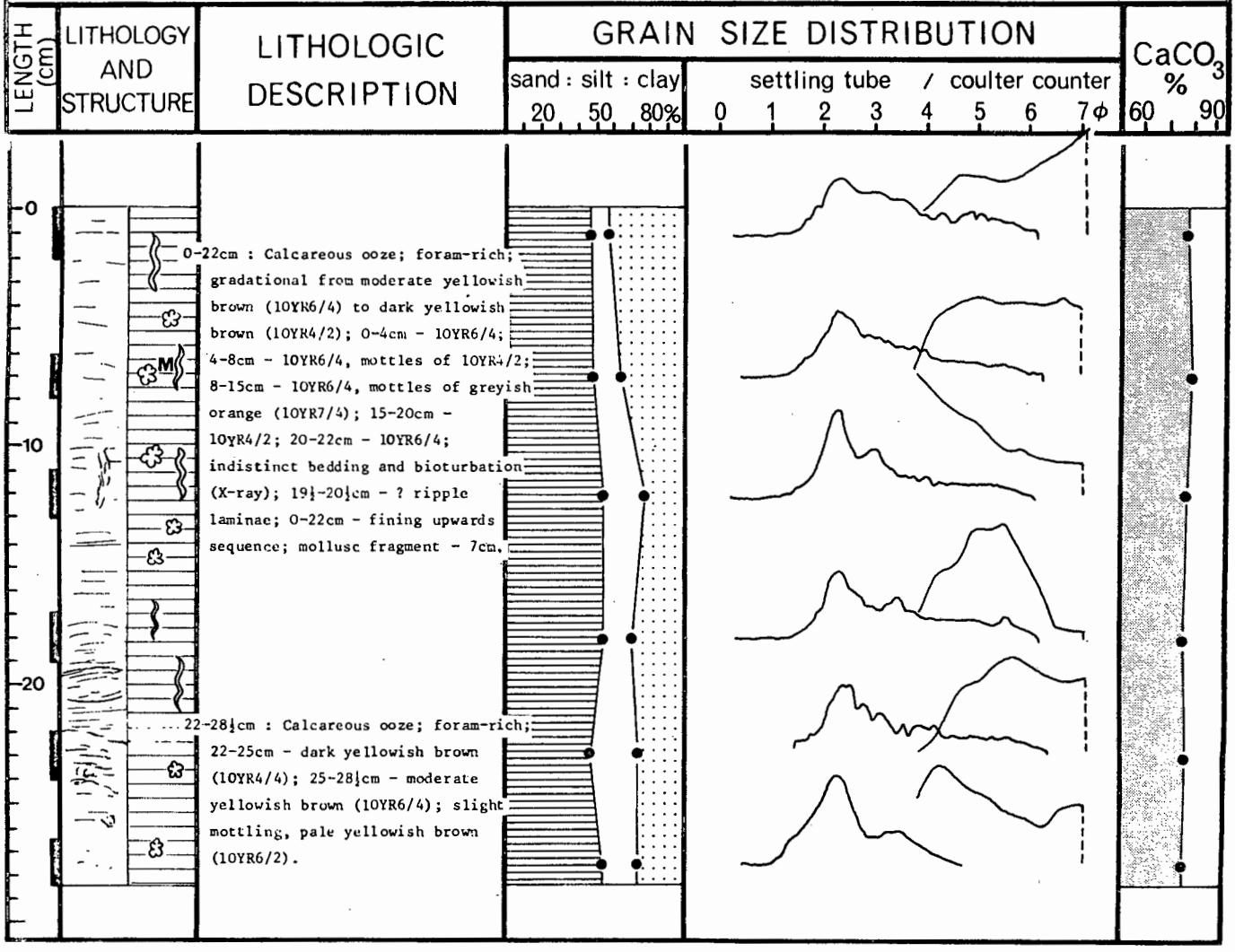

CORE NO. 20 POSITION: 29° 29.7′S 33° 13.0′E WATER DEPTH: 2018m.

LENGTH (cm) | LITHOLOGY AND STRUCTURE | LITHOLOGIC DESCRIPTION | GRAIN SIZE DISTRIBUTION | $CaCO_3$ %

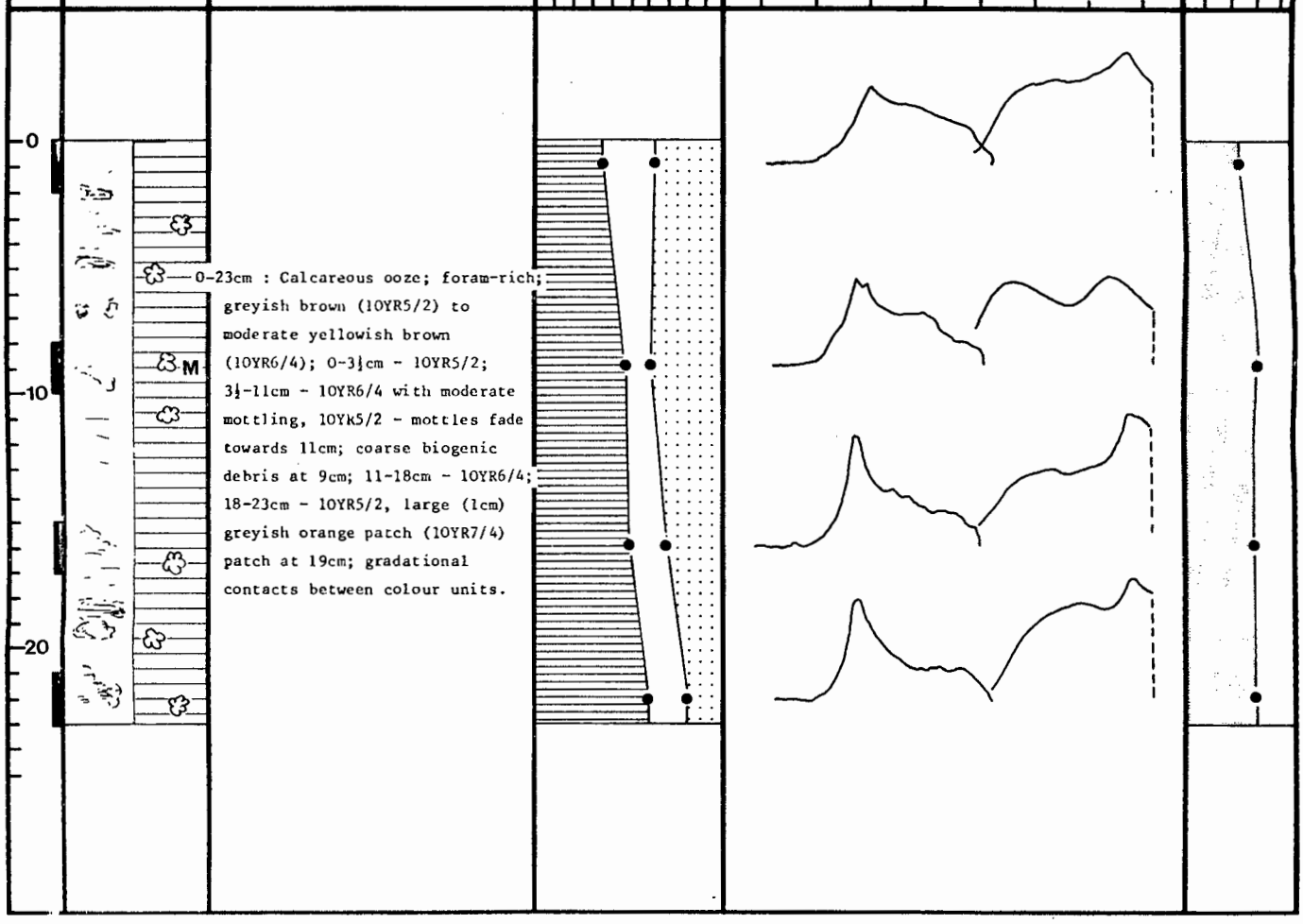

0-23cm : Calcareous ooze; foram-rich; greyish brown (10YR5/2) to moderate yellowish brown (10YR6/4); 0-3½cm - 10YR5/2; 3½-11cm - 10YR6/4 with moderate mottling, 10YR5/2 - mottles fade towards 11cm; coarse biogenic debris at 9cm; 11-18cm - 10YR6/4; 18-23cm - 10YR5/2, large (1cm) greyish orange patch (10YR7/4) patch at 19cm; gradational contacts between colour units.

CORE NO. 24 POSITION: 29° 30.1′S 32° 46.9′E WATER DEPTH: 1950m.

LENGTH (cm) | LITHOLOGY AND STRUCTURE | LITHOLOGIC DESCRIPTION | GRAIN SIZE DISTRIBUTION | $CaCO_3$ %

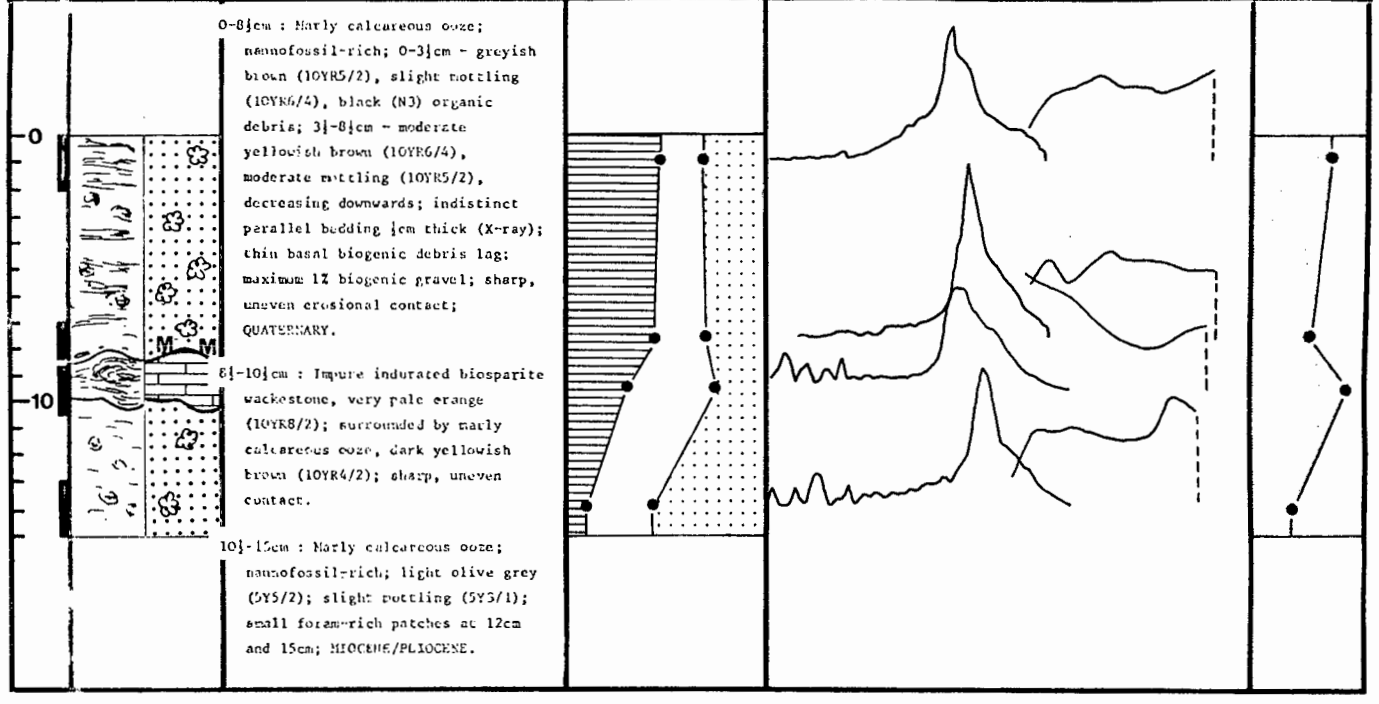

0-8½cm : Marly calcareous ooze; nannofossil-rich; 0-3½cm - greyish brown (10YR5/2), slight mottling (10YR6/4), black (N3) organic debris; 3½-8½cm - moderate yellowish brown (10YR6/4), moderate mottling (10YR5/2), decreasing downwards; indistinct parallel bedding ½cm thick (X-ray); thin basal biogenic debris lag; maximum 1% biogenic gravel; sharp, uneven erosional contact; QUATERNARY.

8½-10½cm : Impure indurated biosparite wackestone, very pale orange (10YR8/2); surrounded by marly calcareous ooze, dark yellowish brown (10YR4/2); sharp, uneven contact.

10½-15cm : Marly calcareous ooze; nannofossil-rich; light olive grey (5Y5/2); slight mottling (5Y5/1); small foram-rich patches at 12cm and 15cm; MIOCENE/PLIOCENE.

CORE NO. 23 POSITION: 29° 23.7′S 32° 51.3′E WATER DEPTH: 1850 m.

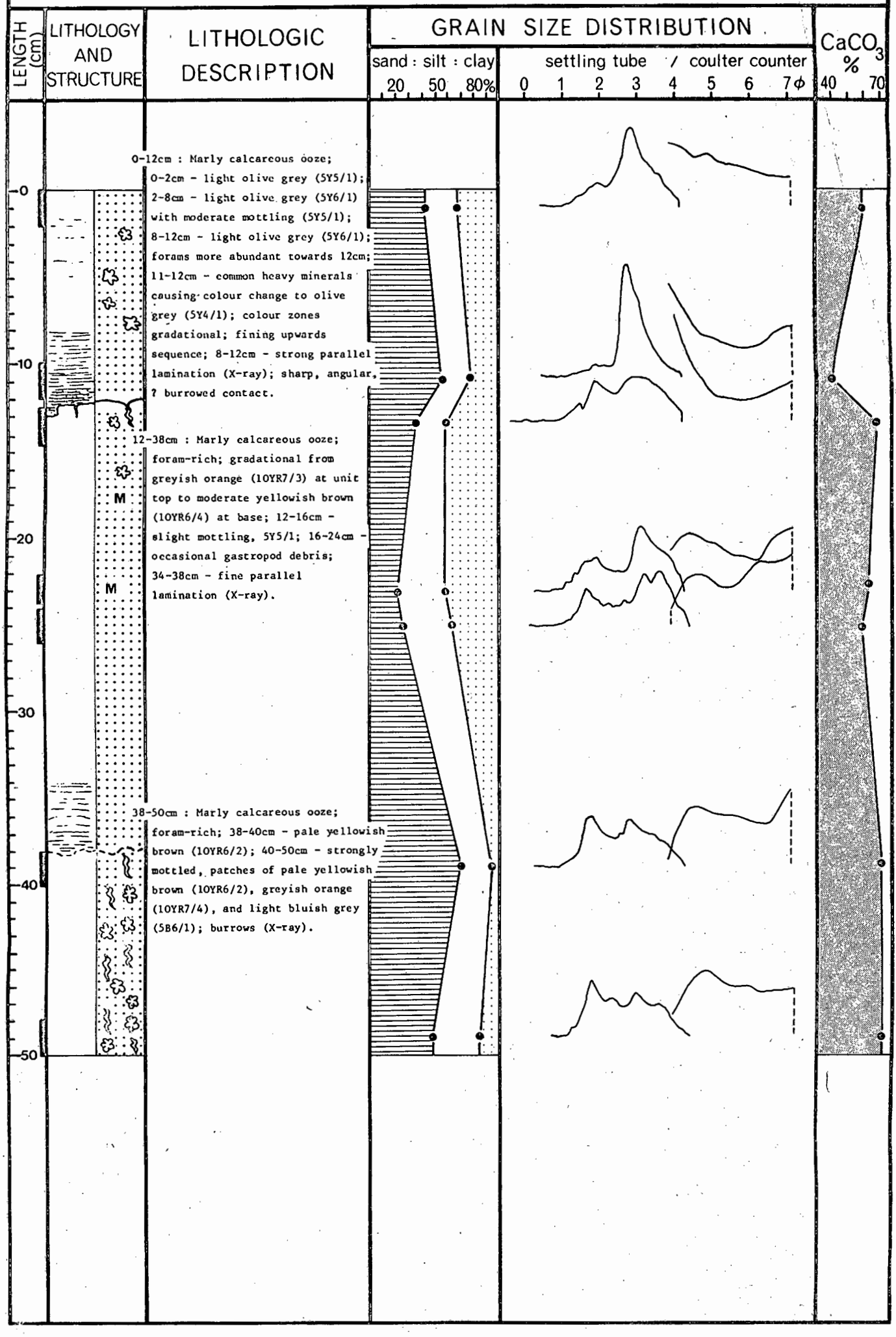

CORE NO. 25 POSITION: 29° 30.3′S 32° 40.7′E WATER DEPTH: 1840m.

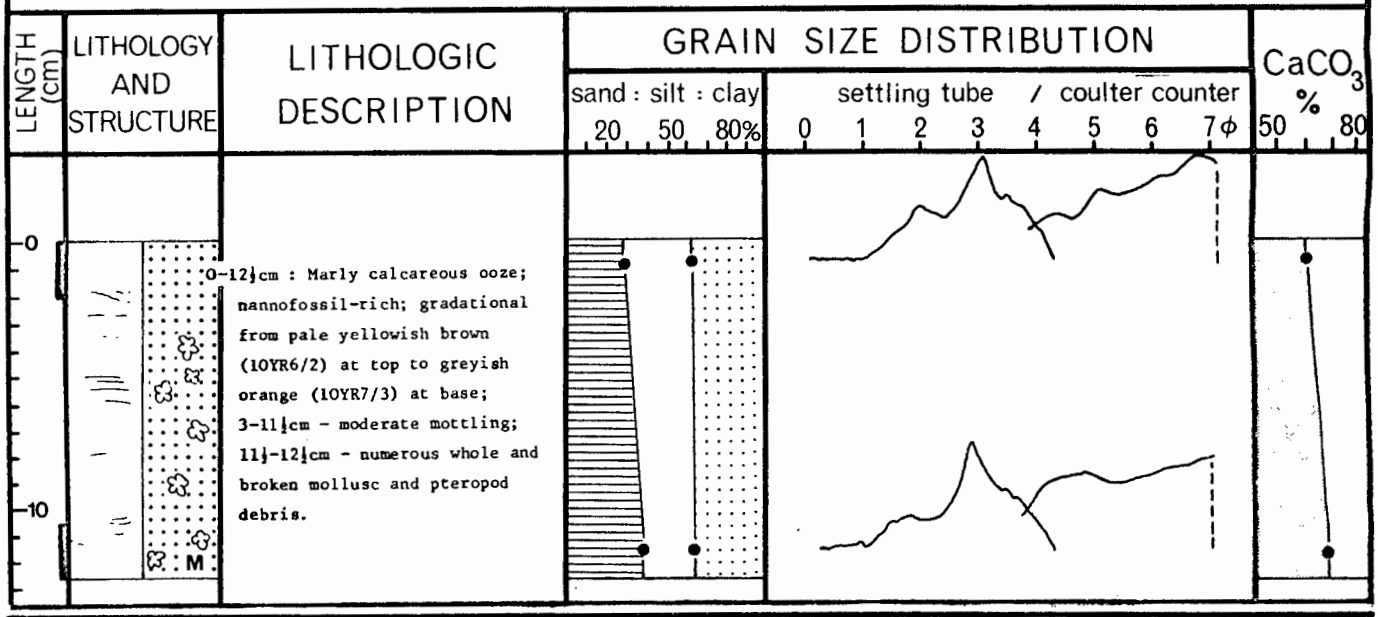

0-12½cm : Marly calcareous ooze; nannofossil-rich; gradational from pale yellowish brown (10YR6/2) at top to greyish orange (10YR7/3) at base; 3-11½cm - moderate mottling; 11½-12½cm - numerous whole and broken mollusc and pteropod debris.

CORE NO. 5116 POSITION: 30° 14.7′S 31° 54.9′E WATER DEPTH: 2010m.

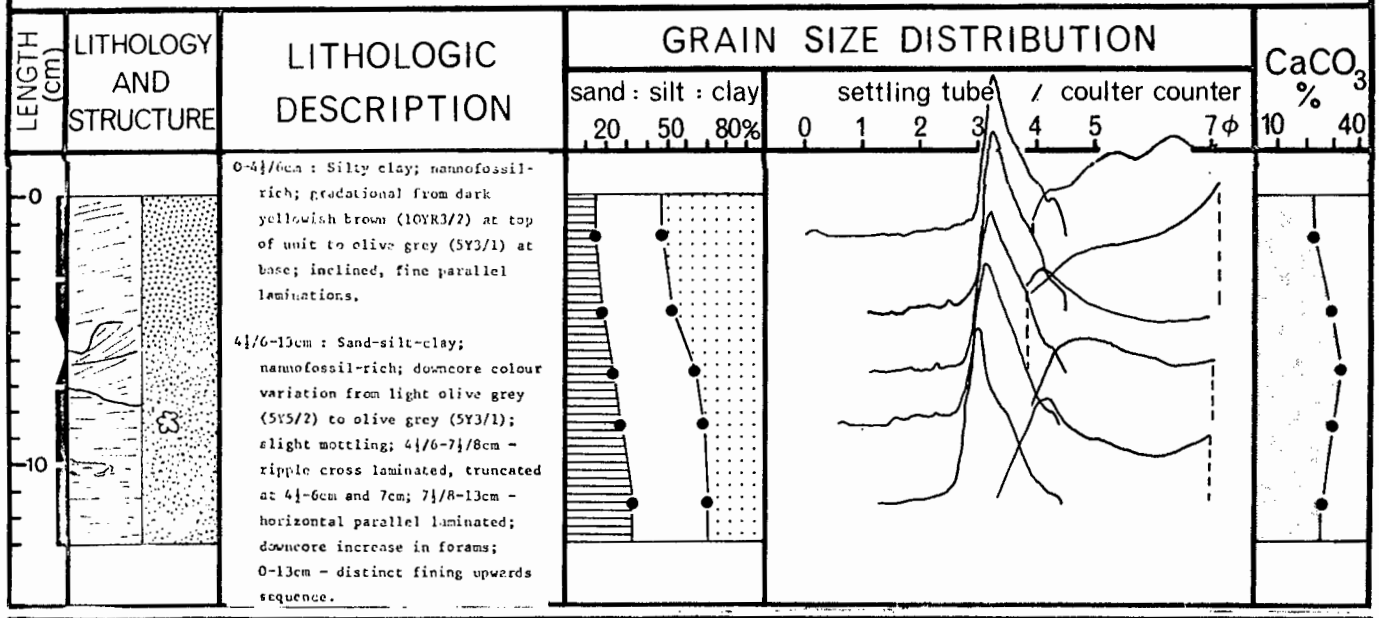

0-4½/6cm : Silty clay; nannofossil-rich; gradational from dark yellowish brown (10YR3/2) at top of unit to olive grey (5Y3/1) at base; inclined, fine parallel laminations.

4½/6-13cm : Sand-silt-clay; nannofossil-rich; downcore colour variation from light olive grey (5Y5/2) to olive grey (5Y3/1); slight mottling; 4½/6-7½/8cm - ripple cross laminated, truncated at 4½-6cm and 7cm; 7½/8-13cm - horizontal parallel laminated; downcore increase in forams; 0-13cm - distinct fining upwards sequence.

CORE NO. 5124 POSITION: 30° 07.8′S 33° 10.0′E WATER DEPTH: 2221m.

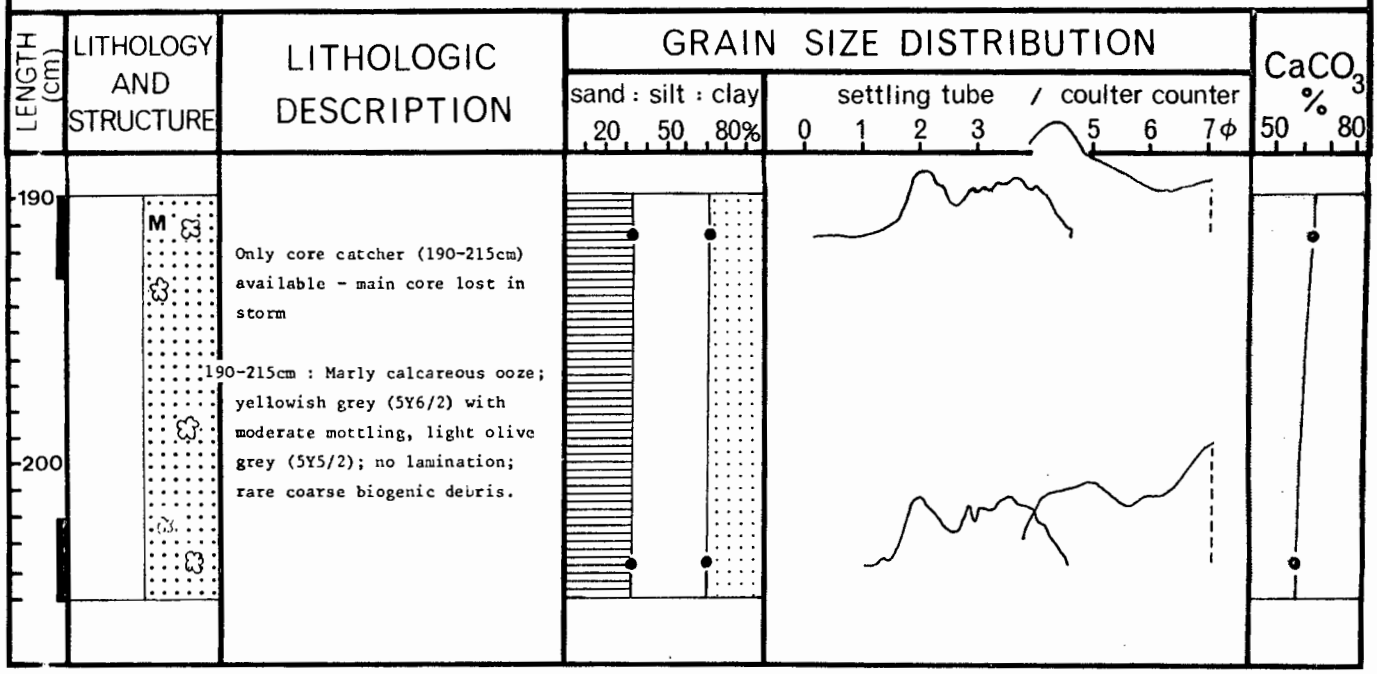

Only core catcher (190-215cm) available - main core lost in storm

190-215cm : Marly calcareous ooze; yellowish grey (5Y6/2) with moderate mottling, light olive grey (5Y5/2); no lamination; rare coarse biogenic debris.

CORE NO. 26 POSITION: 29° 28.8′S 32° 32.8′E WATER DEPTH: 1680m.

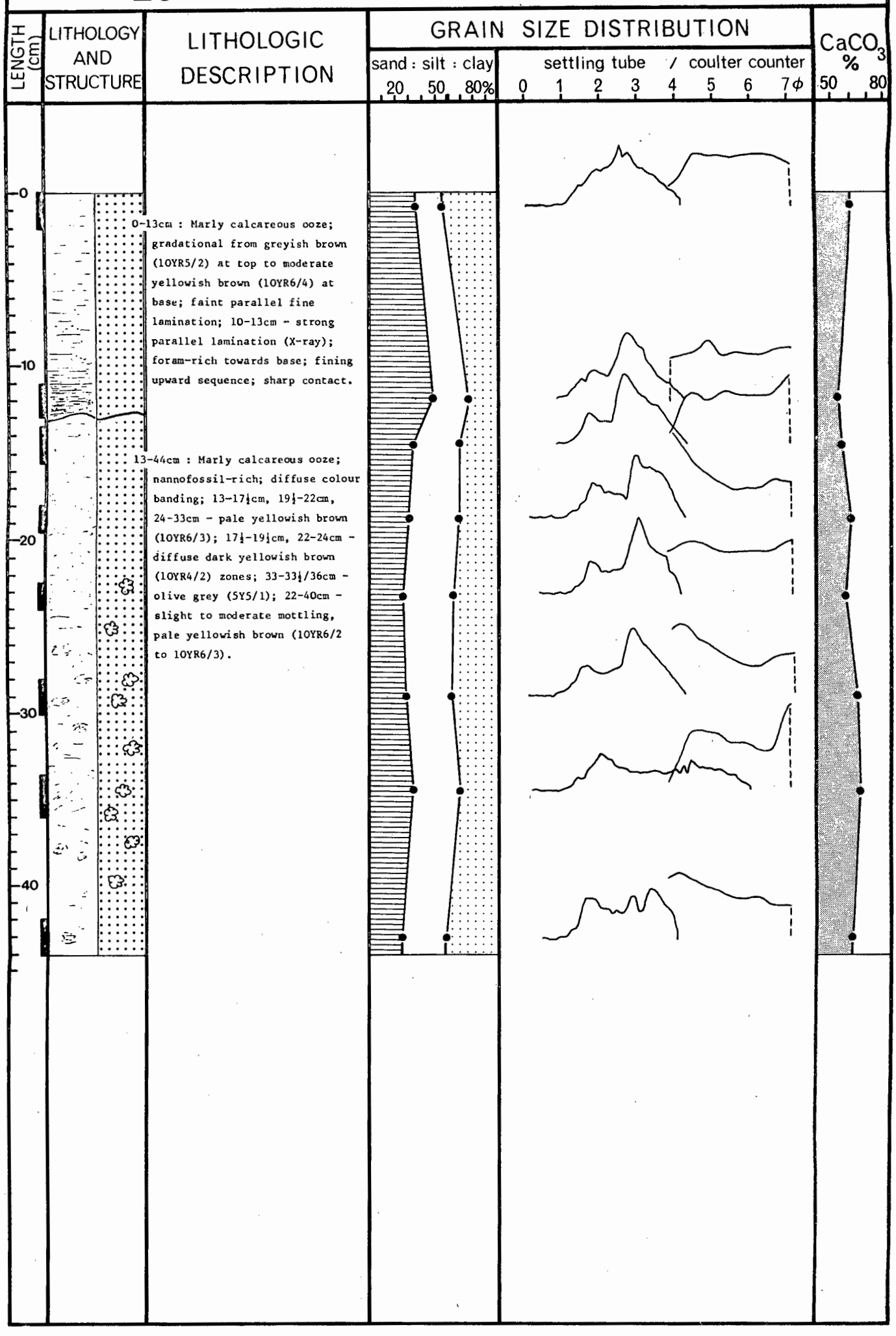

CORE NO. 27 POSITION: 29° 33.4'S 32° 27.1'E WATER DEPTH: 1577m.

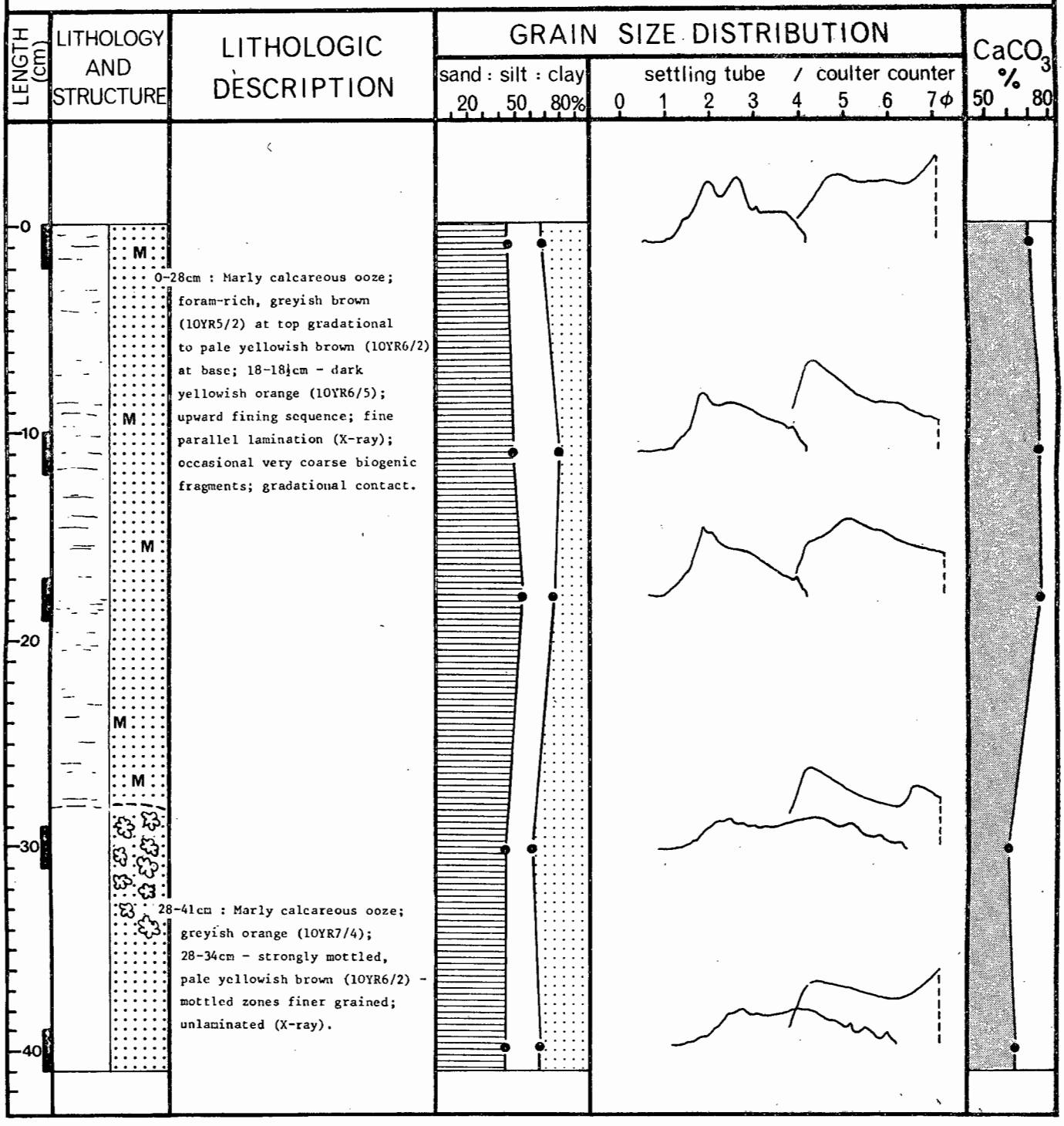

CORE NO. 32 POSITION: 29°42.7'S 31°46.9'E WATER DEPTH: 657m.

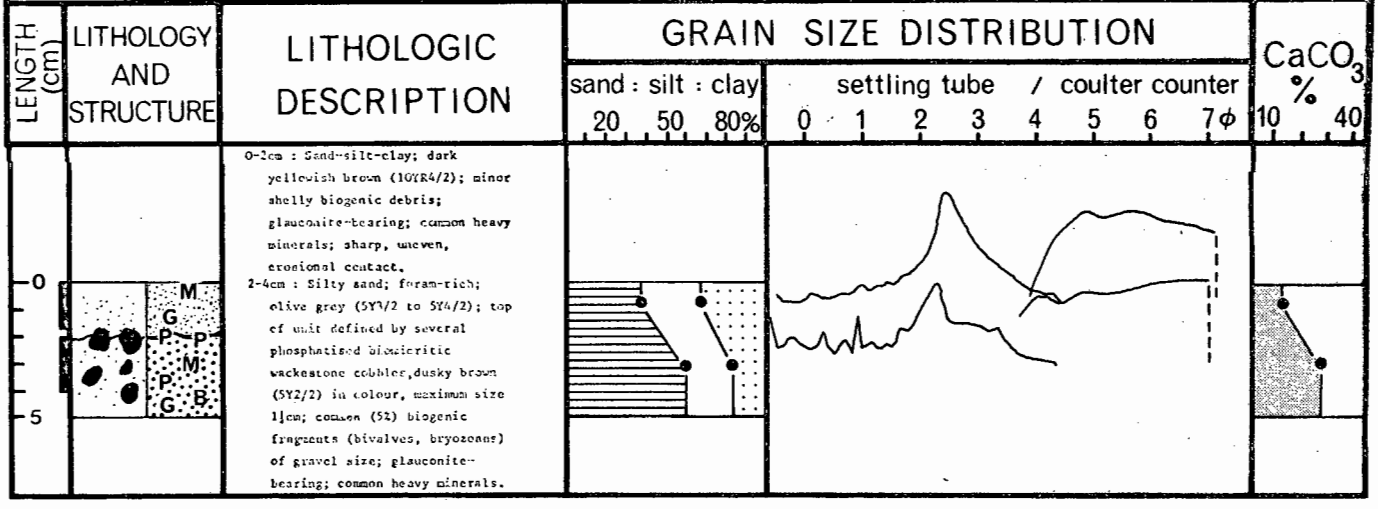

CORE NO. 29 POSITION: 29° 40.9′S 32° 13.0′E WATER DEPTH: 1320m.

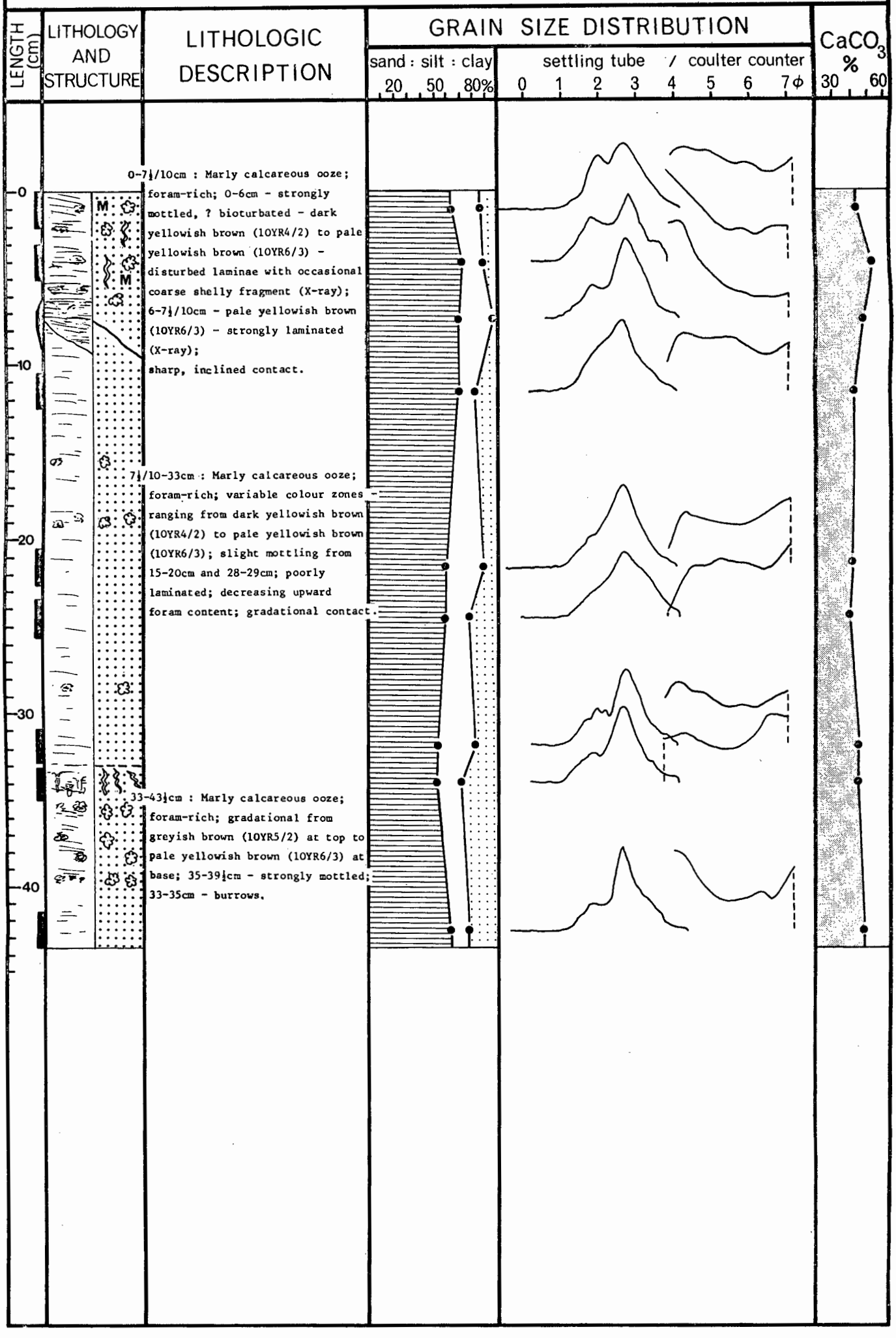

CORE NO. 30 POSITION: 29° 44.2'S 31° 58.2'E WATER DEPTH: 1340m.

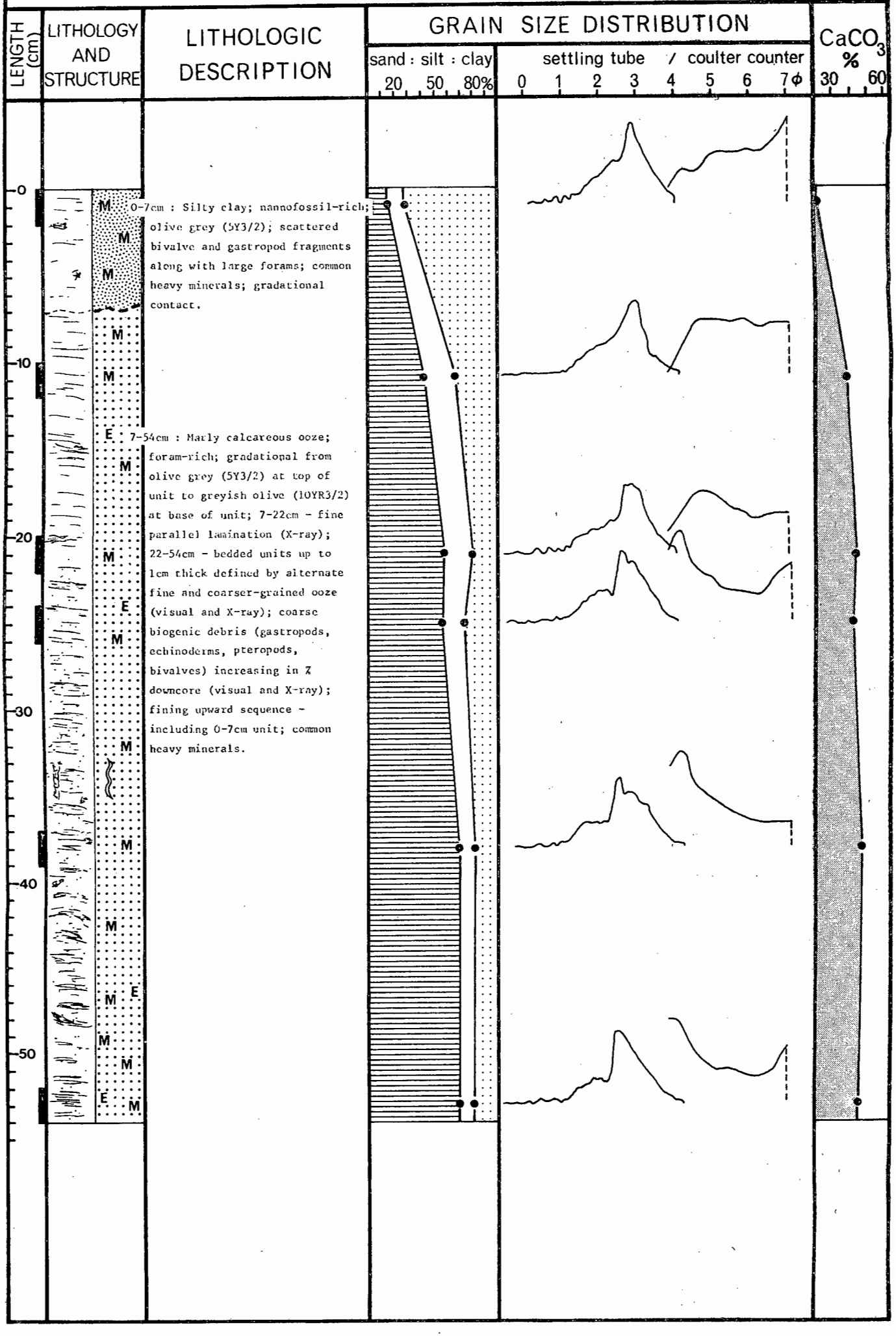

CORE NO. 31 POSITION: 29° 40.3′S 31° 54.8′E WATER DEPTH: 1100m.

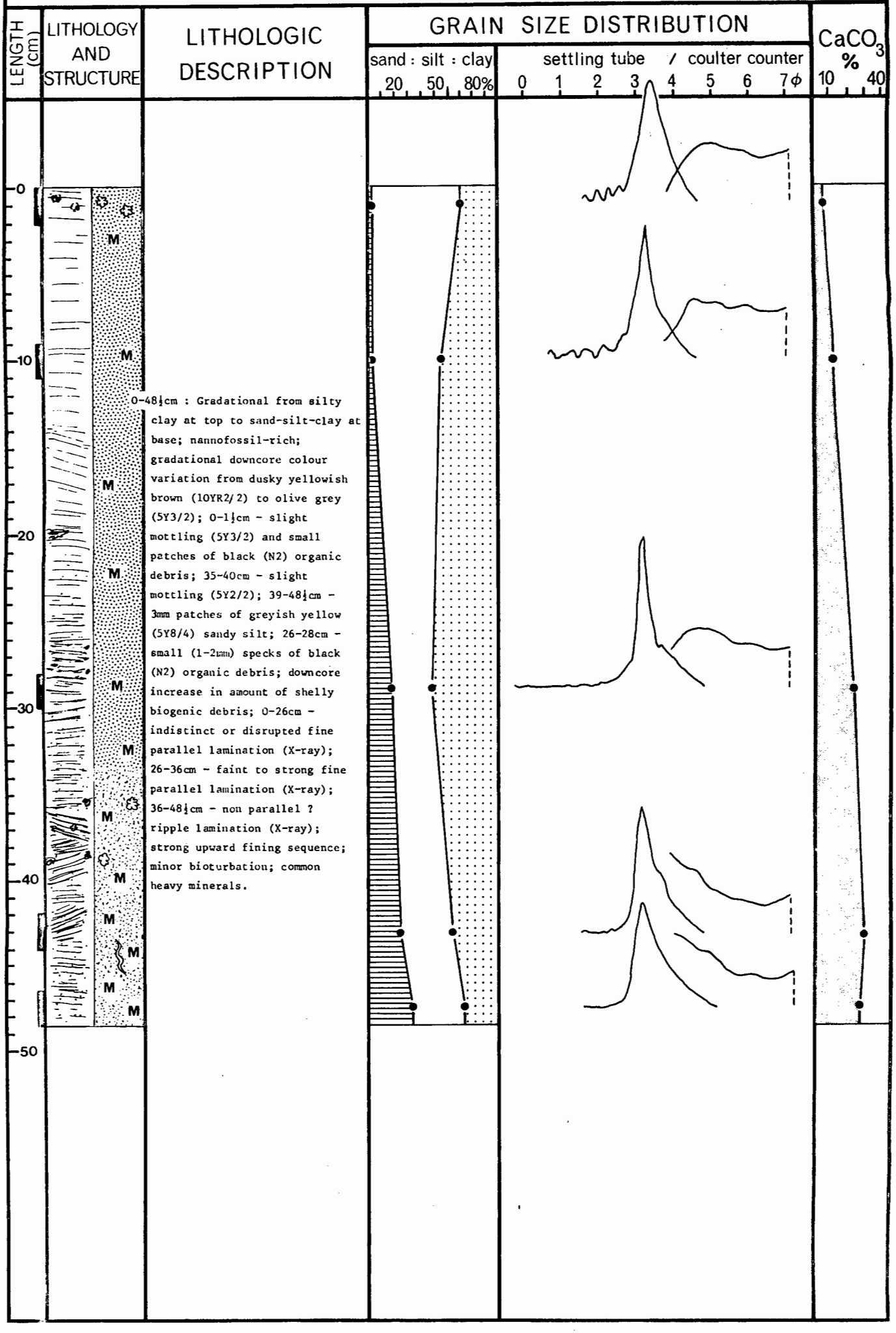

CORE NO. 34 POSITION: 29° 42.3′S 31° 35.0′E WATER DEPTH: 304m.

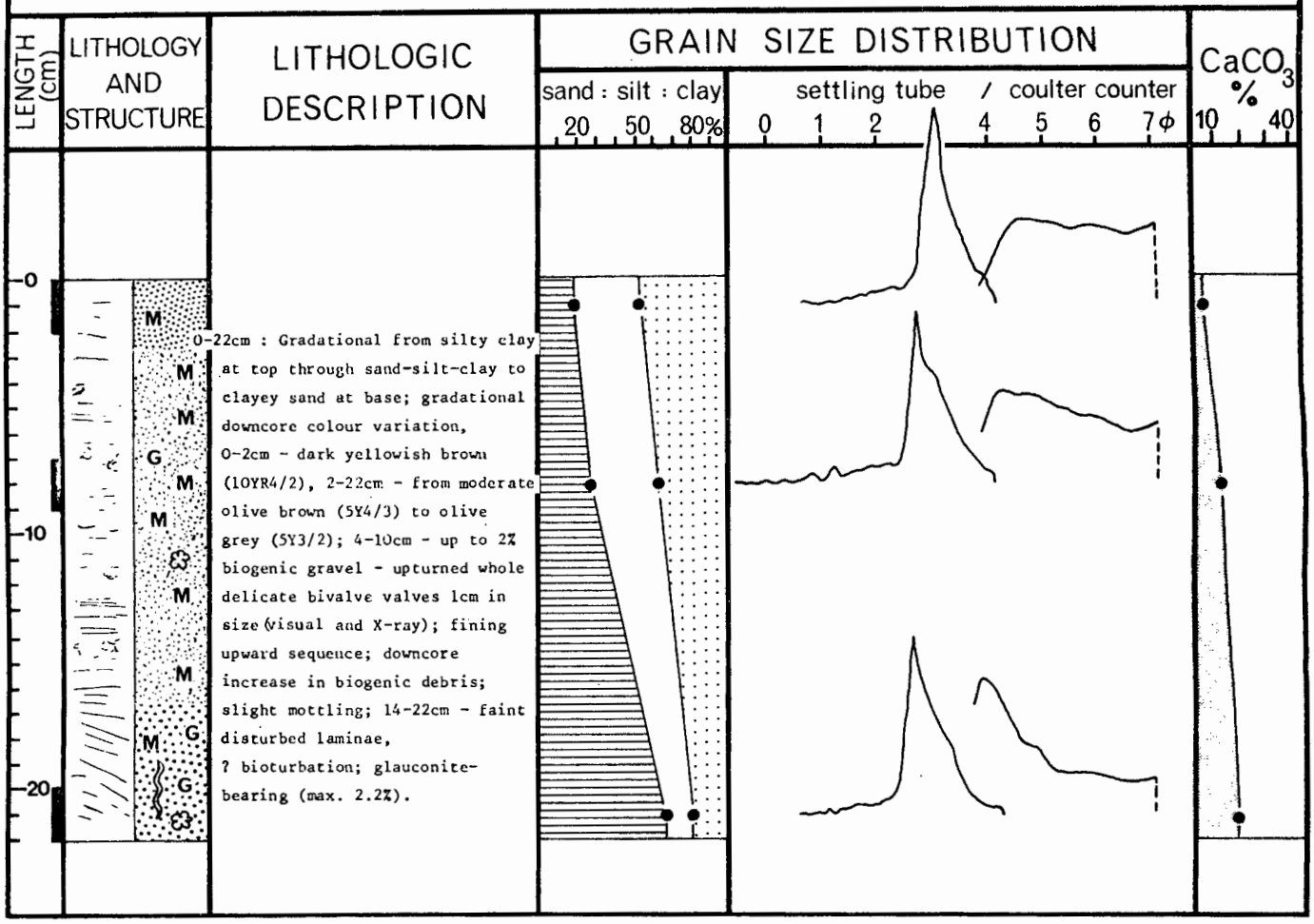

CORE NO. 5115 POSITION: 29° 54.7′S 31° 40.5′E WATER DEPTH: 765m.

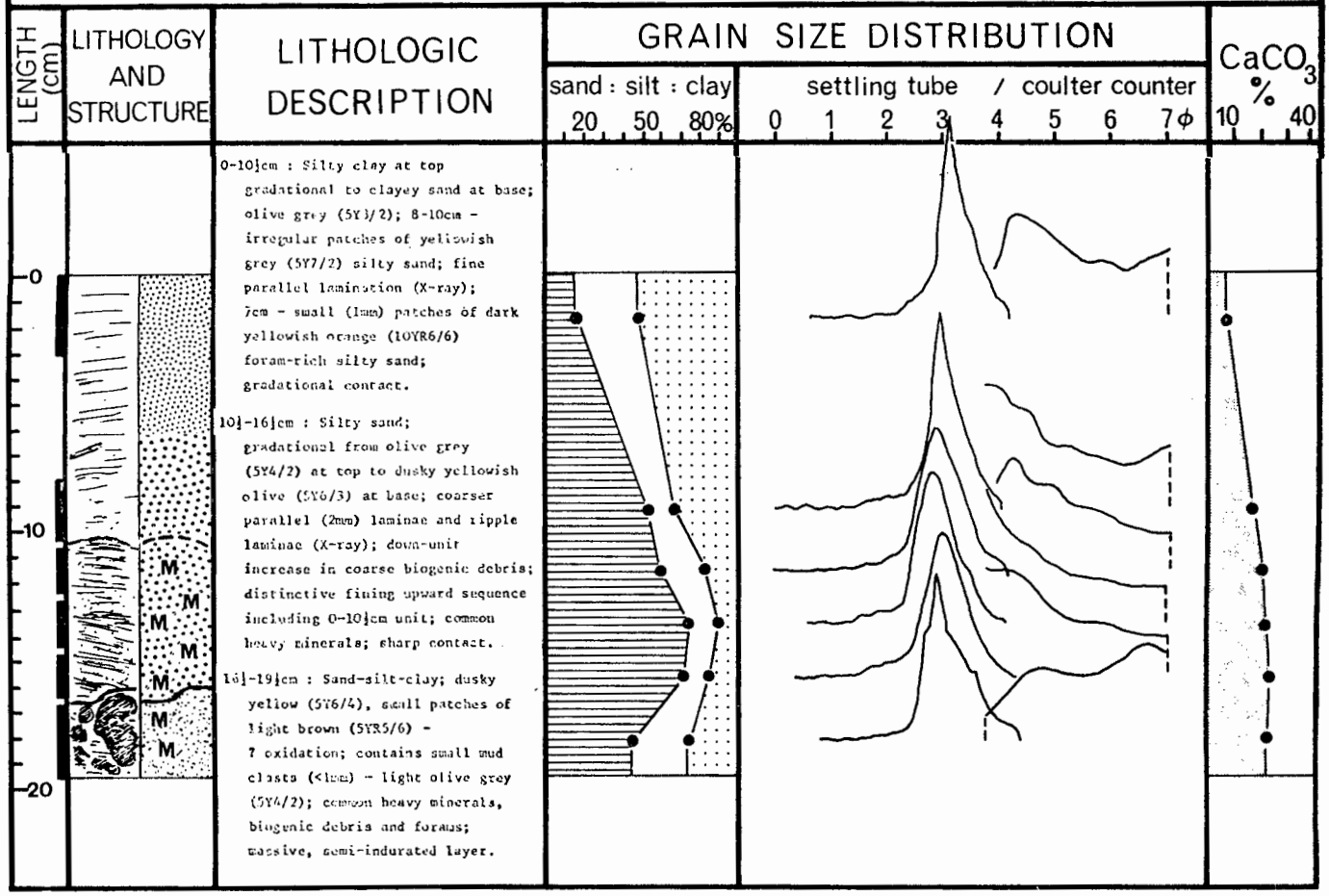

CORE NO. 5117 POSITION: 30° 13.6′S 31° 54.7′ E WATER DEPTH: 1705m.

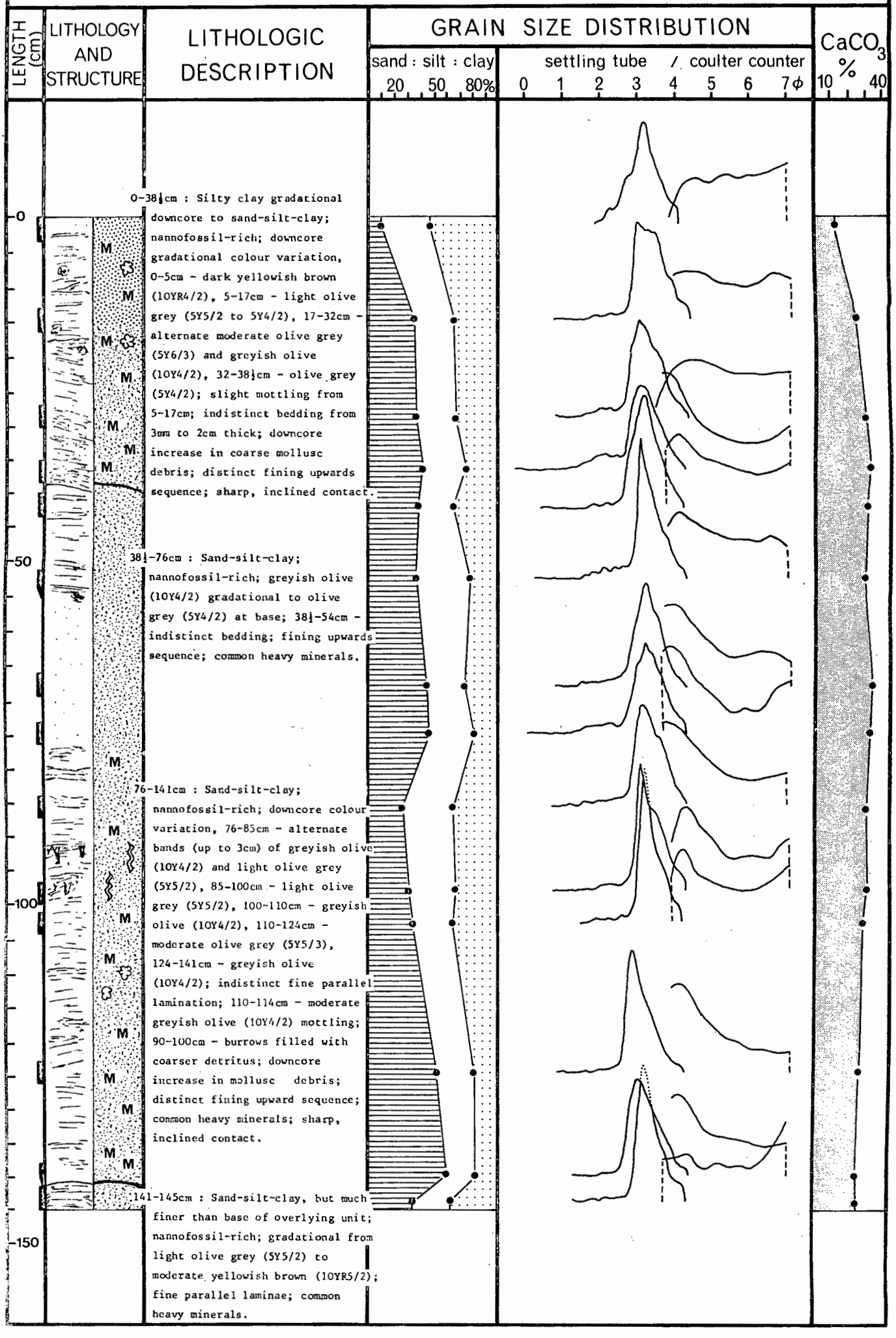

CORE NO. 5119 POSITION: 30° 18.9′ S 32° 32.7′ E WATER DEPTH: 2813m.

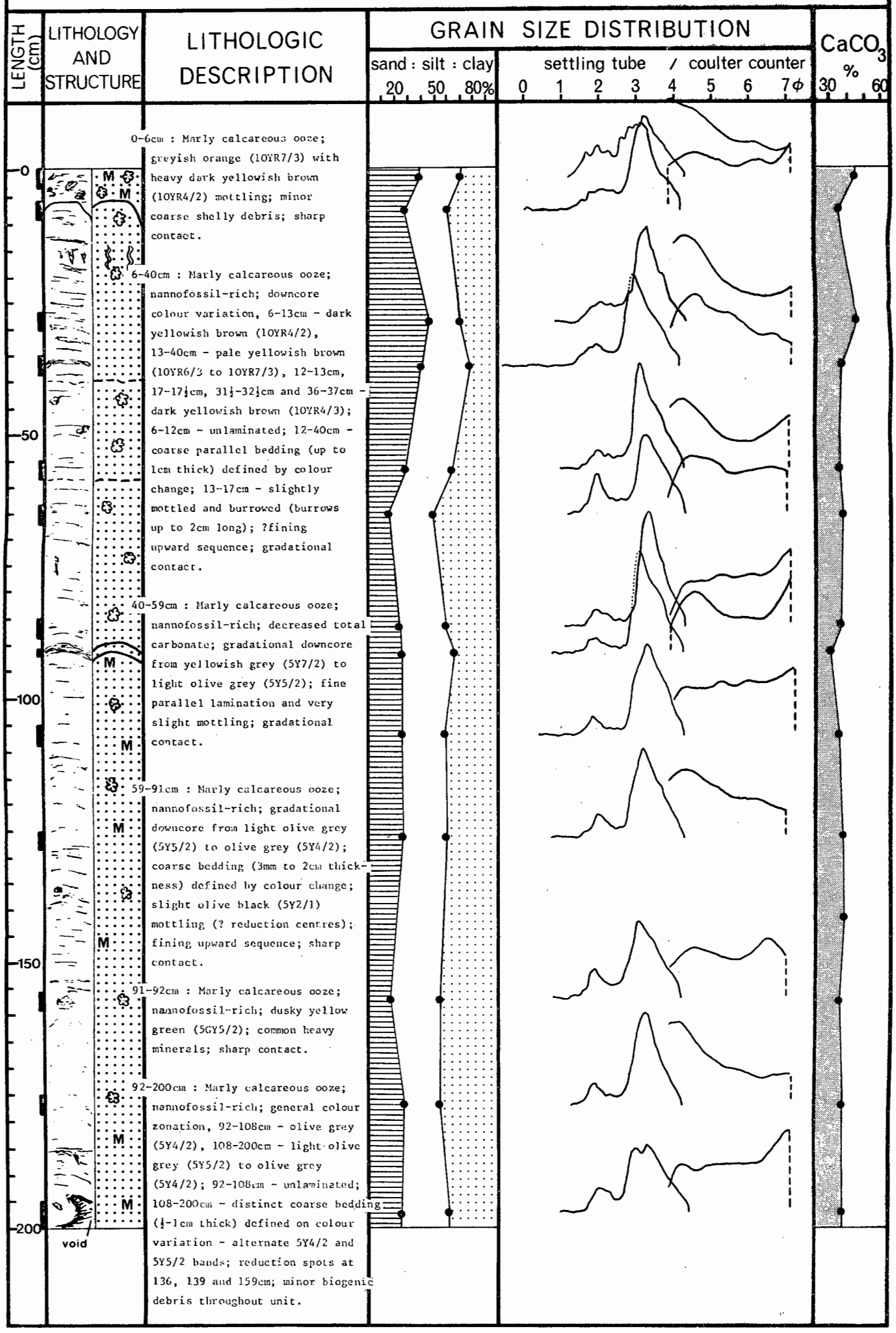

CORE NO. 5121 POSITION: 30° 35.8'S 33° 07.6'E WATER DEPTH: 3030m.

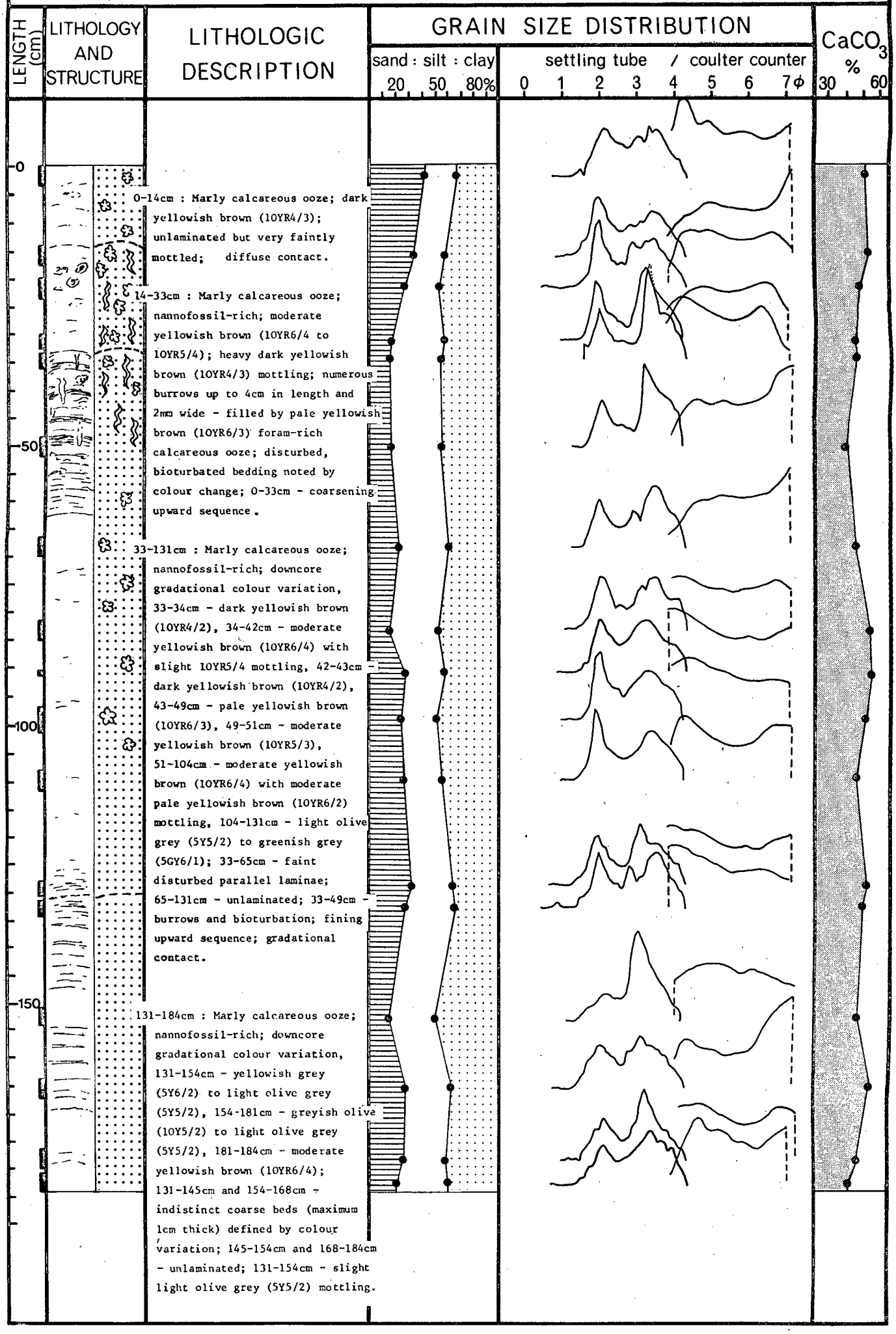

CORE NO. 5127 POSITION: 29° 19.1'S 33° 02.0'E WATER DEPTH: 1940m.

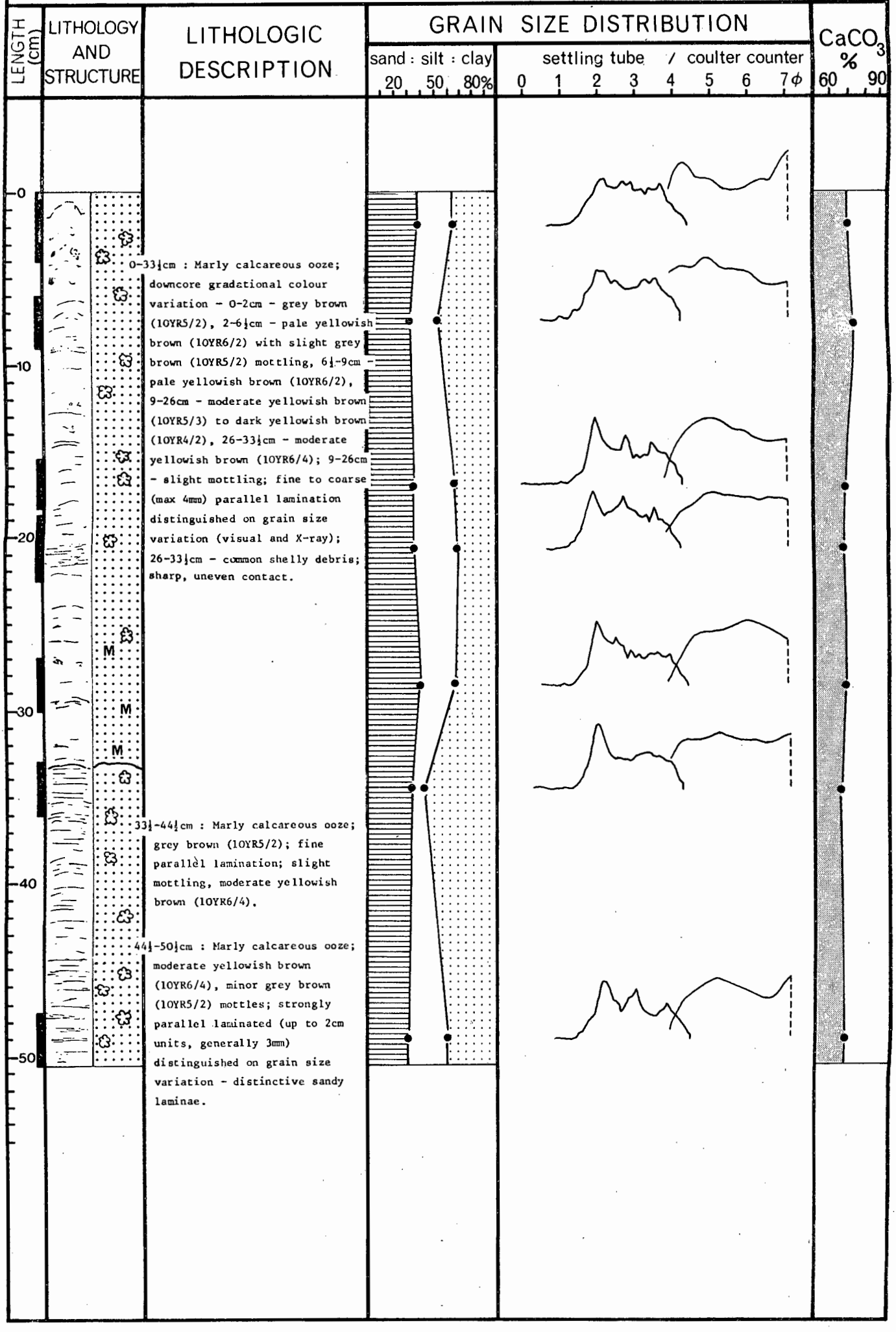

CORE NO. 5751 POSITION: 30° 38.7′S 34° 17.4′E WATER DEPTH: 2778m.

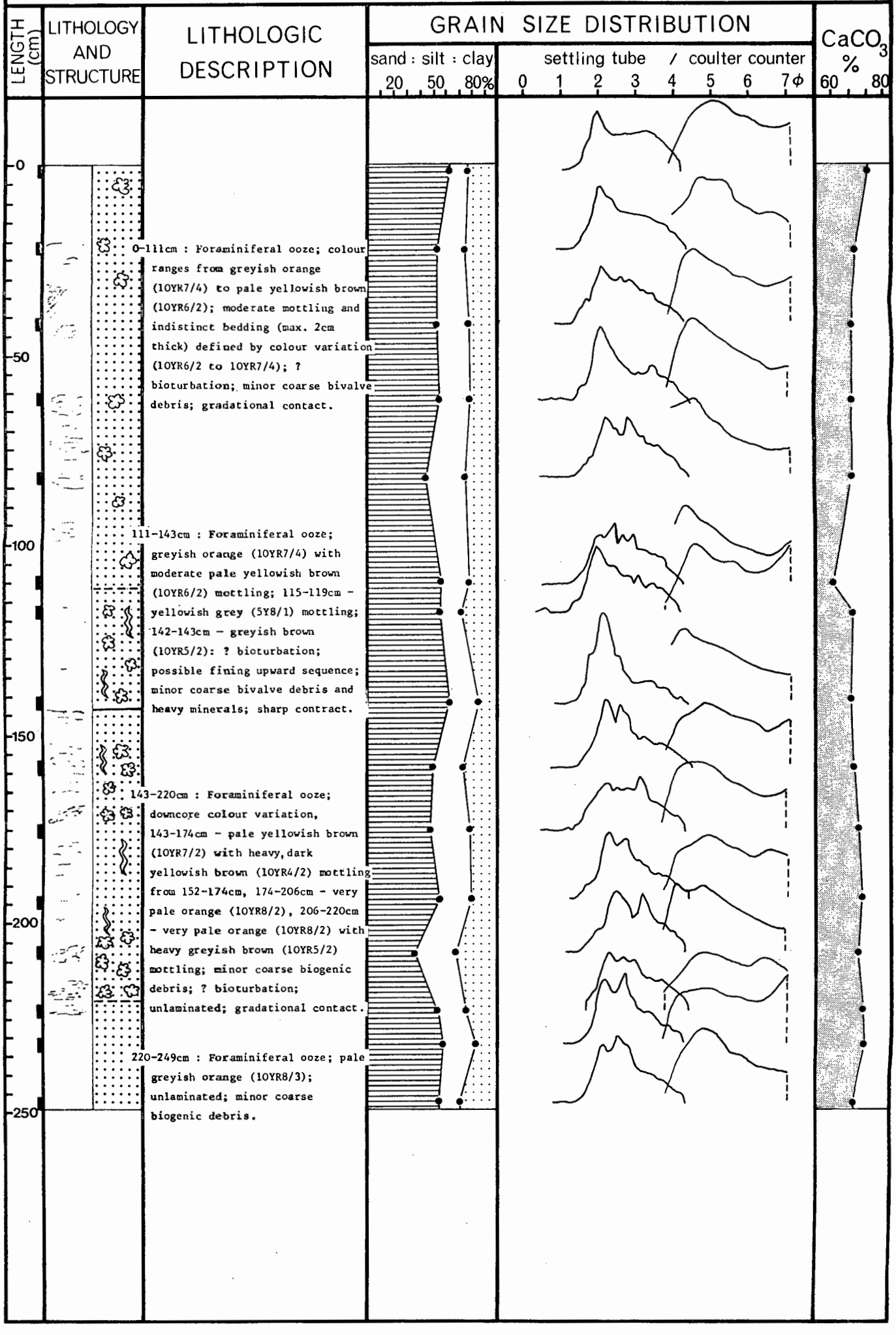

CORE NO. 5753 POSITION: 30° 31.9′ S 32° 42.6′E WATER DEPTH: 2992 m.

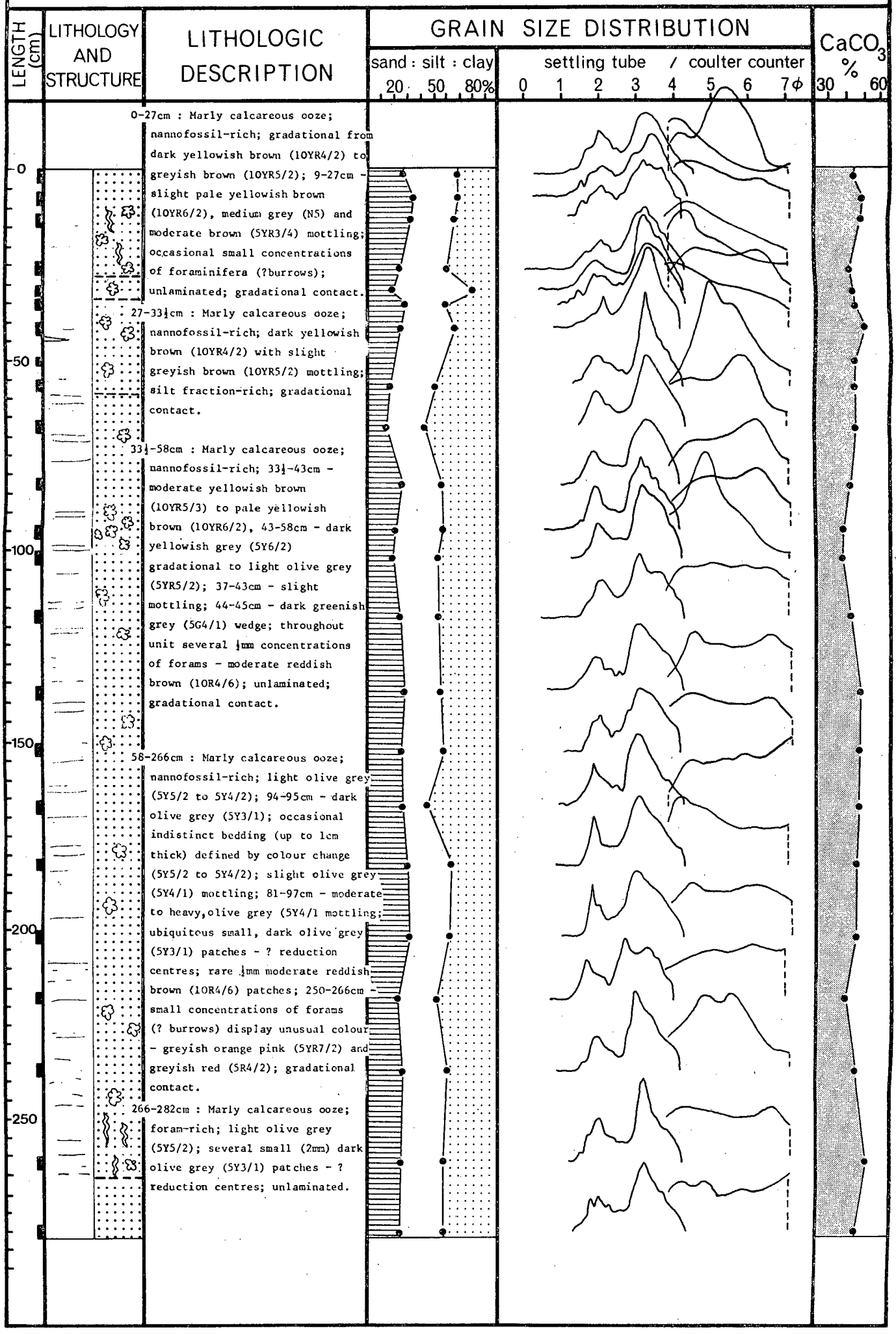

APPENDIX B3 Seismic Profile Photographic Reproductions

Photographic reproductions of eighteen key continuous seismic reflection profiles are presented in this appendix (for profile location see Fig. 6.2). Reproduced profiles are complimentary to line drawings presented throughout the thesis but in particular to those of Figs. 6.6 to 6.9. To reduce expense, individual profiles have been closely packed with only minor regard for physiographic zonation. Most profiles have been reduced to a vertical scale of 20 mm = 1 second two-way travel time. Profiles depicted in each plate are listed below:

Plate B3.1 : 284, 283

Plate B3.2 : 371/8, 520, 519, 76/28/4, 522a, 371/2, 350/1

Plate B3.3 : 76/28/3, 76/28/5, 371/3, 522b, 350/2

Plate B3.4 : 76/28/2, 76/28/1, 371/4, 371/7

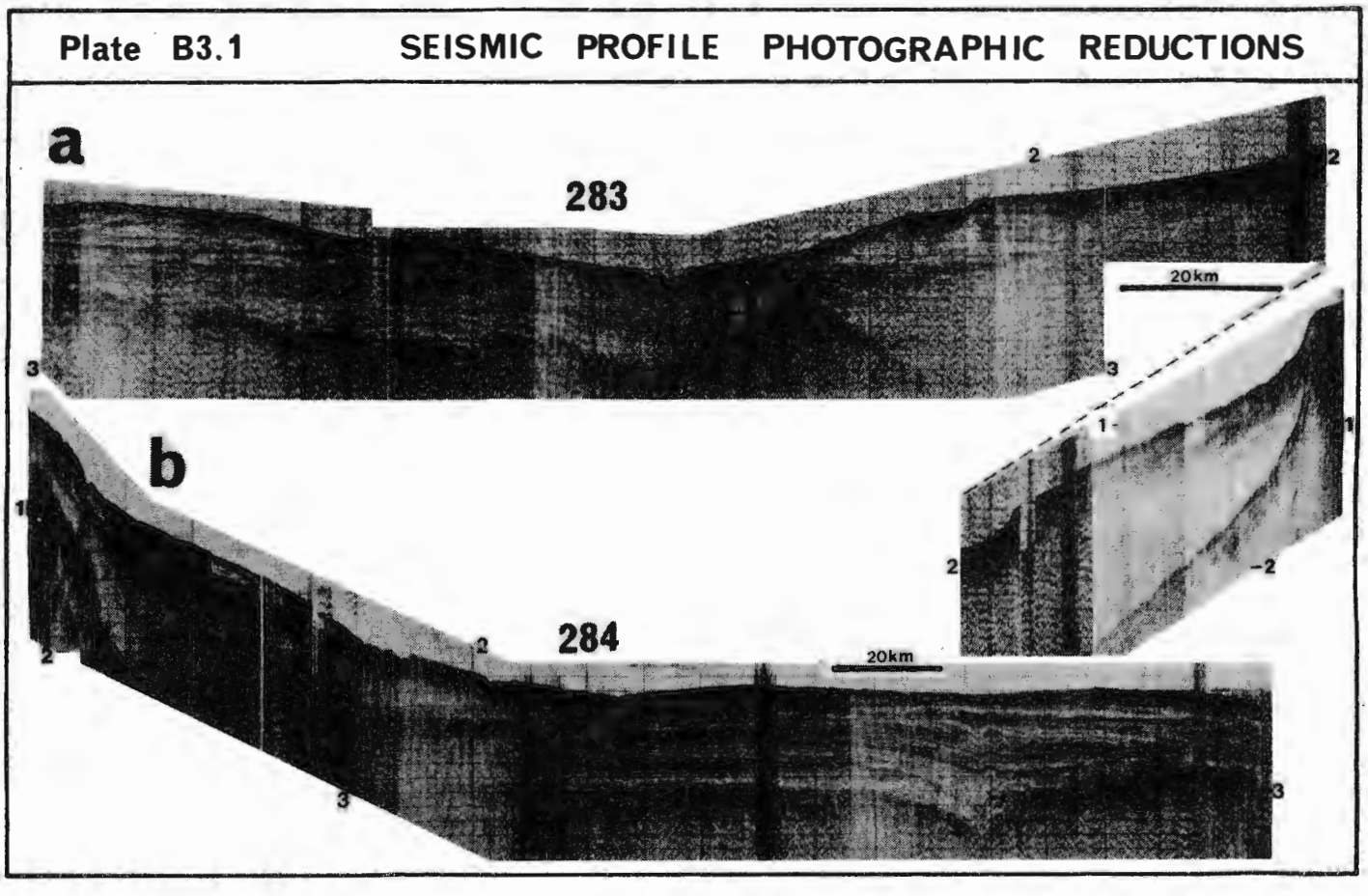

Plate B3.2 SEISMIC PROFILE PHOTOGRAPHIC REDUCTIONS

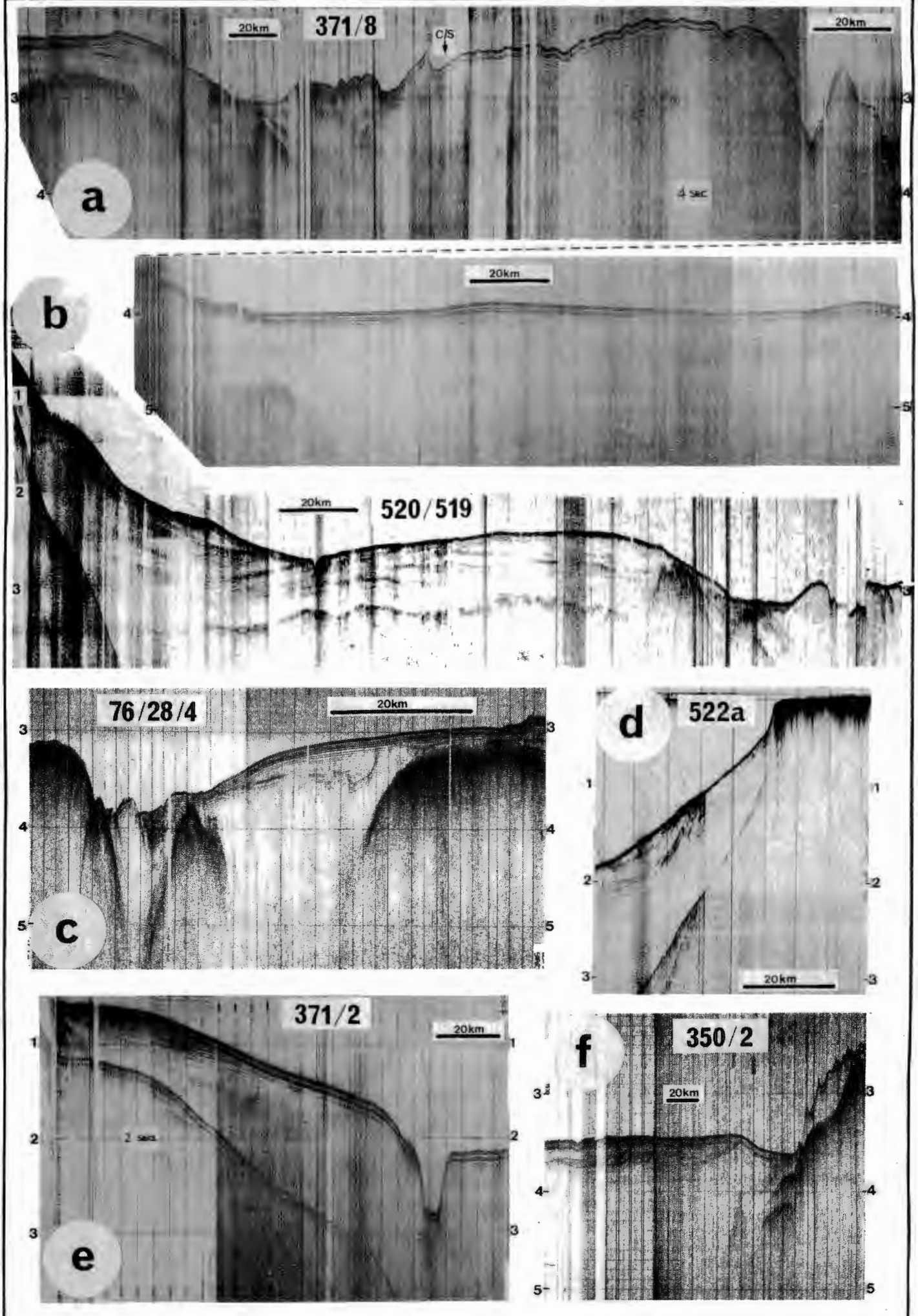

Plate B3.3 SEISMIC PROFILE PHOTOGRAPHIC REDUCTIONS

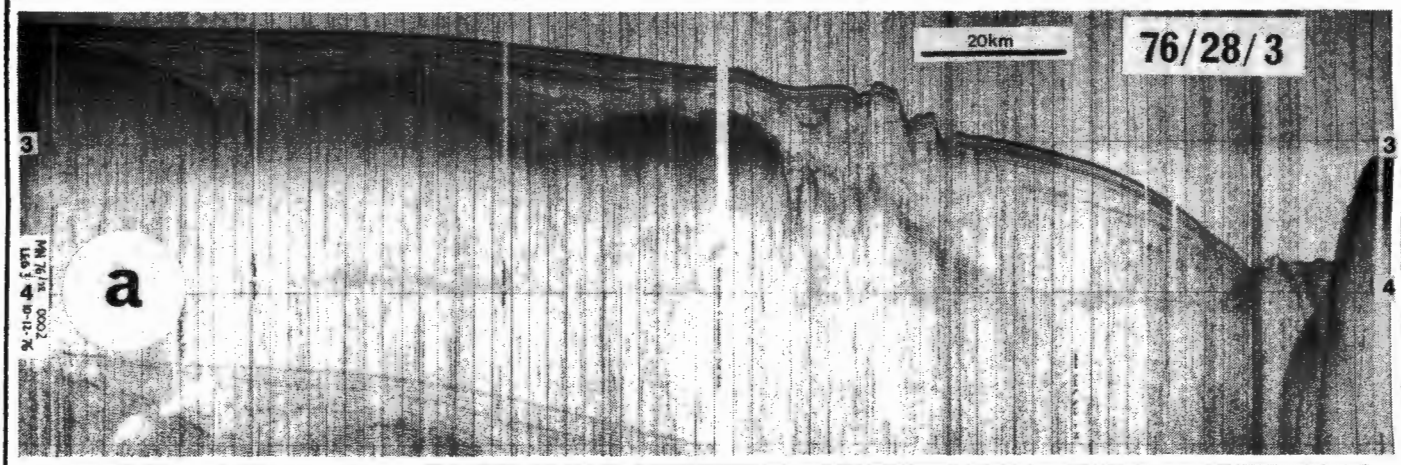

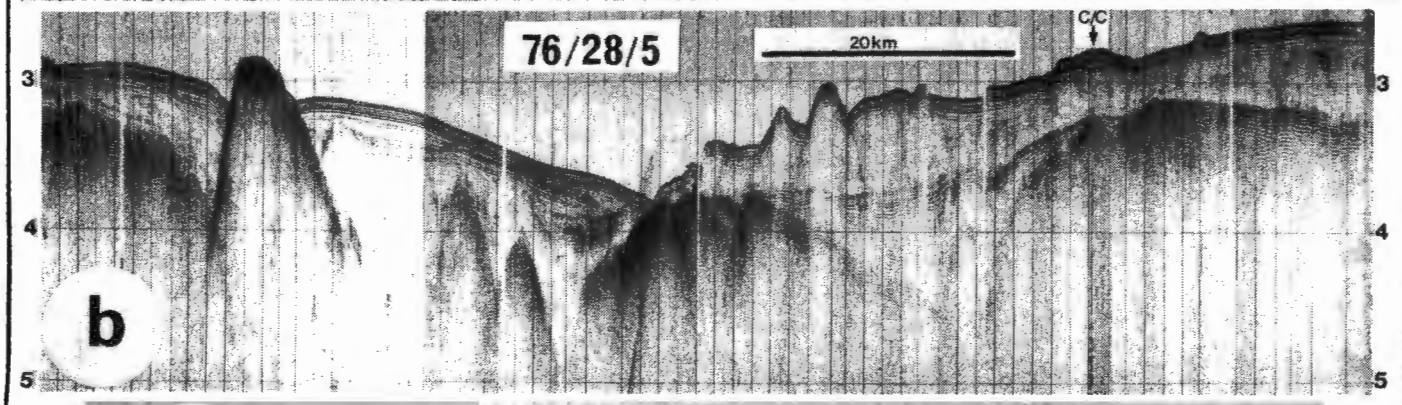

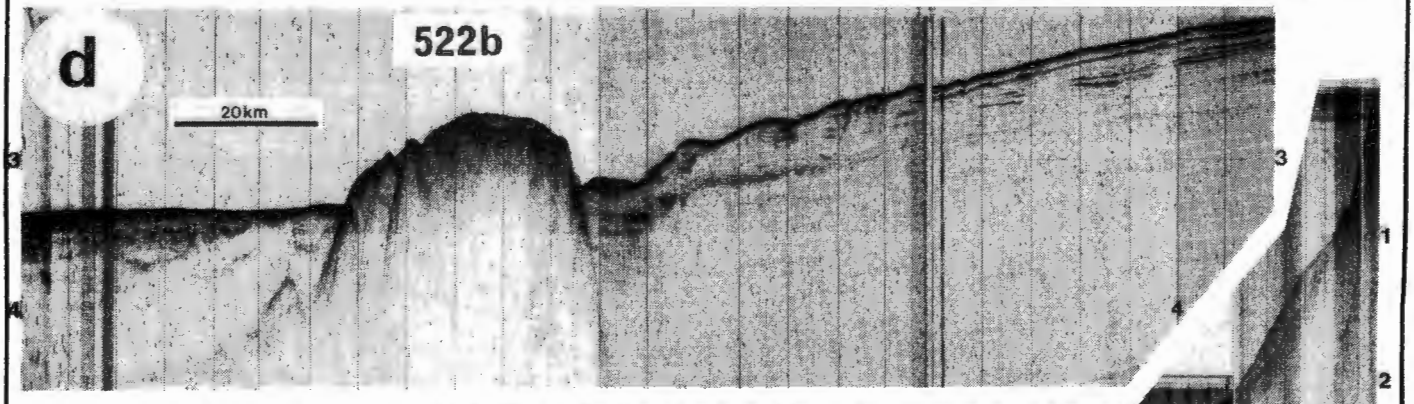

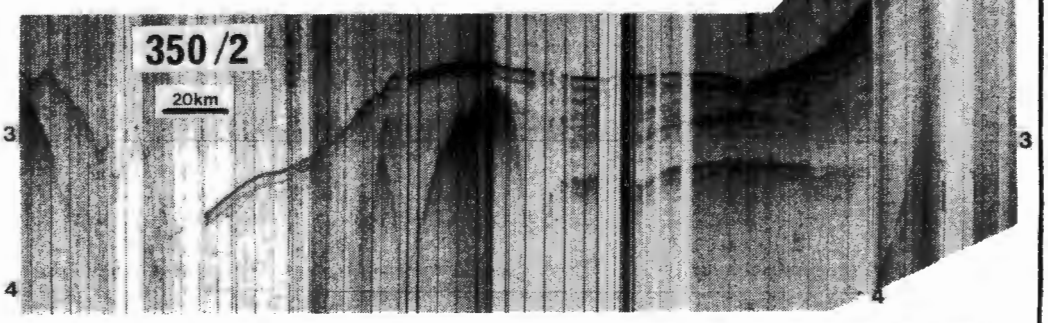

Plate B3.4 SEISMIC PROFILE PHOTOGRAPHIC REDUCTIONS

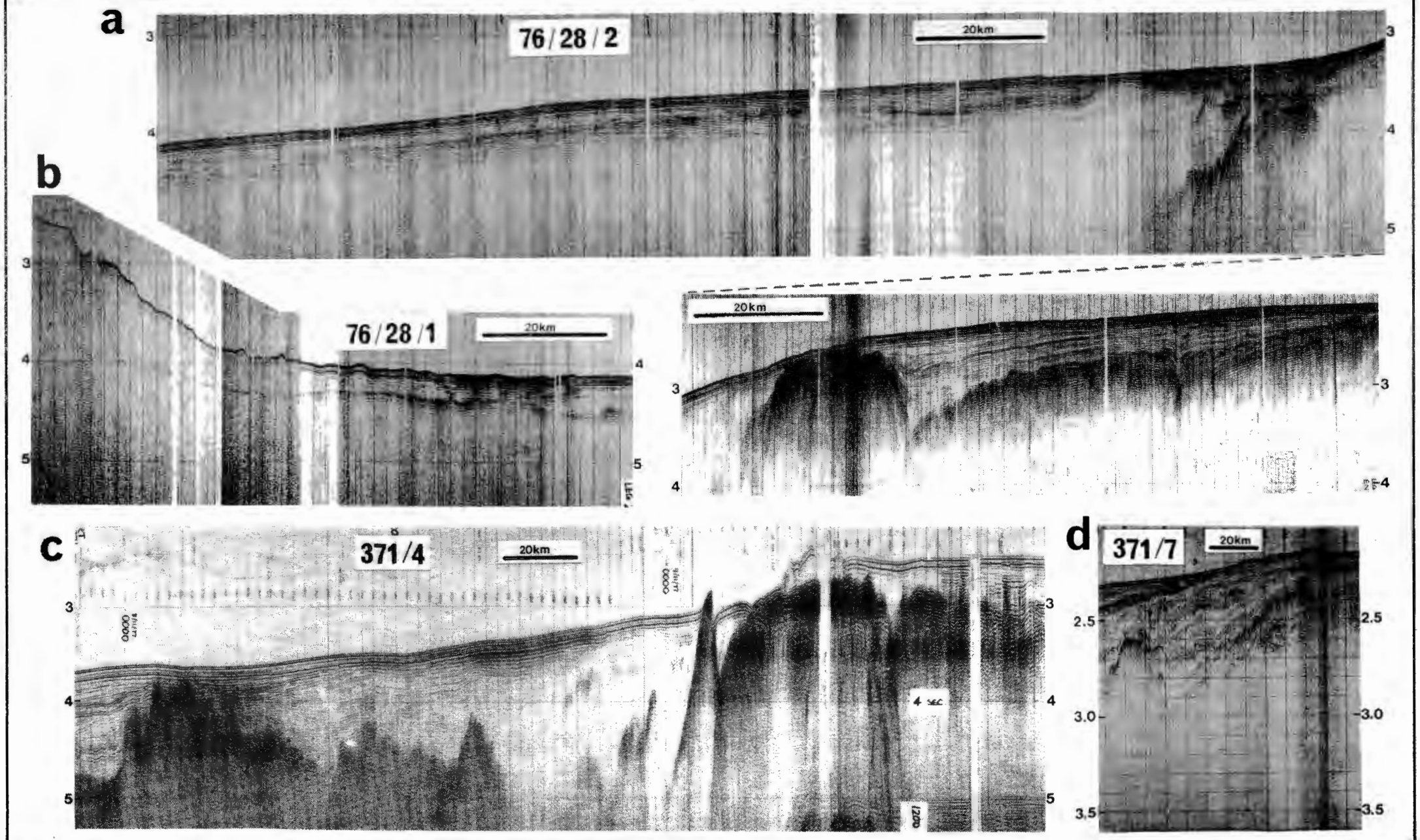

Plate B4.1 CORE PHOTOGRAPHIC REDUCTIONS

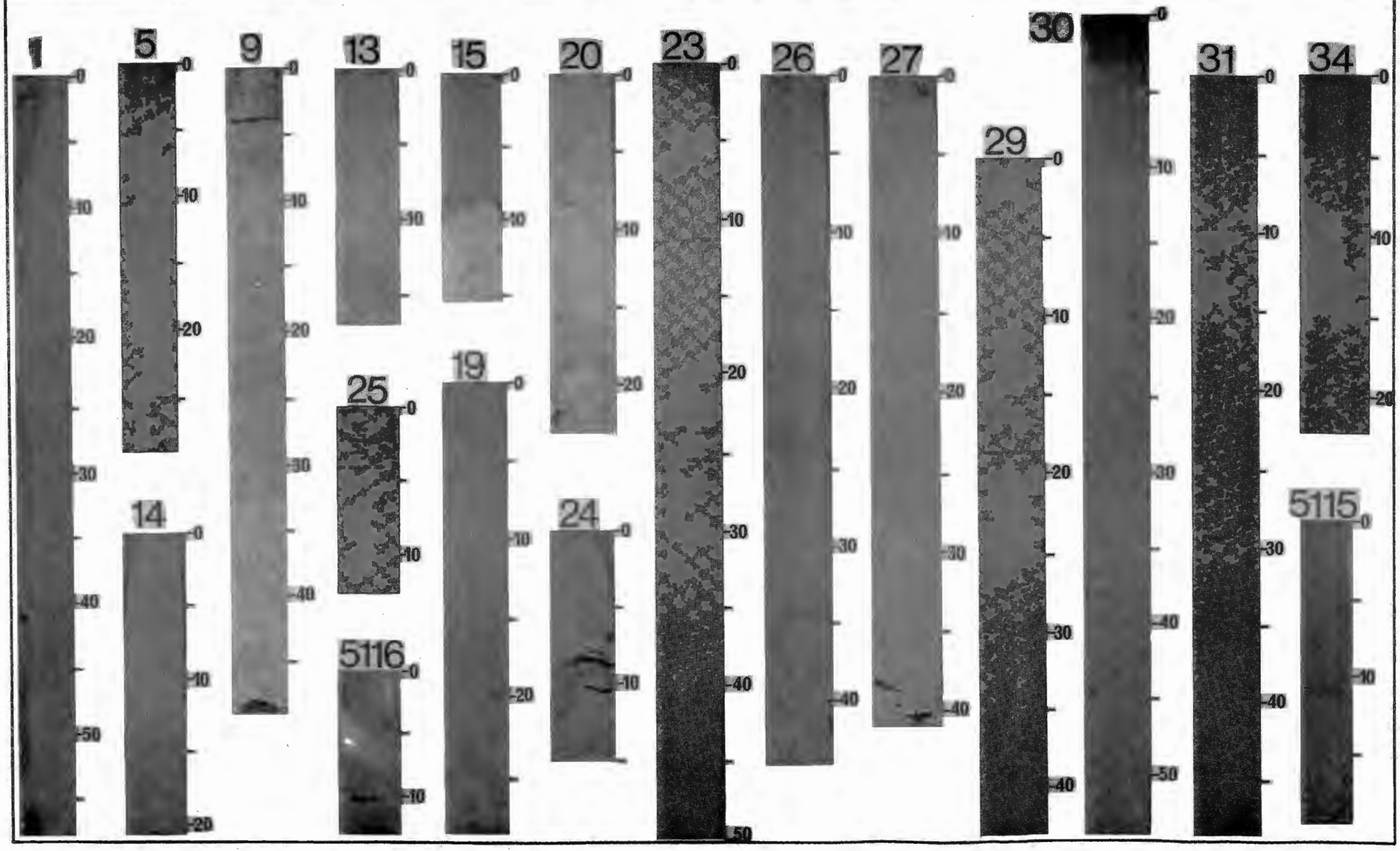

Plate B4.2 CORE PHOTOGRAPHIC REDUCTIONS

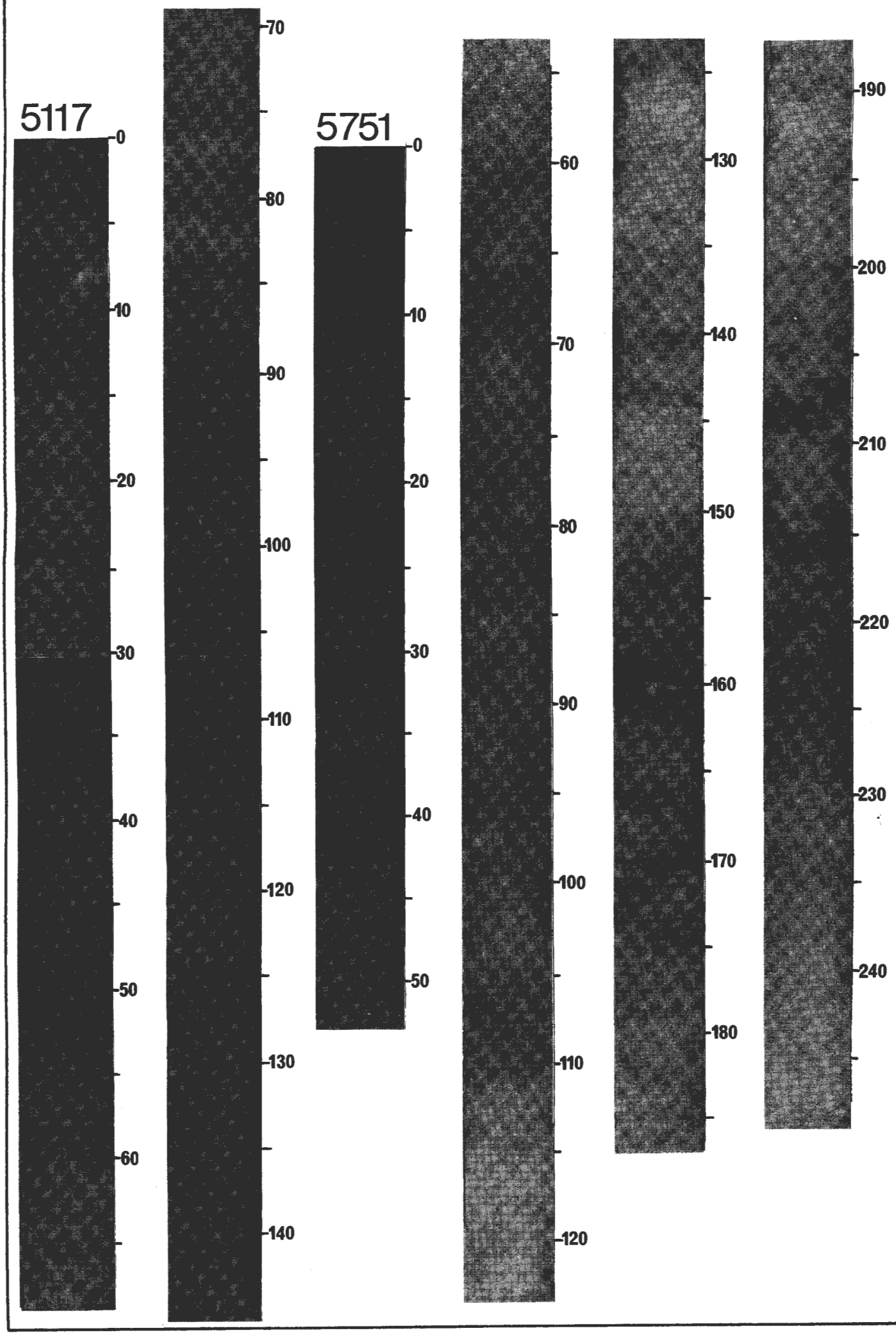

Plate B4.3 CORE PHOTOGRAPHIC REDUCTIONS

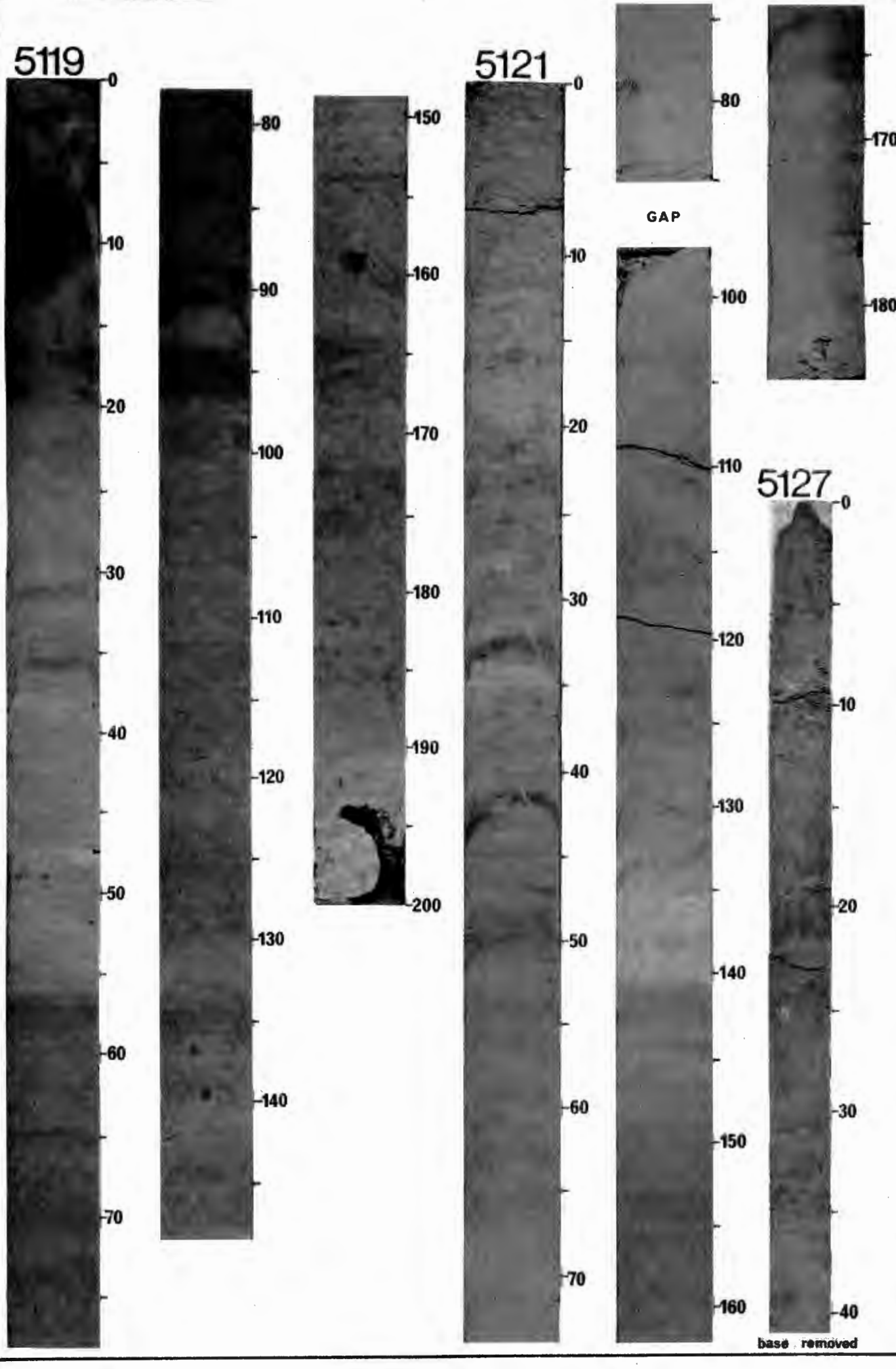

Plate B5.1 CORE X-RADIOGRAPH REDUCTIONS

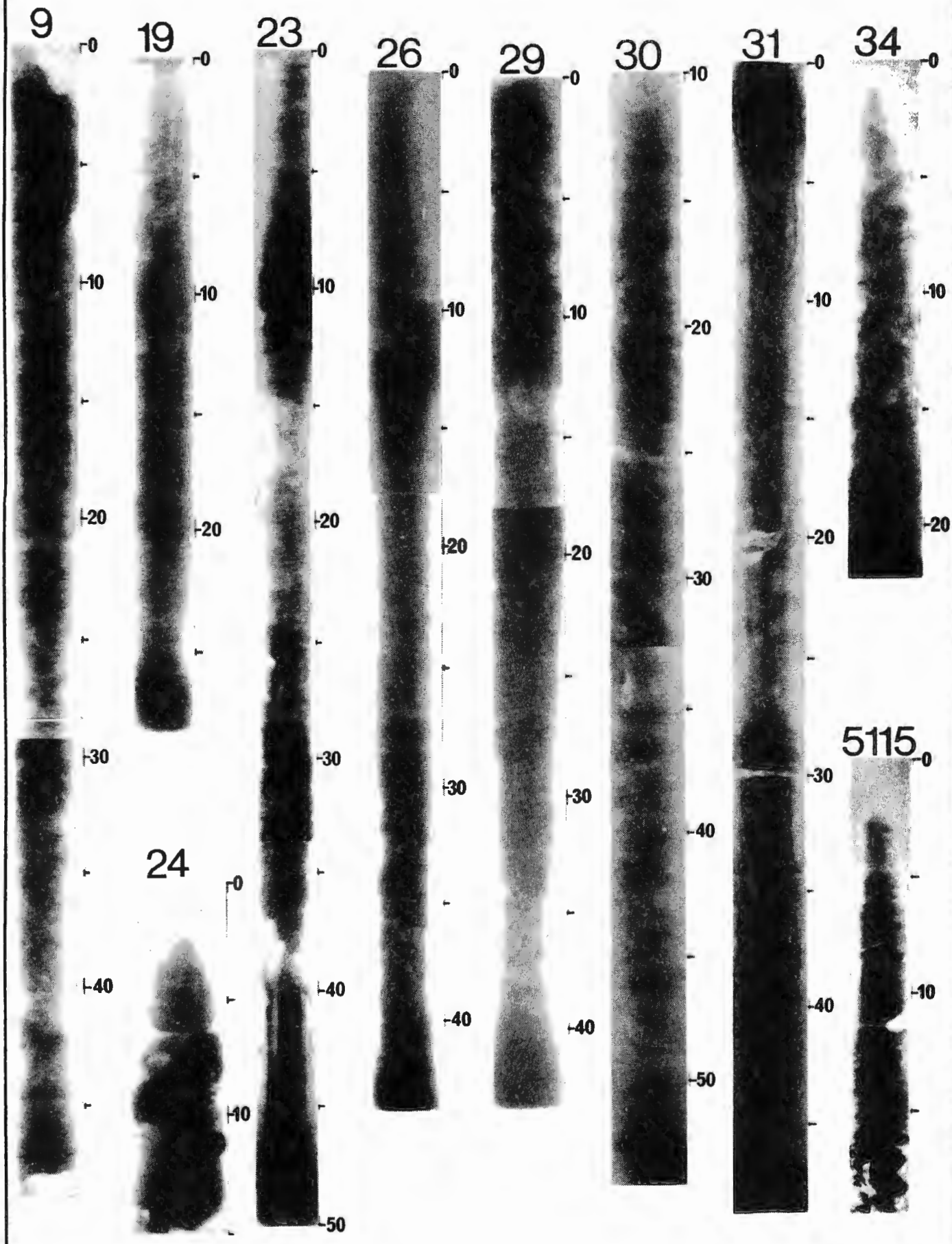

APPENDIX B6 Textural and Geochemical Parameters

CORE	SAMPLE INTERVAL	% GRAVEL	% SAND	% SILT	% CLAY	% $CaCO_3$ TOTAL	% $CaCO_3$ SAND	% $CaCO_3$ MUD	% C_{org}
1	0-2	-	50.8	23.5	25.7	67.8	89.2	45.7	0.27
	6-8	-	54.6	15.0	30.4	69.1	*	*	0.31
	8-10	-	58.2	14.4	27.4	69.1	*	*	0.30
	17½-19½	-	43.4	20.4	36.2	66.4	*	*	0.29
	32-34	-	54.9	23.8	21.3	70.1	91.1	44.6	0.23
	44½-46½	-	53.9	15.8	30.3	57.1	*	*	0.35
	46½-50	-	4.1	43.2	52.7	32.2	*	*	0.23
	55½-57½	-	3.2	38.0	58.8	37.2	40.5	37.1	0.19
5	0-2	-	67.2	9.1	23.7	80.4	88.5	63.8	0.26
	6-8	-	67.7	9.1	23.2	81.8	*	*	0.23
	11½-13½	-	76.8	8.4	14.8	63.7	*	*	0.16
	20-22	-	56.3	18.9	24.8	52.4	*	*	0.19
	27-29	-	64.9	10.4	24.6	51.9	57.7	41.2	0.12
9	0-3	-	62.3	15.7	22.0	71.2	88.7	42.3	0.43
	7-10	-	60.9	12.2	26.9	71.2	*	*	0.29
	19-21	-	65.5	13.9	20.7	70.9	*	*	0.20
	39-41	-	56.4	15.1	28.5	67.8	*	*	0.19
	46-49	-	54.7	20.8	24.5	70.2	88.2	48.4	0.21
12	0-2	-	67.0	11.7	21.3	64.8	71.3	51.6	0.34
	11½-13½	-	70.2	10.2	19.6	60.6	*	*	0.19
13	0-2	-	68.0	2.2	29.8	45.8	44.7	48.1	0.40
	7-9	-	68.0	12.3	19.7	48.3	*	*	0.21
	10½-12½	-	38.4	22.3	39.3	51.4	*	*	0.18
	15-17	-	21.1	24.2	54.7	52.2	*	*	0.22
14	0-2	-	57.4	5.4	37.2	49.5	38.5	64.3	0.35
	10-12	-	67.6	6.4	25.0	50.2	*	*	0.27
	18½-20½	-	57.5	20.0	22.5	62.6	*	*	0.23
15	0-3	-	73.8	9.0	17.2	48.7	39.3	75.2	0.36
	6-8½/9	-	76.0	3.2	20.8	44.3	*	*	0.16
	9½-12½	-	37.2	27.5	35.3	71.3	*	*	0.13
	12½-15½	-	38.4	24.4	37.2	70.3	83.6	62.0	0.17
16	0-2	-	66.2	15.2	18.6	50.6	31.7	87.5	0.44
	10½-12½	-	81.1	6.6	12.3	47.5	*	*	0.24
18	0-2	-	48.3	25.7	26.0	76.2	92.3	61.2	0.41
	10½-12½	-	39.0	27.7	33.3	71.8	*	*	0.38
	20½-22½	-	54.6	13.4	32.0	77.0	*	*	0.34
19	0-2	-	46.2	11.7	42.1	76.7	90.9	64.5	0.47
	6-8	-	48.5	14.8	36.7	80.2	*	*	0.29
	11-13	-	53.2	23.0	23.8	76.2	*	*	0.23
	17-19	-	52.9	16.2	30.9	76.2	*	*	0.23
	22-24	-	45.4	28.0	26.6	76.7	*	*	0.21
	26½-28½	-	50.3	20.5	29.2	75.2	92.5	63.5	0.30

APPENDIX B6 (cont.)

CORE	SAMPLE INTERVAL	% GRAVEL	% SAND	% SILT	% CLAY	% $CaCO_3$ TOTAL	% $CaCO_3$ SAND	% $CaCO_3$ MUD	% C_{org}
20	0-2	-	34.7	28.0	37.3	73.3	92.1	63.3	0.37
	8-10	-	46.3	14.9	38.8	78.2	*	*	0.27
	15-17	-	48.0	20.2	31.8	77.7	*	*	0.29
	21-23	-	59.3	20.9	19.8	78.2	*	*	0.23
21	0-2½	-	58.8	20.5	20.7	49.5	47.3	52.6	0.35
	2½-3½	-	58.7	27.0	14.3	47.5	*	*	0.34
	3½-7	-	64.9	7.5	27.6	47.5	*	*	0.33
23	0-2	-	42.0	24.5	33.5	57.4	64.4	52.3	0.53
	10-12	-	56.3	20.0	23.7	39.6	23.7	60.1	0.23
	12½-14½	-	35.3	24.8	39.9	65.3	*	*	0.34
	22-24	-	21.3	38.0	40.7	58.9	*	*	0.40
	24-26	-	24.2	38.9	36.9	56.4	*	*	0.33
	38-40	-	68.6	26.6	4.8	67.8	*	*	0.23
	48-50	-	45.6	36.2	13.2	68.1	87.4	52.0	0.41
24	0-2	1.1	46.0	21.8	31.1	50.5	44.2	57.7	0.41
	7-8½	-	42.8	26.4	30.8	42.1	*	*	0.22
	8½-10½	1.3	29.3	42.7	26.7	57.4	*	*	0.41
	13-15	0.8	7.9	33.0	58.3	36.1	47.7	35.4	0.41
25	0-2	-	29.9	32.9	37.2	60.4	76.0	53.7	0.63
	10½-12½	0.3	38.2	25.2	36.6	67.4	*	*	0.34
26	0-2	-	34.0	21.2	44.8	61.2	81.2	50.9	0.50
	11-12	-	48.1	27.7	24.2	53.4	*	*	0.28
	13½-15½	-	32.7	35.4	31.9	55.9	*	*	0.35
	18-19½	-	29.8	37.7	32.5	60.6	*	*	0.33
	22½-24	-	24.9	39.3	35.8	56.9	*	*	0.42
	28-30	-	26.9	36.2	36.9	62.7	*	*	0.31
	33½-36	-	32.1	37.9	30.0	65.2	87.2	54.8	0.32
	42-44	-	23.9	33.7	42.4	60.9	86.1	53.0	0.39
27	0-2	-	47.1	21.8	31.1	71.5	88.4	56.4	0.42
	10-12	-	48.2	31.2	20.6	74.5	*	*	0.35
	17-19	-	55.4	21.9	22.7	74.5	*	*	0.21
	29-31	-	43.1	17.5	39.4	59.3	*	*	0.26
	39-41	-	43.2	22.3	34.5	61.9	65.8	58.9	0.26
29	0-2	-	62.0	24.0	14.0	43.4	48.1	35.7	0.36
	3-5	-	70.4	17.0	12.6	52.4	*	*	0.39
	6½/7-7½/9	-	68.6	26.6	4.8	45.7	*	*	0.27
	10½-12½	-	68.0	12.9	19.1	41.7	*	*	0.21
	20½-22½	-	58.0	30.9	11.1	41.0	*	*	0.12
	23½-25½	-	56.6	18.3	25.1	38.6	38.5	38.7	0.26
	31-33	-	52.7	25.4	21.9	43.1	*	*	0.21
	33-35	-	51.0	19.3	13.7	43.2	*	*	0.36
	41½-43½	-	62.6	16.5	20.9	46.3	43.3	51.3	0.26

APPENDIX B6 (cont.)

CORE	SAMPLE INTERVAL	% GRAVEL	% SAND	% SILT	% CLAY	% $CaCO_3$ TOTAL	% $CaCO_3$ SAND	% $CaCO_3$ MUD	% C_{org}
30	0-2	-	14.4	13.7	71.9	22.2	41.6	18.9	0.85
	10-12	-	42.2	23.7	34.1	36.8	*	*	0.55
	20-22	0.5	56.5	21.4	21.6	42.8	*	*	0.56
	24-26	-	56.8	15.4	27.8	40.2	*	*	0.50
	37-39	-	69.0	12.3	18.7	46.1	*	*	0.44
	52-54	-	68.1	11.9	20.0	45.3	39.6	57.5	0.35
31	0-2	-	3.7	39.6	56.7	7.9	21.4	7.4	1.09
	9-11	-	3.1	42.5	54.4	11.1	*	*	1.22
	28-30	-	17.9	30.2	51.9	20.7	*	*	1.08
	42-44	-	23.1	40.9	36.0	28.9	23.7	30.5	1.11
	46½-48½	-	31.2	41.8	27.0	25.6	*	*	1.04
32	0-1½	-	36.8	29.5	33.7	13.0	17.3	10.5	0.62
	2-4	4.5	59.5	22.2	13.8	28.1	28.3	31.3	0.43
34	0-2	-	18.9	32.0	49.1	5.4	9.5	4.4	1.10
	7-9	1.4	29.4	33.2	36.0	11.8	*	*	0.95
	20-22	-	66.9	13.1	20.0	17.7	13.2	26.8	0.49
5115	0-3	-	17.4	31.3	51.3	8.5	14.3	7.3	1.00
	8-10½	-	53.9	13.0	33.1	18.6	*	*	0.64
	10½-12½	-	59.7	24.7	15.6	22.3	*	*	0.42
	12½-14½	-	73.3	16.3	11.4	23.4	*	*	0.31
	14½-16½	-	68.8	24.5	6.7	24.8	*	*	0.41
	16½-19½	-	44.1	26.6	29.3	23.4	18.6	27.2	0.17
5116	0-3	-	13.4	34.9	51.7	23.6	26.3	22.4	0.82
	3-4½/7	-	19.2	33.3	47.5	30.2	*	*	0.72
	4½/7-7	-	23.0	40.9	36.1	32.7	*	*	0.60
	7-10	-	27.3	41.6	31.1	29.7	*	*	0.60
	10-13	-	32.5	37.7	29.8	25.9	19.0	29.2	0.57
5117	0-3	-	9.1	35.8	55.1	13.2	30.0	11.5	1.00
	13-16	-	33.7	31.6	34.7	25.4	30.2	23.0	0.70
	27-30	-	34.8	32.9	32.3	28.9	*	*	0.75
	35.38	-	41.3	33.1	25.6	31.6	33.6	30.2	0.62
	40-43	-	38.0	28.6	33.4	30.7	*	*	0.65
	52.54	-	34.1	33.3	32.6	27.2	*	*	0.67
	66-69	-	43.0	29.2	28.8	31.9	22.6	38.9	0.57
	73-76	-	45.6	34.0	20.4	30.7	*	*	0.49
	84-87	-	27.3	37.2	35.5	30.2	25.3	33.4	0.56
	97-100	-	30.4	35.0	34.6	30.7	*	*	0.70
	101-104	-	32.7	31.6	35.7	28.5	27.7	28.8	0.76
	123-126	-	49.9	28.2	21.9	25.0	17.9	32.2	0.39
	138-140	-	58.1	22.8	19.1	25.4	*	*	0.54
	142-145	-	33.1	28.5	38.4	26.3	19.2	29.8	0.57

APPENDIX B6 (cont.)

CORE	SAMPLE INTERVAL	% GRAVEL	% SAND	% SILT	% CLAY	% $CaCO_3$ TOTAL	% $CaCO_3$ SAND	% $CaCO_3$ MUD	% C_{org}
5119	0-3	-	39.6	30.5	29.9	43.1	50.6	38.2	0.52
	6-9	-	27.0	33.1	39.9	36.2	53.2	29.9	0.62
	27-30	-	45.8	24.4	29.8	44.0	*	*	0.34
	35-38	-	40.0	38.3	21.7	37.1	40.1	35.1	0.62
	55-58	-	29.3	32.6	38.1	35.3	39.2	33.7	0.42
	69-72	-	14.9	34.8	50.3	37.5	46.7	35.9	0.83
	85-88	-	22.5	39.0	38.5	36.6	*	*	0.50
	91-92	-	23.2	43.0	33.8	30.2	28.3	30.8	0.57
	105-108	-	26.9	31.2	41.9	34.5	35.3	34.2	0.59
	125-128	-	25.9	34.5	39.6	37.9	*	*	0.50
	156-159	-	18.9	35.5	45.6	36.2	54.2	32.0	0.57
	175-178	-	26.4	29.3	44.3	37.1	*	*	0.62
	195-200	-	28.6	33.7	37.7	38.8	39.6	38.5	0.61
5120	~200	-	17.8	43.7	38.5	36.6	35.4	36.9	0.39
5121	0-3	-	41.6	26.1	32.3	50.9	69.3	37.9	0.58
	14-17	-	32.9	25.4	41.7	53.0	*	*	0.36
	20-23	-	26.9	26.6	46.5	47.8	79.5	36.1	0.38
	30-33	-	18.9	39.3	41.8	43.1	*	*	0.32
	33-36	-	17.4	38.4	44.2	44.8	62.2	41.1	0.44
	49.52	-	17.9	37.6	44.5	39.5	61.0	34.8	0.45
	67-70	-	21.5	39.2	39.3	45.2	68.4	38.9	0.46
	82-85	-	16.7	35.1	48.2	53.5	*	*	0.36
	91	-	28.5	31.0	40.5	54.0	*	*	0.40
	97-101	-	23.9	26.6	49.5	50.9	78.7	42.2	0.32
	108-111	-	27.3	27.1	45.6	46.1	*	*	0.40
	128-131	-	32.3	32.0	35.7	50.4	72.4	39.9	0.43
	131-134	-	27.3	37.0	35.7	48.3	*	*	0.25
	151-154	-	15.8	33.9	50.3	44.8	70.5	40.0	0.37
	164-167	-	28.7	33.8	37.5	53.9	71.6	46.8	0.30
	177-180	-	25.7	33.6	40.7	45.7	*	*	0.50
	181-184	-	20.0	40.6	39.4	40.5	*	*	0.24
5124	190-193	-	32.5	28.2	39.3	63.7	93.8	49.2	0.31
	202-205	-	31.6	39.2	29.2	59.4	*	*	0.29
5127	0-4	-	38.0	28.3	33.7	69.9	91.1	56.9	0.30
	6-9	-	31.8	21.4	46.8	72.6	*	*	0.33
	15½-18½	-	36.3	31.1	32.6	68.1	*	*	0.30
	18½-22½	-	37.8	30.7	31.5	66.6	*	*	0.31
	27-30	-	40.5	27.1	32.4	68.3	91.5	52.5	0.28
	34-37	-	33.4	9.5	57.1	64.9	*	*	0.27
	47½-50½	-	32.0	25.9	42.1	66.0	89.3	55.1	0.31
5751	0-3	-	62.1	14.7	23.2	81.0	85.6	73.5	0.27
	20-23	-	52.7	20.1	27.2	73.3	82.7	62.8	0.20
	40-43	-	52.8	24.0	23.2	71.6	*	*	0.23
	60-63	-	54.2	24.0	21.8	71.1	*	*	0.32
	81-84	-	42.5	29.2	28.3	70.4	85.6	59.2	0.22
	108-111	-	55.0	22.9	22.1	60.9	70.0	49.8	0.22

APPENDIX B6 (cont.)

CORE	SAMPLE INTERVAL	% GRAVEL	% SAND	% SILT	% CLAY	% $CaCO_3$ TOTAL	% $CaCO_3$ SAND	% $CaCO_3$ MUD	% C_{org}
5751	116-119	-	52.2	18.4	29.4	71.3	89.1	51.9	0.25
	140-143	-	60.2	24.7	15.1	70.9	*	*	0.23
	157-160	-	48.2	24.2	27.6	73.9	91.3	58.1	0.08
	174-177	-	46.9	31.9	21.2	75.7	*	*	0.19
	193-196	-	53.4	25.5	21.1	78.7	92.1	63.4	0.17
	206-209	-	34.1	31.9	34.0	75.2	96.3	64.2	0.13
	221-224	-	52.3	23.8	23.9	77.4	*	*	0.21
	230-233	-	56.2	25.5	18.3	79.1	*	*	0.21
	246-249	-	52.0	18.3	29.7	72.2	94.7	47.8	0.13
5752	0-5	-	84.3	5.7	10.0	54.8	48.1	90.7	0.23
	20-24	-	65.9	17.7	16.4	65.7	*	*	0.25
	32-35	-	51.9	25.2	22.9	54.8	40.4	70.3	0.17
5753	0-3	-	26.9	41.1	32.0	43.2	61.7	36.4	0.58
	6-9	-	32.9	34.0	33.1	47.8	*	*	0.40
	12-15	-	30.8	32.9	36.3	47.4	*	*	0.42
	24-27	-	23.4	35.2	41.4	40.9	54.3	36.8	0.41
	30-33	-	14.0	66.4	19.6	41.4	*	*	0.42
	34-37	-	28.0	31.5	40.5	43.2	*	*	0.49
	40-43	-	24.2	41.9	33.9	47.4	57.0	44.3	0.40
	49-51	*	*	*	*	47.4	*	*	0.40
	55-58	-	17.9	32.7	49.4	42.8	63.0	38.4	0.45
	66-69	-	13.5	29.0	57.5	43.3	65.4	39.8	0.63
	81-84	-	24.4	31.1	44.5	40.0	*	*	0.60
	94-97	-	21.4	35.9	42.7	35.8	*	*	0.46
	100-103	-	19.9	32.4	47.7	35.3	55.1	30.4	0.50
	116-119	-	24.1	27.7	48.2	40.0	*	*	0.47
	136-139	-	29.3	25.0	45.7	45.6	65.0	37.5	0.40
	150-153	-	25.7	34.0	40.3	45.6	*	*	0.46
	166-169	-	25.8	18.3	55.9	44.6	68.3	36.4	0.45
	181-184	-	30.7	32.2	37.1	43.7	*	*	0.42
	200-203	-	31.3	32.7	36.0	41.9	61.9	32.8	0.43
	216-219	-	22.1	31.2	46.7	35.8	*	*	0.47
	235-238	-	28.8	32.5	38.7	41.9	*	*	0.43
	260-263	-	26.9	32.1	41.0	47.0	58.3	42.9	0.34
	278-282	-	26.7	30.3	43.0	42.8	61.3	36.1	0.41

GRAB	% GRAVEL	% SAND	% SAND	% CLAY	% $CaCO_3$ TOTAL	% $CaCO_3$ SAND	% $CaCO_3$ MUD	% C_{org}
4	-	66.4	11.6	22.0	82.7	90.9	66.5	0.23
5726	-	81.1	7.2	11.7	41.7	38.5	55.4	0.31
5727	-	74.8	16.3	8.9	60.0	63.3	50.2	0.27

LEGEND :

% GRAVEL - wt.% gravel (>2mm) in total sediment

% SAND - wt.% sand (63µm-2mm) in total sediment

% SILT - wt.% silt (4µm-63µm) in total sediment

% CLAY - wt.% clay (<4µm) in total sediment

* - not determined

% $CaCO_3$ TOTAL - wt.% $CaCO_3$ in total sediment

% $CaCO_3$ SAND - wt.% $CaCO_3$ in sand fraction

% $CaCO_3$ MUD - wt.% $CaCO_3$ in mud fraction

% C_{org} - wt.% organic carbon in total sediment

APPENDIX B7 Grain Size Parameters of the Total Sand Fraction

CORE	SAMPLE INTERVAL	MEAN	MD	QD	QH	SK	K	%VCS	%CS	%MS	%FS	%VFS	%CSi	%MSi	%FSi	1%
1	0-2	2.51	2.34	0.68	3.78	0.34	-0.47	-	0.1	24.5	52.4	20.4	2.8	-	-	1.30
	6-8	2.50	2.32	0.66	3.67	0.32	-0.29	-	0.4	22.5	54.7	20.3	2.1	-	-	1.30
	8-10	2.40	2.23	0.64	3.56	0.36	-0.09	-	0.4	30.7	50.7	17.3	1.0	-	-	1.20
	17½-19½	2.46	2.30	0.63	3.50	0.30	-0.48	-	0.2	26.4	52.7	20.5	0.2	-	-	1.35
	32-34	2.44	2.28	0.66	3.67	0.36	-0.42	-	0.3	28.1	50.9	19.2	1.5	-	-	1.25
	44½-46½	2.48	2.27	0.70	3.89	0.38	-0.08	-	0.6	25.2	52.0	18.5	3.7	-	-	1.15
	46½-50	3.28	3.46	0.54	2.16	-0.63	1.22	-	0.2	3.1	21.3	72.9	2.4	-	-	1.45
	55½-57½	3.30	3.48	0.59	2.27	-0.60	1.51	-	-	3.2	22.6	68.9	5.3	-	-	1.25
5	0-2	2.39	2.19	0.64	3.56	0.47	0.20	-	-	32.1	50.2	15.7	2.0	-	-	1.35
	6-8	2.31	2.14	0.57	3.00	0.59	0.97	-	0.1	31.9	54.9	12.2	0.9	-	-	1.40
	11½-13½	2.59	2.52	0.50	2.78	0.42	0.82	-	-	8.7	73.9	15.9	1.5	-	-	1.60
	20-22	2.73	2.68	0.51	2.68	0.16	0.60	-	0.1	5.8	69.4	23.0	1.6	-	-	1.55
	27-29	2.69	2.63	0.50	2.63	0.23	0.90	-	0.1	7.0	71.3	19.9	1.6	-	-	1.55
9	0-3	2.41	2.32	0.55	3.06	0.39	0.30	-	-	23.2	61.8	14.7	0.3	-	-	1.45
	7-10	2.41	2.30	0.58	3.22	0.43	0.52	-	0.1	26.2	58.4	13.9	1.4	-	-	1.45
	19-21	2.77	2.61	0.91	4.79	0.61	1.74	-	0.4	15.0	56.4	17.9	6.5	3.8	0.1	1.35
	39-41	2.75	2.54	0.84	4.42	0.71	2.24	-	0.1	12.4	61.7	16.7	6.1	3.0	-	1.45
	46-49	2.93	2.70	0.86	4.30	0.54	0.96	-	-	9.1	54.9	23.5	8.8	3.7	-	1.50
12	0-2	3.00	2.84	0.81	3.86	0.60	1.71	-	-	5.4	54.4	28.8	8.5	2.5	0.4	1.65
	11½-13½	2.88	2.74	0.86	4.30	0.52	1.27	-	-	12.7	50.2	27.0	6.9	3.1	0.1	1.40
13	0-2	3.58	3.52	0.86	2.69	0.10	0.28	-	-	3.6	17.9	50.1	22.0	6.1	0.3	1.55
	7-9	3.42	3.38	0.92	3.29	0.05	0.09	-	0.5	5.7	23.6	45.6	19.0	5.7	-	1.35
	10½-12½	3.58	3.60	1.03	3.22	0.08	0.72	-	-	5.5	25.2	35.3	23.6	10.3	-	1.50
	15-17	3.56	3.43	1.20	3.87	0.14	0.94	-	0.4	6.4	32.5	25.3	19.4	14.9	1.0	1.45
14	0-2	3.49	3.49	0.85	2.83	0.04	0.97	-	0.4	4.4	17.1	56.7	15.9	5.3	0.2	1.45
	10-12	3.46	3.39	0.84	2.90	0.15	0.67	-	0.3	3.8	18.4	56.0	15.8	5.5	0.2	1.55
	18½-20½	3.23	3.03	1.02	4.08	0.32	0.26	-	0.2	7.2	41.8	29.2	14.5	7.3	0.1	1.45
15	0-3	3.63	3.56	0.82	2.34	0.13	0.75	-	0.2	2.3	18.1	50.4	22.6	6.0	0.4	1.60
	6-8½/9	3.70	3.64	0.73	1.97	0.11	1.01	-	-	1.9	8.7	60.9	23.2	5.0	0.3	1.75
	9½-12½	3.66	3.62	0.94	2.61	0.07	0.07	-	0.5	2.2	21.7	43.0	22.8	9.6	0.2	1.50
	12½-15½	3.67	3.52	0.92	2.56	0.21	0.09	-	0.1	2.2	19.1	47.7	21.0	8.9	1.0	1.65
16	0-2	3.44	3.32	0.87	3.00	0.23	0.45	-	0.2	4.0	24.8	49.0	16.2	5.6	0.3	1.45
	10½-12½	3.36	3.19	0.85	3.15	0.35	0.72	-	0.1	3.2	34.2	42.7	14.8	4.5	0.5	1.55
18	0-2	3.34	3.30	1.00	3.70	0.16	-0.14	-	0.4	7.4	29.0	41.7	14.5	7.1	-	1.40
	10½-12½	3.18	2.90	1.13	4.71	0.32	-0.57	-	0.2	10.4	42.3	22.8	14.7	9.4	0.1	1.40
	20½-22½	3.10	2.82	1.08	4.70	0.49	0.16	-	0.1	8.3	49.6	22.6	10.9	7.9	0.7	1.50
19	0-2	3.33	3.10	1.17	4.50	0.26	-0.64	-	0.3	8.7	37.7	25.9	15.2	11.2	1.0	1.35
	6-8	3.20	2.95	1.16	4.83	0.32	-0.36	-	0.6	11.2	39.8	25.0	13.0	9.1	1.2	1.15
	11-13	3.14	2.85	1.11	4.83	0.40	-0.30	-	0.1	9.1	46.9	21.4	13.7	8.2	0.5	1.40
	17-19	3.34	3.13	1.19	4.41	0.26	-0.76	-	0.2	8.5	38.4	23.9	16.5	12.0	0.8	1.45
	22-24	3.36	3.04	1.21	4.48	0.33	-0.60	-	-	7.8	40.8	22.6	15.4	11.3	2.2	1.45
	26½-28½	2.41	2.26	0.74	4.11	0.27	-0.81	-	0.2	36.3	39.6	22.7	1.3	-	-	1.15
20	0-2	2.59	2.56	0.73	4.06	0.01	-0.59	-	0.7	23.3	45.2	29.1	1.8	-	-	1.05
	8-10	2.40	2.30	0.73	4.06	0.15	-0.82	-	1.1	35.2	40.3	22.6	0.7	-	-	0.95
	15-17	2.40	2.27	0.73	4.06	0.18	-0.70	-	0.9	36.5	39.2	22.8	0.6	-	-	0.95
	21-23	2.39	2.23	0.74	4.11	0.25	-0.63	-	0.6	37.2	38.6	22.5	1.2	-	-	1.05

APPENDIX B7 (cont.)

CORE	SAMPLE INTERVAL	MEAN	MD	QD	QH	SK	K	%VCS	%CS	%MS	%FS	%VFS	%CSi	%MSi	%FSi	1%
21	0-2½	2.50	2.46	0.68	3.78	-0.02	0.06	-	1.7	2.0	56.1	21.5	1.1	-	-	0.75
	2½-3½	2.48	2.50	0.69	3.83	-0.02	-0.36	-	2.3	20.6	55.8	20.3	1.1	-	-	0.75
	3½-7	2.78	2.74	0.52	2.74	0.09	0.09	-	0.2	5.1	63.5	29.9	1.3	-	-	1.65
23	0-2	2.84	2.91	0.63	3.32	-0.18	-0.50	-	0.2	12.4	44.7	40.9	1.8	-	-	1.25
	10-12	2.87	2.85	0.50	2.50	-0.27	1.58	-	0.2	6.0	57.3	35.4	1.0	-	-	1.35
	12½-14½	2.68	2.74	0.78	4.11	-0.17	-0.26	-	1.1	21.3	39.7	35.2	2.5	-	-	0.75
	22-24	2.79	2.98	0.83	4.37	-0.18	-1.01	-	1.0	22.6	27.5	45.1	3.8	-	-	0.95
	24-26	2.88	3.09	0.85	4.25	-0.23	-0.82	-	0.9	20.9	24.2	48.2	5.9	-	-	1.00
	38-40	2.60	2.64	0.76	4.22	0.02	-0.94	-	0.5	27.7	38.8	30.9	2.2	-	-	1.10
	48-50	2.61	2.60	0.75	4.17	0.10	-1.08	-	0.2	27.4	39.8	30.4	2.3	-	-	1.20
24	0-2	2.56	2.59	0.76	4.22	-0.48	2.78	-	2.0	14.8	57.9	22.8	1.3	-	-	-0.25
	7-8½	2.84	2.87	0.65	3.42	-0.60	2.79	-	2.4	6.4	53.1	36.4	1.6	-	-	0.50
	8½-10½	2.27	2.65	1.20	6.32	-0.51	-0.07	-	9.6	8.3	44.6	27.6	0.9	-	-	0.60
	13-15	2.47	3.00	1.33	7.39	-0.70	0.95	-	8.0	8.4	26.3	48.6	1.3	-	-	-0.95
25	0-2	2.70	2.83	0.70	3.68	-0.24	-0.38	-	0.7	18.8	41.3	39.2	-	-	-	1.05
	10½-12½	2.78	2.88	0.78	4.11	-0.27	-0.23	-	2.3	16.0	39.7	38.5	3.4	-	-	0.70
26	0-2	2.63	2.62	0.71	3.94	-0.02	-0.54	-	0.8	20.4	48.1	28.9	1.8	-	-	1.05
	11-13	2.69	2.74	0.68	3.58	-0.11	-0.44	-	0.4	17.9	48.1	31.8	1.8	-	-	1.15
	13½-15½	2.83	2.87	0.69	3.63	-0.10	-0.61	-	0.1	15.1	42.6	38.9	3.3	-	-	1.35
	18-19½	2.90	3.03	0.75	3.75	-0.24	-0.53	-	0.7	16.0	31.5	48.4	3.5	-	-	1.15
	22½-24	2.85	2.99	0.70	3.50	-0.22	-0.69	-	0.5	16.0	34.4	47.1	1.9	-	-	1.15
	28-30	2.77	2.87	0.76	4.00	-0.17	-0.63	-	0.6	19.2	37.1	40.0	3.0	-	-	1.05
	33½-36	3.57	3.51	1.29	4.03	0.05	-1.19	-	0.4	10.9	29.0	18.8	23.3	16.8	0.8	1.25
	42-44	2.70	2.79	0.79	4.16	-0.09	-1.10	-	0.5	25.0	34.1	39.5	1.0	-	-	1.10
27	0-2	2.57	2.51	0.72	4.00	0.12	-0.71	-	0.3	23.0	48.5	26.3	1.9	-	-	1.15
	10-12	2.57	2.53	0.71	3.94	0.06	-0.77	-	0.5	25.1	44.9	28.3	1.2	-	-	1.15
	17-19	2.51	2.45	0.70	3.89	0.13	-0.70	-	0.3	27.5	45.6	25.5	1.1	-	-	1.15
	29-31	3.75	3.78	1.17	3.00	0.10	-0.87	-	0.2	6.4	23.7	26.2	27.1	14.4	1.9	1.45
	39-41	3.65	3.67	1.03	2.94	0.07	-0.66	-	-	3.9	26.3	59.3	25.8	10.8	0.3	1.55
29	0-2	2.53	2.55	0.63	3.50	-0.08	0.26	-	0.6	19.8	57.4	21.4	0.6	-	-	1.05
	3-5	2.51	2.59	0.64	3.56	-0.04	-0.96	-	0.5	25.2	50.4	23.9	-	-	-	1.05
	6½/7-7½/9	2.60	2.69	0.62	3.44	-0.15	-0.24	-	0.6	18.5	53.8	26.5	0.7	-	-	1.05
	10½-12½	2.49	2.50	0.59	3.28	-0.02	-0.47	-	0.7	20.7	58.9	19.5	0.1	-	-	1.05
	20½-22½	2.54	2.58	0.61	3.39	-0.17	0.34	-	0.4	19.3	58.3	21.7	0.2	-	-	1.10
	23½-25½	2.62	2.65	0.64	3.56	-0.16	0.23	-	0.5	17.4	53.7	27.8	0.5	-	-	1.10
	31-33	2.58	2.64	0.61	3.39	-0.08	-0.47	-	0.4	19.8	56.0	23.4	0.4	-	-	1.15
	33-35	2.57	2.59	0.63	3.50	-0.07	-0.04	-	0.5	18.7	57.0	22.6	1.2	-	-	1.15
	41½-43½	2.54	2.56	0.64	3.56	-0.15	0.46	-	0.9	19.3	57.1	21.7	1.0	-	-	0.95
30	0-2	2.61	2.72	0.65	3.61	-0.27	-0.06	-	2.1	15.3	55.1	27.5	-	-	-	0.65
	10-12	2.56	2.66	0.73	4.06	-0.46	1.76	-	2.5	16.4	51.9	27.7	0.8	-	-	0.15
	20-22	2.57	2.72	0.74	4.11	-0.42	0.45	-	3.3	16.4	49.5	29.6	0.4	-	-	0.25
	24-26	2.54	2.64	0.72	4.00	-0.44	1.54	-	2.5	18.2	52.4	26.0	0.3	-	-	0.35
	37-39	2.48	2.53	0.71	3.94	-0.24	0.34	-	2.5	20.4	52.9	23.1	0.8	-	-	0.45
	52-54	2.57	2.65	0.73	4.06	-0.42	1.51	-	3.1	15.7	53.1	26.7	1.0	-	-	0.25

APPENDIX B7 (cont.)

CORE	SAMPLE INTERVAL	MEAN	MD	QD	QH	SK	K	%VCS	%CS	%MS	%FS	%VFS	%CSi	%MSi	%FSi	1%
31	0-2	3.24	3.32	0.42	1.68	-0.66	2.10	-	-	2.4	18.4	79.2	-	-	-	1.65
	9-11	3.06	3.21	0.62	2.82	-0.89	3.45	-	1.7	5.6	22.7	70.1	-	-	-	0.70
	28-30	3.25	3.20	0.50	2.00	-0.70	8.00	-	0.3	1.1	18.0	73.9	6.6	-	-	1.45
	42-44	3.37	3.31	0.38	1.41	-0.03	1.11	-	-	0.4	10.7	82.1	6.8	-	-	2.35
	46½-48½	3.41	3.34	0.48	1.71	0.11	-0.20	-	-	0.3	19.6	66.2	13.9	-	-	2.30
32	0-1½	2.42	2.50	0.85	4.72	-0.37	1.06	-	6.1	16.2	53.0	21.8	1.8	-	-	-0.05
	2-4	1.85	2.12	1.20	5.00	-0.22	-0.74	-	15.1	18.4	37.9	16.2	1.0	-	-	-0.55
34	0-2	3.00	3.01	0.49	2.33	-0.58	3.04	-	0.4	4.6	43.4	51.2	0.4	-	-	1.25
	7-9	2.86	2.91	0.64	3.20	-0.65	3.15	-	2.2	7.1	48.4	40.7	1.5	-	-	0.65
	20-22	2.88	2.86	0.49	2.45	-0.26	1.93	-	0.4	4.6	56.5	42.0	1.5	-	-	1.30
5115	0-3	3.16	3.17	0.43	1.79	-0.59	4.67	-	0.3	1.5	25.0	71.3	1.8	-	-	1.65
	8-10½	2.98	3.01	0.54	2.57	-0.68	6.09	-	1.2	4.0	43.5	50.6	0.6	-	-	0.60
	10½-12½	3.04	3.05	0.47	2.14	-0.33	2.09	-	0.2	2.5	42.8	52.7	1.8	-	-	1.55
	12½-14½	2.91	2.90	0.49	2.45	-0.35	1.75	-	0.4	4.6	54.0	40.3	0.7	-	-	1.35
	14½-16½	2.95	3.00	0.50	2.38	-0.39	1.17	-	0.6	4.7	44.6	49.3	1.0	-	-	1.25
	16½-19½	3.18	3.11	0.49	2.04	-0.06	1.32	-	0.1	1.7	36.5	56.0	5.7	-	-	1.75
5116	0-3	3.38	3.38	0.57	2.04	-0.98	8.93	0.1	1.1	1.4	8.5	78.0	11.0	-	-	0.25
	3-4½/7	3.44	3.43	0.47	1.62	-0.31	1.98	-	-	1.4	8.2	78.8	11.7	-	-	1.85
	4½/7-7	3.45	3.43	0.45	1.55	-0.31	1.82	-	-	1.4	7.1	81.0	10.5	-	-	1.80
	7-10	3.24	3.27	0.49	1.96	-0.64	4.22	-	0.4	2.5	20.3	73.2	3.6	-	-	1.55
	10-13	3.23	3.18	0.44	1.76	-0.07	1.28	-	-	1.3	29.3	64.9	4.5	-	-	1.85
5117	0-3	3.16	3.17	0.44	1.83	-0.11	-0.26	-	-	0.4	32.2	65.6	1.8	-	-	2.05
	13-16	3.31	3.30	0.45	1.73	-0.25	1.83	-	0.1	1.2	20.2	72.3	6.2	-	-	1.85
	27-30	3.21	3.21	0.49	2.04	-0.39	1.68	-	0.3	2.6	25.5	67.8	3.9	-	-	1.65
	35-38	3.09	3.15	0.58	2.52	-0.53	2.12	0.1	0.3	5.9	30.2	59.5	3.9	-	-	1.35
	40-43	3.25	3.26	0.45	1.80	-0.48	3.58	-	0.2	1.7	22.8	69.2	6.1	-	-	1.75
	52-54	3.18	3.20	0.50	2.08	-0.64	3.45	-	0.3	3.2	18.8	75.1	2.6	-	-	1.55
	66-69	3.21	3.24	0.49	2.04	-0.47	2.33	-	0.3	2.7	28.5	65.8	2.7	-	-	1.55
	73-76	3.15	3.21	0.57	2.38	-0.56	2.12	-	0.4	5.0	25.9	64.9	3.8	-	-	1.35
	84-87	3.22	3.24	0.50	2.08	-0.55	2.60	-	0.1	3.2	21.7	71.5	8.6	-	-	1.50
	97-100	3.28	3.27	0.47	1.81	-0.51	3.38	-	0.2	1.9	16.0	76.6	5.3	-	-	1.65
	101-104	3.31	3.28	0.36	1.38	0.10	-5.00	-	-	1.2	9.6	85.8	3.4	-	-	1.90
	123-126	3.12	3.07	0.38	1.65	0.01	1.42	-	-	0.7	41.7	55.8	1.8	-	-	2.05
	138-140	3.13	3.10	0.40	1.74	0.07	0.03	-	-	0.7	40.7	56.5	2.1	-	-	2.05
	142-145	3.28	3.25	0.41	1.58	-0.34	2.80	-	-	1.4	16.0	77.9	4.7	-	-	1.80
5119	0-3	2.87	2.96	0.69	3.45	-0.15	-0.77	-	-	15.1	37.2	44.6	3.1	-	-	1.35
	6-9	3.00	3.12	0.67	3.19	-0.45	1.02	-	0.7	9.7	32.1	86.5	3.1	-	-	1.15
	27-30	3.07	3.16	0.57	2.59	-0.36	0.07	-	-	7.2	27.1	63.0	2.7	-	-	1.55
	35-38	2.94	3.04	0.74	3.70	-1.00	9.65	0.2	0.6	10.3	36.4	50.3	2.2	-	-	1.15
	55-58	3.17	3.23	0.55	2.29	-0.37	0.21	-	-	5.7	22.8	67.6	3.9	-	-	1.65
	69-72	3.04	3.17	0.68	3.09	-0.27	-0.71	-	-	13.4	23.1	58.7	4.8	-	-	1.55
	85-88	3.27	3.33	0.54	2.16	-0.60	1.75	-	-	5.5	10.9	78.7	5.0	-	-	1.65
	91-92	3.21	3.25	0.55	2.29	-0.44	0.32	-	-	6.0	17.4	71.8	4.7	-	-	1.60
	105-108	3.23	3.32	0.61	2.54	-0.63	1.87	-	0.4	7.1	15.9	71.4	5.1	-	-	1.45
	125-128	3.14	3.20	0.57	2.48	-0.38	0.35	-	0.1	6.2	26.2	63.4	4.0	-	-	1.55
	156-159	3.08	3.18	0.64	2.78	-0.32	-0.13	-	0.3	9.2	28.8	56.9	5.0	-	-	1.45
	175-178	3.19	3.28	0.58	2.42	-0.45	0.48	-	-	6.9	18.2	70.4	4.5	-	-	1.65
	195-200	3.02	3.09	0.61	2.90	-0.25	-0.23	-	-	9.1	35.2	52.4	3.2	-	-	1.60

APPENDIX B7 (cont.)

CORE	SAMPLE INTERVAL	MEAN	MD	QD	QH	SK	K	%VCS	%CS	%MS	%FS	%VFS	%CSi	%MSi	%FSi	1%
5120	∿200	3.15	3.21	0.63	2.63	-0.29	0.09	-	0.1	6.9	27.2	58.6	7.3	-	-	1.55
5121	0-3	2.84	2.89	0.71	3.74	-0.04	-1.09	-	0.1	14.6	40.0	41.8	3.4	-	-	1.35
	14-17	2.78	2.79	0.75	3.95	0.02	-1.26	-	0.1	20.5	36.5	39.4	3.6	-	-	1.35
	20-23	2.81	2.86	0.73	3.84	-0.02	-1.06	-	0.3	19.6	36.1	40.2	3.7	-	-	1.45
	30-33	2.89	3.08	0.71	3.55	-0.13	-1.33	-	-	18.2	26.6	52.3	2.9	-	-	1.55
	33-36	3.01	3.22	0.72	3.43	-0.21	-1.03	-	-	14.3	23.8	56.7	5.2	-	-	1.55
	49-52	3.06	3.21	0.67	3.05	-0.13	-1.67	-	-	9.8	27.0	58.4	4.8	-	-	1.65
	67-70	3.00	3.16	0.71	3.38	-0.15	-1.18	-	-	13.0	31.1	81.7	5.4	-	-	1.65
	82-85	2.89	3.00	0.75	3.75	-0.05	-1.23	-	-	16.5	33.3	44.2	6.0	-	-	1.45
	91	2.86	2.91	0.73	3.65	0.02	-1.32	-	0.1	16.0	38.8	39.7	5.4	-	-	1.45
	97-101	2.78	2.82	0.71	3.74	0.02	-1.27	-	-	19.9	37.1	41.0	2.0	-	-	1.55
	108-111	2.80	2.86	0.77	4.05	-0.06	-1.32	-	0.1	22.6	35.5	42.1	3.7	-	-	1.40
	128-131	2.85	2.98	0.74	3.70	-0.09	-1.10	-	0.1	19.1	31.8	45.0	4.0	-	-	1.35
	131-134	2.87	2.97	0.77	3.85	-0.16	-0.74	-	1.2	16.8	32.9	44.7	4.5	-	-	0.85
	151-154	3.10	3.16	0.58	2.52	-0.23	-0.39	-	-	5.3	29.5	61.3	3.9	-	-	1.65
	164-167	2.81	2.90	0.72	3.79	-0.06	-1.00	-	0.2	17.2	37.5	41.8	3.4	-	-	1.35
	177-180	2.89	3.05	0.69	3.45	-0.16	-0.82	-	0.1	13.4	33.4	49.7	3.4	-	-	1.35
	181-184	2.91	2.99	0.71	3.55	-0.11	-0.95	-	0.1	13.3	37.2	45.5	3.9	-	-	1.40
5124	190-193	2.94	3.00	0.84	4.20	-0.04	-1.04	-	0.2	17.0	32.9	38.3	11.6	-	-	1.25
	202-205	3.00	3.07	0.79	3.76	-0.05	-1.14	-	-	14.4	32.7	42.3	10.6	-	-	1.45
5127	0-4	2.80	2.78	0.73	3.84	0.11	-0.87	-	0.3	15.5	43.7	36.2	4.4	-	-	1.30
	6-9	2.70	2.67	0.75	3.95	0.10	-0.92	-	0.7	19.8	40.8	36.2	2.5	-	-	1.05
	15½-18½	2.73	2.69	0.76	4.00	0.03	-0.73	0.1	0.5	20.0	42.7	32.9	3.9	-	-	1.25
	18½-22½	2.81	2.78	0.72	3.79	0.07	-0.98	-	0.1	14.8	45.8	34.4	4.9	-	-	1.45
	27-30	2.73	2.61	0.75	3.95	0.13	-0.99	-	0.1	19.8	43.7	31.8	4.6	-	-	1.35
	34-37	2.77	2.76	0.75	3.95	0.14	-0.81	-	0.5	17.5	39.8	38.2	4.1	-	-	1.35
	47½-50½	2.70	2.69	0.73	3.84	0.08	-0.88	-	0.2	19.6	44.9	31.8	3.5	-	-	1.25
5751	0-3	2.69	2.67	0.70	3.68	0.08	-1.08	-	-	21.1	43.6	33.3	1.3	-	-	1.40
	20-23	2.65	2.57	0.68	3.58	0.16	-0.78	-	-	19.8	48.7	28.7	2.7	-	-	1.45
	40-43	2.66	2.62	0.67	3.53	0.12	-0.67	-	0.1	17.8	52.9	26.6	2.6	-	-	1.35
	60-63	2.62	2.49	0.72	4.00	0.11	-0.36	-	0.8	18.9	49.7	27.8	2.9	-	-	1.30
	81-84	2.76	2.73	0.66	3.47	0.09	-0.65	-	0.1	11.4	53.6	31.8	3.2	-	-	1.45
	108-111	2.70	2.64	0.65	3.42	0.10	-0.68	-	0.1	15.4	52.6	29.8	2.1	-	-	1.40
	116-119	2.43	2.33	0.70	3.89	0.12	-0.58	-	0.9	32.1	43-4	23.5	0.1	-	-	1.05
	140-143	2.49	2.32	0.63	3.50	0.38	-0.22	-	-	21.6	55.4	21.3	1.7	-	-	1.45
	157-160	2.73	2.61	0.67	3.53	0.24	-0.50	-	0.1	11.7	57.0	26.6	4.7	-	-	1.50
	174-177	2.74	2.73	0.70	3.68	0.05	-0.64	-	0.2	15.7	46.7	33.4	4.0	-	-	1.35
	193-196	2.76	2.67	0.64	3.37	0.23	-0.50	-	-	9.2	58.4	28.1	4.4	-	-	1.55
	206-209	2.78	2.69	0.62	3.26	0.08	-0.66	-	-	9.8	52.7	35.2	2.2	-	-	1.50
	221-224	2.77	2.70	0.65	3.42	0.16	-0.76	-	-	10.9	55.4	30.1	3.6	-	-	1.55
	230-233	2.64	2.57	0.61	3.39	0.23	-0.48	-	-	15.6	57.6	24.9	1.9	-	-	1.50
	246-249	2.68	2.59	0.63	3.32	0.20	-0.51	-	0.1	13.4	70.0	24.8	3.9	-	-	1.45
5752	0-5	2.58	2.48	0.62	3.44	0.21	-0.23	-	-	11.9	60.5	25.1	2.5	-	-	1.30
	20-24	2.56	2.45	0.69	3.83	0.22	-0.43	-	0.3	21.7	52.0	23.4	2.6	-	-	1.25
	32-35	2.68	2.55	0.72	3.79	0.11	-0.71	-	0.4	17.1	48.9	30.0	3.5	-	-	1.15
5753	0-3	2.87	3.00	0.79	3.95	-0.07	-0.86	-	0.6	16.2	32.2	42.7	7.6	-	-	1.15
	6-9	2.99	3.15	0.75	3.57	-0.27	-0.49	-	0.5	12.6	30.4	50.8	5.7	-	-	1.20
	12-15	3.04	3.17	0.72	3.27	-0.21	-0.79	-	-	11.1	30.2	51.9	6.8	-	-	1.45
	24-27	2.93	3.03	0.70	3.50	-0.29	-0.04	-	0.7	12.0	35.5	48.1	3.8	-	-	1.25
	30-33	3.00	3.18	0.75	3.57	-0.35	-0.27	-	0.8	13.6	21.9	59.1	4.6	-	-	1.15

APPENDIX B7 (cont.)

CORE	SAMPLE INTERVAL	MEAN	MD	QD	QH	SK	K	%VCS	%CS	%MS	%FS	%VFS	%CSi	%MSi	%FSi	1%
5753	34-37	3.02	3.13	0.70	3.33	-0.24	-0.74	-	-	12.1	31.0	52.5	4.4	-	-	1.45
	40-43	3.10	3.20	0.62	2.70	-0.34	-0.05	-	0.2	6.1	29.6	60.3	3.8	-	-	1.45
	55-58	3.03	3.22	0.70	3.33	-0.29	-0.69	-	-	12.5	23.2	59.7	4.6	-	-	1.40
	66-69	3.04	3.14	0.72	3.43	-0.20	-0.90	-	-	13.7	25.8	53.1	7.5	-	-	1.55
	81-84	3.00	3.12	0.68	3.24	-0.26	-0.76	-	-	13.1	27.8	55.8	3.3	-	-	1.45
	94-97	2.96	3.10	0.68	3.24	-0.17	-1.22	-	0.1	13.6	30.2	53.0	3.2	-	-	1.45
	100-103	3.16	3.15	0.63	2.86	-0.25	-0.74	-	-	9.1	29.3	58.4	3.3	-	-	1.65
	116-119	2.96	3.03	0.69	3.29	-0.17	-0.54	-	0.5	10.6	36.6	47.8	4.6	-	-	1.45
	136-139	2.97	3.08	0.71	3.38	-0.25	-0.54	-	0.2	14.0	30.7	51.5	4.2	-	-	1.35
	150-153	3.03	3.13	0.64	3.05	0.18	-0.92	-	-	9.7	32.4	53.7	4.3	-	-	1.65
	166-169	2.88	2.98	0.69	3.45	-0.21	-0.42	-	0.2	15.3	36.4	44.7	3.4	-	-	1.30
	181-184	2.96	3.04	0.68	3.24	-0.14	-0.91	-	0.2	14.4	33.8	47.1	4.6	-	-	1.55
	200-203	3.01	3.12	0.68	3.24	-0.17	-0.88	-	-	12.5	32.5	50.0	5.0	-	-	1.65
	216-219	2.92	3.01	0.70	3.50	-0.18	-0.79	-	0.3	14.8	34.2	47.2	3.5	-	-	1.45
	235-238	2.98	3.07	0.64	3.05	-0.20	-0.82	-	0.1	11.6	33.8	51.1	3.3	-	-	1.50
	260-263	2.88	3.06	0.70	3.50	-0.15	-1.07	-	-	17.0	28.3	52.2	2.4	-	-	1.45
	278-282	2.94	3.06	0.70	3.50	-0.16	-0.93	-	-	14.8	30.8	50.8	3.6	-	-	1.45

GRAB	MEAN	MD	QD	QH	SK	K	%VCS	%CS	%MS	%FS	%VFS	%CSi	%MSi	%FSi	1%
4	2.74	2.77	0.72	3.79	0.03	-1.20	-	0.2	20.5	40.4	35.9	3.2	-	-	1.35
5726	2.71	2.72	0.57	3.00	-0.04	-0.19	-	0.1	11.4	56.3	31.0	1.1	-	-	1.35
5727	2.60	2.52	0.64	3.56	0.13	-0.65	-	0.1	18.4	53.1	26.9	1.5	-	-	1.35

LEGEND :

MEAN - mean settling diameter in phi
MD - median grain size (50th percentile) in phi
QD - standard sorting coefficient in phi
QH - relative sorting coefficient
SK - skewness of the size distribution
K - kurtosis of the size distribution
%VCS - proportion of very coarse sand in the total sediment
%CS - proportion of coarse sand
%MS - proportion of medium sand
%FS - proportion of fine sand
%VFS - proportion of very fine sand
%CSi - proportion of coarse silt
%MSi - proportion of medium silt
%FSi - proportion of fine silt
(%CSi, %MSi, %FSi: see text for explanation)
1% - first percentile in phi

APPENDIX B8 Grain Size Frequencies in the Silt Fraction (∿4-7ϕ)

CORE	SAMPLE INTERVAL	14	13	12	11	10	9	8	7	6	5	4
1	0-2	-	8.5	13.9	13.8	11.9	12.0	9.1	8.3	6.7	6.0	9.8
	6-8	-	5.3	9.2	11.1	13.4	12.4	11.2	11.3	11.0	8.6	6.5
	8-10	-	6.5	11.3	9.7	10.6	11.0	9.9	10.5	8.6	9.1	12.8
	17½-19½	-	2.1	7.2	12.2	13.2	13.0	11.8	11.3	10.5	9.4	9.3
	32-34	-	1.4	9.2	10.7	12.6	13.9	12.6	11.5	10.0	9.7	8.4
	44½-46½	-	8.6	10.6	10.7	12.7	12.6	9.9	9.9	8.8	7.6	8.6
	46½-50	-	6.1	9.5	12.1	13.3	13.1	10.9	10.1	8.5	8.1	8.3
	55½-57½	-	3.1	10.3	10.9	13.4	11.4	10.6	9.9	8.8	10.0	11.6
5	0-2	-	4.2	17.3	14.7	14.8	11.5	9.1	8.8	7.5	6.5	5.6
	6-8	-	3.3	10.3	13.3	13.3	12.6	10.4	10.1	8.5	10.0	8.2
	11½-13½	-	7.1	12.0	10.4	8.6	9.1	14.2	15.4	11.9	5.9	5.4
	20-22	-	1.7	4.8	7.9	11.4	13.6	13.9	13.4	11.4	9.4	12.3
	22-29	0.5	5.4	11.1	10.8	13.5	12.1	10.5	9.6	9.2	9.8	7.5
9	0-3	-	9.3	10.9	16.2	19.6	13.4	8.7	6.6	5.6	5.7	4.0
	7-10	-	3.1	9.0	17.7	15.2	14.3	11.0	10.2	7.8	6.0	5.5
	19-21	-	1.1	9.2	13.4	14.5	14.1	12.2	11.2	9.0	7.7	7.6
	39-41	-	2.0	8.6	8.9	10.8	11.1	11.3	11.8	10.7	11.0	13.8
	46-49	0.5	5.0	7.7	10.3	13.8	11.4	11.0	10.5	10.7	9.0	10.1
12	0-2	-	12.0	8.8	3.3	8.2	8.9	10.8	12.3	12.1	11.8	11.8
	11½-13½	-	2.6	6.9	9.1	11.3	10.2	10.3	11.5	11.1	12.6	14.4
13	0-2	-	12.3	9.8	10.9	8.3	9.0	9.4	11.8	11.1	9.6	7.8
	7-9	-	17.4	15.2	12.3	10.2	9.0	8.7	8.0	6.7	6.0	6.5
	10½-12½	-	11.3	12.2	12.8	11.8	10.5	8.3	7.7	7.4	9.4	8.6
	15-17	-	2.3	3.4	7.7	8.9	10.4	10.2	12.3	13.8	15.3	15.7
14	0-2	-	1.2	5.7	6.5	4.9	11.0	17.2	21.4	15.1	8.8	8.2
	10-12	-	7.6	6.8	8.3	12.0	11.9	11.3	10.8	10.5	10.5	10.3
	18½-20½	-	2.0	7.9	14.0	13.9	12.3	11.0	10.5	9.5	10.6	8.3
15	0-3	-	16.4	10.2	5.4	9.2	8.6	12.0	15.2	11.4	6.1	5.5
	6-8½/9	-	6.0	9.8	14.0	14.4	11.1	11.4	10.4	7.9	8.3	6.7
	9½-12½	-	4.3	7.1	9.7	10.6	11.3	11.0	11.4	11.9	10.7	12.0
	12½-15½	-	9.5	17.0	26.0	20.7	10.8	7.7	4.6	2.7	0.6	0.4
16	0-2	-	2.1	15.6	8.4	9.7	12.6	10.7	11.7	10.1	9.5	9.6
	10½-12½	-	15.6	13.2	11.6	11.7	9.4	7.5	7.9	6.7	7.6	8.8
18	0-2	-	10.9	17.4	14.9	10.7	9.5	8.9	8.0	6.9	6.2	6.6
	10½-12½	-	7.6	16.1	15.7	13.2	11.1	8.6	7.9	6.4	6.8	6.6
	20½-22½	-	4.2	8.5	10.8	13.0	12.0	10.6	10.0	9.2	9.3	12.4

APPENDIX B8 (contd.)

CORE	SAMPLE INTERVAL	14	13	12	11	10	9	8	7	6	5	4
19	0-2	-	3.1	6.9	9.1	10.1	9.0	8.5	10.3	12.5	13.3	17.2
	6-8	-	-	8.4	10.9	12.1	12.1	11.4	11.5	10.5	12.1	11.0
	11-13	0.9	19.3	15.7	13.4	11.3	9.3	7.2	6.9	5.6	5.4	5.0
	17-19	-	3.6	10.2	10.7	16.4	16.4	17.7	13.2	8.5	1.9	1.4
	22-24	-	-	3.2	9.5	11.7	13.7	14.8	13.5	12.1	10.5	11.0
	26½-28½	-	10.8	15.1	13.9	11.8	10.3	8.1	6.8	5.9	8.4	8.9
20	0-2	-	0.4	5.5	9,1	10.9	10.9	11.3	11.6	13.1	15.5	11.7
	8-10	-	5.3	11.2	11.7	10.1	9.0	8.7	11.0	12.8	11.0	9.2
	15-17	-	1.6	3.9	8.7	9.2	10.1	9.7	10.4	11.5	17.6	17.3
	21-23	-	-	1.9	6.2	9.7	11.8	12.2	13.3	12.6	17.0	15.3
21	0-2½	-	14.4	12.7	11.0	10.0	9.4	8.3	9.3	8.0	7.8	9.1
	2½-3½	-	9.8	15.3	11.5	11.3	10.7	8.6	9.6	8.4	7.2	7.6
	3½-7	-	3.0	9.1	11.8	11.8	11.5	12.2	11.6	8.9	8.7	11.4
23	0-2	1.6	13.4	12.9	10.5	11.6	9.6	9.5	8.9	7.7	7.5	6.8
	10-12	-	19.6	15.3	10.1	8.6	8.0	6.4	6.1	6.5	9.2	10.2
	12½-14½	1.9	28.6	16.7	10.7	6.3	5.0	4.8	4.3	5.5	6.5	9.7
	22-24	0.3	8.1	11.6	12.5	10.9	9.7	7.8	7.6	6.8	11.9	12.8
	24-26	-	0.6	8.9	10.5	10.5	8.6	8.3	10.9	14.4	13.5	13.8
	38-40	-	2.0	9.0	13.0	12.1	10.8	11.0	10.3	9.2	9.3	13.3
	48-50	-	4.6	8.8	12.9	13.6	11.4	10.3	10.6	9.0	9.3	9.5
24	0-2	-	4.2	8.6	10.0	10.8	12.1	10.4	10.8	10.1	10.9	12.1
	7-8½	-	8.0	11.1	8.0	10.0	12.2	10.6	11.2	9.9	9.8	9.2
	8½-10½	-	15.4	14.1	12.8	10.4	8.4	7.0	6.6	6.7	8.9	9.7
	13-15	-	4.3	10.5	10.0	10.5	9.4	9.0	8.7	9.2	15.3	13.1
25	0-2	-	4.9	6.8	6.0	9.8	9.2	9.8	12.1	12.4	15.1	13.9
	10½-12½	-	5.8	9.2	9.7	10.6	9.5	9.7	9.9	11.7	11.9	12.2
26	0-2	1.2	4.0	6.6	11.6	11.2	11.4	10.7	11.5	11.7	10.7	9.4
	11-13	-	8.7	9.4	9.8	12.2	9.2	9.8	9.8	9.5	10.8	10.8
	13½-15½	-	3.0	9.4	10.5	9.6	11.4	10.8	10.7	10.2	10.6	13.8
	18-19½	-	18.9	16.0	11.8	9.3	8.3	6.1	6.5	6.3	8.6	8.3
	22½-24	-	9.1	11.1	11.9	11.3	9.3	8.8	9.0	9.2	9.2	11.1
	28-30	0.7	14.2	15.2	12.7	10.5	8.8	7.2	6.9	6.4	8.3	8.7
	33½-36	-	2.1	8.0	12.5	12.4	12.3	10.1	10.4	8.6	8.3	15.3
	42-44	-	12.8	13.8	12.4	11.1	10.4	8.5	8.3	8.5	7.2	7.0
27	0-2	-	3.5	6.6	10.5	11.6	10.8	10.6	11.0	10.5	11.1	13.8
	10-12	-	7.4	15.3	15.2	12.7	10.4	8.9	8.6	8.5	6.8	6.2
	17-19	-	2.9	9.3	10.7	12.6	13.3	12.0	11.8	9.8	9.6	8.0
	29-31	1.1	6.1	13.3	13.5	11.4	10.0	8.5	8.0	7.4	11.0	9.7
	39-41	-	3.9	10.9	11.5	11.7	10.9	9.9	9.3	8.9	10.4	12.6
29	0-2	-	11.2	12.7	11.8	11.8	10.3	9.0	9.5	7.9	7.2	8.6
	3-5	-	19.2	16.3	13.9	10.9	8.0	6.5	6.5	5.4	6.5	6.8
	6½/7-7½/9	-	20.1	20.6	14.1	10.6	8.0	6.3	5.9	4.7	4.7	5.0

APPENDIX B8 (contd.)

CORE	SAMPLE INTERVAL	14	13	12	11	10	9	8	7	6	5	4
29	10½-12½	-	6.3	11.9	11.9	10.9	11.8	11.8	9.7	8.3	7.9	9.5
	20½-22½	-	4.2	11.4	9.9	9.8	9.3	9.3	9.1	10.4	12.3	14.3
	23½-25½	-	1.7	7.8	10.3	10.9	12.0	11.6	11.1	10.3	9.9	14.4
	31-33	0.8	10.3	13.4	11.6	11.0	9.1	8.1	8.3	7.5	9.3	10.6
	33-35	-	9.2	8.7	10.5	8.7	7.5	7.3	7.9	10.1	14.8	14.3
	41½-43½	-	17.3	16.1	11.1	8.2	6.6	6.7	7.2	8.0	7.1	11.7
30	0-2	-	3.8	7.0	6.5	9.8	10.7	10.4	11.1	10.7	13.0	17.0
	10-12	-	1.4	6.8	11.4	11.6	11.9	11.8	12.0	10.8	11.1	11.2
	20-22	-	6.7	9.6	12.9	13.5	12.2	10.2	9.7	7.8	8.6	8.8
	24-26	-	16.2	18.8	10.8	9.0	6.8	6.2	6.2	5.7	8.8	11.5
	37-39	-	17.3	19.4	13.8	10.4	9.3	7.3	5.9	5.6	5.5	5.5
	52-54	-	17.8	17.6	11.9	8.5	7.1	7.5	6.3	5.6	6.1	11.6
31	0-2	-	3.0	8.5	11.6	12.7	12.2	10.7	11.1	9.6	9.9	10.7
	9-11	-	4.8	8.2	12.2	11.5	11.7	10.6	11.0	10.2	9.6	10.2
	28.30	0.4	7.9	11.6	12.4	12.4	11.2	9.7	9.4	8.6	7.7	8.7
	42-44	2.7	16.8	13.9	12.5	10.0	8.7	7.4	7.2	6.5	6.6	7.7
	46½-48½	1.5	15.9	14.4	12.6	11.6	8.6	7.0	7.2	6.6	6.4	7.3
32	0-1¾	-	0.4	8.0	10.7	12.4	11.6	12.3	12.4	11.5	10.9	9.8
	2-4	-	6.8	9.6	8.4	9.8	9.5	10.5	11.1	11.2	11.3	11.8
34	0-2	-	3.2	8.5	12.4	11.6	11.4	10.6	11.0	10.7	10.0	10.6
	7-9	0.2	7.7	13.3	12.8	12.4	11.2	9.7	9.2	8.2	7.2	8.1
	20-22	7.3	19.5	17.0	10.4	9.5	7.2	6.6	6.6	5.6	4.9	5.4
5115	0-3	1.8	7.4	14.1	14.3	12.4	10.8	8.0	8.2	6.8	7.4	8.8
	8-10½	-	17.8	14.8	14.0	9.1	8.5	7.2	7.1	6.3	6.5	8.7
	10½-12½	-	13.0	16.1	12.9	12.6	9.7	8.4	8.3	6.6	6.1	6.3
	12½-14½	0.8	25.4	14.2	12.4	9.8	8.1	6.3	6.2	5.7	5.6	5.5
	14½-16½	-	15.5	15.3	15.3	10.8	8.4	7.8	7.9	7.0	6.2	5.8
	16½-19½	-	4.4	7.7	10.5	9.6	10.0	9.2	10.2	11.1	13.8	13.5
5116	0-3	-	1.5	5.6	6.4	9.7	11.2	11.0	13.1	14.8	13.0	13.7
	3-4½/7	-	2.5	4.6	7.3	8.9	9.7	10.0	11.8	11.9	14.6	18.7
	4½/7-7	-	12.8	15.5	12.3	10.9	9.1	7.9	7.7	7.3	7.5	8.0
	7-10	-	2.6	10.3	12.2	12.8	12.7	10.8	10.4	9.0	9,0	10.2
	10-13	1.3	10.7	15.7	12.7	10.5	9.3	8.0	7.4	6.5	7.9	10.0
5117	0-3	-	1.2	8.6	9.9	9.3	11.1	10.7	11.6	11.8	12.0	13.8
	13-16	-	10.3	11.7	10.9	10.4	9.2	8.4	8.1	8.9	11.4	10.7
	27-30	0.4	9.0	11.4	11.9	11.7	9.9	9.1	9.1	9.0	9.2	9.3
	35-38	-	23.8	17.4	11.5	8.4	6.9	6.0	5.7	5.6	5.9	8.8
	40-43	0.7	13.1	16.1	11.0	10.7	9.0	8.0	7.7	6.8	7.6	9.3
	52-54	1.2	12.6	13.8	11.4	10.3	9.6	8.5	8.3	8.1	9.7	6.5
	66-69	3.0	17.8	15.9	12.1	9.3	7.7	6.5	6.7	7.7	7.3	6.0
	73-76	0.6	19.8	16.1	12.0	9.0	6.9	5.4	5.5	5.0	9.3	10.4

APPENDIX B8 (contd.)

CORE	SAMPLE INTERVAL	14	13	12	11	10	9	8	7	6	5	4
5117	84-87	2.1	20.9	16.7	13.0	9.9	7.7	6.2	5.9	5.4	5.5	6.7
	97-100	-	10.2	18.6	13.2	11.1	8.5	7.0	7.1	7.8	6.7	9.8
	101-104	-	9.8	15.5	10.4	9.3	7.8	7.3	7.4	7.5	9.0	16.0
	123-126	-	22.9	17.6	14.0	10.7	8.0	6.4	5.8	5.3	4.7	4.6
	138-140	-	15.0	16.6	14.0	8.9	8.6	8.1	7.9	6.6	6.5	7.8
	142-145	-	9.8	10.3	10.8	7.9	9.3	8.2	8.4	7.9	11.7	15.7
5119	0-3	-	18.1	14.6	14.1	10.5	9.4	7.6	7.3	6.6	5.7	6.1
	6-9	-	8.6	10.2	11.5	10.5	9.8	8.7	9.3	10.2	9.1	12.1
	27-30	1.8	16.9	17.9	16.3	10.6	7.6	6.5	6.0	5.2	4.9	6.9
	35-38	-	8.2	13.6	14.6	12.4	11.2	10.9	8.5	6.9	7.2	6.5
	55-58	0.3	13.5	15.3	13.2	9.8	7.7	6.6	6.4	6.6	9.1	11.5
	69-72	1.1	5.0	11.7	12.2	11.3	10.7	9.0	9.4	9.4	10.1	9.7
	85-88	-	3.1	9.0	9.1	9.2	10.0	9.9	10.5	10.4	12.3	16.5
	91-92	-	5.2	11.9	13.3	10.2	8.8	7.8	8.1	7.5	9.8	17.4
	105-108	0.8	6.7	10.3	9.5	9.9	10.5	9.8	10.1	9.9	10.4	12.1
	125-128	0.3	11.5	14.0	14.0	12.0	10.5	8.7	8.5	7.5	7.0	6.0
	156-159	-	6.4	9.2	11.1	10.9	9.7	8.5	9.0	10.2	13.5	11.5
	175-178	4.0	17.2	16.6	13.0	10.1	8.1	7.0	6.4	5.6	6.0	6.0
	195-200	-	4.5	9.7	8.4	9.3	9.9	9.5	9.5	9.8	13.0	16.4
5120	~200	0.1	8.7	11.0	9.5	10.7	9.4	8.5	9.6	8.4	10.9	13.2
5121	0-3	-	9.4	16.5	9.4	11.9	8.9	9.1	8.9	7.7	7.8	10.4
	14-17	-	4.8	7.7	9.0	10.7	10.4	9.6	9.8	9.5	10.6	17.9
	20-23	-	5.4	11.7	11.1	11.3	10.5	9.6	9.6	10.1	11.5	9.2
	30-33	-	4.6	8.7	10.8	11.2	10.9	10.6	11.2	12.2	12.2	7.6
	33-36	0.5	10.7	13.4	11.7	10.2	9.3	8.7	9.9	12.0	9.3	4.3
	49-52	-	2.8	8.7	9.8	8.7	9.3	8.5	9.7	10.2	15.5	16.8
	67-70	-	3.1	6.0	9.4	10.0	11.4	10.3	10.9	10.7	12.6	15.6
	82-85	-	11.5	11.5	10.0	9.2	8.9	8.7	9.7	10.1	11.1	9.3
	91	3.1	14.8	12.5	11.5	9.3	8.4	7.8	7.9	7.4	8.2	9.1
	97-101	0.6	11.5	12.8	12.2	10.8	10.3	8.6	8.3	8.2	8.6	8.0
	108-111	-	7.7	14.6	12.1	9.5	8.5	7.8	8.1	8.2	11.5	12.0
	128-131	2.5	12.9	11.5	11.5	9.8	8.5	8.1	8.2	7.4	9.3	10.3
	131-134	0.9	13.9	13.8	12.4	11.0	9.1	8.0	7.8	8.5	8.4	6.2
	151-154	0.2	8.2	11.0	11.7	11.8	11.1	9.9	10.4	10.0	8.7	7.0
	164-167	-	6.0	9.4	7.7	7.7	6.6	7.0	7.5	12.5	16.6	19.0
	177-180	0.7	11.4	11.6	12.0	10.2	8.2	7.7	7.9	8.8	11.4	10.1
	181-184	-	6.4	11.7	13.7	11.1	11.1	8.7	8.6	7.4	9.9	11.4
5124	190-193	-	12.8	16.0	14.9	10.6	10.3	8.0	7.5	6.4	6.5	7.0
	202-205	-	3.8	9.2	10.2	10.8	10.0	8.9	9.5	9.7	11.7	16.2
5127	0-4	-	7.5	13.6	10.4	9.9	8.3	7.5	8.0	9.9	9.5	15.4
	6-9	-	9.7	11.5	11.1	13.3	10.7	10.2	10.3	8.2	7.2	7.8
	15½-18½	-	2.0	9.6	12.0	13.6	13.1	11.4	10.7	9.4	8.6	9.6
	18½-22½	-	4.9	8.1	9.4	11.9	11.8	11.0	11.3	10.3	10.9	10.4
	27-30	-	-	5.0	10.7	11.3	11.8	12.4	13.8	13.4	11.6	10.0
	34-37	-	6.2	10.1	10.5	10.3	11.7	10.9	10.1	9.8	9.6	10.8
	47½-50½	-	2.4	8.1	9.8	11.9	12.3	10.9	10.7	9.3	8.9	15.7

APPENDIX B8 (contd.)

CORE	SAMPLE INTERVAL	14	13	12	11	10	9	8	7	6	5	4
5751	0-3	-	1.1	9.5	12.8	14.1	14.1	11.2	10.6	9.1	8.5	9.0
	20-23	-	7.1	9.6	14.8	14.3	14.6	10.3	8.7	7.2	7.6	5.8
	40-43	-	1.2	13.4	15.5	13.1	11.8	10.2	9.6	7.7	7.8	9.7
	60-63	-	4.0	12.6	16.6	14.5	12.8	10.2	9.2	7.9	5.9	6.3
	81-84	-	14.0	14.9	15.8	12.0	11.0	8.1	7.6	6.4	5.2	5.0
	108-111	-	12.7	16.0	13.4	12.5	9.7	8.3	7.3	6.2	5.3	8.6
	116-119	-	2.8	9.7	13.9	12.1	9.9	10.6	8.9	8.3	9.2	14.6
	140-143	-	12.1	15.7	12.4	12.3	11.3	9.7	8.5	7.0	5.7	5.3
	157-160	-	3.4	10.6	11.8	13.5	13.2	10.8	9.6	9.6	7.9	9.6
	174-177	-	2.2	13.5	13.6	14.6	13.3	10.5	9.6	7.9	6.8	8.0
	193-196	-	2.5	10.1	11.4	13.4	13.0	11.0	10.3	8.8	10.2	9.3
	206-209	-	5.6	13.7	13.2	15.0	12.1	10.3	9.6	8.3	6.4	5.8
	221-224	-	3.6	7.2	11.2	12.6	12.3	11.0	10.5	9.9	12.2	9.5
	230-233	-	1.1	10.7	11.5	11.9	12.1	10.5	10.1	9.0	9.7	13.4
	246-249	-	2.3	10.8	13.3	16.0	14.1	10.9	10.1	8.2	7.3	7.0
5752	0-5	-	28.4	20.9	13.5	9.1	6.5	5.1	5.3	4.3	3.6	3.3
	20-24	-	2.6	8.1	9.7	12.0	13.8	11.2	11.4	10.5	9.8	10.9
	32-35	-	10.9	12.7	11.1	12.2	9.8	8.8	8.8	7.8	7.6	10.3
5753	0-3	-	6.6	9.5	7.5	14.0	18.5	18.5	13.4	8.3	2.2	1.5
	6-9	-	17.1	16.2	13.3	10.9	9.4	7.8	6.5	5.5	5.9	7.4
	12-15	1.5	11.0	13.1	12.5	10.7	9.9	8.7	8.6	9.0	8.1	6.9
	24-27	-	11.4	13.8	14.1	13.7	11.6	9.4	8.3	7.4	5.9	4.4
	30-33	-	13.7	16.5	15.7	11.3	10.3	7.8	7.1	6.0	5.7	5.9
	34-37	-	6.3	10.5	12.2	11.6	11.0	10.2	11.0	12.2	10.0	5.0
	40-43	1.6	14.5	13.8	12.5	11.0	9.8	8.7	8.5	8.1	6.8	4.7
	55-58	-	1.4	4.3	11.4	26.0	17.3	17.9	12.5	7.4	1.3	0.5
	66-69	-	9.4	9.9	10.2	9.8	11.1	16.0	14.9	10.7	4.3	3.7
	81-84	-	4.2	8.4	10.4	10.6	10.8	11.4	13.3	14.5	9.9	6.5
	94-97	-	6.9	9.0	10.4	11.3	11.2	10.8	12.1	12.9	8.7	6.7
	100-103	-	8.3	10.7	18.7	23.0	12.4	12.3	8.8	4.7	0.8	0.3
	116-119	-	5.7	10.2	10.6	10.9	11.1	10.9	11.0	10.4	10.3	8.9
	136-139	-	3.8	7.6	13.6	10.8	10.6	9.6	10.1	10.6	13.0	10.3
	150-153	-	9.6	11.6	11.7	10.9	9.9	8.9	9.1	9.5	11.2	7.6
	166-169	-	3.4	9.0	10.5	8.9	10.2	10.2	11.6	10.7	11.4	14.1
	181-184	-	9.3	14.6	12.6	12.4	10.0	8.5	8.0	8.3	7.5	8.8
	200-203	0.1	7.6	10.0	11.8	9.4	9.8	9.8	10.9	11.1	10.8	8.7
	216-219	-	7.3	7.3	8.6	10.5	10.8	10.5	11.2	11.7	11.2	10.9
	235-238	-	6.4	10.1	12.6	16.2	14.0	16.7	13.1	8.2	1.9	0.8
	260-263	-	9.1	10.8	11.1	10.7	10.0	9.1	9.3	10.0	11.5	8.3
	278-282	-	9.3	11.4	9.4	11.4	8.4	8.7	9.6	8.7	10.0	13.1

APPENDIX B8 (contd.)

GRAB	14	13	12	11	10	9	8	7	6	5	4
4	-	12.5	19.6	18.9	12.3	12.2	8.0	6.7	4.5	3.1	2.2
5726	-	11.2	11.6	11.2	10.5	11.1	9.9	9.6	8.3	7.8	8.8
5727	-	8.7	14.0	13.1	14.0	9.5	11.0	9.5	7.1	6.3	6.8

LEGEND :

Analyses conducted on Coulter Counter Model TA II using channels 14 to 4 inclusive

14 - Particle volume % in the range 3.3ϕ - 3.63ϕ
13 - Particle volume % in the range 3.63ϕ - 3.97ϕ
12 - Particle volume % in the range 3.97ϕ - 4.3ϕ
11 - Particle volume % in the range 4.3ϕ - 4.63ϕ
10 - Particle volume % in the range 4.63ϕ - 4.96ϕ
9 - Particle volume % in the range 4.96ϕ - 5.3ϕ
8 - Particle volume % in the range 5.3ϕ - 5.63ϕ
7 - Particle volume % in the range 5.63ϕ - 5.97ϕ
6 - Particle volume % in the range 5.97ϕ - 6.3ϕ
5 - Particle volume % in the range 6.3ϕ - 6.63ϕ
4 - Particle volume % in the range 6.63ϕ - 6.96ϕ

APPENDIX B9 Upper Slope Grab Samples - Location, Texture, Chemistry and Clay Mineralogy[1]

STATION	LAT. (S)	LONG. (E)	WATER DEPTH(m)	% GRAVEL	% SAND	% SILT	% CLAY	% $CaCO_3$	% C_{org}	SMECT+	ILL+	KAOL+
4121	28°05.4'	32°43.2'	692	0.5	59.5	25.0	15.0	41.0	0.5	70	19	11
4129	28°18.6'	32°39.6'	730	0.0	20.7	26.2	53.1	25.2	0.3	*	*	*
4130	28°28.2'	32°36.0'	753	0.0	26.7	26.3	47.1	20.7	0.2	*	*	*
4139	28°49.8'	32°26.4'	840	0.2	78.5	10.8	10.5	33.4	0.1	*	*	*
4150	29°52.2'	31°19.8'	377	*	*	*	*	*	*	*	*	*
4151	29°52.2'	31°27.0'	411	0.0	24.0	17.8	58.2	20.2	0.6	*	*	*
4152	29°57.6'	31°36.0'	650	0.0	58.9	16.5	24.6	24.1	0.4	17	39	45
4153	30°07.8'	31°38.4'	920	*	*	*	*	*	*	*	*	*
4155	29°57.6'	31°45.6'	931	0.0	80.5	13.2	6.3	29.0	0.3	*	*	*
4156	29°52.2'	31°37.2'	591	0.2	69.6	15.5	14.7	21.5	0.5	*	*	*
4171	29°43.2'	31°45.6'	669	0.2	75.4	13.1	11.3	18.8	0.3	*	*	*
4172	29°36.0'	31°52.8'	740	0.0	35.2	30.7	34.1	2.4	0.9	38	39	23
4189	29°28.2'	32°00.0'	810	0.0	40.5	32.2	27.3	22.2	0.3	*	*	*
4190	29°19.2'	32°07.2'	1195	1.4	55.8	18.9	23.9	*	*	37	35	28
4203	29°13.2'	32°10.8'	779	0.0	64.3	16.3	19.4	11.2	0.3	*	*	*
4212	29°40.8'	32°03.0'	1002	2.2	58.4	26.9	12.6	35.4	0.2	*	*	*
4213	29°51.0'	31°58.2'	1118	0.1	70.5	15.1	14.3	27.5	0.3	39	28	33
4214	30°02.4'	31°54.0'	1111	0.0	71.4	12.9	15.7	21.1	0.1	*	*	*
4234	30°53.4'	30°35.4'	1435	0.0	46.1	18.2	35.7	*	*	*	*	*

LEGEND:

1 - data from Birch (in press, a and b)

% GRAVEL - wt. % gravel (>2 mm) in total sediment

% SAND - wt. % sand (63µm-2 mm) in total sediment

% SILT - wt. % silt (4µm-63µm) in total sediment

% CLAY - wt. % clay (<4µm) in total sediment

% $CaCO_3$ - wt. % $CaCO_3$ in total sediment

% C_{org} - wt. % organic carbon in total sediment

SMECT - % abundance of smectite (montmorillonite) in the clay fraction (<2µm)

ILL - % abundance of illite in the clay fraction (<2µm)

KAOL - % abundance of kaolinite in the clay fraction (<2µm)

+ - semi-quantitative clay mineralogy analyses (X-ray diffraction)

* - not determined

APPENDIX B10 Component Modal Analyses (Volume %) of the Sand Fraction (63μm-2mm)

CORE	SAMPLE INTERVAL	BIOGENIC						TERRIGENOUS					AUTH
		Benth	Plank	Brok	Spic	Moll	Other	Qtz	Feld	Mica	Heav	Opaq	Glauc
1	0-2	0.7	78.3	10.3	-	-	0.3	6.0	1.7	0.7	1.0	1.0	-
	32-34	-	77.3	10.0	1.0	-	-	7.0	1.0	0.3	2.7	0.7	-
	55½-57½	-	20.0	58.3	-	-	0.3	16.3	2.0	-	3.0	-	-
5	0-2	0.3	81.3	6.0	-	-	-	9.0	1.0	-	2.0	0.3	-
	27-29	0.3	36.3	6.3	0.3	-	1.3	32.3	12.0	0.7	9.0	1.3	-
9	0-3	0.3	65.3	16.7	-	1.0	-	9.3	3.3	0.3	3.3	0.3	-
	46-49	1.3	59.3	19.7	-	-	0.3	13.3	4.3	0.3	0.7	0.7	-
12	0-2	0.3	42.0	7.0	-	-	0.7	36.0	7.0	-	5.7	1.3	-
13	0-2	0.3	33.7	5.3	-	0.7	-	41.3	7.7	-	9.7	1.0	0.3
14	0-2	-	43.7	2.3	-	-	1.0	36.0	7.3	0.3	8.0	1.3	-
15	0-3	-	46.7	4.7	1.0	1.0	1.3	28.3	-	9.0	-	7.3	-
	12½-15½	0.3	82.0	11.3	-	-	-	3.3	1.0	-	1.3	-	-
16	0-2	1.3	40.0	4.7	-	1.3	2.0	35.3	7.3	0.3	6.3	1.3	-
18	0-2	0.3	84.7	6.0	-	-	0.3	5.7	-	2.3	-	0.7	-
19	0-2	-	86.3	9.3	-	-	0.3	1.3	1.7	-	1.0	-	-
	22-24	-	83.0	11.0	-	-	-	4.3	-	0.7	-	0.7	0.3
20	0-2	-	88.3	4.7	0.3	-	1.0	3.7	0.7	-	1.3	-	-
21	0-2½	0.3	44.7	5.0	-	1.0	-	34.7	10.0	-	3.7	0.7	-
23	0-2	-	56.3	7.7	-	2.0	2.7	23.0	3.3	-	3.7	0.3	-
	10-12	0.7	22.0	3.7	0.3	0.7	1.7	50.3	7.0	-	3.3	0.3	-
	48-50	-	83.0	5.0	1.0	-	0.3	6.7	2.3	-	1.3	0.3	-
24	0-2	0.3	42.0	3.3	-	1.3	1.7	35.3	9.0	-	6.3	0.7	-
	13-15	1.7	34.0	6.7	-	0.3	1.0	46.3	5.0	-	4.7	-	0.3
25	0-2	0.7	74.0	5.3	0.7	-	0.7	10.0	5.7	-	2.7	0.3	-
26	0-2	1.3	76.0	5.7	0.3	-	0.3	10.7	3.3	1.0	1.3	-	-
	33½-36	0.7	85.0	7.0	0.3	-	-	4.0	1.7	-	1.3	-	-
	42-44	-	89.7	4.7	-	-	-	4.3	0.3	-	1.0	-	-
27	0-2	1.0	84.3	7.3	-	-	-	5.7	0.7	-	1.0	-	-
	39-41	-	59.3	15.0	-	-	-	15.6	6.7	-	2.7	0.7	-
29	0-2	0.7	37.0	8.0	0.3	1.3	2.7	33.3	11.0	0.3	3.3	2.0	0.3
	23½-25½	-	18.3	10.3	0.7	-	1.0	49.3	13.0	0.3	5.7	1.0	0.3
	41½-43½	1.0	24.0	5.3	0.7	1.3	0.7	52.7	8.0	-	5.7	0.7	-
30	0-2	0.7	33.0	5.3	-	0.7	4.0	43.7	6.0	1.3	14.0	2.0	0.3
	52-54	1.3	17.7	16.7	2.3	1.3	3.7	38.0	5.0	1.3	11.0	1.3	0.3

APPENDIX B10 (contd.)

CORE	SAMPLE INTERVAL	BIOGENIC						TERRIGENOUS					AUTH
		Benth	Plank	Brok	Spic	Moll	Other	Qtz	Feld	Mica	Heav	Opaq	Glauc
31	0-2	0.7	21.0	3.0	1.3	-	1.3	46.3	11.0	-	12.0	2.7	0.3
	42-44	2.7	15.0	3.3	3.0	0.7	1.3	50.7	11.3	0.3	9.7	1.7	0.3
32	0-1½	1.7	8.3	4.7	-	2.3	-	55.3	12.3	-	9.3	2.3	3.3
	2-4	0.7	3.0	2.7	0.3	4.3	1.7	64.3	7.7	-	11.3	3.0	1.0
34	0-2	1.0	6.0	6.0	-	3.0	2.3	60.7	8.0	-	7.3	0.3	5.4
	20-22	0.7	3.7	3.0	1.0	0.7	0.3	61.0	13.3	-	11.7	1.3	3.3
5115	0-3	0.7	12.0	5.0	0.7	-	-	58.7	12.7	-	9.7	0.7	-
	16½-19½	2.0	12.7	2.7	-	-	4.3	61.0	6.3	-	10.7	0.3	-
5116	0-3	0.7	21.3	4.0	2.7	0.3	0.3	48.0	6.7	3.3	10.0	2.7	-
	10-13	1.0	16.3	5.7	0.3	0.3	1.7	55.0	10.7	-	7.3	0.7	1.0
5117	3	1.0	9.7	1.3	1.0	-	0.7	65.3	9.3	1.0	9.0	1.7	-
	17	1.3	21.7	4.0	6.7	0.7	1.7	42.0	5.7	2.3	13.7	0.3	-
	38	1.3	16.3	3.3	2.0	0.3	2.7	53.0	7.3	0.7	11.7	1.3	-
	66	1.3	20.3	6.0	1.7	0.3	4.0	41.0	12.3	0.7	11.0	1.3	0.3
	87	0.7	15.7	6.0	1.7	0.7	2.3	51.0	10.3	0.3	9.7	1.0	0.7
	101	1.0	14.7	3.3	0.3	-	2.7	55.0	10.7	-	11.3	1.0	-
	122	1.3	14.3	1.7	-	1.7	-	61.3	6.0	-	13.3	0.3	-
	143	1.0	12.0	2.3	1.7	-	0.7	60.0	9.7	-	11.7	0.3	0.7
5119	5	1.0	38.7	3.7	1.3	-	1.0	37.0	5.0	3.0	9.0	0.3	-
	12	1.0	39.7	4.3	1.0	-	1.0	38.3	5.3	0.3	9.0	-	-
	33	5.3	16.0	5.3	1.0	3.3	1.3	47.7	11.7	-	8.0	0.3	-
	54	0.7	21.0	2.7	2.0	0.7	3.3	51.7	6.0	-	-	1.0	0.3
	75	1.3	45.3	5.3	3.0	-	0.3	30.3	5.7	1.3	7.0	0.3	-
	91-92	0.3	28.7	4.0	-	-	0.3	43.3	7.0	-	14.7	1.3	0.3
	110	1.0	36.0	8.0	1.3	-	1.3	37.3	8.3	0.7	4.7	0.7	0.7
	159	3.3	39.7	4.7	4.0	-	0.7	33.0	5.7	2.7	6.3	0.7	-
	194	1.7	49.3	4.0	0.7	-	2.3	29.0	4.3	-	7.7	0.7	0.3
5120	∿200	1.0	63.7	4.0	1.3	-	0.3	18.7	2.3	1.3	7.0	0.3	-
5121	3	0.3	65.0	4.7	0.7	-	-	17.6	5.7	-	5.3	0.7	-
	24	-	62.3	6.3	-	-	0.7	19.6	6.0	0.3	4.7	-	-
	38	-	62.0	5.7	1.0	-	1.0	17.7	5.0	2.3	5.0	0.3	-
	45	-	61.3	4.3	0.7	-	-	18.0	4.0	4.3	6.3	1.0	-
	73	0.7	45.7	3.7	2.0	-	-	30.0	9.3	0.3	8.3	-	-
	101	-	53.7	8.0	2.0	-	1.0	24.7	2.0	0.3	7.3	-	-
	121	-	63.3	3.3	0.7	-	0.3	20.7	6.7	2.3	2.7	-	-
	142	1.0	81.7	3.3	1.3	-	0.7	4.7	1.7	-	5.7	-	-
	170	0.7	53.7	4.0	1.3	-	0.7	26.7	4.7	-	8.3	-	-
5124	190-193	-	81.0	10.0	1.0	-	-	7.0	-	-	-	0.3	-
5127	0-4	-	84.7	7.7	-	-	-	7.0	-	-	-	0.7	-
	27-30	0.3	84.0	10.3	0.7	-	-	2.7	1.0	-	0.3	0.7	-
	47½-50½	0.3	78.3	5.0	-	-	0.3	8.3	3.0	-	4.0	0.3	-

APPENDIX B10 (contd.)

CORE	SAMPLE INTERVAL	BIOGENIC						TERRIGENOUS					AUTH
		Benth	Plank	Brok	Spic	Moll	Other	Qtz	Feld	Mica	Heav	Opaq	Glauc
5751	10	-	91.0	4.3	-	-	0.7	2.0	1.0	-	1.0	-	-
	24	0.3	84.0	4.3	-	-	0.3	7.3	2.0	0.3	1.3	-	-
	80	0.3	72.3	2.7	0.3	-	-	20.0	1.7	-	2.7	-	-
	108	1.0	59.0	3.3	0.3	-	-	22.7	7.7	-	5.7	0.3	-
	129	-	71.0	4.0	0.3	-	-	15.7	4.0	-	4.7	0.3	-
	157	0.7	83.0	10.7	1.0	-	-	2.6	0.7	-	1.3	-	-
	185	-	93.3	4.7	-	-	-	1.7	-	-	0.3	-	-
	213	0.3	86.7	8.7	0.3	-	-	3.3	-	-	0.7	-	-
	241	0.7	89.0	6.0	-	-	-	3.0	0.3	-	1.0	-	-
5752	0-5	-	35.7	11.0	2.3	-	-	30.0	7.7	1.0	12.3	-	-
	32-35	0.3	57.7	4.0	0.7	-	1.3	22.3	7.7	-	5.7	0.3	-
5753	2	6.0	53.3	9.0	0.3	0.3	2.7	19.7	3.0	-	5.7	-	-
	20	1.0	60.0	6.3	0.7	0.7	1.3	17.7	3.0	-	9.3	-	-
	40	0.7	49.3	7.0	0.3	0.3	3.0	30.0	3.7	-	5.0	-	0.7
	50	2.0	50.0	7.3	2.0	2.3	0.3	23.0	5.7	-	7.0	0.3	-
	70	1.0	47.3	6.0	0.3	-	2.0	29.0	6.0	0.7	7.7	-	-
	100	2.0	44.0	4.0	1.0	0.7	0.7	28.7	9.3	1.3	8.0	0.3	-
	130	1.0	46.3	5.0	1.3	0.3	0.3	24.6	8.0	-	2.7	0.3	-
	170	1.0	66.7	4.7	1.3	-	1.3	18.0	4.3	0.7	1.7	0.3	-
	210	1.0	46.3	5.7	3.7	-	2.0	25.6	5.3	1.0	7.0	2.3	-
	250	1.3	47.3	5.7	0.7	0.3	2.0	28.6	4.7	-	7.0	1.3	-
	280	1.7	52.7	3.7	1.7	-	1.3	28.0	6.0	0.7	3.7	0.7	-

GRAB	BIOGENIC						TERRIGENOUS					AUTH
	Benth	Plank	Brok	Spic	Moll	Other	Qtz	Feld	Mica	Heav	Opaq	Glauc
4	-	50.7	19.3	-	-	-	20.3	2.0	1.0	3.7	3.0	-
5726	0.3	25.0	4.7	-	0.7	-	56.7	4.0	-	6.7	2.0	-
5727	0.3	46.0	7.7	0.3	0.7	1.7	31.7	5.3	-	5.3	0.3	0.7

LEGEND:

Benth	-	Benthic Foraminifera
Plank	-	Planktic Foraminifera
Brok	-	Broken Planktic Foraminifera
Spic	-	Sponge spicules
Moll	-	Mollusc valves and debris
Other	-	Other biogenic components (Ostracods, Radiolaria, Echinoid Fragments etc)
Qtz	-	Quartz
Feld	-	Feldspar
Mica	-	Micaceous minerals
Heav	-	Heavy minerals (Garnet, Pyroxene, Amphibole etc)
Opaq	-	Opaque minerals (Magnetite, Ilmenite etc)
Glauc	-	Glauconite

Minimum of 300 grains counted for each sample

APPENDIX B11 Component Modal Analyses (Volume %) of the Sand Fraction (63μm-2mm)*

	BIOGENIC						TERRIGENOUS						AUTH
SAMPLE	Benth	Plank	Brok	Spic	Moll	Other	Qtz	Feld	Mica	Heav	Opaq	Rock	Glauc
2	Tr	95.0	4.0	-	-	1.0	Tr	-	-	Tr	-	-	-
3	1.0	85.0	12.0	-	-	-	2.0	Tr	-	Tr	-	-	-
6	-	60.0	22.0	-	-	-	13.0	1.0	-	3.0	1.0	-	-
7	1.0	75.0	7.0	1.0	-	1.0	13.0	1.0	-	1.0	Tr	-	Tr
8	4.0	63.0	10.0	-	2.0	2.0	18.0	-	-	1.0	Tr	-	-
10	3.0	47.0	45.0	-	-	-	4.0	1.0	-	-	-	-	-
11	Tr	77.0	19.0	-	-	-	4.0	-	-	Tr	-	-	-
17	1.0	61.0	19.0	-	-	-	6.0	10.0	-	3.0	Tr	-	-
22	-	79.0	16.0	-	-	-	5.0	-	-	-	-	-	-
28	2.0	73.0	20.0	-	1.0	-	3.0	-	-	1.0	Tr	-	-
33	3.0	2.0	9.0	-	8.0	1.0	29.0	11.0	-	11.0	4.0	15.0	7.0
5118	3.0	16.0	5.0	2.0	-	-	58.0	7.0	-	9.0	Tr	-	-
5122	Tr	14.0	9.0	1.0	-	1.0	56.0	10.0	-	9.0	Tr	-	-
5728	Tr	18.0	7.0	1.0	1.0	Tr	49.0	16.0	-	6.0	1.0	-	1.0
5748	-	83.0	10.0	-	Tr	-	6.0	-	-	1.0	Tr	-	-
5750	1.0	88.0	10.0	-	-	-	1.0	-	-	-	-	-	-
5754	2.0	83.0	4.0	-	-	-	6.0	2.0	-	2.0	Tr	-	-
5755	0.5	72.0	4.0	-	-	-	17.0	4.0	-	1.5	1.0	-	-

LEGEND:

*	-	Unsuccessful core stations - samples may have been partly winnowed during recovery process
Benth	-	Benthic Foraminifera
Plank	-	Planktic Foraminifera
Brok	-	Broken Planktic Foraminifera
Spic	-	Sponge spicules
Moll	-	Mollusc valves and debris
Other	-	Other biogenic components (Ostracods, Radiolaria, Echinoid Fragments etc)
Qtz	-	Quartz
Feld	-	Feldspar
Mica	-	Micaceous minerals
Heav	-	Heavy minerals (Garnet, Pyroxene, Amphibole etc)
Opaq	-	Opaque minerals (Magnetite, Ilmenite etc)
Rock	-	Rock fragments
Glauc	-	Glauconite
Tr	-	Trace amounts detectable (<1 grain in 300)

Minimum of 300 grains counted for each sample

APPENDIX B12 Mineralogy of the Silt Fraction (2-63μm)*

CORE	SAMPLE INTERVAL	Qtz	Calc	Plag	K-fe	Mica	Clay	Phill	Talc	Dol	Arag	Gibb	Amph
1	0-2	A	A	C	C	Tr	-	-	-	Tr	-	-	Tr
	55½-57½	A	A	C	P	P	Tr	-	-	Tr	-	-	Tr
5	0-2	A	A	C	C	-	-	Tr	-	-	-	-	Tr
9	7-10	A	C	C	C	P	Tr	-	-	Tr	-	-	P
	46-49	A	A	C	C	Tr	-	-	-	Tr	-	-	Tr
12	0-2	A	A	C	C	P	P	Tr	-	Tr	-	-	P
13	0-2	A	A	C	P	P	Tr	-	-	Tr	-	-	P
14	0-2	A	A	C	P	P	Tr	-	Tr	-	-	-	Tr
15	0-3	A	A	C	C	P	Tr	-	Tr	-	-	-	P
	12½-15½	C	M	C	P	P	Tr	-	Tr	-	-	-	Tr
16	0-2	A	A	C	C	P	P	-	-	-	-	-	P
18	0-2	A	A	C	C	P	Tr	-	-	-	-	-	Tr
19	0-2	A	A	C	P	-	-	-	-	-	-	-	-
	22-24	A	A	C	C	P	-	-	-	-	-	-	Tr
20	0-2	C	M	C	P	Tr	Tr	-	-	-	-	Tr	-
21	0-2½	A	A	C	P	Tr	-	-	-	-	Tr	-	Tr
23	0-2	A	A	C	C	P	Tr	-	-	-	Tr	Tr	Tr
	48-50	A	A	C	P	Tr	Tr	-	Tr	Tr	-	-	Tr
24	0-2	A	A	C	C	Tr	Tr	-	-	Tr	-	-	-
25	0-2	C	M	C	C	P	Tr	Tr	-	-	-	Tr	Tr
26	0-2	A	A	C	P	P	Tr	-	Tr	Tr	-	-	Tr
27	0-2	A	A	C	C	P	Tr	-	-	Tr	Tr	-	Tr
29	0-2	M	Tr	C	C	P	-	-	-	Tr	-	-	P
30	0-2	M	-	C	C	P	Tr	-	-	Tr	-	-	Tr
31	0-2	M	-	C	P	P	Tr	-	Tr	Tr	Tr	-	Tr
32	0-1¾	M	-	C	P	P	-	-	Tr	Tr	-	-	-
34	0-2	M	-	C	P	P	Tr	-	Tr	Tr	-	-	-
5115	0-3	M	-	C	C	P	-	Tr	Tr	Tr	Tr	-	Tr
5116	0-3	M	C	C	C	P	Tr	-	Tr	Tr	-	-	Tr
5117	0-3	M	-	C	C	C	Tr	-	Tr	Tr	-	-	P
	40-43	M	C	C	C	P	Tr	Tr	-	Tr	Tr	-	Tr
	101-104	A	A	C	C	C	P	-	Tr	-	-	-	Tr
	142-145	M	C	A	C	P	Tr	-	-	-	-	-	P
5119	0-3	M	C	C	C	P	Tr	-	-	Tr	Tr	Tr	Tr
	35-38	M	C	C	C	Tr	Tr	-	Tr	-	-	-	Tr
	91-92	M	C	C	C	P	Tr	-	-	-	Tr	Tr	P
	156-159	A	A	C	P	P	P	-	Tr	Tr	Tr	-	Tr
	195-200	A	A	C	P	P	Tr	-	Tr	-	-	-	Tr
5120	∿200	A	A	C	C	P	P	Tr	-	Tr	-	Tr	P
5121	0-3	A	A	C	C	P	Tr	-	Tr	Tr	Tr	Tr	Tr
	49-52	A	A	C	C	C	P	-	Tr	Tr	Tr	-	Tr
	108-111	A	A	C	P	P	P	-	-	Tr	Tr	Tr	Tr
	181-184	A	A	C	P	P	P	-	-	-	Tr	Tr	Tr

APPENDIX B12 (Contd.)

CORE	SAMPLE INTERVAL	Qtz	Calc	Plag	K-fe	Mica	Clay	Phill	Talc	Dol	Arag	Gibb	Amph
5124	190-193	A	A	C	Tr	Tr	Tr	-	-	Tr	-	Tr	Tr
5127	0-4	A	A	C	C	P	Tr	-	-	Tr	-	-	Tr
5751	20-23	C	M	C	C	Tr	-	-	Tr	Tr	-	-	Tr
	81-84	A	A	C	P	Tr	Tr	-	-	Tr	-	-	-
	157-160	A	A	C	P	Tr	-	-	-	-	-	-	Tr
	246-249	A	A	C	P	Tr	Tr	-	-	Tr	-	-	-
5752	32-35	A	A	C	C	P	Tr	-	-	Tr	-	-	Tr
5753	0-3	M	C	C	P	P	Tr	Tr	-	Tr	-	-	Tr
	66-69	A	A	C	P	P	Tr	-	Tr	Tr	Tr	-	Tr
	166-169	A	A	C	C	C	P	-	-	Tr	Tr	-	Tr
	278-282	A	A	C	C	P	Tr	Tr	Tr	Tr	Tr	-	Tr

GRAB	Qtz	Calc	Plag	K-fe	Mica	Clay	Phill	Talc	Dol	Arag	Gibb	Amph
4	A	A	C	C	Tr	-	-	Tr	Tr	-	-	Tr
5726	M	Tr	C	P	-	-	-	-	-	-	-	Tr
5727	M	Tr	C	P	Tr	-	-	Tr	Tr	-	-	Tr

LEGEND:

*	-	X-ray diffraction analyses
Qtz	-	Quartz
Calc	-	Calcite
Plag	-	Plagioclase Feldspar
K-fe	-	K-Feldspar
Mica	-	Illite and Mica
Clay	-	Kaolinite, Chlorite and Smectite
Phill	-	Phillipsite
Talc	-	Talc/Pyrophyllite
Dol	-	Dolomite
Arag	-	Aragonite
Gibb	-	Gibbsite
Amph	-	Amphibole

Ranked, semi-qualitative abundance scale (modified after Matti et al, 1974):

Tr	-	trace (<1%)
P	-	present (1-5%)
C	-	common (5-25%)
A	-	abundant (25-65%)
M	-	major (>65%)

APPENDIX B13 Semi-Quantative Mineralogical Analyses of the Clay Fraction (<2μm)*

a) MARINE SAMPLES

CORE	SAMPLE INTERVAL	17Å	10Å	7Å	V/P
1	0-2	34	43	23	0.16
	55½-57½	47	46	7	0.20
5	0-2	38	34	28	0.26
9	7-10	39	35	26	0.34
	46-49	48	34	18	0.40
12	0-2	48	28	24	0.49
13	0-2	35	40	25	0.47
14	0-2	24	49	27	0.16
15	0-3	29	43	28	0.20
	12½-15½	54	32	14	0.49
16	0-2	27	43	30	0.32
18	0-2	36	37	27	0.31
19	0-2	31	36	33	0.40
	22-24	23	43	34	0.38
20	0-2	28	46	26	0.25
21	0-2½	53	29	18	0.44
23	0-2	56	28	16	0.27
	48-50	52	32	16	0.39
24	0-2	27	54	19	0.26
25	0-2	56	27	17	0.42
26	0-2	52	29	19	0.43
27	0-2	50	33	17	0.46
29	0-2	44	38	18	0.29
30	0-2	12	72	16	0.04
31	0-2	45	42	13	0.13
32	0-1½	15	70	15	0.17
34	0-2	8	75	17	0.08
5115	0-3	3	80	17	0.03
5116	0-3	48	37	15	0.23
5117	0-3	22	55	23	0.21
	40-43	37	39	24	0.09
5117	101-104	54	33	13	0.18
	142-145	29	48	23	0.24
5119	0-3	17	58	25	0.29
	35-38	22	59	19	0
	91-92	45	41	14	0.01
	156-159	62	22	16	0.28
	195-200	52	33	15	0.05
5120	∿200	73	17	10	0.5
5121	0-3	32	47	21	0.19
	49-52	48	33	19	0.36
	108-111	59	28	13	0.38
	181-184	46	33	21	0.25
5124	190-193	65	24	11	0.38
5127	0-4	38	47	15	0.35
5751	20-23	33	45	22	0.28
	81-84	39	38	23	0.37
	157-160	44	38	18	0.31
	246-249	38	47	15	0.31
5752	32-35	51	31	18	0.26
5753	0-3	29	41	30	0.32
	66-69	60	26	14	0.45
	166-169	56	32	12	0.23
	278-282	45	38	17	0.24

GRAB	17Å	10Å	7Å	V/P
4	20	54	26	0.23
5726	38	40	22	0.39
5727	27	48	25	0.4

b) RIVERINE SAMPLES

SAMPLE	17Å	10Å	7Å	V/P
MGR 174	-	51	49	-
175	34	48	18	0.24
176	36	38	26	0.33
177	20	65	15	0.16
178A	50	28	22	0.16
178B	26	49	25	-0.01
179	25	55	20	-0.07
181	16	53	31	-0.18
185	13	34	53	0.17
MGR 186	15	45	40	-0.08
187	24	57	19	0.18
188	6	31	63	0.26
190	31	59	10	0.27
191	-	64	36	-
192	4	41	55	0.07
193	1	59	40	0.14
194	-	30	70	-
195	8	47	45	0.24

LEGEND:

* - X-ray diffraction analyses (glycolated traces)

17Å - % abundance of smectite (montmorillonite)

10Å - % abundance of illite

7Å - % abundance of kaolinite (with very small amounts of chlorite)

V/P - Smectite crystallinity index

APPENDIX C MULTI-AUTHOR PUBLICATIONS

Several sections of the thesis have been published in both international journals and annual reports of the Marine Geoscience Unit. Inferences, conclusions and sections of three multi-authored papers are used in this thesis and thus warrant special mention to note the contribution of the various authors.

In the early stages of the Natal Valley project, a preliminary account of the bathymetry and acoustic stratigraphy was published as Dingle, Goodlad and Martin (1978). This paper was based on seismic interpretation and bathymetry compilations carried out jointly by Mr Martin and myself. Professor Dingle acted as project supervisor, wrote the script and handled editorial duties.

After having identified the M0-M12 Mesozoic magnetic anomaly sequence, I was informed by Mr Martin that he had come to a similar conclusion while working in my study area unbeknown to me. The subsequent paper was published as Goodlad, Martin and Hartnady (1982) which is incorporated in this thesis as section 5.3.4. I personally handled all aspects of manuscript production including data reduction, diagram draughting, text writing and editorial duties. Mr Martin was included as a junior author because he had arrived at similar conclusions while overlapping my work. Dr Hartnady was included since he formed part of the east coast tectonic study group working in close conjunction with Mr Martin.

A discussion of the significance of regional hiatuses in the mid Natal Valley is presented in section 7.3. Hypotheses outlined in sections 7.3.2.3 and 7.3.2.4 have in part been published in Martin, Goodlad and Salmon (1982). Although joint discussion and critical review formulated the content and structure of this paper, Mr Martin undertook the majority of the script writing acting as senior author.